UNIVERSIDADE FEDERAL DO RIO GRANDE DO SUL

INSTITUTO DE BIOCIÊNCIAS

PROGRAMA DE PÓS-GRADUAÇÃO EM ECOLOGIA

Tese de Doutorado

Evolução morfológica na radiação dos roedores sigmodontíneos: ecologia e história evolutiva

RENAN MAESTRI

Porto Alegre, março de 2017

Evolução morfológica na radiação dos roedores sigmodontíneos: ecologia e história evolutiva

Renan Maestri

Tese de Doutorado apresentada ao Programa de Pós-Graduação em Ecologia, do Instituto de Biociências da Universidade Federal do Rio Grande do Sul, como parte dos requisitos para a obtenção do título de Doutor em Ciências com ênfase em Ecologia.

Orientador: Prof. Dr. Thales Renato Ochotorena de Freitas

Coorientador: Prof. Dr. Rodrigo Fornel

Comissão Examinadora

Profa. Dra. Maria João Ramos Pereira (UFRGS)

Prof. Dr. Nelson Jurandi Rosa Fagundes (UFRGS)

Prof. Dr. José Alexandre Felizola Diniz-Filho (UFG)

Porto Alegre, março de 2017

"In fact, evolution is so messy that a faithful description of real cases converts the science into natural history, in which unique details are as important as the principles by which they are explained."

Edward O. Wilson
(1992) The Diversity of Life

AGRADECIMENTOS

Escrever uma tese de doutorado é um imenso privilégio. Foram incontáveis horas lendo, pensando, criando e podendo me dedicar aquilo que eu gosto de fazer, e na maior parte do tempo sem interrupções ou outros afazeres. E eu ainda tive muita ajuda direta e indireta durante todo o tempo. Certo de não conseguir expressar toda a ajuda que recebi, ficam aqui alguns breves agradecimentos:

À minha mãe por todo apoio, carinho e amor desde sempre.

Ao meu pai por me ensinar firmeza e persistência.

À Raissa, Arthur e Ivete pela alegria, descontração e suporte.

À Kamila Correa pelo amor, equilíbrio, apoio emocional, paciência e confiança.

Ao Thales Freitas, pela orientação, oportunidade, confiança, amizade, liberdade, e por todas as histórias e os ensinamentos biológicos e de vida.

Ao Rodrigo Fornel por me apresentar a morfometria geométrica, pela parceria nas viagens, amizade e confiança.

Ao Bruce Patterson pelo aprendizado durante o sanduíche e depois dele, por ampliar minha visão sobre ciência, pela constante motivação e pela confiança e amizade.

Ao Leandro Monteiro pela parceria e oportunidade de aprender mais sobre evolução e métodos filogenéticos comparativos.

Ao Leandro Duarte pelo incentivo desde o início do doutorado, e por me apresentar a ecologia filogenética de comunidades.

À Sandra Hartz por todos os ensinamentos ecológicos e didáticos, e por todo o suporte operacional durante o doutorado.

À Lena Geise pela confiança e pela oportunidade de entrar no mundo da filogeografia e dos *Akodon*.

À Gislene Gonçalves e à Ana Carolina Carnaval pelos ensinamentos, oportunidades de aprendizado e pela insistência em mim na fase menos desenvolvida do meu doutorado.

Ao André Luís Luza, Augusto Ferrari, Lurdiana Barros e Nate Upham pelas discussões e ajuda em momentos essenciais da tese.

Ao Bruno Kubiak, Daniel Galiano e Leandro Borges pela amizade, cervejas e discussões sobre ciência e carreira.

Ao Jorge Reppold Marinho pelo incentivo e por todos os ensinamentos mesmo de longe.

À todos os colegas do Laboratório de Citogenética e Evolução com que convivi durante esses quatros anos, pela energia, discussões, companhia e ajuda de diversos tipos em vários momentos.

À Lucia Nunes e ao Luciano Silva pela eficiência e suporte no laboratório, e à Silvana Barzotto pelo apoio junto ao PPG.

Ao Marco Mello, por inspiração científica geral, conselhos bem-vindos e motivação para trilhar a jornada do cientista: https://marcoarmello.wordpress.com/.

Aos curadores de coleções dos museus que visitei, devidamente apresentados ao longo da tese, sempre atenciosos e dispostos a ajudar durante uma etapa essencial do doutorado.

Ao programa de Pós-Graduação em Ecologia da UFRGS pela formação e inúmeras oportunidades de crescimento, e à CAPES pela bolsa de doutorado e do PDSE.

SUMÁRIO

RESUMO

Radiações evolutivas estão entre os eventos mais fascinantes da evolução. Grande parte da diversidade da vida, tanto de espécies como ecológica, surgiu nos breves intervalos temporais de rápida especiação que configuram as radiações. As causas ecológicas e não-ecológicas do surgimento da diversidade em radiações evolutivas, em especial nas radiações adaptativas, são tema de pesquisa há muito tempo, pelo menos desde que Darwin observou a imensa diversidade de um grupo de pássaros nas ilhas Galápagos. Desde então, as ilhas têm sido os ambientes ideais para o estudo desse fenômeno, e foi a partir das observações e experimentos em ilhas que toda a teoria ecológica das radiações evolutivas surgiu. Contudo, as causas ecológicas das radiações explosivas ocorridas em amplas escalas continentais permanecem tema de constante debate. Nesta tese, foram investigados os determinantes ecológicos e não-ecológicos (e.g., geografia, contingências históricas, efeitos filogenéticos) da evolução morfológica dos roedores sigmodontíneos durante sua radiação na região Neotropical, em especial no continente sul-americano. Para isso, foi quantificada a morfologia do crânio e mandíbula de mais de dois mil exemplares do grupo, e foram investigadas variações ecomorfológicas nos níveis interespecífico (I), intraespecífico (II), e entre assembleias de sigmodontíneos (III). Na Parte I da tese, foram investigadas duas predições da teoria da radiação adaptativa, a correlação-fenótipo ambiente (capítulo 1) e a funcionalidade do fenótipo através da força da mordida (capítulo 2), permitindo determinar o papel da divergência ecológica na evolução morfológica das espécies. Na Parte II (capítulo 3), foram investigadas as contribuições relativas de processos determinísticos e neutros sobre a variação morfológica entre populações de uma espécie de roedor sigmodontíneo amplamente distribuída, *Akodon cursor*. Na Parte III, a influência da variação ambiental e da distribuição espacial das linhagens filogenéticas de sigmodontíneos sobre o tamanho

corporal (capítulo 4) e forma do crânio e mandíbula (capítulo 5), foram investigados no contexto biogeográfico da variação no tamanho e forma média entre assembleias de sigmodontíneos. As contribuições originais desta tese foram: (i) mostrar que a radiação evolutiva dos roedores sigmodontíneos foi guiada principalmente por fatores históricos e geográficos ao invés de fatores ecológicos; (ii) sugerir que radiações evolutivas ocorridas em escalas continentais, especialmente de roedores, têm um componente geográfico e histórico mais determinante do que o componente ecológico; (iii) revelar que a força da mordida varia pouco entre roedores sigmodontíneos herbívoros e granívoros, o que provavelmente é resultado do fenótipo generalista desses roedores; (iv) apontar que sigmodontíneos com dieta insetívora têm uma taxa de evolução mais rápida, e parecem estar evoluindo sua forma do crânio/mandíbula e sua força da mordida em uma direção diferente das demais espécies; (v) demonstrar que, dentro de uma espécie de sigmodontíneo (*Akodon cursor*), fluxo gênico e deriva genética explicam melhor a forma do crânio entre populações, enquanto a variação ambiental explica melhor o tamanho do crânio, indicando que o tamanho é uma característica mais lábil e mais sujeita a pressões ambientais do que a forma do crânio; (vi) mostrar que a variação biogeográfica, tanto do tamanho quanto da forma média do crânio/mandíbula entre assembleias de sigmodontíneos, está sob influência da distribuição diferencial das linhagens filogenéticas ao longo do espaço geográfico, bem como de variáveis ambientais; o que indica conservação filogenética de nicho à nível de metacomunidades. De modo geral, ao investigar as contribuições relativas dos componentes adaptativo e não-adaptativo da evolução morfológica, foram obtidas informações importantes para conhecer as causas da diversificação morfológica em Sigmodontinae, aumentando nosso conhecimento sobre as origens de toda a diversidade biológica.

Palavras-chave: Adaptação, biogeografia funcional, ecologia filogenética de comunidades, evolução morfológica, história evolutiva, morfometria geométrica, métodos filogenéticos comparativos, macroecologia, macroevolução, Neotrópicos, radiações evolutivas, seleção natural.

ABSTRACT

Evolutionary radiations are among the most fascinating phenomena of evolution. Most of the biological diversity on the planet, both in terms of species and ecological diversity, appeared during these brief intervals of rapid speciation. The ecological and non-ecological causes of the emergence of diversity in evolutionary radiations, especially in adaptive radiations, have long been the subject of research, beginning with Darwin and his notice of the astonishing diversity of bird forms in the Galapagos Islands. Islands have since been ideal environments in which to study evolutionary and adaptive radiations, and indeed it was from observations and experiments on islands that all ecological theory of evolutionary radiations arose. However, the ecological causes of explosive radiations occurring on large continental scales are still a matter of debate. In this dissertation, I investigated the ecological and non-ecological (e.g., geography, historical contingencies, phylogenetic effects) determinants of morphological evolution in sigmodontine rodents during their radiation in the Neotropical region, particularly on the South-American continent. The skull and mandible morphology of more than two thousand specimens was quantified, and ecomorphological variation was investigated on three levels: interspecific (I), intraspecific (II), and among sigmodontine assemblages (III). In part I, two predictions from the ecological theory of adaptive radiation were investigated: the phenotype-environment correlation (chapter 1), and the trait utility through the bite force (chapter 2). This approach enabled determination of the role of ecological divergence in species morphological evolution. In part II (chapter 3), I investigated the relative contributions of deterministic and neutral processes to morphological variation among populations of one widely distributed sigmodontine species, *Akodon cursor*. In part III, I investigated the influence of environmental variation and spatial distribution of phylogenetic lineages on body size (chapter 4) and on shape of the skull and mandible

(chapter 5), in the context of biogeographical variation of mean size and shape in sigmodontine assemblages. The original contributions of this dissertation are as follows: (i) to demonstrate that the evolutionary radiation of sigmodontines was driven mainly by historical and geographical factors instead of ecological factors; (ii) to suggest that evolutionary radiations on continental scales, especially rodent radiations, have a more determinant historical and geographical component than an ecological one; (iii) to show small variation in bite force between sigmodontine herbivores and granivores, which is likely a consequence of the generalist phenotype of these rodents; (iv) to highlight that insectivorous sigmodontines have a faster rate of morphological evolution than other diet groups, and that skull and mandible morphology and bite force are evolving in different directions than in other species; (v) to demonstrate that within a sigmodontine species (*Akodon cursor*), gene flow and genetic drift better explain variation in skull shape among populations, while environmental variation better explains variation in skull size, which suggests that size is more labile feature than shape and thus more prone to change with environmental pressures; and (vi) to show that biogeographical variation in mean body size, mean skull shape, and mean mandible shape across sigmodontine assemblages is influenced by the different distributions of phylogenetic lineages over geographical space, as well by environmental variables, which indicates phylogenetic niche conservatism at the metacommunity level. These results shed light on some of the factors driving morphological diversification in Sigmodontinae. Further, the analytical approach(es) utilized may be useful for general investigations of the relative contributions of adaptive and non-adaptive components of morphological evolution, thereby potentially increasing our knowledge of the origins of all biological diversity.

Keywords: Adaptation, evolutionary history, evolutionary radiation, functional biogeography, geometric morphometrics, macroecology, macroevolution, morphological evolution, natural selection, Neotropics, phylogenetic community ecology, phylogenetic comparative methods.

LISTA DE TABELAS

Capítulo 1

Capítulo 2

Capítulo 3

Capítulo 4

Capítulo 5

LISTA DE FIGURAS

Introdução Geral

Capítulo 1

Capítulo 2

Capítulo 3

Capítulo 4

Capítulo 5

INTRODUÇÃO GERAL

Durante meu doutorado, eu investiguei a evolução morfológica de um grupo de roedores (Rodentia, Cricetidae, Sigmodontinae) que colonizou a região Neotropical e partes da América do Norte. Na América do Sul, o grupo sofreu uma extensa radiação, que resultou no surgimento de aproximadamente 400 espécies em um período de tempo relativamente curto – cerca de 10 milhões de anos. Os capítulos desta tese buscam compreender os fatores históricos e ecológicos envolvidos durante o processo de evolução morfológica do grupo, dentro do escopo teórico das radiações evolutivas no nível de espécies, e da biogeografia funcional no nível de comunidades. A tese é melhor compreendida dentro de quatro quadros conceituais: 1) o estudo da adaptação conforme analisado pelos métodos filogenéticos comparativos atuais, 2) a ecologia das radiações evolutivas e das radiações adaptativas, 3) a evolução fenotípica e a radiação dos roedores sigmodontíneos, e 4) a biogeografia funcional no nível de metacomunidades. Acredito que a tese consegue avançar o conhecimento nesses quatro tópicos, fornecendo informações inéditas para o estudo da adaptação de forma geral e especialmente dentro de radiações evolutivas, aumentando nosso conhecimento sobre a história evolutiva e ecológica dos roedores sigmodontíneos, e ajudando a compreender os fatores históricos e ecológicos responsáveis pela variação morfológica no nível de metacomunidades. Uma breve revisão destes tópicos compõe a próxima seção da introdução. Após, segue uma seção com os objetivos e a estrutura da tese, onde são apresentados os capítulos que a compõem.

Revisão bibliográfica

Evolução biológica e o estudo da adaptação

Um dos principais objetivos da biologia evolutiva é atribuir à seleção natural e à história evolutiva os seus respectivos papéis na explicação de processos evolutivos ou estruturas biológicas de interesse (Stearns & Hoekstra, 2005). A seleção natural continua sendo a principal explicação para a adaptação, embora o papel das restrições evolutivas seja cada vez melhor entendido e apreciado (Futuyma, 2010). Fatores como contingências históricas, correlações genéticas entre caracteres e limites nos caminhos de desenvolvimento, entre outros, podem limitar ou impedir a adaptação (Gould & Lewontin, 1979; Futuyma, 2010).

Convergências evolutivas são especialmente bem explicadas por seleção natural, e constituem uma das principais evidências para a adaptação (embora convergências também possam ser consideradas evidência de restrições evolutivas, veja Losos 2011a para uma revisão). Uma convergência é definida, da maneira mais simples, sempre que espécies distantemente aparentadas evoluem soluções fenotípicas similares para um mesmo problema ecológico. Esse fenômeno é bastante comum, e o raciocínio (adaptativo) para a evolução de convergência é simples: dada uma mesma pressão seletiva (e.g., ambientes similares), espécies diferentes vão evoluir para uma mesma direção no espaço fenotípico, levando à um aumento na sua aptidão (Stayton, 2015).

Por outro lado, longos períodos de estase em caracteres fenotípicos constituem um dos fenômenos mais difíceis de explicar. Falta de variação genética, baixas taxas de mutação, alta correlação genética levando a alta integração em caracteres complexos, são todos fatores intrínsecos que podem explicar longos períodos de estase em caracteres fenotípicos (Futuyma, 2010). No entanto, fatores externos também podem estar envolvidos. A seleção natural estabilizadora tem sido invocada como uma potencial explicação para conservação de caracteres por longos períodos (Estes & Arnold, 2007).

Distinguir entre tais fatores intrínsecos e extrínsecos é particularmente difícil, especialmente em um cenário de longo prazo temporal (Jablonski, 2000).

Por exemplo, sabemos hoje que a evolução pode ocorrer de forma bastante rápida. Um dos exemplos mais marcantes nos mostra que os tentilhões das ilhas galápagos podem sofrer seleção que conduza a bicos pequenos em um ano e grandes no outro (Grant & Grant, 2008). Com efeito, isso também altera nossa interpretação da evolução em longos períodos de tempo. Mesmo a detecção de aparente restrição ou evolução neutra de um caráter pode na verdade ser resultado de múltiplas e rápidas oscilações na direção e na força da seleção natural (O'Meara et al., 2006). No nível macroevolutivo, atribuir corretamente os papéis relativos da seleção natural e de restrições evolutivas é desafiador.

O próprio conceito de adaptação entra na discussão ainda não resolvido. A escola cladística tradicionalmente considera adaptação apenas os eventos de evolução independentes, ao custo de considerar as plesiomorfias (retenção de caracteres ancestrais) unicamente como tal, sem que estas produzam evidência suficiente para serem consideradas adaptação. No entanto, outra visão (Hansen, 1997) sugere que se houve manutenção de caráter por longos períodos de tempo, esse atributo resistente à mudança deve estar sob efeito de seleção natural estabilizadora, e portanto, configura uma adaptação (Hansen, 2014). De outro modo, se o atributo não estivesse sob seleção, seria esperado que, ao longo do tempo, o caráter se modificasse ao acaso e assumisse outras formas. Por exemplo, apesar das penas nas aves terem surgido uma única vez, ninguém argumentaria que elas não são uma adaptação. O uso de filogenias junto com os métodos comparativos surge para ajudar a distinguir eventos de adaptações independentes (e detectar convergências) daqueles de conservação do atributo por longos períodos, e para ajudar a inferir quais processos evolutivos deram origem aos atuais padrões observados – o resultado da evolução (Monteiro, 2013; Stayton, 2015).

A partir das restrições evolutivas surgem os efeitos filogenéticos. No modelo mais simples de evolução de um atributo, que imita a evolução neutra (i.e. por deriva genética), quanto mais próximas duas espécies forem filogeneticamente, mais provável que elas sejam similares fenotipicamente (evolução por movimento Browniano – Felsenstein, 1985). Esse modelo Browniano de evolução descreve mudanças não direcionais no fenótipo ao longo do tempo, que podem surgir como resultado de deriva genética ou de seleção natural com mudança constante nos ótimos evolutivos (seleção natural flutuante – O'Meara, 2006). O papel da história evolutiva em moldar o fenótipo ao longo do tempo torna necessária a consideração da história (exemplificada em uma árvore filogenética) no estudo da adaptação (Felsenstein, 1985, Harvey & Pagel, 1991).

Outros fatores também podem levar a efeitos filogenéticos. A seleção natural estabilizadora com diferentes ótimos adaptativos (quando espécies próximas filogeneticamente sofrem pressão de seleção similar e diferentes pressões seletivas existem para clados diferentes ao longo da filogenia) pode levar a um grande efeito filogenético (a.k.a. alto sinal filogenético), onde o fenótipo está bem agrupado ao longo da árvore filogenética (Losos, 2011b). Um modelo evolutivo que considere, além do componente de deriva (Browniano – Felsenstein, 1985), também esse componente seletivo, imitando a presença de diferentes ótimos adaptativos ao longo de uma filogenia, foi proposto por Hansen & Martins (1996) e Hansen (1997) – e chamado de modelo de Ornstein-Uhlenbeck (OU). O uso frequente desse modelo em estudos de evolução fenotípica começa a partir de Butler & King (2004), que propõem uma maneira de usar o modelo para comparar distintas hipóteses para a evolução de um atributo, a partir da alteração dos parâmetros do modelo para imitar a seleção natural ocorrendo em distintos ótimos ao longo da árvore.

O uso de filogenias e de métodos filogenéticos comparativos para o estudo da adaptação é hoje ubíquo. Testes de sinal filogenético (i.e. a quantificação do quanto espécies filogeneticamente próximas possuem atributos similares) e correção filogenética (e.g. contrastes independentes – Felsenstein, 1985, regressão filogenética – Grafen, 1989) são amplamente empregados no estudo da evolução fenotípica. No entanto, os métodos filogenéticos em geral, e o teste de sinal filogenético em particular, ajudam a entender padrões, mas dizem pouco ou nada sobre processos (Revell et al., 2008). Diferentes processos evolutivos podem gerar o mesmo padrão de distribuição no atributo na filogenia, tornando as filogenias necessárias, mas não suficientes para inferir processos evolutivos (Losos, 2011b).

Por exemplo, sob forte seleção estabilizadora para um único ótimo, seria natural pensar que o sinal filogenético seria forte, indicando grande conservação filogenética de nicho ecológico. No entanto, o que se observa é que quanto maior a força de atração para um único ótimo de seleção estabilizadora, menor é o sinal filogenético (Ackerly, 2009). Isso acontece porque como todas as espécies são atraídas para uma mesma média, os efeitos da história evolutiva (i.e. a posição relativa na filogenia) são perdidos, e o atributo pode assumir valores imprevisíveis pela posição da espécie na filogenia (Losos, 2011b). Por outro lado, em um clado apresentando forte convergência no atributo entre espécies distantemente relacionadas, e grande labilidade, um baixo sinal filogenético também é esperado (Revell et al., 2008; Ackerly, 2009; Wiens et al., 2010). Desta forma, outras alternativas além do sinal filogenético devem ser usadas para inferir processos evolutivos. Uma delas pode ser o teste de hipóteses prévias a partir da seleção de diferentes modelos evolutivos (Monteiro, 2013). Modelos OU com múltiplos ótimos adaptativos, que remetem às paisagens adaptativas de Simpson (1953), por exemplo, podem ser interessantes para explorar relações ecológicas implicadas na evolução fenotípica.

Idealmente, o entendimento do processo de evolução de uma característica fenotípica deve levar em conta o maior número de fatores possíveis, incluindo não só a filogenia, o atributo e correlações ecológicas, mas também dados de história natural e diversidade e distribuição das espécies no espaço geográfico.

Radiações Evolutivas

Radiações evolutivas são eventos onde um grande número de espécies surge em um período de tempo relativamente curto (Schluter, 2000). A especiação rápida dentro de uma radiação pode ser resultado de oportunidade ecológica—radiação adaptativa—ou de múltiplos eventos de alopatria sem um papel predominante do ambiente na especiação—radiação não-adaptativa— (Gittenberger, 1991). Contudo, a distinção binária entre radiação adaptativa ou não-adaptativa pode ser enganosa, já que a maioria dos clados que sofreram radiação provavelmente se localizam em um lugar intermediário dentro desse espectro (Losos & Maher, 2010). Por isso, quantificar o grau de adaptação das espécies é o principal fator na busca por entender o processo conjunto de diversificação de espécies e diversificação fenotípica em uma linhagem que sofreu radiação.

O entendimento do quão adaptativa foi uma radiação nos permite saber o quanto de seleção natural divergente esteve envolvido durante o processo de especiação do grupo. Normalmente, dado um cenário de alta correlação entre uma característica fenotípica e o ambiente, infere-se que a seleção natural divergente teve um papel fundamental durante o processo de especiação do grupo (Schluter, 2000; Rundle & Nosil, 2005). Por outro lado, em linhagens onde a diversificação fenotípica não acompanha um gradiente ambiental, e/ou onde houve pouca diversificação fenotípica, infere-se que a seleção natural não foi predominante durante a especiação do grupo (Rundell & Price, 2009). No último caso, extensa especiação não-ecológica pode ser resultado do

surgimento de barreiras levando a alopatria (Gittenberger, 1991; Rundell & Price, 2009), ou de formas de seleção (e.g. seleção sexual) que não foram causadas por divergência entre ambientes (Rundle & Nosil, 2005).

Dentro do espectro geral das radiações evolutivas, a ênfase é dada ao processo de radiação adaptativa. Futuyma (1998) define esse processo como: "divergência evolutiva dos membros de uma única linhagem filogenética em uma variedade de diferentes formas adaptativas". Isso implica a diferenciação de um ancestral em uma variedade de espécies habitando distintos ambientes, e diferindo nos atributos fenotípicos usados para explorar esses ambientes (Losos & Mahler, 2010). Em um trabalho clássico, Schluter (2000) estabelece quatro critérios para classificar uma radiação como adaptativa: (1) ancestralidade comum, (2) correlação fenótipo-ambiente, (3) utilidade do atributo fenotípico, e (4) especiação rápida. Preencher esses critérios, na busca de entender as causas da diferenciação fenotípica em radiações explosivas, tem sido o foco de inúmeros estudos macroevolutivos com diversos táxons (e.g. Grant & Grant, 2008; Losos, 2009; Maher et al., 2013), embora, em sua imensa maioria, estes estudos tenham sido conduzidos em ilhas, devido à facilidade teórica e prática, comparado com a complexidade deste tipo de estudo em escalas continentais (Schluter, 2000; Harmon et al., 2010). Desta forma, permanece em aberto a questão sobre o quão extenso é o papel da adaptação nas radiações explosivas ocorridas em amplas escalas continentais.

Evidências prévias sugerem que fatores ecológicos distintos influenciam a presença de morfotipos em ilhas versus continente para lagartos *Anolis* (Irschick et al., 1997). Em escala continental, a geografia pode ser um fator mais importante do que variáveis ecológicas para explicar a variação morfológica em esquilos (Zelditch et al., 2015). Por outro lado, um forte componente ecológico (dieta) está implicado na variação morfológica gerada na radiação dos morcegos phyllostomídeos no continente Sul-

Americano (Monteiro & Nogueira, 2011). Deste modo, enquanto as radiações em ilhas com frequência aparentam ser adaptativas (Losos, 2010), ainda não sabemos a frequência com que radiações adaptativas ocorrem em escalas continentais.

Os roedores sigmodontíneos

Os roedores são o grupo de maior sucesso (i.e. maior riqueza de espécies) entre os mamíferos. Mais de 40% das espécies de mamíferos viventes são roedores, e eles ocupam quase todos os ambientes terrestres, com exceção da Antártica (Lacher, 2016). Mais de 60% das espécies de roedores (~ 1400 espécies) estão distribuídas dentro de duas famílias: Muridae e Cricetidae (Fabre et al., 2012). Membros dessas famílias são conhecidos popularmente como ratos e camundongos, e compartilham um ancestral comum datado de aproximadamente 40 milhões de anos, provavelmente originário da Eurásia (Schenk et al., 2013). Devido à sua grande diversidade de espécies, e os múltiplos eventos de especiação rápida (especialmente dentro de Cricetidae e Muridae), os roedores são um grupo interessante para investigar os efeitos da divergência ecológica sobre o fenótipo dentro de radiações ocorridas em escalas continentais.

Os roedores sigmodontíneos (família Cricetidae, subfamília Sigmodontinae) são um grupo monofilético (Lessa et al., 2014) que provavelmente teve origem na América do Norte e colonizou a América do Sul algum tempo antes do fechamento do istmo do Panamá (~ 10 milhões de anos – Vilela et al., 2013). Dentro desse curto período de tempo, o grupo sofreu uma radiação rápida, dando origem a aproximadamente 86 gêneros e 400 espécies no continente sul-americano (Patton et al., 2015). Isso preenche os critérios (1) ancestralidade comum, e (4) especiação rápida, propostos por Schluter (2000) para identificar uma radiação adaptativa. A extensão da correlação fenótipo-ambiente (2), bem como a utilidade do atributo fenotípico (3), serão itens investigados nesta tese.

No continente sul-americano, os sigmodontíneos ocorrem em diversos ambientes: desde florestais até desérticos, e desde o nível do mar até o alto dos Andes (Figura 1; Patton et al., 2015; Maestri & Patterson, 2016). Somada à diversidade de ambientes, os sigmodontíneos apresentam distintas morfologias e distintos modos de vida, onde incluem-se espécies semiaquáticas, fossoriais, arbóreas e terrestres (Patton et al., 2015). Essas evidências empíricas levaram alguns autores a sugerir que a radiação dos sigmodontíneos tenha provavelmente sido adaptativa (Hershkovitz, 1969; Reig, 1981; Engel et al., 1998; Steppan et al., 2004; Parada et al., 2013). Na mesma linha de pensamento, outros estudos com o grupo apontam que a diversificação de espécies pode ter sido fruto de oportunidade ecológica (Schenk et al., 2013; Parada et al., 2015). Se essa conjectura está correta, a maior parte da variação fenotípica entre as espécies deve estar associada à algum gradiente ecológico relevante. Isso sugeriria que a divergência de espécies dentro da radiação esteve associada à divergência ecológica, conforme a teoria da radiação adaptativa (Schluter, 2000).

Embora vários estudos tenham analisado a diversificação de espécies de sigmodontíneos em ampla escala taxonômica (e.g. Parada et al., 2013; Schenk et al., 2013; Leite et al., 2014; Parada et al., 2015), e alguns tenham incluído a diversificação fenotípica com algumas medidas morfológicas externas (Carrizo et al., 2014; Tulli et al., 2016; Alhajeri et al., 2016), nenhum estudo até o momento analisou a extensão da associação entre mudanças morfológicas da forma e tamanho do crânio e variáveis ambientais, testou as predições da radiação adaptativa, ou analisou o tempo e modo da evolução morfológica do grupo em grande escala taxonômica e espacial. Desta forma, nós ainda não sabemos quanto de divergência evolutiva e/ou convergência ecológica está presente no fenótipo das espécies, ou quando a evolução fenotípica foi mais rápida ou mais lenta durante a radiação do grupo.

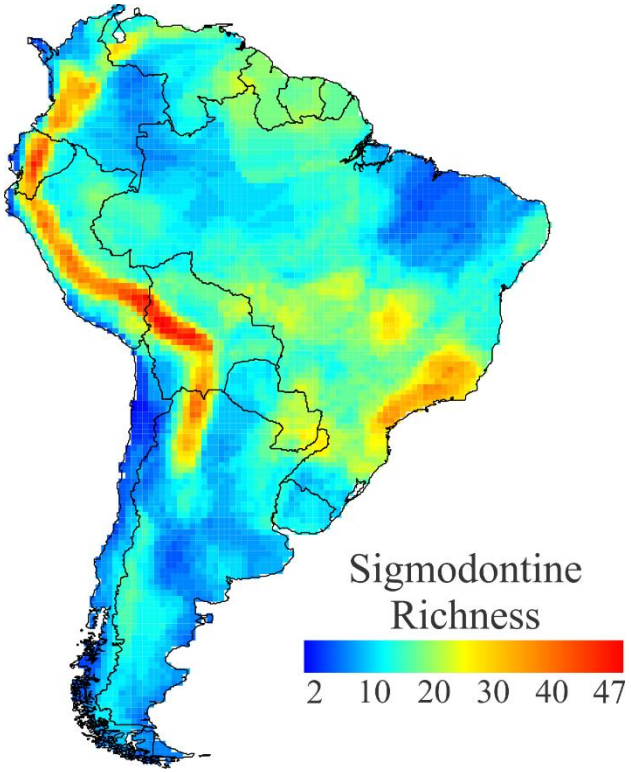

Figura 1. Riqueza de espécies de roedores sigmodontíneos (Rodentia, Cricetidae, Sigmodontinae) na América do Sul. Figura extraída de Maestri & Patterson (2016).

Biogeografia funcional

A biogeografia estuda a distribuição dos organismos ao longo do espaço e do tempo, e busca entender os processos bióticos e abióticos subjacentes à essa distribuição (Brown & Lomolino, 1998). Em conjunto a dados filogenéticos, a biogeografia evolutiva tem um papel integrador, que combina conceitos já conhecidos da biogeografia ecológica e histórica (e.g., filtros ambientais, dispersão e vicariância) com ideias da ecologia filogenética e biologia evolutiva (Morrone, 2009), na busca por elucidar padrões e processos biogeográficos em um contexto histórico-evolutivo.

Tradicionalmente, a biogeografia é centrada na distribuição das espécies e de sua diversidade. Nas últimas décadas, contudo, o estudo da distribuição dos atributos ao longo do espaço e do tempo tem se mostrado promissor, ajudando a descrever e explicar a diversidade de forma dos organismos em escala biogeográfica. Com isso, emerge a

disciplina de biogeografia funcional – "a análise dos padrões, causas e consequências da distribuição geográfica da diversidade de forma e função" (Violle et al., 2014).

Entre as múltiplas abordagens que podem ser empregadas para entender a distribuição de atributos ao longo do espaço, uma delas é o estudo de atributos médios de comunidades (*community-weighted means* – CWM) (Garnier et al., 2004). O CWM é pensado como um atributo funcional agregado, que pode integrar escalas organizacionais de diversidade (Violle et al., 2014). Quando calculado para um conjunto de comunidades conectadas por dispersão entre espécies que interagem mutuamente (uma metacomunidade – Leibold et al., 2004), o CWM pode expressar a dominância funcional de determinado atributo, consequentemente permitindo descobrir quais gradientes ambientais ou históricos estão relacionados com a distribuição funcional. Ao mesmo tempo, entender quais funções os organismos desempenham no seu ambiente pode nos ajudar a descobrir mais sobre as regras de montagem das comunidades.

A distribuição de atributos médios em metacomunidades é portanto o resultado de processos ecológicos e históricos atuando tanto no nível das espécies quanto no do agregado de espécies que formam as comunidades. Ambos os gradientes ambientais e a história evolutiva das linhagens que colonizaram determinada área ajudam a explicar o padrão de distribuição do CWM observado (Pillar & Duarte, 2010).

A história evolutiva (representada pela filogenia) normalmente é considerada no nível de espécies. Cálculos como sinal filogenético, autocorrelação filogenética (Cheverud et al., 1985) e regressão de auto-vetores filogenéticos (Diniz-Filho et al., 1998) podem ser usados para inferir indiretamente o papel relativo da filogenia versus gradientes ecológicos, permitindo explorar também o papel da conservação filogenética de nicho nos atributos (i.e. a fração do atributo conservada ao longo da história evolutiva em função da retenção de nicho ecológico entre espécies aparentadas – Wiens, 2004).

Uma alternativa mais robusta estatisticamente para explorar a correlação fenótipo-ambiente é o uso de regressão filogenética (e.g. *Phylogenetic Generalised Least Squares* - PGLS) (Rohlf, 2001). No entanto, como a regressão filogenética "remove" o componente filogenético, é impossível saber o quanto do atributo é explicado simultaneamente por variação ambiental e história compartilhada (a parte de conservação filogenética de nicho) (Desdevises et al. 2003). No contexto do estudo de atributos funcionais em metacomunidades, essa porção da variação pode ser particularmente interessante.

O papel da história evolutiva, ecologia e conservação filogenética de nicho é, portanto, bem menos entendida no nível funcional de metacomunidades do que no nível de espécies. Enquanto a filogenia é hoje indispensável na explicação da composição e diversidade das comunidades (Webb, 2002; Cavender-Bares et al., 2009), e na explicação da adaptação no nível de espécies (Harvey & Pagel, 1991), ainda não sabemos se a filogenia é importante para explicar o CWM (Pillar & Duarte, 2010; de Bello et al., 2015; Lawing et al., 2016). Algumas das estratégias empregadas nessa direção envolveram a remoção da não-independência filogenética antes de calcular o CWM (Diniz-Filho et al., 2007; Olalla-Tárraga et al., 2010). No entanto, essa abordagem também não permite investigar quanto do CWM é explicado simultaneamente pelo ambiente e pela distribuição histórica das linhagens.

Uma vez que a distribuição de membros de linhagens filogenéticas distintas (ao longo do espaço geográfico) pode determinar quais espécies estão presentes em uma comunidade, e por extensão o CWM, talvez seja importante considerar a distribuição dessas linhagens de maneira explícita (Pillar & Duarte, 2010). Por exemplo, se um clado e todos os seus descendentes são similares morfologicamente, e ocorrem somente na parte sul e fria do continente, enquanto outro clado e seus descendentes, com morfologia

diferente, ocorrem somente na parte norte e quente do continente, uma correlação entre CWM e temperatura irá surgir (Lawing et al., 2016). Essa correlação, no entanto, pode ser espúria, já que pode simplesmente ser resultado da distribuição histórica dos ancestrais que originaram os clados atuais (Lawing et al., 2016).

Para acessar o quanto da variação no CWM é resultado de fatores ambientais, o quanto é explicado pela distribuição histórica das linhagens, e o quanto é compartilhado entre ambos (i.e. conservação filogenética de nicho ao nível de metacomunidades – Pillar & Duarte, 2010), uma estratégia interessante pode ser o uso de uma métrica que capture a variação na composição filogenética das comunidades, permitindo acessar a variação na distribuição de diferentes linhagens entre comunidades ao longo do espaço. As coordenadas principais de estrutura filogenética (*Principal Coordinates of Phylogenetic Structure* – PCPS – Duarte, 2011) capturam essa variação, que pode entrar em um modelo linear junto com variáveis ambientais, permitindo segregar os componentes históricos e ambientais que influenciam o CWM (Pillar & Duarte, 2010).

Objetivos e estrutura da tese

O objetivo principal da tese foi investigar a variação morfológica na forma e tamanho do crânio em roedores sigmodontíneos, ao longo do tempo e do espaço geográfico. Essa investigação foi conduzida em três níveis: i) interespecífico ou macroevolutivo, compreendendo a variação morfológica entre espécies e gêneros de sigmodontíneos, ii) intraespecífico ou microevolutivo, compreendendo a variação morfológica entre populações de uma única espécie amplamente distribuída (*Akodon cursor*) e iii) a nível de metacomunidades, onde a variação morfológica entre assembleias compostas por roedores sigmodontíneos foi investigada. Em todos os níveis, a pergunta principal e subjacente que guiou a tese pode ser resumida como: são as variáveis

ecológicas (i.e. processos determinísticos) ou as contingências históricas que melhor explicam a evolução morfológica do grupo? Responder a essa pergunta exigiu, primeiro, conhecer os padrões de variação morfológica, e depois entender se a variação está mais associada com variáveis ecológicas relevantes ou com simples relações de parentesco entre indivíduos ou espécies, além de variáveis históricas. A partir daí, foi possível inferir quais processos foram potencialmente responsáveis pela evolução morfológica no grupo, e consequentemente geraram a atual diversidade morfológica nos roedores sigmodontíneos.

No capítulo 1, foi investigada a influência da dieta e do modo de vida sobre a variação morfológica de 176 espécies de sigmodontíneos. Dados de mais de dois mil espécimes foram analisados a partir de amostras de museus, dados ecológicos foram coletados a partir da literatura, e uma nova filogenia para o grupo foi apresentada. O objetivo desse capítulo foi investigar o quanto de divergência ecológica está refletido no fenótipo das espécies, o que permitiu inferir o quão adaptativa foi a radiação dos roedores sigmodontíneos. No capítulo 2, foi analisada uma característica funcionalmente importante no desempenho das espécies: a força de mordida. As relações entre a força da mordida, dieta, e a morfologia do crânio e da mandíbula das espécies permitiram avaliar as relações funcionais entre dieta e força da mordida. Esses dois capítulos compõem a Parte I da tese, que investigou a evolução e ecologia morfológica entre espécies e gêneros de sigmodontíneos.

O capítulo 3, que compõe a Parte II da tese, intraespecífica, investigou a evolução e ecologia morfológica de uma espécie de sigmodontíneo (*Akodon cursor*) com ampla distribuição geográfica. Os resultados desse artigo permitiram avaliar os papéis relativos da ecologia e de processos neutros na explicação da variação morfológica entre populações, e comparar se os resultados encontrados são semelhantes entre os níveis

hierárquicos (i.e. entre populações – parte II – e entre espécies, investigados na Parte I da tese).

Os capítulos 4 e 5 abordam a variação ecomorfológica entre sítios (i.e. assembleias ou "comunidades") compostas por roedores sigmodontíneos. O termo comunidade é usado de maneira livre ao longo da tese para indicar uma diversa assembleia de roedores (i.e. comunidade, assembleia ou sítio representam o mesmo), todos consumidores primários ou secundários. Esses dois capítulos compõem a Parte III da tese, que investigou a ecologia morfológica do tamanho e forma entre metacomunidades, e sua relação com variáveis ambientais e com a composição filogenética de comunidades.

Referências

Ackerly, D. (2009) Conservatism and diversification of plant functional traits: evolutionary rates versus phylogenetic signal. *PNAS*, **106**, 19699-19706.

Alhajeri, B.H., Schenk, J. J. & Steppan, S.J. (2016) Ecomorphological diversification following continental colonization in muroid rodents (Rodentia: Muroidea). *Biological Journal of the Linnean Society*, **117**, 463-481.

Brown, J.H. & Lomolino, M.V. (1998) *Biogeography*. 2nd ed. Sinauer Associates, Sunderland, Massachusetts.

Butler, M.A. & King, A.A. (2004) Phylogenetic comparative analysis: a modeling approach for adaptive evolution. *The American Naturalist*, **164**, 683-695.

Carrizo, L.V., Tulli, M.J. & Abdala, V. (2014) An ecomorphological analysis of forelimb musculotendinous system in sigmodontine rodents (Rodentia, Cricetidae, Sigmodontinae). *Journal of Mammalogy*, **95**, 843-854.

Cavender-Bares, J., Kozak, K.H., Fine, P.V.A. & Kembel, S.W. (2009) The merging of community ecology and phylogenetic biology. *Ecology Letters*, **12**, 693-715.

Cheverud, J.M., Dow, M.M. & Leutenegger, W. (1985) The quantitative assessment of phylogenetic constraints in comparative analyses: sexual dimorphism in body weight in primates. *Evolution*, **39**, 1335-1351.

De Bello, F., Berg, M.P., Dias, A.T.C., Diniz-Filho, J.A.F., Götzenberger, L., Hortal, J., Ladle, R.J. & Leps, J. (2015) On the need for phylogenetic 'corrections' in functional trait-based approaches. *Folia Geobot*, **50**, 349-357.

Desdevises, Y., Legendre, P., Azouzi, L. & Morand, S. (2003) Quantifying phylogenetically structured environmental variation. *Evolution*, **57**, 2647-2652.

Diniz-Filho, J.A.F., Sant'Ana, C.E.R. & Bini, L.M. (1998) An eigenvector method for estimating phylogenetic inertia. *Evolution*, **52**, 1247-1262.

Diniz-Filho, J.A.F., Bini, L.M., Rodríguez, M.Á., Rangel, T.F.L.V.B. & Hawkins, B.A. (2007) Seeing the forest for the trees: partitioning ecological and phylogenetic components of Bergmann's rule in European Carnivora. *Ecography*, **30**, 598-608.

Duarte, L.D.S. (2011) Phylogenetic habitat filtering influences forest nucleation in grasslands. *Oikos*, **120**, 208-215.

Duarte, L.D.S., Debastiani, V.J., Freitas, A.V.L. & Pillar, V.D. (2016) Dissecting phylogenetic fuzzy weighting: theory and application in metacommunity phylogenetics. *Methods in Ecology and Evolution*, **7**, 937-946.

Engel, S.R., Hogan, K.M., Taylor, J.F. & Davis, S.K. (1998) Molecular systematics and paleobiogeography of the south American sigmodontine rodents. *Molecular Biology and Evolution*, **15**, 35-49.

Estes, S. & Arnold, S.J. (2007) Resolving the paradox of stasis: models with stabilizing selection explain evolutionary divergence on all timescales. *The American Naturalist*, **169**, 227-244.

Fabre, P., Hautier, L., Dimitrov, D. & Douzery, E.J.P. (2012) A glimpse on the pattern of rodent diversification: a phylogenetic approach. *BMC Evolutionary Biology*, **12**, 88.

Felsestein, J. 1985. Phylogenies and the comparative method. *The American Naturalist*, **125**, 1-15.

Futuyma, D.J. (1998) *Evolutionary Biology*. 3rd ed. Sinauer Associates, Sunderland, Massachusetts.

Futuyma, D.J. (2010) Evolutionary constraint and ecological consequences. *Evolution*, **64**, 1865-1884.

Garnier, E., Cortez, J., Billès, G., Navas, M.L., Roumet, C., Debussche, M., Laurent, G., Blanchard, A., Aubry, D. & Bellmann, A. (2004) Plant functional markers capture ecosystem properties during secondary succession. *Ecology*, **85**, 2630-2637.

Gittenberger, E. (1991) What about non-adaptive radiation? *Biological Journal of the Linnean Society*, **43**, 263-272.

Gould, S.J., & Lewontin, R.C. (1979) The spandrels of San Marco and the Panglossian paradigm: a critique of the adaptationist programme. *Proceedings of the Royal Society B*, **205**, 581-598.

Grafen, A. (1989) The phylogenetic regression. *Philosophical Transactions of the Royal Society of London*, **326**, 119-157.

Grant, P.R. & Grant, B.R. (2008) *How and why species multiply: the radiation of Darwin's finches*. Princeton University Press, 272p.

Hansen, T.F. (1997) Stabilizing selection and the comparative analysis of adaptation. *Evolution*, **51**, 1341-1351.

Hansen, T.F. (2014) Use and misuse of comparative methods in the study of adaptation. *Modern phylogenetic comparative methods and their application in evolutionary biology* (ed. by L.Z. Garamszegi), pp. 351-380. Springer-Verlag, Berlin.

Hansen, T.F., & Martins, E.P. (1996) Translating between microevolutionary process and macroevolutionary patterns: the correlation structure of interspecific data. *Evolution*, **50**, 1404-1417.

Harmon, L.J., Losos, J.B., Davies, T.J., Gillespie, R.G., Gittleman, J.L., Jennings, W.B., Kozak, K.H., McPeek, M.A., Moreno-Roark, F., Near, T.J., Purvis, A., Ricklefs, R.E., Schluter, D., Schulte II, J.A., Seehausen, O., Sidlauskas, B.L., Torres-Carvajal, O., Weir, J.T. & Mooers, A.Ø. (2010) Early bursts of body size and shape evolution are rare in comparative data. *Evolution*, **64**, 2385-2396.

Harvey, P.H. & Pagel, M.D. (1991) *The comparative method in evolutionary biology*. Oxford University Press, Oxford.

Hershkovitz, P. (1969) The recent mammals of the Neotropical region: a zoogeographic and ecological review. *Quaternary Review of Biology*, **44**, 1-70.

Irschick, D.J., Vitt, L.J., Zani, P.A. & Losos J.B. (1997) A comparison of evolutionary radiations in mainland and Caribbean Anolis lizards. *Ecology*, **78**, 2191-2203.

Jablonski, D. (2000) Micro- and macroevolution: scale and hierarchy in evolutionary biology and paleobiology. *Paleobiology*, **26**, 15-52.

Lacher, T.E., Murphy, W.J., Rogan, J., Smith, A.T. & Upham N.S. (2016) Evolution, phylogeny, ecology, and conservation of the Clade Glires: Lagomorpha and Rodentia. *Handbook of Mammals of the World, Volume 6: Lagomorphs and Rodents* (ed. by D.E. Wilson, J.T.E. Lacher and R.A. Mittermeier), pp. 15-26. Lynx Ediciones, Barcelona.

Lawing, A.M., Eronen, J.T., Blois, J.L., Graham, C.H. & Polly, P.D. (2016) Community functional trait composition at the continental scale: the effects of non-ecological processes. *Ecography*, doi: 10.1111/ecog.01986.

Leibold, M.A., Holyoak, M., Mouquet, N., Amarasekare, P., Chase, J.M., Hoopes, M.F., Holt, R.D., Shurin, J.B., Law, R., Tilman, D., Loreau, M. & Gonzalez, A. (2004) The metacommunity concept: a framework for multi-scale community ecology. *Ecology Letters*, **7**, 601-613.

Leite, R.N., Kolokotronis, S., Almeida, F.C., Werneck, F.P., Rogers, D. & Weksler, M. (2014) In the wake of invasion: tracing the historical biogeography of the South American cricetid radiation (Rodentia, Sigmodontinae). *PLoS ONE*, **9**, e100687.

Lessa, E.P., Cook, J.A., D'Elía G. & Opazo J.C. (2014) Rodent diversity in South America: transitioning into the genomics era. *Frontiers in Ecology and Evolution*, **2**, 39.

Losos, J.B. (2010) Adaptive radiation, ecological opportunity, and evolutionary determinism. *The American Naturalist*, **175**, 623-639.

Losos, J.B. (2011a) Convergence, adaptation, and constraint. *Evolution*, **65**, 1827-1840.

Losos, J.B. (2011b) Seeing the forest for the trees: the limitations of phylogenies in comparative biology. *The American Naturalist*, **177**, 709-727.

Losos, J.B. & Mahler, D.L. (2010) Adaptive radiation: the interaction of ecological opportunity, adaptation, and speciation. *Evolution Since Darwin: the first 150 years* (ed. by M.A. Bell, D.J. Futuyma, W.F. Eanes and J.S. Levinton), pp. 381-420. Sinauer Associates, Sunderland, MA.

Maestri, R. & Patterson, B.D. (2016) Patterns of species richness and turnover for the South American rodent fauna. *PLoS ONE*, **11**, e0151895.

Mahler, D.L., Ingram, T., Revell, L.J. & Losos, J.B. (2013) Exceptional convergence on the macroevolutionary landscape in island lizard radiations. *Science*, **341**, 292-295.

Monteiro, L.R. (2013) Morphometrics and the comparative method: studying the evolution of biological shape. *Hystrix*, **24**, 25-32.

Monteiro, L.R. & Nogueira, M.R. (2011) Evolutionary patterns and processes in the radiation of phyllostomid bats. *BMC Evolutionary Biology*, **11**, 137.

Morrone, J.J. (2009) *Evolutionary Biogeography: an integrative approach with case studies*. Columbia University Press, New York.

Olalla-Tárraga, M.Á., Bini, L.M., Diniz-Filho, J.A.F. & Rodríguez, M.Á. (2010) Cross-species and assemblage-based approaches to Bergmann's rule and the biogeography of body size in Plethodon salamanders of eastern North America. *Ecography*, **33**, 362–368.

O'Meara, B.C., Ané, C., Sanderson, M.J. & Wainwright, P.C. (2006) Testing for different rates of continuous trait evolution using likelihood. *Evolution*, **60**, 922-933.

Parada, A., Pardiñas, U.F.J., Salazar-Bravo, J, D'Elía, G. & Palma, R.E. (2013) Dating an impressive Neotropical radiation: molecular time estimates for the Sigmodontinae (Rodentia) provide insights into its historical biogeography. *Molecular Phylogenetics and Evolution*, **66**, 960-968.

Parada, A., D'Elía, G. & Palma, R.E. (2015) The influence of ecological and geographical context in the radiation of Neotropical sigmodontine rodents. *BMC Evolutionary Biology*, **15**, 172.

Patton, J.L., Pardiñas, U.F.J. & D'Elia G. eds. (2015) *Mammals of South America, Vol. 2: rodents*. University of Chicago Press, Chicago.

Pillar, V.D. & Duarte, L.D.S. (2010) A framework for metacommunity analysis of phylogenetic structure. *Ecology Letters*, **13**, 587–596.

Reig, O.A. (1981) Teoría del origen y desarrollo de la fauna de mamíferos de America del Sur. *Monographiae Naturae*, Museo Municipal de Ciencias Naturales "Lorenzo Scaglia", **1**, 1-162.

Revell, L.J., Harmon, L. & Collar, D.C. (2008) Phylogenetic signal, evolutionary process, and rate. *Systematic Biology*, **57**, 591-601.

Rohlf, F.J. (2001) Comparative methods for the analysis of continuous variables: geometric interpretations. *Evolution*, **55**, 2143-2160.

Rundell, R.J. & Price T. D. (2009) Adaptive radiation, nonadaptive radiation, ecological speciation and nonecological speciation. *Trends in Ecology and Evolution*, **24**, 394-399.

Rundle, H.D. & Nosil, P. (2005) Ecological speciation. *Ecology Letters*, **8**, 336-352.

Schenk, J.J., Rowe, K.C. & Steppan, S.J. (2013) Ecological opportunity and incumbency in the diversification of repeated continental colonizations by muroid rodents. *Systematic Biology*, **62**, 837-864.

Schluter, D. (2000) *The ecology of adaptive radiation*. Oxford University Press, New York.

Simpson, G.G. (1953) *The major features of evolution*. Columbia University Press, New York.

Stayton, C.T. (2015) The definition, recognition, and interpretation of convergent evolution, and two new measures for quantifying and assessing the significance of convergence. *Evolution*, **69**, 2140-2153.

Stearns, S.C. & Hoekstra, R.F. (2005) *Evolution: an introduction*. 2nd ed. Oxford University Press, New York.

Steppan, S.J., Adkins, R.M. & Anderson, J. (2004) Phylogeny and divergence-date estimates of rapid radiations in muroid rodents based on multiple nuclear genes. *Systematic Biology*, **53**, 533-553.

Tulli, M.J., Carrizo, L.V. & Samuels, J.X. (2016) Morphological variation of the forelimb and claw in Neotropical sigmodontine rodents (Rodentia: Cricetidae). *Journal of Mammalian Evolution*, **23**, 81-91.

Vilela, J.F., Mello, B., Voloch, C.M. & Schrago, C.G. (2013) Sigmodontine rodents diversified in South America prior to the complete rise of the Panamanian Isthmus. *Journal of Zoological Systematics and Evolutionary Research*, **52**, 249-256.

Violle, C., Reich, P.B., Pacala, S.W., Enquist, B.J. & Kattge, J. (2014) The emergence and promise of functional biogeography. *Proceedings of the National Academy of Science*, **111**, 38.

Webb, C.O., Ackerly, D.D., McPeek, M.A. & Donoghue, M.J. (2002) Phylogenies and community ecology. *Annual Review of Ecology and Systematics*, **33**, 475-505.

Wiens, J.J. (2004) Speciation and ecology revisited: phylogenetic niche conservatism and the origin of species. *Evolution*, **58**, 193-197.

Wiens, J.J., Ackerly, D.D., Allen, A.P., Anacker, B.L., Buckley, L.B., Cornell, H.V., Damschen, E.I., Davies, T.J., Grytnes, J., Harrison, S.P., Hawkins, B.A., Holt, R.D., McCain, C.M. & Stephens, P.R. (2010) Niche conservatism as an emerging principle in ecology and conservation biology. *Ecology Letters*, **13**, 1310-1324.

Zelditch, M.L., Li, J., Tran, L.A.P. & Swiderski, D.L. (2015) Relationships of diversity, disparity, and their evolutionary rates in squirrels (Sciuridae). *Evolution*, **69**, 1284-1300.

PARTE I

MACROEVOLUÇÃO: VARIAÇÃO ECOMORFOLÓGICA ENTRE ESPÉCIES

PART I

MACROEVOLUTION: ECOMORPHOLOGICAL VARIATION AMONG SPECIES

Capítulo 1

The ecology of a continental evolutionary radiation: is the radiation of sigmodontine rodents adaptive?**

Renan Maestri[1,5*], Leandro Rabello Monteiro[2], Rodrigo Fornel[3], Nathan S Upham[4,5], Bruce D Patterson[5], Thales Renato Ochotorena de Freitas[1,6]

[1]*Programa de Pós-Graduação em Ecologia, Universidade Federal do Rio Grande do Sul, Porto Alegre, RS 91501-970, Brazil.*

[2]*Laboratório de Ciências Ambientais, CBB, Universidade Estadual do Norte Fluminense, Campos dos Goytacazes, RJ 28013-620, Brazil.*

[3]*Programa de Pós-Graduação em Ecologia, Universidade Regional Integrada do Alto Uruguai e das Missões, Campus Erechim, Erechim RS 99709-910, Brazil.*

[4]*Ecology and Evolutionary Biology, Yale University, New Haven, CT 06511, USA.*

[5]*Integrative Research Center, Field Museum of Natural History, Chicago, IL 60605, USA.*

[6]*Departamento de Genética, Universidade Federal do Rio Grande do Sul, Porto Alegre, RS 91501-970, Brazil.*

* *Correspondence*: renanmaestri@gmail.com

** Artigo publicado no periódico *Evolution* (2017) 71: 610-632 (doi: 10.1111/evo.13155)

Abstract

Evolutionary radiations on continents are less well understood and appreciated than those occurring on islands. The extent of ecological influence on species divergence can be evaluated to determine whether a radiation was ultimately the outcome of divergent natural selection or else arose mainly by non-ecological divergence. Here, we used phylogenetic comparative methods to test distinct hypotheses corresponding to adaptive and non-adaptive evolutionary scenarios for the morphological evolution of sigmodontine rodents. Results showed that ecological variables (diet and life-mode) explain little of the shape and size variation of sigmodontine skulls and mandibles. A Brownian model with varying rates for insectivory versus all other diets was the most likely evolutionary model. The insectivorous sigmodontines have a faster rate of morphological evolution than mice feeding on other diets, possibly due to stronger selection for features that aid insectivory. We also demonstrate that rapid early-lineage diversification is not accompanied by high morphological divergence among sub-clades, contrasting with island results. The geographic size of continents permits spatial segregation to a greater extent than on islands, allowing for allopatric distributions and escape from interspecific competition. We suggest that continental radiations of rodents are likely to produce a pattern of high species diversification coupled with a low degree of phenotypic specialization.

Keywords: disparity through time, evolutionary models, evolutionary rates, macroevolution, macroevolutionary adaptive landscape, Neotropics, non-adaptive radiation, tempo and mode of evolution.

Introduction

Understanding the processes of speciation and the origin of adaptive forms has long attracted the attention of biologists (e.g., Darwin 1859). Events where many species appear over short time periods are termed evolutionary radiations (Schluter 2000). Such radiations can be either adaptive or non-adaptive. Species may arise following ecological specialization with concurrent phenotypic diversification (Simpson 1944) or else may arise mainly by allopatric effects and historical contingencies without disruptive selection (Gould and Lewontin 1979; Rundell and Price 2009). A radiation is considered adaptive if it involves the differentiation of a single ancestor into an array of species that occupy a variety of niches and differ in the phenotypic traits used to exploit these resources (Futuyma 1998; Losos 2010; Losos and Mahler 2010). Rapid speciation resulting in many species that lack accompanying phenotypic diversification is best termed a non-adaptive radiation (Gittenberger 1991; Rundell and Price 2009).

Schluter (2000) established four criteria to define a radiation as adaptive: common ancestry, phenotype-environment correlation, trait functionality, and rapid speciation. Assessing these criteria and understanding the drivers of phenotypic differentiation in major radiations have been the focus of several macroevolutionary investigations (e.g. Grant and Grant 2008; Losos and Ricklefs 2009; Mahler et al. 2013). Most of these studies have been conducted on islands, because of the theoretical and practical advantages of simple insular systems (Whittaker and Fernández-Palacios 2007) compared to the complexities of this kind of study with richer biotas at continental scales (Schluter 2000; Claramunt 2010; Harmon et al. 2010). Continental radiations may also present different macroevolutionary patterns from those studied in islands, offering new and more extensive empirical information for the study of evolutionary radiations. At continental scales, studies on Neotropical lizards (Pincheira-Donoso et al. 2015), passerines

(Claramunt 2010), and bats (Monteiro and Nogueira 2011) showed that ecological opportunity (the exploitation of resources underutilized by other species) plays a strong role in determining morphological evolution through the existence of distinct adaptive peaks. These studies are among the first to apply the concept of Simpson's macroevolutionary landscape to the phylogenies of continental radiations.

Other studies on continental radiations have shown a more varied relationship between adaptive divergence and ecological opportunity. Derryberry et al. (2011) found constrained morphological evolution in the radiation of Furnariidae, Tran (2014) detected a possible lack of ecological opportunity in the radiation of African colobine monkeys, and Zelditch et al. (2015) found that geography is a very important component in the speciation of diverse and rapidly diversifying continental squirrels. At continental scales, patterns of species and morphological diversification are sometimes found to be decoupled, leading, for instance, to clades with high species diversity but limited ecological variability (Kozak et al. 2006; Burbrink et al. 2012). The role of ecological opportunity in continental radiations is still to be better elucidated, and requires an investigation of both ecomorphological associations and temporal changes in diversity and morphological diversification.

Temporal changes in a radiation explored via cumulative patterns of lineage and morphological disparity through time can inform about the tempo of morphological diversification. Radiations that are considered adaptive are thought to exhibit an "early-burst" model of evolution (Simpson 1944, 1953). An adaptive radiation is predicted to undergo rapid diversification early in its evolutionary course, followed by a slowing in the rate of morphological evolution as niches become filled (Schluter 2000; Tran 2014). Ancestors would have abundant resources and many vacant niches to fill, and speciation would produce descendants that occupy distinct niches in various adaptive zones; later,

when the niches are almost all filled and the rate of novel niche occupation declines, there should be a corresponding decline in rates of phenotypic diversification (Simpson 1944; Schluter 2000; Losos 2010). Recent evidence suggests that this phenomenon may be rarer than previously thought (Harmon et al. 2010; Venditti et al. 2011). Early-Burst is also not a necessary feature of adaptive radiations (Givnish 2015) and its generality needs to be further tested (Stroud & Losos 2016). Harmon et al. (2003) proposed that if taxa rapidly diversify early in their history, they should quickly fill ecological niches, so that little subsequent ecological diversification is expected inside the extant sub-clades. Under this hypothesis, most morphological variation would exist among sub-clades, characterizing a mostly adaptive radiation (Tran 2014). On the other hand, for taxa that diversify gradually throughout their history, species may diversify independently of each other, leading to greater disparity within rather than among sub-clades, a pattern mostly characteristic of non-adaptive radiations. We test that hypothesis by comparing patterns of lineages through time and morphological disparity through time to a major radiation of rodents that colonized and diversified over the entire Neotropical region and adjacent parts of North America.

Rodents are the most successful group in the 200 million-year history of mammals. They comprise more than 40% of all living species and occupy most terrestrial environments (Lacher et al. 2016). The rodent skull characteristically features an elongated rostrum, a pair of chisel-like and ever-growing upper and lower incisors that is separated by a diastema from a battery of cheekteeth, and enlarged masseter muscles (Korth 1994). Rodents are widespread, abundant, and highly diversified. Nevertheless, the extent of morphological specializations of rodents has seldom been explored at large taxonomic and geographic scales. Although most rodents have generalized diets, highly specialized forms, such as strict carnivores, insectivores, and herbivores, can show

convergences in morphology (Samuels 2009; Rowe et al. 2016). The convergence of ecology and morphology is especially well documented for rodents living on different continents (Wood 1947; Samuels and Van Valkenburgh 2008; Rodrigues et al. 2015). Wood (1935: 250) once observed "'Parallelism, parallelism, more parallelism and still more parallelism' is the evolutionary motto of the rodents".

We studied one of the most impressive rodent radiations, which took place during the Neogene in the Neotropical region. The sigmodontine rodents (Cricetidae, Sigmodontinae) are a monophyletic group (Lessa et al. 2014) that likely originated in North America and colonized South America sometime before the closure of the Panamanian isthmus (~10Ma, Vilela et al. 2013). The group has diversified into 86 extant genera and about 400 species in South America (Patton et al. 2015), occurring from sea level to the high Andes and from humid Amazonia to the world's driest desert, the Atacama (Lessa et al. 2014; Maestri and Patterson 2016). Their lifestyles include semiaquatic, fossorial, arboreal, cursorial, and scansorial habits (Patton et al. 2015). Empirical evidence of its Neogene diversification and apparent ecological specialization has led many to suggest that the sigmodontine radiation was probably adaptive (e.g., Hershkovitz 1966; Reig, 1981; Engel et al. 1998; Steppan et al. 2004; Parada et al. 2013). In the same fashion, other studies have shown that species diversification was likely triggered by ecological opportunity (Schenk et al. 2013; Parada et al. 2015). If this is correct, under the theory of adaptive radiation (Schluter 2000), much of phenotypic variation must be linked to a relevant ecological gradient. However, a recent study suggested that muroid morphological diversification seems to be not associated with ecological opportunity, as patterns of disparity through time show a high within-clade disparity, as opposed to an early-burst pattern (Alhajeri et al. 2016). Despite the lack of support for ecological opportunity across all muroid clades, support was strongest for

sigmodontines (in particular for the predominantly South American subclade Oryzomyalia), and ecological variables were not expressly evaluated (Alhajeri et al. 2016).

Despite the remarkable range of habitats used by sigmodontines, no studies have evaluated the extent of skull and mandible shape and size changes during this ecological radiation in association with ecological variables, or explored the tempo and mode of the evolution of these traits at a broad scale. So we still do not know how or whether species have become adapted to specific environments, whether evolutionary divergences and/or ecological convergences have occurred in this group of mammals, and when rates of phenotypic evolution have been faster or slower during their evolutionary history. A few recent investigations of sigmodontine ecomorphology are relevant here. Parada et al. (2015) found no evidence that a tetra-or-pentalophodont molar plan influenced species diversification. Tulli et al. (2016) analyzed the claw morphology of 25 sigmodontine species and showed that only highly specialized forms (natatorial and fossorial) deviated from a generalist claw morphotype. Analyzing bite force, Maestri et al. (2016) found that only insectivorous sigmodontines differed strongly from other diet classes, suggesting that sigmodontines are mostly generalists with respect to this feature. More extensive ecomorphological associations, in terms of both traits and taxonomic sampling, are needed to shed light on the question of how adaptive was the sigmodontine radiation.

Our principal objective here is to determine whether the sigmodontine radiation can be considered an adaptive radiation in terms of cranial and mandibular morphology. This determination hinges on the extent (i.e. the degree) of adaptive disparity involved in the radiation of living species (Losos and Maher 2010). Therefore, we use a combination of morphometrics and comparative methods based on model selection and trait simulation to assess the relationship between morphology and ecological variables (diet and habit)

during sigmodontine evolution. The resulting information can shed light on the role of natural selection in driving divergences during rapid continental radiations. If divergent natural selection was responsible for driving the radiation, we expect a close relationship between morphological variation and ecological variables. We test alternative evolutionary scenarios based on different models—Brownian motion, Ornstein-Uhlenbeck with single and multiple peaks, and Early Burst—to determine the most probable evolutionary course.

Materials and Methods

Sample, morphological, and ecological data

We analyzed 2420 specimens of 176 species and 64 genera of sigmodontine rodents (Table S1). This corresponds to nearly 75% of living genera within the clade. The number of species sampled for each genus was generally proportional, that is, more species were sampled in more diverse genera (see Leite et al. 2014). Nomenclature and classification followed accounts in Patton et al. (2015), updated where necessary (Pardiñas et al. 2016; Teta et al. 2016). Only adult specimens were examined, identified by the complete eruption of the third molar (in occlusion). We took images of skulls in ventral and lateral views and of mandibles in lateral view using a digital camera (Nikon Coolpix P100). All specimens were positioned in the same plane, and the same distance was used from the camera to the subject. On each specimen, 56 landmarks were digitized on the skull in ventral view, 19 landmarks on the skull in lateral view, and 13 landmarks on the mandible (Fig. 1, Table S2). The digitization of landmarks was made in TpsDig2 software (Rohlf 2015). Landmarks were chosen to identify both structural and functional differences among skulls, including some associated with lever arms and others with muscle attachment sites, covering the whole structure. For each view, images were

eliminated if a digitized structure was broken, resulting in 2402 specimens with ventral views, 2401 with lateral views, and 2241 involving mandibles. Views of the skull and mandible were each treated separately in analyses. The matrices of landmark coordinates were superimposed with a Generalized Procrustes Analysis (GPA) that removes undesirable effects of scale, position, and orientation. The ventral view was constrained to symmetry in order to eliminate noise caused by bilateral asymmetry. Size was measured for each view as the centroid size – the square root of the sum of squared distances of each landmark from the centroid of the configuration (Bookstein 1991). A mean shape (i.e. matrices of coordinates after GPA) and size (i.e. log of centroid size) was calculated for each species. An average of centroid size for each species was measured as the arithmetic mean of log centroid size of all skull and mandible views. Mean values of shape and size by species were used in all subsequent analyses, except where a reduction of dimensionality was needed (see *Evolutionary Model Selection* below). GPA was performed using *geomorph* package (Adams and Otarola-Castillo 2013) in the R environment (R Core Team 2016). A list of museums housing the specimens examined, the catalogue numbers of these specimens, and the number of individuals analyzed for each species are found in Table S1.

Two qualitative ecological variables were assessed alongside morphology: diet and life-mode. Dietary information was classified as a factor with four levels representing species which are predominantly herbivores (feeding mainly on vegetation, herbs, leaves and green plant material in general), frugivores/granivores (feeding mainly on seeds, grain, and fruits), insectivores (including carnivores, feeding mainly on insects and/or small vertebrates), or omnivores. As most species are omnivorous and scant information exists regarding the feeding habits of these rodents, we searched the natural history literature to find likely diets of each species, and classified each according to the most

common food resource utilized. Those species without clear feeding preferences were classified as omnivores. The same literature documented the life-mode (habit) variable, classified into six categories: cursorial, scansorial, arboreal, semiaquatic, semifossorial, and fossorial. Diet and habit variables were based on Reid (1997), Nowak (1999), Marinho-Filho et al. (2002), Tirira (2007), Iriarte (2008), Bonvicino et al. (2008), Paglia et al. (2012), Leite et al. (2015), and Patton et al. (2015), supplemented by personal experience (B.D. Patterson).

Phylogeny and timetree

To provide a temporal and evolutionary framework for conducting comparative analyses, we estimated a multi-gene phylogeny for 279 of 413 extant species in Sigmodontinae (including 26 species described since the ~2008 cutoff to the IUCN list; IUCN 2015). We built this timetree from a supermatrix alignment of 11 genes as extracted from a more inclusive 31-gene supermatrix from an unpublished species-level mammalian phylogeny (Upham, Esselstyn, and Jetz, in prep). Here we briefly describe how those DNA data sequences were gathered, curated, and aligned from public databases. The BLAST algorithm (Basic Local Alignment Search Tool; Altschul et al. 1997) was used to efficiently query a local copy of NCBI's "nt" database downloaded on 20 April 2015 and subset to the NCBI GI list for mammals (unix *blastn* executable v2.2.31; Camacho et al. 2009). Aligned hits and taxonomic metadata were returned from BLAST on a per-gene basis and subsequently parsed for redundancy and quality, yielding the single longest sequence for each NCBI taxon ID. Species and subspecies names were then matched to accepted species in the IUCN list (2015), first referencing against a synonym list compiled from several sources (e.g., Wilson and Reeder 2005), and then doing manual verification. Sequence alignments were then performed using MACSE v1.0

(Ranwez et al. 2011) to verify coding frame, plus MAFFT v7.245 (Katoh and Standley 2013) and manual checking.

For Sigmodontinae, the 11 gene fragments we targeted ranged in species sampling from 261 (CYTB) to 10 (RAG2), with a mean of 72.2 species/gene, and included eight nuclear exons and three mitochondrial regions (see Table S3 for details of gene and taxon sampling). The concatenated site-by-taxon supermatrix of 12,330 base pairs (bp) was 21.4% complete, which is a level of missing data (78.6%) comparable to other recent studies (e.g., 81% for squamates in Pyron et al. 2013) and not expected to interfere with accurate phylogeny estimation (Wiens and Morrill 2011; Roure et al. 2013). To root our tree, we also included five species from Tylomyinae (of 10 extant; tylomyines are the closest sister subfamily to Sigmodontinae – Fabre et al. 2012) and designated *Rattus norvegicus* as the primary outgroup (best-sampled member of the Muridae sister lineage – Churakov et al. 2010) to arrive at a total of 285 taxa in the full tree (Fig. S1).

We estimated the topology and relative branch lengths of the phylogeny using MrBayes v3.2.6 (Ronquist et al. 2012). Parameters for the GTR+ Γ model of nucleotide substitution were estimated independently among six character partitions: first-, second-, and third-codon positions grouped across nuclear (nDNA) genes, and the same for mitochondrial (mtDNA) genes. We allowed partition-specific rate variation and set the relaxed clock model (independent gamma rates – Lepage et al. 2007) as a birth-death process, using exponential distributions on the priors for clock rate variance and speciation (with mean of 0.1), a beta prior (0 to 1) on the relative extinction rate, and ingroup sampling probability to 0.671 (=284/423; sigmodontines and tylomyines). We performed four parallel runs of MrBayes on the XSEDE online computing cluster accessed via the CIPRES Science Gateway (Miller et al. 2010), each run consisting of four MCMC chains (three heated and one cold), and sampled every 10,000 steps for

33,330,000 generations. Burn-in of 25% was sufficient for all four runs and resulted in a combined posterior sample of exactly 10,000 independent trees.

The resulting Sigmodontinae phylogeny had ultrametric branch lengths in relative units (expected substitutions/site), which allowed us to perform a multiplicative re-scaling to absolute time (millions of years, Ma). Tree-wide re-scaling usefully allowed for post-hoc flexibility in divergence dating as well as future modularity to larger phylogenies (e.g., as in Jetz et al. 2012; Tonini et al. 2016), so for this study it was preferable to using node age priors. We performed simple branch multiplication from root-to-tip across each tree of the posterior using R. The global mean divergence time of 25.88 Ma (19.09, 34.04) between *Mus*/*Cricetus* (i.e., Muridae/Cricetidae) from the mammalian family-level study of Meredith et al. (2011) served as our root re-scaling point between *Rattus* and the remainder of the tree. We then summarized our posterior sample of timetrees using TreeAnnotator v1.8.2 (Drummond et al. 2012), generating a maximum clade credibility (MCC) tree setting node heights to mean ages. That full MCC tree was then pruned to match the 176 species with morphological data for downstream analyses. See Supplemental Files S1 and S2 for the DNA alignments and resulting tree from these analyses.

Phylogenetic Comparative Analyses

Phylogenetic signal

Phylogenetic signal for each dataset (size, shape of skull in ventral and lateral views, and mandible shape) was calculated using the generalized K statistics (Adams 2014a). The K statistic measures deviations from a Brownian model of evolution (K = 1), where values of K > 1 indicate greater similarity in the attribute than expected under Brownian evolution (usually interpreted as being conserved), and K values < 1 indicate

less similarity in the attribute than expected under Brownian evolution (usually interpreted as being labile) (Blomberg et al. 2003). Phylogenetic signal was calculated using *geomorph* package (Adams and Otarola-Castillo 2013) in the R environment (R Core Team 2016).

Evolutionary Model selection

The use of Ornstein-Uhlenbeck (OU) models to understand the dynamic evolution of traits was first proposed by Hansen and Martins (1996) and Hansen (1997) as an alternative to the simple Brownian model. The OU formula estimates parameters that can express: (i) the "rate of adaptation" (α) towards the optimum θ, which is 0 under Brownian motion, (ii) the intensity of random fluctuations during trait evolution (σ), and (iii) the optimum trait value (θ), which can accommodate more than one optimum (Butler and King 2004; Hansen and Bartoszek 2012). Therefore, whereas trait variance under a Brownian process is simply a function of the time elapsed from root to tips without changes in the trait's mean value over time (Felsenstein 1985), an OU process can incorporate distinct rates of selection as well as variable numbers of selective optima (Beaulieu et al. 2012). Hence, by changing OU parameters, the fit of distinct evolutionary models on continuous traits can be compared to understand phenotypic evolution (Collar et al. 2009; Monteiro and Nogueira 2011; Astudillo-Clavijo et al. 2015; Princheira-Donoso et al. 2015; Scales and Butler 2016). This model-based approach allows a researcher to establish adaptive optima according to *a priori* biological hypotheses and then compare the fit of the hypotheses with actual empirical data (Monteiro 2013).

Here, we estimate adaptive optima according to the hypotheses of diet and life-mode diversification (Fig. 2). We performed stochastic character mapping to estimate ancestral states via likelihood using the make.simmap function of the *phytools* package

(Revell 2012) for the R environment (R Core Team 2016). The optima estimation for each branch on each hypothesis (Fig. 2) was used to test the fit of these multivariate models with size and shape variables (all selected PCs), using functions implemented in *mvMORPH* package (Clavel et al. 2015) in R (R Core Team 2016). The log of centroid size of each species (an arithmetic mean of skull and mandible views) was used as a measure of size. Because the high dimensionality of shape data in the form of aligned coordinates would preclude the use of mean shape data on evolutionary model selection (Monteiro 2013), we reduced its dimensionality by conducting a principal components analysis of shape. We then used a selection of PC's as new shape variables. Principal components selection was based on Horn parallel analysis (Peres-Neto et al. 2005) – five PC's were retained for both skull shape in ventral view and mandible shape, and six components for skull in lateral view. All models fitted were multivariate, because using PC's as univariate variables is potentially problematic, causing an artificial appearance of "early burst", even with data simulated under a Brownian model of evolution (Uyeda et al. 2015). Hypotheses for diet gradually increased in complexity, starting from simple models of two adaptive peaks, separating insectivores from the rest (Diet OU.2In) or herbivores from the rest (Diet OU.2Hb), and progressing to a model (Diet OU.3) segregating herbivores and insectivores from the rest, as these two feeding classes proved to contain specialized rodent species (Samuels 2009). Diet OU.4 discriminated all four feeding classes (Fig. 2). Model hypotheses for life mode also followed a trend of progressive complexity, distinguishing first the specialized arboreal and fossorial genera from the most cursorial ones (Habit OU.3), passing through a hypothesis where groups included scansorial + arboreal, semifossorial + fossorial, cursorial, and semiaquatic forms (Habit OU.4), and ending with all life-mode classes treated separately (Habit OU.6; Fig. 2). Model OU.1 accounts for the hypothesis of single peak of stabilizing selection.

According to the same OU hypotheses, we define Brownian motion models with multiple varying rates (BMMs; Fig. 2). A single rate Brownian motion model was also evaluated (BM1). Finally, the hypothesis of an early-burst model of trait evolution was explored with a model (EB) where the evolutionary rates decrease exponentially with time. Identifying the best scenarios for multivariate trait evolution used model-selection techniques based on information theory (Burham and Anderson 2002). We used Akaike's Information Criterion (AIC) corrected for small sample sizes (AICc), along with estimates of ΔAICc and AICc weights, to rank the models.

Techniques for selecting evolutionary models can be criticized on theoretical and statistical grounds. Cooper et al. (2016) found that OU models are usually favored over simple models like Brownian motion in trees having fewer than 200 taxa. It is also well known that the number of parameters being estimated is limited by the number of species in the tree, a special concern when dealing with highly-dimensional morphometric data (Monteiro 2013). Also, as trait dimensionality increases, larger type I error rates are expected in likelihood tests for evolutionary rate differences based on covariance matrices (Adams 2014b). Even the mitigating solution of using a few PC's can be problematic, as important shape dimensions may be excluded. To investigate whether our model-selection results are reliable and unbiased by these issues, we performed trait simulation and compared simulated data with our empirical data by exploring the shape of Phylogenetic Signal Representation (PSR) curves.

Simulation analysis in PSR plots

Phylogenetic Eigenvector Regression (PVR) was proposed as a method to estimate the amount of phylogenetic signal in data and to distinguish trait variation due to phylogeny from that attributable to other causes (i.e. the specific component, Diniz-

Filho et al. 1998). This is done by regressing the trait against eigenvectors extracted by a principal coordinate analysis of a pairwise phylogenetic distance matrix (Diniz-Filho et al. 1998). The R^2 of the regression between the trait and selected eigenvectors offers an estimate of phylogenetic signal. However, if all eigenvectors are used, the R^2 inevitably reaches 1, and if some eigenvectors are omitted, parts of the phylogeny are ignored (Rohlf 2001). Diniz-Filho et al. (2012) found that if one performs successive PVRs incrementally increasing the eigenvectors by one, and plots the R^2 of the PVRs against the cumulative eigenvalues (in percentage) of the associated eigenvectors, a linear relationship (45° line) is obtained under a Brownian motion model of evolution. This approach, called Phylogenetic Signal-Representation (PSR), also indicates other evolutionary models, such as Ornstein-Uhlenbeck when the shape of the PSR curve becomes curvilinear and falls below the Brownian line (Diniz-Filho et al. 2012). Therefore, PSR offers the ability to visualize the pattern of trait variation along the phylogeny, rather than simply describing it as a number, as do K statistics (Blomberg et al. 2003). This attribute is especially useful when complex patterns are involved, such as OU with multiple adaptive peaks (Diniz-Filho et al. 2012). Indeed, PSR curves have been used to find complex non-stationary patterns in dinosaur data (Diniz-Filho et al. 2015) and to compare the relationship between patterns in trait evolution with OU simulations having different α values (Bini et al. 2014).

Here, we employed the flexibility of the PSR to examine empirical data in comparison with simulated data derived from Brownian and OU (with single and multiple peaks) expectations, simultaneously released to use all shape space. PSR curves for our empirical data were generated either by plotting cumulative phylogenetic eigenvalues against R^2 obtained by multiple regression for size (i.e. log centroid size against the eigenvectors of the PVR), or by Procrustes distance regression of shape against PVR

eigenvectors (i.e. through the procD.lm function of the *geomorph* package), using the full shape space (Adams and Otarola-Castillo 2013). Therefore, the steps of the analysis involved: 1) decompose the phylogenetic distance matrix into eigenvectors (using the PVRdecomp function of the *PVR* package); 2) conduct a sequential regression between response variables (size and shape on each view) and the eigenvectors (i.e. Y ~ eig1; Y ~ eig1+eig2; Y ~ eig1+eig2+eig3; etc. – Diniz-Filho et al. 2012), where the function procD.lm was used when shape was a response variable; and 3) plot the R^2 of each regression of traits on eigenvectors against the cumulative eigenvalues associated with the eigenvectors.

We simulated data using the rTraitCont function (package *ape*, Paradis et al. 2004) over the sigmodontine phylogeny to mimic a trait under Brownian evolution, under OU with a single peak, and under OU with peaks (θ) according to the identified diet and life-mode hypotheses (Fig. 2), treated as different θ values. The alpha parameter was arbitrarily set to 2.0 for all simulated traits. We plotted the PSR curves for the empirical data and for 10,000 simulations of each model, compared the curves visually, and measured the Euclidean distances between the empirical and the average simulated curve for each model, ranked from smaller to larger distances. Euclidean distances were calculated by taking the square root of the sum of the square distances between corresponding points along the y-axis, for two given curves. The OU evolutionary model with a single peak was used to generate simulations varying the alpha parameter (1,2,4,6,8,10), plus a null curve obtained by 10,000 randomizations of trait values, and then compared to the empirical data, following the same procedures described above.

Phylogenetic evolutionary rates

We also quantified and compared rates of morphological evolution among ecological categories shown to be important in model selection (see *Results* section). These rates of trait evolution over time are related to the intensity of random fluctuations during evolution (σ), and not with the "rate of adaptation" (α), both previously described. Therefore, differences in the rate of evolution may be linked with models hypothesizing Brownian evolution with multiple varying rates (BMM; Fig. 2). Quantification of the rate of evolution was conducted for size and shape with the multi-dimensional distance method proposed by Adams (2014b). The rate of evolution (σ^2) describes the accumulation of phenotype variation per unit of time, for each ecological group, and then simulations of phenotypic datasets are used to calculate the probability that each evolutionary rate differ statistically ($p < 0.05$) from others (Adams 2014b). Evolutionary rates were computed using *geomorph* package (Adams and Otarola-Castillo 2013) in the R environment (R Core Team 2016).

Lineage and morphological disparity through time

We evaluated the tempo of sigmodontine diversification using a set of taxonomically completed trees where species unsampled for DNA were imputed to trees based on their known phylogenetic placement. Given our taxon sampling completeness of ~70%, and the non-random location of those missing taxa on the tree (speciose vs depauperate clades) and in space (tropical vs. temperate), this step was essential to obtain an accurate estimate of the rate at which lineages accumulated in Sigmodontinae (e.g., Cusimano and Renner 2010; Brock et al. 2011; Sanmartín and Meseguer 2016). Along with our 279 species sampled for one or more genes (type 1 species), we had 134 missing species in categories of either type 2 (unsampled but in a sampled genus; 115 species) or type 3 (unsampled and in an unsampled genus; 19 species). We constrained missing

species to their assigned genus (type 2) and tribe (type 3), thereby assuming monophyly at the genus and tribe levels, respectively. Taxon assignments are noted in Table S3. The R package PASTIS (Thomas et al. 2013) was used to form the necessary taxonomic constraints for input to MrBayes, where missing species were imputed randomly within those type 2 or 3 constraints and branch lengths were drawn from the same underlying birth-death distribution as the rest of the tree (Jetz et al. 2012; Thomas et al. 2013). The resulting completed posterior trees (413 species each) thus tended conservatively to a birth-death process, and so provided a conservative test of the null hypothesis of constant rate (pure-birth) diversification across the tree. A main advantage of phylogeny-based completion using PASTIS, as compared to other methods of tree completion (e.g., Cusimano et al. 2012), is that it preserves the taxonomically-expected tree shape for downstream applications (Thomas et al. 2013).

We randomly selected 100 completed trees from the PASTIS posterior sample to perform lineage diversification analyses of Sigmodontinae. We generated a lineage-through-time (LTT) plot to visualize the rates of lineage accumulation and detect if they depart from the constant-rates null model. For instance, lineages may have diversified at a faster rate early in their evolution with subsequent decline, which is a prediction of niche-filling in island adaptive radiations (Phillimore and Price 2008). We used the gamma statistic (γ-test, Pybus and Harvey 2000) to empirically evaluate the distribution of internode distances (i.e. waiting times to speciation) throughout the sample of completed timetrees. This two-tailed test measures whether most of the branching events are concentrated closer to the root of the phylogeny ($\gamma<0$), or instead closer to the tips ($\gamma>0$); $\gamma= 0$ when lineage diversification follows constant pure-birth diversification (Pybus and Harvey 2000; Pincheira-Donoso et al. 2015). The LTT plot of 100 trees, 10,000 simulations of a pure-birth model, and the gamma test were performed in the

phytools package (Revell 2012) in the R environment (R Core Team 2016). The sample of posterior completed trees for all sigmodontines and the group's principal subclade Oryzomyalia are available in Supplemental Files S3 and S4.

The mode of morphological diversification was evaluated as morphological disparity through time (DTT), plotted for the accumulation of morphological variation among clades (size and shape of skull and mandible). Disparity was measured as the average squared Euclidean distance among pairs of species. The DTT plots were calculated independently for log size, skull shape in ventral and lateral views, and mandible shape. DTT calculates mean phenotypic disparity through each step in time (i.e. each divergence event) and compares the observed disparity with a pattern of disparity simulated under a Brownian model of evolution (Harmon et al. 2003). At each step, DTT measures the disparity within sub-clades (i.e. those sub-clades present at that time) in relation to total disparity (Rowe et al. 2011). Values of observed relative disparity range from 0 to 1 at each step. Values near 0 imply that the phenotypic variation is concentrated *among* sub-clades, so that little variation is present *within* sub-clades, while values near 1 indicate that variation is high within sub-clades, with less variation among them (Harmon et al. 2003). Accordingly, if variation is high within sub-clades, it indicates high overlap of sub-clades in morphological space (Harmon et al. 2003). Empirical DTT patterns were compared to the average of 10,000 simulations under Brownian motion. Significance testing was performed using the Morphological Disparity Index (MDI) statistics. MDI measures the area between the empirical and the median of the simulated curves, and provide a *P*-value by calculating proportions of deviations of the empirical from the 10,000 simulated curves. A two-tailed test was performed following Slater et al. (2010). DTT plots were generated in the *geiger* package (Harmon et al. 2008) of R

environment (R Core Team 2016), and MDI tests used the Slater's dttFullCIs function (available at http://fourdimensionalbiology.com/code/).

The Oryzomyalia radiation

The explosive radiation of sigmodontine rodents is hypothesized to be at the base of its subclade Oryzomyalia (Schenk et al. 2013; Leite et al. 2014; Parada et al. 2015), which includes all tribes save the Sigmodontini and Ichthyomyini, instead of the subfamily as a whole. To check for differences between all sigmodontines and the Oryzomyalia radiation, we repeated most of the analyses (K statistics, evolutionary model selection, evolutionary rates, LTT and DTT) excluding non-Oryzomyalia sigmodontines.

Results

Phylogenetic signal

Phylogenetic signal for all morphological datasets returned a similar low value (size – K= 0.79; skull shape ventral – K= 0.72; skull shape lateral – K= 0.74; shape mandible – K= 0.63; all statistically significant at $P< 0.05$), indicating that morphology is slightly less structured by phylogeny than expected under a Brownian model of evolution. Each dietary and life-mode category is distributed over the entire phylogeny (Fig. 2), with notable exceptions being the absence of insectivores in the tribes Oryzomyini and Phyllotini, and of herbivores and frugivores/granivores in the tribe Akodontini. Convergences in diet and life mode across the phylogenetic tree seem not to be accompanied by morphological specializations of the skull, as both diet and life mode have visible overlaps on size (Fig. 3) and shape spaces (Fig. 4). Size differentiation was mainly driven by the large size of herbivorous species, as well as semiaquatic (e.g. *Nectomys*, *Holochilus*, *Lundomys*) and semifossorial ones (e.g. *Kunsia*, which was also

considered to have semiaquatic habits by Bonvicino et al. 2008; Fig. 3). The PCA of skull and mandible shape variation (Fig. 4) showed an overall tendency for insectivores to lie in a different direction from frugivores/granivores and herbivores in the shape space of the first and second principal components, while omnivores were scattered over this state space.

Evolutionary Model selection

Results of the evolutionary model selection are presented in Tables 1 and 2. For size, the Brownian model with 6 varying rates--corresponding to the six-habit hypothesis (Fig. 2)-- was found to be the best model (i.e. the one with ΔAICc= 0) compared to other models of diet and life mode (Table 1). Nevertheless, the two subsequent models differ from the best model by ΔAICc<4 and can be considered to have similar statistical support. There is also a tendency for models with more parameters to receive highest support. A roughly similar number of BM and OU models with diet and habit received high statistical support, but those with habit ranked better. For shape data, the best model was the two-rates Brownian model (Diet BMM.2In – with different rates for insectivores and the remainder) for all views (Table 2). Overall, Brownian models were favored over OU, and models with diet were favored over models with habit. Notably, the early-burst model received low support in all cases.

Simulation analysis in PSR plots

The patterns of PSR curves were similar for all morphological data (Fig. 5). Skull shape and mandible curves are very close, and the curve for size differs only slightly (Fig. 5). The results of comparing simulated curves (the mean of 10,000 simulations under distinct evolutionary models of trait evolution with α= 2) on morphological data is given

in Table 3. A model segregating insectivores from others (OU.2In) was closest to all empirical morphological curves, possibly indicating a degree of specialization in morphology accompanying an insectivorous diet. The comparisons of OU with distinct alphas on morphological data is shown in Table 4, with curves presented in Fig. 5C. Overall, a weak pull towards a single optimum was detected in morphological data (α= 1), with the empirical curves falling mostly inside the confidence interval of the Brownian curve in the first few eigenvectors, and approaching an OU curve in the last ones.

Phylogenetic evolutionary rates

We compared differences in evolutionary rates between insectivores and others (see Fig. 2 – BMM.2In). The evolutionary rates differ statistically among this two diet groups for shape (ventral: $\sigma^{2max/min}$=2.04, *P*= 0.001; lateral: $\sigma^{2max/min}$= 2.24, *P*= 0.001; mandible: $\sigma^{2max/min}$= 2.94, *P*= 0.001), but not for size ($\sigma^{2max/min}$= 1.03, *P*= 0.96). Insectivores have a higher evolutionary rate when compared to others, for all shape views (ventral: In σ^2= 5.14×10^{-6}, On σ^2= 2.52×10^{-6}; lateral: In σ^2= 2.20×10^{-5}, On σ^2= 9.81×10^{-6}; mandible: In σ^2= 6.94×10^{-5}, On σ^2= 2.36×10^{-5}).

Lineage and morphological disparity through time

The lineages-through-time plot (Fig. S2) suggests that sigmodontine lineages have accumulated roughly as expected given constant rates of lineage birth and death through time. Across 100 completed trees we calculated a γ mean of -1.75 (95% confidence interval: -2.97, -0.63), which is slightly lower but statistically equivalent to the critical value of $\gamma < -1.645$ expected if branching was concentrated early in evolution. Use of taxonomically complete trees in this case allows for direct comparison to the critical value, rather than simulating a null distribution with random incompleteness (i.e., the

MCCR test; Pybus and Harvey 2000). Considered individually, 52 of the 100 completed trees had $\gamma < -1.645$ (range: -3.55 to -0.35). Pruning to just the Oryzomyalia portion of the phylogenies yields similar results with mean $\gamma = -1.90$ (-3.25, -0.72), see Fig. S3.

Morphological diversification through time analyses found similar patterns for both skull and mandible shape (skull ventral MDI= 0.016, skull lateral MDI= 0.002, mandible MDI= 0.035; $P > 0.05$ in all cases – Fig. S4, Fig. 6), and slightly different results for size (MDI= -0.04; $P > 0.05$). The patterns agreed with a Brownian model of evolution through time. Early in their evolution, morphological variation was concentrated among sub-clades, and then peaks of morphological disparity (i.e. a higher proportion of total shape morphological variation become concentrated within sub-clades) took place about 9 to 7 Ma, remaining roughly constant until the present.

The Oryzomyalia radiation

Results of K statistics, evolutionary model selection, evolutionary rates and DTT for the Oryzomyalia radiation are presented in Supplemental File S5. All results are similar to those for the Sigmodontinae as a whole. Noteworthy differences are the highest values for MDI statistics in all datasets, indicating variation is more concentrated within sub-clades of the Oryzomyalia radiation.

Discussion

Morphological variation (size and shape of the skull and mandible) was weakly related to diet and habit, and models of evolution based on adaptive optima in these ecological scenarios over long periods of time were poorly supported (i.e. the OU models), indicating that these variables have little power to explain skull and mandible shape. These results are remarkable given the recently reported biases in multivariate

model selection based on comparative data towards artificially supporting more complex models (Uyeda et al., 2015; Adams, 2014b; Cooper et al., 2016). Thus, speciation during the radiation of sigmodontines seems to have been driven mostly by factors unrelated to an adaptive process involving these variables. Morphological differences among species are usually taken as the primary evidence to consider a radiation as mostly adaptive (e.g., Grant 1986) or mostly non-adaptive (Rundell and Price 2009). Extraordinary phenotypic and ecological disparity is expected for a clade to be considered a case of adaptive radiation (i.e. for divergent natural selection to be implied as important during the course of its radiation; Schluter 2000; Givnish 2015), and the evidence in this direction is weak for sigmodontines. Moreover, the clade did not experience an early burst of phenotypic accumulation. Both phylogenetic signal and the high support of Brownian models indicate that long-term adaptive processes are absent. This suggests that neither diet nor life-mode has played a primary role influencing skull and mandible shape and size variation in sigmodontines over long periods.

Given the remarkable species richness of sigmodontines, this is a surprising result, but species diversity can theoretically be unrelated to morphological diversity (Losos and Miles 2002; Alfaro et al. 2004), as well as to their rates of diversification (Adams et al. 2009). For example, species richness is not a good predictor of morphological disparity among squirrels of the world (Zelditch et al. 2015), a pattern that may characterize continental radiations. A predisposition to speciate in allopatric isolation should often result in species richness without great morphological variation (Kozak et al. 2006; Losos and Mahler 2010). Even in the absence of distinct adaptive peaks, fragmented landscapes can produce speciation (Gittenberger 1991), and karyotypic repatterning can quickly lead to reproductive isolation (Patton and Sherwood 1983). Though sigmodontine morphological variation is not small (Fig. 4; Maestri et al. 2016) when compared with all

rodent variation (Samuels 2009), it lacks conspicuous association with the ecological variables analyzed here, both across the entire tree and within the Oryzomyalia radiation. Debate on how adaptive was the sigmodontine radiation is on-going (Schenk et al. 2013; Parada et al. 2015; Alhajeri et al. 2016; Tulli et al. 2016), without a clear consensus. We suggest the pattern of high species richness coupled with a lack of clear association between morphological and ecological divergence may be common in rapid rodent radiations (e.g., in the *Rattus* radiation – Rowe et al. 2011, and in the worldwide muroid radiation – Alhajeri et al. 2016), despite some remarkable instances of rodent convergence involving dietary shifts when distinct radiations are compared (Samuels 2009).

The LTT-based results (mean γ = -1.75) contrast to those reported in earlier studies of Sigmodontinae (γ = -5.91, Parada et al. 2015; and γ = -5.81, Schenk et al. 2013), possibly because those studies used different molecular markers (CYTB and IRBP only) and imputed missing species differently. Parada et al. (2015) used the CorSiM method and Schenk et al. (2013) used an alpha-corrected MCCR test, both of which are post hoc methods of accounting for biased taxon sampling, while we used the PASTIS method to impute unsampled species during the phylogeny estimation process. The latter approach has the advantage of drawing branch lengths from the same underlying birth-death distribution as the rest of the tree, and thus adds biological realism to the inference (Thomas et al. 2013). In general, our timing estimates for the crown of Sigmodontinae 12.7 Ma (11.3, 14.2) and Oryzomyalia 9.3 Ma (8.4, 10.4) are in line with the divergence times of other recent phylogenies (means of 8.1-11.8 Ma and 7.3-9.8 Ma, respectively; Parada et al. 2013, 2015; Schenk et al. 2013; Leite et al. 2014). The topology recovered in the MCC tree suggests that, inside Oryzomyalia, the Oryzomyini branched off first prior to the divergence of other tribes, as in Schenk et al. (2013) but not in others (Parada et al. 2013; Leite et al. 2014; Parada et al. 2015). Tribes Akodontini and Thomasomyini

were recovered as sister to each other, and this group was sister to a speciose clade of Phyllotini and other tribes. Nevertheless, the statistical support for tribal interrelationships was generally low (< 0.95 PP), as consistently found in other studies (Smith and Patton 1999; Steppan et al. 2004; Parada et al. 2013; Schenk et al. 2013; Leite et al. 2014). Full divergence time information and nodal support information from our analyses can be found in Supplemental File S1 and Figure S1.

The patterns of morphological and lineage diversification through time somehow contrasts with the hypothesis proposed by Harmon et al. (2003), despite its resemblance with a Brownian pattern. In clades that underwent rapid lineage diversification early in history (such as the sigmodontines), phenotypic diversification should be high among sub-clades, because ecological niches would be filled rapidly, leading to reduced opportunities for subsequent ecological diversification inside each sub-clade. Sigmodontines seem to refute this generality, because phenotype diversification follows a Brownian pattern and there is high disparity within sub-clades (more evident in Oryzomyalia – Supplemental File S5; see also Alhajeri et al. 2016); an early burst of morphological evolution received low support in our analyses (Tables 1 and 2). A possible explanation resides in the fact that ecological opportunity played a secondary role in sigmodontine radiation, as indicated here, unlike most adaptive lizard radiations analyzed (Harmon et al. 2003). Moreover, the great expanse of a continental region, sharply contrasting with the spatial confinement of islands, could offer opportunities for reduced geographical overlap among species, allowing independent but simultaneous diversification of species without corresponding ecological change. Therefore, interspecific competition would be low, and the resulting species could occupy similar regions in both ecological and morphological space. Perhaps a central feature of mainland

radiations is that speciation events can be ecologically incompatible (under the principle of competitive exclusion), but it does not matter because the species remain in allopatry.

Radiations on continents may indeed result in different patterns than expected for islands. In *Anolis*, different ecological morphotypes were found in islands when compared to the mainland (Irschick et al. 1997), suggesting different ecological factors influence morphology in each system. Neotropical birds studied by Derryberry et al. (2011) showed constant rates of speciation with limited phenotypic disparity, a result reminiscent of our own study. Studying continental squirrels, Zelditch et al. (2015) suggested that such rapidly diversifying clades may be the ones on which geography is a more important component in speciation than ecological diversification. Allopatry following geographic speciation is also taken as the main explanation for the highly diverse but phenotypic similar group of North-American salamanders (Kozak et al. 2006). Following our own evidence that geographical variation leading to speciation is more common in sigmodontines than are ecological influences, we are tempted to suggest that non-adaptive radiations may prove to be more common on continents than on islands.

Circumstantial evidence suggests the primary explanation for sigmodontine morphological variation is the divergence associated with a simple process of speciation in allopatry. Garzione et al. (2008) analyzed oxygen isotopes, fossil-leaf physiognomy, and volcanic activity and suggested that the main period of rising elevation in the central Andes (between 19ºS and 26°S) lasted from 9 to 6 Mya. This period coincides with increased morphological disparity within subclades (Fig. 6). The central Andes is the region where the highest species richness and turnover of sigmodontine rodents can be found, and is an area where the discrete but complementary distributions of the major sigmodontine tribes all overlap (Maestri and Patterson 2016). As Andean uplift transformed the landscape, shifting and fragmenting species distributions, many daughter

populations would have been produced, with little cause for ecological and morphological divergence. The uplift of the Andes was responsible for a great recent radiation of *Lupinus* species (Hughes and Eastwood 2006); in the process of uplift, the Andes created discrete environments, which led to an island-like diversification process unfolding on a continent. The similarity with insular radiation helps to explain the high diversity in *Lupinus* (Hughes and Eastwood 2006). In the same fashion, uplift in the Andes could have triggered speciation in sigmodontines. As the central Andes are a region of range overlap for all the main clades of sigmodontines, morphological variation inside each sub-clade was shaped in similar environments, leading to little morphological disparity among clades (Fig. 6). Additionally, as the richness patterns of the main tribes are largely allopatric (Maestri and Patterson 2016), each clade may have exploited a similar set of resources in distinct parts of the continent since their likely radiation from the Andes. Morphological differences among species were then possibly generated by neutral evolution, historical contingencies and simple allopatric speciation, a pattern that may occur even for highly complex structures such as the mammalian skull (Marroig & Cheverud 2004).

The South and Central Andes have already been suggested to be the area of original differentiation for most of the main tribes of sigmodontines (Reig 1986). Other studies acknowledge the influence of the Andes in the diversification of sigmodontines, especially Oryzomyalia (Engel et al. 1998; Smith and Patton 1999; Alhajeri et al. 2016), and Maestri and Patterson (2016) showed that the only region with high overlap in the distribution of main tribes is the South Central Andes. Others cast doubt on the Andes as a center of diversification. Prado et al. (2014) found high endemicity of oryzomines in both the Andes and Atlantic Forest, and Leite et al. (2014), analyzing 66 species that represent 54 genera, found eastern South America to be the area of main differentiation

for the Oryzomyalia. Salazar-Bravo et al. (2013) recently showed the association of phyllotines with South Central Andes, but noted that lowland habitats played a major role on this tribe's diversification. In a recent review, D'Elía and Pardiñas (2015) recognized eastern South America as more important than previously thought (e.g., Reig 1986) for sigmodontine biogeographical history, and implicated the lowlands as the most important area for akodontine diversification. Likewise, Parada et al. (2015) found high speciation rates in lowlands. Thus, there is no consensus concerning the ancestral area of occurrence and original differentiation areas for the sigmodontines and their main tribes. Our data on the timing of morphological diversification (skull and mandible shape and size) seem to favor the Andean biogeographical hypothesis.

Another interesting result of this study is its compelling evidence that insectivorous mice evolve at a faster rate than other groups. This suggests that diet can affect the rate of evolution, although not necessarily leading to convergent evolution (e.g., Alfaro et al. 2004). Insectivorous sigmodontines typically share general resemblance, such as an elongated, gracile rostrum (Fig. 4), but insectivorous genera like *Rhagomys* and *Blarinomys* lack these features. Such obvious within-group disparities may help to explain their faster evolutionary pace. Fast divergence among insectivores can also result from the consuming of very different items, as for instance, beetles, grasshoppers, earthworms and fish, each presumably requiring different strategies of hunting, prey handling, and food processing.

On the other hand, convergence for diet might help to explain the morphological variation associated with the first principal component (Fig. 4), which in turn is related to bite force (Maestri et al. 2016). Moreover, simulated models of evolution with a separate peak for insectivorous rodents closely resemble the empirical ones in the PSR curves (Table 3). These differences are mainly associated with the elongated rostrum that

distinguishes insectivores from granivores and herbivores. Elongation of the rostrum is common among mammals and may arise in response to selective processes (e.g. Freeman 2000; Christiansen and Wroe 2007; Monteiro and Nogueira 2011; Rowe et al. 2016). Similar patterns of rostral elongation in insectivores has also been observed in other rodent families (Samuels 2009).

Nevertheless, the first principal component explains only 30.64% to 35.94% of total shape variation, suggesting a modest degree of specialization and a still-ongoing process of adaptation. Overall morphological variation seems neither influenced by ecological processes (or else responds to ecological variables not analyzed here) nor subject to phylogenetic "constraints", as the morphological variation is only weakly structured by phylogeny. The challenges of an actively hunting mode of feeding may cause natural selection to act faster, leading to an "adapt or die" state where any feature that promotes advantage in feeding may be selected. This would potentially explain both the convergences and the divergences of insectivores, driven by the faster evolutionary rate of phenotypic change in order to adapt to an insectivorous mode of feeding.

Given the low specialization levels in phenotype, then why are some species restricted to particular habitat types in the absence of physical barriers? The answer may be the generalist nature of the muroid rodent phenotype (Wood 1965; Cox et al. 2012; Maestri et al. 2016). For complex morphological structures, it is possible that a single phenotype is well adapted to many functions, or the opposite (the many to-one-mapping – Alfaro et al. 2005; Wainwright et al. 2005). As trait complexity increases, the number of possible morphological solutions to a particular challenge also increases (Alfaro et al. 2004), which can lead to functional versatility (Bellwood et al. 2006) or functional redundancy (Alfaro et al. 2005). In such cases, clades with exceptional species diversity but limited morphological diversity can arise (Alfaro et al. 2004), and the detection of

convergence and ecological specialization is compromised. Radical changes in the morphology of sigmodontines are absent, even if coupled with ecological specialization (Coutinho et al. 2013; Maestri et al. 2016; Tulli et al. 2016). Previous studies have shown that sigmodontines show limited ecological specialization in features such as claw morphology (Tulli et al. 2016), forelimb musculature (Carrizo et al. 2014), and bite force (Maestri et al. 2016). This strongly contrasts with phyllostomid bats, for instance, which have optimal phenotypes for each diet classes (Monteiro & Nogueira 2011). If sigmodontines retain a phenotype that permits them to exploit a wide range of dietary resources in a given area (i.e. functional versatility), then convergence is unlikely. Still, diet preferences and a degree of habitat/functional specialization may exist, as a generalist morphology can be coupled with functional specialization (Bellwood et al. 2006). We here provide evidence that skull and mandible shape and size are in line with these studies, favoring a probable one-to-many mapping between form and function (i.e. one form, many functions).

Although dietary and life-mode preferences are not strongly associated with the main axis of morphological changes in sigmodontines, it is impossible to measure every aspect of the ecological attributes of species. Other traits, such as behavioral or physiological attributes may be involved in the speciation and ecological diversification of sigmodontines and deserve further attention. Indeed, some habitats, such as tropical lowlands and mixed vegetation habitats (i.e. open and forested areas), evidently promoted faster speciation in sigmodontines (Parada et al. 2015). Ecological or trait characteristics not evaluated here might be coupled with diversification events, which would produce a pattern closer to an adaptive radiation. Alternatively, a series of events of changes in the direction of adaptive peaks may lead to a process of fluctuating directional selection, which is also consistent with a Brownian model of evolution (O'Meara et al. 2006).

Moreover, the framing of our dietary hypothesis may also influence the results. Among primates, feeding behavior and material proprieties of food are better reflected in mandibular morphology than are dietary categories (Ross et al. 2012). However, given the scant information on diet of sigmodontines, more refined variables are not currently available. Evaluation of the ecological features of other rodent radiations can reveal whether the patterns found here might be generalized. An obvious candidate is the radiation of Murinae rodents in the Paleotropics, as they are similar to sigmodontines both in age and biological characteristics (Schenk et al. 2013).

We demonstrated that continental radiations can produce a pattern of high species diversification coupled with a low degree of ecological specialization as this is reflected in the skull and mandible shape and size. This pattern may prove to be more common among rodent radiations (e.g. Rowe et al. 2011; Alhajeri et al. 2016) than for other mammal groups, as South American bats (Monteiro and Nogueira 2011) and monkeys (Meloro et al. 2015), which both seem to have a strong selective component to their morphologies. The vast geographical expanse of the South American continent and the habitat diversity and fragmentation generated by Andean uplift provided the opportunity for allopatric speciation in sigmodontines without competitive elimination, resulting in a high within-clade morphological disparity despite an early-burst of species diversification. The age and complexity of continental evolutionary radiations presumably hide other patterns that may be fundamental to a complete understanding of the ecology of rapid and diverse radiations.

Aknowledgments

We thank Miriam Zelditch, Emma Sherratt, and three anonymous reviewers for their insightful and helpful suggestions on a previous version of this paper. We are grateful to

the curators and collection managers that provided access to specimens and assistance in finding specimens in their institutions: in addition to FMNH, these include João A. de Oliveira (MNUFRJ), Mario de Vivo and Juliana Gualda (MZUSP), Diego H. Verzi and A. Itatí Olivares (MLP), Eileen Westwig (AMNH), and Darrin Lunde (NMNH). RM is supported by CAPES, and TROF is supported by CAPES, CNPq, and FAPERGS. NSU is supported by the NSF VertLife Terrestrial grant (#1441737).

Literature cited

Adams, D. C. 2014a. A generalized K statistic for estimating phylogenetic signal from shape and other high-dimensional multivariate data. Syst. Biol. 63:685-697.

Adams, D. C. 2014b. Quantifying and comparing phylogenetic evolutionary rates for shape and other high-dimensional phenotypic data. Syst. Biol. 63:166-177.

Adams, D. C., and E. Otarola-Castillo. 2013. geomorph: an R package for the collection and analysis of geometric morphometric shape data. Methods Ecol. Evol. 4:393-399.

Adams, D. C., C. M. Berns, K. H. Kozak, and J. J. Wiens. 2009. Are rates of species diversification correlated with rates of morphological evolution? Proc. R. Soc. B. 276:2729-2738.

Alfaro, M. E., D. I. Bolnick, and P. C. Wainwright. 2004. Evolutionary dynamics of complex biomechanical systems: an example using the four-bar mechanism. Evolution 58:495-503.

Alfaro, M. E., D. I. Bolnick, and P. C. Wainwright. 2005. Evolutionary consequences of many-to-one mapping of jaw morphology to mechanics in labrid fishes. Am. Nat. 165:E140-E154.

Alhajeri, B. H., J. J. Schenk, and S. J. Steppan. 2016. Ecomorphological diversification following continental colonization in muroid rodents (Rodentia: Muroidea). Biol. J. Linn. Soc. 117:463-481.

Altschul, S. F., T. L. Madden, A. A. Schaffer, J. Zhang, Z. Zhang, W. Miller, and D. J. Lipman. 1997. Gapped BLAST and PSI-BLAST: A new generation of protein database search programs. Nucleic Acids Res. 25:3389–3402.

Astudillo-Clavijo, V., J. H. Arbour, and H. López-Fernández. 2015. Selection towards different adaptive optima drove the early diversification of locomotor phenotypes in the radiation of Neotropical geophagine cichlids. BMC Evol. Biol. 15:77.

Beaulieu, J. M., D. Jhwueng, C. Boettiger, and B. C. O'Meara. 2012. Modeling stabilizing selection: expanding the Ornstein-Uhlenbeck model of adaptive evolution. Evolution 66:2369-2383.

Bellwood, D. R., P. C. Wainwright, C. J. Fulton, and A. S. Hoey. 2006. Functional versatility supports coral reef biodiversity. Proc. R. Soc. B. 273:101-107.

Bini, L. M., F. Villalobos, and J. A. F. Diniz-Filho. 2014. Explorando patrones em rasgos macroecológicos utilizando regresión secuencial de autovectores filogenéticos. Ecosistemas 23:21-26.

Blomberg, S. P., T. Garland, and A. R. Ives. 2003. Testing for phylogenetic signal in comparative data: behavioral traits are more labile. Evolution 57:717-745.

Bonvicino, C. R., J. A. de Oliveira, and P. S. D'Andrea. 2008. Guia dos roedores do Brasil. Centro Pan-Americano de Febre Aftosa, Rio de Janeiro.

Bookstein, F. L. 1991. Morphometric tools for landmark data. Cambridge Univ. Press, UK.

Brock, C. D., L. J. Harmon, and M. E. Alfaro. 2011. Testing for temporal variation in diversification rates when sampling is incomplete and nonrandom. Syst. Biol. 60:410-419.

Burbrink, F. T., X. Chen, E. A. Myers, M. C. Brandley, and R. A. Pyron. 2012. Evidence for determinism in species diversification and contingency in phenotypic evolution during adaptive radiation. Proc. R. Soc. B 279:4817-4826.

Burham, K. P., and D. R. Anderson. 2002. Model selection and multimodel inference: a practical information-theoretic approach. Springer, New York.

Butler, M. A., and A. A. King. 2004. Phylogenetic comparative analysis: a modeling approach for adaptive evolution. Am. Nat. 164:683-695.

Camacho, C., G. Coulouris, V. Avagyan, N. Ma, J. Papadopoulos, K. Bealer, and T. L. Madden. 2009. BLAST+: architecture and applications. BMC Bioinformatics 10:421.

Carrizo, L. V., M. J. Tulli, and V. Abdala. 2014. An ecomorphological analysis of forelimb musculotendinous system in sigmodontine rodents (Rodentia, Cricetidae, Sigmodontinae). J. Mamm. 95:843-854.

Churakov, G., M. K. Sadasivuni, K. R. Rosenbloom, D. Huchon, J. Brosius, and J. Schmitz. 2010. Rodent evolution: back to the root. Mol. Biol. Evol. 27:1315–1326.

Claramunt, S. 2010. Discovering exceptional diversification at continental scales: the case of the endemic families of Neotropical suboscine passerines. Evolution 64:2004-2019.

Clavel, J., G. Escarguel, and G. Merceron. 2015. Mvmorph: an R package for fitting multivariate evolutionary models to morphometric data. Methods Ecol. Evol. 6:1311-1319.

Collar, D. C., B. C. O'Meara, P. C. Wainwright, and T. J. Near. 2009. Piscivory limits diversification of feeding morphology in centrarchid fishes. Evolution 63:1557-1573.

Cooper, N., G. H. Thomas, C. Venditti, A. Meade, and R. P. Freckleton. 2016. A cautionary note on the use of Ornstein Uhlenbeck models in macroevolutionary studies. Biol. J. Linn. Soc. 118:64-77.

Coutinho, L. C., J. A. de Oliveira, and L. M. Pessôa. 2013. Morphological variation in the appendicular skeleton of Atlantic Forest sigmodontine rodents. J. Morphol. 274:779-792.

Cox, P. G., E. J. Rayfield, M. J. Fagan, A. Herrel, T. C. Pataky, and N. Jeffery. 2012. Functional evolution of the feeding system in rodents. PLoS ONE 7:e36299.

Cusimano, N., and S. S. Renner. 2010. Slowdowns in diversification rates from real phylogenies may not be real. Syst. Biol. 59:458–464.

Cusimano, N., T. Stadler, and S. S. Renner. 2012. A new method for handling missing species in diversification analysis applicable to randomly or nonrandomly sampled phylogenies. Syst. Biol. 61:785–792.

Darwin, C. 1859. On the origin of species by means of natural selection, or the preservation of favoured races in the struggle for life. John Murray, London.

D'Elía, G., and U. F. J. Pardiñas. 2015. Subfamily Sigmodontinae Wagner, 1843. Pp. 63-70 *in* J. L. Patton, U. F. J. Pardiñas, and G. D'Elia, eds. Mammals of South America, Vol. 2: Rodents. Univ. Chicago Press, Chicago.

Derryberry, E. P., S. Claramunt, G. Derryberry, R. T. Chesser, J. Cracraft, A. Aleixo, J. Pérez-Emán, J. V. Remsen Jr, and R. T. Brumfield. 2011. Lineage diversification and morphological evolution in a large-scale continental radiation: the

Neotropical ovenbirds and woodcreepers (Aves: Furnariidae). Evolution 65:2973-2986.

Diniz-Filho, J. A. F., C. E. R. Sant'Ana, and L. M. Bini. 1998. An eigenvector method for estimating phylogenetic inertia. Evolution 52:1247-1262.

Diniz-Filho, J. A. F., T. F. Rangel, T. Santos, and L. M. Bini. 2012. Exploring patterns of interspecific variation in quantitative traits using sequential phylogenetic eigenvector regressions. Evolution 66:1079-1090.

Diniz-Filho, J. A. F., D. M. C. C. Alves, F. Villalobos, M. Sakamoto, S. L. Brusatte, and L. M. Bini. 2015. Phylogenetic eigenvectors and nonstationarity in the evolution of

theropod dinosaur skulls. J. Evol. Biol. 28:1410-1416.

Drummond, A. J., M. A. Suchard, D. Xie, and A. Rambaut. 2012. Bayesian phylogenetics with BEAUti and the BEAST 1.7. Mol. Biol. Evol. 29:1969–1973.

Engel, S. R., K. M. Hogan, J. F. Taylor, and S. K. Davis. 1998. Molecular systematics and paleobiogeography of the South American sigmodontine rodents. Mol. Biol. Evol. 15:35-49.

Fabre, P.-H., L. Hautier, D. Dimitrov, and E. J. P. Douzery. 2012. A glimpse on the pattern of rodent diversification: a phylogenetic approach. BMC Evol. Biol. 12:88.

Felsestein, J. 1985. Phylogenies and the comparative method. Am. Nat. 125:1-15.

Freeman, P. W. 2000. Macroevolution in Microchiroptera: recoupling morphology and ecology with phylogeny. Evol. Ecol. Res. 2:317-335.

Futuyma, D.J. 1998. Evolutionary Biology (3rd ed.). Sinauer Associates, Sunderland, MA.

Garzione, C. N., G. D. Hoke, J. C. Libarkin, S. Withers, B. MacFadden, J. Eiler, P. Ghosh, and A. Mulch. 2008. Rise of the Andes. Science 320:1304-1307.

Gittenberger, E. 1991. What about non-adaptive radiation? Biol. J. Linn. Soc. 43:263-272.

Givnish, T. J. 2015. Adaptive radiation versus ‘radiation’ and ‘explosive diversification’: why conceptual distinctions are fundamental to understanding evolution. New Phytol. 207:297-303.

Gould, S. J., and R. C. Lewontin. 1979. The spandrels of San Marco and the Panglossian paradigm: a critique of the adaptationist programme. Proc. R. Soc. B 205:581-598.

Grant, P. R. 1986. Ecology and evolution of Darwin’s finches. Princeton Univ. Press, Princeton.

Grant, P. R., and R. G. Grant. 2008. How and why species multiply: the radiation of Darwin’s finches. Princeton Univ. Press, Princeton.

Hansen, T. F., and E. P. Martins. 1996. Translating between microevolutionary process and macroevolutionary patterns: the correlation structure of interspecific data. Evolution 50:1404-1417.

Hansen, T. F. 1997. Stabilizing selection and the comparative analysis of adaptation. Evolution 51:1341-1351.

Hansen, T. F., and K. Bartoszek. 2012. Interpreting the evolutionary regression: the interplay between observational and biological errors in phylogenetic comparative studies. Syst. Biol. 61:413-425.

Harmon, L. J., J. A. Schulte II, A. Larson, and J. B. Losos. 2003. Tempo and mode of evolutionary radiation in iguanian lizards. Science 301:961-964.

Harmon, L. J., J. T. Weir, C. D. Brock, R. E. Glor, and W. Challenger. 2008. GEIGER: investigating evolutionary radiations. Bioinformatics 24:129-131.

Harmon, L. J., J. B. Losos, T. J. Davies, R. G. Gillespie, J. L. Gittleman, W. B. Jennings, K. H. Kozak, M. A. McPeek, F. Moreno-Roark, T. J. Near, et al. 2010. Early bursts of body size and shape evolution are rare in comparative data. Evolution 64:2385-2396.

Hershkovitz, P. 1966. Mice, land bridges and Latin American faunal interchange. Pp. 725-751 *in* Wenzel, R. L. & Tipton, V. J. eds. Ectoparasites of Panama. Field Museum of Natural History, Chicago.

Iriarte, A. 2008. Mamíferos de Chile. Lynx Edicions, Barcelona.

Irschick, D. J., L. J. Vitt, P. A. Zani, and J. B. Losos. 1997. A comparison of evolutionary radiations in mainland and Caribbean *Anolis* lizards. Ecology 78:2191-2203.

IUCN. 2015. IUCN Redlist of Threatened Species. Version 2015.1. Available at www.iucnredlist.org. Accessed April 15, 2015.

Jetz, W., G. H. Thomas, J. B. Joy, K. Hartmann, and A. O. Mooers. 2012. The global diversity of birds in space and time. Nature 491:444–448.

Katoh, K., and D. M. Standley. 2013. MAFFT multiple sequence alignment software version 7: improvements in performance and usability. Mol. Biol. Evol. 30:772–780.

Korth, W. W. 1994. The Tertiary record of rodents in North America. Springer Science, New York.

Kozak, K. H., D. W. Weisrock, and A. Larson. 2006. Rapid lineage accumulation in a non-adaptive radiation: phylogenetic analysis of diversification rates in eastern North American woodland salamanders (Plethodontidae: Plethodon). Proc. R. Soc. B 273:539-546.

Lacher, T. E., W. J. Murphy, J. Rogan, A. T. Smith, and N. S. Upham. 2016. Evolution, phylogeny, ecology, and conservation of the Clade Glires: Lagomorpha and

Rodentia. Pp. 15-26 *in* D. E. Wilson, J. T. E. Lacher and R. A. Mittermeier, eds. Handbook of Mammals of the World, Volume 6: Lagomorphs and Rodents. Lynx Ediciones, Barcelona.

Leite, R. N., S. Kolokotronis, F. C. Almeida, F. Werneck, D. S. Rogers, and M. Weksler. 2014. In the wake of invasion: tracing the historical biogeography of the South American cricetid radiation (Rodentia, Sigmodontinae). PLoS ONE 9:e100687.

Leite, Y. L. R., P. J. R. Kok, and M. Weksler. 2015. Evolutionary affinities of the "Lost World" mouse suggest a late Pliocene connection between the Guiana and Brazilian shields. J. Biogeogr. 42:706-715.

Lepage, T., D. Bryant, H. Philippe, and N. Lartillot. 2007. A general comparison of relaxed molecular clock models. Mol. Biol. Evol. 24:2669–2680.

Lessa, E. P., J. A. Cook, G. D'Elía, and J. C. Opazo. 2014. Rodent diversity in South America: transitioning into the genomics era. Front. Ecol. Evol. 2:39.

Losos, J. B. 2010. Adaptive radiation, ecological opportunity, and evolutionary determinism. Am. Nat. 175:623-639.

Losos, J. B. 2011. Convergence, adaptation, and constraint. Evolution 65:1827-1840.

Losos, J. B., and D. B. Miles. 2002. Testing the hypothesis that a clade has adaptively radiated: iguanid lizard clades as a case study. Am. Nat. 160:147-157.

Losos, J. B., and R. E. Ricklefs. 2009. Adaptation and diversification on islands. Nature 457:830-836.

Losos, J. B., and D. L. Mahler. 2010. Adaptive radiation: the interaction of ecological opportunity, adaptation, and speciation. Pp. 381-420 *in* M. A. Bell, D. J. Futuyma, W. F. Eanes and J. S. Levinton, eds. Evolution Since Darwin: the first 150 years. Sinauer Associates, Sunderland, MA.

Maestri, R., and B. D. Patterson. 2016. Patterns of species richness and turnover for the South American rodent fauna. PLoS ONE 11:e0151895.

Maestri, R., B. D. Patterson, R. Fornel, L. R. Monteiro, and T. R. O. de Freitas. 2016. Diet, bite force, and skull morphology in the generalist rodent morphotype. J. Evol. Biol. 29:2191-2204.

Mahler, D. L., T. Ingram, L. J. Revell, and J. B. Losos. 2013. Exceptional convergence on the macroevolutionary landscape in island lizard radiations. Science 341:292-295.

Marinho-Filho, J., F. H. G. Rodrigues, and K. M. Juarez. 2002. The Cerrado mammals: diversity, ecology, and natural history. Pp. 266-286 *in* P. S. Oliveira and R. J. Marquis, eds. The Cerrados of Brazil. Columbia University Press, New York.

Marroig, G., and J. M. Cheverud. 2004. Did natural selection or genetic drift produce the cranial diversification of Neotropical monkeys? Am. Nat. 163:417-428.

Meloro, C., N. C. Cáceres, F. Carotenuto, J. Sponchiado, G. L. Melo, F. Passaro, and P. Raia. 2015. Chewing on the trees: Constraints and adaptation in the evolution of the primate mandible. Evolution 69:1690-1700.

Meredith, R. W., J. E. Janečka, J. Gatesy, O. A. Ryder, C. A. Fisher, E. C. Teeling, A. Goodbla, E. Eizirik, T. L. L. Simão, T. Stadler, et al. 2011. Impacts of the Cretaceous terrestrial revolution and KPg extinction on mammal diversification. Science 334:521–524.

Miller, M. A., W. Pfeiffer, and T. Schwartz. 2010. Creating the CIPRES science gateway for inference of large phylogenetic trees. Proceedings of the Gateway Computing Environments Workshop (GCE), 14 Nov. 2010, New Orleans, LA pp 1-8.

Monteiro, L. R., and M. R. Nogueira. 2011. Evolutionary patterns and processes in the radiation of phyllostomid bats. BMC Evol. Biol. 11:137.

Monteiro, L. R. 2013. Morphometrics and the comparative method: studying the evolution of biological shape. Hystrix 24:25-32.

Nowak, R. M. 1999. Walker's mammals of the world, 6th ed. John Hopkins Univ. Press, Baltimore.

O'Meara, B. C., C. Ané, M. J. Sanderson, and P. C. Wainwright. 2006. Testing for different rates of continuous trait evolution using likelihood. Evolution 60:922-933.

Paglia, A. P., G. A. B. Fonseca, A. B. Rylands, G. Herrmann, L. M. S. Aguiar, A. G. Chiarello, Y. L. R. Leite, L. P. Costa, S. Siciliano, M. C. M. Kierulff, et al. 2012. Annotated checklist of Brazilian mammals 2º edition. Conservation International, Arlington.

Parada, A., U. F. J. Pardiñas, J. Salazar-Bravo, G. D'Elía, and R. E. Palma. 2013. Dating an impressive Neotropical radiation: molecular time estimates for the Sigmodontinae (Rodentia) provide insights into its historical biogeography. Mol. Phylogenet. Evol. 66:960-968.

Parada, A., G. D'Elía, and R. E. Palma. 2015. The influence of ecological and geographical context in the radiation of Neotropical sigmodontine rodents. BMC Evol. Biol. 15:172.

Paradis, E., J. Claude, and K. Strimmer. 2004. APE: analysis of phylogenetics and evolution in R language. Bioinformatics 20:289-290.

Pardiñas, U. F. J., L. Geise, K. Ventura, and G. Lessa. 2016. A new genus for *Habrothrix angustidens* and *Akodon serrensis* (Rodentia, Cricetidae): again paleontology meets neontology in the legacy of Lund. Mastozool. Neotrop. 23:93-115.

Patton, J. L., and S. W. Sherwood. 1983. Chromosome evolution and speciation in rodents. Ann. Rev. Ecol. Syst. 14:139-158.

Patton, J. L., U. F. J. Pardiñas, and G. D'Elia, eds. 2015. Mammals of South America, Vol. 2: Rodents. Univ. Chicago Press, Chicago.

Peres-Neto, P. R., D. A. Jackson, and K. M. Somers. 2005. How many principal components? Stopping rules for determining the number of non-trivial axes revisited. Comput. Stat. Data Anal. 49:974-997.

Phillimore, A. B., and T. D. Price. 2008. Density-dependent cladogenesis in birds. PLoS Biol. 6:e71.

Pincheira-Donoso, D., L. P. Harvey, and M. Ruta. 2015. What defines an adaptive radiation? Macroevolutionary diversification dynamics of an exceptionally species-rich continental lizard radiation. BMC Evol. Biol. 15:153.

Prado, J. R., P. G. G. Brennand, L. P. Godoy, G. S. Libardi., E. F. Abreu-Júnior, P. R. O. Roth, E. A. Chiquito, and A. R. Percequillo. 2014. Species richness and areas of endemism of oryzomyine rodents (Cricetidae, Sigmodontinae) in South America: an ndm/vndm approach. J. Biogeogr. 42:540-551.

Pybus, O. G., and P. H. Harvey. 2000. Testing macro-evolutionary models using incomplete molecular phylogenies. Proc. R. Soc. B 267:2267-2272.

Pyron, R. A., F. T. Burbrink, and J. J. Wiens. 2013. A phylogeny and revised classification of Squamata, including 4161 species of lizards and snakes. BMC Evol. Biol. 13:93.

R Core Team. 2016. R: a language and environment for statistical computing. R Foundation for Statistical Computing, Vienna, Austria.

Ranwez, V., S. Harispe, F. Delsuc, and E. J. P. Douzery. 2011. MACSE: Multiple Alignment of Coding SEquences accounting for frameshifts and stop codons. PLoS ONE 6:e22594.

Reid, F. A. 1997. A field guide to the mammals of Central America and southeast Mexico. Oxford Univ. Press, New York.

Reig, O. A. 1981. Teoría del origen y desarrollo de la fauna de mamíferos de America del Sur. Monographiae Naturae, Museo Municipal de Ciencias Naturales "Lorenzo Scaglia" 1:1-162.

Reig, O. A. 1986. Diversity patterns and differentiation of high Andean rodents. Pp. 404-439 *in* F. Vuilleumier and M. Monasterio, eds. High altitude tropical biogeography. Oxford Univ. Press, New York.

Revell, L. J. 2012. phytools: an R package for phylogenetic comparative biology (and other things). Methods Ecol. Evol. 3:217-223.

Rodrigues, H. G., R. Šumbera, and L. Hautier. 2015. Life in burrows channelled the morphological evolution of the skull in rodents: the case of African mole-rats (Bathyergidae, Rodentia). J. Mamm. Evol. 23:175-189.

Rohlf, F. J. 2001. Comparative methods for the analysis of continuous variables: geometric interpretations. Evolution 55:2143-2160.

Rohlf, F. J. 2015. The tps series of software. Hystrix 26:9-12.

Ronquist, F., M. Teslenko, P. V. D. Mark, D. L. Ayres, A. Darling, S. Höhna, B. Larget, L. Liu, M. A. Suchard, and J. P. Huelsenbeck. 2012. MrBayes 3.2: efficient Bayesian phylogenetic inference and model choice across a large model space. Syst. Biol. 61:539-542.

Ross, C. F., J. Iriarte-Diaz, and C. L. Nunn. 2012. Innovative approaches to the relationship between diet and mandibular morphology in Primates. Int. J. Primatol. 33:632-660.

Roure, B., D. Baurain, and H. Philippe. 2013. Impact of missing data on phylogenies inferred from empirical phylogenomic data sets. Mol. Biol. Evol. 30:197–214.

Rowe, K. C., K. P. Aplin, P. R. Baverstock, and C. Moritz. 2011. Recent and rapid speciation with limited morphological disparity in the genus *Rattus*. Syst. Biol. 60:188-203.

Rowe, K. C., A. S. Achmadi, and J. A. Esselstyn. 2016. Repeated evolution of carnivory among Indo-Australian rodents. Evolution 70:653-665.

Rundell, R. J., and T. D. Price. 2009. Adaptive radiation, nonadaptive radiation, ecological speciation and nonecological speciation. Trends Ecol. Evol. 24:394-399.

Salazar-Bravo, J., U. F. J. Pardiñas, and G. D'Elía. 2013. (Rodentia, Cricetidae) with emphasis on phyllotine genera: systematics and biogeography. Zool. Scr. 42:250-261.

Samuels, J. X. 2009. Cranial morphology and dietary habits of rodents. Zool. J. Linn. Soc. 156:864-888.

Samuels, J. X., and B. Van Valkenburgh. 2008. Skeletal indicators of locomotor adaptations in living and extinct rodents. J. Morphol. 269:1387-1411.

Sanmartín, I., and A. S. Meseguer. 2016. Extinction in phylogenetics and biogeography: from timetrees to patterns of biotic assemblage. Front. Genet. 7:35.

Scales, J. A., and M. A. Butler. 2016. Adaptive evolution in locomotor performance: How selective pressures and functional relationships produce diversity. Evolution 70:48-61.

Schenk, J. J., K. C. Rowe, and S. J. Steppan. 2013. Ecological opportunity and incumbency in the diversification of repeated continental colonizations by muroid rodents. Syst. Biol. 62:837-864.

Schluter, D. 2000. The ecology of adaptive radiation. Oxford Univ. Press.

Simpson. G. G. 1944. Tempo and mode in evolution. Columbia Univ. Press.

Simpson, G. G. 1953. The major features of evolution. Columbia Univ. Press.

Slater, G. J., S. A. Price, F. Santini, and M. E. Alfaro. 2010. Diversity versus disparity and the radiation of modern cetaceans. Proc. R. Soc. Lond. B 277:3097-3104.

Smith, M. F., and J. L. Patton. 1999. Phylogenetic relationships and the radiation of sigmodontine rodents in South America: evidence from cytochrome *b*. J. Mamm. Evol. 6:89-128.

Steppan, S. J., R. M. Adkins, and J. Anderson. 2004. Phylogeny and divergence-date estimates of rapid radiations in muroid rodents based on multiple nuclear genes. Syst. Biol. 53:533-553.

Stroud, J. T., and Losos, J. B. 2016. Ecological opportunity and adaptive radiation. Annu. Rev. Ecol. Evol. Syst. 47:507-532.

Teta, P., C. Cañón, B. D. Patterson and U. F. J. Pardiñas. 2016. Phylogeny of the tribe Abrotrichini (Cricetidae, Sigmodontinae): integrating morphological and molecular evidence into a new classification. Cladistics http://dx.doi.org/10.1111/cla.12164.

Thomas, G. H., K. Hartmann, W. Jetz, J. B. Joy, A. Mimoto, and A. O. Mooers. 2013. PASTIS: an R package to facilitate phylogenetic assembly with soft taxonomic inferences. Methods Ecol. Evol. 4:1011–1017.

Tirira, D. 2007. Mamíferos del Ecuador: Guia de campo. Ediciones Murcielago Blanco, Quito, Ecuador.

Tonini, J. F. R., K. H. Beard, R. B. Ferreira, W. Jetz, and R. A. Pyron. 2016. Fully-sampled phylogenies of squamates reveal evolutionary patterns in threat status. Biol. Cons. doi:10.1016/j.biocon.2016.03.039.

Tran, L. A. P. 2014. The role of ecological opportunity in shaping disparate diversification trajectories in a bicontinental primate radiation. Proc. R. Soc. B. 281:20131979.

Tulli, M. J., L. V. Carrizo, and J. X. Samuels. 2016. Morphological variation of the forelimb and claw in Neotropical sigmodontine rodents (Rodentia: Cricetidae). J. Mammal. Evol. 23:81-91.

Uyeda, J. C., D. S. Caetano, and M. W. Pennell. 2015. Comparative analysis of principal components can be misleading. Syst. Biol. 64:677-689.

Venditti, C., A. Meade, and M. Pagel. 2011. Multiple rotes to mammalian diversity. Nature 479:393-396.

Vilela, J. F., B. Mello, C. M. Voloch, and C. G. Schrago. 2013. Sigmodontine rodents diversified in South America prior to the complete rise of the Panamanian isthmus. J. Zool. Sys. Evol. Res. 52:249-256.

Wainwright, P. C., M. E. Alfaro, D. I. Bolnick, and C. D. Hulsey. 2005. Many-to-one mapping of form to function: A general principle in organismal design? Integr. Comp. Biol. 45:256-262.

Whittaker, R. J., and J. M. Fernández-Palacios. 2007. Island biogeography: ecology, evolution, and conservation, 2nd ed. Oxford University Press, Oxford.

Wiens, J. J., and M. C. Morrill. 2011. Missing data in phylogenetic analysis: reconciling results from simulations and empirical data. Syst. Biol. 60:719-731.

Wilson, D. E., and D. M. Reeder, eds. 2005. Mammal species of the world: a taxonomic and geographic reference, 3rd ed. Johns Hopkins Univ. Press, Baltimore, MD.

Wood, A. E. 1935. Evolution and relationship of the heteromyid rodents with new forms from the Tertiary of western North America. Ann. Carnegie Mus. 24:73-262.

Wood, A. E. 1947. Rodents – a study in evolution. Evolution 1:154-162.

Wood, A. E. 1965. Grades and clades among rodents. Evolution 19:115-130.

Zelditch, M. L., J. Li, L. A. P. Tran, and D. L. Swiderski. 2015. Relationships of diversity, disparity, and their evolutionary rates in squirrels (Sciuridae). Evolution 69:1284-1300.

Data archiving

The doi for our data is 10.5061/dryad.k5777.

Supporting information

Additional Supporting Information may be found in the online version of this article:

Table S1. Number of specimens sampled for each species and museum catalogue numbers.

Table S2. Definition of landmarks on the skull and mandible.

Table S3. Details of gene and taxon sampling used for tree construction.

Figure S1. Phylogenetic relationships for 279 species of sigmodontines and outgroups.

Figure S2. Lineages-through-time (LTT) plot for all sigmodontines, and the distribution of γ statistic values.

Figure S3. Lineages-through-time (LTT) plot for Oryzomyalia sigmodontines, and the distribution of γ statistic values.

Figure S4. Average subclade disparity-through-time (DTT) plots for all morphological datasets.

Supplemental File S1. Primary phylogenetic tree used in this study. The tree shows a multi-gene phylogeny of 279 species of sigmodontines and outgroups, see Figure S1.

Supplemental File S2. DNA matrices for the 11 genes used to construct the sigmodontine phylogeny.

Supplemental File S3. Set of 100 posterior taxonomically completed trees for 413 species of sigmodontines.

Supplemental File S4. Set of 100 posterior taxonomically completed trees for 383 species of Oryzomyalia sigmodontines.

Supplemental File S5. Results of analyses for the Oryzomyalia radiation.

Tables

Table 1. Comparison of the fit of alternative models for the evolution of size based on distinct diet and life mode hypotheses.

Model	Size			
	AICc	ΔAICc	AICc*wi*	Np
Habit BMM.6	-228.27	0.00	0.551	7
Habit BMM.4	-227.07	1.20	0.303	5
Habit OU.4	-225.10	3.17	0.113	6
Diet OU.4	-220.63	7.64	0.012	6
Diet OU.3	-219.36	8.91	0.006	5
Diet OU.2In	-218.16	10.11	0.004	4
BM.1	-217.46	10.80	0.002	2
Diet BMM.4	-216.96	11.30	0.002	5
Habit OU.6	-216.85	11.42	0.002	8
Diet BMM.2In	-216.10	12.16	0.001	3
Diet BMM.2Hb	-215.41	12.86	0.001	3
OU.1	-215.39	12.87	0.001	3
Diet BMM.3	-213.83	14.44	0.000	4
Diet OU.2Hb	-213.82	14.45	0.000	4
Habit BMM.3	-213.67	14.60	0.000	4
Habit OU.3	-211.24	17.03	0.000	5
EB	-131.38	96.88	0.000	3

Model acronyms as in Figure 2. See text and Fig. 2 for details on diet and habit hypothesis. EB corresponds to an early-burst model of evolution. Np are the numbers of parameters estimated by each model.

Table 2. Comparison of the fit of alternative models based on distinct diet and hypothesis for the evolution of skull and mandible shape using principal components.

Model	**Skull shape ventral 5 PCs (75.40)%**			
	AICc	ΔAICc	AICc*wi*	Np
Diet BMM.2In	-5594.04	0.00	0.960	35
Diet BMM.3	-5587.31	6.73	0.033	50
BM.1	-5583.81	10.23	0.006	20
Diet BMM.2Hb	-5579.53	14.50	0.001	35
Diet BMM.4	-5579.29	14.75	0.001	65
Habit BMM.3	-5528.66	65.37	0.000	50
Habit BMM.4	-5526.49	67.55	0.000	65
Habit OU.6	-5446.55	147.49	0.000	60
Habit OU.4	-5435.62	158.41	0.000	50
Diet OU.2In	-5431.71	162.32	0.000	40
OU.1	-5411.29	182.74	0.000	35
Habit OU.3	-5348.64	245.40	0.000	45
Diet OU.3	-5342.50	251.54	0.000	45
Habit BMM.6	-5320.20	273.84	0.000	95
Diet OU.4	-5310.62	283.42	0.000	50
Diet OU.2Hb	-5180.04	414.00	0.000	40
EB	-5001.56	592.48	0.000	21
Model	**Skull shape lateral 6 PCs (82.46%)**			
	AICc	ΔAICc	AICc*wi*	Np
Diet BMM.2In	-6345.35	0.00	1.000	48
BM.1	-6311.43	33.92	0.000	27
Diet BMM.2Hb	-6302.11	43.24	0.000	48
Diet BMM.3	-6279.10	66.25	0.000	69
Habit BMM.3	-6247.85	97.50	0.000	69
Diet BMM.4	-6204.03	141.33	0.000	90
Habit OU.3	-6189.20	156.15	0.000	60
Diet OU.4	-6150.20	195.15	0.000	66
Diet OU.2Hb	-6148.66	196.69	0.000	54
Habit BMM.4	-6138.92	206.43	0.000	90
OU.1	-6099.01	246.34	0.000	48
Diet OU.3	-6091.91	253.44	0.000	60
Diet OU.2In	-6074.67	270.68	0.000	54
Habit OU.6	-6025.22	320.13	0.000	78
Habit OU.4	-6008.98	336.37	0.000	66
EB	-5761.48	583.87	0.000	28
Habit BMM.6	-5490.54	854.81	0.000	132
Model	**Mandible shape 5 PCs (80.37%)**			
	AICc	ΔAICc	AICc*wi*	Np

Diet BMM.2In	-4720.03	0.00	1.000	35
Diet BMM.3	-4704.57	15.46	0.000	50
Diet BMM.4	-4653.33	66.70	0.000	65
Diet OU.2In	-4650.13	69.91	0.000	40
Diet OU.2Hb	-4645.22	74.81	0.000	40
Habit OU.3	-4645.05	74.99	0.000	45
Habit OU.4	-4638.71	81.32	0.000	50
OU.1	-4632.12	87.91	0.000	35
Diet OU.4	-4619.56	100.47	0.000	50
Diet BMM.2Hb	-4617.20	102.83	0.000	35
BM.1	-4612.72	107.32	0.000	20
Habit OU.6	-4612.06	107.97	0.000	60
Diet OU.3	-4591.80	128.24	0.000	45
Habit BMM.3	-4584.74	135.30	0.000	50
Habit BMM.4	-4528.99	191.04	0.000	65
Habit BMM.6	-4349.72	370.31	0.000	95
EB	-4245.20	474.83	0.000	21

Model acronyms as in Figure 2. See text and Fig. 2 for details on diet and habit hypothesis. EB corresponds to an early-burst model of evolution. Np are the numbers of parameters estimated by each model.

Table 3. Comparison of the Euclidean distances between empirical and simulated traits under distinct evolutionary models based on diet and habit hypothesis for the evolution of skull and mandible shape and size.

Model	Size	Shape Ventral	Shape Lateral	Shape Mandible
Diet.OU.2In	0.567	0.430	0.538	0.623
OU.1	1.005	0.839	0.877	1.002
BM	1.463	1.513	1.525	1.436
Diet.OU.3	1.590	1.666	1.744	1.717
Diet.OU.2Hb	1.712	1.799	1.866	1.825
Diet.OU.4	2.018	2.104	2.149	2.081
Habit.OU.3	2.268	2.365	2.420	2.361
Habit.OU.6	2.303	2.384	2.425	2.354
Habit.OU.4	2.392	2.473	2.517	2.447

Euclidean distances were calculated by comparing the Phylogenetic Signal-Representation curves (PSR curves) for traits simulated under distinct evolutionary models, with empirical PSR curves for morphological data. Distances are ranked from smallest to largest. Models acronyms correspond to: BM – Brownian motion; OU – Ornstein-Uhlenbeck with one optimum (OU.1), and with varying numbers of optima according to diet and habit hypothesis. See text and Fig. 2 for details on diet and habit hypothesis.

Table 4. Comparison of the Euclidean distances between empirical and simulated traits under an Ornstein-Uhlenbeck model with a single optimum varying α parameter for the evolution of skull and mandible shape and size.

Model	Size	Shape Ventral	Shape Lateral	Shape Mandible
OU α=1	0.478	0.370	0.443	0.454
OU α=2	1.119	0.989	1.026	1.183
BM	1.391	1.421	1.433	1.299
OU α=4	2.126	1.992	2.000	2.111
OU α=6	2.639	2.510	2.512	2.618
OU α=8	2.945	2.819	2.818	2.921
OU α=10	3.100	2.975	2.973	3.074
Null	3.508	3.386	3.380	3.476

Euclidean distances were calculated by comparing the Phylogenetic Signal-Representation curves (PSR curves) for traits simulated under Ornstein-Uhlenbeck model with distinct values of the α parameter, with empirical PSR curves for morphological data. Distances are ranked from smallest to largest. Models acronyms correspond to: BM – Brownian motion; OU – Ornstein-Uhlenbeck with a restraining force of α=1, α=2, α=4, α=6, α=8 and α=10. The null curve correspond to trait simulated at random.

Figures

Figure 1. Position of the landmarks (circles) digitized on ventral and lateral views of the skull and on the mandible of sigmodontine rodents. See Table S2 for landmark definitions.

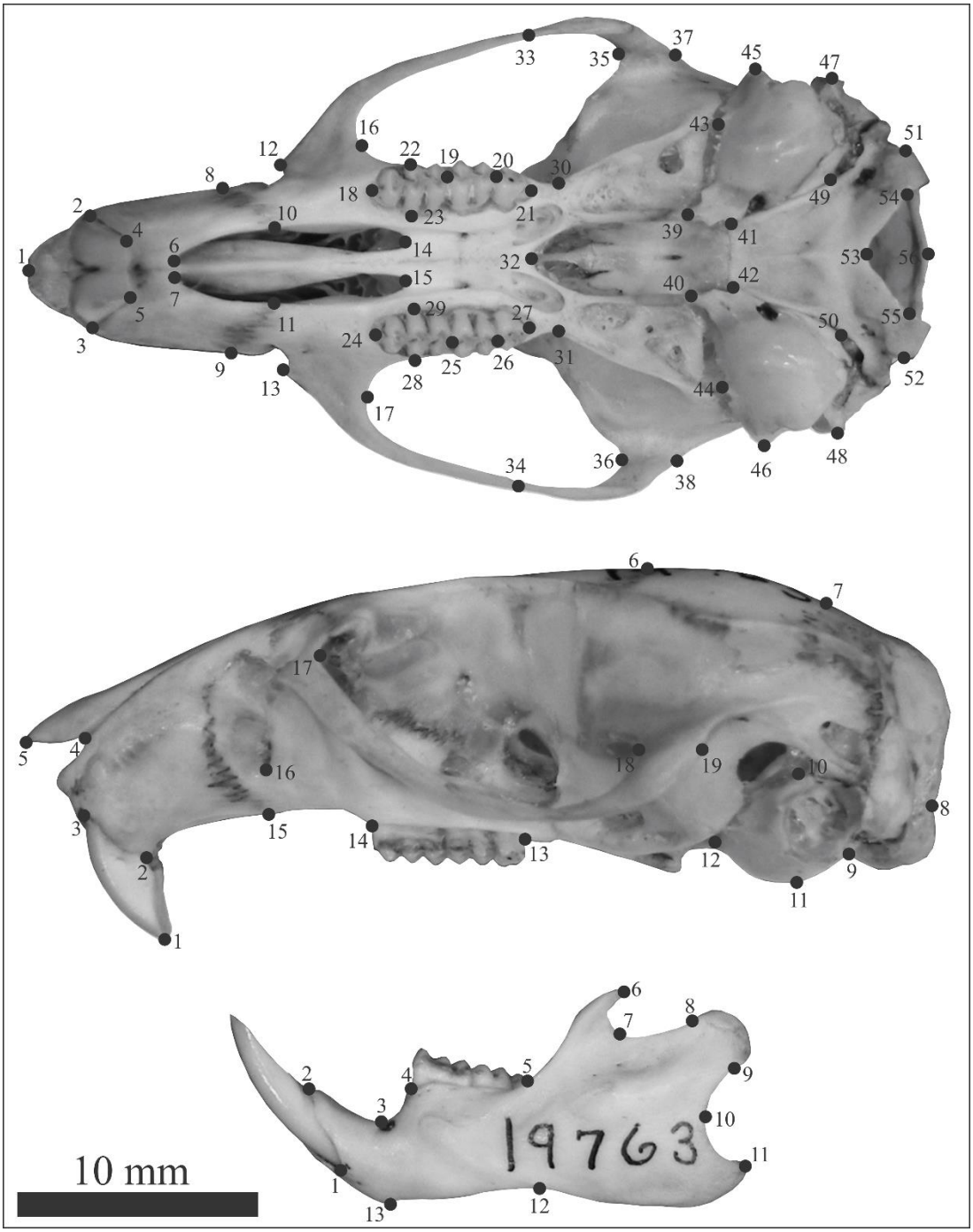

Figure 2. Adaptive evolutionary hypotheses for testing the association of diet and life mode with morphology. Ancestral states were estimated by maximum likelihood. See text for explanation.

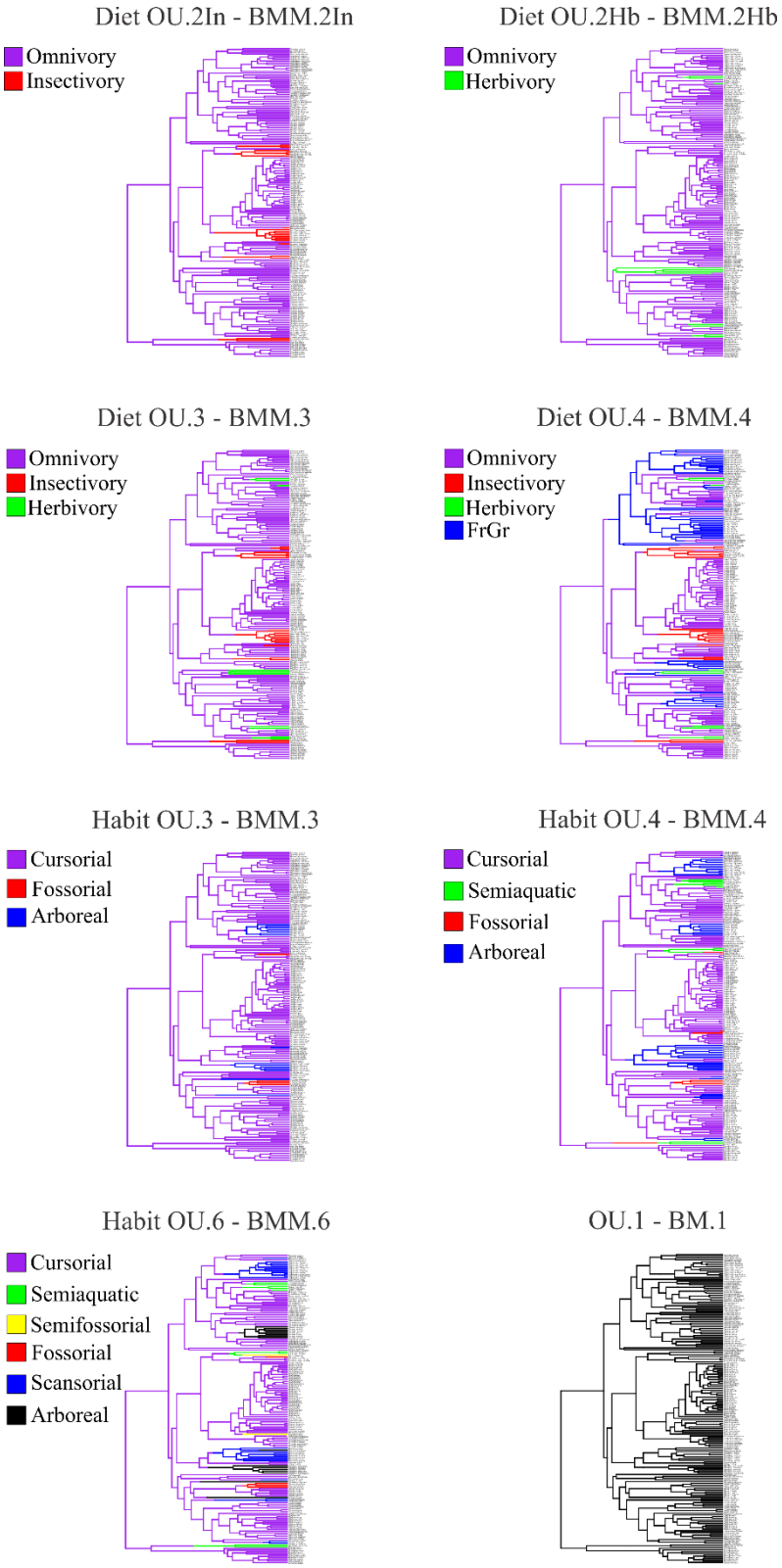

Figure 3. Boxplot showing size variation among dietary (A) and life mode classes (B) for the sigmodontine species. Size was calculated as the arithmetic average of centroid size (log) in skull ventral and lateral views plus mandible.

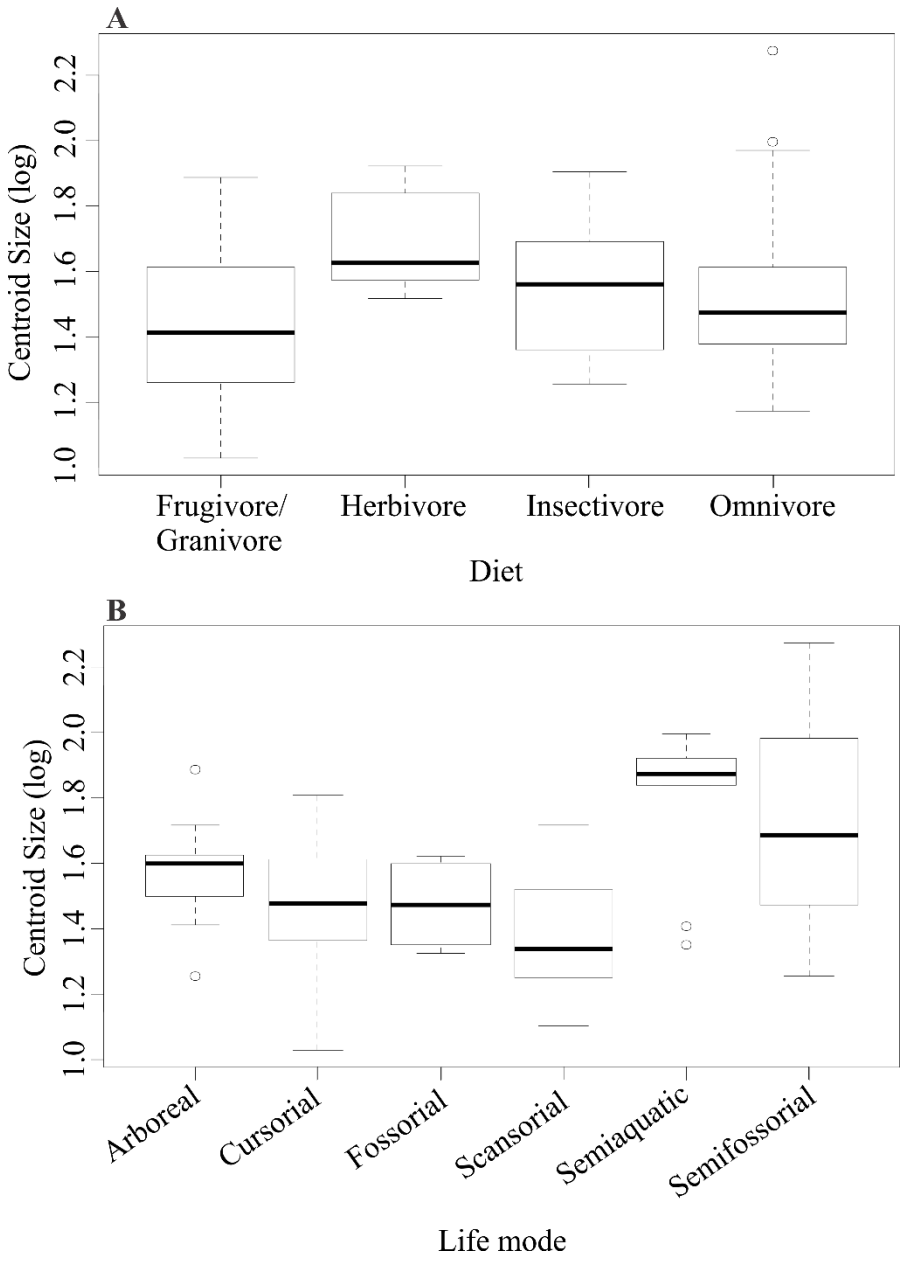

Figure 4. Phylomorphospace of skull (A: ventral view, B: lateral view) and mandible (C) shape variation on the phylogeny of sigmodontine rodents. Shapes at internal nodes were reconstructed by squared-change parsimony. Genera at the periphery of the scatter were named, as far as space permits. Below the scatter, shapes changes associated with positive and negative values for each axis are shown.

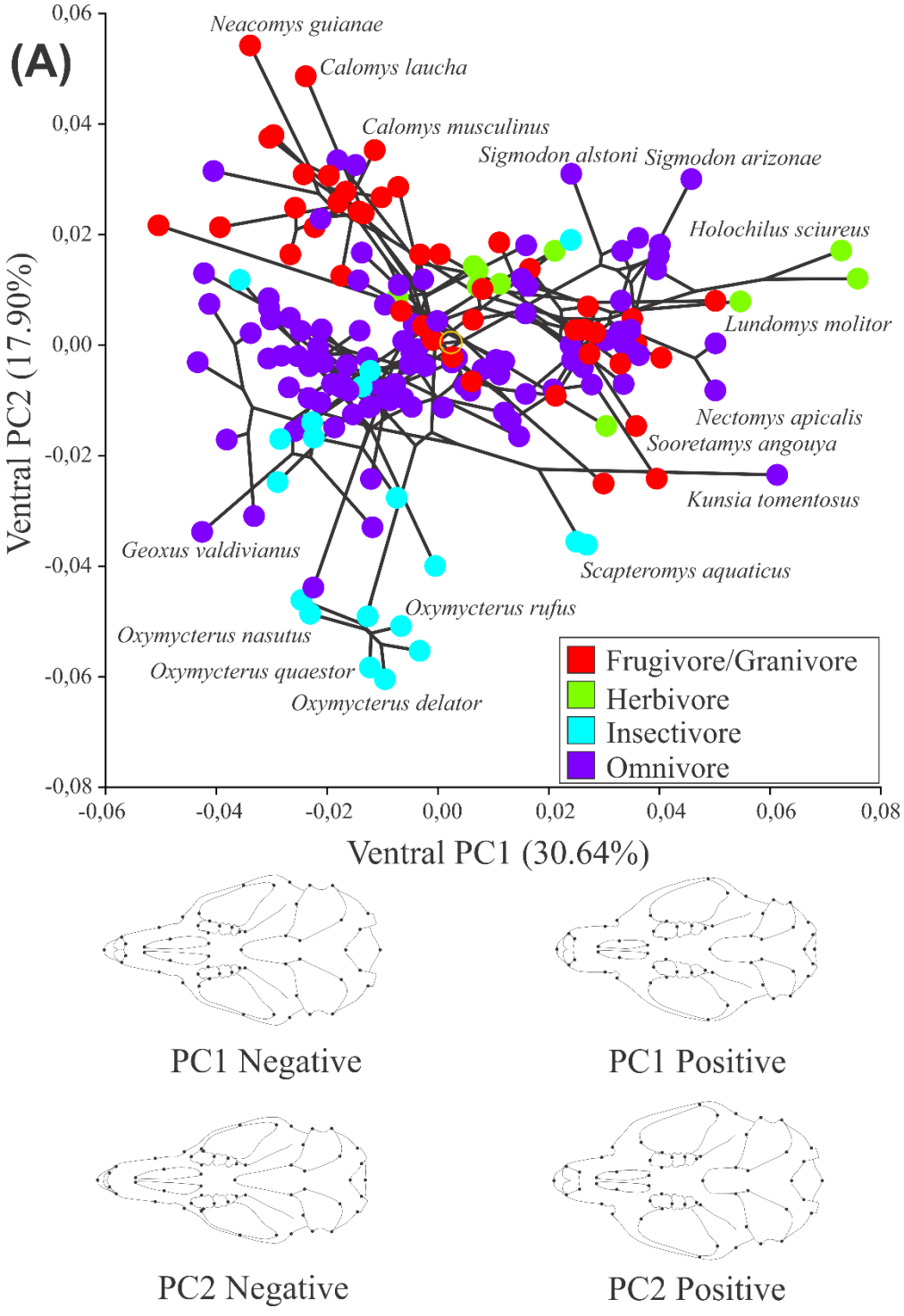

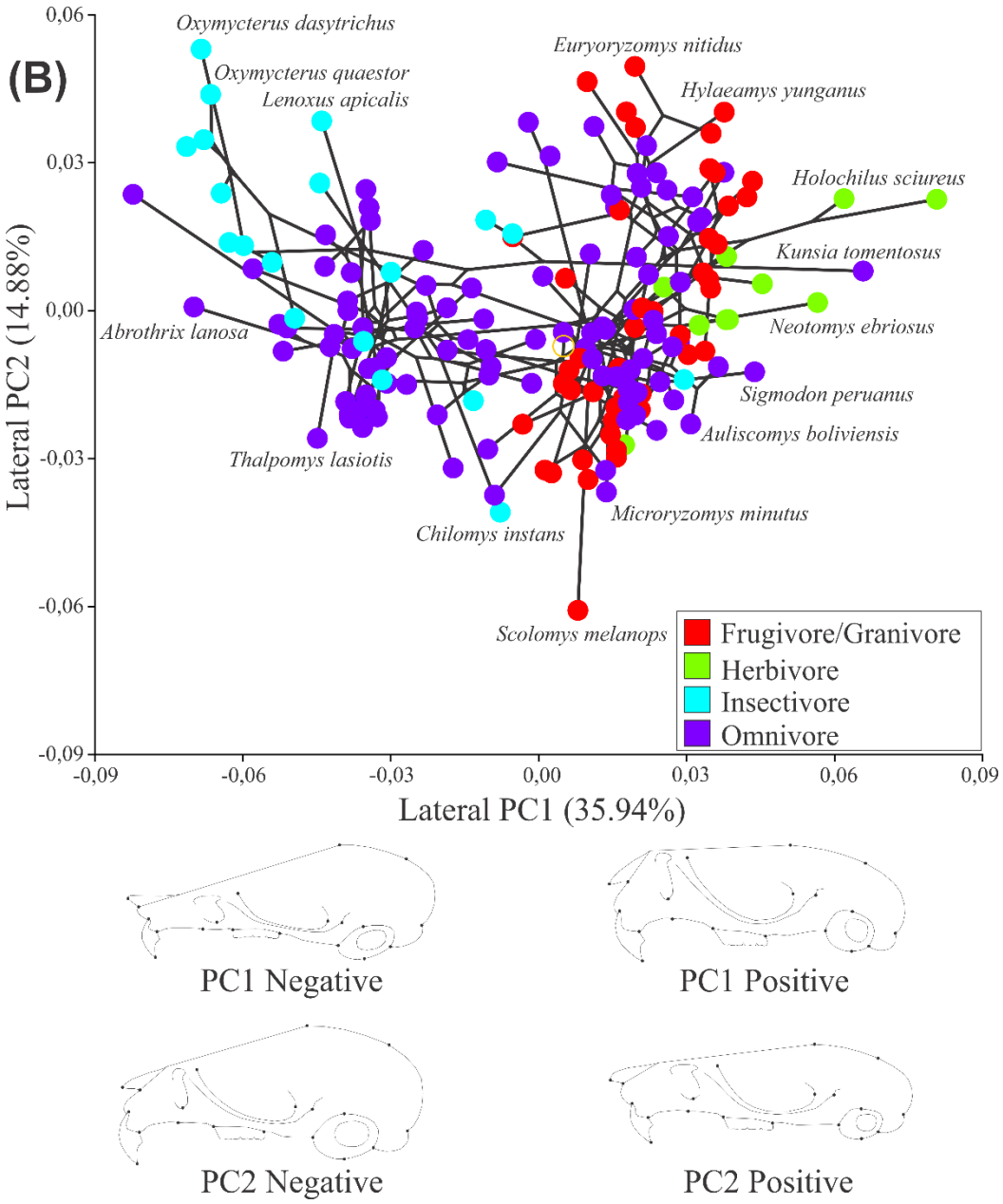
(B)
Oxymycterus dasytrichus
Oxymycterus quaestor
Lenoxus apicalis
Euryoryzomys nitidus
Hylaeamys yunganus
Holochilus sciureus
Kunsia tomentosus
Neotomys ebriosus
Sigmodon peruanus
Auliscomys boliviensis
Microryzomys minutus
Scolomys melanops
Chilomys instans
Thalpomys lasiotis
Abrothrix lanosa
Frugivore/Granivore
Herbivore
Insectivore
Omnivore
Lateral PC2 (14.88%)
Lateral PC1 (35.94%)
0,06
0,03
0,00
-0,03
-0,06
-0,09
-0,09
-0,06
-0,03
0,00
0,03
0,06
0,09
PC1 Negative
PC1 Positive
PC2 Negative
PC2 Positive

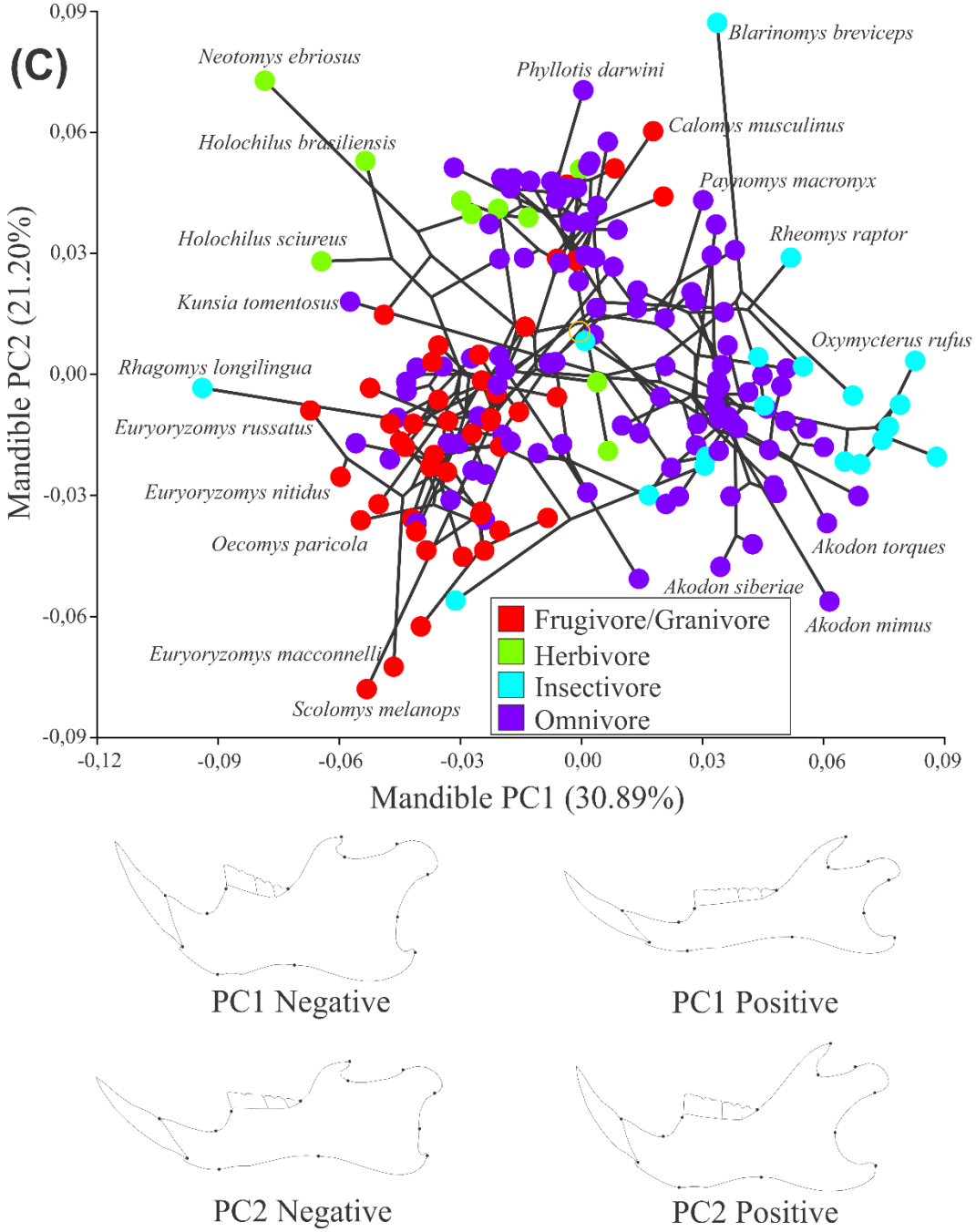
(C)
Mandible PC2 (21.20%)
Mandible PC1 (30.89%)
0,09
0,06
0,03
0,00
-0,03
-0,06
-0,09
-0,12
-0,09
-0,06
-0,03
0,00
0,03
0,06
0,09
Neotomys ebriosus
Holochilus brasiliensis
Holochilus sciureus
Kunsia tomentosus
Rhagomys longilingua
Euryoryzomys russatus
Euryoryzomys nitidus
Oecomys paricola
Euryoryzomys macconnelli
Scolomys melanops
Phyllotis darwini
Blarinomys breviceps
Calomys musculinus
Paynomys macronyx
Rheomys raptor
Oxymycterus rufus
Akodon torques
Akodon siberiae
Akodon mimus
Frugivore/Granivore
Herbivore
Insectivore
Omnivore
PC1 Negative
PC1 Positive
PC2 Negative
PC2 Positive

Figure 5. Phylogenetic signal-representation (PSR) curves for skull and mandible size and shape of sigmodontine rodents. Empirical curves are compared with curves resulting from 10,000 simulations under distinct evolutionary models: Brownian motion (BM), and Ornstein-Uhlenbeck (OU) models with a constant α value, and θ values set according to distinct diet (A) and life-mode (B) hypothesis (Fig. 2). In (C) empirical curves are compared with curves resulting from 10,000 simulations of a single peak Ornstein-Uhlenbeck (OU) models with varying values of α. Brownian motion (BM) corresponds to OU with α=0, and the null curve results from a randomization of trait values across the tips.

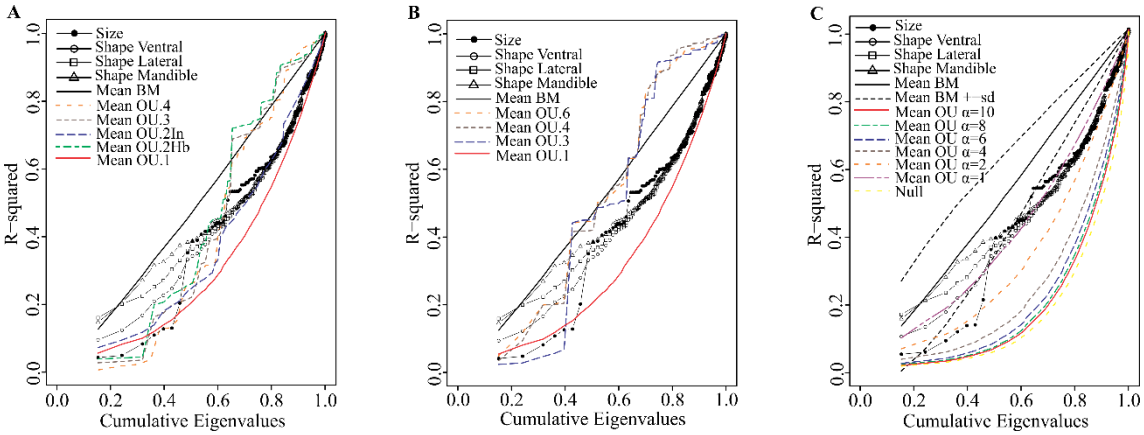

Figure 6. Tempo of morphological evolution in sigmodontine rodents. The combined plot shows the observed morphological disparity through time (DTT plots) for all morphological variables. In the bottom, a time estimate of the Andes' rise in elevation, as shown in Garzione et al. (2008). The phylogenetic tree of sigmodontines appears as the background.

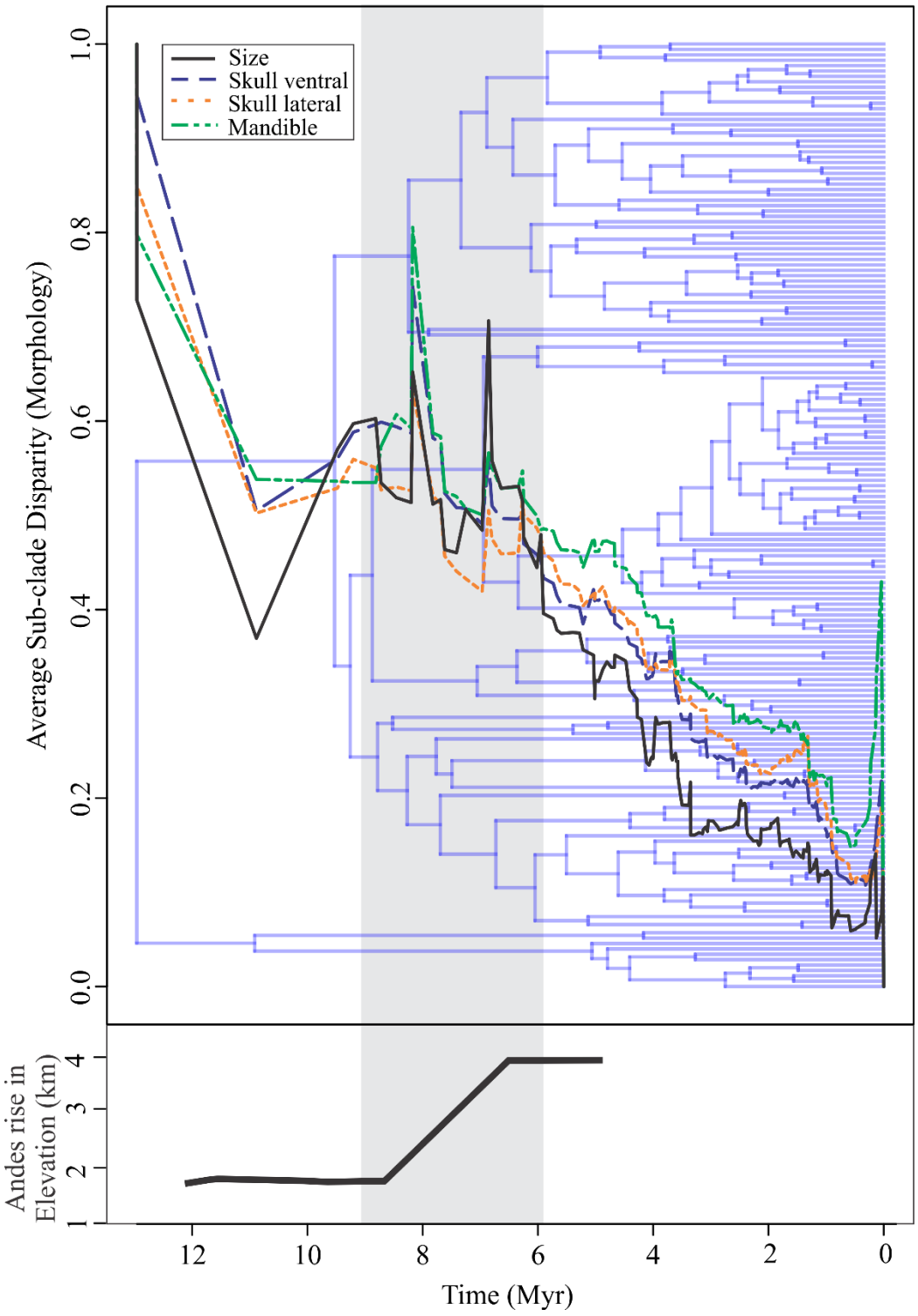

Supporting Information

Table S1. Number of specimens by species and genus of sigmodontine rodents, and the list of museums and catalogue numbers of specimens examined.

Genus	Species	Number of Individuals
Abrothrix		
	Abrothrix andina	4
	Abrothrix jelskii	5
	Abrothrix lanosa	6
	Abrothrix longipilis	5
	Abrothrix olivacea	10
Aegialomys		
	Aegialomys galapagoensis	11
	Aegialomys xanthaeolus	17
Aepeomys		
	Aepeomys lugens	13
Akodon		
	Akodon aerosus	142
	Akodon affinis	9
	Akodon albiventer	88
	Akodon azarae	101
	Akodon boliviensis	45
	Akodon budini	14
	Akodon cursor	94
	Akodon dayi	30
	Akodon dolores	19
	Akodon fumeus	20
	Akodon iniscatus	4
	Akodon juninensis	20
	Akodon kofordi	5
	Akodon lindberghi	13
	Akodon lutescens	8
	Akodon mimus	11
	Akodon mollis	48
	Akodon montensis	81
	Akodon mystax	32
	Akodon orophilus	23
	Akodon paranaensis	50
	Akodon reigi	2
	Akodon serrensis	33
	Akodon siberiae	7
	Akodon simulator	25
	Akodon spegazzinii	13
	Akodon subfuscus	65
	Akodon sylvanus	2
	Akodon toba	36
	Akodon torques	67
	Akodon varius	10
Andalgalomys		
	Andalgalomys pearsoni	10
Andinomys		
	Andinomys edax	14
Auliscomys		
	Auliscomys boliviensis	10
	Auliscomys pictus	8
	Auliscomys sublimis	11
Blarinomys		

	Blarinomys breviceps	2
Brucepattersonius		
	Brucepattersonius iheringi	3
	Brucepattersonius soricinus	2
Calomys		
	Calomys callosus	13
	Calomys laucha	6
	Calomys lepidus	5
	Calomys musculinus	9
	Calomys sorellus	8
	Calomys venustus	2
Cerradomys		
	Cerradomys langguthi	3
	Cerradomys maracajuensis	11
	Cerradomys scotti	5
Chelemys		
	Chelemys megalonyx	2
Chilomys		
	Chilomys instans	10
Delomys		
	Delomys dorsalis	5
	Delomys sublineatus	6
Deltamys		
	Deltamys kempi	16
Eligmodontia		
	Eligmodontia morgani	10
Eremoryzomys		
	Eremoryzomys polius	7
Euneomys		
	Euneomys chinchilloides	8
Euryoryzomys		
	Euryoryzomys macconnelli	8
	Euryoryzomys nitidus	10
	Euryoryzomys russatus	10
Galenomys		
	Galenomys garleppi	7
Geoxus		
	Geoxus valdivianus	16
Graomys		
	Graomys domorum	6
	Graomys griseoflavus	20
Handleyomys		
	Handleyomys alfaroi	17
	Handleyomys intectus	5
Holochilus		
	Holochilus brasiliensis	9
	Holochilus sciureus	5
Hylaeamys		
	Hylaeamys megacephalus	9
	Hylaeamys perenensis	10
	Hylaeamys yunganus	8
Irenomys		
	Irenomys tarsalis	24
Juliomys		
	Juliomys pictipes	1
Juscelinomys		
	Juscelinomys huanchacae	7
Kunsia		
	Kunsia tomentosus	4
Lenoxus		

	Lenoxus apicalis	17
Loxodontomys		
	Loxodontomys micropus	24
Lundomys		
	Lundomys molitor	5
Melanomys		
	Melanomys caliginosus	15
Microryzomys		
	Microryzomys minutus	18
Neacomys		
	Neacomys guianae	1
	Neacomys spinosus	21
Necromys		
	Necromys amoenus	8
	Necromys lactens	2
	Necromys lasiurus	11
	Necromys lenguarum	10
	Necromys obscurus	1
	Necromys urichi	6
Nectomys		
	Nectomys apicalis	13
	Nectomys squamipes	10
Neotomys		
	Neotomys ebriosus	16
Nephelomys		
	Nephelomys albigularis	9
	Nephelomys keaysi	7
	Nephelomys levipes	9
Nesoryzomys		
	Nesoryzomys fernandinae	1
	Nesoryzomys swarthi	1
Neusticomys		
	Neusticomys monticolus	12
Oecomys		
	Oecomys bicolor	11
	Oecomys concolor	1
	Oecomys mamorae	7
	Oecomys paricola	8
	Oecomys roberti	6
	Oecomys superans	10
	Oecomys trinitatis	2
Oligoryzomys		
	Oligoryzomys andinus	3
	Oligoryzomys chacoensis	10
	Oligoryzomys destructor	10
	Oligoryzomys flavescens	10
	Oligoryzomys fulvescens	9
	Oligoryzomys longicaudatus	19
	Oligoryzomys magellanicus	11
	Oligoryzomys microtis	11
	Oligoryzomys nigripes	26
	Oligoryzomys vegetus	2
Oreoryzomys		
	Oreoryzomys balneator	1
Oryzomys		
	Oryzomys couesi	13
	Oryzomys palustris	8
Oxymycterus		
	Oxymycterus dasytrichus	42
	Oxymycterus delator	7

	Oxymycterus nasutus	5
	Oxymycterus paramensis	13
	Oxymycterus quaestor	8
	Oxymycterus rufus	6
Paynomys		
	Paynomys macronyx	19
Phyllotis		
	Phyllotis amicus	12
	Phyllotis andium	11
	Phyllotis caprinus	4
	Phyllotis darwini	9
	Phyllotis gerbillus	12
	Phyllotis limatus	10
	Phyllotis magister	11
	Phyllotis osilae	7
	Phyllotis xanthopygus	10
Podoxymys		
	Podoxymys roraimae	2
Pseudoryzomys		
	Pseudoryzomys simplex	6
Rhagomys		
	Rhagomys longilingua	1
Rheomys		
	Rheomys raptor	4
Rhipidomys		
	Rhipidomys latimanus	7
	Rhipidomys leucodactylus	10
	Rhipidomys maconnelli	2
	Rhipidomys macrurus	1
	Rhipidomys mastacalis	1
Scapteromys		
	Scapteromys aquaticus	4
	Scapteromys tumidus	13
Scolomys		
	Scolomys melanops	5
Sigmodon		
	Sigmodon alstoni	10
	Sigmodon arizonae	6
	Sigmodon fulviventer	1
	Sigmodon hirsutus	13
	Sigmodon hispidus	10
	Sigmodon leucotis	4
	Sigmodon mascotensis	4
	Sigmodon peruanus	6
	Sigmodon toltecus	4
Sigmodontomys		
	Sigmodontomys alfari	11
Sooretamys		
	Sooretamys angouya	12
Thalpomys		
	Thalpomys lasiotis	2
Thaptomys		
	Thaptomys nigrita	49
Thomasomys		
	Thomasomys aureus	13
	Thomasomys baeops	12
	Thomasomys daphne	1
	Thomasomys gracilis	4
	Thomasomys ischyurus	11
	Thomasomys notatus	6

	Thomasomys oreas	6
Transandinomys		
	Transandinomys bolivaris	4
	Transandinomys talamancae	15
Wiedomys		
	Wiedomys pyrrhorhinus	8
Zygodontomys		
	Zygodontomys brevicaudata	21
Total		**2420**

Box S1. List of museums housing the specimens examined with their catalogue numbers, organized by column. AMNH: American Museum of Natural History; FMNH: Field Museum of Natural History; MCNU: Museu de Ciências Naturais da Ulbra; MLP: Museo de la Plata; MN: Museu Nacional do Rio de Janeiro; MZUSP: Museu de Zoologia da Universidade de São Paulo; USNM: U.S. National Museum of Natural History.

Abrothrix	***Akodon cont.***	***Calomys***	***Oligoryzomys cont.***
FMNH23143	FMNH49697	FMNH23341	FMNH27654
FMNH23144	FMNH21559	FMNH23393	FMNH27651
FMNH23146	FMNH50975	FMNH23377	FMNH162807
FMNH23147	FMNH20899	FMNH23376	FMNH162809
FMNH49386	FMNH20902	FMNH23373	FMNH162811
FMNH48389	FMNH20905	FMNH23430	FMNH19768
FMNH49392	FMNH20909	FMNH26790	FMNH19778
FMNH49394	FMNH20908	FMNH26792	FMNH19779
FMNH49395	FMNH20910	FMNH26796	FMNH19780
FMNH50174	FMNH21144	FMNH26799	FMNH19781
FMNH50379	FMNH81350	FMNH26795	FMNH19782
FMNH50380	FMNH24481	FMNH28361	FMNH19783
FMNH50382	FMNH24487	FMNH28362	FMNH143301
FMNH50383	FMNH24489	FMNH23404	FMNH143300
FMNH50384	FMNH24425	FMNH23405	FMNH143299
FMNH127506	FMNH24427	FMNH23407	FMNH143298
FMNH127507	FMNH24429	FMNH23409	FMNH143297
FMNH127504	FMNH24431	FMNH23410	FMNH143295
FMNH127503	FMNH24439	FMNH23413	FMNH143293
FMNH127502	FMNH24441	FMNH49551	FMNH29240
FMNH131540	FMNH24440	FMNH49552	FMNH27650
FMNH131642	FMNH24438	FMNH49553	FMNH27649
FMNH131643	FMNH24434	FMNH75420	FMNH27645
FMNH131645	FMNH24432	FMNH54743	FMNH29230
FMNH131647	FMNH24426	FMNH164672	FMNH29231
FMNH131649	FMNH24430	FMNH164723	FMNH29232
FMNH131651	FMNH26817	FMNH164724	FMNH29234
FMNH131652	FMNH26834	FMNH164737	FMNH29236
FMNH131654	FMNH26838	FMNH157322	FMNH1305
FMNH131655	FMNH26846	FMNH157342	FMNH73550
Aegialomys	FMNH26847	FMNH157343	FMNH73551
FMNH179528	FMNH26848	FMNH157352	FMNH73554
FMNH51756	FMNH26851	FMNH157364	FMNH72555
FMNH49012	FMNH26850	FMNH140812	FMNH73557
FMNH51761	FMNH26853	FMNH140813	FMNH73561
FMNH51763	FMNH26855	FMNH23751	FMNH73518
FMNH51764	FMNH26858	FMNH23752	FMNH73519
FMNH51765	FMNH29146	FMNH23654	FMNH89332

FMNH51766	FMNH29145	FMNH23753	FMNH133211
FMNH51767	FMNH35243	FMNH23757	FMNH133217
FMNH51769	FMNH24535	FMNH23758	FMNH133215
FMNH51768	FMNH24500	FMNH23760	FMNH133218
FMNH107377	FMNH24495	FMNH23763	FMNH25312
FMNH107378	FMNH24774	***Cerradomys***	FMNH25313
FMNH107379	FMNH24773	FMNH19507	FMNH22644
FMNH107380	FMNH19754	FMNH25246	FMNH22645
FMNH107381	FMNH129234	FMNH26446	FMNH22646
FMNH107383	FMNH129236	FMNH116909	FMNH22647
FMNH107386	FMNH19718	FMNH116822	FMNH22649
FMNH81389	FMNH19717	FMNH116823	FMNH22651
FMNH81390	FMNH19728	FMNH116824	FMNH133469
FMNH81391	FMNH19726	FMNH116825	FMNH133470
FMNH81392	FMNH19721	FMNH116826	FMNH133471
FMNH81393	FMNH19722	FMNH116827	FMNH133473
FMNH81394	FMNH19725	FMNH116887	FMNH133475
FMNH81403	FMNH19729	FMNH116888	FMNH133476
FMNH81404	FMNH29138	FMNH116889	FMNH133478
FMNH81405	FMNH19135	FMNH116895	FMNH50698
FMNH81407	FMNH30131	FMNH128310	FMNH50699
Aepeomys	FMNH30122	FMNH128311	FMNH50700
FMNH22154	FMNH30128	FMNH128312	FMNH124339
FMNH22155	FMNH30109	FMNH128313	FMNH127353
USNM579496	FMNH30110	FMNH128315	FMNH50685
USNM579498	FMNH30113	***Chelemys***	FMNH50686
USNM579492	FMNH30115	FMNH22494	FMNH50690
USNM579494	FMNH30117	FMNH23901	FMNH50691
USNM387954	FMNH29142	***Chilomys***	FMNH50693
USNM387957	FMNH30119	FMNH71600	FMNH50695
USNM387961	FMNH30120	FMNH71621	FMNH139838
USNM374597	FMNH122686	FMNH71607	FMNH139844
USNM374598	FMNH29122	FMNH71606	FMNH139839
USNM374603	FMNH29123	FMNH71604	FMNH139842
USNM374600	FMNH30181	FMNH71602	FMNH139845
Akodon	FMNH30182	FMNH71605	FMNH139847
USNM236310	FMNH30184	FMNH71499	FMNH139848
USNM236315	FMNH30189	FMNH71495	FMNH84341
USNM274275	FMNH107797	FMNH71496	FMNH84342
USNM274276	FMNH107794	***Delomys***	FMNH84343
USNM236259	FMNH107793	FMNH26597	FMNH84344
USNM236261	FMNH107787	FMNH26598	FMNH26593
USNM236266	FMNH107727	FMNH141628	FMNH26599
USNM236268	FMNH107721	FMNH145383	FMNH26600
USNM236299	FMNH107719	FMNH141629	FMNH26601
USNM236263	FMNH107544	FMNH143287	FMNH26604
USNM236269	FMNH107549	FMNH136932	FMNH26612
USNM236276	FMNH107546	FMNH136934	FMNH26613
USNM236300	FMNH107530	FMNH136936	FMNH26613
USNM271407	FMNH107772	FMNH136937	FMNH26616
USNM259611	FMNH107777	FMNH136939	FMNH26617
USNM259612	FMNH107760	***Deltamys***	FMNH26618
USNM236314	FMNH107754	MCNU15	FMNH14304
USNM172966	FMNH107751	MCNU2	FMNH18519
USNM259622	FMNH107747	MCNU9	***Oreoryzomys***
USNM259623	FMNH107744	MCNU8	USNM513570
USNM331060	FMNH107703	MCNU6	***Oryzomys***
USNM276608	FMNH107704	MCNU7	FMNH5347
USNM276609	FMNH107705	MCNU22	FMNH44702
USNM290926	FMNH107717	MCNU14	FMNH54160
USNM390141	FMNH107718	MCNU5	FMNH54161
USNM390699	FMNH170485	MCNU10	FMNH54162
USNM584503	FMNH170487	MCNU11	FMNH54163
USNM584504	FMNH170489	MCNUPCE5	FMNH56006

USNM584505	FMNH107803	MCNU15	FMNH56007
USNM584506	FMNH107805	MCNU7	FMNH56008
USNM390160	FMNH107807	MCNU25	FMNH73521
USNM390161	FMNH107810	MCNU44	FMNH73522
USNM390162	FMNH107814	***Eligmodontia***	FMNH73523
USNM271433	FMNH107817	FMNH133029	FMNH73525
USNM290907	FMNH107818	FMNH133034	FMNH171227
USNM290927	FMNH164159	FMNH133035	FMNH171228
USNM236238	FMNH164160	FMNH133036	FMNH171230
USNM236241	FMNH164161	FMNH133037	FMNH171231
USNM238127	FMNH164164	FMNH133038	FMNH171232
USNM259603	FMNH164168	FMNH133041	FMNH7818
USNM141453	FMNH164169	FMNH133044	FMNH7819
USNM181333	FMNH157211	FMNH133045	FMNH7811
USNM181335	FMNH164101	FMNH133046	***Oxymycterus***
USNM181338	FMNH164118	***Eremoryzomys***	MZUSP10777
USNM259615	FMNH164119	FMNH19763	MZUSP2089
USNM259616	FMNH164136	FMNH19764	MZUSP10721
USNM259617	FMNH157192	FMNH19766	MZUSP29368
USNM259618	FMNH157194	FMNH19767	MZUSP29374
USNM259619	FMNH157197	FMNH129243	MZUSP29375
USNM302998	FMNH157199	FMNH129245	MZUSP9891
USNM303000	FMNH157201	FMNH129242	MZUSP9832
USNM303001	FMNH157203	***Euneomys***	MZUSP10207
USNM304548	FMNH157206	FMNH134186	MZUSP10189
USNM279457	FMNH172223	FMNH134182	MZUSP10188
USNM279459	FMNH172221	FMNH133088	MZUSP10187
USNM279461	FMNH171861	FMNH134183	MZUSP10190
USNM513598	FMNH171862	FMNH133083	MZUSP29364
USNM513599	FMNH172231	FMNH133085	MZUSP29365
USNM513600	FMNH172225	FMNH134181	MZUSP29366
USNM513601	FMNH172227	FMNH133089	MZUSP29367
USNM513602	FMNH172229	***Euryoryzomys***	MZUSP29369
USNM513603	FMNH172233	FMNH136915	MZUSP29370
USNM513604	FMNH170501	FMNH136906	MZUSP22483
USNM513605	FMNH170503	FMNH136905	MZUSP22487
USNM364531	FMNH170506	FMNH136911	MZUSP22488
USNM181334	FMNH170508	FMNH136909	MZUSP22490
USNM181336	FMNH170509	FMNH136913	MZUSP22491
USNM121380	FMNH170510	FMNH143318	MZUSP22492
USNM121386	FMNH170511	FMNH143319	MZUSP21572
USNM259279	FMNH170517	FMNH117111	MZUSP21573
USNM259632	FMNH170519	FMNH117113	MZUSP21574
USNM194753	FMNH170523	FMNH26786	MZUSP10208
USNM194752	FMNH170524	FMNH117110	MZUSP21575
USNM194758	FMNH170526	FMNH139874	MZUSP26794
USNM194757	FMNH175021	FMNH141637	MZUSP21595
USNM195760	FMNH175023	FMNH141638	MZUSP21594
USNM194762	FMNH175025	FMNH141639	MZUSP23751
USNM194763	FMNH170029	FMNH141640	MZUSP22461
USNM194666	FMNH175031	FMNH141641	MZUSP845
USNM196941	FMNH175033	FMNH141642	MZUSP10085
USNM259272	FMNH50980	FMNH141643	MZUSP35158
USNM259273	FMNH50983	FMNH141644	MZUSP35157
USNM259274	FMNH20981	FMNH141646	MZUSP2771
USNM259275	MN33681	FMNH141648	MZUSP10650
USNM259277	MN33681	MZUSP1844	MZUSP10651
USNM259278	MN33681	MZUSP1841	FMNH145443
USNM194658	MN33681	MZUSP1894	FMNH145442
USNM194672	MN33681	MZUSP20559	FMNH145441
USNM194673	MN33681	MZUSP20560	FMNH145438
USNM194675	MN33681	***Galenomys***	FMNH145437
USNM194727	MN33703	AMNH262814	FMNH53875
USNM194735	MN48026	AMNH246941	FMNH53874

USNM194736	MN67123	AMNH246942	FMNH27652
USNM194739	MN48882	AMNH246943	FMNH29250
USNM194742	MN48882	AMNH246945	FMNH29253
USNM194743	MN48882	AMNH246947	FMNH52623
USNM194744	MN48882	AMNH246946	FMNH52630
USNM194746	MN48882	***Geoxus***	FMNH52624
USNM194749	MN48882	FMNH133125	FMNH52633
USNM194751	MN48888	FMNH133115	FMNH52625
USNM194750	MN48889	FMNH133116	FMNH52626
USNM324907	MN50241	FMNH133124	FMNH52631
USNM324908	MN63121	FMNH134949	FMNH162837
USNM390146	MN48890	FMNH134948	FMNH162839
USNM390147	MN48891	FMNH127724	FMNH162841
USNM390148	MN50255	FMNH133097	FMNH162843
USNM390150	MN50281	FMNH133103	FMNH162845
USNM390151	MN50282	FMNH133104	FMNH26592
USNM390152	MN50283	FMNH124059	FMNH26595
USNM390153	MN50256	FMNH22499	FMNH26587
USNM390155	MN50257	FMNH22496	FMNH35354
USNM390157	MN50258	FMNH22495	FMNH34383
USNM390158	MN50259	FMNH133094	FMNH23843
USNM555668	MN50260	FMNH50538	FMNH26757
USNM555669	MN50261	***Graomys***	FMNH26754
USNM194581	MN50262	FMNH50961	FMNH128320
USNM194583	MN50263	FMNH50962	FMNH128321
USNM194586	MN50264	FMNH50963	FMNH128322
USNM194593	MN50265	FMNH50968	FMNH128323
USNM194594	MN50266	FMNH50969	FMNH128324
USNM194595	MN50267	FMNH21525	FMNH122697
USNM194596	MN50269	FMNH157386	FMNH95138
USNM194599	MN50270	FMNH157387	FMNH136928
USNM194600	MN50271	FMNH157388	FMNH136929
USNM194601	MN50272	FMNH157393	***Paynomys***
USNM194604	MN50273	FMNH157394	FMNH132990
USNM194609	MN50274	FMNH164754	FMNH132979
USNM194610	MN50275	FMNH164749	FMNH132940
USNM194612	MN50276	FMNH164750	FMNH132988
USNM194613	MN69565	FMNH157385	FMNH132987
USNM194614	MN69566	FMNH157382	FMNH132983
USNM194615	MN69567	FMNH164836	FMNH50530
USNM194618	MN69568	FMNH164837	FMNH50529
USNM194619	MN69569	FMNH164838	FMNH46153
USNM194621	MN69570	FMNH164841	FMNH46154
USNM194623	MN69571	FMNH164842	FMNH46155
USNM194626	MN69572	FMNH164843	FMNH132927
USNM194627	MN69573	FMNH164844	FMNH132931
USNM194628	MN69574	FMNH164846	FMNH132944
USNM194629	MN69575	FMNH164850	FMNH132956
USNM194630	MN69576	FMNH164857	FMNH132924
USNM194631	MN69585	***Handleyomys***	FMNH132930
USNM194633	MN69586	FMNH64541	FMNH132942
USNM194635	MN69587	FMNH73543	FMNH132953
USNM194636	MN69588	FMNH73562	***Phyllotis***
USNM582136	MN69589	FMNH73545	FMNH81260
USNM582137	MN69590	FMNH73560	FMNH81261
USNM582138	MN69596	FMNH61679	FMNH81263
USNM582139	MN69599	FMNH61680	FMNH19258
USNM582141	MN59113	FMNH5371	FMNH19259
USNM582142	MN69602	FMNH70296	FMNH19261
USNM582143	MN69605	FMNH70302	FMNH107390
USNM582169	MN69606	FMNH70303	FMNH107392
USNM582171	MN69609	FMNH70304	FMNH107391
USNM182175	MN69613	FMNH70305	FMNH107393
USNM290909	MN69623	FMNH55904	FMNH107394

AMNH268750	MN69627	FMNH56033	FMNH107396
AMNH268743	MN69628	FMNH55896	FMNH19839
AMNH268744	MN69629	FMNH55900	FMNH19841
AMNH268751	MN69644	FMNH11137	FMNH19842
AMNH268745	MN69645	FMNH11138	FMNH19843
AMNH268746	MN69660	FMNH11139	FMNH81208
AMNH268747	MN69664	FMNH11142	FMNH81207
AMNH268748	MN69665	FMNH14111	FMNH81206
AMNH268752	MN48029	***Holochilus***	FMNH81205
AMNH268738	MN48066	FMNH145308	FMNH81204
AMNH268739	MN75283	FMNH53948	FMNH81203
AMNH268740	MN75282	FMNH53949	FMNH81202
AMNH268741	MN48031	FMNH23307	FMNH41287
AMNH268742	MN48032	FMNH23308	FMNH85847
AMNH67428	MN48033	FMNH23311	FMNH85848
AMNH67431	MN48034	FMNH23313	FMNH85849
AMNH67462	MN48035	FMNH23314	FMNH119508
AMNH67466	MN48036	FMNH23315	FMNH119507
AMNH47567	MN48041	FMNH118811	FMNH22325
AMNH47568	MN48067	FMNH118819	FMNH22326
AMNH47566	MN48070	FMNH118816	FMNH22328
AMNH47556	MN63110	FMNH118820	FMNH133896
AMNH47558	MN69675	FMNH118825	FMNH119512
AMNH47563	MN69676	***Hylaeamys***	FMNH35902
AMNH231302	MN69677	FMNH143304	FMNH119505
AMNH231298	MN69679	FMNH143305	FMNH21916
AMNH231296	MN69681	FMNH143306	FMNH81265
AMNH231300	MN69682	FMNH143308	FMNH81266
AMNH71230	MN69683	FMNH143309	FMNH81269
AMNH71220	MN69685	FMNH143310	FMNH81270
AMNH71227	MN69686	FMNH143313	FMNH81271
AMNH71226	MN69687	FMNH143315	FMNH81275
AMNH76691	MN69695	FMNH143316	FMNH81274
AMNH92456	MN69700	FMNH75222	FMNH81273
AMNH260436	MN69701	FMNH75241	FMNH81272
AMNH260439	MN69705	FMNH75243	FMNH107609
AMNH260438	MN69710	FMNH75244	FMNH107574
AMNH260440	MN69714	FMNH75246	FMNH107575
AMNH260441	MN69715	FMNH75247	FMNH107598
AMNH260442	MN69716	FMNH75248	FMNH49481
AMNH260445	MN69719	FMNH75273	FMNH49482
AMNH268759	MN69724	FMNH75269	FMNH49484
AMNH268757	MN69735	FMNH75270	FMNH49485
AMNH262681	MN69727	FMNH66401	FMNH49487
AMNH262680	MN69726	FMNH75242	FMNH49488
AMNH262678	MN69737	FMNH75253	FMNH35360
AMNH262677	MN69741	FMNH72051	FMNH49475
AMNH262682	MN69745	FMNH58778	FMNH107683
AMNH206049	MN71897	FMNH58779	FMNH107690
AMNH206047	MN62119	FMNH87970	FMNH107691
AMNH206046	MN62120	FMNH72067	FMNH107692
AMNH206040	MN54491	***Irenomys***	FMNH107561
AMNH206041	MN69584	FMNH134969	FMNH107611
AMNH206042	MN69597	FMNH134970	FMNH107612
AMNH206043	MN69621	FMNH134964	FMNH107613
AMNH206056	MN60640	FMNH134967	FMNH107616
AMNH206050	MN60654	FMNH134963	FMNH22342
AMNH206052	MN69655	FMNH133137	FMNH50964
AMNH262690	MN69657	FMNH133139	FMNH74870
AMNH262718	MN69666	FMNH133140	FMNH50966
AMNH626692	MN69667	FMNH133154	FMNH74871
AMNH262717	MN69669	FMNH133155	FMNH74872
AMNH262714	MN69673	FMNH133142	FMNH74873
AMNH262711	MN63113	FMNH50554	FMNH107898

AMNH248998	MN63114	FMNH50567	FMNH107900
AMNH263640	MN51644	FMNH50555	FMNH107901
AMNH263630	MN71903	FMNH50557	FMNH107902
AMNH263632	MN48065	FMNH50561	FMNH107903
AMNH263631	MN77791	FMNH50563	FMNH107904
AMNH263642	MN71942	FMNH50564	FMNH107905
AMNH263641	MN48027	FMNH50565	FMNH107929
AMNH262648	MN48028	FMNH50568	FMNH107936
AMNH262685	MN42011	FMNH133166	FMNH107939
AMNH262687	MN48030	FMNH133164	USNM121143
AMNH262695	MN60680	FMNH133148	USNM121145
AMNH262719	MN60711	FMNH133143	***Podoxymys***
AMNH262704	MN35912	***Juliomys***	AMNH75584
AMNH247794	MN35919	FMNH94552	AMNH75585
AMNH247789	MN35921	***Juscelinomys***	***Pseudoryzomys***
AMNH247795	MN35922	USNM584510	FMNH118810
AMNH247796	MN35923	USNM584508	FMNH34236
AMNH247797	MN35924	USNM584509	USNM584585
AMNH263300	MN35926	USNM584511	USNM584586
AMNH263298	MN35927	USNM584512	USNM390668
AMNH263295	MN32637	USNM584514	AMNH262048
AMNH263294	MN24592	USNM584513	***Rhagomys***
AMNH263291	MN24594	***Kunsia***	FMNH170687
AMNH262745	MN24595	FMNH122711	***Rheomys***
AMNH262746	MN24616	FMNH122710	USNM565826
AMNH262747	MN24617	USNM584515	USNM396585
AMNH262748	MN24627	USNM584516	USNM396586
AMNH262751	MN24630	***Lenoxus***	USNM520769
AMNH262753	MN24631	FMNH20106	***Rhipidomys***
AMNH262754	MN24632	FMNH52613	FMNH70235
AMNH268777	MN24639	FMNH52612	FMNH70237
AMNH268776	MZUSP29114	AMNH72624	FMNH70238
AMNH268773	MZUSP29112	AMNH72620	FMNH70241
AMNH268772	MZUSP29100	AMNH72622	FMNH70244
AMNH268771	MZUSP29102	AMNH72618	FMNH70247
AMNH268780	MZUSP29103	AMNH72616	FMNH70249
AMNH268783	MZUSP29104	AMNH72615	FMNH43211
AMNH268779	MZUSP29105	AMNH72611	FMNH41477
AMNH268788	MZUSP29106	AMNH72610	FMNH125049
AMNH268787	MZUSP29107	AMNH72609	FMNH53401
AMNH268786	MZUSP29108	AMNH264855	FMNH41478
AMNH268785	MZUSP29109	AMNH264854	FMNH68652
AMNH231341	MZUSP29110	AMNH16553	FMNH75229
AMNH231340	MZUSP29111	AMNH16065	FMNH24820
AMNH231338	MZUSP29113	AMNH16558	FMNH24819
AMNH231337	MZUSP29088	***Loxodontomys***	FMNH24816
AMNH231334	MZUSP29089	FMNH132689	FMNH53982
AMNH231331	MZUSP29090	FMNH132692	FMNH53983
AMNH231329	MZUSP29091	FMNH132706	FMNH211417
AMNH231328	MZUSP29092	FMNH132746	FMNH128325
AMNH231326	MZUSP29093	FMNH132747	FMNH140806
AMNH231325	MZUSP29094	FMNH132749	FMNH140807
AMNH231324	MZUSP29096	FMNH132751	FMNH140808
AMNH231322	MZUSP29097	FMNH132752	***Scapteromys***
AMNH231318	MZUSP29098	FMNH132668	FMNH29160
AMNH231317	MZUSP29099	FMNH132666	FMNH98288
AMNH231403	MZUSP29119	FMNH132665	FMNH98287
AMNH231400	MZUSP29120	FMNH132787	FMNH122714
AMNH231399	MZUSP29121	FMNH132785	FMNH122713
AMNH268766	MZUSP29122	FMNH132783	USNM
AMNH262724	MZUSP29123	FMNH132782	AMNH206221
AMNH268803	MZUSP29124	FMNH132780	AMNH206223
AMNH268809	MZUSP29126	FMNH132779	AMNH206222
AMNH268810	MZUSP29101	FMNH132778	AMNH206216

AMNH268816	MZUSP29115	FMNH132789	AMNH206209
AMNH268818	MZUSP29116	FMNH132791	AMNH206219
AMNH268819	MZUSP29117	FMNH132792	AMNH206230
AMNH268820	MZUSP29118	FMNH132800	AMNH206244
AMNH268795	MZUSP938	FMNH132804	AMNH206245
AMNH268797	MZUSP939	FMNH132807	AMNH206240
AMNH268801	MZUSP942	***Lundomys***	AMNH206231
AMNH268802	MZUSP30951	FMNH29257	***Scolomys***
AMNH47486	MZUSP31013	FMNH29260	USNM513582
AMNH47494	MZUSP30997	FMNH29261	USNM513583
AMNH47501	MZUSP1773	FMNH29263	USNM548381
AMNH231476	MZUSP1796	USNM259641	USNM513581
AMNH231475	MZUSP27226	***Melanomys***	AMNH57522
AMNH231472	MZUSP27223	FMNH128471	***Sigmodon***
AMNH231469	MZUSP1794	FMNH128472	FMNH18683
AMNH60594	MZUSP27225	FMNH128476	FMNH18686
AMNH264231	MZUSP9469	FMNH128477	FMNH18682
AMNH264232	MZUSP2772	FMNH128488	FMNH18693
AMNH264233	MZUSP29127	FMNH92459	FMNH22138
AMNH264238	MZUSP29128	FMNH70358	FMNH18648
AMNH264239	MZUSP30947	FMNH70364	FMNH20040
AMNH264274	MZUSP28965	FMNH70366	FMNH20041
AMNH264272	MZUSP28966	FMNH70370	FMNH20042
AMNH91561	MZUSP626	FMNH70347	FMNH20038
AMNH91565	MZUSP29255	FMNH70350	FMNH890
AMNH91564	MZUSP29256	FMNH70352	FMNH891
AMNH91569	MZUSP29257	FMNH70354	FMNH892
AMNH91577	MZUSP29259	FMNH70355	FMNH893
AMNH91575	MZUSP29260	***Microryzomys***	FMNH894
AMNH91574	MZUSP29261	FMNH175045	FMNH895
AMNH91578	MZUSP29262	FMNH175047	FMNH889
AMNH41816	MZUSP29263	FMNH175049	FMNH13223
AMNH41803	MZUSP29264	FMNH175051	FMNH13224
AMNH41682	MZUSP29247	FMNH175053	FMNH13226
AMNH41692	MZUSP29225	FMNH175055	FMNH44865
AMNH264296	MZUSP28388	FMNH175057	FMNH69157
AMNH264288	MZUSP28379	FMNH175059	FMNH54008
AMNH264281	MZUSP28357	FMNH71951	FMNH54007
AMNH264293	MZUSP29239	FMNH71950	FMNH34962
AMNH264282	MZUSP29240	FMNH71956	FMNH5005
AMNH264290	MZUSP29241	FMNH71957	FMNH34960
AMNH264295	MZUSP29242	FMNH71964	FMNH44009
AMNH262294	MZUSP29243	FMNH71958	FMNH44010
AMNH264292	MZUSP29244	FMNH71966	FMNH34972
AMNH264285	MZUSP29245	FMNH71960	FMNH7930
AMNH41752	MZUSP29246	FMNH71959	FMNH7931
AMNH41832	MZUSP29218	FMNH71954	FMNH7934
AMNH41835	MZUSP29219	***Neacomys***	FMNH7918
AMNH41675	MZUSP29228	FMNH95643	FMNH7920
AMNH41648	MZUSP29229	FMNH125030	FMNH7923
AMNH41651	MZUSP29230	FMNH125033	FMNH7925
AMNH41656	MZUSP29231	FMNH125036	FMNH7926
AMNH268857	MZUSP29232	FMNH125038	FMNH7944
AMNH268856	MZUSP29233	FMNH125039	FMNH7938
AMNH268855	MZUSP29234	FMNH125041	FMNH15181
AMNH268850	MZUSP29235	FMNH75364	FMNH14090
AMNH268851	MZUSP29237	FMNH75362	FMNH14089
AMNH268854	MZUSP29238	FMNH75360	FMNH14363
FMNH65705	MZUSP32429	FMNH75359	FMNH8653
FMNH66402	MZUSP32424	FMNH75361	FMNH8656
FMNH68609	MZUSP32427	FMNH75363	FMNH8658
FMNH68612	MZUSP29227	FMNH23746	FMNH8662
FMNH68614	MZUSP29226	FMNH24761	FMNH81341
FMNH68616	MZUSP3520	FMNH24762	FMNH19216

FMNH78709	MLP5.xi.92.37	FMNH24763	FMNH81344
FMNH41474	MLP5.xi.92.14	FMNH20088	FMNH81345
FMNH43229	MLP5.xi.92.28	FMNH20089	FMNH81346
FMNH43232	MLP5.xi.92.23	FMNH52711	FMNH81347
FMNH19265	MLP5.xi.92.38	FMNH19360	FMNH106540
FMNH19268	MLP5.xi.92.24	FMNH19691	FMNH106541
FMNH19266	MLP5.xi.92.19	***Necromys***	FMNH106542
FMNH19757	MLP5.xi.92.21	AMNH259916	FMNH106544
FMNH78715	MLP5.xi.92.18	AMNH259917	***Siqmodontomys***
FMNH78714	MLP5.xi.92.13	AMNH259919	FMNH70530
FMNH78710	MLP5.xi.92.17	AMNH259920	FMNH70534
FMNH78720	MLP5.xi.92.1	AMNH259921	FMNH70535
FMNH75481	MLP10.iii.79.1	AMNH259922	FMNH70536
FMNH75480	MLP10.iii.79.5	FMNH162771	FMNH90282
FMNH75479	MLP24.v.77.1	FMNH23366	FMNH89563
FMNH75478	MLP20.xii.00.16	FMNH122687	FMNH70532
FMNH75477	MLP16.v.01.10	FMNH107836	FMNH69193
FMNH75476	MLP16.v.01.9	FMNH107838	FMNH69196
FMNH75475	MLP30.v.02.2	FMNH107862	FMNH21829
FMNH75474	MLP14.xii.73.3	FMNH107864	FMNH53999
FMNH75473	MLP28.ix.95.5	FMNH107866	***Sooretamys***
FMNH75472	MLP1.x.70.18	FMNH10875	FMNH26752
FMNH75471	MLP11.ii.36.7	FMNH107680	FMNH26751
FMNH75470	MLP18.viii.74.2	FMNH107699	FMNH26750
FMNH75479	MLP18.viii.74.6	FMNH25197	FMNH26749
FMNH75565	MLP18.viii.74.4	FMNH25198	FMNH26748
FMNH75225	MLP18.viii.74.8	FMNH25200	FMNH26747
FMNH24522	MLP9.ii.99.1	FMNH26201	FMNH136919
FMNH24525	MLP24.v.96.2	FMNH128339	FMNH136920
FMNH24526	MLP30.viii.99.8	FMNH128337	FMNH136922
FMNH24532	MLP14.ix.99.34	FMNH128336	FMNH18165
FMNH24534	MLP14.ix.99.35	FMNH128335	FMNH18166
FMNH24536	MLP14.ix.99.3	FMNH128334	FMNH18167
FMNH24538	MLP14.ix.99.17	FMNH128333	***Thalpomys***
FMNH24540	MLP14.ix.99.37	FMNH128331	FMNH128327
FMNH24542	MLP14.ix.99.45	FMNH164415	FMNH128326
FMNH24543	MLP14.ix.99.42	FMNH164416	***Thaptomys***
FMNH24502	MLP14.ix.99.43	FMNH164414	MN8780
FMNH24506	MLP14.ix.99.30	FMNH164413	MN8778
FMNH24503	MLP14.ix.99.1	FMNH164411	MN8775
FMNH24510	MLP18.v.74.7	FMNH164426	MN8771
FMNH24512	FMNH23341	FMNH164422	MN8769
FMNH78376	FMNH23340	FMNH164421	MN8767
FMNH78375	FMNH23328	FMNH164419	MN8764
FMNH78377	FMNH23329	FMNH164418	MN8763
FMNH52539	FMNH23330	***Nectomys***	MN8805
FMNH52523	FMNH23333	FMNH43208	MN8804
FMNH52522	FMNH23334	FMNH43210	MN8803
FMNH52593	FMNH23332	FMNH41465	MN8797
FMNH52294	FMNH23335	FMNH41466	MN8795
FMNH52527	FMNH23336	FMNH41467	MN8792
FMNH52526	FMNH23337	FMNH65687	MN8788
FMNH52525	FMNH23339	FMNH65690	MN8787
FMNH52524	FMNH22233	FMNH65691	MN8785
FMNH52528	FMNH98283	FMNH78696	MN8735
FMNH52529	FMNH98282	FMNH68643	MN8734
FMNH52541	FMNH95140	FMNH68640	MN8731
FMNH18180	FMNH23344	FMNH68639	MN8730
FMNH52538	FMNH23345	FMNH65694	MN8729
FMNH52107	FMNH23346	FMNH19645	MN2727
FMNH52531	FMNH23347	FMNH19644	MN8724
FMNH72100	FMNH23348	FMNH19643	MN8721
FMNH170423	FMNH23349	FMNH19649	MN8720
FMNH170427	FMNH23350	FMNH18549	MN29100

FMNH170428	FMNH29218	FMNH46213	MN29101
FMNH170429	FMNH29220	FMNH18542	MN29104
FMNH170431	FMNH29222	FMNH20710	MN29110
FMNH170408	FMNH29223	FMNH20711	MN29096
FMNH170413	FMNH29215	FMNH20712	MN29097
FMNH170414	FMNH29214	FMNH20713	MN29098
FMNH170415	FMNH29213	FMNH94390	MN29099
FMNH170416	FMNH29211	FMNH94387	MN69838
FMNH170417	FMNH29209	FMNH94380	MN77795
FMNH170412	FMNH29207	FMNH94385	MN7041
FMNH170420	FMNH29205	FMNH94377	MN7037
FMNH170388	FMNH29200	FMNH93049	MN7025
FMNH170393	FMNH29199	***Neotomys***	MN7033
FMNH170396	FMNH29196	FMNH24775	MN7096
FMNH170397	FMNH29195	FMNH81238	MZUSP29384
FMNH170399	FMNH27612	FMNH24776	MZUSP29385
FMNH170400	FMNH29204	FMNH75580	MZUSP29386
FMNH170403	FMNH29188	FMNH49708	MZUSP29387
FMNH170368	FMNH29189	FMNH51262	MZUSP29388
FMNH170369	FMNH27614	FMNH51263	MZUSP29383
FMNH170371	FMNH27615	USNM541802	MZUSP23850
FMNH170377	FMNH27616	AMNH231645	MZUSP24008
FMNH170379	FMNH27617	AMNH231644	***Thomasomys***
FMNH170380	FMNH27620	AMNH231641	FMNH70320
FMNH170384	FMNH27621	AMNH231640	FMNH70322
FMNH170385	FMNH27624	AMNH231639	FMNH70323
FMNH170351	FMNH27625	AMNH231637	FMNH70327
FMNH170353	FMNH27626	AMNH231636	FMNH70328
FMNH170357	FMNH27627	AMNH231634	FMNH70329
FMNH170359	FMNH27628	***Nephelomys***	FMNH70331
FMNH170360	FMNH27630	FMNH71840	FMNH70307
FMNH170361	FMNH27631	FMNH71845	FMNH70308
FMNH172197	FMNH27632	FMNH71846	FMNH70309
FMNH172195	FMNH27633	FMNH71847	FMNH70310
FMNH172193	FMNH27635	FMNH71848	FMNH70311
FMNH172192	FMNH27636	FMNH71849	FMNH70316
FMNH172190	FMNH27641	FMNH71851	FMNH90333
FMNH129981	FMNH27670	FMNH53342	FMNH90334
FMNH129982	FMNH27662	FMNH53344	FMNH90335
FMNH129983	FMNH23352	FMNH170640	FMNH90339
FMNH129986	FMNH23355	FMNH170645	FMNH71478
FMNH129992	FMNH23351	FMNH170649	FMNH71480
FMNH129993	FMNH23361	FMNH170651	FMNH71481
FMNH129995	FMNH21581	FMNH170654	FMNH71482
FMNH107876	FMNH21578	FMNH170655	FMNH71475
FMNH52575	FMNH21575	FMNH170658	FMNH71474
FMNH107880	FMNH21588	FMNH172358	FMNH71471
FMNH107879	FMNH74880	FMNH172360	FMNH71467
FMNH107890	FMNH74879	FMNH172362	FMNH172378
FMNH53622	FMNH74874	FMNH171884	FMNH43393
FMNH53623	FMNH74876	FMNH175171	FMNH43392
FMNH53624	FMNH74875	FMNH174173	FMNH70342
FMNH107472	FMNH41284	FMNH175175	FMNH71489
FMNH107475	FMNH41285	FMNH175177	FMNH53244
FMNH107479	FMNH29127	FMNH175179	FMNH53407
FMNH107478	FMNH23673	***Nesoryzomys***	FMNH92000
FMNH107543	FMNH75561	FMNH179526	FMNH92001
FMNH107488	FMNH23671	FMNH179527	FMNH92002
FMNH107491	FMNH52544	***Neusticomys***	FMNH92003
FMNH107492	FMNH52556	FMNH71218	FMNH93148
FMNH107497	FMNH52555	FMNH71220	FMNH93150
FMNH107528	FMNH75483	FMNH71222	FMNH93152
FMNH107533	FMNH128296	FMNH71223	FMNH94991
FMNH107470	FMNH49696	FMNH71225	FMNH94993

FMNH107441	FMNH23362	AMNH64632	FMNH170693
FMNH107439	FMNH23363	AMNH64633	FMNH170796
FMNH170630	FMNH23364	AMNH64629	FMNH170697
FMNH107627	FMNH23365	AMNH62920	FMNH170699
FMNH107624	FMNH23360	AMNH63376	FMNH170701
FMNH107593	FMNH23359	AMNH244609	FMNH172380
FMNH107594	FMNH23357	AMNH244608	FMNH75224
FMNH107597	FMNH23356	***Oecomys***	FMNH172376
FMNH107600	***Andalgalomys***	FMNH116934	FMNH170707
FMNH107601	FMNH157341	FMNH116936	FMNH175241
FMNH107618	FMNH164192	FMNH116933	FMNH175243
FMNH107619	FMNH164190	FMNH116979	FMNH175245
FMNH107621	FMNH164184	FMNH116973	***Transandinomys***
FMNH107633	FMNH164188	FMNH116974	FMNH128493
FMNH107554	FMNH151997	FMNH116966	FMNH128490
FMNH107568	AMNH262344	FMNH116926	FMNH128491
FMNH107570	AMNH262345	FMNH116927	FMNH128492
FMNH107573	AMNH262347	FMNH116947	FMNH70504
FMNH107578	AMNH262346	FMNH116946	FMNH70496
FMNH107579	***Andinomys***	FMNH87968	FMNH70497
FMNH107580	FMNH23435	FMNH51913	FMNH70526
FMNH107587	FMNH132648	FMNH21522	FMNH70522
FMNH162735	FMNH132647	FMNH25267	FMNH70492
FMNH162737	FMNH132651	FMNH21524	FMNH70489
FMNH162745	FMNH162757	FMNH21523	FMNH69207
FMNH162645	FMNH162759	FMNH117061	FMNH60211
FMNH162647	FMNH162761	FMNH117060	FMNH69203
FMNH162679	FMNH51281	FMNH94024	FMNH69204
FMNH162681	FMNH51283	FMNH136894	FMNH69205
FMNH162685	FMNH51282	FMNH143292	FMNH71057
FMNH162683	FMNH51279	FMNH136943	FMNH72058
FMNH162687	FMNH29156	FMNH143288	FMNH72059
FMNH162689	FMNH29157	FMNH143291	***Wiedomys***
FMNH162693	FMNH74869	FMNH143289	FMNH25249
FMNH162699	***Auliscomys***	FMNH143290	FMNH136941
FMNH162707	FMNH49769	FMNH175097	FMNH136942
FMNH162713	FMNH49768	FMNH84303	USNM538314
FMNH162721	FMNH49771	FMNH175099	USNM538306
FMNH162723	FMNH49773	FMNH88937	USNM555761
FMNH162725	FMNH49774	FMNH72024	USNM304584
FMNH23342	FMNH49599	FMNH72030	USNM555760
FMNH27642	FMNH49600	FMNH41460	***Zygodontomys***
FMNH27638	FMNH49601	FMNH41458	FMNH20051
FMNH27664	FMNH49602	FMNH41459	FMNH20052
FMNH27619	FMNH49604	FMNH72013	FMNH20053
FMNH27669	FMNH81284	FMNH72025	FMNH20054
FMNH52551	FMNH81228	FMNH72089	FMNH20055
FMNH64339	FMNH81282	FMNH72020	FMNH87990
FMNH52543	FMNH107764	FMNH72027	FMNH87999
FMNH52545	FMNH107748	FMNH72042	FMNH88004
FMNH52544	FMNH107716	FMNH72033	FMNH88006
FMNH162753	FMNH107694	FMNH24574	FMNH88008
FMNH162751	FMNH107678	FMNH24576	FMNH89014
FMNH162749	FMNH107767	***Oligoryzomys***	FMNH18482
FMNH107829	FMNH107769	FMNH20962	FMNH18483
FMNH107834	FMNH49550	FMNH20961	FMNH18487
FMNH107840	FMNH107696	FMNH20963	FMNH18484
FMNH107841	FMNH107674	FMNH157391	FMNH18485
FMNH107848	FMNH107675	FMNH164910	FMNH18486
FMNH107850	FMNH107711	FMNH164911	FMNH18568
FMNH107853	FMNH107763	FMNH164913	FMNH18630
FMNH107856	FMNH49546	FMNH164914	FMNH21832
FMNH10858	FMNH49540	FMNH164915	FMNH54010
FMNH107863	FMNH49544	FMNH164924	

FMNH107865	***Blarinomys***	FMNH145314	
FMNH107928	MZUSP34269	FMNH26641	
FMNH107940	USNM304577	FMNH26805	
FMNH107943	***Brucepattersonius***	FMNH29238	
FMNH107944	MZUSP34665	FMNH122692	
FMNH107969	FMNH94499	FMNH27671	
FMNH52564	MZUSP27227	FMNH27668	
FMNH49699	MZUSP10661	FMNH27667	
FMNH49700	MZUSP21129	FMNH27655	

Table S2. Definition of landmarks on the skull and mandible views of all sigmodontine specimens. See Figure 1 in the main paper.

Description of landmarks of skull-ventral view:

L1: anteriormost point of the suture between nasals; **L2,3**: lateralmost point of the alveolus of the incisor; **L4,5**: lateral tip of the incisor; **L6,7**: anteriormost point of the incisive foramen; **L14,15**: posteriormost point of the incisive foramen; **L10,11**: medial extent of the suture between the premaxilla and maxilla lateral to the incisive foramen as seen in the ventral view; **L8,9**: lateralmost extent of suture between the premaxilla and maxilla; **L12,13**: anterodorsal tip of zygomatic plate; **L16,17**: anteriormost point of the orbit; **L18,24**: anteriormost point of the molar row; **L19,25**: contact point between first and second molars; **L20,26**: contact point between second and third molars; **L21,27**: posteriormost point of the third molar; **L22,28**: lateral paracone of first molar; **L23,29**: medial paracone of first molar; **L30,31**: least post-palatal distance across the palatines; **L32**: posteriormost extent of palate at the midline; **L33,34**: suture between jugal and squamosal in the zygomatic arch as seen in the ventral view; **L35-36**: anteriormost point of the glenoid fossa; **L37,38**: posterior end of squamosal root of zygomatic bar; **L39-40**: anteriormost point of the eustachian tube; **L41,42**: suture between basisphenoid and basioccipital at point of contact with the auditory bulla; **L43-44**: anteriormost border of the paramastoid process; **L45,46:** anteriormost external border of the ectotympanic; **L47,48**: posteriormost margin of the masseteric tubercle; **L49,50**: opening of the basioccipital at the level of the occipital condyle; **L51,52**: lateralmost point of the occipital condyle; **L53**: anteriormost point of the foramen magnum along the midline; **L54**: posteriormost point of the foramen magnum on the midline; **L55,56**: anteriormost margin of the occipital condyle.

Description of landmarks of skull lateral view:

L1: tip of the incisor; **L2:** posteriormost point of the upper incisive alveolus; **L3:** inferiormost point of the upper incisive alveolus; **L4:** anteriormost point of the suture between the nasal and the premaxilla; **L5:** anterior tip of the nasal; **L6:** dorsalmost point of the suture between the frontal and the parietal; **L7:** dorsalmost point of the suture between the parietal and the interparietal; **L8:** curvature at the limit between the occipital condyle and the occipital bone; **L9:** inferior extremity on the boundary between the occipital condyle and the tympanic bulla; **L10:** superiormost point at the middle of the tympanic bulla; **L11:** ventralmost point at the middle of the tympanic bulla; **L12:** anteroventral limit of the tympanic bulla; **L13:** posteriormost point of the molar row; **L14:** anteriormost point of the molar row; **L15:** ventral extent of the suture between maxilla and premaxilla; **L16:** ventral extent of intraorbital foramen; **L17:** anteriormost point of the orbit; **L18:** anteriormost point of the glenoid fossa in the zygomatic bar; **L19:** posterior end of zygomatic bar.

Description of landmarks of mandible view:

L1: Anteroventral border of incisive alveolus; **L2:** Upper extreme anterior border of incisor alveolus; **L3:** Position of greatest inflection of the diastema; **L4:** Anterior edge of the alveolus of first molar; **L5:** Intersection between molar crown and coronoid process in lateral view; **L6:** Tip of the coronoid process; **L7:** Point of maximum curvature between the coronoid and condylar process; **L8:** Dorsal margin of the anterior edge of the articular surface of the condylar process; **L9:** Ventral edge of the articular surface of the condylar process; **L10:** Point of maximum curvature between condylar and angular process; **L11:** Tip of the angular process; **L12:** Intersection between mandibular body and masseteric crest; **L13:** Ventral limits of the mandibular symphysis.

Figure S1. Phylogenetic relationships for 279 species of the subfamily Sigmodontinae. Species of Tylominae and *Rattus norvegicus* were used to root the tree. The MCC tree was constructed based on a supermatrix alignment of 11 genes. See main text for details on tree construction. *,** synonym names.

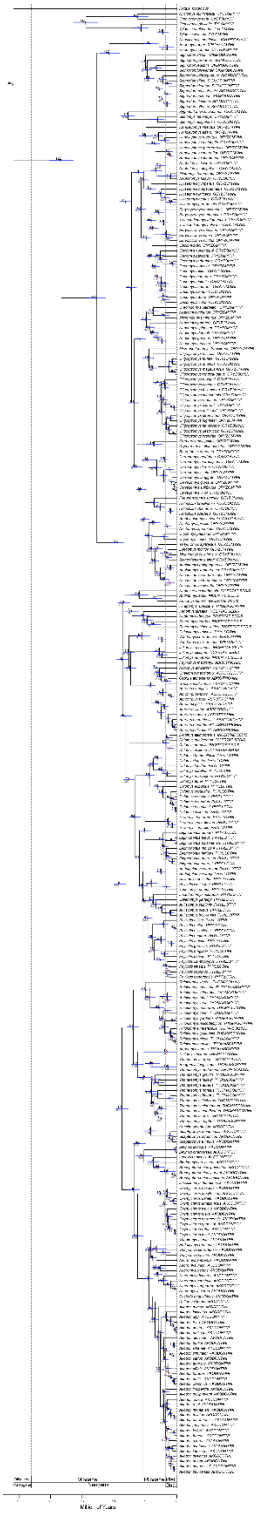

Figure S2. Lineages-through-time (LTT) plot for all sigmodontines, and the distribution of γ statistic values.

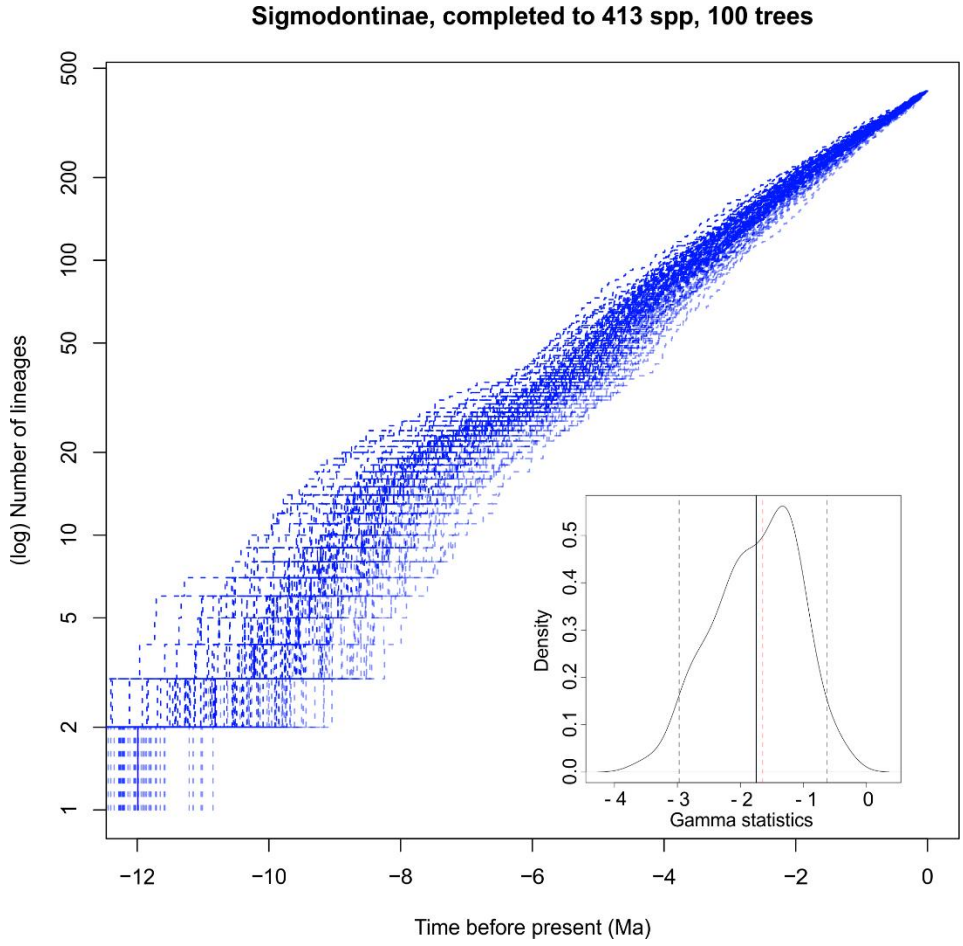

Figure S3. Lineages-through-time (LTT) plot for Oryzomyalia sigmodontines, and the distribution of γ statistic values.

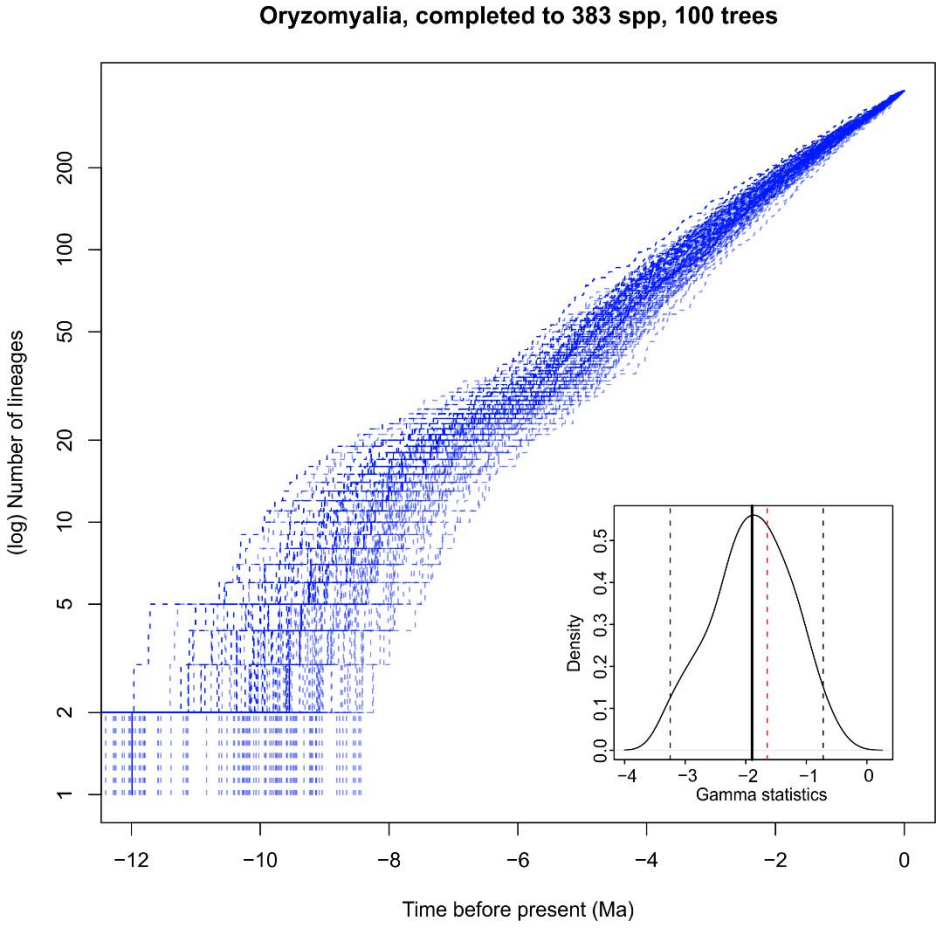

Figure S4. Average subclade disparity-through-time (DTT) plots for size, skull shape in ventral and lateral view, and mandible shape. The solid lines shows the observed disparity, and the dashed lines shows the average disparity of 10,000 simulations of a trait under Brownian motion. The gray shaded areas represent the 95% confidence interval for the simulated trait.

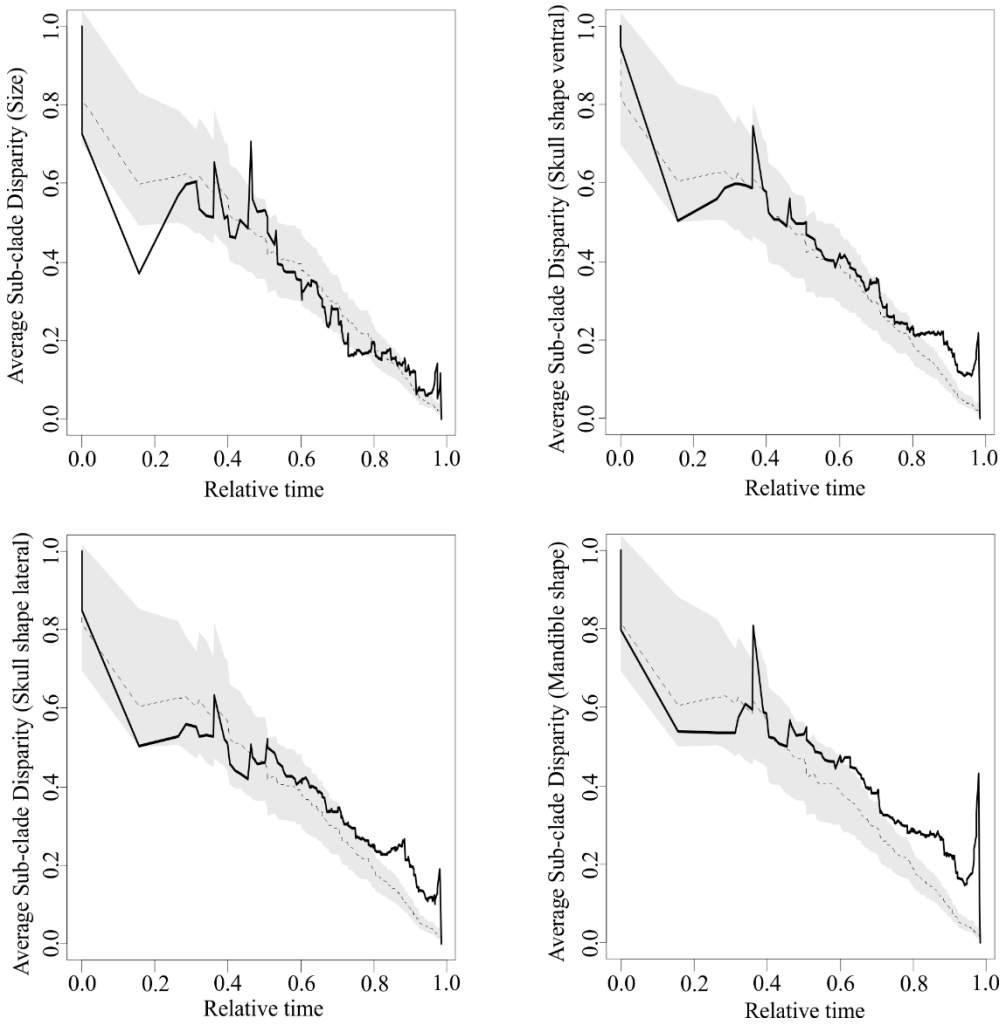

Supplemental File S5. Results of comparative analyses using Oryzomyalia sigmodontines only. Details on methods are fully presented in the main paper.

Phylogenetic signal for size and shape of Oryzomyalia was similar to the results using all tree (size – K= 0.90; skull shape ventral – K= 0.78; skull shape lateral – K= 0.79; shape mandible – K= 0.68; all statistical significant at $P< 0.05$), albeit all K values were a little higher for the Oryzomyalia radiation than for all sigmodontines.

Evolutionary model selection results are presented in Tables 1 and 2. Overall, shape results are similar between Oryzomyalia and all sigmodontines, with the highest support given to the Brownian model with two varying rates segregating insectivorous from others. For size evolution, model selection of Oryzomyalia selected models with life-mode as better than models with diet, in the same fashion that of all sigmodontines. Life-mode might be more important than diet for size evolution, and the opposite for shape.

Table 1. Comparison of the fit of alternative models for the evolution of size based on distinct diet and life mode hypotheses. The Oryzomyalia radiation was considered, other sigmodontines were excluded.

Model	**Size**			
	AICc	ΔAICc	AICc*wi*	Np
Habit OU.4	-213.96	0.00	0.769	6
Habit BMM.6	-210.43	3.53	0.131	7
Habit BMM.4	-209.30	4.66	0.075	5
Diet OU.2Hb	-205.18	8.78	0.010	4
Diet BMM.4	-203.71	10.24	0.005	5
Diet OU.4	-202.57	11.39	0.003	6
Habit OU.6	-202.54	11.42	0.003	8
BM.1	-201.29	12.66	0.001	2
Diet OU.3	-200.75	13.21	0.001	5
Diet BMM.2Hb	-200.71	13.25	0.001	3
Diet BMM.3	-199.77	14.19	0.001	4
Diet BMM.2In	-199.30	14.66	0.001	3

OU.1	-199.22	14.74	0.000	3
Diet OU.2In	-197.33	16.63	0.000	4
Habit BMM.3	-197.33	16.63	0.000	4
Habit OU.3	-195.29	18.66	0.000	5
EB	-122.65	91.30	0.000	3

Model acronyms as in Figure 2 in the main paper. See text and Fig. 2 for details on diet and habit hypothesis. EB corresponds to an early-burst model of evolution. Np are the numbers of parameters estimated by each model.

Table 2. Comparison of the fit of alternative models based on distinct diet and hypothesis for the evolution of skull and mandible shape using principal components. The Oryzomyalia radiation was considered, other sigmodontines were excluded.

Model	**Skull shape ventral 5 PC's (76.18)%**			
	AICc	ΔAICc	AICc*wi*	Np
Diet BMM.2In	-5224.19	0.00	0.980	35
Diet BMM.3	-5215.95	8.24	0.016	50
BM.1	-5213.40	10.79	0.004	20
Diet BMM.2Hb	-5205.31	18.88	0.000	35
Diet BMM.4	-5173.94	50.25	0.000	65
Habit BMM.3	-5165.04	59.16	0.000	50
Habit BMM.4	-5117.69	106.50	0.000	65
OU.1	-5071.09	153.11	0.000	35
Diet OU.2Hb	-4983.74	240.46	0.000	40
Habit OU.6	-4974.02	250.17	0.000	60
Habit OU.4	-4969.79	254.41	0.000	50
Diet OU.3	-4940.28	283.92	0.000	45
Diet OU.4	-4912.35	311.84	0.000	50
Habit BMM.6	-4903.85	320.35	0.000	95
Habit OU.3	-4859.85	364.35	0.000	45
Diet OU.2In	-4797.03	427.17	0.000	40
EB	-4702.34	521.85	0.000	21
Model	**Skull shape lateral 6 PC's (83.53%)**			
	AICc	ΔAICc	AICc*wi*	Np
Diet BMM.2In	-5940.80	0.00	1.000	48
BM.1	-5907.46	33.34	0.000	27
Diet BMM.2Hb	-5876.42	64.38	0.000	48
Diet BMM.3	-5861.08	79.72	0.000	69
Diet OU.3	-5835.38	105.42	0.000	60
Habit BMM.3	-5821.69	119.11	0.000	69
Habit OU.4	-5786.27	154.53	0.000	66
Diet OU.2In	-5782.75	158.05	0.000	54

Habit OU.6	-5780.93	159.87	0.000	78
Diet BMM.4	-5746.72	194.08	0.000	90
OU.1	-5734.82	205.98	0.000	48
Habit OU.3	-5732.15	208.65	0.000	60
Habit BMM.4	-5725.74	215.06	0.000	90
Diet OU.4	-5676.41	264.39	0.000	66
Diet OU.2Hb	-5670.00	270.80	0.000	54
EB	-5404.44	536.36	0.000	28
Habit BMM.6	-4804.99	1135.81	0.000	132

Model	**Mandible shape 5 PC's (80.25%)**			
	AICc	ΔAICc	AICc*wi*	Np
Diet BMM.2In	-4440.20	0.00	1.000	35
Diet BMM.3	-4419.52	20.69	0.000	50
Diet BMM.4	-4370.45	69.75	0.000	65
Diet OU.2In	-4369.64	70.57	0.000	40
Habit OU.3	-4359.06	81.14	0.000	45
Diet OU.4	-4353.74	86.47	0.000	50
Diet OU.2Hb	-4349.38	90.83	0.000	40
Diet OU.3	-4347.02	93.18	0.000	45
Habit OU.4	-4346.63	93.57	0.000	50
OU.1	-4343.96	96.24	0.000	35
BM.1	-4328.69	111.52	0.000	20
Diet BMM.2Hb	-4319.52	120.68	0.000	35
Habit OU.6	-4307.90	132.30	0.000	60
Habit BMM.3	-4285.86	154.34	0.000	50
Habit BMM.4	-4266.60	173.61	0.000	65
EB	-4036.10	404.11	0.000	21
Habit BMM.6	-4030.70	409.50	0.000	95

Model acronyms as in Figure 2 in the main paper. See text and Fig. 2 for details on diet and habit hypothesis. EB corresponds to an early-burst model of evolution. Np are the numbers of parameters estimated by each model.

Evolutionary rates between insectivorous and others proved statistical significant for shape (ventral: $\sigma^{2max/min}$=2.15, *P*= 0.003; lateral: $\sigma^{2max/min}$= 2.35, *P*= 0.001; mandible: $\sigma^{2max/min}$= 3.13, *P*= 0.001) but not for size ($\sigma^{2max/min}$= 1.06, *P*= 0.89). Once again, insectivorous had a much faster evolutionary rate than others did (ventral: In σ^2= 5.50×10^{-6}, On σ^2= 2.55×10^{-6}; lateral: In σ^2= 2.37×10^{-5}, On σ^2= 1.01×10^{-5}; mandible: In σ^2= 7.54×10^{-5}, On σ^2= 2.04×10^{-5}).

Morphological diversification through time analyses indicated that MDI for all morphological datasets were higher (i.e. more variation concentrated within sub-clades) than the MDI for all sigmodontines (skull ventral MDI= 0.051 *P*= 0.01; skull lateral MDI= 0.033 *P*= 0.06; skull mandible MDI= 0.083 *P*= 0.001; size MDI= 0.023 *P*= 0.17). For skull shape on ventral view and mandible shape, *P* values achieved significance, indicating more variation concentrated within sub-clades than expected under Brownian evolution; other two datasets showed no significance. See Figure 1 for morphological disparity curves.

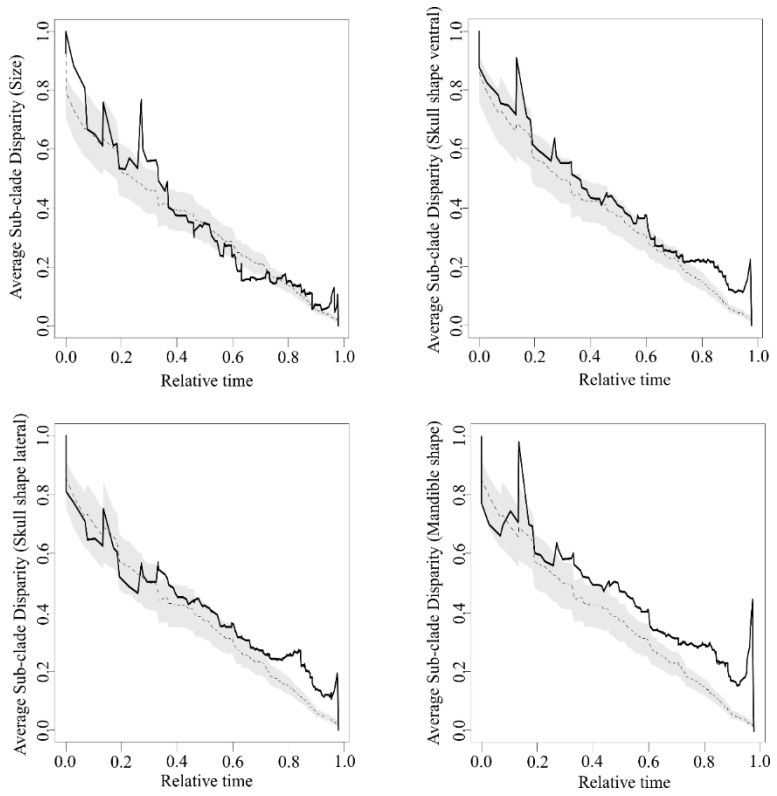

Figure 2. Average subclade disparity-through-time (DTT) plots for size, skull shape in ventral and lateral view, and mandible shape, for the Oryzomyalia radiation. The solid lines shows the observed disparity, and the dashed lines shows the average disparity of 10,000 simulations of a trait under Brownian motion. The gray shaded areas represent the 95% confidence interval for the simulated trait.

Capítulo 2

Diet, bite force and skull morphology in the generalist rodent morphotype**

Renan Maestri[1*], Bruce D Patterson[2], Rodrigo Fornel[3], Leandro Rabello Monteiro[4], Thales Renato Ochotorena de Freitas[1,5]

[1]*Programa de Pós-Graduação em Ecologia, Universidade Federal do Rio Grande do Sul, Porto Alegre, RS 91501-970, Brazil.*

[2]*Integrative Research Center, Field Museum of Natural History, Chicago, IL 60605, USA.*

[3]*Programa de Pós-Graduação em Ecologia, Universidade Regional Integrada do Alto Uruguai e das Missões, Campus Erechim, Erechim RS 99709-910, Brazil.*

[4]*Laboratório de Ciências Ambientais, CBB, Universidade Estadual do Norte Fluminense, Campos dos Goytacazes, RJ 28013-620, Brazil.*

[5]*Departamento de Genética, Universidade Federal do Rio Grande do Sul, Porto Alegre, RS 91501-970, Brazil.*

* *Correspondence*: renanmaestri@gmail.com

** Artigo publicado no periódico *Journal of Evolutionary Biology* (2016) 29: 2191-2204 (doi: 10.1111/jeb.12937)

Abstract

For many vertebrate species, bite force plays an important functional role. Ecological characteristics of a species' niche, such as diet, are often associated with bite force. Previous evidence suggests a biomechanical trade-off between rodents specialized for gnawing, which feed mainly on seeds, and those specialized for chewing, which feed mainly on green vegetation. We test the hypothesis that gnawers are stronger biters than chewers. We estimated bite force and measured skull and mandible shape and size in 63 genera of a major rodent radiation (the myomorph sigmodontines). Analysis of the influence of diet on bite force and morphology were made in a comparative framework. We then used phylogenetic path analysis to uncover the most probable causal relationships linking diet and bite force. Both granivores (gnawers) and herbivores (chewers) have a similar high bite force, leading us to reject the initial hypothesis. Path analysis reveals that bite force is more likely influenced by diet than the reverse causality. Absence of a trade-off between herbivores and granivores may be associated with the generalist nature of the myomorph condition seen in sigmodontine rodents. Both gnawing and chewing sigmodontines exhibit similar, intermediate phenotypes, at least compared to extreme gnawers (squirrels) and chewers (chinchillas). Only insectivorous rodents appear to be moving towards a different direction in the shape space, through some notable changes in morphology. In terms of diet, natural selection alters bite force though changes in size and shape, indicating that organisms adjust their bite force in tandem with changes in food items.

Keywords: chew, diet evolution, feeding, functional morphology, gnaw, phylogenetic path analysis, myomorph, natural selection, Rodentia, sigmodontines.

Introduction

Ecological morphology seeks to understand the association between morphological variation and ecology in a functional context (James, 1982). Understanding the mechanistic relationship between morphology and the way it functions in the environment is thus a major aim of functional morphology (Wainwright, 1994). By studying ecologically relevant functions of organisms, one can shed light on the relationships between ecology and function – it thus provides primary evidence of adaptation. One such trait of obvious performance relevance and clear ecological function is bite force (Aguirre *et al.*, 2003; Herrel *et al.*, 2005; Anderson *et al.*, 2008; Santana *et al.*, 2010).

Bite force is an attribute related to numerous types of functional demands in vertebrates (e.g. feeding, mating, defense, competition) and may reflect the strength of ecological challenges that organisms face (Anderson *et al.*, 2008). Demands related to feeding are usually the primary selective agents determining bite force (Christiansen & Wroe, 2007; Nogueira *et al.*, 2009), although intra- and interspecific competitive interactions can also play a role (Herrel *et al.*, 2007, Anderson *et al.*, 2008; Cornette *et al.*, 2015). Bite force is also known to be highly correlated with body size in vertebrates (Wroe *et al.*, 2005; Freeman & Lemen, 2008), although exceptions to this rule are most interesting. Skull shape, which configures the position and arrangement of muscle masses and lever arms, may similarly play a role in influencing bite force (Herrel *et al.*, 2001; Nogueira *et al.*, 2009; Cornette *et al.*, 2015; Wittorski *et al.*, 2016). Studies relating bite force with ecological functions have been extensively investigated in lizards (Herrel *et al.*, 2001; Wittorski *et al.*, 2016), turtles (Herrel *et al.*, 2002), birds (Herrel *et al.*, 2005), and in several mammal orders (Wroe *et al.*, 2005; Nogueira *et al.*, 2009; Cornette *et al.*, 2015), including rodents (Van Daele *et al.*, 2009; Willians *et al.*, 2009; Blanco *et al.*,

2012; Cox *et al.*, 2012; Cox *et al.*, 2013; Becerra *et al.*, 2014; Cox *et al.*, 2015; Druzinsky, 2015; Vassallo *et al.*, 2015). However, investigations of bite force in rodents have been limited to one or a few species, so that comparative assessments using large datasets are still lacking.

The order Rodentia is considered the most successful group in the 210 Ma history of mammals (Meredith *et al.*, 2011). More than 40% of living mammal species are rodents (Wilson & Reeder, 2005; IUCN, 2016), and they occupy nearly all terrestrial ecosystems. Although their species richness exceeds that of other mammalian orders, their morphological variation is thought to be relatively conserved (Hautier *et al.*, 2011). Disparity in diet among living species may result from changes in size and shape (Samuels, 2009), as well as in bite force (Hautier *et al.*, 2011; Cox *et al.*, 2012; Hautier *et al.*, 2012; Cox *et al.*, 2013).

Rodents are specialized towards a peculiar form of mastication, resulting in a characteristic skull that has a pair of ever-growing teeth, elongated rostrum, and large masseter muscles (Wood, 1965; Korth, 1994). All rodent species have a single incisor on each side of the jaw that is separated from the cheekteeth by a diastema. Occlusion of the incisors (for gnawing) and of the cheekteeth (for grinding and chewing) take place in alternation, so that when the incisors are engaged, the cheekteeth do not contact each other and vice versa. This fundamental characteristic of rodents sets the stage for an interesting trade-off between rodents specialized in gnawing (incisor engaged) or in chewing (cheekteeth engaged) (Cox *et al.*, 2012), which is accompanied by changes in morphology. Rodents that use mostly the incisors (gnawers) are expected to have stronger bite forces at the incisor, these rodents are prone to feed on seeds and nuts; conversely, rodents that use mostly the cheekteeth to feed (chewers) are expected to have weaker bite forces at the incisor, these rodents are prone to be herbivorous.

Living rodents were traditionally divided into three morphotypes based on masseter muscle configurations: sciuromorph, hystricomorph, and myomorph (Brandt, 1855; Simpson, 1945). These three groups are no longer considered to be monophyletic (Wood, 1965; Blanga-Kanfi *et al.*, 2009; Fabre *et al.*, 2012), although they still reflect important and well-defined differences in skull and mandible morphology (Cox *et al.*, 2012). The sciuromorph condition is characterized by a large masseter lateralis muscle that extends onto the rostrum, and associated changes in the mandible's angular process (Wood, 1965; Koth, 1994). These changes amplify the gnawing abilities of sciuromorph rodents (Druzinsky, 2010; Cox *et al.*, 2012), giving them stronger bites than other rodents. On the other hand, the hystricomorph condition represents a specialization for chewing. Morphological specialization involves the enlargement of the masseter medialis, which passes through the infraorbital foramen (greatly enlarging it) and inserts onto the rostrum (Wood, 1965; Koth, 1994). This condition allows rodents to be more effective at feeding with the molars (Hautier *et al.*, 2011; Cox *et al.*, 2012). Hystricomorph rodents feed mainly on vegetation, and most strictly herbivorous rodents have this morphotype; on the other hand, sciuromorphous rodents feed mainly on seeds and nuts and are therefore granivorous.

Finally, rats and mice--members of the highly successful Muroidea, which account for more than half of all rodent species--are characterized by the myomorphous condition. This condition involves shifts and extensions of both masseter medialis and lateralis, effectively combining features of both the sciuromorph and hystricomorph conditions (Wood, 1965; Koth, 1994). Myomorphy is thought to represent a compromise between gnawing and chewing specializations, producing a generalist "jack-of-all-trades" phenotype that has proven to be very successful.

Here, we explore the relationship between diet, bite force, skull, and mandible morphology in one of the world's most explosive radiations (Schenk *et al.*, 2013). Sigmodontines comprise a Neotropical subfamily of the muroid family Cricetidae, and hence share the myomorphous condition. Most of these rats and mice have generalist, omnivorous diets, feeding on fruits, seeds, and insects in different proportions (Nowak, 1999; Patton *et al.*, 2015). However, others have more specialized diets, such as the insectivorous and carnivorous members of the tribe Ichthyomyini or the obligately herbivorous rats of the genera *Andinomys* and *Chinchillula* (Patton *et al.*, 2015). Given the established relationships among morphotypes and diet in rodents, here we ask whether these patterns hold true for this radiation of myomorphs. Do sigmodontines with specialized herbivorous diets (resembling hystricomorphs) have weaker bite forces than their relatives feeding on hard foods such as seeds (resembling sciuromorphs)? These morphotypes are usually associated with shape changes, particularly in mandibular morphology, so we also expect that sigmodontines with herbivorous diets that place a premium on chewing will have the angular process of the mandible dorsoventrally flattened, with a longer, straighter diastema, and other associated changes, while hard-food specialists eating seeds and fruits will have a strong angular process to the mandible (Hautier *et al.*, 2011).

Rarely addressed in concert, the causal links between bite force, skull size and shape, and diet are investigated here though phylogenetic path analysis (PPA - Gonzalez-Voyer & von Hardenberg, 2014). Because bite force is expected to scale with changing size and shape, a question that remains is whether diet can change size and shape via selection on individuals with high or low bite force, or do changes in bite force happen first, leading to changes in diet? PPA is used to explore the direction of the causal relationships among bite force and diet changes. From this, insights are gained on the

targets of natural selection. Here, we reject the hypothesis that gnawers are stronger biters than chewers, and we demonstrate that natural selection acts to change bite force after organisms change their food items.

Materials and Methods

Morphological dataset

Bite force estimates were generated from 427 specimens representing 63 genera of sigmodontine rodents, using an index proposed by Freeman & Lemen (2008). The authors analysed five different indexes based on jaw bending and resistance, and compared them to actual (*in vivo*) bite forces of related cricetid rodents. The selected index involves taking two measurements of the lower incisor at the alveolus level: anterior-posterior length and medial-lateral width. By applying the formula (Zi= ((anterior-posterior length) ^{2} × (medial-lateral width))/6), one can have a reliable estimate of bite force (where Zi is the incisor strength index). Freeman & Lemen (2008) discovered that this index is correlated with bite force taken from live specimens ($R^2 = 0.96$) using a piezo-resistive sensor. After determining Zi for each individual, we averaged the values by genus (see Appendix S1 for number of specimens, species, and bite force for each genus), and transformed the units to Newtons (N) following the regression equation provided by Freeman & Lemen (2008). All incisor measurements were taken from specimens deposited in the Recent mammal collections of the Field Museum of Natural History, Chicago, USA.

We obtained size and shape variables from a sample of 2808 skulls (2763 skulls in ventral view and 2753 skulls in lateral view) and 2567 mandibles representing 63 genera of sigmodontine rodents. A list of visited mammal collections, the specimens consulted, and number of individuals by species and by genus can be found in Appendix

S2. Discrepancies in the number of specimens are due to damaged skulls, which caused specimens and views to be eliminated from the sample. Photographs of skulls in ventral and lateral view, and of the mandible in lateral view were taken with a digital camera (Nikon Coolpix P100, Tokyo, Japan). We positioned all specimens in the same plane and used the same distance from the camera to the subject. For each specimen, 56 landmarks were digitized on the ventral view of the skull, 19 landmarks and 1 semilandmark on the lateral view of the skull, and 13 landmarks and 47 semilandmarks on the mandible (Fig. 1; see Appendix S3 for landmark definitions). Landmarks and semilandmarks were digitized in TpsDig2 software (New York, USA; Rohlf, 2015). After digitization, matrices of coordinates were superimposed with a Procrustes superimposition (Adams *et al.*, 2013). The ventral view was rendered symmetrical to avoid noise caused by bilateral asymmetry. Semilandmarks were slid to minimize bending energy (Perez *et al.*, 2006). Minimizing the Procrustes distance caused some semilandmarks to slide beyond fixed landmarks (an unrealistic shape deformation). In this situation, minimizing bending energy may be a better choice (Gunz & Mittereocker, 2013). Size was obtained for each view as the centroid size – the square root of the sum of squared distances of each landmark from the centroid of the configuration (Bookstein, 1991). Average sizes and shapes were calculated for each genus by first calculating an arithmetic average of all specimens of a species, then of all species of a genus. After this generic compilation, an average of size was calculated to summarize the three views (skull plus mandible) and then used (log-transformed) as a unified measure of size per genus. Mean values by genus is justifiable because most morphological and ecological variation of sigmodontines is concentrated among genera, and taking a mean of different species allows for a more reliable estimation than using an exemplar species to represent the genus. After digitalization, all geometric morphometric procedures were implemented using the

geomorph package (Adams & Otárola-Castillo, 2013) in the R environment (R Core Team, 2016).

Diet and phylogeny

Diet data was obtained from literature summaries: Reid (1997), Nowak (1999), Marinho-Filho *et al.* (2002), Tirira (2007), Iriarte (2008), Bonvicino *et al.* (2008), Paglia *et al.* (2012), Leite *et al.* (2015), and Patton *et al.* (2015), supplemented by personal observations (B.D. Patterson). The diet variable was constructed by assigning a feeding category to each genus based on the principal food item in its diet: vegetation, herbs, leaves, and green plant material in general (Herbivore); seeds, nuts, grain, fruits (Granivore/Frugivore); insects and/or small vertebrates (Insectivores); and genera feeding on various categories without clear food preferences (Omnivores). Diet information can be found in Appendix S1.

We pruned a molecular tree derived from Parada *et al.* (2013) to use as a phylogenetic hypothesis (Fig. 2). Genera missing from that phylogeny were included following Machado *et al.* (2015) for *Neomicroxus* and *Wilfredomys*, Parada *et al.* (2015) for *Chilomys*, and Teta *et al.* (2016) for *Paynomys*. Relationships among members of the tribe Ichthyomyini still lacking genetic information (*Chibchanomys*, *Anotomys* and *Ichthyomys*) were fixed according to Voss (1988). Dates in millions of years were set according to Parada *et al.* (2013) to nodes present in that phylogeny, and extrapolated over non-dated nodes using the *bladj* algorithm implemented in Phylocom 4.2 (Webb *et al.*, 2008). Phylogenetic representation and heat-map (Fig. 2) was made in *phytools* package (Revell, 2012) of R environment (R Core Team, 2016).

Statistical analyses

We used a sequential phylogenetic ANCOVA (Grafen, 1989) to test the relationship between bite force (log N – dependent variable), size (log of centroid size), diet, and principal components (PCs) of shape variables (for shape on skull ventral and lateral views, and the mandible). Twenty-four models were evaluated, including: 1) bite force against (=) the intercept (a null model where size and diet have no influence on bite force); 2) bite force = size; 3) bite force = size plus diet; and 4) bite force = size interacting with diet; then followed by models including PCs of shape in a sequential manner, in models with and without diet, and with and without interactions. Size was included as a covariate in all models. The phylogenetic covariance matrix included as the error term was estimated according to the Ornstein-Uhlenbeck model (Martins & Hansen, 1997), where $V_{ij} = \gamma \exp(-\alpha t_{ij})$. The parameter γ is a constant similar to the variance (σ) of a Brownian process, and t_{ij} refers to phylogenetic distance between taxa *i* and *j*. The parameter α can be interpreted as the rate of adaptation towards an optimum phenotype, and its value determines the covariance structure among species. This approach was developed in a microevolutionary context by Martins and Hansen (1997) and provides substantial flexibility in the choice of evolutionary assumptions -- as α approaches zero, the covariance estimates approach those of a Brownian motion model, and the correlations among species caused by shared branches decrease exponentially for larger α. The parameter α was estimated using a maximum likelihood iteration procedure (Paradis *et al.*, 2004). The model selection was performed through comparisons of Akaike Information Criteria corrected for small sample sizes (AICc – Burham & Anderson, 2002).

For the visualization of shape changes associated with the Phylogenetic Generalized Least Squares (PGLS) models described above, a principal component analysis (PCA) was used to show the distribution of genera with distinct diets on the main

axes of morphological variation. We projected the phylogeny onto the shape space of the principal components, reconstructing internal shapes by square-change parsimony. This type of plot was first proposed by Klingenberg & Ekau (1996) and later named phylomorphospace by Sidlauskas (2008). Shape changes associated with bite force were visualized by first taking the regression coefficients of the PGLS (BF = Size + PC1 + PC2), and plotting shape changes associated with the combination of PC1 and PC2 scores determined by the regression coefficients that represented the strongest and weakest biters. Shape visualization was obtained using outline interpolation (Klingenberg, 2013).

Phylogenetic regressions were performed using the packages *ape* (Paradis *et al.*, 2004) and *nlme* (Pinheiro *et al.*, 2015), AICc were calculated using the package *AICcmodavg* (Mazerolle, 2016), all in the R environment (R Core Team, 2016).

Phylogenetic path analysis

The linear models described above are sufficient to identify associations between diet and bite force, size or shape. However, some classes of questions are difficult to answer with simple associations. For instance, does diet select for bite force through changes in size and shape? Alternatively, do changes in bite force (a necessary consequence of changes in size and shape) drive changes in diet? To postulate cause-effect relationships among these variables is therefore challenging. To address the causal links between variables, we use confirmatory phylogenetic path analysis using the *d*-separation method (von Hardenberg & Gonzalez-Voyer, 2013; Gonzalez-Voyer & von Hardenberg, 2014). The *d*-separation method on path analysis was proposed by Shipley (2000) to select among distinct hypotheses of causal relationships in data. The fit of a given model to the data is evaluated by testing the minimum set of conditional independencies (Appendix S4) that must be fulfilled by the observational data (Shipley

2000). This offers a basis for selecting or rejecting a postulated causal model (each model in Fig. 3). Goodness-of-fit for each model is assessed combining the *p* values of the conditional independencies in the Fisher's *C* statistic (Shipley, 2000); if the *p*-value reaches significance at a specified alpha, the postulated causal model is rejected (i.e., it does not provide a good fit). Models can also be ranked by using *C* statistics to generate the *C* statistic information criterion corrected for small sample sizes (CICc – Cardon *et al.*, 2011; Shipley, 2013; von Hardenberg & Gonzalez-Voyer, 2013), which is similar to the Akaike information criterion (AIC – Burham & Anderson, 2002; see Shipley, 2013 for mathematical proof of the CIC). Accordingly, we calculated ΔCICc and CICc weights to rank the models (von Hardenberg & Gonzalez-Voyer, 2013), where causal models with the lowest ΔCICc values are considered to have highest support. Models with ΔCICc less than 2 units are considered to be equally supported by the data (Gonzalez-Voyer & von Hardenberg, 2014). Based on the hypotheses of causal models depicted in the DAGs in Fig. 3, we calculated the C statistic and CICc for each model under the framework proposed by von Hardenberg & Gonzalez-Voyer (2013), using PGLS analyses with the error structure following an Ornstein-Uhlenbeck model (Martins & Hansen, 1997), as described in the *Statistical Analyses* section. Variables used were the logarithm of bite force (log N) as bite force (BF), logarithm of centroid size as size (SZ), the diet variable (DI), and a set PC shape vectors (SH) selected by Horn's parallel analysis (Horn, 1965; Peres-Neto *et al.*, 2005). A total of seven PCs were used for both skull ventral (83.92% of variation explained) and mandible (91%), and six PCs for skull lateral (82.8%). The full set of conditional independences and associated linear models for each hypothesized causal model (Fig. 3) can be checked in Appendix S4. Models are described as: model A) bite force is driven by diet through changes in both size and shape; B) bite force is driven by diet only through shape changes (and by size through allometry in shape); C) bite force

is driven by diet only through size changes; D) diet is driven by size and shape through changes in bite force; E) diet is driven by shape though changes in bite force (and by the effects of size on shape); and F) diet is driven by size through changes in bite force.

Phylogenetic path analysis was conducted in the R environment (R Core Team, 2016) using the packages *ape* (Paradis et al. 2004), and *nlme* (Pinheiro *et al.*, 2015), and Horn's parallel analysis was performed with the package *paran* (Dinno, 2012). Readers are referred to Gonzalez-Voyer & von Hardenberg (2014) for a review of phylogenetic path analysis and R codes to implement the method.

Results

As expected, bite force variation is predicted by size (R^2= 0.82; F= 278.1; *P*= 0.01). The regression scatterplot (Fig. 4) shows that both herbivores and granivores are generally above the prediction line, with stronger bites for their sizes. Conversely, most insectivores are below the line, with weaker bites for their size (Fig. 4). Results of the sequential phylogenetic ANCOVA are presented in Tables 1, 2, and 3. The models with strongest statistical support mostly included the independent influences of size, at least one shape PC, and/or diet. For ventral shape PCs (Table 1), the least complex models within the group with higher statistical support (ΔAICc < 6) included size + diet or size + PC1 as predictors, suggesting that shape and diet are interchangeable predictors. The first ventral shape PC ordinates species with stronger relative bite forces having positive scores and weaker species with negative scores (Fig. 6). For lateral skull PCs (Table 2), size and shape are the most relevant predictors in the models. The best fitting model included size+PC1+PC2, and the least complex model within the supported set excluded PC2. The evidence ratio (ratio between AICc differences) between these two models was 8.29, so there is some evidence that lateral PC2 is a relevant variable in the model. The

lateral shape PC ordination shows a stronger relative bite force gradient along the first PC (Fig. 7), and it can be argued that a weaker gradient can be observed along the second PC. For mandible shape PCs, the least complex model within the supported set predicts bite force based on size+PC1 (Table 3). The ordination of species on the first two mandible shape PCs shows a clear gradient of increasing relative bite force from positive to negative scores along PC1 (Fig 8). Models including the interaction between size, shape and diet, as well as models including multiple shape PCs were always less supported than models without interaction. These results do not necessarily mean that diet is not a relevant factor. In fact, most variation in relative bite force is between granivores and insectivores, the strongest and the weakest biters, respectively (Fig. 5). However, because (as shown below) dietary categories with extreme bite force differences have scores of different signs on PC1, the information contained in the diet factor is already conveyed by PC scores in all views studied. All models within supported groups presented high coefficients of determination ($R^2 > 0.85$). This statistic was not used as a criterion for selection, but indicates that the best fitting models were actually explaining variation in bite force.

Skull shape changes associated with relative bite force showed that herbivores and granivores (typically stronger biters) have a shorter and wider rostrum, wider incisors, larger maxillae, and wider zygomatic arches in comparison with weaker biters (insectivores), as can be seen in ventral view (Fig. 6). Skull lateral view showed the same tendency of stronger biters having a shorter, more arched rostrum, a heightened skull at the level of the zygomatic plate, and a more anterodorsal location of the antorbital bridge of the maxillary, compared with weaker biters (Fig. 7). Mandible shape changes revealed that higher values of relative bite force are associated with a shortening of the mandible, as opposed to the elongation that occurs in forms with low values (Fig. 8). Mandibles of

stronger biters have a shorter coronoid process, a wider condyloid process, a wider and shorter angular process, and the ramus at the diastema is shorter and more curved than weaker biters (Fig. 8). In summary, stronger biters have a more compact and robust skull and mandible, whereas weaker biters are more gracile and elongate. Because the direction of shape differences associated with high and low relative bite forces is generally represented by the axis between diets, notably the axis between granivores-insectivores for the ventral and lateral views (the mandible view seem to be associated with a granivore-omnivore axis), diet is a somewhat redundant term with shape PCs in the PGLS models, which explains why models that include diet have similar levels of statistical support as those without diet but with shape PCs.

Results of the phylogenetic path analysis are presented in Table 4. Only results using shape of ventral view are presented, as the other shape variables returned similar results; results for other shape views can be found in Appendix S4. The causal model depicted in A (Fig. 3) received the highest support (i.e. is deemed most probable to reflect the true causal relationships for these data than other models). In this model, bite force is driven by diet through (i.e. conditioned by) changes in size and shape. Models D, E and F, with lower support, describe models where changes in diet are influenced by size and shape through changes in bite force.

Discussion

Contrary to our expectations, we found that both herbivores and granivores/frugivores have similar bite forces, and similar associated skull and mandible shape changes. Still, granivores and frugivores have slightly stronger (although statistically non-significant) relative bites than herbivores. Most variation in both bite force and related skull and mandible shape lies between the insectivores and all others.

Insectivores had longer snouts and a slender and elongated skull and mandible, which make them weaker biters due to lever-arm mechanical constraints. The same weaker bite force due to an insectivorous diet is observed among mammals of the order Carnivora (Christianensen & Wroe, 2007). Unsurprisingly, omnivores exhibit the greatest variation in relative bite force values.

Wider and taller skulls of sigmodontines were associated with stronger bites. Head width and height are indeed among the best predictors of bite force for lemurs (Chazeau *et al.*, 2013) and bats (Aguirre *et al.*, 2002). Species of phyllostomid bats with shorter and taller skulls and mandibles are stronger biters than species with elongated skulls and mandibles (Nogueira *et al.*, 2009), similar to the pattern observed here. These common morphological attributes related to bite force reflect fundamental biomechanical properties, as shorter jaws produce higher force outputs (Anderson *et al.*, 2008), and shorter but wider and taller skulls can house a higher volume of muscles. Muscle size can be even more important than lever-arm mechanical advantages in explaining bite force (Becerra *et al.*, 2014).

Values of bite force (N) for sigmodontines were similar to those found by Freeman & Lemen (2008) for related cricetid rodents of similar size, although we predicted bite forces through the proxy of incisor strength whereas they used a piezo-resistive sensor on live animals. Measures of the only genus (*Sigmodon*) common to both studies returned a value of 20.61 N in our study and 19.87 N in Freeman & Lemen (2008). Herbivorous sigmodontines presented bite force values higher than the herbivorous hystricomorph *Octodon degus* (21.87 N) and *Chinchilla laniger* (23.49 N) (Becerra *et al.*, 2014), when taking size into account – two of the largest herbivorous sigmodontines (*Holochilus* and *Lundomys*), which are still smaller than the degu and the chinchilla, have bite forces of 24.63 N and 24.80 N, respectively (Appendix S1). These values are similar to those of

seed-eating rodents (e.g. squirrel – Cox *et al.*, 2012). Herbivorous sigmodontines seem to follow a different evolutionary path from hystricomorphs with the same diet, resulting in distinct morphologies and thus striking differences in bite force. Druzinsky (2010) may have anticipated this when showing that the muscle anterior lateral masseter (present in sigmodontines but absent in hystricomorphs) is important for bite force production.

The general herbivorous bauplan found in hystricomophs then contrasts with the morphology of myomorphs (sigmodontines) that have the same diet. However, some hystricomorphs, such as *Laonastes*, exhibit high bite force on the incisors because of its specialized folivorous diet (Cox *et al.*, 2013). The mandible shape of *Laonastes* also presents features similar to herbivorous sigmodontines, such as the robust angular process. Cox *et al.* (2013) suggested that a uniform bite force across all teeth may be beneficial for folivorous species. Moreover, cricetid grazers bite about 10% harder than omnivores according to Freeman & Lemen (2008). Such observations help to explain the stronger bites of herbivorous sigmodontines in comparison to insectivores and omnivores.

Another expectation, that the angular process of the mandible would be narrower and thinner in herbivorous species when compared with granivores/frugivores, does not hold true. It is, however, worth noting that we analyzed shape in two dimensions. Analyses in three dimensions or taking other mandible views might show different results (Hautier *et al.*, 2011). In our two-dimensional study, both the shape of the skull and mandible were similar between herbivores and granivores/frugivores species. From a rodent phenotype that already is a compromise between gnawing and chewing, becoming a herbivore or a granivore/frugivore seems to require few or no changes in morphology. This can explain the high efficacy of the myomorph condition in feeding with incisors and molars (Cox *et al.*, 2012). This morphology also agrees with the strong relative bite force of herbivorous sigmodontines. The mechanical features seem to be consistent

among all rodents, but herbivorous sigmodontines are stronger biters than same-sized herbivorous hystricomorphs.

The morphological trend observed here points to a particular phenotype of insectivore species. Mammal specialization towards eating insects is sometimes followed by an elongated rostrum (and nose), as observed in the stink badger (*Mydaus*) and sloth bear (*Ursus ursinus*) (Carnivora), which also have weak bite forces for their size (Christiansen & Wroe, 2007). This pattern is also observed in several shrew species (Nowak, 1999) and reaches an extreme in the anteater (*Myrmecophaga*) (Naples, 1999). Rodent specializations towards eating insects seem to follow the same path. Moreover, really specialized insect eaters (and carnivores) arise in rodents only from the myomorph condition, so that no parallel exists among other rodents – the sciuromorph and hystricomorph conditions have no meat eaters. Diet explains a smaller proportion of bite force (because of the associated shape changes) in sigmodontines than among phyllostomid bats (Nogueira *et al.*, 2009). However, the radiation of sigmodontines is younger (8 to 12 Ma – Parada *et al.*, 2013; Vilela *et al.*, 2013; Leite *et al.*, 2014; cf. Rojas *et al.*, 2016), so it is possible that dietary specialization, especially towards insectivory, is still incipient in this group. The compromise between chewing and gnawing could be responsible for an ecological release of morphology, because a generalist morphotype is more prone to exploit new and unprecedented diets than a morphology specialized for gnawing or chewing.

The method recently proposed by von Hardenberg & Gonzalez-Voyer (2013) to test among causal hypotheses in a phylogenetic context produced interesting results here. It was previously used to conclude that mammal range size is more strongly driven by biological properties than by human impacts (Ollala-Tárraga *et al.*, 2015), and clutch size influences the intensity of aggression in birds (von Hardenberg & Gonzalez-Voyer,

2013). Using PPA, we have an indication of the most likely causal models (Gonzalez-Voyer & von Hardenberg, 2014), although they do not definitively differentiate among hypotheses of causality.

The path model having the highest support in our PPA indicates that changes in diet are more likely to be influencing changes in bite force than the reverse. Although provisional, this suggests that the primary features in an organism's environment are proportions of food items, which require changes in morphology to produce adequate bite force. Therefore, as food items change in abundance or availability, organisms are selected by having an adequate bite force to perform feeding. Maladapted organisms, those whose bite force is not adequate to feeding, are then penalized. These findings help to shed light on the direction of the morphological-ecological influences, as well as can offer some clues on the course of natural selection. Evidence to selection on bite force have been suggested in other groups (Kiltie, 1982; Christiansen & Wroe, 2007; Cornette *et al.*, 2015), and here we provide evidence that this may be the case. Future studies can explore further the directions of causality, and analyse other possible selective agents beyond diet.

Acknowledgements

We thank Chris Klingenberg, Philip Cox, and an anonymous reviewer for the helpful suggestions and comments that have improved this manuscript. We are grateful to all curators and collection managers that provide access to specimens and assistance in finding specimens in their institutions: João A. de Oliveira (MNUFRJ), Mario de Vivo e Juliana Gualda (MZUSP), Diego H. Verzi and A. Itatí Olivares (MLP), Eileen Westwig (AMNH) and Darrin Lunde (NMNH). RM is supported by CAPES through regular and

sandwich fellowship (4087/14-3). TROF is supported by CAPES, CNPq, and FAPERGS. LRM is supported by CNPq and FAPERJ.

References

Adams, D.C. & Otárola-Castillo, E. 2013. geomorph: and R package for the collection and analysis of geometric morphometric shape data. *Methods Ecol. Evol.* **4**: 393-399.

Adams, D.C., Rohlf, F.J. & Slice, D.E. 2013. A field comes of age: geometric morphometrics in the 21st century. *Hystrix* **24**: 7-14.

Aguirre, L.F., Herrel, A., van Damme, R. & Matthysen, E. 2002. Ecomorphological analysis of trophic niche partitioning in a tropical savannah bat community. *Proc. R. Soc. B* **269**: 1271-1278.

Aguirre, L.F., Herrel, A., van Damme, R. & Matthysen, E. 2003. The implications of food hardness for diet in bats. *Funct. Ecol.* **17**: 201-212.

Anderson, R.A., Macbrayer, L.D. & Herrel, A. 2008. Bite force in vertebrates: opportunities and caveats for use of a nonpareil whole-animal performance measure. *Biol. J. Linn. Soc.* **93**: 709-720.

Becerra, F., Echeverría, A.I., Casinos, A. & Vassallo, A.I. 2014. Another one bites the dust: bite force and ecology in three caviomorph rodents (Rodentia, Hystricognathi). *J. Exp. Zool.* **321**: 220-232.

Blanco, R.E., Rinderknecht, A. & Lecuona, G. 2012. The bite force of the largest fossil rodent (Hystricognathi, Caviomorpha, Dinomyidae). *Lethaia* **45**: 157-163.

Blanga-Kanfi, S., Miranda, H., Penn, O., Pupko, T., DeBry, R.W. & Huchon, D. 2009. Rodent phylogeny revised: analysis of six nuclear genes from all major rodent clades. *BMC Evol. Biol.* **9**: 71.

Bonvicino, C.R., de Oliveira, J.A. & D'Andrea, P.S. 2008. *Guia dos roedores do Brasil*. Centro Pan-Americano de Febre Aftosa, Rio de Janeiro.

Bookstein, F.L. 1991. *Morphometric tools for landmark data*. Cambridge University Press, UK.

Brandt, J.F. 1855. Beiträge zur nähern Kenntniss der Säugethiere Russlands. *Mém. Acad. Imp. Sci.* **9**: 1–375.

Burham, K.P. & Anderson, D.R. 2002. *Model selection and multimodel inference: a pratical information-theoretic approach*. Springer, New York.

Cardon, M., Loot, G., Grenouillet, G. & Blanchet, S. 2011. Host characteristics and environmental factors differentially drive the burden and pathogenicity of an ectoparasite: a multilevel causal analysis. *J. Anim. Ecol.* **80**: 657-667.

Chazeau, C., Marchal, J., Hackert, R., Perret, M. & Herrel, A. 2013. Proximate determinants of bite force capacity in the mouse lemur. *J. Zool.* **290**: 42-48.

Christiansen, P. & Wroe, S. 2007. Bite forces and evolutionary adaptations to feeding ecology in carnivores. *Ecology* **88**: 347-358.

Cornette, R., Tresset, A., Houssin, C., Pascal, M. & Herrel, A. 2015. Does bite force provide a competitive advantage in shrews? The case of the greater white-toothed shrew. *Biol. J. Linn. Soc.* **114**: 795-807.

Cox, P.G., Rayfield, E.J., Fagan, M.J., Herrel, A., Pataky, T.C. & Jeffery, N. 2012. Functional evolution of the feeding system in rodents. *Plos One* **7**: e36299.

Cox, P.G., Kirkham, J. & Herrel, A. 2013. Masticatory biomechanics of the Laotian rock rat, *Laonastes aenigmamus*, and the function of the zygomaticomandibularis muscle. *PeerJ* **1**: e160.

Cox, P.G., Rinderknecht, A. & Blanco, R.E. 2015. Predicting bite force and cranial biomechanics in the largest fossil rodent using finite element analysis. *J. Anat.* **226**: 215-223.

Dinno, A. 2012. paran: Horn's test of principal components/factors. R package version 1.5.1. http://CRAN.R-project.org/package=paran.

Druzinsky, R.E. 2010. Functional anatomy of incisal biting in *Aplodontia rufa* and sciuromorph rodents – part 2: sciuromorphy is efficacious for production of force at the incisors. *Cells Tissues Organs* **192**: 50-63.

Druzinsky, R.E. 2015. The oral apparatus of rodents: variations on the theme of a gnawing machine. *Evolution of the Rodents: Advances in Phylogeny, Functional Morphology and Development* (P.G. Cox & L. Hautier, eds.), pp. 232-349. Cambridge University Press, Cambridge.

Fabre, P., Hautier, L., Dimitrov, D. & Douzery, E.J.P. 2012. A glimpse on the pattern of rodent diversification: a phylogenetic approach. *BMC Evol. Biol.* **12**: 88.

Freeman, P.W. & Lemen, C.A. 2008. A simple morphological predictor of bite force in rodents. *J. Zool.* **275**: 418-422.

Gonzalez-Voyer, A. & von Hardenberg, A. 2014. An introduction to phylogenetic path analysis. In: *Modern phylogenetic comparative methods and their application in evolutionary biology* (L.Z. Garamszegi, ed.), pp. 201-229. Springer Heidelberg, New York.

Grafen, A. 1989. The phylogenetic regression. *Philos. Trans. R. Soc. Lond. B* **326**: 119-157.

Gunz, P. & Mitteroecker, P. 2013. Semilandmarks: a method for quantifying curves and surfaces. *Hystrix* **24**: 103-109.

Hautier, L., Lebrun, R., Saksiri, S., Michaux, J., Vianey-Liaud, M. & Marivaux, L. 2011. Hystricognathy vs sciurognathy in the Rodent Jaw: A new morphometric assessment of hystricognathy applied to the living fossil *Laonastes* (Diatomyidae). *Plos One* **6**: e18698.

Hautier, L., Lebrun, R. & Cox, P.G. 2012. Patterns of covariation in the masticatory apparatus of hystricognathous rodents: implications for evolution and diversification. *J. Morphol.* **273**: 1319-1337.

Herrel, A., Van Damme, R., Vanhooydonck, B. & De Vree, F. 2001. The implications of bite performance for diet in two species of lacertid lizards. *Can. J. Zool.* **79**: 662-670.

Herrel, A., O'Reilly, J.C., Richmond, A.M. 2002. Evolution of bite force performance in turtles. *J. Evol. Biol.* **15**: 1083-1094.

Herrel, A., Podos, J., Huber, S.K. & Hendry, A.P. 2005. Bite performance and morphology in a population of Darwin's finches: implications for the evolution of beak shape. *Funct. Ecol.* **19**: 43-48.

Herrel, A., Macbrayer, L.D. & Larson, P.M. 2007. Functional basis for sexual differences in bite force in the lizard *Anolis carolinensis*. *Biol. J. Linn. Soc.* **91**: 111-119.

Horn, J.L. 1965. A rationale and test for the number of factors in factor analysis. *Psychometrika* **30**: 179-185.

Iriarte, A. 2008. *Mamíferos de Chile*. Lynx Edicions, Barcelona.

IUCN 2016. *IUCN Red List of Threatened Species*. Version 2016.1. Accessed in February 18, 2016. http://www.iucnredlist.org/.

James, F.C. 1982. The ecological morphology of birds. *Ann. Zool. Fenn.* **19**: 265-275.

Kiltie, R.A. 1982. Bite force as a basis for niche differentiation between rain forest peccaries (*Tayassu tajacu* and *Tayassu pecari*). *Biotropica* **14**:188-195

Klingenberg, C.P. 2013. Visualizations in geometric morphometrics: how to read and make graphs showing shape changes. *Hystrix* **24**: 15-24.

Klingenberg, C.P. & Ekau, W. 1996. A combined morphometric and phylogenetic analysis of an ecomorphological trend: pelagization in Antarctic fishes (Perciformes: Nototheniidae). *Biol. J. Linn. Soc.* **59**: 143-177.

Korth, W.W. 1994. *The tertiary record of rodents in North America*. Springer Science, New York.

Leite, R.N., Kolokotronis, S., Almeida, F.C., Werneck, F., Rogers, D.S. & Weksler, M. 2014. In the wake of invasion: tracing the historical biogeography of the south american cricetid radiation (Rodentia, Sigmodontinae). *Plos One* **9**: e100687.

Leite, Y.L.R., Kok, P.J.R. & Weksler, M. 2015. Evolutionary affinities of the "Lost World" mouse suggest a late Pliocene connection between the Guiana and Brazilian shields. *J. Biogeogr.* **42**: 706-715.

Machado, L.F., Passaia, M.H., Rodrigues, F.P., Peters, F.B., Sponchiado, J., Valiati, V.H. *et al.* 2015. Molecular phylogenetic position of endangered *Wilfredomys* within Sigmodontinae (Cricetidae) based on mitochondrial and nuclear DNA sequences and comments on Wiedomyini. *Zootaxa* **3986**: 421-434.

Marinho-Filho, J., Rodrigues, F.H.G., & Juarez, K.M. 2002. The Cerrado mammals: diversity, ecology, and natural history. *The Cerrados of Brazil* (P.S. Oliveira & R.J. Marquis, eds.), pp. 266-286. Columbia University Press, New York.

Martins, E.P. & Hansen, T.F. 1997. Phylogenies and the comparative method: a general approach to incorporating phylogenetic information into the analysis of interspecific data. *Am. Nat.* **149**: 646-667.

Mazerolle, M.J. 2016. AICcmodavg: model selection and multimodel inference based on (Q)AIC(c). R package version 2.0-4. http://CRAN.R-project.org/package=AICcmodavg.

Meredith, R.W., Janečka, J.E., Gatesy, J., Ryder, O.A., Fisher, C.A., Teeling, E.C. *et al.* 2011. Impacts of the Cretaceous terrestrial revolution and KPg extinction on mammal diversification. *Science* **334**: 521-524.

Naples, V.L. 1999. Morphology, evolution and function of feeding in the giant anteater (*Myrmecophaga tridactyla*). *J. Zool.* **249**: 19-41.

Nogueira, M.R., Peracchi, A.L. & Monteiro, L.R. 2009. Morphological correlates of bite force and diet in the skull and mandible of phyllostomid bats. *Funct. Ecol.* **23**: 715-723.

Nowak, R.M. 1999. *Walker's mammals of the world*, 6th edn. John Hopkins University Press, Baltimore.

Olalla-Tárraga, M.A., Torres-Romero, E.J., Amado, T.F. & Martinez, P.A. 2015. Phylogenetic path analysis reveals the importance of niche-related biological traits on geographic range size in mammals. *Global Change Biol.* **21**: 3194-3196.

Paglia, A.P., Fonseca, G.A.B., Rylands, A.B., Herrmann, G., Aguiar, L.M.S., Chiarello, A.G. *et al.* 2012. *Annotated checklist of Brazilian Mammals 2º edition*. Conservation International, Arlington.

Parada, A., Pardiñas, U.F.J., Salazar-Bravo, J, D'Elía, G. & Palma, R.E. 2013. Dating an impressive Neotropical radiation: molecular time estimates for the Sigmodontinae (Rodentia) provide insights into its historical biogeography. *Mol. Phylogenet. Evol.* **66**: 960-968.

Parada, A., D'Elía, G. & Palma, R.E. 2015. The influence of ecological and geographical context in the radiation of Neotropical sigmodontine rodents. *BMC Evol. Biol.* **15**: 172.

Paradis, E., Claude, J. & Strimmer, K. 2004. APE: analysis of phylogenetics and evolution in R language. *Bioinformatics* **20**: 289-290.

Patton, J.L., Pardiñas, U.F.J. & D'Elia G. eds. 2015. *Mammals of South America, Vol. 2: rodents*. University of Chicago Press, Chicago.

Peres-Neto, P.R., Jackson, D.A. & Somers, K.M. 2005. How many principal components? Stopping rules for determining the number of non-trivial axes revisited. *Comput. Stat. Data Anal.* **49**: 974-997.

Perez, S.I., Bernal, V. & Gonzalez, P.N. 2006. Differences between sliding semi-landmark methods in geometric morphometrics, with an application to human craniofacial and dental variation. *J. Anat.* **208**: 769-784.

Pinheiro, J., Bates, D., DebRoy, S., Sarkar, D. & R Core Team 2015. nlme: linear and nonlinear mixed effects models. R package version 3.1-121.

R Core Team 2016. *R: a language and environment for statistical computing*. R Foundation for Statistical Computing, Vienna, Austria.

Reid, F.A. 1997. *A field guide to the mammals of Central America & southeast Mexico*. Oxford University Press, New York.

Revell, L.J. 2012. phytools: an R package for phylogenetic comparative biology (and other things). *Methods Ecol. Evol.* **3**: 217-223.

Rohlf, F.J. 2015. The tps series of software. *Hystrix* **26**: 9-12.

Rojas, D., Warsi, O.M. & Dávalos, L. 2016. Bats (Chiroptera: Noctilionoidea) challenge a recent origin of extant neotropical diversity. *Syst. Biol.* **65**: 432-448.

Samuels, J.X. 2009. Cranial morphology and dietary habits of rodents. *Zool. J. Linn. Soc.* **156**: 864-888.

Santana, S.E., Dumont, E.R. & Davis, J.L. 2010. Mechanics of bite force production and its relationship to diet in bats. *Funct. Ecol.* **24**: 776-784.

Schenk, J.J., Rowe, K.C. & Steppan, S.J. 2013. Ecological opportunity and incumbency in the diversification of repeated continental colonizations by muroid rodents. *Syst. Biol.* **62**: 837-864.

Shipley, B. 2000. A new inferential test for path models based on directed acyclic graphs. *Struct. Equ. Modeling* **7**: 206-218.

Shipley, B. 2013. The AIC model selection method applied to path analytic models compared using a d-separation test. *Ecology* **94**: 560-564.

Sidlauskas, B. (2008) Continuous and arrested morphological diversification in sister clades of characiform fishes: a phylomorphospace approach. *Evolution* **62**: 3135-3156.

Simpson, G.G. 1945. The principles of classification and a classification of mammals. *Bull. Am. Mus. Nat. Hist.* **85**: 1–350.

Teta, P., Cañón, C., Patterson, B.D. & Pardiñas, U.F.J. In press. Phylogeny of the tribe Abrotrichini (Cricetidae, Sigmodontinae): integrating morphological and molecular evidence into a new classification. *Cladistics.* DOI: 10.1111/cla.12164

Tirira, D. 2007. *Mamíferos del Ecuador: Guia de campo*. Ediciones Murcielago Blanco, Quito, Ecuador.

Van Daele, P.A.A.G., Herrel, A. & Adriaens, D. 2009. Biting performance in teeth-digging African mole-rats (Fukomys, Bathyergidae, Rodentia). *Physiol. Biochem. Zool.* **82**: 40-50.

Vassallo, A.I., Becerra, F., Escheverría, A.I. & Casinos, A. 2015. Ontogenetic integration between force production and force reception: a case study in *Ctenomys* (Rodentia:Caviomorpha). *Acta Zool.* **97**: 232-340.

Vilela, J.F., Mello, B., Voloch, C.M. & Schrago, C.G. 2013. Sigmodontine rodents diversified in South America prior to the complete rise of the Panamanian Isthmus. *Journal of J. Zool. Sys. Evol. Res.* **52**: 249-256.

Von Hardenberg, A. & Gonzalez-Voyer, A. 2013. Disentangling evolutionary cause-effect relationships with phylogenetic confirmatory path analysis. *Evolution* **67**: 378-387.

Voss, R.S. 1988. Systematics and ecology of ichthyomyine rodents (Muroidea): patterns of morphological evolution in a small adaptive radiation. *Bull. Am. Mus. Nat. Hist.* **188**: 259-493.

Wainwright, P.C. 1994. Functional morphology as a tool in ecological research. *Ecological Morphology: integrative organismal biology* (P.C. Wainwright & S.M. Reilly, eds.), pp. 42-59. The University of Chicago Press, Chicago.

Webb, C.O., Ackerly, D.D. & Kembel, S.W. 2008. Phylocom: software for the analysis of phylogenetic community structure and trait evolution. *Bioinformatics* **24**: 2098-2100.

Willians, S.H., Peiffer, E. & Ford, S. 2009. Gape and bite force in the rodents *Onychomys leucogaster* and *Peromyscus maniculatus*: does jaw-muscle anatomy predict performance? *J. Morphol.* **270**: 1338-1347.

Wilson, D.E. & Reeder, D.M. eds. 2005. *Mammal species of the world: a taxonomic and geographic reference*, 3rd edn. Johns Hopkins University Press, Baltimore, MD.

Wittorski, A., Losos, J.B. & Herrel, A. 2016. Proximate determinants of bite force in *Anolis* lizards. *J. Anat.* **228**: 85-95.

Wood, A.E. 1965. Grades and clades among rodents. *Evolution* **19**: 115-130.

Wroe, S., McHenry, C. & Thomason, J. 2005. Bite club: comparative bite force in big biting mammals and the prediction of predatory behaviour in fossil taxa. *Proc. R. Soc. B* **272**: 619-625.

Supporting Information

Additional Supporting Information may be found online in the supporting information tab for this article:

Appendix S1. Number of specimens, species, and bite force for each genus.

Appendix S2. A list of visited mammal collections and specimens sampled for geometric morphometrics.

Appendix S3. Landmark definitions.

Appendix S4. Data on phylogenetic path analyses.

Tables

Table 1. Sequential phylogenetic ANCOVA of log bite force (BF, N) on log centroid size (SZ, cm), diet (DI), and principal components of shape (PC) for the skull in ventral view. Model notation omitted parameters for shortness and depicted interactions as products (*). Only the predicted, E(BF) part is presented. The phylogenetic covariance matrix included as the error term was estimated according to the Ornstein-Uhlenbeck model (Martins & Hansen 1997). Models were ranked according to AICc values.

Model	AICc	ΔAICc	AICc*wi*	R^2	LL	K
E(BF)=SZ+PC1+DI	-143.49	0.00	0.17	0.872	81.08	8
E(BF)=SZ+PC1+PC2+DI	-142.70	0.78	0.12	0.876	82.05	9
E(BF)=SZ+DI	-142.60	0.88	0.11	0.865	79.32	7
E(BF)=SZ+PC1+PC2+PC3+PC4+DI	-142.41	1.08	0.10	0.886	84.79	11
E(BF)=SZ+PC1+PC2+PC3+PC4	-142.27	1.22	0.09	0.870	80.47	8
E(BF)=SZ+PC1	-142.14	1.35	0.09	0.853	76.59	5
E(BF)=SZ+PC1+PC2	-141.86	1.63	0.08	0.858	77.68	6
E(BF)=SZ+DI+SZ*DI+PC1	-141.16	2.32	0.05	0.884	84.17	11
E(BF)=SZ+DI+SZ*DI	-141.04	2.45	0.05	0.878	82.63	10
E(BF)=SZ+DI+SZ*DI+PC1+PC2	-140.52	2.97	0.04	0.888	85.38	12
E(BF)=SZ+PC1+PC2+PC3+DI	-140.42	3.06	0.04	0.877	82.33	10
E(BF)=SZ+PC1+PC2+PC3	-139.46	4.03	0.02	0.858	77.75	7
E(BF)=SZ+DI+SZ*DI+PC1+PC2+PC3	-137.95	5.54	0.01	0.890	85.69	13
E(BF)=SZ+PC1+DI+PC1*DI	-137.91	5.57	0.01	0.878	82.54	11
E(BF)=SZ+DI+SZ*DI+PC1+PC2+PC3+PC4	-137.19	6.30	0.01	0.894	86.97	14
E(BF)=SZ+PC1+DI+SZ*DI+PC1*DI	-136.38	7.11	0.00	0.893	86.56	14
E(BF)=SZ	-133.78	9.71	0.00	0.825	71.23	4
E(BF)=SZ+PC1+PC2+DI+PC1*DI+PC2*DI	-133.23	10.26	0.00	0.893	86.72	15
E(BF)=SZ+PC1+PC2+DI+SZ*DI+PC1*DI+PC2*DI	-129.79	13.69	0.00	0.906	90.67	18
E(BF)=SZ+PC1+PC2+PC3+DI+PC1*DI+PC2*DI+PC3*DI	-124.73	18.75	0.00	0.904	90.2	19
E(BF)=SZ+PC1+PC2+PC3+DI+SZ*DI+PC1*DI+PC2*DI+PC3*DI	-116.01	27.47	0.00	0.911	92.66	22
E(BF)=SZ+PC1+PC2+PC3+PC4+DI+PC1*DI+PC2*DI+PC3*DI+PC4*DI	-111.49	32.00	0.00	0.912	92.9	23
E(BF)=SZ+PC1+PC2+PC3+PC4+DI+SZ*DI+PC1*DI+PC2*DI+PC3*DI+PC4*DI	-100.75	42.74	0.00	0.920	95.88	26
E(BF)=1	-30.05	113.44	0.00	0.002	18.23	3

Table 2. Sequential phylogenetic ANCOVA of log bite force (BF, N) on log centroid size (SZ, cm), diet (DI), and principal components of shape (PC) for the skull in lateral view. Model notation omitted parameters for shortness and depicted interactions as products (*). Only the predicted, E(BF) part is presented. The phylogenetic covariance matrix included as the error term was estimated according to the Ornstein-Uhlenbeck model (Martins & Hansen 1997). Models were ranked according to AICc values.

Model	AICc	ΔAICc	AIC *cwi*	R^2	LL	K
E(BF)=SZ+PC1+PC2	-159.54	0.00	0.58	0.893	86.52	6
E(BF)=SZ+PC1+PC2+PC3	-157.07	2.47	0.17	0.894	86.55	7
E(BF)=SZ+PC1	-155.16	4.38	0.07	0.881	83.11	5
E(BF)=SZ+PC1+PC2+PC3+PC4	-155.14	4.40	0.06	0.895	86.9	8
E(BF)=SZ+PC1+PC2+DI	-155.10	4.44	0.06	0.899	88.25	9
E(BF)=SZ+PC1+PC2+PC3+DI	-152.97	6.57	0.02	0.900	88.6	10
E(BF)=SZ+PC1+DI	-152.70	6.84	0.02	0.890	85.68	8
E(BF)=SZ+PC1+PC2+PC3+PC4+DI	-150.64	8.90	0.01	0.901	88.91	11
E(BF)=SZ+DI+SZ*DI+PC1+PC2	-148.89	10.66	0.00	0.903	89.56	12
E(BF)=SZ+DI+SZ*DI+PC1	-148.56	10.98	0.00	0.897	87.87	11
E(BF)=SZ+DI+SZ*DI+PC1+PC2+PC3	-146.44	13.11	0.00	0.904	89.93	13
E(BF)=SZ+PC1+DI+PC1*DI	-144.53	15.02	0.00	0.890	85.85	11
E(BF)=SZ+DI+SZ*DI+PC1+PC2+PC3+PC4	-143.72	15.83	0.00	0.905	90.23	14
E(BF)=SZ+DI	-142.60	16.94	0.00	0.865	79.32	7
E(BF)=SZ+DI+SZ*DI	-141.04	18.51	0.00	0.878	82.63	10
E(BF)=SZ+PC1+DI+SZ*DI+PC1*DI	-140.35	19.20	0.00	0.899	88.55	14
E(BF)=SZ+PC1+PC2+DI+PC1*DI+PC2*DI	-137.85	21.69	0.00	0.901	89.03	15
E(BF)=SZ	-133.78	25.77	0.00	0.825	71.23	4
E(BF)=SZ+PC1+PC2+DI+SZ*DI+PC1*DI+PC2*DI	-129.85	29.69	0.00	0.906	90.7	18
E(BF)=SZ+PC1+PC2+PC3+DI+PC1*DI+PC2*DI+PC3*DI	-124.37	35.18	0.00	0.904	90.02	19
E(BF)=SZ+PC1+PC2+PC3+DI+SZ*DI+PC1*DI+PC2*DI+PC3*DI	-116.76	42.79	0.00	0.913	93.03	22
E(BF)=SZ+PC1+PC2+PC3+PC4+DI+PC1*DI+PC2*DI+PC3*DI+PC4*DI	-115.04	44.50	0.00	0.917	94.67	23
E(BF)=SZ+PC1+PC2+PC3+PC4+DI+SZ*DI+PC1*DI+PC2*DI+PC3*DI+PC4*DI	-101.10	58.45	0.00	0.921	96.05	26
E(BF)=1	-30.05	129.49	0.00	0.002	18.23	3

Table 3. Sequential phylogenetic ANCOVA of log bite force (BF, N) on log centroid size (SZ, cm), diet (DI), and principal components of shape (PC) for the mandible. Model notation omitted parameters for shortness and depicted interactions as products (*). Only the predicted, E(BF) part is presented. The phylogenetic covariance matrix included as the error term was estimated according to the Ornstein-Uhlenbeck model (Martins & Hansen 1997). Models were ranked according to AICc values.

Model	**AICc**	**ΔAICc**	**AICc *wi***	**R^2**	**LL**	**K**
E(BF)=SZ+PC1+DI	-151.23	0	0.37	0.887	84.95	8
E(BF)=SZ+PC1	-150.28	0.95	0.23	0.871	80.66	5
E(BF)=SZ+PC1+PC2+DI	-148.63	2.59	0.1	0.887	85.01	9
E(BF)=SZ+PC1+PC2	-148.35	2.87	0.09	0.872	80.93	6
E(BF)=SZ+PC1+DI+PC1*DI	-147.89	3.34	0.07	0.896	87.53	11
E(BF)=SZ+PC1+PC2+PC3	-146.88	4.34	0.04	0.874	81.46	7
E(BF)=SZ+PC1+PC2+PC3+DI	-146.03	5.2	0.03	0.888	85.13	10
E(BF)=SZ+DI+SZ*DI+PC1	-145.73	5.5	0.02	0.892	86.45	11
E(BF)=SZ+PC1+PC2+PC3+PC4	-145.19	6.04	0.02	0.876	81.93	8
E(BF)=SZ+PC1+PC2+PC3+PC4+DI	-143.78	7.45	0.01	0.889	85.48	11
E(BF)=SZ+DI+SZ*DI+PC1+PC2	-142.94	8.29	0.01	0.893	86.59	12
E(BF)=SZ+DI	-142.6	8.62	0	0.865	79.32	7
E(BF)=SZ+PC1+DI+SZ*DI+PC1*DI	-142.28	8.95	0	0.902	89.51	14
E(BF)=SZ+DI+SZ*DI	-141.04	10.19	0	0.878	82.63	10
E(BF)=SZ+DI+SZ*DI+PC1+PC2+PC3	-139.86	11.37	0	0.893	86.64	13
E(BF)=SZ+DI+SZ*DI+PC1+PC2+PC3+PC4	-136.69	14.54	0	0.893	86.72	14
E(BF)=SZ+PC1+PC2+DI+PC1*DI+PC2*DI	-135.54	15.68	0	0.897	87.88	15
E(BF)=SZ	-133.78	17.45	0	0.825	71.23	4
E(BF)=SZ+PC1+PC2+DI+SZ*DI+PC1*DI+PC2*DI	-130.85	20.38	0	0.907	91.2	18
E(BF)=SZ+PC1+PC2+PC3+DI+PC1*DI+PC2*DI+PC3*DI	-124.3	26.92	0	0.904	89.99	19
E(BF)=SZ+PC1+PC2+PC3+DI+SZ*DI+PC1*DI+PC2*DI+PC3*DI	-117.27	33.96	0	0.913	93.28	22
E(BF)=SZ+PC1+PC2+PC3+PC4+DI+PC1*DI+PC2*DI+PC3*DI+PC4*DI	-111.63	39.59	0	0.912	92.97	23
E(BF)=SZ+PC1+PC2+PC3+PC4+DI+SZ*DI+PC1*DI+PC2*DI+PC3*DI+PC4*DI	-100.62	50.61	0	0.920	95.81	26
E(BF) = 1	-30.05	121.18	0	0.002	18.23	3

Table 4. Phylogenetic path analysis results. Hypothesized causal models are ranked according to a theoretical information criterion (*ΔCICc*). *q* corresponds to the number of parameters estimated in each model. Causal models are depicted in Fig. 3.

Model	*q*	CICc	ΔCICc	CICc*wi*
A	9	23.432	0	0.61
D	7	26.231	2.799	0.15
E	7	26.317	2.885	0.14
F	7	27.492	4.061	0.08
C	8	30.322	6.891	0.02
B	7	45.091	21.659	0.00

Figures

Figure 1. Position of the landmarks (circles) and semilandmarks (squares) digitized on the skull on ventral and lateral views, and on the mandible of sigmodontine rodents. See Appendix S3 for landmark definitions.

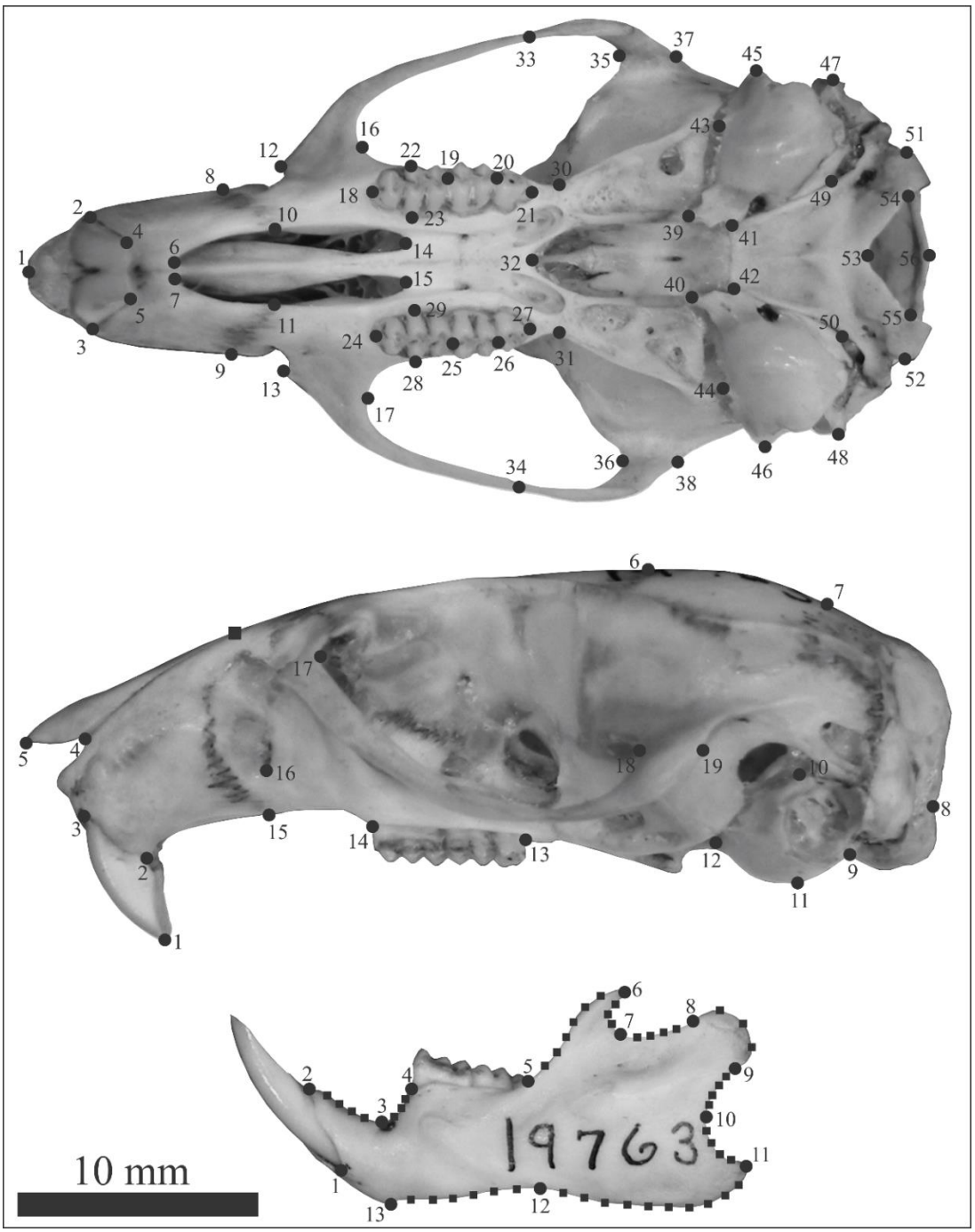

Figure 2. Phylogenetic relationships among sigmodontine rodents. A heat-map represents the standardized values for relative bite force (Rs – residuals of the regression between log bite force and log of centroid size), log of bite force (N), and log of centroid size (CS).

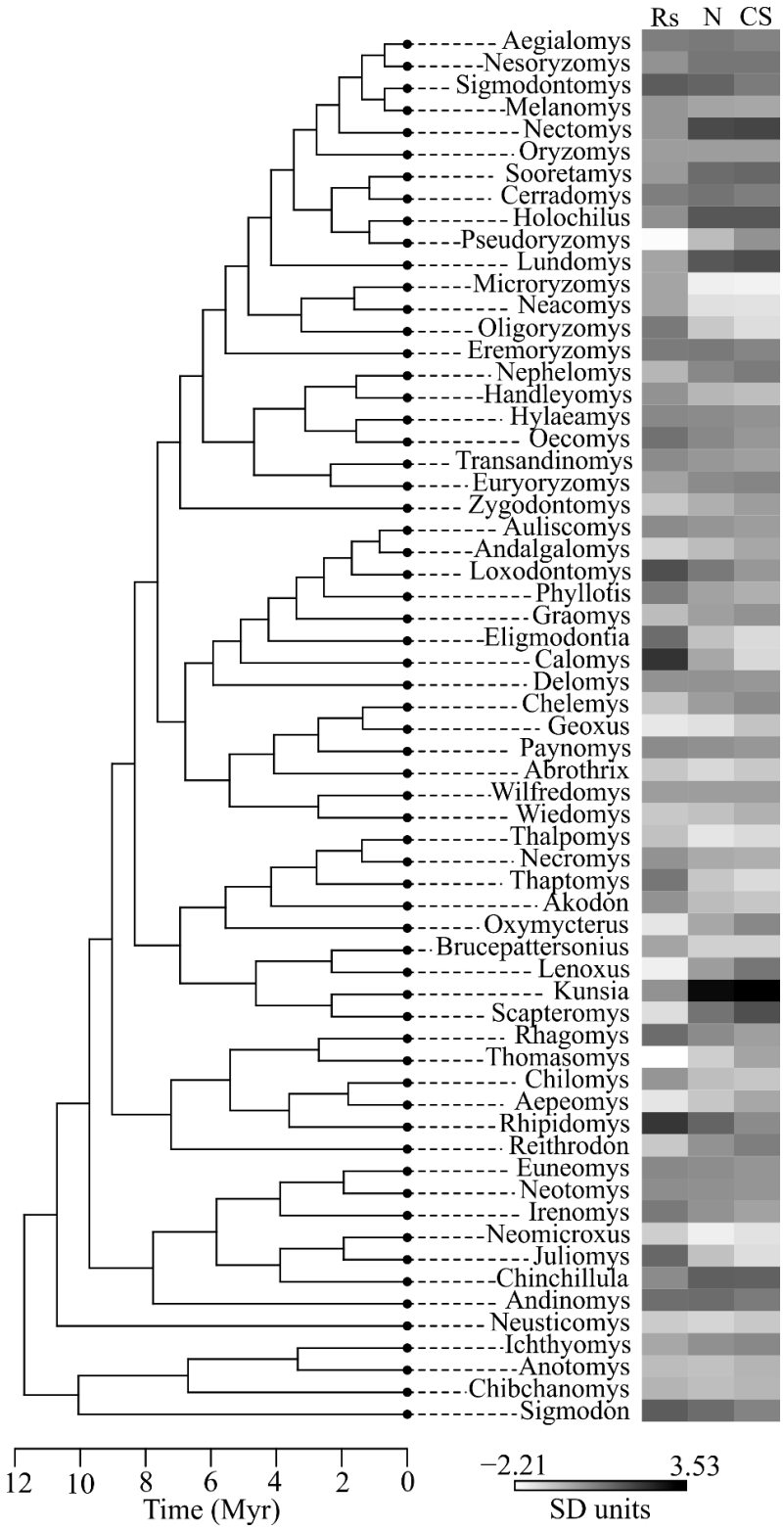

Figure 3. Direct acyclic graphs representing the alternative hypotheses of causal relationships among diet (DI), log of bite force (BF), log of centroid size (SZ), and PCs of shape (SH).The results of the rankings of alternative path models are presented in Table 2. Models represented by the path A is deemed superior/the best.

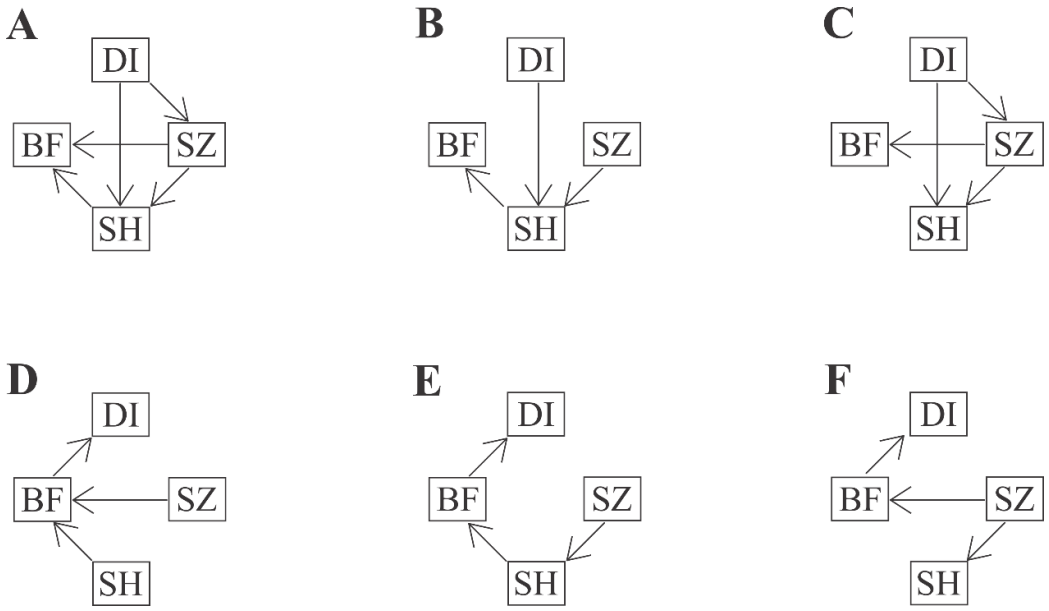

Figure 4. Phylogenetic regression (PGLS) of bite force (Newtons) on centroid size (cm), in a log-scale, for sigmodontine rodents. Solid line represents the PGLS predicted line and dashed lines represents the 95% confidence interval.

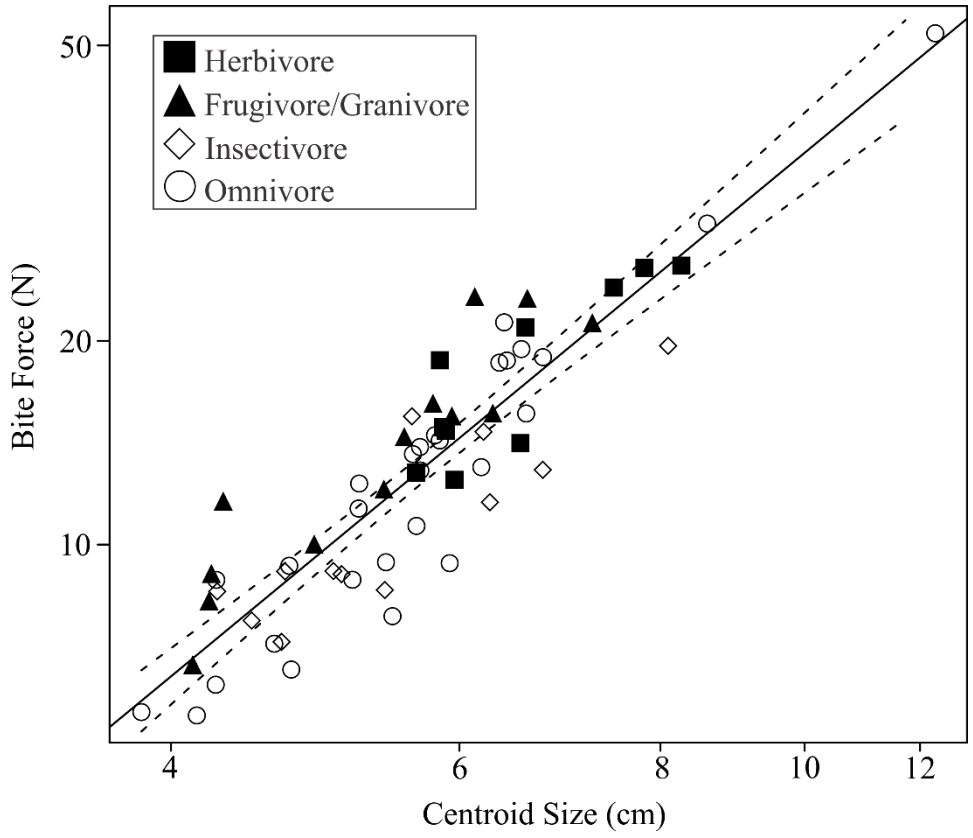

Figure 5. Boxplot representing variation in relative bite force among diet classes. Boxes represent the third and first quartiles, plus the median (bold line), and upper and lower limits. Solid triangles show the mean and open triangles the standard deviations of relative bite force for each diet class. Acronyms of diets are Frugivore/Granivore (FrGr), Herbivore (Hb), Insectivore (In), and Omnivore (On). Letters above plots indicate statistical significance (at α= 0.05) in PGLS pairwise comparisons between diets (equal letters mean no significance, distinct letters mean significance).

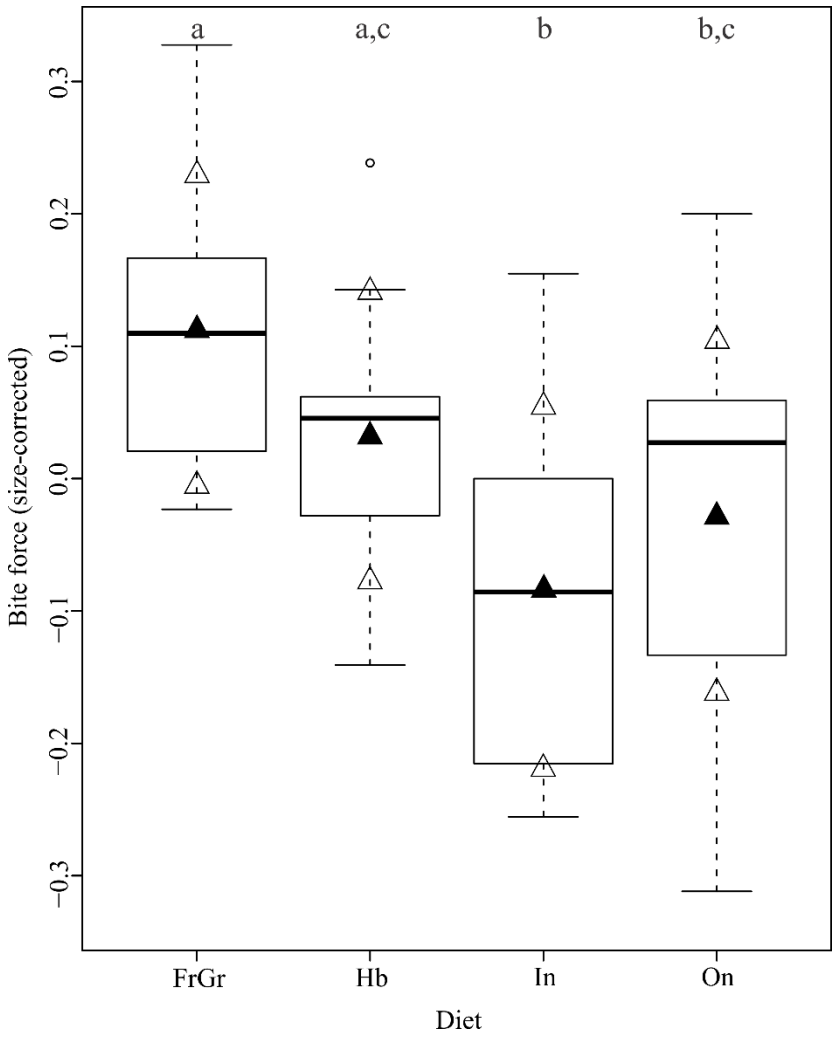

Figure 6. Principal Component Analysis of skull shape in ventral view with phylogeny and diet mapped. The connecting lines are determined by phylogeny, with shape at nodes estimated by square-change parsimony. The gradient of relative bite force (residuals from the regression of BF on size) is depicted by coloring symbol background as gray scale from weakest (lighter tones) to strongest (darker tones). Shape changes associated with positive values in both PCs (high relative BF) and negative values in both PCs (low relative BF) are shown.

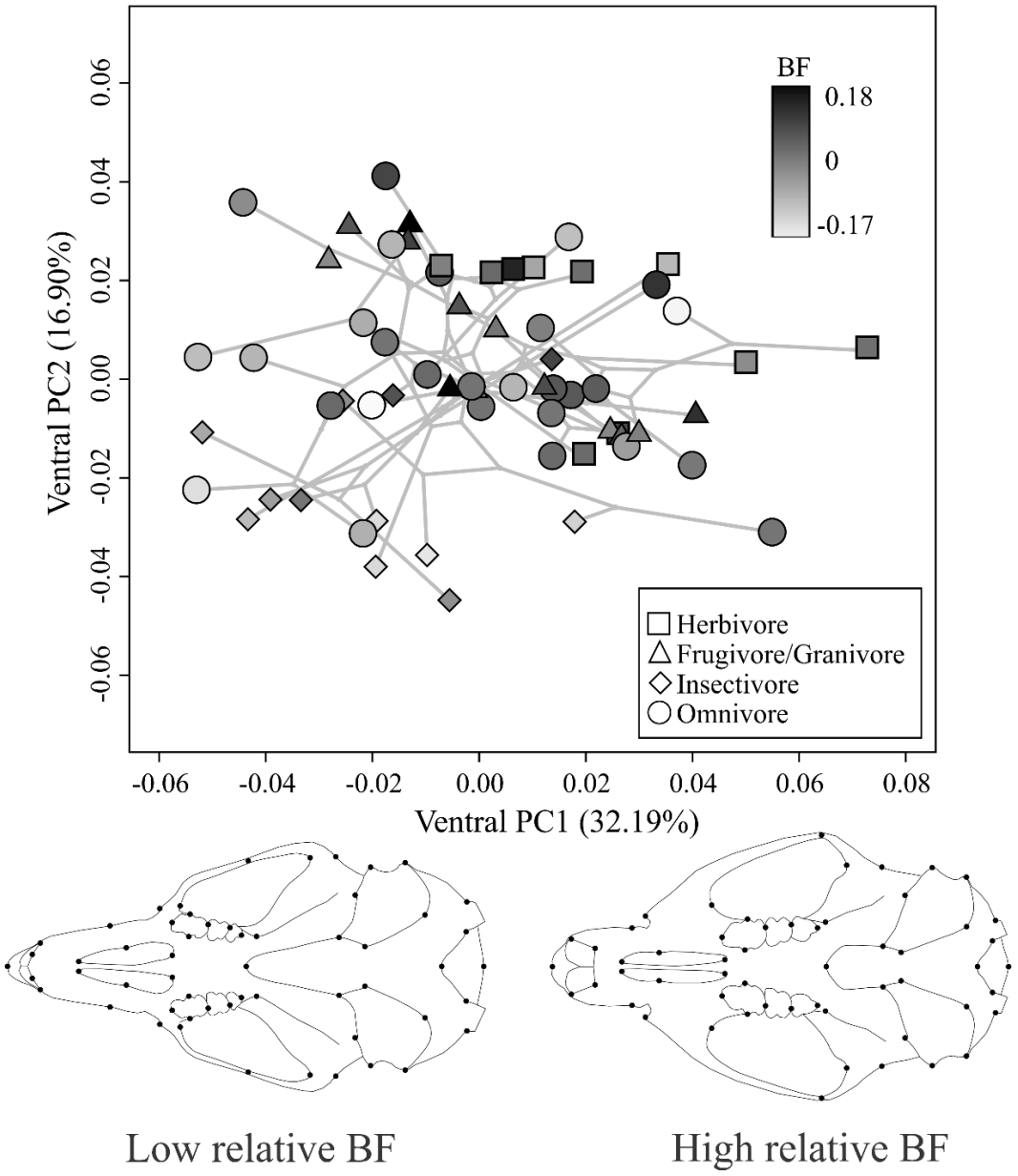

Figure 7. Principal Component Analysis of skull shape in lateral view with phylogeny and diet mapped. The connecting lines are determined by phylogeny, with shape at nodes estimated by square-change parsimony. The gradient of relative bite force (residuals from the regression of BF on size) is depicted by coloring symbol background as gray scale from weakest (lighter tones) to strongest (darker tones). Shape changes associated with positive values of PC1 and negative values of PC2 (high relative BF), and with negative values of PC1 and positive values of PC2 (low relative BF) are shown.

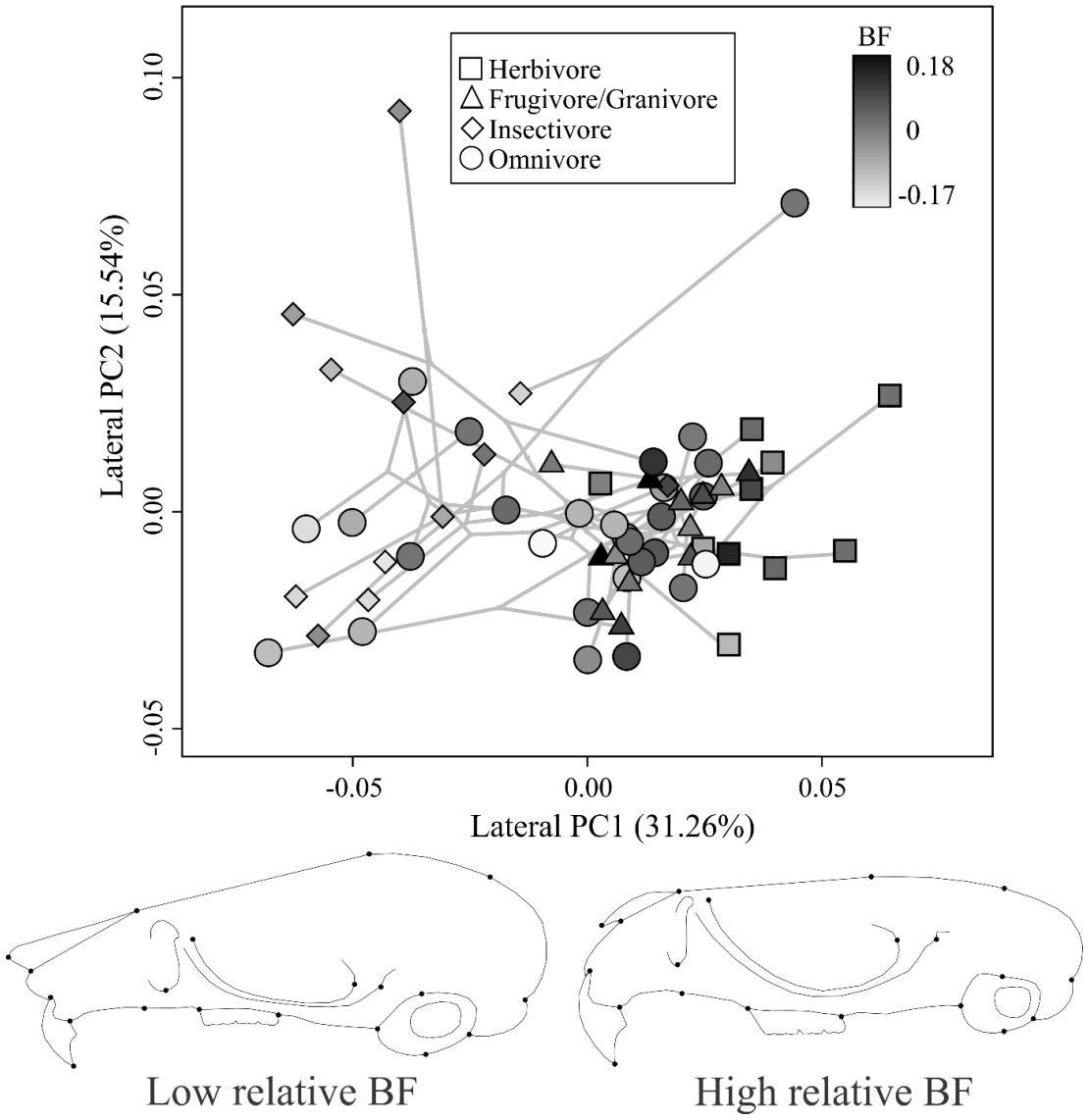

Figure 8. Principal Component Analysis of mandible shape with phylogeny and diet mapped. The connecting lines are determined by phylogeny, with shape at nodes estimated by square-change parsimony. The gradient of relative bite force (residuals from the regression of BF on size) is depicted by coloring symbol background as gray scale from weakest (lighter tones) to strongest (darker tones). Shape changes associated with negative values in both PCs (high relative BF) and positive values in both PCs (low relative BF) are shown.

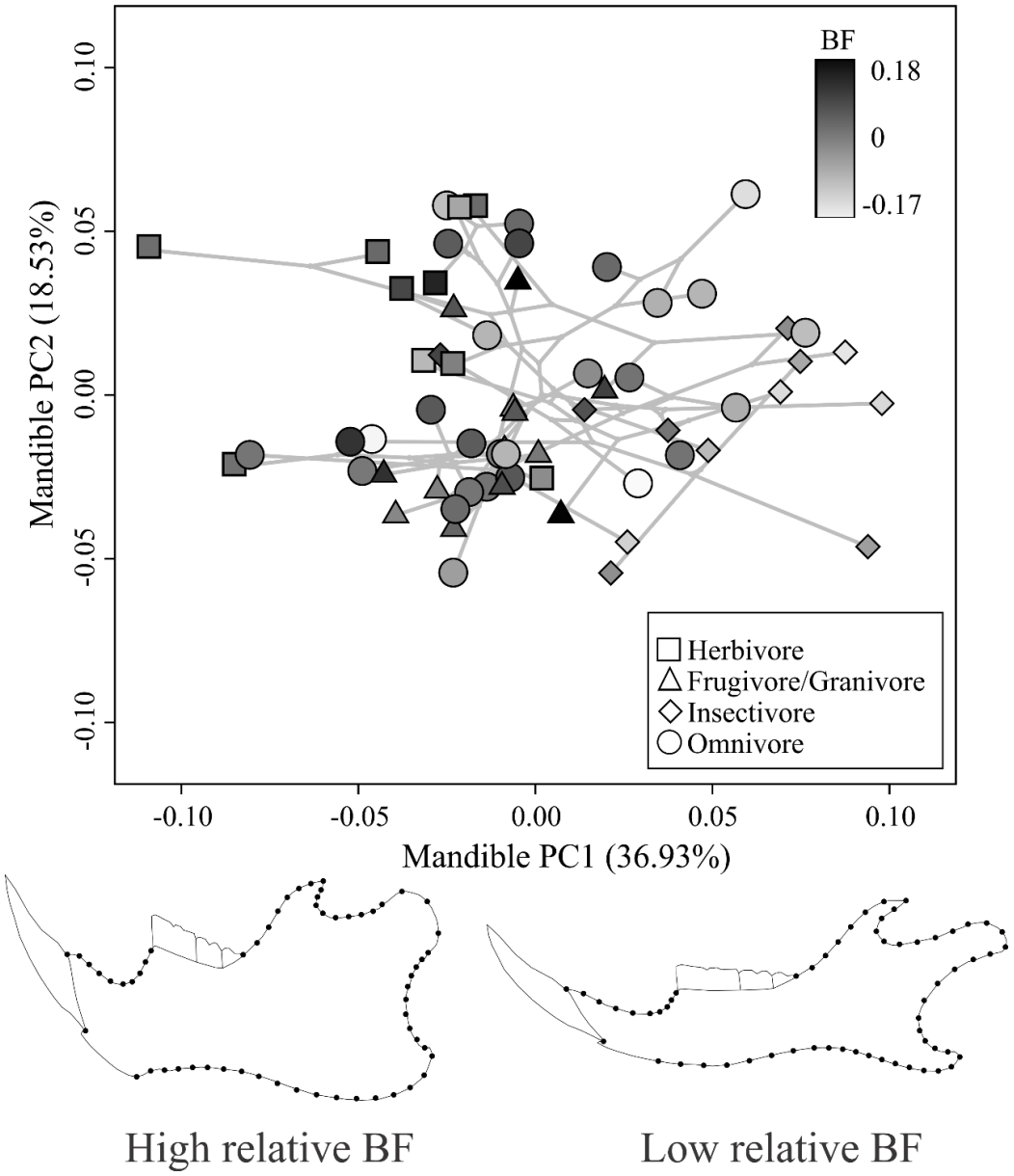

Supporting Information

Appendix S1. Number of specimens from which bite force estimates were taken, along with respective species and genus. A mean of log centroid size (cm) and of predicted bite force (N) is provided. The diet of each genus is shown: On (Omnivore), In (Insectivore), Hb (Herbivore), and FrGr (Frugivore/Granivore).

Species	**Genus**	**Number of Specimens**	**Mean CS (log)**	**Mean predicted BF (N)**	**Diet**
Abrothrix olivaceus brachiotis	*Abrothrix*	9	4.63	7.21	On
Aegialomys galapagoensis	*Aegialomys*	10	6.48	18.20	On
Aepeomys lugens	*Aepeomys*	3	5.43	8.59	In
Akodon aerosus baliolus	*Akodon*	10	4.73	9.30	On
Andalgalomys pearsoni	*Andalgalomys*	6	5.44	9.41	On
Andinomys edax	*Andinomys*	8	6.65	20.28	Hb
Anotomys leander	*Anotomys*	1	5.11	9.05	In
Auliscomys boliviensis flavidor	*Auliscomys*	8	5.72	13.71	On
Brucepattersonius soricinus	*Brucepattersonius*	5	4.49	7.78	In
Calomys callosus callosus	*Calomys*	9	4.31	11.38	FrGr
Cerradomys maracajuensis	*Cerradomys*	9	6.61	18.89	On
Chelemys megalonyx	*Chelemys*	3	6.24	12.84	On
Chibchanomys trichotis	*Chibchanomys*	1	5.05	9.14	In
Chilomys instans instans	*Chilomys*	10	4.71	9.13	In
Chinchillula sahamae	*Chinchillula*	8	7.56	23.09	Hb
Delomys collinus	*Delomys*	8	5.88	14.01	On
Eligmodontia morgani	*Eligmodontia*	10	4.26	8.88	On
Eremoryzomys polius	*Eremoryzomys*	8	6.41	18.07	On
Euneomys chinchilloides	*Euneomys*	6	5.91	14.63	Hb
Euryoryzomys macconelli	*Euryoryzomys*	10	6.35	15.17	FrGr
Geoxus valdivianus	*Geoxus*	6	4.75	6.63	On
Graomys griseoflavus	*Graomys*	5	6.01	12.31	Hb
Handleyomys intectus	*Handleyomys*	10	4.91	9.90	FrGr
Holochilus brasiliensis balnearum	*Holochilus*	10	7.90	24.63	Hb
Hylaeamys megacephalus capito	*Hylaeamys*	10	5.98	15.03	FrGr
Ichthyomys hydrobates	*Ichthyomys*	1	6.26	14.41	In
Irenomys tarsalis	*Irenomys*	6	5.59	14.03	FrGr
Juliomys pictipes	*Juliomys*	1	4.24	8.97	FrGr
Kunsia tomentosus tomentosus	*Kunsia*	2	12.00	53.03	On

Lenoxus apicalis	*Lenoxus*	3	6.82	12.73	In
Loxodontomys micropus fumipes	*Loxodontomys*	5	5.88	18.21	Hb
Lundomys molitor	*Lundomys*	5	8.33	24.81	Hb
Melanomys calliginosus	*Melanomys*	10	5.43	11.83	FrGr
Microryzomys minutus	*Microryzomys*	9	3.83	5.77	On
Neacomys spinosus	*Neacomys*	9	4.12	6.67	FrGr
Necromys lasiurus lasiurus	*Necromys*	9	5.23	11.22	On
Nectomys squamipes	*Nectomys*	9	8.64	28.46	On
Neomicroxus bogotensis	*Neomicroxus*	10	4.15	5.70	On
Neotomys ebriosus	*Neotomys*	6	5.93	14.46	Hb
Nephelomys albigularis	*Nephelomys*	10	6.66	15.30	On
Nesoryzomys indefessus narboroughi	*Nesoryzomys*	10	6.82	18.40	On
Neusticomys monticolus	*Neusticomys*	7	4.68	7.25	In
Oecomys mamorae	*Oecomys*	10	5.83	15.64	FrGr
Oligoryzomys destructor	*Oligoryzomys*	9	4.22	8.28	FrGr
Oryzomys couesi couesi	*Oryzomys*	10	5.72	12.70	On
Oxymycterus judex	*Oxymycterus*	8	6.32	11.45	In
Paynomys macronyx	*Paynomys*	10	5.84	14.25	On
Phyllotis darwini darwini	*Phyllotis*	9	5.24	12.17	On
Pseudoryzomys simplex	*Pseudoryzomys*	1	5.97	9.38	On
Reithrodon auritus pachycephalus	*Reithrodon*	6	6.61	13.89	Hb
Rhagomys longilingua	*Rhagomys*	1	5.65	15.16	In
Rhipidomys leucodactylus	*Rhipidomys*	8	6.19	22.23	FrGr
Scapteromys tumidus aquaticus	*Scapteromys*	5	8.17	19.09	In
Sigmodon arizonae cienegae	*Sigmodon*	7	6.45	20.61	On
Sigmodontomys alfari	*Sigmodontomys*	6	6.67	22.07	FrGr
Sooretamys angouya paraguanus	*Sooretamys*	7	7.33	20.37	FrGr
Thalpomys lasiotis	*Thalpomys*	2	4.26	6.31	On
Thaptomys nigrita	*Thaptomys*	6	4.27	8.55	In
Thomasomys incanus	*Thomasomys*	10	5.49	7.89	On
Transandinomys talamancae	*Transandinomys*	5	5.66	13.40	On
Wiedomys pyrrhorhinus	*Wiedomys*	3	5.19	8.89	On
Wilfredomys oenax	*Wilfredomys*	1	5.68	12.61	Hb
Zygodontomys brevicaudata	*Zygodontomys*	8	5.69	10.60	On

Appendix S2. Number of specimens by species and by genera of sigmodontine rodents, the percentage of species sampled in relation to the total in the genus, and the list of museums housing the specimens examined with the catalogue numbers of these specimens.

Genus	Species	Number of Individuals	Number of Species	Species Representation (%)
Abrothrix			**5**	**62.5**
	Abrothrix andina	4		
	Abrothrix jelskii	5		
	Abrothrix lanosa	6		
	Abrothrix longipilis	5		
	Abrothrix olivacea	10		
Aegialomys			**2**	**100**
	Aegialomys galapagoensis	11		
	Aegialomys xanthaeolus	17		
Aepeomys			**1**	**50**
	Aepeomys lugens	13		
Akodon			**34**	**87.18**
	Akodon aerosus	142		
	Akodon affinis	9		
	Akodon albiventer	88		
	Akodon azarae	101		
	Akodon boliviensis	45		
	Akodon budini	14		
	Akodon caenosus	13		
	Akodon cursor	94		
	Akodon dayi	30		
	Akodon dolores	19		
	Akodon fumeus	20		
	Akodon iniscatus	4		
	Akodon juninensis	20		
	Akodon kofordi	5		
	Akodon lindberghi	13		
	Akodon lutescens	8		
	Akodon mimus	11		
	Akodon mollis	48		
	Akodon montensis	81		
	Akodon mystax	32		
	Akodon orophilus	23		
	Akodon paranaensis	50		
	Akodon reigi	2		
	Akodon sanctipaulensis	14		
	Akodon serrensis	33		
	Akodon siberiae	7		
	Akodon simulator	25		
	Akodon spegazzinii	13		
	Akodon subfuscus	65		
	Akodon surdus	14		
	Akodon sylvanus	2		
	Akodon toba	36		
	Akodon torques	67		

	Akodon varius	10		
Andalgalomys			**1**	**33.33**
	Andalgalomys pearsoni	10		
Andinomys			**1**	**100**
	Andinomys edax	14		
Anotomys			**1**	**100**
	Anotomys leander	5		
Auliscomys			**3**	**100**
	Auliscomys boliviensis	10		
	Auliscomys pictus	8		
	Auliscomys sublimis	11		
Brucepattersonius			**2**	**28.57**
	Brucepattersonius iheringi	3		
	Brucepattersonius soricinus	2		
Calomys			**6**	**46.15**
	Calomys callosus	13		
	Calomys laucha	6		
	Calomys lepidus	5		
	Calomys musculinus	9		
	Calomys sorellus	8		
	Calomys venustus	2		
Cerradomys			**3**	**42.86**
	Cerradomys langguthi	3		
	Cerradomys maracajuensis	11		
	Cerradomys scotti	5		
Chelemys			**1**	**100**
	Chelemys megalonyx	2		
Chibchanomys			**1**	**50**
	Chibchanomys trichotis	2		
Chilomys			**1**	**50**
	Chilomys instans	10		
Chinchillula			**1**	**100**
	Chinchillula sahamae	11		
Delomys			**2**	**100**
	Delomys dorsalis	5		
	Delomys sublineatus	6		
Eligmodontia			**1**	**14.29**
	Eligmodontia morgani	10		
Eremoryzomys			**1**	**100**
	Eremoryzomys polius	7		
Euneomys			**2**	**50**
	Euneomys chinchilloides	8		
	Euneomys petersoni	6		
Euryoryzomys			**4**	**66.67**
	Euryoryzomys legatus	6		
	Euryoryzomys macconnelli	8		
	Euryoryzomys nitidus	10		
	Euryoryzomys russatus	10		
Geoxus			**1**	**100**
	Geoxus valdivianus	16		
Graomys			**2**	**50**
	Graomys domorum	6		
	Graomys griseoflavus	20		

Handleyomys		**22**	**2**	**66.67**
	Handleyomys alfaroi	17		
	Handleyomys intectus	5		
Holochilus			**2**	**40**
	Holochilus brasiliensis	9		
	Holochilus sciureus	5		
Hylaeamys			**4**	**57.14**
	Hylaeamys megacephalus	9		
	Hylaeamys oniscus	1		
	Hylaeamys perenensis	10		
	Hylaeamys yunganus	8		
Ichthyomys			**3**	**75**
	Ichthyomys hydrobates	10		
	Ichthyomys pittieri	2		
	Ichthyomys tweedii	7		
Irenomys			**1**	**100**
	Irenomys tarsalis	24		
Juliomys			**1**	**33.33**
	Juliomys pictipes	1		
Kunsia			**1**	**100**
	Kunsia tomentosus	4		
Lenoxus			**1**	**100**
	Lenoxus apicalis	17		
Loxodontomys			**1**	**100**
	Loxodontomys micropus	24		
Lundomys			**1**	**100**
	Lundomys molitor	5		
Melanomys			**3**	**75**
	Melanomys caliginosus	15		
	Melanomys robustulus	3		
	Melanomys zunigae	3		
Microryzomys			**2**	**100**
	Microryzomys altissimus	8		
	Microryzomys minutus	18		
Neacomys			**3**	**42.86**
	Neacomys guianae	1		
	Neacomys spinosus	21		
	Neacomys tenuipes	6		
Necromys			**6**	**85.71**
	Necromys amoenus	8		
	Necromys lactens	2		
	Necromys lasiurus	11		
	Necromys lenguarum	10		
	Necromys obscurus	1		
	Necromys urichi	6		
Nectomys			**4**	**80**
	Nectomys apicalis	13		
	Nectomys palmipes	3		
	Nectomys rattus	9		
	Nectomys squamipes	10		
Neomicroxus			**1**	**50**
	Neomicroxus bogotensis	25		
Neotomys			**1**	**100**
	Neotomys ebriosus	16		
Nephelomys			**10**	**90.91**

	Nephelomys albigularis	9		
	Nephelomys auriventer	1		
	Nephelomys devius	9		
	Nephelomys keaysi	7		
	Nephelomys levipes	9		
	Nephelomys maculiventer	6		
	Nephelomys meridensis	7		
	Nephelomys moerex	2		
	Nephelomys pectoralis	2		
	Nephelomys pirrensis	1		
Nesoryzomys			**4**	**80**
	Nesoryzomys darwini	1		
	Nesoryzomys fernandinae	1		
	Nesoryzomys indefessus	15		
	Nesoryzomys swarthi	1		
Neusticomys			**2**	**33.33**
	Neusticomys monticolus	12		
	Neusticomys venezuelae	1		
Oecomys			**10**	**62.5**
	Oecomys bicolor	11		
	Oecomys concolor	1		
	Oecomys flavicans	9		
	Oecomys mamorae	7		
	Oecomys paricola	8		
	Oecomys phaeotis	7		
	Oecomys roberti	6		
	Oecomys speciosus	1		
	Oecomys superans	10		
	Oecomys trinitatis	2		
Oligoryzomys			**12**	**63.16**
	Oligoryzomys andinus	3		
	Oligoryzomys arenalis	11		
	Oligoryzomys chacoensis	10		
	Oligoryzomys destructor	10		
	Oligoryzomys flavescens	10		
	Oligoryzomys fulvescens	9		
	Oligoryzomys griseolus	9		
	Oligoryzomys longicaudatus	19		
	Oligoryzomys magellanicus	11		
	Oligoryzomys microtis	11		
	Oligoryzomys nigripes	26		
	Oligoryzomys vegetus	2		
Oryzomys			**2**	**100**
	Oryzomys couesi	13		
	Oryzomys palustris	8		
Oxymycterus			**7**	**46.67**

	Oxymycterus dasytrichus	42		
	Oxymycterus delator	7		
	Oxymycterus inca	7		
	Oxymycterus nasutus	5		
	Oxymycterus paramensis	13		
	Oxymycterus quaestor	8		
	Oxymycterus rufus	6		
Paynomys			**1**	**100**
	Paynomys macronyx	19		
Phyllotis			**11**	**73.33**
	Phyllotis amicus	12		
	Phyllotis andium	11		
	Phyllotis caprinus	4		
	Phyllotis darwini	9		
	Phyllotis definitus	3		
	Phyllotis gerbillus	12		
	Phyllotis haggardi	1		
	Phyllotis limatus	10		
	Phyllotis magister	11		
	Phyllotis osilae	7		
	Phyllotis xanthopygus	10		
Pseudoryzomys			**1**	**100**
	Pseudoryzomys simplex	6		
Reithrodon			**1**	**50**
	Reithrodon auritus	15		
Rhagomys			**1**	**50**
	Rhagomys longilingua	1		
Rhipidomys			**11**	**47.83**
	Rhipidomys austrinus	3		
	Rhipidomys caucensis	3		
	Rhipidomys fulviventer	11		
	Rhipidomys latimanus	7		
	Rhipidomys leucodactylus	10		
	Rhipidomys maconnelli	2		
	Rhipidomys macrurus	1		
	Rhipidomys mastacalis	1		
	Rhipidomys modicus	4		
	Rhipidomys venezuelae	5		
	Rhipidomys venustus	13		
Scapteromys			**2**	**100**
	Scapteromys aquaticus	4		
	Scapteromys tumidus	13		
Sigmodon			**10**	**76.92**
	Sigmodon alstoni	10		
	Sigmodon arizonae	6		
	Sigmodon fulviventer	1		
	Sigmodon hirsutus	13		
	Sigmodon hispidus	10		
	Sigmodon leucotis	4		
	Sigmodon mascotensis	4		
	Sigmodon peruanus	6		
	Sigmodon toltecus	4		
	Sigmodon zanjonensis	7		
Sigmodontomys			**1**	**100**
	Sigmodontomys alfari	11		
Sooretamys			**1**	**100**

	Sooretamys angouya	12		
Thalpomys			**1**	**50**
	Thalpomys lasiotis	2		
Thaptomys			**1**	**100**
	Thaptomys nigrita	49		
Thomasomys			**19**	**43.18**
	Thomasomys aureus	13		
	Thomasomys baeops	12		
	Thomasomys cinereiventer	14		
	Thomasomys cinereus	14		
	Thomasomys daphne	1		
	Thomasomys gracilis	4		
	Thomasomys hylophilus	11		
	Thomasomys incanus	6		
	Thomasomys ischyurus	11		
	Thomasomys kalinowskii	7		
	Thomasomys laniger	10		
	Thomasomys monochromus	1		
	Thomasomys niveipes	12		
	Thomasomys notatus	6		
	Thomasomys oreas	6		
	Thomasomys paramarum	10		
	Thomasomys pyrrhonotus	4		
	Thomasomys taczanowskii	2		
	Thomasomys vulcani	3		
Transandinomys			**2**	**100**
	Transandinomys bolivaris	4		
	Transandinomys talamancae	15		
Wiedomys			**1**	**50**
	Wiedomys pyrrhorhinus	8		
Wilfredomys			**1**	**100**
	Wilfredomys oenax	2		
Zygodontomys			**2**	**100**
	Zygodontomys brevicaudata	21		
	Zygodontomys brunneus	12		
Total		**2808**	**227**	

Box S2. List of museums housing the specimens examined with the catalogue numbers of these specimens, organized by column. FMNH: Field Museum of Natural History; AMNH: American Museum of Natural History; NMNH: National Museum of Natural

History; MLP: Museo de la Plata; MZUSP: Museu de Zoologia da Universidade de São Paulo, MN: Museu Nacional do Rio de Janeiro.

Abrothrix	***Akodon***	***Akodon cont.***	***Euneomys***	***Nephelomys cont.***	***Phyllotis cont.***
FMNH23143	FMNH75474	MN50282	FMNH134186	FMNH128469	FMNH107900
FMNH23144	FMNH75473	MN50283	FMNH134182	FMNH128470	FMNH107901
FMNH23146	FMNH75472	MN50256	FMNH133088	FMNH170640	FMNH107902
FMNH23147	FMNH75471	MN50257	FMNH134183	FMNH170645	FMNH107903
FMNH49386	FMNH75470	MN50258	FMNH133083	FMNH170649	FMNH107904
FMNH48389	FMNH75479	MN50259	FMNH133085	FMNH170651	FMNH107905
FMNH49392	FMNH75565	MN50260	FMNH134181	FMNH170654	FMNH107929
FMNH49394	FMNH75225	MN50261	FMNH133089	FMNH170655	FMNH107936
FMNH49395	FMNH24522	MN50262	FMNH50587	FMNH170658	FMNH107939
FMNH50174	FMNH24525	MN50263	FMNH50590	FMNH172358	NMNH121143
FMNH50379	FMNH24526	MN50264	FMNH50591	FMNH172360	NMNH121145
FMNH50380	FMNH24532	MN50265	FMNH50592	FMNH172362	***Pseudoryzomys***
FMNH50382	FMNH24534	MN50266	FMNH50593	FMNH171884	FMNH118810
FMNH50383	FMNH24536	MN50267	FMNH50596	FMNH175171	FMNH34236
FMNH50384	FMNH24538	MN50269	***Euryoryzomys***	FMNH174173	NMNH584585
FMNH127506	FMNH24540	MN50270	FMNH162819	FMNH175175	NMNH584586
FMNH127507	FMNH24542	MN50271	FMNH162821	FMNH175177	NMNH390668
FMNH127504	FMNH24543	MN50272	FMNH162823	FMNH175179	AMNH262048
FMNH127503	FMNH24502	MN50273	FMNH129265	FMNH13213	***Reithrodon***
FMNH127502	FMNH24506	MN50274	FMNH129267	FMNH13214	FMNH134180
FMNH131540	FMNH24503	MN50275	FMNH129266	FMNH13215	FMNH134188
FMNH131642	FMNH24510	MN50276	FMNH136915	FMNH13217	FMNH134189
FMNH131643	FMNH24512	MN69565	FMNH136906	FMNH13220	FMNH134190
FMNH131645	FMNH78376	MN69566	FMNH136905	FMNH13222	FMNH134225
FMNH131647	FMNH78375	MN69567	FMNH136911	FMNH18646	FMNH134211
FMNH131649	FMNH78377	MN69568	FMNH136909	FMNH18650	FMNH134222
FMNH131651	FMNH52539	MN69569	FMNH136913	FMNH18651	FMNH134224
FMNH131652	FMNH52523	MN69570	FMNH143318	FMNH18652	FMNH50577
FMNH131654	FMNH52522	MN69571	FMNH143319	FMNH18653	FMNH50578
FMNH131655	FMNH52593	MN69572	FMNH117111	FMNH18654	FMNH124418
Aegialomys	FMNH52294	MN69573	FMNH117113	FMNH18655	FMNH124420
FMNH179528	FMNH52527	MN69574	FMNH26786	FMNH54004	FMNH124417
FMNH51756	FMNH52526	MN69575	FMNH117110	FMNH93133	FMNH35339
FMNH49012	FMNH52525	MN69576	FMNH139874	FMNH93134	FMNH18192
FMNH51761	FMNH52524	MN69585	FMNH141637	FMNH20087	***Rhagomys***
FMNH51763	FMNH52528	MN69586	FMNH141638	FMNH20085	FMNH170687
FMNH51764	FMNH52529	MN69587	FMNH141639	***Nesoryzomys***	***Rhipidomys***
FMNH51765	FMNH52541	MN69588	FMNH141640	FMNH179526	FMNH72882
FMNH51766	FMNH18180	MN69589	FMNH141641	FMNH30831	FMNH72881
FMNH51767	FMNH52538	MN69590	FMNH141642	FMNH30843	FMNH72883
FMNH51769	FMNH52107	MN69596	FMNH141643	FMNH30832	FMNH71738
FMNH51768	FMNH52531	MN69599	FMNH141644	FMNH30835	FMNH71736
FMNH107377	FMNH72100	MN59113	FMNH141646	FMNH30838	FMNH71744
FMNH107378	FMNH170423	MN69602	FMNH141648	FMNH30839	FMNH71487
FMNH107379	FMNH170427	MN69605	MZUSP1844	FMNH30840	FMNH71488
FMNH107380	FMNH170428	MN69606	MZUSP1841	FMNH30841	FMNH71720
FMNH107381	FMNH170429	MN69609	MZUSP1894	FMNH179527	FMNH71722
FMNH107383	FMNH170431	MN69613	MZUSP20559	FMNH30848	FMNH71723
FMNH107386	FMNH170408	MN69623	MZUSP20560	FMNH30855	FMNH71724
FMNH81389	FMNH170413	MN69627	***Geoxus***	FMNH30854	FMNH71725
FMNH81390	FMNH170414	MN69628	FMNH133125	FMNH30852	FMNH71726
FMNH81391	FMNH170415	MN69629	FMNH133115	FMNH30856	FMNH71727
FMNH81392	FMNH170416	MN69644	FMNH133116	FMNH30859	FMNH71728
FMNH81393	FMNH170417	MN69645	FMNH133124	FMNH30873	FMNH71729
FMNH81394	FMNH170412	MN69660	FMNH134949	FMNH30871	FMNH70235
FMNH81403	FMNH170420	MN69664	FMNH134948	***Neusticomys***	FMNH70237
FMNH81404	FMNH170388	MN69665	FMNH127724	FMNH71218	FMNH70238

FMNH81405	FMNH170393	MN48029	FMNH133097	FMNH71220	FMNH70241
FMNH81407	FMNH170396	MN48066	FMNH133103	FMNH71222	FMNH70244
Aepeomys	FMNH170397	MN75283	FMNH133104	FMNH71223	FMNH70247
FMNH22154	FMNH170399	MN75282	FMNH124059	FMNH71225	FMNH70249
FMNH22155	FMNH170400	MN48031	FMNH22499	NMNH406123	FMNH43211
NMNH579496	FMNH170403	MN48032	FMNH22496	AMNH64632	FMNH41477
NMNH579498	FMNH170368	MN48033	FMNH22495	AMNH64633	FMNH125049
NMNH579492	FMNH170369	MN48034	FMNH133094	AMNH64629	FMNH53401
NMNH579494	FMNH170371	MN48035	FMNH50538	AMNH62920	FMNH41478
NMNH387954	FMNH170377	MN48036	***Graomys***	AMNH63376	FMNH68652
NMNH387957	FMNH170379	MN48041	FMNH50961	AMNH244609	FMNH75229
NMNH387961	FMNH170380	MN48067	FMNH50962	AMNH244608	FMNH24820
NMNH374597	FMNH170384	MN48070	FMNH50963	***Oecomys***	FMNH24819
NMNH374598	FMNH170385	MN63110	FMNH50968	FMNH116934	FMNH24816
NMNH374603	FMNH170351	MN69675	FMNH50969	FMNH116936	FMNH53982
NMNH374600	FMNH170353	MN69676	FMNH21525	FMNH116933	FMNH53983
Akodon	FMNH170357	MN69677	FMNH157386	FMNH116979	FMNH211417
NMNH236310	FMNH170359	MN69679	FMNH157387	FMNH116973	FMNH128325
NMNH236315	FMNH170360	MN69681	FMNH157388	FMNH116974	FMNH140806
NMNH274275	FMNH170361	MN69682	FMNH157393	FMNH116966	FMNH140807
NMNH274276	FMNH172197	MN69683	FMNH157394	FMNH116926	FMNH140808
NMNH236259	FMNH172195	MN69685	FMNH164754	FMNH116927	FMNH19363
NMNH236261	FMNH172193	MN69686	FMNH164749	FMNH116947	FMNH70261
NMNH236266	FMNH172192	MN69687	FMNH164750	FMNH116946	FMNH7048
NMNH236268	FMNH172190	MN69695	FMNH157385	FMNH87968	FMNH21826
NMNH236299	FMNH129981	MN69700	FMNH157382	FMNH69198	FMNH21828
NMNH236263	FMNH129982	MN69701	FMNH164836	FMNH69199	FMNH29443
NMNH236269	FMNH129983	MN69705	FMNH164837	FMNH69200	FMNH71705
NMNH236276	FMNH129986	MN69710	FMNH164838	FMNH92521	FMNH71706
NMNH236300	FMNH129992	MN69714	FMNH164841	FMNH92525	FMNH71708
NMNH271407	FMNH129993	MN69715	FMNH164842	FMNH92526	FMNH71712
NMNH259611	FMNH129995	MN69716	FMNH164843	FMNH92527	FMNH71713
NMNH259612	FMNH107876	MN69719	FMNH164844	FMNH92528	FMNH71714
NMNH236314	FMNH52575	MN69724	FMNH164846	FMNH92530	FMNH71715
NMNH172966	FMNH107880	MN69735	FMNH164850	FMNH51913	FMNH71716
NMNH259622	FMNH107879	MN69727	FMNH164857	FMNH21522	FMNH71717
NMNH259623	FMNH107890	MN69726	***Handleyomys***	FMNH25267	FMNH71719
NMNH331060	FMNH53622	MN69737	FMNH64541	FMNH21524	FMNH19831
NMNH276608	FMNH53623	MN69741	FMNH73543	FMNH21523	FMNH18188
NMNH276609	FMNH53624	MN69745	FMNH73562	FMNH117061	FMNH21825
NMNH290926	FMNH107472	MN71897	FMNH73545	FMNH117060	***Scapteromys***
NMNH390141	FMNH107475	MN62119	FMNH73560	FMNH94024	FMNH29160
NMNH390699	FMNH107479	MN62120	FMNH61679	FMNH136894	FMNH98288
NMNH584503	FMNH107478	MN54491	FMNH61680	FMNH143292	FMNH98287
NMNH584504	FMNH107543	MN69584	FMNH5371	FMNH136943	FMNH122714
NMNH584505	FMNH107488	MN69597	FMNH70296	FMNH143288	FMNH122713
NMNH584506	FMNH107491	MN69621	FMNH70302	FMNH143291	NMNH
NMNH390160	FMNH107492	MN60640	FMNH70303	FMNH143289	AMNH206221
NMNH390161	FMNH107497	MN60654	FMNH70304	FMNH143290	AMNH206223
NMNH390162	FMNH107528	MN69655	FMNH70305	FMNH84314	AMNH206222
NMNH271433	FMNH107533	MN69657	FMNH55904	FMNH68637	AMNH206216
NMNH290907	FMNH107470	MN69666	FMNH56033	FMNH68638	AMNH206209
NMNH290927	FMNH107441	MN69667	FMNH55896	FMNH170604	AMNH206219
NMNH236238	FMNH107439	MN69669	FMNH55900	FMNH172269	AMNH206230
NMNH236241	FMNH170630	MN69673	FMNH11137	FMNH170599	AMNH206244
NMNH238127	FMNH107627	MN63113	FMNH11138	FMNH170602	AMNH206245
NMNH259603	FMNH107624	MN63114	FMNH11139	FMNH175097	AMNH206240
NMNH141453	FMNH107593	MN51644	FMNH11142	FMNH84303	AMNH206231
NMNH181333	FMNH107594	MN71903	FMNH14111	FMNH175099	***Sigmodon***
NMNH181335	FMNH107597	MN48065	***Holochilus***	FMNH88937	FMNH18683
NMNH181338	FMNH107600	MN77791	FMNH145308	FMNH72024	FMNH18686
NMNH259615	FMNH107601	MN71942	FMNH53948	FMNH72030	FMNH18682
NMNH259616	FMNH107618	MN48027	FMNH53949	FMNH62056	FMNH18693
NMNH259617	FMNH107619	MN48028	FMNH23307	FMNH41460	FMNH22138

NMNH259618	FMNH107621	MN42011	FMNH23308	FMNH41458	FMNH18648
NMNH259619	FMNH107633	MN48030	FMNH23311	FMNH41459	FMNH20040
NMNH302998	FMNH107554	MN60680	FMNH23313	FMNH72013	FMNH20041
NMNH303000	FMNH107568	MN60711	FMNH23314	FMNH72025	FMNH20042
NMNH303001	FMNH107570	MN35912	FMNH23315	FMNH72089	FMNH20038
NMNH304548	FMNH107573	MN35919	FMNH118811	FMNH72020	FMNH890
NMNH279457	FMNH107578	MN35921	FMNH118819	FMNH72027	FMNH891
NMNH279459	FMNH107579	MN35922	FMNH118816	FMNH72042	FMNH892
NMNH279461	FMNH107580	MN35923	FMNH118820	FMNH72033	FMNH893
NMNH513598	FMNH107587	MN35924	FMNH118825	FMNH24574	FMNH894
NMNH513599	FMNH162735	MN35926	***Hylaeamys***	FMNH24576	FMNH895
NMNH513600	FMNH162737	MN35927	FMNH143304	***Oligoryzomys***	FMNH889
NMNH513601	FMNH162745	MN32637	FMNH143305	FMNH20962	FMNH13223
NMNH513602	FMNH162645	MN24592	FMNH143306	FMNH20961	FMNH13224
NMNH513603	FMNH162647	MN24594	FMNH143308	FMNH20963	FMNH13226
NMNH513604	FMNH162679	MN24595	FMNH143309	FMNH19409	FMNH44865
NMNH513605	FMNH162681	MN24616	FMNH143310	FMNH19414	FMNH69157
NMNH364531	FMNH162685	MN24617	FMNH143313	FMNH19415	FMNH54008
NMNH181334	FMNH162683	MN24627	FMNH143315	FMNH19416	FMNH54007
NMNH181336	FMNH162687	MN24630	FMNH143316	FMNH19418	FMNH34962
NMNH121380	FMNH162689	MN24631	FMNH63778	FMNH19419	FMNH5005
NMNH121386	FMNH162693	MN24632	FMNH75222	FMNH19421	FMNH34960
NMNH541492	FMNH162699	MN24639	FMNH75241	FMNH19423	FMNH44009
NMNH304606	FMNH162707	MZUSP29114	FMNH75243	FMNH19424	FMNH44010
NMNH304607	FMNH162713	MZUSP29112	FMNH75244	FMNH19425	FMNH34972
NMNH309160	FMNH162721	MZUSP29100	FMNH75246	FMNH19426	FMNH7930
NMNH462077	FMNH162723	MZUSP29102	FMNH75247	FMNH157391	FMNH7931
NMNH462078	FMNH162725	MZUSP29103	FMNH75248	FMNH164910	FMNH7934
NMNH484227	FMNH23342	MZUSP29104	FMNH75273	FMNH164911	FMNH7918
NMNH484229	FMNH23341	MZUSP29105	FMNH75269	FMNH164913	FMNH7920
NMNH484230	FMNH23340	MZUSP29106	FMNH75270	FMNH164914	FMNH7923
NMNH484521	FMNH23328	MZUSP29107	FMNH66401	FMNH164915	FMNH7925
NMNH485107	FMNH23329	MZUSP29108	FMNH75242	FMNH164924	FMNH7926
NMNH485110	FMNH23330	MZUSP29109	FMNH75253	FMNH145314	FMNH7944
NMNH485115	FMNH23333	MZUSP29110	FMNH72051	FMNH26641	FMNH7938
NMNH259279	FMNH23334	MZUSP29111	FMNH58778	FMNH26805	FMNH15181
NMNH259632	FMNH23332	MZUSP29113	FMNH58779	FMNH29238	FMNH14090
NMNH194753	FMNH23335	MZUSP29088	FMNH87970	FMNH122692	FMNH14089
NMNH194752	FMNH23336	MZUSP29089	FMNH72067	FMNH27671	FMNH14363
NMNH194758	FMNH23337	MZUSP29090	***Ichthyomys***	FMNH27668	FMNH8653
NMNH194757	FMNH23339	MZUSP29091	FMNH90293	FMNH27667	FMNH8656
NMNH195760	FMNH22233	MZUSP29092	NMNH513625	FMNH27655	FMNH8658
NMNH194762	FMNH98283	MZUSP29093	NMNH151288	FMNH27654	FMNH8662
NMNH194763	FMNH98282	MZUSP29094	NMNH115315	FMNH27651	FMNH81341
NMNH194666	FMNH95140	MZUSP29096	NMNH460684	FMNH162807	FMNH19216
NMNH196941	FMNH23344	MZUSP29097	NMNH461078	FMNH162809	FMNH81344
NMNH259272	FMNH23345	MZUSP29098	NMNH461094	FMNH162811	FMNH81345
NMNH259273	FMNH23346	MZUSP29099	NMNH294985	FMNH19768	FMNH81346
NMNH259274	FMNH23347	MZUSP29119	NMNH562980	FMNH19778	FMNH81347
NMNH259275	FMNH23348	MZUSP29120	NMNH562981	FMNH19779	FMNH106540
NMNH259277	FMNH23349	MZUSP29121	AMNH71382	FMNH19780	FMNH106541
NMNH259278	FMNH23350	MZUSP29122	AMNH71383	FMNH19781	FMNH106542
NMNH194658	FMNH29218	MZUSP29123	AMNH71384	FMNH19782	FMNH106544
NMNH194672	FMNH29220	MZUSP29124	AMNH71385	FMNH19783	FMNH73614
NMNH194673	FMNH29222	MZUSP29126	AMNH46732	FMNH143301	FMNH73615
NMNH194675	FMNH29223	MZUSP29101	AMNH46730	FMNH143300	FMNH73616
NMNH194727	FMNH29215	MZUSP29115	AMNH46731	FMNH143299	FMNH73617
NMNH194735	FMNH29214	MZUSP29116	AMNH39594	FMNH143298	FMNH73618
NMNH194736	FMNH29213	MZUSP29117	AMNH64624	FMNH143297	FMNH73619
NMNH194739	FMNH29211	MZUSP29118	***Irenomys***	FMNH143295	FMNH73613
NMNH194742	FMNH29209	MZUSP938	FMNH134969	FMNH143293	***Sigmodontomys***
NMNH194743	FMNH29207	MZUSP939	FMNH134970	FMNH29240	FMNH70530
NMNH194744	FMNH29205	MZUSP942	FMNH134964	FMNH27650	FMNH70534
NMNH194746	FMNH29200	MZUSP30951	FMNH134967	FMNH27649	FMNH70535

NMNH194749	FMNH29199	MZUSP31013	FMNH134963	FMNH27645	FMNH70536
NMNH194751	FMNH29196	MZUSP30997	FMNH133137	FMNH29230	FMNH90282
NMNH194750	FMNH29195	MZUSP1773	FMNH133139	FMNH29231	FMNH89563
NMNH194645	FMNH27612	MZUSP1796	FMNH133140	FMNH29232	FMNH70532
NMNH194644	FMNH29204	MZUSP27226	FMNH133154	FMNH29234	FMNH69193
NMNH194655	FMNH29188	MZUSP27223	FMNH133155	FMNH29236	FMNH69196
NMNH194643	FMNH29189	MZUSP1794	FMNH133142	FMNH1305	FMNH21829
NMNH194694	FMNH27614	MZUSP27225	FMNH50554	FMNH73550	FMNH53999
NMNH194641	FMNH27615	MZUSP9469	FMNH50567	FMNH73551	***Sooretamys***
NMNH194657	FMNH27616	MZUSP2772	FMNH50555	FMNH73554	FMNH26752
NMNH194639	FMNH27617	MZUSP29127	FMNH50557	FMNH72555	FMNH26751
NMNH194651	FMNH27620	MZUSP29128	FMNH50561	FMNH73557	FMNH26750
NMNH194642	FMNH27621	MZUSP30947	FMNH50563	FMNH73561	FMNH26749
NMNH194656	FMNH27624	MZUSP28965	FMNH50564	FMNH73518	FMNH26748
NMNH324907	FMNH27625	MZUSP28966	FMNH50565	FMNH73519	FMNH26747
NMNH324908	FMNH27626	MZUSP626	FMNH50568	FMNH89332	FMNH136919
NMNH390146	FMNH27627	MZUSP29255	FMNH133166	FMNH18634	FMNH136920
NMNH390147	FMNH27628	MZUSP29256	FMNH133164	FMNH18636	FMNH136922
NMNH390148	FMNH27630	MZUSP29257	FMNH133148	FMNH18637	FMNH18165
NMNH390150	FMNH27631	MZUSP29259	FMNH133143	FMNH18638	FMNH18166
NMNH390151	FMNH27632	MZUSP29260	***Juliomys***	FMNH18641	FMNH18167
NMNH390152	FMNH27633	MZUSP29261	FMNH94552	FMNH71969	***Thalpomys***
NMNH390153	FMNH27635	MZUSP29262	***Kunsia***	FMNH71975	FMNH128327
NMNH390155	FMNH27636	MZUSP29263	FMNH122711	FMNH71967	FMNH128326
NMNH390157	FMNH27641	MZUSP29264	FMNH122710	FMNH71970	***Thaptomys***
NMNH390158	FMNH27670	MZUSP29247	NMNH584515	FMNH133211	MN8780
NMNH555668	FMNH27662	MZUSP29225	NMNH584516	FMNH133217	MN8778
NMNH555669	FMNH27642	MZUSP28388	***Lenoxus***	FMNH133215	MN8775
NMNH194581	FMNH27638	MZUSP28379	FMNH20106	FMNH133218	MN8771
NMNH194583	FMNH27664	MZUSP28357	FMNH52613	FMNH25312	MN8769
NMNH194586	FMNH27619	MZUSP29239	FMNH52612	FMNH25313	MN8767
NMNH194593	FMNH27669	MZUSP29240	AMNH72624	FMNH22644	MN8764
NMNH194594	FMNH52551	MZUSP29241	AMNH72620	FMNH22645	MN8763
NMNH194595	FMNH64339	MZUSP29242	AMNH72622	FMNH22646	MN8805
NMNH194596	FMNH52543	MZUSP29243	AMNH72618	FMNH22647	MN8804
NMNH194599	FMNH52545	MZUSP29244	AMNH72616	FMNH22649	MN8803
NMNH194600	FMNH52544	MZUSP29245	AMNH72615	FMNH22651	MN8797
NMNH194601	FMNH162753	MZUSP29246	AMNH72611	FMNH133469	MN8795
NMNH194604	FMNH162751	MZUSP29218	AMNH72610	FMNH133470	MN8792
NMNH194609	FMNH162749	MZUSP29219	AMNH72609	FMNH133471	MN8788
NMNH194610	FMNH107829	MZUSP29228	AMNH264855	FMNH133473	MN8787
NMNH194612	FMNH107834	MZUSP29229	AMNH264854	FMNH133475	MN8785
NMNH194613	FMNH107840	MZUSP29230	AMNH16553	FMNH133476	MN8735
NMNH194614	FMNH107841	MZUSP29231	AMNH16065	FMNH133478	MN8734
NMNH194615	FMNH107848	MZUSP29232	AMNH16558	FMNH50698	MN8731
NMNH194618	FMNH107850	MZUSP29233	***Loxodontomys***	FMNH50699	MN8730
NMNH194619	FMNH107853	MZUSP29234	FMNH132689	FMNH50700	MN8729
NMNH194621	FMNH107856	MZUSP29235	FMNH132692	FMNH124339	MN2727
NMNH194623	FMNH10858	MZUSP29237	FMNH132706	FMNH127353	MN8724
NMNH194626	FMNH107863	MZUSP29238	FMNH132746	FMNH50685	MN8721
NMNH194627	FMNH107865	MZUSP32429	FMNH132747	FMNH50686	MN8720
NMNH194628	FMNH107928	MZUSP32424	FMNH132749	FMNH50690	MN29100
NMNH194629	FMNH107940	MZUSP32427	FMNH132751	FMNH50691	MN29101
NMNH194630	FMNH107943	MZUSP29227	FMNH132752	FMNH50693	MN29104
NMNH194631	FMNH107944	MZUSP29226	FMNH132668	FMNH50695	MN29110
NMNH194633	FMNH107969	MZUSP3520	FMNH132666	FMNH139838	MN29096
NMNH194635	FMNH52564	MLP5.xi.92.37	FMNH132665	FMNH139844	MN29097
NMNH194636	FMNH49699	MLP5.xi.92.14	FMNH132787	FMNH139839	MN29098
NMNH582136	FMNH49700	MLP5.xi.92.28	FMNH132785	FMNH139842	MN29099
NMNH582137	FMNH23362	MLP5.xi.92.23	FMNH132783	FMNH139845	MN69838
NMNH582138	FMNH23363	MLP5.xi.92.38	FMNH132782	FMNH139847	MN77795
NMNH582139	FMNH23364	MLP5.xi.92.24	FMNH132780	FMNH139848	MN7041
NMNH582141	FMNH23365	MLP5.xi.92.19	FMNH132779	FMNH84341	MN7037
NMNH582142	FMNH23360	MLP5.xi.92.21	FMNH132778	FMNH84342	MN7025

NMNH582143	FMNH23359	MLP5.xi.92.18	FMNH132789	FMNH84343	MN7033
NMNH582169	FMNH23357	MLP5.xi.92.13	FMNH132791	FMNH84344	MN7096
NMNH582171	FMNH23356	MLP5.xi.92.17	FMNH132792	FMNH26593	MZUSP29384
NMNH182175	FMNH23352	MLP5.xi.92.1	FMNH132800	FMNH26599	MZUSP29385
NMNH290909	FMNH23355	MLP10.iii.79.1	FMNH132804	FMNH26600	MZUSP29386
AMNH268750	FMNH23351	MLP10.iii.79.5	FMNH132807	FMNH26601	MZUSP29387
AMNH268743	FMNH23361	MLP24.v.77.1	***Lundomys***	FMNH26604	MZUSP29388
AMNH268744	FMNH21581	MLP20.xii.00.16	FMNH29257	FMNH26612	MZUSP29383
AMNH268751	FMNH21578	MLP16.v.01.10	FMNH29260	FMNH26613	MZUSP23850
AMNH268745	FMNH21575	MLP16.v.01.9	FMNH29261	FMNH26613	MZUSP24008
AMNH268746	FMNH21588	MLP30.v.02.2	FMNH29263	FMNH26616	***Thomasomys***
AMNH268747	FMNH74880	MLP14.xii.73.3	NMNH259641	FMNH26617	FMNH70320
AMNH268748	FMNH74879	MLP28.ix.95.5	***Melanomys***	FMNH26618	FMNH70322
AMNH268752	FMNH74874	MLP1.x.70.18	FMNH66576	FMNH14304	FMNH70323
AMNH268738	FMNH74876	MLP11.ii.36.7	FMNH65577	FMNH18519	FMNH70327
AMNH268739	FMNH74875	MLP18.viii.74.2	FMNH65578	***Oryzomys***	FMNH70328
AMNH268740	FMNH41284	MLP18.viii.74.6	FMNH29454	FMNH5347	FMNH70329
AMNH268741	FMNH41285	MLP18.viii.74.4	FMNH41475	FMNH44702	FMNH70331
AMNH268742	FMNH29127	MLP18.viii.74.8	FMNH43228	FMNH54160	FMNH70307
AMNH67428	FMNH23673	MLP9.ii.99.1	FMNH128471	FMNH54161	FMNH70308
AMNH67431	FMNH75561	MLP24.v.96.2	FMNH128472	FMNH54162	FMNH70309
AMNH67462	FMNH23671	MLP30.viii.99.8	FMNH128476	FMNH54163	FMNH70310
AMNH67466	FMNH52544	MLP14.ix.99.34	FMNH128477	FMNH56006	FMNH70311
AMNH47567	FMNH52556	MLP14.ix.99.35	FMNH128488	FMNH56007	FMNH70316
AMNH47568	FMNH52555	MLP14.ix.99.3	FMNH92459	FMNH56008	FMNH90333
AMNH47566	FMNH75483	MLP14.ix.99.17	FMNH70358	FMNH73521	FMNH90334
AMNH47556	FMNH128296	MLP14.ix.99.37	FMNH70364	FMNH73522	FMNH90335
AMNH47558	FMNH128298	MLP14.ix.99.45	FMNH70366	FMNH73523	FMNH90339
AMNH47563	FMNH128293	MLP14.ix.99.42	FMNH70370	FMNH73525	FMNH71478
AMNH231302	FMNH128297	MLP14.ix.99.43	FMNH70347	FMNH171227	FMNH71480
AMNH231298	FMNH128295	MLP14.ix.99.30	FMNH70350	FMNH171228	FMNH71481
AMNH231296	FMNH30195	MLP14.ix.99.1	FMNH70352	FMNH171230	FMNH71482
AMNH231300	FMNH30194	MLP18.v.74.7	FMNH70354	FMNH171231	FMNH71475
AMNH71230	FMNH23384	***Andalgalomys***	FMNH70355	FMNH171232	FMNH71474
AMNH71220	FMNH23390	FMNH157341	***Microryzomys***	FMNH7818	FMNH71471
AMNH71227	FMNH23392	FMNH164192	FMNH24698	FMNH7819	FMNH71467
AMNH71226	FMNH23389	FMNH164190	FMNH24700	FMNH7811	FMNH71344
AMNH76691	FMNH23388	FMNH164184	FMNH24704	***Oxymycterus***	FMNH71348
AMNH92456	FMNH23387	FMNH164188	FMNH24703	MZUSP10777	FMNH71347
AMNH260436	FMNH49696	FMNH151997	FMNH24705	MZUSP2089	FMNH71351
AMNH260439	FMNH49697	AMNH262344	FMNH24685	MZUSP10721	FMNH71329
AMNH260438	FMNH21559	AMNH262345	FMNH24686	MZUSP29368	FMNH71336
AMNH260440	FMNH50975	AMNH262347	FMNH24694	MZUSP29374	FMNH71337
AMNH260441	FMNH20899	AMNH262346	FMNH175045	MZUSP29375	FMNH71339
AMNH260442	FMNH20902	***Andinomys***	FMNH175047	MZUSP9891	FMNH71352
AMNH260445	FMNH20905	FMNH23435	FMNH175049	MZUSP9832	FMNH71353
AMNH268759	FMNH20909	FMNH132648	FMNH175051	MZUSP10207	FMNH71354
AMNH268757	FMNH20908	FMNH132647	FMNH175053	MZUSP10189	FMNH71355
AMNH262681	FMNH20910	FMNH132651	FMNH175055	MZUSP10188	FMNH71356
AMNH262680	FMNH21144	FMNH162757	FMNH175057	MZUSP10187	FMNH81332
AMNH262678	FMNH81350	FMNH162759	FMNH175059	MZUSP10190	FMNH81333
AMNH262677	FMNH24481	FMNH162761	FMNH71951	MZUSP29364	FMNH81337
AMNH262682	FMNH24487	FMNH51281	FMNH71950	MZUSP29365	FMNH81338
AMNH206049	FMNH24489	FMNH51283	FMNH71956	MZUSP29366	FMNH81339
AMNH206047	FMNH24425	FMNH51282	FMNH71957	MZUSP29367	FMNH83444
AMNH206046	FMNH24427	FMNH51279	FMNH71964	MZUSP29369	FMNH81334
AMNH206040	FMNH24429	FMNH29156	FMNH71958	MZUSP29370	FMNH81330
AMNH206041	FMNH24431	FMNH29157	FMNH71966	MZUSP22483	FMNH81329
AMNH206042	FMNH24439	FMNH74869	FMNH71960	MZUSP22487	FMNH81328
AMNH206043	FMNH24441	***Anotomys***	FMNH71959	MZUSP22488	FMNH81327
AMNH206056	FMNH24440	FMNH53367	FMNH71954	MZUSP22490	FMNH83446
AMNH206050	FMNH24438	AMNH244607	***Neacomys***	MZUSP22491	FMNH83449
AMNH206052	FMNH24434	AMNH244606	FMNH95643	MZUSP22492	FMNH83450
AMNH262690	FMNH24432	AMNH244605	FMNH125030	MZUSP21572	FMNH172378

AMNH262718	FMNH24426	AMNH66202	FMNH125033	MZUSP21573	FMNH43393
AMNH626692	FMNH24430	***Auliscomys***	FMNH125036	MZUSP21574	FMNH43392
AMNH262717	FMNH26817	FMNH49769	FMNH125038	MZUSP10208	FMNH70342
AMNH262714	FMNH26834	FMNH49768	FMNH125039	MZUSP21575	FMNH71489
AMNH262711	FMNH26838	FMNH49771	FMNH125041	MZUSP26794	FMNH18565
AMNH248998	FMNH26846	FMNH49773	FMNH75364	MZUSP21595	FMNH18576
AMNH263640	FMNH26847	FMNH49774	FMNH75362	MZUSP21594	FMNH18578
AMNH263630	FMNH26848	FMNH49599	FMNH75360	MZUSP23751	FMNH18580
AMNH263632	FMNH26851	FMNH49600	FMNH75359	MZUSP22461	FMNH18584
AMNH263631	FMNH26850	FMNH49601	FMNH75361	MZUSP845	FMNH18586
AMNH263642	FMNH26853	FMNH49602	FMNH75363	MZUSP10085	FMNH18588
AMNH263641	FMNH26855	FMNH49604	FMNH23746	MZUSP35158	FMNH18587
AMNH262648	FMNH26858	FMNH81284	FMNH24761	MZUSP35157	FMNH92554
AMNH262685	FMNH29146	FMNH81228	FMNH24762	MZUSP2771	FMNH92558
AMNH262687	FMNH29145	FMNH81282	FMNH24763	MZUSP10650	FMNH92560
AMNH262695	FMNH35243	FMNH107764	FMNH20088	MZUSP10651	FMNH23725
AMNH262719	FMNH24535	FMNH107748	FMNH20089	FMNH145443	FMNH23731
AMNH262704	FMNH24500	FMNH107716	FMNH52711	FMNH145442	FMNH23728
AMNH247794	FMNH24495	FMNH107694	FMNH19360	FMNH145441	FMNH23730
AMNH247789	FMNH24774	FMNH107678	FMNH19691	FMNH145438	FMNH23732
AMNH247795	FMNH24773	FMNH107767	FMNH70116	FMNH145437	FMNH23734
AMNH247796	FMNH19754	FMNH107769	FMNH70123	FMNH53875	FMNH53244
AMNH247797	FMNH129234	FMNH49550	FMNH70124	FMNH53874	FMNH53407
AMNH263300	FMNH129236	FMNH107696	FMNH70125	FMNH175211	FMNH92000
AMNH263298	FMNH19718	FMNH107674	FMNH70126	FMNH179217	FMNH92001
AMNH263295	FMNH19717	FMNH107675	FMNH19653	FMNH175213	FMNH92002
AMNH263294	FMNH19728	FMNH107711	***Necromys***	FMNH175215	FMNH92003
AMNH263291	FMNH19726	FMNH107763	AMNH259916	FMNH172366	FMNH93148
AMNH262745	FMNH19721	FMNH49546	AMNH259917	FMNH52622	FMNH93150
AMNH262746	FMNH19722	FMNH49540	AMNH259919	FMNH84365	FMNH93152
AMNH262747	FMNH19725	FMNH49544	AMNH259920	FMNH27652	FMNH94991
AMNH262748	FMNH19729	***Brucepattersonius***	AMNH259921	FMNH29250	FMNH94993
AMNH262751	FMNH94520	MZUSP34665	AMNH259922	FMNH29253	FMNH23738
AMNH262753	FMNH94515	FMNH94499	FMNH162771	FMNH52623	FMNH23724
AMNH262754	FMNH29138	MZUSP27227	FMNH23366	FMNH52630	FMNH23739
AMNH268777	FMNH19135	MZUSP10661	FMNH122687	FMNH52624	FMNH23736
AMNH268776	FMNH30131	MZUSP21129	FMNH107836	FMNH52633	FMNH23737
AMNH268773	FMNH30122	***Calomys***	FMNH107838	FMNH52625	FMNH23735
AMNH268772	FMNH30128	FMNH23341	FMNH107862	FMNH52626	FMNH23723
AMNH268771	FMNH30109	FMNH23393	FMNH107864	FMNH52631	FMNH71452
AMNH268780	FMNH30110	FMNH23377	FMNH107866	FMNH162837	FMNH71457
AMNH268783	FMNH30113	FMNH23376	FMNH10875	FMNH162839	FMNH71458
AMNH268779	FMNH30115	FMNH23373	FMNH107680	FMNH162841	FMNH71459
AMNH268788	FMNH30117	FMNH23430	FMNH107699	FMNH162843	FMNH71461
AMNH268787	FMNH29142	FMNH26790	FMNH25197	FMNH162845	FMNH71454
AMNH268786	FMNH30119	FMNH26792	FMNH25198	FMNH26592	FMNH71455
AMNH268785	FMNH30120	FMNH26796	FMNH25200	FMNH26595	FMNH71456
AMNH231341	FMNH122686	FMNH26799	FMNH26201	FMNH26587	FMNH71443
AMNH231340	FMNH29122	FMNH26795	FMNH128339	FMNH35354	FMNH71444
AMNH231338	FMNH29123	FMNH28361	FMNH128337	FMNH34383	FMNH71445
AMNH231337	FMNH30181	FMNH28362	FMNH128336	FMNH23843	FMNH71446
AMNH231334	FMNH30182	FMNH23404	FMNH128335	FMNH26757	FMNH71408
AMNH231331	FMNH30184	FMNH23405	FMNH128334	FMNH26754	FMNH71409
AMNH231329	FMNH30189	FMNH23407	FMNH128333	FMNH128320	FMNH71413
AMNH231328	FMNH107797	FMNH23409	FMNH128331	FMNH128321	FMNH71414
AMNH231326	FMNH107794	FMNH23410	FMNH164415	FMNH128322	FMNH71416
AMNH231325	FMNH107793	FMNH23413	FMNH164416	FMNH128323	FMNH71415
AMNH231324	FMNH107787	FMNH49551	FMNH164414	FMNH128324	FMNH71417
AMNH231322	FMNH107727	FMNH49552	FMNH164413	FMNH122697	FMNH71419
AMNH231318	FMNH107721	FMNH49553	FMNH164411	FMNH95138	FMNH71420
AMNH231317	FMNH107719	FMNH75420	FMNH164426	FMNH136928	FMNH71423
AMNH231403	FMNH107544	FMNH54743	FMNH164422	FMNH136929	FMNH69190
AMNH231400	FMNH107549	FMNH164672	FMNH164421	***Paynomys***	FMNH170693
AMNH231399	FMNH107546	FMNH164723	FMNH164419	FMNH132990	FMNH170796

AMNH268766	FMNH107530	FMNH164724	FMNH164418	FMNH132979	FMNH170697
AMNH262724	FMNH107772	FMNH164737	***Nectomys***	FMNH132940	FMNH170699
AMNH268803	FMNH107777	FMNH157322	FMNH43208	FMNH132988	FMNH170701
AMNH268809	FMNH107760	FMNH157342	FMNH43210	FMNH132987	FMNH172380
AMNH268810	FMNH107754	FMNH157343	FMNH41465	FMNH132983	FMNH75224
AMNH268816	FMNH107751	FMNH157352	FMNH41466	FMNH50530	FMNH172376
AMNH268818	FMNH107747	FMNH157364	FMNH41467	FMNH50529	FMNH170707
AMNH268819	FMNH107744	FMNH140812	FMNH65687	FMNH46153	FMNH175241
AMNH268820	FMNH107703	FMNH140813	FMNH65690	FMNH46154	FMNH175243
AMNH268795	FMNH107704	FMNH23751	FMNH65691	FMNH46155	FMNH175245
AMNH268797	FMNH107705	FMNH23752	FMNH78696	FMNH132927	FMNH53236
AMNH268801	FMNH107717	FMNH23654	FMNH68643	FMNH132931	FMNH91984
AMNH268802	FMNH107718	FMNH23753	FMNH68640	FMNH132944	FMNH91986
AMNH47486	FMNH170485	FMNH23757	FMNH68639	FMNH132956	FMNH91987
AMNH47494	FMNH170487	FMNH23758	FMNH65694	FMNH132924	FMNH91988
AMNH47501	FMNH170489	FMNH23760	FMNH19645	FMNH132930	FMNH91989
AMNH207963	FMNH107803	FMNH23763	FMNH19644	FMNH132942	FMNH91992
AMNH207966	FMNH107805	***Cerradomys***	FMNH19643	FMNH132953	FMNH91993
AMNH207965	FMNH107807	FMNH19507	FMNH19649	***Phyllotis***	FMNH91991
AMNH260579	FMNH107810	FMNH25246	FMNH18549	FMNH81260	FMNH44309
AMNH260594	FMNH107814	FMNH26446	FMNH46213	FMNH81261	FMNH81296
AMNH260578	FMNH107817	FMNH116909	FMNH18542	FMNH81263	FMNH84439
AMNH260431	FMNH107818	FMNH116822	FMNH61896	FMNH19258	FMNH84438
AMNH260428	FMNH43371	FMNH116823	FMNH20110	FMNH19259	FMNH81295
AMNH260434	FMNH43372	FMNH116824	FMNH61892	FMNH19261	FMNH43249
AMNH260430	FMNH83476	FMNH116825	FMNH26442	FMNH107390	FMNH93146
AMNH231476	FMNH164159	FMNH116826	FMNH140805	FMNH107392	FMNH94992
AMNH231475	FMNH164160	FMNH116827	FMNH20710	FMNH107391	FMNH53980
AMNH231472	FMNH164161	FMNH116887	FMNH20711	FMNH107393	FMNH74867
AMNH231469	FMNH164164	FMNH116888	FMNH20712	FMNH107394	FMNH74866
AMNH60594	FMNH164168	FMNH116889	FMNH20713	FMNH107396	***Transandinomys***
AMNH264231	FMNH164169	FMNH116895	FMNH94390	FMNH19839	FMNH128493
AMNH264232	FMNH157211	FMNH128310	FMNH94387	FMNH19841	FMNH128490
AMNH264233	FMNH164101	FMNH128311	FMNH94380	FMNH19842	FMNH128491
AMNH264238	FMNH164118	FMNH128312	FMNH94385	FMNH19843	FMNH128492
AMNH264239	FMNH164119	FMNH128313	FMNH94377	FMNH81208	FMNH70504
AMNH264274	FMNH164136	FMNH128315	FMNH93049	FMNH81207	FMNH70496
AMNH264272	FMNH157192	***Chelemys***	***Neomicroxus***	FMNH81206	FMNH70497
AMNH91561	FMNH157194	FMNH22494	FMNH71235	FMNH81205	FMNH70526
AMNH91565	FMNH157197	FMNH23901	FMNH71239	FMNH81204	FMNH70522
AMNH91564	FMNH157199	***Chibchanomys***	FMNH71240	FMNH81203	FMNH70492
AMNH91569	FMNH157201	FMNH71226	FMNH71243	FMNH81202	FMNH70489
AMNH91577	FMNH157203	NMNH442606	FMNH71244	FMNH41287	FMNH69207
AMNH91575	FMNH157206	***Chilomys***	FMNH71247	FMNH85847	FMNH60211
AMNH91574	FMNH172223	FMNH71600	FMNH18573	FMNH85848	FMNH69203
AMNH91578	FMNH172221	FMNH71621	FMNH18574	FMNH85849	FMNH69204
AMNH41816	FMNH171861	FMNH71607	FMNH18671	FMNH119508	FMNH69205
AMNH41803	FMNH171862	FMNH71606	FMNH18673	FMNH119507	FMNH71057
AMNH41682	FMNH172231	FMNH71604	FMNH18675	FMNH22325	FMNH72058
AMNH41692	FMNH172225	FMNH71602	NMNH374609	FMNH22326	FMNH72059
AMNH264296	FMNH172227	FMNH71605	NMNH374611	FMNH22328	***Wiedomys***
AMNH264288	FMNH172229	FMNH71499	NMNH374613	FMNH133896	FMNH25249
AMNH264281	FMNH172233	FMNH71495	NMNH387966	FMNH119512	FMNH136941
AMNH264293	FMNH170501	FMNH71496	NMNH387967	FMNH35902	FMNH136942
AMNH264282	FMNH170503	***Chinchillula***	NMNH387969	FMNH119505	NMNH538314
AMNH264290	FMNH170506	FMNH49401	NMNH579559	FMNH21126	NMNH538306
AMNH264295	FMNH170508	FMNH49402	NMNH579560	FMNH21127	NMNH555761
AMNH262294	FMNH170509	FMNH49403	NMNH579562	FMNH21128	NMNH304584
AMNH264292	FMNH170510	FMNH49404	NMNH579563	FMNH21916	NMNH555760
AMNH264285	FMNH170511	FMNH49405	NMNH579564	FMNH81265	***Wilfredomys***
AMNH41752	FMNH170517	FMNH49406	NMNH579565	FMNH81266	FMNH104933
AMNH41832	FMNH170519	FMNH49409	NMNH579566	FMNH81269	AMNH206020
AMNH41835	FMNH170523	FMNH49410	NMNH579567	FMNH81270	***Zygodontomys***
AMNH41675	FMNH170524	FMNH49411	***Neotomys***	FMNH81271	FMNH20051

AMNH41648	FMNH170526	FMNH49417	FMNH24775	FMNH81275	FMNH20052
AMNH41651	FMNH175021	FMNH49418	FMNH81238	FMNH81274	FMNH20053
AMNH41656	FMNH175023	***Delomys***	FMNH24776	FMNH81273	FMNH20054
AMNH268857	FMNH175025	FMNH26597	FMNH75580	FMNH81272	FMNH20055
AMNH268856	FMNH170029	FMNH26598	FMNH49708	FMNH53306	FMNH87990
AMNH268855	FMNH175031	FMNH141628	FMNH51262	FMNH107609	FMNH87999
AMNH268850	FMNH175033	FMNH145383	FMNH51263	FMNH107574	FMNH88004
AMNH268851	FMNH50980	FMNH141629	NMNH541802	FMNH107575	FMNH88006
AMNH268854	FMNH50983	FMNH143287	AMNH231645	FMNH107598	FMNH88008
FMNH65705	FMNH20981	FMNH136932	AMNH231644	FMNH49481	FMNH89014
FMNH66402	MN33681	FMNH136934	AMNH231641	FMNH49482	FMNH18482
FMNH68609	MN33681	FMNH136936	AMNH231640	FMNH49484	FMNH18483
FMNH68612	MN33681	FMNH136937	AMNH231639	FMNH49485	FMNH18487
FMNH68614	MN33681	FMNH136939	AMNH231637	FMNH49487	FMNH18484
FMNH68616	MN33681	***Eliqmodontia***	AMNH231636	FMNH49488	FMNH18485
FMNH78709	MN33681	FMNH133029	AMNH231634	FMNH35360	FMNH18486
FMNH41474	MN33681	FMNH133034	***Nephelomys***	FMNH49475	FMNH18568
FMNH43229	MN33703	FMNH133035	FMNH71840	FMNH107683	FMNH18630
FMNH43232	MN48026	FMNH133036	FMNH71845	FMNH107690	FMNH21832
FMNH19265	MN67123	FMNH133037	FMNH71846	FMNH107691	FMNH54010
FMNH19268	MN48882	FMNH133038	FMNH71847	FMNH107692	FMNH70193
FMNH19266	MN48882	FMNH133041	FMNH71848	FMNH107561	FMNH70194
FMNH19757	MN48882	FMNH133044	FMNH71849	FMNH107611	FMNH70188
FMNH78715	MN48882	FMNH133045	FMNH71851	FMNH107612	FMNH70187
FMNH78714	MN48882	FMNH133046	FMNH53342	FMNH107613	FMNH70205
FMNH78710	MN48882	***Eremoryzomys***	FMNH53344	FMNH107616	FMNH70204
FMNH78720	MN48888	FMNH19763	FMNH53336	FMNH22342	FMNH70202
FMNH75481	MN48889	FMNH19764	FMNH123996	FMNH50964	FMNH70201
FMNH75480	MN50241	FMNH19766	FMNH128415	FMNH74870	FMNH70199
FMNH75479	MN63121	FMNH19767	FMNH128467	FMNH50966	FMNH70198
FMNH75478	MN48890	FMNH129243	FMNH128462	FMNH74871	FMNH70206
FMNH75477	MN48891	FMNH129245	FMNH128464	FMNH74872	FMNH70226
FMNH75476	MN50255	FMNH129242	FMNH128466	FMNH74873	
FMNH75475	MN50281		FMNH128468	FMNH107898	

Appendix S3. Definition of landmarks placed in the two skull views and in the mandible of all sigmodontine specimens. See Figure 1 in the main paper.

Description of landmarks of skull-ventral view:

L1: anteriormost point of the suture between nasals; **L2,3**: lateralmost point of the alveolus of the incisor; **L4,5**: lateral tip of the incisor; **L6,7**: anteriormost point of the incisive foramen; **L14,15**: posteriormost point of the incisive foramen; **L10,11**: medial extent of the suture between the premaxilla and maxilla lateral to the incisive foramen as seen in the ventral view; **L8,9**: lateralmost extent of suture between the premaxilla and maxilla; **L12,13**: anterodorsal tip of zygomatic plate; **L16,17**: anteriormost point of the orbit; **L18,24**: anteriormost point of the molar row; **L19,25**: contact point between first and second molars; **L20,26**: contact point between second and third molars; **L21,27**: posteriormost point of the third molar; **L22,28**: lateral paracone of first molar; **L23,29**: medial paracone of first molar; **L30,31**: least post-palatal distance across the palatines; **L32**: posteriormost extent of palate at the midline; **L33,34**: suture between jugal and squamosal in the zygomatic arch as seen in the ventral view; **L35-36**: anteriormost point of the glenoid fossa; **L37,38**: posterior end of squamosal root of zygomatic bar; **L39-40**: anteriormost point of the eustachian tube; **L41,42**: suture between basisphenoid and basioccipital at point of contact with the auditory bulla; **L43-44**: anteriormost border of the paramastoid process; **L45,46:** anteriormost external border of the ectotympanic; **L47,48**: posteriormost margin of the masseteric tubercle; **L49,50**: opening of the basioccipital at the level of the occipital condyle; **L51,52**: lateralmost point of the occipital condyle; **L53**: anteriormost point of the foramen magnum along the midline; **L54**: posteriormost point of the foramen magnum on the midline; **L55,56**: anteriormost margin of the occipital condyle.

Description of landmarks of skull lateral view:

L1: tip of the incisor; **L2:** posteriormost point of the upper incisive alveolus; **L3:** inferiormost point of the upper incisive alveolus; **L4:** anteriormost point of the suture between the nasal and the premaxilla; **L5:** anterior tip of the nasal; **SL6:** end of nasal line at lateral view; **L6:** dorsalmost point of the suture between the frontal and the parietal; **L7:** dorsalmost point of the suture between the parietal and the interparietal; **L8:** curvature at the limit between the occipital condyle and the occipital bone; **L9:** inferior extremity on the boundary between the occipital condyle and the tympanic bulla; **L10:** superiormost point at the middle of the tympanic bulla; **L11:** ventralmost point at the middle of the tympanic bulla; **L12:** anteroventral limit of the tympanic bulla; **L13:** posteriormost point of the molar row; **L14:** anteriormost point of the molar row; **L15:** ventral extent of the suture between maxilla and premaxilla; **L16:** ventral extent of infraorbital foramen; **L17:** anteriormost point of the orbit; **L18:** anteriormost point of the glenoid fossa in the zygomatic bar; **L19:** posterior end of zygomatic bar.

Description of landmarks of mandible view:

L1: Anteroventral border of incisive alveolus; **L2:** Upper extreme anterior border of incisor alveolus; **L3:** Position of greatest inflection of the diastema; **L4:** Anterior edge of the alveolus of first molar; **L5:** Intersection between molar crown and coronoid process in lateral view; **L6:** Tip of the coronoid process; **L7:** Point of maximum curvature between the coronoid and condylar process; **L8:** Dorsal margin of the anterior edge of the articular surface of the condylar process; **L9:** Ventral edge of the articular surface of the condylar process; **L10:** Point of maximum curvature between condylar and angular process; **L11:** Tip of the angular process; **L12:** Intersection between mandibular body and masseteric crest; **L13:** Ventral limits of the mandibular symphysis.

Appendix S4. List of Direct Acyclic Graphs (DAG; see Figure 3 in the main paper) models with its lists of variable considered conditionally independent and the associated linear models. Results of the Phylogenetic Path Analysis (PPA) for all skull views and mandible are presented below. Acronyms: BF= log bite force (N); DI= diet; SZ= log centroid size (cm); SH= principal components of shape.

Model (DAG)	**Conditional Independencies**	**Linear Models**
A	(BF,DI) {SH,SZ}	BF~SZ+SH+DI
B	(BF,DI) {SH}	BF~SH+DI
	(BF,SZ) {SH}	BF~SH+SZ
C	(BF,DI) {SZ}	BF~SZ+DI
D	(DI,SZ) {BF}	DI~BF+SZ
	(DI,SH) {BF}	DI~BF+SH
E	(DI,SZ) {BF,SH}	DI~BF+SH+SZ
	(DI,SH) {BF}	DI~BF+SH
F	(DI,SZ) {BF}	DI~BF+SZ

RESULTS

Results Ventral View	**Model**	**C statistic**	**CICc**	**ΔCICc**	**CICc*wi***	***q***
	A	4.765	23.432	0	0.61	9
	D	10.195	26.231	2.799	0.15	7
	E	10.28	26.317	2.885	0.14	7
	F	8.825	27.492	4.06	0.08	7
	C	11.656	30.322	6.89	0.02	8
	B	29.055	45.091	21.659	0.00	7
Results Lateral View	**Model**	**C statistic**	**CICc**	**ΔCICc**	**CICc*wi***	***q***
	A	1.875	20.542	0	0.87	9
	E	10.256	26.292	5.75	0.05	7
	F	10.28	26.317	5.775	0.05	7
	D	9.075	27.742	7.2	0.02	7
	C	11.656	30.322	9.78	0.01	8
	B	38.851	54.888	34.346	0.00	7
Results Mandible	**Model**	**C statistic**	**CICc**	**ΔCICc**	**CICc*wi***	***q***
	A	2.601	21.268	0	0.66	9
	E	7.923	23.96	2.692	0.17	7
	D	6.189	24.855	3.587	0.11	7
	F	10.28	26.317	5.049	0.05	7
	C	11.656	30.322	9.054	0.01	8
	B	35.348	51.384	30.116	0.00	7

PARTE II

MICROEVOLUÇÃO: VARIAÇÃO ECOMORFOLÓGICA ENTRE POPULAÇÕES

PART II

MICROEVOLUTION: ECOMORPHOLOGICAL VARIATION AMONG POPULATIONS

Capítulo 3

Predictors of intraspecific morphological variability in a tropical hotspot: comparing the influence of random and non-random factors**

Renan Maestri[1*], Rodrigo Fornel[2], Gislene Lopes Gonçalves[3,4], Lena Geise[5], Thales Renato Ochotorena de Freitas[3,6], Ana Carolina Carnaval[7]

[1]*Programa de Pós-Graduação em Ecologia, Universidade Federal do Rio Grande do Sul, Porto Alegre, RS 91501-970, Brazil.*

[2]*Programa de Pós-Graduação em Ecologia, Universidade Regional Integrada do Alto Uruguai e das Missões, Campus Erechim, Erechim RS 99709-910, Brazil.*

[3]*Programa de Pós-Graduação em Biologia Animal, Universidade Federal do Rio Grande do Sul, Porto Alegre, RS 91501-970, Brazil.*

[4]*Instituto de Alta Investigación, Universidad de Tarapacá, Antofagasta 1520, Arica, Chile*.

[5]*Laboratório de Mastozoologia, Departamento de Zoologia, Universidade do Estado do Rio de Janeiro, Rio de Janeiro, RJ 20550-900, Brazil.*

[6]*Departamento de Genética, Universidade Federal do Rio Grande do Sul, Porto Alegre, RS 91501-970, Brazil.*

[7]*City University of New York and CUNY Graduate Center, Marshak Science Building, New York, NY 10031, USA.*

* *Correspondence*: renanmaestri@gmail.com

** Artigo publicado no periódico *Journal of Biogeography* (2016) 43: 2160-2172 (doi: 10.1111/jbi.12815)

Abstract

Aim We describe patterns of skull size and shape variation in an Atlantic forest endemic rodent to test the influence of genetic structure, historical, and environmental variables upon intraspecific morphological variability.

Location South America, Brazil, Atlantic forest.

Methods We analyze subtle differences in skull morphology of *Akodon cursor* through geometric morphometrics applied to 324 individuals from 12 localities distributed throughout the species range. Using cytochrome-*b* gene (cyt-*b*) sequences from 125 individuals (38 localities), we describe underlying patterns of genetic structure and transform them into distance measures that are included in our morphological analyses. We estimate the relative importance of genetic structure, historical variables, and environmental variables on skull size and shape through mixed model selection and Akaike's information criterion.

Results Geographical patterns in skull size are mainly explained by non-random factors related to primary productivity and precipitation, whereas spatial shifts in shape correlate with mitochondrial divergence. Cytochrome-*b* data revealed a phylogeographic break around the Jequitinhonha River, yet striking morphological shifts were observed further south. Differences in palaeostability between regions, and the configuration of rivers, appear as secondary sources of explanation for observed patterns.

Main conclusions Multiple forces explain morphological variation within *A. cursor*. Teasing apart the effects of local adaptation and gene flow may be difficult, but is key to improve our understanding of the drivers of intraspecific morphological variation. Our findings support the view that size is a more labile feature than shape, and that it may more easily break away from constraints imposed by gene flow. The combination of random and non-random factors, together with documented breaks in the distribution of

the Atlantic forest over the Late Quaternary, account for the majority of morphological differences observed in *A. cursor*.

Keywords: *Akodon cursor*, Cytochrome-*b*, environmental variables, geographical barrier, geographical variation, geometric morphometrics, model selection, Quaternary refugia, riverine barrier hypothesis.

Introduction

Although intraspecific patterns of genetic variation in geographical space have been studied extensively over the last decades (Moritz, 1994; Moritz *et al.*, 2000), the mechanisms underlying spatial variation in morphology are particularly difficult to investigate. In part, this complexity stems from the fact that spatial heterogeneity in morphological traits is thought to be maintained both by random and non-random evolutionary forces, tied to past and contemporary conditions (Perez & Monteiro, 2008; Perez *et al*., 2010). Within a species, three elements stand out as important sources of geographical differences in morphology: (1) local natural selection and (2) phenotypic plasticity, imposed by variation in the abiotic or biotic environment, both of which can lead to distinct morphological traits exhibited across populations, and (3) population connectivity, often measured by geographic patterns of neutral genetic variation, whenever shared haplotypes lead to greater morphological similarity.

Previous studies have partially addressed the causes of geographical patterns of morphological change by focusing on non-random causes of trait variation (Mullen *et al.*, 2009; Wang *et al.*, 2013). However, joint analyses of random and non-random evolutionary processes underlying patterns are rarely performed (Perez & Monteiro, 2008; Alvarado-Serrano *et al.*, 2013). In particular, it remains unclear how and why

phenotypic variation is geographically structured in widely distributed species, especially in tropical regions (Monteiro *et al*., 2003; Alvarado-Serrano *et al*., 2013). Understanding the processes that underlie trait variation in these areas is important from a theoretical perspective, though not exclusively. By enabling a deeper understanding of the degree to which distinct phenotypes respond to local environmental pressures (West-Eberhard, 2005), which vary along tropical areas and are expected to keep on changing in multiple ways (Loarie *et al.*, 2009), studies of spatial trait variation can be of conservation relevance (McGuire, 2010).

We investigate the potential roles of historical gene flow (neutral) and selective processes (non-neutral) in structuring geographical patterns of morphological variation in a widely distributed mammal endemic to the Atlantic forest (Ribeiro *et al.*, 2009). In this region, geographic patterns of neutral molecular diversity have been associated with demographic responses to riverine barriers (Pellegrino *et al.*, 2005; Brunes *et al.*, 2010) and the location of putative forest refugia during Late Quaternary climatic shifts (Carnaval & Moritz, 2008; Carnaval *et al.*, 2009; Martins, 2011; Valdez & D'Elia, 2013). However, non-neutral processes are also likely important in shaping both genetic and trait diversity in the Atlantic forest. Because the large area of this biome exposes the local fauna and flora to a wide latitudinal range, it is possible that diverse local environmental conditions may act upon and select for distinct genotypes and phenotypes within species. While taking patterns of neutral gene flow in consideration, we ask whether local patterns of morphological variation within a widespread species of rodent correlate with environmental shifts along the biome.

We describe the spatial patterns of variation in morphology (skull size and shape) and in a neutral genetic marker (within the mitochondrial DNA) along the entire range of the small-bodied *Akodon cursor* (Winge, 1887; Rodentia, Cricetidae, ca. 50 g; Geise,

2012). Gathering data from multiple localities across the range, we apply geometric morphometrics and mitochondrial DNA analysis to explore the association between phenotypes, haplotypes and environmental variables under current and past climates. Our main question asks what variables best predict the spatial patterns of morphological variation observed within this species. If historical population demography and mitochondrial gene flow are important correlates of morphological shifts in space, we expect that divergence in neutral markers across sites will closely match morphological distances. Conversely, if adaptations to local and present-day environmental conditions are mostly responsible for spatial patterns of morphological variation, we expect that variation in primary productivity, climatic conditions, or topography will best predict morphological variation in geographic space.

Expanding on previous observations of how size and shape change in geographical space, we use our data to evaluate the hypothesis that skull size alone is a more labile feature than skull shape, and therefore more prone to be influenced by recent changes in environment - whereas shape variables independent of size are more constrained and reflect genetic-based evolutionary units (Patton & Brylski, 1987; Cardini & Elton, 2009). Simultaneously, we evaluate two potential explanations that account for variation in body size: (1) the hypothesis that decreased temperatures lead to increased body size (Bergmann, 1847; Meiri, 2011), and (2) the hypothesis that increases in primary productivity and precipitation lead to increased size (Cardini *et al.*, 2007; Rodríguez *et al.*, 2008; Cardini *et al.*, 2013). Given the documented links between genetic structure, riverine barriers, and former forest stability in the Atlantic forest (Pellegrino et al., 2005; Thomé *et al.*, 2010; Martins, 2011; Carnaval *et al.*, 2014), we also ask whether the location of rivers, or Late Quaternary forest refugia, adequately predict the spatial distribution of observed morphological shifts.

Materials and Methods

To ask if (and to what extent) neutral genetic variation and environmental conditions explain geographic patterns of morphological shifts in *Akodon cursor*, we performed mixed model comparisons and used Akaike's information criterion (AIC) for model selection (Burnham & Anderson, 2002). In the models, morphological measurements taken from individuals across multiple localities (skull size and shape, analyzed separately) were used as response variables. Predictor variables reflected (1) the neutral genetic distance between localities, measured through mitochondrial DNA (mtDNA) haplotype frequency differences, (2) the spatial configuration of local rivers, (3) the spatial configuration of hypothesized areas of forest refugia throughout the last 120,000 years (120 kyrs), (4) environmental measurements that summarize temperature and topography, and (5) environmental measurements that summarize precipitation and primary productivity. All models included spatial filters to correct for the impact of geographical proximity (spatial autocorrelation) on the patterns observed.

Quantifying spatial patterns of morphological diversity: morphometric analyses

Morphometric analyses were performed on 324 adult specimens of *A. cursor*, all deposited in museum collections and representing 12 localities that cover nearly the entire geographical distribution of the species (Fig. 1). Morphological variation within each locality was assessed with a large number of specimens (17+), hence ensuring that our interpretations were not biased or compromised by insufficient samples. Within each locality, samples of males and females were pooled once we ensured that the sex ratio was not statistically significantly skewed (Appendix S1 in Supporting Information).

On each specimen, 40 landmarks were digitized in the ventral view of the skull with TPSDIG 2 software (Rohlf, 2010), by a single person (RM; see Figure S2 in Appendix S2). After digitalization, the matrix of landmark coordinates was superimposed through a generalized procrustes analysis (GPA) in MORPHOJ 1.06b (Klingenberg, 2011). The GPA was used to remove effects not related to shape (position, orientation, and scale). The size of each individual was assessed through the centroid size (CS) – the square root of the sum of squared distances of each landmark from the centroid of the configuration (Bookstein, 1991). We used the symmetrical component of morphological variation to avoid any noise caused by bilateral asymmetry. We ran a multivariate regression analysis in MORPHOJ 1.06b (Klingenberg, 2011), plotting shape against CS, to test for the presence of allometry in the sample. Because the relationship was significant (P<0.001), with size predicting 17.46% of shape variation, we used the residuals of the regression analysis to create a size-corrected shape matrix that was used in all further analyses.

Quantifying spatial patterns of diversity in a neutral molecular marker

Sequences of the complete cytochrome-*b* gene (1140 bp) were gathered for 125 individuals of *A. cursor* across 38 localities within the Atlantic forest (Geise, 2012, Fig. 1, see Appendix S3). Mitochondrial DNA (mtDNA) has been broadly used in evolutionary studies due to its high probability of recovery and its appropriateness for population-level analyses (Avise, 1994). Given its high mutation rate and lack of recombination, mtDNA is highly sensitive to the effects of subdivision resulting from small population sizes or barriers to gene flow (Moritz, 1994). Because mtDNA is maternally inherited and haploid, it is also more strongly affected by genetic drift (Dodson *et al.*, 1995). In sigmodontine rodents, the mtDNA gene cytochrome *b* (cyt-*b*) has been frequently used for intra and interspecific analyses of genetic variation due to its high

levels of polymorphism (e.g. Geise *et al*. 2001, Valdez & D'Elía, 2013). Sex-biased dispersal presents a concern to mtDNA-based inferences, as the marker can indicate deep divergences despite the presence of gene flow through males (Dávalos & Russell, 2014). Yet nuclear DNA loci, presenting slower rates of evolution and lineage sorting, have been of limited use in intraspecific studies of mammals (e.g. *Deltamys kempi*; Montes *et al.*, 2008). In the absence of sub-genomic data for this species, we here use cyt-*b* information as a proxy for neutral (mitochondrial) gene flow. Because gene flow is inversely correlated with genetic distance (Allendorf & Luikart, 2009), we specifically used Nei (1972) D_A distance among pooled cyt-*b* sequences from each locality as a proxy for neutral gene flow. Distance measures were calculated for each pair of localities based on haplotype frequencies, using DNASP 5.10 (Librado & Rozas, 2009).

Mitochondrial DNA sequence alignment was performed in the Clustal X algorithm implemented in MEGA 6 (Tamura *et al*., 2013). A Bayesian mtDNA tree of *A. cursor* was reconstructed in BEAST 2.0.1 (Drummond & Rambaut, 2007). *Akodon montensis* and *A. lindberghi*, both closely related to *A. cursor* (Geise *et al*., 2001), were used to root the tree. A GTR substitution model with four gamma categories (Tavaré, 1986) was used in the analysis, as it was shown as most appropriate based on an AIC analysis in jMODELTEST 2 (Posada, 2008). The Bayesian tree was estimated with a Yule branching rate prior, assuming uncorrelated and log-normally distributed rate variation across branches (Drummond *et al*., 2006). Each Markov chain was run for 10^7 iterations (burn-in 10,000), with parameters sampled every 1,000 steps. Examination of the Markov chain samples using TRACER 1.4.8 (Rambaut & Drummond, 2007) suggested that the independent chains adequately sampled the same probability distribution, and effective sample sizes (ESS) for all parameters of interest were greater than 200.

To describe the amount of genetic divergence across a major mtDNA break observed in the data set (along the Rio Jequitinhonha), we performed an analysis of molecular variance (AMOVA; Excoffier *et al*., 1992).

Spatial interpolation of genetic distances

Because localities with existing genetic data differed from those with morphometric information (Fig. 1), we were unable to directly compare the patterns of morphological and genetic variance in our study system. To circumvent this issue, we interpolated Nei's D_A genetic distances estimated across all pairs of localities for which the molecular data were available, and used the interpolated values as estimates of divergence across sites for which we only had morphological data (see Figure S3 in Appendix S3). For this, we conducted a principal coordinate analysis (PCoA) on a matrix of genetic distances estimated from the molecular data. Because the first principal component explained 53.02% of variance, and was the only PCo retained under a broken stick criterion (Jackson, 1993), we used the PCo1 scores as z values in an interpolation function ran with an ordinal kriging algorithm (Matheron, 1963). The kriging model has been proven advantageous over other interpolation methods when applied to genetic data (Xue *et al.*, 2005), and it is commonly used to produce genetic maps of spatial variation (Hill *et al.*, 2007). To interpolate the data, we drew a grid of squared cells over the map of the Atlantic forest, and selected a grid cell size based on the average distance between nearest neighbour localities (201.05 km). We then ran the kriging function, using a spherical semivariogram, in QUANTUM GIS 2.2.0 (Nanni *et al*., 2014). The function spatially interpolated the z values using linear combinations whose weights were derived from the semivariogram models, considering both the spatial correlation and the relative position of the data points (Cardini *et al.*, 2013).

Explanatory variables

We generated four sets of explanatory variables for the analysis of morphological variation in space: one depicting the amount of genetic distance across sites, one describing the location of major local rivers, one providing estimates of Late Quaternary climatic stability within the Atlantic forest domain, and one describing contemporary climatic conditions. As proxy for genetic distances between localities, we used the output of the interpolation of PCo1, as previously described. Because it has been proposed that rivers may act (or have acted) as barriers to gene flow in the Atlantic forest (e.g. Pellegrino *et al.*, 2005; Brunes *et al.*, 2010), we also investigated whether the existence of rivers between two given localities predicts their level of morphological similarity. For that, we built a weighted categorical variable by assigning values from 1 to 5 to each locality. Localities within the same interfluvial (i.e., with no rivers between them) received the same value. We weighted the values according to the geographical position of the localities, so that the net difference between each pair of localities equaled the number of rivers that flow between them. For example, if one river flows amidst two localities, the numeric difference between their values was one; if three rivers flows amidst them, the numeric difference was three. Focusing only on the four main rivers associated with genetic breaks in other Atlantic forest species (Fig. 1; Pellegrino *et al.*, 2005; Brunes *et al.*, 2010; Thomé *et al*., 2010), we assigned value one for localities 1 and 2, value two for localities 3 and 4, value four for localities 5, and 8 to 12, and value five for localities 6 and 7 (Fig. 1).

To delimit potential areas of Late Quaternary refugia that may have been isolated from each other and hence prevented gene flow in the past, we used Carnaval *et al*.'s (2014) map of inferred climatic stability of the Atlantic forest over the last 120 kyr. Using

Carnaval *et al*.'s (2014) hypothesis of forest palaeostability for the entire Atlantic forest (available at Dryad: doi:10.5061/dryad.8kclv), we constructed a weighted categorical variable by assigning the values 1 to 7 to each forest refuge, depending on which refuge a locality is located in. To threshold Carnaval *et al*.'s (2014) continuous map, we considered all areas with stability levels of 0.80 or higher as stable, and delimited a refuge as the largest group of adjoining stable grid cells. All localities within a single forest refuge thus received the same value in a reconstructed refuge affiliation variable.

To describe present-day climatic conditions, we extracted environmental data at each locality (Fig. 1) based on maps at 30 arc second resolution. The following four environmental variables were used: annual mean temperature and annual mean precipitation (obtained from the Worldclim bioclimatic database available at http://www.worldclim.org/download), altitude (from ESA GlobCover, available at http://www.esa.int/ESA), and primary productivity (from the Atlas of the Biosphere; http://nelson.wisc.edu/sage/data-and-models/atlas/). These variables were selected because they have been shown to affect mammal size and shape (Monteiro *et al.*, 2003; Cardini *et al.*, 2007; Martínez & Cola, 2011). To minimize the problem of collinearity between variables, and to avoid over-fitting the full model, we ran a principal component analysis (PCA) on the correlation matrix of these four data sets and used the scores of the first two orthogonal axes, selected under broken stick criterion, in our analysis. The main environmental information summarized by each component is presented in Table 1. The first PC accounts for variation in temperature and topography, while second PC is mainly related with primary productivity and precipitation. We extracted the environmental variables by locality on QUANTUM GIS 2.2.0 (Nanni *et al*., 2014), and conducted the PCA on SAM 4.0 (Rangel *et al*., 2010).

Statistical analyses

Size

We tested for differences in size among localities and between males and females using an analysis of variance (ANOVA), including the interaction term between populations and sex. Because the interaction between factors was not significant (stating that sexual dimorphism is uniform across localities, F= 0.95; *P*= 0.49), we pooled all individuals from each locality in our subsequent analyses. With a Tukey's test, we analyzed size differences across every locality pair. In all subsequent analyses, we averaged all size data within localities to avoid pseudoreplication.

To test for the presence of spatial autocorrelation in size, we ran a Moran's I index (Sokal *et al*., 1998), estimating a Moran's correlogram based on six distance classes set up according to a criterion of equal number of pairs within each class. Significant values were identified through 250 permutations. To control for the effects of spatial autocorrelation (Legendre, 1993; Perez *et al.*, 2010), we calculated principal coordinates of neighborhood matrices (PCNM) through a PCoA on a matrix of truncated distances across all pairs of sites (Griffith & Peres-Neto, 2006), which was estimated from georeferenced locality data (the truncation distance defines the neighbourhood boundaries, and was estimated as the maximum distance connecting all sites under a minimum spanning tree criterion). A linear combination of these PCNM variables were then used as spatial filters in the analyses below (Diniz-Filho *et al.*, 2008), to eliminate spatial autocorrelation in the (Moran's I) residuals.

To estimate the importance of genetic structure, rivers, forest refugia and environmental variables on skull size, we ran a mixed model selection using AIC (Burnham & Anderson, 2002), also including the linear combination of spatial filters as a fixed explanatory variable (present in all models) to eliminate the spatial autocorrelation

in the residuals (Diniz-Filho *et al*., 2008). ANOVA and Tukey's test were ran in R 3.03 (R Core Team, 2014). The software SAM 4.0 (Rangel *et al*., 2010) was used for Moran's I analysis, PCNM extraction, and model selection.

Skull shape

We evaluated shape differences among localities and between males and females using a multivariate analysis of variance (MANOVA), including an interaction term between localities and sex. Because the interaction between factors was not significant (λ_{Wilks}= 0.62; Fapprox= 1.21; *P*= 0.054), all individuals from each locality were pooled in the subsequent analyses. Using Mahalanobis distances (Mahalanobis, 1936) and a Neighbour-Joining algorithm of clustering (Saitou & Nei, 1987), we created a tree of morphological distance between localities. To portray shape changes along geographic space, we estimated the consensus shape for each group of localities (defined based on morphological similarity). Shape visualization was obtained using outline interpolation (Klingenberg, 2013).

We tested for spatial autocorrelation in skull shape, using a Mantel test (999 permutations) that employed a matrix of shape distance based on the Mahalanobis distances across the 12 localities and a matrix of geographic distance based on Euclidean distances estimated from the geo-referenced locality data. To control for the effects of spatial autocorrelation, we extracted PCNM variables as previously described. To that end, we averaged the shape data across individuals within each locality, and extracted a linear combination of spatial filters as described for the size analyses.

As a response variable in the shape analysis, we used the regression scores from the size versus shape interaction (Drake & Klingenberg, 2008), exported from the MORPHOJ 1.06b (Klingenberg, 2011), to summarize the shape matrix in one vector.

Thereby, we avoided over-fitting in the full model. Those regression scores are variables associated with shape changes predicted by a regression model (Drake & Klingenberg, 2008). We chose to use the regression scores because they proved to be effective descriptors of shape variation: the association between a matrix of shape distances among each pair of locality (based on Mahalanobis distance) and a distance matrix based on the regression scores among localities was considerably stronger than that between the former and a distance matrix based on the PC1 of shape (r=0.68, and a significant *p* value, compared to r=0.12 and p=0.42). Because the regression scores captured more information than any PC of shape alone, we proceeded to use the former in our analyses.

As in the analyses of size, we ran a mixed model selection using AIC (Burnham & Anderson, 2002) to estimate the importance of genetic structure, rivers, forest refugia and environmental variables on skull shape. As before, we included the linear combination of spatial filters as a fixed explanatory variable to eliminate the spatial autocorrelation in the residuals (Diniz-Filho *et al*., 2008).

MANOVAs, Mantel tests, and morphological trees were conducted with the package "vegan" (Oksanen *et al*., 2013) on R v3.03 (R Core Team, 2014). PCNM extraction and model selection were performed with SAM 4.0 (Rangel *et al*., 2010).

Results

Phylogeography

A Bayesian tree built from cyt-*b* sequences (350 polymorphic sites) demonstrates a well-defined phylogeographic structure within *A. cursor* and depicts two haplogroups (with 5% of divergence; Fig. 2). One of the mitochondrial lineages includes individuals collected south of the Jequitinhonha River (i.e., specimens from the states of São Paulo, Rio de Janeiro, Minas Gerais [except locality XI] and Espírito Santo). The other lineage

is mostly present north of the river (specimens from Paraíba, Pernambuco, Bahia and locality XI in Minas Gerais; Fig. 1). A total of 48.9% of the total genetic variance can be explained by this genetic turnover around the Jequitinhonha river, and significant differentiation is found across localities (ϕ_{ST} = 0.48, P < 0.001; observed variance component = 17.98).

Size

There is significant difference in size between localities (F= 11.94; P< 0.001; Fig. 3). Individuals in the central area of the species distribution (sites 5, 6, and 7) present the largest skulls, individuals from the north (1 to 4) shown intermediate skull sizes, whereas southernmost specimens have smaller skulls. Moran's I coefficient indicate significant positive spatial autocorrelation in the first distance class (~163 km – Moran's I: 0.695, P= 0.004), and negative autocorrelation in the second distance class (~355 km – Moran's I: -0.807, P= 0.004). Other classes showed no spatial autocorrelation.

A mixed model selection analysis indicated that skull size is better explained by environmental variables predominantly associated with primary productivity and precipitation (environmental PC2, Table 2): there is a positive relationship between skull size and both precipitation and primary productivity. The relative AIC weight of this model relative to others suggests a 39% chance that it is the best one to explain overall patterns in skull size. Configuration of forest refugia under Late Quaternary conditions was selected as a predictor of skull size in the model ranked as second-best. River configuration was selected as a predictor in the model ranked in third place. Second and third models are very similar regarding its AICc values, generating a low confidence that one is really better than the other.

Skull shape

Individuals also differ in skull shape across localities (MANOVA λ_{Wilks}= 0.001; Fapprox: 6.00; *P*< 0.001). A tree of morphological distance (Fig. 4) identifies three major groups within the species: (i), individuals from the southern range of the species (localities 8 to 12) compose one group, characterized by proportionally longer snout and incisive foramen than the species mean, (ii) individuals from the central localities (5 to 7) form a second cluster, with proportionally shorter snout and incisive foramen, and larger foramen magnum, and (iii) individuals in the north (localities 1 to 4) are relatively narrower, with a wider maxilla and a shorter snout. Greater morphological distance is observed between the southern and central groups than between the central and northern groups: the skull shape of individuals in the central range is more similar to that of animals living in the northern part of Atlantic forest than with those in the (geographically closer) southern region. There is significant spatial autocorrelation in skull shape (Mantel r= 0.33; *P*= 0.02), indicating that geographically close sites have animals with more similar skull shape than localities further apart.

Skull shape seems to be better predicted by neutral genetic divergence between localities. Nei's D_A genetic distance was the sole predictor in the model showing the lowest AICc (Table 2). AIC weight comparisons indicate a 47% chance that this model best explain skull shape variation in this system. The model ranking in second place placed the configuration of historical forest refugia as the strongest predictor variable. River configuration was selected as a predictor variable in the model that ranked in third place. Historical forest refugia and river configuration returned a roughly equal AICc, placing both variables with virtually the same effect.

Discussion

Recent cross-species eco-morphological comparisons demonstrated that temperature, precipitation and productivity affect the distribution of mammal body size and shape in tropical regions (Rodríguez *et al.*, 2008; Martínez & Cola, 2011; Cardini *et al.*, 2013). Yet, studies addressing this question at the intra-specific level are still rare (Cardini *et al.*, 2007; Marchán-Rivadeneira *et al.*, 2012; O'Keefe *et al.*, 2013; Alvarado-Serrano *et al.*, 2013), and, until now, nonexistent for the Atlantic forest fauna.

Previous studies of the mechanisms driving geographic variation in skull morphology used information about spatial gradients (e.g. latitude and longitude), or spatial correlation, as proxies for genetic distance (Monteiro *et al.*, 2003; Cardini *et al.*, 2007). Implicit in those exercises was the assumption that genetic isolation by distance is pervasive. In *A. cursor*, we found marked geographic structure in the distribution of mitochondrial lineages and explored the use of empirically measured genetic distances between pairwise localities, along with quantifications of environmental differences (present and past), to explore the relative roles of genetic isolation and local adaptation on species traits.

One of our major findings is that the major predictors of morphological shifts along geographical space differ between traits: variation in skull size is better explained by shifts in precipitation and productivity, whereas changes in skull shape are better predicted by genetic divergence. Such discrepancy is remarkable, yet makes sense in the light of previous findings. Our observation that skull size tracks environmental conditions more closely than shape agrees with the general statement that size is a more labile feature (Patton & Brylski, 1987; Cardini & Elton, 2009; Cardini *et al.*, 2013), and, perhaps, easier to change over time.

Mitochondrial DNA sequences suggest that gene flow is geographically structured. Data show a well-marked break between the north and south of the Jequitinhonha River (Fig. 2). This river has also been correlated with genetic structure in *Thamnophilus* passerines (Lacerda *et al*., 2007) and *Gymnodactylus* lizards (Pellegrino *et al.*, 2005). Yet, other Atlantic forest rivers which have been associated with intraspecific genetic structuring - including the Doce River (Pellegrino *et al*., 2005; Brunes *et al*., 2010; Thomé *et al*., 2010) - do not seem to be associated with breaks in the distribution of mitochondrial lineages in the case of *A. cursor*.

In *A. cursor* we do not find strong correspondence between geographic patterns of mitochondrial structure and spatial patterns of variation in size. Instead, we found support for a stronger relation between spatial patterns of variation in size and environmental variation – suggesting a role of local selection pressures as drivers of size evolution. Larger individuals are found in regions of greater primary productivity and greater precipitation; size is also weakly positively associated with temperature, and negative related with topography (Table 1). These findings are at odds with Bergmann's rule, which states that body size and temperature are negatively correlated (Bergmann, 1847; Meiri, 2011). Instead, they are well aligned with recent arguments in favour of a more relevant role of precipitation and productivity in determining size patterns in tropical regions (Cardini *et al.*, 2007; Medina *et al.*, 2007). Since productivity is likely related to the availability of food (e.g. Ashton *et al.*, 2000), it is possible that highly productive environments result in individuals able to better explore the availability of food, shown a prolonged growth, therefore increasing its skull size. In a short-time scale, increases in size would occur via phenotypic plasticity, as more food would result in large individuals at each developmental stage. At a long-time scale, plasticity can lead to adaptation (Travis, 1994), as variation in cranial bones (size and shape of the skull and

mandible) is highly heritable in mice (Palladares *et al.*, 2015), which suggests a genetic basis for differences in bone growth among localities.

Phenotypic plasticity is therefore a potential source of explanation for the observed size changes across localities. This phenomenon is widespread, and may be the first step to produce adaptation (Travis, 1994), yet its effects are difficult to access without controlled experiments, where genetic differences between individuals are keep constant. Even in the presence of only small genetic differences between specimens, like in widespread gene flow, recent evidence suggest that parts of the genome may be kept intact through selection, therefore maintaining different phenotypes across a species range (Poelstra *et al.*, 2014). Consequently, disentangle between plasticity or local adaptation in our scenario is a hard task.

Although speculative, it may be that regional differences in size were also magnified due to allopatry. Despite of the absence of current geographical barrier between the central (5-7) and southern (8-12) localities, these two areas include individuals with contrastingly different sizes – and it has been proposed that they harboured distinct forest refugia during the Pleistocene (Carnaval *et al*., 2009; Martins, 2011). This may explain why forest refugia configuration appears as a major predictor variable of size in the second-best model selected by the AIC. Such morphological difference between central and southern groups also helps to explain the small inferred contribution of genetic differentiation as a predictor of size differences, given that the strongest haplotype break observed within this species is located between the northern group (1-4) and all of those sites south of the Jequitinhonha river.

Selective pressures due to environmental shifts are frequently targeted in intraspecific ecomorphological investigations (Marchán-Rivadeneira *et al*., 2012; O'Keefe *et al*., 2013). Yet, many studies that have detected correlations between skull

shape and ecological settings had failed to consider or account the influence of genetic factors (Monteiro *et al*., 2003; Cardini *et al.*, 2007; Fornel *et al.*, 2010). Contrary to our findings regarding size variation, we found the geographic distribution of shape differences within *A. cursor* to be only slightly related to changes in environmental variables. Our results suggest that neutral genetic structure and gene flow better explain shape changes in space. Random processes related to genetic drift and gene flow have been implied in human skull variation (Relethford, 1994), despite recent evidence of strong influence of non-random factors (Perez & Monteiro, 2008). Moreover, an intraspecific study of *Akodon mollis* demonstrated limited morphological differentiation related to ecological variables, yet found that genetic variables explained a small percentage of skull size and shape variation (Avarado-Serrano *et al*., 2013).

Still, the geographic pattern of skull shape variation was not completely concordant with the distribution of mitochondrial lineages. While southern and northern individuals differ morphologically and genetically, skull shape of those from the central areas is more similar to those living in geographically more distant localities, and genetically more divergent from the sites north of the Jequitinhonha river. As observed for skull size, morphological differences in skull shape are flagged between the southernmost areas and the central plus northern localities. Recent environmental analyses of the entire Atlantic forest demonstrated that the southern range of the forest is climatically distinct from central and northern areas (Carnaval *et al.*, 2014). Moreover, distinctions have been reported in the climate dynamics between the southernmost areas of the forest relative to northern sites (Cheng *et al.*, 2013). Because this shift matches inferred interruptions in the distribution of forest refugia (Martins, 2011) and the approximate location of the Paraíba do Sul river, it is not surprising to find that models

based on forest refugia or river configurations as independent variables were ranked highly (though not highest) as predictors of both size and shape patterns in *A. cursor*.

We demonstrate that multiple forces affect morphological variation within *A. cursor*. Geographically structured gene flow, inferred from mitochondrial DNA lineages, best explain differences in skull shape across localities. Studies that only take environmental information into account when explaining morphological variation in geographical space may hence be missing an important piece of the puzzle. Teasing apart the effects of local adaptation and gene flow may be difficult, but is key to improve our understanding of the drivers of intraspecific morphological variation. In contrast to skull shape, we find that skull size is most strongly tracking differential environmental conditions along the Atlantic forest, likely providing evidence of a response to productivity – either through phenotypically plastic responses, or local adaptation. Our findings support the view that size is a more labile feature than shape (Patton & Brylski, 1987). Further studies are needed to test the generality of our findings and shed light on the drivers of morphological variation in higher taxonomic groups and biogeographical realms.

Acknowledgments

João Alves de Oliveira provided access to specimens in the mammal collection Museu Nacional da Universidade Federal do Rio de Janeiro (MNRJ); Mario de Vivo and Juliana Gualda assisted with collection access at Museu de Zoologia da Universidade de São Paulo (MZUSP). Pedro C. Estrela helped with valuable tips on skull photography, Daniel Galiano assisted with environmental layers, and Sandra M. Hartz, Maria J. Pereira and Leandro D.S. Duarte provided valuable comments on early drafts. Luciana Guedes Pereira helped with DNA sequencing. This research was supported by the Coordenação

de Aperfeiçoamento Pessoal (CAPES) and Conselho Nacional de Desenvolvimento Científico e Tecnológico (CNPq), through fellowships for R. Maestri and G. L. Gonçalves (150115/2014-8), respectively. L. Geise was supported by CAPES, CNPq, Fundação de Amparo à Pesquisa do Estado do Rio de Janeiro (FAPERJ) and UERJ/Prociência. T.R.O. Freitas received financial support from CNPq, CAPES, and Fundação de Amparo à Pesquisa do Estado do RS (FAPERGS). A. Carnaval acknowledges funding by NSF (DEB-1120487, 1343578), FAPESP (BIOTA, 2013/50297-0), and NASA, through the Dimensions of Biodiversity Program.

References

Allendorf, F. W., Luikart, G. (2006) Conservation and the Genetics of Populations. Blackwell Publishing, 642p.

Alvarado-Serrano, D.F., Luna, L. & Knowles, L.L. (2013) Localized versus generalist phenotypes in a broadly distributed tropical mammal: how is intraspecific variation distributed across disparate environments? *BMC Evolutionary Biology*, **13**, 160.

Ashton, K.G., Tracy, M.C. & Queiroz, A. (2000) Is Bergmann's rule valid for Mammals? *The American Naturalist*, **156**, 390-415.

Avise, JC. (1994). Molecular markers, natural history, and evolution. New York: Chapman & Hall.

Bergmann, C. (1847) Über die Verhältnisse der Wärmeokönomie der Thiere zu ihrer Grösse. *Göttinger Studien*, **3**, 595-708.

Bookstein, F.L. (1991) *Morphometric tools for landmark data: Geometry and biology*. Cambridge University Press, Cambridge, UK.

Brunes, T.O., Sequeira, F., Haddad, C.F.B. & Alexandrino, J. (2010) Gene and species trees of a Neotropical group of treefrogs: Genetic diversification in the Brazilian

Atlantic Forest and the origin of a polyploidy species. *Molecular Phylogenetics and Evolution*, **57**, 1120-1133.

Burnham, K.P. & Anderson, D.R. (2002) *Model selection and multimodel inference: a practical information-theoretic approach*. Springer-Verlag, New York.

Cardini, A., Jansson, A. & Elton. S. (2007) A geometric morphometric approach to the study of ecogeographical and clinal variation in vervet monkeys. *Journal of Biogeography*, **34**, 1663-1678.

Cardini, A. & Elton, S. (2009) Geographical and taxonomic influences on cranial variation in red colobus monkeys (Primates, Colobinae): introducing a new approach to 'morph' monkeys. *Global Ecology and Biogeography*, **18**, 248-263.

Cardini, A., Dunn, J., O'Higgins, P. & Elton, S. (2013) Clines in Africa: does size vary in the same way among widespread sub-Saharan monkeys? *Journal of Biogeography*, **40**, 370-381.

Carnaval, A.C. & Moritz, C. (2008) Historical climate modelling predicts patterns of current biodiversity in the Brazilian Atlantic forest. *Journal of Biogeography*, **35**, 1187-1201.

Carnaval, A.C., Hickerson, M.J., Haddad, C.F.B., Rodrigues, M.T. & Moritz, C. (2009) Stability Predicts Genetic Diversity in the Brazilian Atlantic Forest Hotspot. *Science*, **323**: 785-789.

Carnaval, A.C., Waltari, E., Rodrigues, M.T., Rosauer, D., VanDerWal, J., Damasceno, R., Prates, I., Strangas, M., Spanos, Z., Rivera, D., Pie, M.R., Firkowski, C.R., Bornschein, M.R., Ribeiro, L.F. & Moritz, C. (2014) Prediction of phylogeographic endemism in an environmentally complex biome. *Proceedings of the Royal Society B*, **281**, 20141461.

Cheng, H., Sinha, A., Cruz, F.W., Wang, X., Edwards, R.L., d'Horta, F.M., Ribas, C.C., Vuille, M., Stott L.D. & Auler, A.S. (2013) Climate change patterns in Amazonia and biodiversity. *Nature Communications*, **4**: 1411.

Dávalos, L.M. & Russell, A.L. (2014) Sex-biased dispersal produces high error rates in mitochondrial distance-based and tree-based species delimitation. *Journal of Mammalogy*, **95**:781–791.

Diniz-Filho, J.A.F., Rangel, T.F.L.V.B. & Bini, L.M. (2008) Model selection and information theory in geographical ecology. *Global Ecology and Biogeography*, **17**, 479-488.

Dodson, J.J., Colombani, F. & NG, P.K.L. (1995) Phylogeographic structure in mitochondrial DNA of a south-east Asian freshwater fish, *Hemibagrus nemurus* (Siluroidei; Bagridae) and Pleistocene sea-level changes on the Sunda shelf. *Molecular Ecology*, **4**, 331-346.

Drake, A.G. & Klingenberg, C.P. (2008) The pace of morphological change: historical transformation of skull shape in St Bernard dogs. *Proceedings of the Royal Society B*, **275**, 71-76.

Drummond, A.J. & Rambaut, A. (2007) Bayesian evolutionary analysis by sampling trees. *BMC Evolutionary Biology*, **7**, 214.

Drummond, A.J., Ho, S.Y.W., Phillips, M.J. & Rambaut, A. (2006) Relaxed phylogenetics and dating with confidence. *PLoS Biology*, **4**, e88.

Excoffier, L., Smouse, P.E. & Quattro, J.M. (1992) Analysis of molecular variance inferred from metric distances among DNA haplotypes: application to human mitochondrial DNA restriction data. *Genetics*, **131**, 479-491.

Fornel, R., Cordeiro-Estrela, P. & Freitas, T.R.O. (2010) Skull shape and size variation in *Ctenomys minutus* (Rodentia: Ctenomyidae) in geographical, chromosomal

polymorphism, and environmental contexts. *Biological Journal of the Linnean Society*, **101**, 705-720.

Geise, L. (2012) *Akodon cursor* (Rodentia: Cricetidae). *Mammalian Species*, **44**, 33-43.

Geise, L., Smith, M.F. & Patton, J.L. (2001) Diversification in the genus Akodon (Rodentia, Sigmodontinae) in southeastern South America: mitochondrial DNA sequence analysis. *Journal of Mammalogy*, **82**, 92-101.

Griffith, D.A. & Peres-Neto, P.R. (2006) Spatial modeling in ecology: the flexibility of eigenfunction spatial analyses. *Ecology*, **87**, 2603-2613.

Hill, C., Soares, P., Mormina, M., Macaulay, V., Clarke, D., Blumbach, P.B., Vizuete-Forster, M., Forster, P., Bulbeck, D., Oppenheimer, S. & Richards, M. (2007) A mitochondrial stratigraphy for island southeast Asia. *The American Journal of Human Genetics*, **80**, 29-43.

Jackson, D.A. (1993) Stopping rules in Principal Component Analysis: a comparison of heuristical and statistical approaches. *Ecology*, **74**, 2204-2214.

Klingenberg, C.P. (2011) MorphoJ: an integrated software package for geometric morphometrics. *Molecular Ecology Resources*, **11**, 353-357.

Klingenberg, C.P. (2013) Visualizations in geometric morphometrics: how to read and how to make graphs showing shape changes. *Hystrix, the Italian Journal of Mammalogy*, **24**, 15-24.

Lacerda, D.R., Marini, M.A. & Santos, F.R. (2007) Mitochondrial DNA corroborates the species distinctiveness of the Planalto (*Thamnophilus pelzini* Hellmayr, 1924) and the Sooretama (*T. ambiguus* Swainson, 1825) Slaty-antshrikes (Passeriformes: Thamnophilidae). *Brazilian Journal of Biology*, **67**, 873-882.

Legendre, P. (1993) Spatial autocorrelation: trouble or new paradigm? *Ecology*, **74**, 1659-1673.

Librado, P., Rozas, J. 2009. DnaSP v5: A software for comprehensive analysis of DNA polymorphism data. *Bioinformatics* 25: 1451-1452

Loarie, S.R., Duffy, P.B., Hamilton, H., Asner, G.P., Field, C.B. & Ackerly, D.D. (2009) The velocity of climate change. *Nature*, **462**, 1052-1055.

Mahalanobis, P.C. (1936) On the generalized distance in statistics. *Proceedings of the National Institute of Sciences of India*, **2**, 49-55.

Marchán-Rivadeneira, M.R., Larsen, P.A., Phillips, C.J., Strauss, R.E. & Baker R.J. (2012) On the association between environmental gradients and skull size variation in the great fruit-eating bat, *Artibeus lituratus* (Chiroptera: Phyllostomidae). *Biological Journal of the Linnean Society*, **105**, 623-634.

Martínez, J.J. & Cola, V.D. (2011) Geographic distribution and phonetic skull variation in two close species of *Graomys* (Rodentia, Cricetidae, Sigmodontinae). *Zoologischer Anzeiger*, **250**, 175-194.

Martins, F.M. (2011) Historical biogeography of the Brazilian Atlantic forest and the Carnaval-Moritz model of Pleistocene refugia: what do phylogeographical studies tell us? *Biological Journal of the Linnean Society*, **104**, 499-509.

Matheron, G. (1963) Principles of geostatistics. *Economic Geology*, **58**, 1246-1266.

McGuire, J.L. (2010) Geometric morphometrics of vole (*Microtus californicus*) dentition as a new palaeoclimate proxy: shape change along geographic and climatic clines. *Quaternary International*, **212**, 198-205.

Medina, A.I., Martí, D.A. & Bidau, C.J. (2007) Subterranean rodents of the genus *Ctenomys* (Caviomorpha, Ctenomyidae) follow the converse to Bergmann's rule. *Journal of Biogeography*, **34**, 1439-1454.

Meiri, S. (2011) Bergmann's Rule – what's in name? *Global Ecology and Biogeography*, **20**, 203-207.

Monteiro, L.R., Duarte, L.C. & Reis, S.F. (2003) Environmental correlates of geographical variation in skull and mandible shape of the punaré rat *Thrichomys apereoides* (Rodentia, Echimyidae). *Journal of Zoology*, **261**, 47-57.

Montes, M.A., Oliveira, L.F B., Bonatto, S. L., Callegari-Jacques, S.M. & Mattevi, M.S. (2008) DNA sequence analysis and the phylogeographical history of the rodent *Deltamys kempi* (Sigmodontinae, Cricetidae) on the Atlantic Coastal Plain of south of Brazil. *Journal of Evolutionary Biology*, **21**, 1823–1835.

Moritz, C., 1994. Applications of mitochondrial DNA analysis in conservation: critical review. *Molecular Ecology*, **3**, 401-411.

Moritz, C., Patton, J.L., Schneider CJ. & Smith, T.B. (2000) Diversification of rainforest faunas: an integrated molecular approach. *Annual Review of Ecology and Systematics*, **31**, 533-563.

Mullen, L.M., Vignieri, S.N., Gore, J.A. & Hoekstra, H.E. (2009) Adaptive basis of geographic variation: genetic, phenotypic and environmental differences among beach mouse populations. *Proceedings of the Royal Society B*, **276**, 3809-3818.

Nanni, A.S., Descovi-Filho, L., Virtuoso, M.A., Montenegro, D., Willrich, G., Machado, P.H., Sperb, R., Dantas, G.S. & Calazans, Y. (2014) *Quantum GIS*, Guia do Usuário, version 2.2.0 "Valmiera". http://qgis.org/en/site/index.html.

Nei, M., Tajima F. & Tateno Y. (1983) Accuracy of estimated phylogenetic trees from molecular data. II. Gene frequency data. *Journal of Molecular Evolution*, **19**:153-170.

Nei, M. (1972). Genetic distance between populations. Am. Nat. 106: 283–292.

O'Keefe, F.R., Meachen, J., Fet, E.V. & Brannick, A. (2013) Ecological determinants of clinal variation in the cranium of the North American gray wolf. *Journal of Mammalogy*, **94**, 1223-1236.

Oksanen, J., Blanchet, G., Kindt, R., Legendre, P., Minchin, P.R., O'Hara, R.B., Simpson, G.L., Solymos, P., Stevens, M.H.H. & Wagner, H. (2013) *Vegan: Community Ecology Package*. R package version 2.0-7.

Palladares, L.F., Carbonetto, P., Gopalakrishnan, S., Parker, C.C., Ackert-Bicknell, C.L., Palmer, A.A. & Tautz, D. (2015) Mapping of craniofacial traits in outbred mice identifies major developmental genes involved in shape determination. *Plos Genetics*, **11**, e1005607.

Patton, J.L. & Brylski, P.V. (1987) Pocket gophers in alfalfa fields: causes and consequences of habitat-related body size variation. *The American Naturalist*, **130**, 493-506.

Pellegrino, K.C.M., Rodrigues. M.T., Waite, A.N., Morando, M., Yassuda, Y.Y. & Sites JR, J.W. (2005) Phylogeography and species limits in the *Gymnodactylus darwinii* complex (Gekkonidae, Squamata): genetic structure coincides with river systems in the Brazilian Atlantic forest. *Biological Journal of the Linnean Society*, **85**, 13-26.

Perez, S.I. & Monteiro, L.R. (2008) Nonramdom factors in modern human morphological diversification: a study of craniofacial variation in southern south American populations. *Evolution*, **64**, 978-993.

Perez, S.I., Diniz-Filho, J.A.F., Bernal, V. & Gonzalez, P.N. (2010) Spatial regression techniques for inter-population data: studying the relationships between morphological and environmental variation. *Journal of Evolutionary Biology*, **23**, 237-248.

Poelstra, J.W., Vijay, N., Bossu, C.M., Lantz, H., Ryll, B., Müller, I., Baglione, V., Unnenberg, P., Wikelski, M., Grabherr, M.G. & Wolf, J.B.W. (2014) The genomic landscape underlying phenotypic integrity in the face of gene flow in crows. *Science*, **344**, 1410.

Posada, D. (2008) jModelTest: phylogenetic model averaging. *Molecular Biology and Evolution*, **709**, 1253-1256.

R Core Team. (2014) *R: A language for statistical computing*. R Foundation for Statistical Computing, Vienna, Austria. http://www.R-project.org/.

Rambaut, A. & Drummond, A.J. (2007) *Tracer v1.4*. Available from: http://beast.bio.ed.ac.ak/Tracer.

Rangel, T.F., Diniz-Filho, J.A.F. & Bini L.M. (2010) SAM: A comprehensive application for Spatial Analysis in Macroecology. *Ecography*, **33**, 1-5.

Relethford, J.H. (1994) Craniometric variation among modern human populations. *American Journal of Physical Anthropology*, **95**, 53-62.

Ribeiro, M.C., Metzger, J.P., Martensen, A.C., Ponzoni, F.J. & Hirota, M.M. (2009) The Brazilian Atlantic Forest: How much is left, and how is the remaining forest distributed? Implications for conservation. *Biological Conservation*, **142**, 1141-1153.

Rodríguez, M.Á., Olalla-Tárraga, M.Á. & Hawkins, B.A. (2008) Bergmann's rule and the geography of mammal body size in the Western Hemisphere. *Global Ecology and Biogeography*, **17**, 274-283.

Rohlf, F.J. (2010) *TpsDig2*. Departament of Ecology and Evolution, State University of New York, Stony Brook, NY, USA. http://life.bio.sunysb.edu/morph/.

Saitou, N. & Nei, M. (1987) The Neighbor-joining method: a new method for reconstructing phylogenetic trees. *Molecular Biology and Evolution*, **4**, 406-425.

Sokal, R.R., Oden, N.L. & Thomson B.A. (1998) Local spatial autocorrelation in biological variables. *Biological Journal of the Linnean Society*, **65**, 41-62.

Tamura, K., Peterson, D., Peterson, N., Stecher, G., Nei, M. & Kumar, S. (2011) MEGA5: Molecular Evolutionary Genetics Analysis using Maximum Likehood, Evolutionary

Distance, and Maximum Parsimony Methods. *Molecular Biology and Evolution*, **28**, 2731-2739.

Tavaré, S. (1986) Some probabilistic and statistical problems in the analysis of DNA sequences. *Lectures on Mathematics in the Life Sciences*, **17**, 57-86.

Thomé, M.T.C., Zamudio, K.R., Giovanelli, J.G.R., Haddad, C.F.B., Baldissera, F.A. & Alexandrino, J. (2010) Phylogography of endemic toads and post-Pliocene persistence of the Brazilian Atlantic Forest. *Molecular Phylogenetics and Evolution*, **55**, 1018-1031.

Travis, J. (1994) Evaluating the adaptive role of morphological plasticity. *Ecological Morphology* (ed. by P.C. Wainwright and S.M. Reilly), pp. 99-122. The University of Chicago Press, Chicago.

Valdez, L. & D'Elía, G. (2013) Differentiation in the Atlantic Forest: phylogeography of *Akodon montensis* (Rodentia, Sigmodontinae) and the Carnaval-Moritz model of Pleitocene refugia. *Journal of Mammalogy*, **94**, 911-922.

Wang, I.J., Glor, R.E. & Losos, J.B. (2013) Quantifying the roles of ecology and geography in spatial genetic divergence. *Ecology Letters*, **16**, 175-182.

West-Eberhard, M.J. (2005) Developmental plasticity and the origin of species differences. *Proceedings of the National Academy of Sciences*, **102**, 6543-6549.

Xue, F.Z., Wang, J.Z., Hu, P. & Li G.R. (2005) The "Kriging" model of spatial genetic structure in human population genetics. *Acta Genetica Sinica*, **32**, 219-233.

Supporting Information

Additional Supporting Information can be found in the online version of this article:

Appendix S1. Image capture details and specimens by locality.

Appendix S2. Description of the forty landmarks digitized in the skull.

Appendix S3. Specimens and localities used in the Bayesian genetic tree.

Tables

Table 1. Environmental information summarized by principal components 1 and 2 for 12 localities along the Atlantic forest biome.

Climatic Variables	**Component Loadings**	
	PC1	**PC2**
Annual mean temperature	-0.945	0.258
Annual precipitation	0.502	0.695
Topography	0.762	-0.62
Mean primary productivity	0.502	0.732
Proportion explained	**49.4%**	**36.8%**

Table 2. Influence of genetic, historical and environmental variables on skull size and shape of Akodon cursor in the Atlantic forest. Variable selection models based on Akaike information criterion. Acronyms: Gen = genetic distance; River = river hypothesis; P.120kyr = palaeostability over the last 120 kyr; Env1 = PC1 environment; Env2 = PC2 environment. In all models, a linear combination of spatial filters was used as fixed variable to control spatial autocorrelation (not shown).

Model: size ~ Gen + River + P.120kyr + Env1 + Env2				
Variables	r^2	AICc	ΔAIC_c	$AIC_c\ w_i$
Env2	0.780	80.25	0	0.397
P.120kyr	0.739	82.27	2.027	0.144
River	0.694	84.19	3.940	0.055
Gen + Env2	0.805	85.05	4.800	0.036
Env2 + P.120kyr	0.803	85.17	4.921	0.033
Model: shape ~ Gen + River + P.120kyr + Env1 + Env2				
Variables	r^2	AICc	ΔAIC_c	$AIC_c\ w_i$
Gen	0.920	-93.373	0	0.478
P.120kyr	0.880	-90.885	2.487	0.137
River	0.878	-90.718	2.654	0.126
Env1	0.859	-88.952	4.420	0.052
Gen + Env1	0.922	-87.382	5.990	0.023

Figures

Figure 1. Distribution of sampling localities of *Akodon cursor*. (a) South America map showing Atlantic forest narrower definition (black) and broader definition (gray), modified from Carnaval & Moritz (2008). (b) Collection points of morphological data (big white circles numbered in Arabic) and collection points of genetic data (small black circles numbered in Roman, see Appendix S3 for a description of each locality). The *Akodon cursor* range of occurrence from IUCN Red List is shown by gray area. The main rivers are shown in dotted lines.

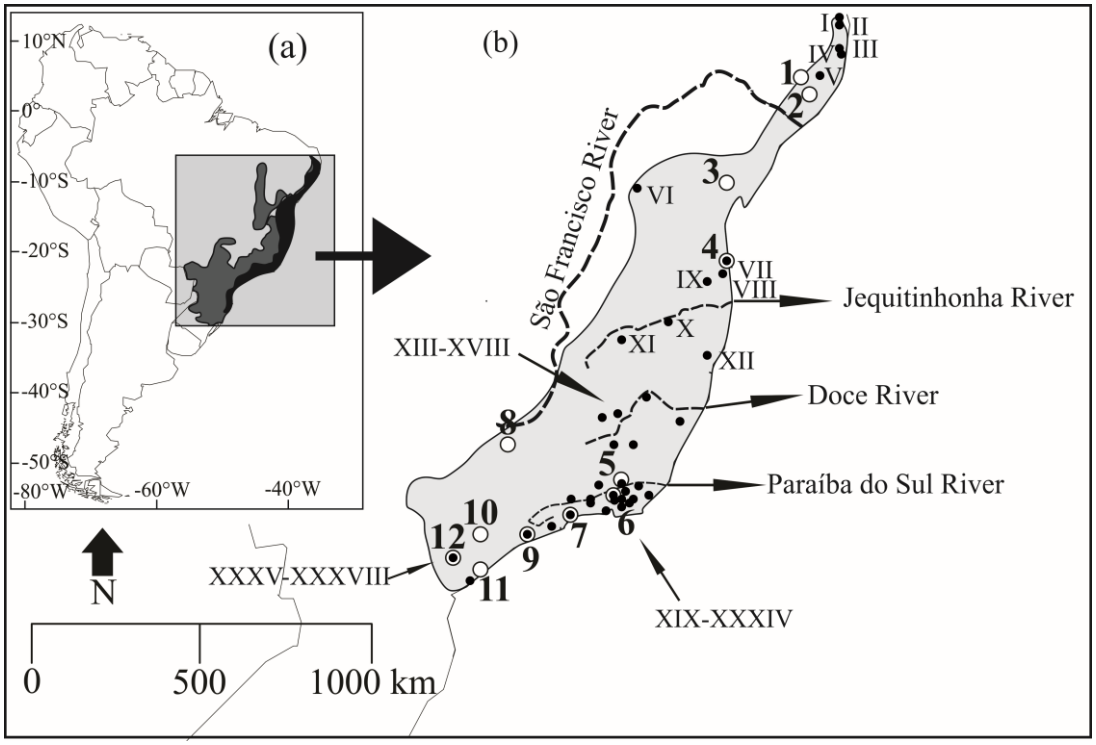

Figure 2. Bayesian inference tree based on complete cytochrome-*b* sequences (1140 bp) showing phylogeographic pattern along the Atlantic forest. Notice major split associated with the location of the Jequitinhonha River (see Figure 1 for locality information).

Figure 3. Boxplots of variability in centroid size among 12 localities, ordered from smallest to largest. Numbers placed under the plots represent localities (see Figure 1). Letters above plots indicate significance in locality comparisons (equal letters mean no significance, distinct letters means significant differences), at $\alpha = 0.05$.

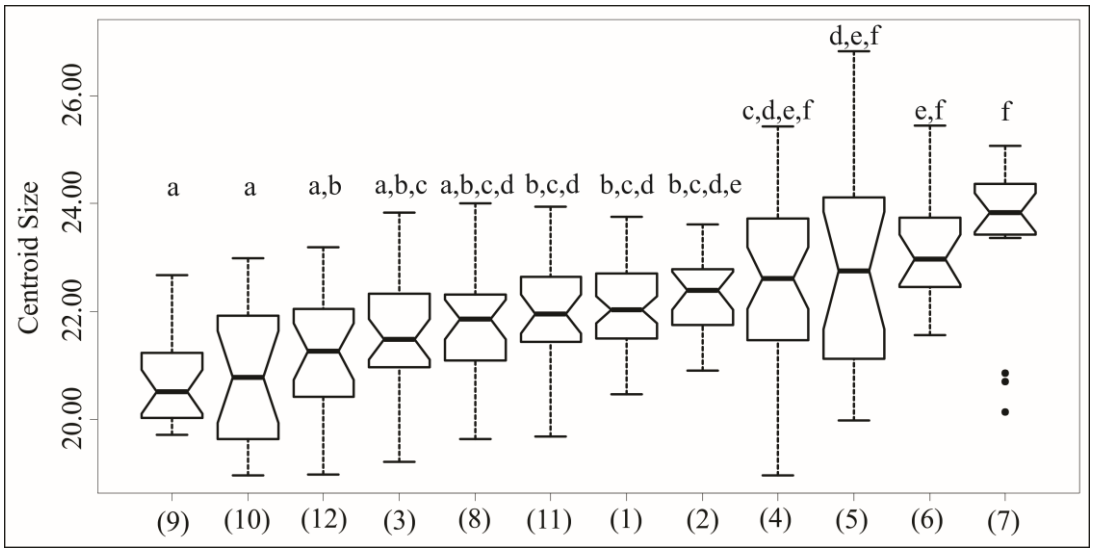

Figure 4. Neighbour-joining tree of Mahalanobis distances showing differences in ventral skull shape (size-corrected) among localities. Shape visualization made from warped outline drawings for a consensus shape for each group (continuous black line). Dashed lines represent the consensus shape for the species. Left: consensus shape of localities 1 to 4; top-right: 8-12; bottom-right: 5-7. Shape differences were increased four times.

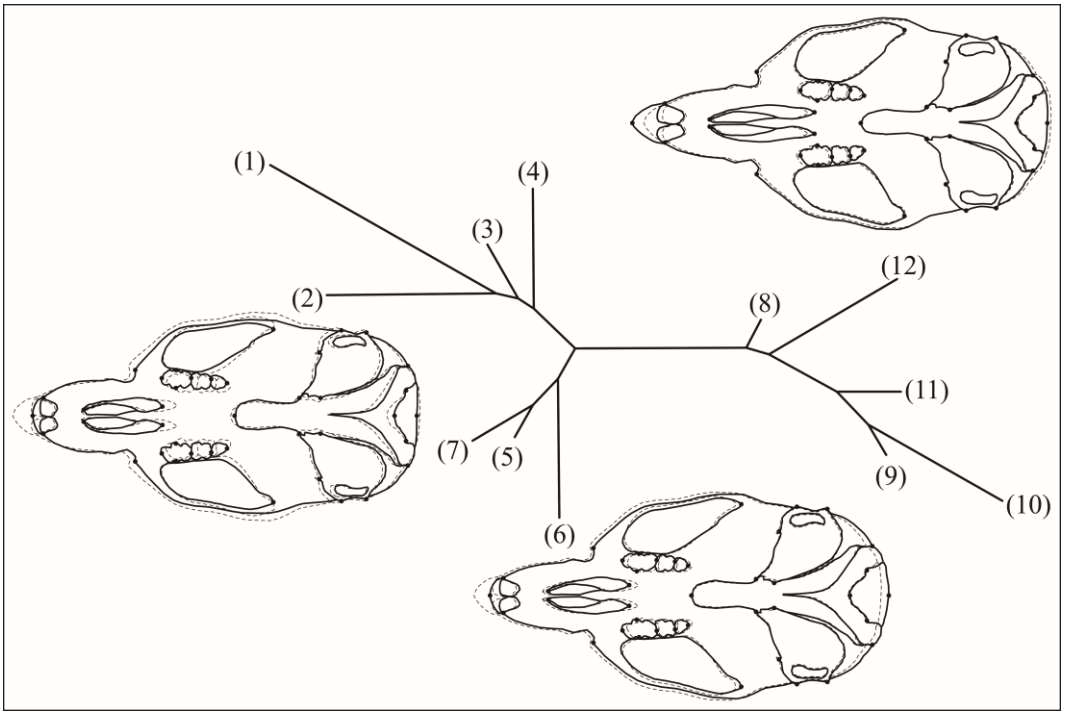

Supporting Information

Appendix S1. Description of the capture of images and lists with the locality number (n), description of the locality, number of individuals by locality, and list of museum collection number of specimens of *Akodon cursor* by locality used in this study:

Digital photographs of the skull in ventral view were taken from specimens deposited in mammal collections at Museu Nacional da Universidade Federal do Rio de Janeiro (MNRJ, Rio de Janeiro, Brazil) and Museu de Zoologia da Universidade de São Paulo (MZUSP, São Paulo, Brazil). Sex and locality data were recorded for all specimens. The sample was composed by 206 males and 118 females. When unavailable in degrees of latitude and longitude, collection sites were recorded as per collection notes, and later georeferenced. To minimize ontogenetic effects, only adult specimens were photographed. Complete eruption of the third molar was used as criterion to distinguish adults from young. Two-dimensional digital images were taken with a Nikon P100 camera with 13.1 megapixel resolution (3648 x 2736), using the macro function of the automatic mode, without flash or zoom. All photos were taken from a standard distance of 50 mm, and specimens were aligned under the same plane.

Because an unequal number of male and female samples could bias our analyses (e.g., sites with proportionally more males could have a mean size higher than sites with proportionally more females), and because we have demonstrated the presence of sexual dimorphism (see text), we tested for the unequal frequency of male and female samples on each site, through chi-square tests. Results of chi-square tests follow: **Garanhuns, Pernambuco:** 23 females, 34 males, χ-squared = 2.12, df = 1, *p*-value = 0.14; **Viçosa, Alagoas:** 8 females, 14 males, χ-squared = 1.63, df = 1, *p*-value = 0.20; **Feira, Bahia:** 12 females, 20 males, χ-squared = 2, df = 1, *p*-value = 0.157; **Ilhéus, Bahia:** 15 females, 24 males, χ-squared = 2.07, df = 1, *p*-value = 0.149; **Além Paraíba, Minas Gerais:** 6

females, 13 males, χ-squared = 2.57, df = 1, *p*-value = 0.108; **Teresópolis, Rio de Janeiro:** 6 females, 13 males, χ-squared = 2.57, df = 1, *p*-value = 0.108; **Angra dos Reis, Rio de Janeiro:** 5 females, 12 males, χ-squared = 2.88, df = 1, *p*-value = 0.089; **Passos, Minas Gerais**: 10 females, 17 males, χ-squared = 1.81, df = 1, *p*-value = 0.179; **Salesópolis, São Paulo:** 7 females, 14 males χ-squared = 2.33, df = 1, *p*-value = 0.126; **Salto de Pirapora, São Paulo:** 6 females, 12 males, χ-squared = 2, df = 1, *p*-value = 0.157; **Iguapé, São Paulo:** 10 females, 19 males, χ-squared = 2.79, df = 1, *p*-value = 0.094; **Capão Bonito, São Paulo:** 9 females, 15 males χ-squared = 1.5, df = 1, *p*-value = 0.22. The results indicate a consistent bias for more males than females in all localities, with deviations toward males ranging between 1.5 to 2.79, with an χ-square mean of 2.18, and a standard deviation of only 0.44. Therefore, unequal presences of males and females are unlikely to affect the estimates of mean size and shape by locality.

List of locality number (in parentheses), locality name and number of individuals by locality:

(1) Garanhuns, Pernambuco 57; (2) Viçosa, Alagoas 22; (3) Feira, Bahia 32; (4) Ilhéus, Bahia 39; (5) Além Paraíba, Minas Gerais 19; (6) Teresópolis, Rio de Janeiro 19; (7) Angra dos Reis, Rio de Janeiro 17; (8) Passos, Minas Gerais 27; (9) Salesópolis, São Paulo 21; (10) Salto de Pirapora, São Paulo 18; (11) Iguapé, São Paulo 29; (12) Capão Bonito, São Paulo 24.

List of museum specimens of *Akodon cursor* used in this study:

Museu Nacional da Universidade Federal do Rio de Janeiro (MN). (1) Garanhuns, Pernambuco: MN - 18928, 18930, 18931, 18933, 18934, 18935, 18936, 18938, 19008, 19009, 19010, 19013, 19014, 19015, 19016, 19017, 19018, 19019, 19020, 19021, 19022, 19023, 19024, 19026, 19027, 19028, 19030, 19031, 19032, 19033, 19034, 19035, 19036, 19038, 19039, 19040, 19041, 19042, 19043, 19044, 19045, 19046, 19047, 19048, 19049,

19114, 19115, 19116, 19118, 19121, 19122, 19123, 19124, 19125, 19126, 19127, 19128. (2) Viçosa, Alagoas: MN – 12944, 13163, 13169, 13175, 13192, 13218, 13228, 18845, 18844, 18846, 18847, 18848, 18849, 18851, 18865, 19055, 19058, 12882, 12887, 12891, 12893, 12894. (3) Feira, Bahia: MN – 18901, 18902, 18903, 18904, 18905, 18906, 18908, 18909, 13124, 18911, 18912, 18913, 18914, 18915, 18916, 18917, 18918, 18919, 18952, 18953, 18954, 18966, 18967, 18968, 18969, 18970, 18971, 18972, 19141, 19142, 19143, 29429. (4) Ilhéus, Bahia: MN - 8867, 8873, 8876, 8887, 8890, 8891, 8895, 8903, 8926, 8941, 8943, 8946, 8953, 8976, 8982, 8983, 8984, 8989, 8990, 8991, 8993, 8994, 8997, 9000, 9011, 9013, 9014, 9028, 9031, 9036, 9039, 9040, 9041, 9042, 9043, 9046, 9047, 9048, 9056. (5) Além Paraíba, Minas Gerais: MN – 5383, 5401, 7325, 7344, 7348, 7384, 7391, 7392,7394, 7396, 7397, 7456, 7458, 7464, 7476, 7478, 7482, 7483, 7486. (6) Teresópolis, Rio de Janeiro: MN – 7106, 7107, 7113, 7114, 7115, 7116, 7117, 7109, 7118, 7119, 7121, 7122, 7123, 7124, 7128, 7130, 7132, 7135, 7136. (7) Angra dos Reis, Rio de Janeiro: MN – 61777, 61778, 61779, 61780, 61781, 61782, 72053, 72065, 72051, 59114, 72071, 72089, 72114, 72115, 72138, 72139, 72101. (8) Passos, Minas Gerais: MN – 12790, 12792, 12793, 12797, 12802, 12805, 12810, 12812, 12813, 12814, 12815, 12816, 12817, 12818, 12825, 12827, 12828, 12830, 12833, 12835, 12836, 12837, 12838, 12840, 12842, 12845, 12846. Museu de Zoologia da Universidade de São Paulo (MZUSP). (9) Salesópolis, São Paulo: MZUSP – 10869, 10881, 10931, 10948, 10864, 24261, 10955, 20947 , 10853, 10823, 10769, 10772, 10854, 10878, 10826, 10856, 10973, 20949, 10843, 10936,10922. (10) Salto de Pirapora, São Paulo: MZUSP – 24527, 24550, 24413, 24610, 24531, 24522, 24563, 24701, 24576, 24526, 24561, 24420, 24534, 24556 , 24530, 24521, 24591, 24542. (11) Iguapé, São Paulo: MZUSP – 10681, 24175, 24169 , 24174, 11450, 26785, 24178, 11417, 26782, 11421, 26797, 26798, 26780, 27410, 26774 , 26784, 26783, 26796, 26781, 22802, 24985, 24981, 24983, 20632,

20635, 20636 , 20637, 20638, 20630. (12) Capão Bonito, São Paulo MZUSP – 29239, 29240, 29241, 29242, 29243, 29244, 29245, 29246, 29218, 29219, 29228, 29229, 29230, 29231, 29232, 29233, 29234 , 29235, 29237, 29238, 27203, 27198, 27204, 27214.

Appendix S2. Description and location of the 40 landmarks digitized on the ventral skull of 324 specimens of *Akodon cursor*.

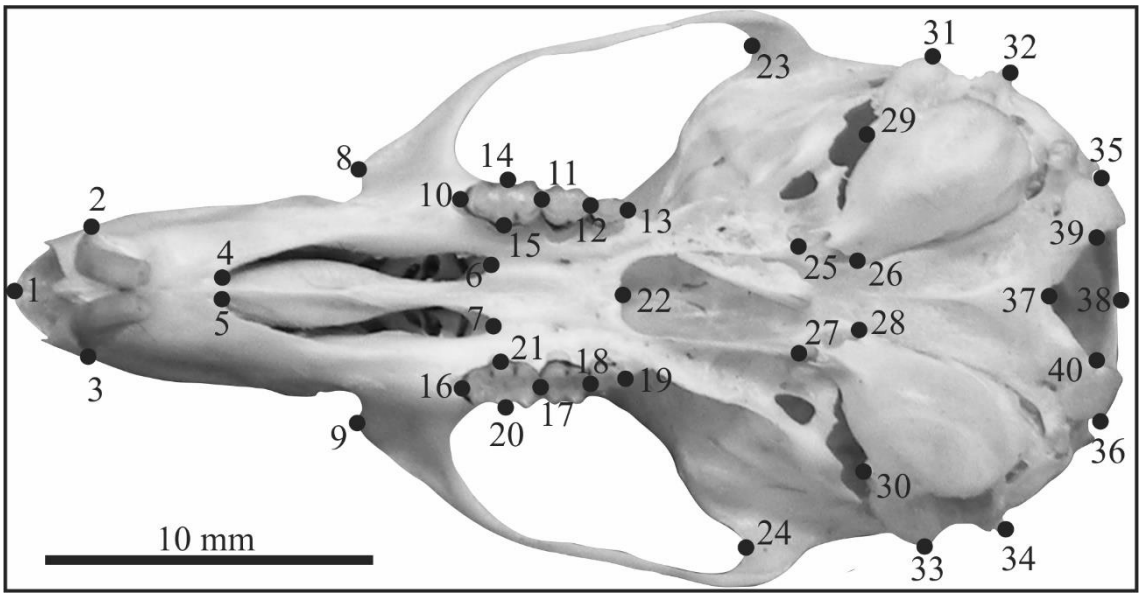

Figure S2 Landmarks digitized in the ventral skull of all *Akodon cursor* specimens. Scale bar= 10 mm.

Landmarks were defined as: 1, anteriormost point of the suture between nasals; 2-3, outermost point of the alveolus of the incisor; 4-5, anteriormost point of the incisive foramen; 6-7, posteriormost point of the incisive foramen; 8-9, rostral end of zygomatic plate; 10-16, anteriormost point of the molar row; 11-17, contact point between first and second molar tooth; 12-19, contact point between second and third molar tooth; 13-19, posteriormost point of the molar row; 14-20, lateral paracone of first molar; 15-21, medial paracone of first molar; 22, posteriormost point of the suture between palatines and the anterior border of the mesopterygoid fossa; 23-24, posteriormost point of the orbit; 25-27, anteriormost point of the eustachian tube; 26-28, suture between basisphenoid and basioccipital at the contact with the auditory bulla; 29-30, anteriormost border of the paramastoid process; 31-33, anteriormost external border of the ectotympanic; 32-34,

posteriormost border of the masseteric tubercle; 35-36, lateralmost point of the occipital condyle; 37, anteriormost point of the foramen magnum; 38, posteriormost point of the foramen magnum; 39-40, anteriormost border of the occipital condyle.

Appendix S3. Specimens of *Akodon cursor* (sampled across the Atlantic Forest) used in the phylogeographical analysis based on cytochrome b sequences. Locality descriptions include acronyms for Brazilian states (e.g. PB) and full names of townships (e.g. Mamanguape). Geographic coordinates are provided in decimal places. Figure S3 shows the spatial distribution of genetic divergence, based on the principal component 1 of a PCoA made using Nei's genetic and geographic distance.

#	Locality	Longitude	Latitude	N	Sample ID
I	PB: Mamanguape	-35.116.667	-6.816.667	1	PB04_0_III
II	PB: Cruz do Espírito Santo	-35.083.333	-7.133.333	4	PHA554, 555, 560, 572
	PB: João Pessoa			1	EF206814
III	PE: Pau D'Alho	-35.166.667	-7.883.333	1	PHA307
IV	PE: Camaragibe	-34.966.667	-8.016.667	16	PHA257, 263, 266, 270, 272, 277, 278, 292, 294, 295, 402,403, 405, 406, 642, 643
V	PE: Jaqueira	-35.783.333	-8.716.667	1	PHA414
VI	BA: Chapada Diamantina	-42.116.667	-12.400.000	20	CD1, 5, 25, 30, 62, 66, 94, 102,103,110,124,137,141,143 157,164,167,178, 219, 242
VII	BA: Ilhéus	-39.056.944	-14.793.056	1	LG173
VIII	BA: Una	-39.183.333	-15.200.000	8	CIT1022, 1023, 929, 930, 931, 933, 934; EDH30
IX	BA: Pau Brasil	-39.650.000	-15.450.000	4	LG190-192, 196
X	MG: Joaíma	-41.016.667	-16.650.000	9	LG747, 477, 485, 500, 501, 503, 506, 524, 527
XI	MG: Turmalina	-42.716.667	-17.283.333	1	YL80
XII	BA: Helvécia	-39.650.000	-17.800.000	1	HGB21
XIII	MG: Capitão Andrade	-41.850.000	-19.066.667	1	LBCE 5552
XIV	MG: Marliéria	-42.733.333	-19.700.000	1	LC98
XV	MG: São Gonçalo do Rio Abaixo	-43.350.000	-19.816.667	1	PE01
XVI	ES: Santa Teresa	-40.600.000	-19.933.333	1	ML124
XVII	MG: Fervedouro	-42.266.667	-20.716.667	7	BRG12, 17, 111, 123, 124,128, 134
XVIII	MG: Viçosa	-42.866.667	-20.750.000	2	GL155; VI17
XIX	RJ: Cambuci	-41.916.667	-21.566.667	5	RBM3_8, 19, 35, 54, 55
XX	MG: Simão Pereira	-43.300.000	-21.950.000	1	BPR7
XXI	RJ: Sumidouro	-42.666.667	-22.033.333	2	LBCE212, 214
XXII	RJ: Nova Friburgo	-42.533.333	-22.283.333	3	LBCE1365, 1367, 1368
XXIII	RJ: Macaé	-41.783.333	-22.350.000	1	GL35
XXIV	RJ: Teresópolis	-42.975.556	-22.417.222	3	LBCE491, 492, 544
XXV	RJ: Cachoeiras de Macau	-42.650.000	-22.450.000	2	FI39; HGBR1
XXVI	RJ: Resende	-44.433.333	-22.466.667	2	HGB55, 56
XXVII	RJ: Casimiro de Abreu	-42.200.000	-22.483.333	2	FU12; SJ24
XXVIII	RJ: Mendes	-43.716.667	-22.516.667	1	LG6
XXIX	RJ: Guapimirim	-42.983.333	-22.533.333	1	ORG46
XXX	RJ: Paracambi	-43.700.000	-22.600.000	3	LBCE734-736
XXXI	RJ: Silva Jardim	-42.383.333	-22.650.000	1	LBCE2358
XXXII	RJ: Rio Bonito	-42.616.667	-22.716.667	2	LG10, 13

XXXIII	RJ: Rio de Janeiro	-43.200.000	-22.916.667	2	LBCE4133, 4139
XXXIV	RJ: Angra dos Reis	-44.447.083	-23.013.278	4	LBCE1315, 1316, 1318; MAM14_2_IV
XXXV	SP: Ubatuba	-45.083.333	-23.400.000	4	LG64; MAM75, 77; MVZ182075
XXXVI	SP: Salesópolis	-45.900.000	-23.650.000	1	MZUSP29257
XXXVII	SP: Capão Bonito	-48.416.667	-24.333.333	3	MAM24, 44; MVZ182072
XXXVIII	SP: Ilha Cardoso	-47.950.000	-25.116.667	2	FMNH141604; HB01

Figure S3. Interpolation of the principal component 1 of a PCoA, using Nei's genetic distance and geographic distance based on 21 localities.

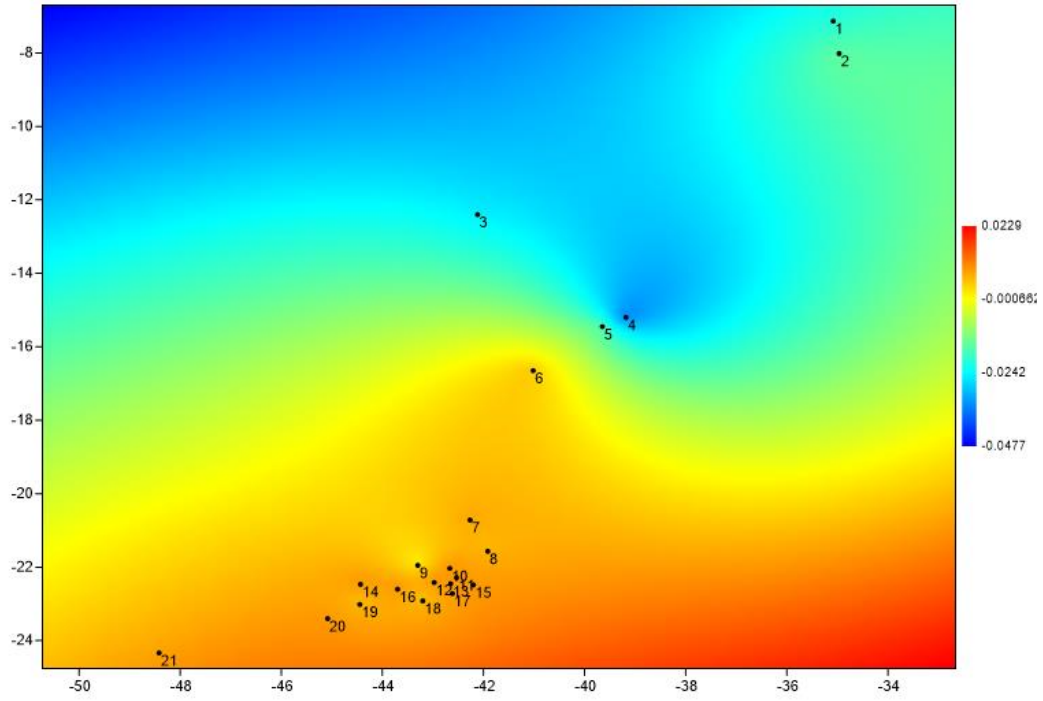

PARTE III

BIOGEOGRAFIA FUNCIONAL: VARIAÇÃO ECOMORFOLÓGICA ENTRE SÍTIOS

PART III

FUNCTIONAL BIOGEOGRAPHY: ECOMORPHOLOGICAL VARIATION AMONG SITES

Capítulo 4

Geographical variation of body size in sigmodontine rodents depends on both environment and phylogenetic composition of communities**

Renan Maestri[1*], André Luís Luza[1], Lurdiana Dayse de Barros[2], Sandra Maria Hartz[1], Augusto Ferrari[3], Thales Renato Ochotorena de Freitas[1,2], Leandro D. S. Duarte[1]

[1]*Programa de Pós-Graduação em Ecologia, Universidade Federal do Rio Grande do Sul, Porto Alegre, RS 91501-970, Brazil.*

[2]*Programa de Pós-Graduação em Biologia Animal, Universidade Federal do Rio Grande do Sul, Porto Alegre, RS 91501-970, Brazil.*

[3]*Instituto de Ciências Biológicas, Universidade Federal do Rio Grande, Rio Grande RS 96203-900, Brazil.*

* *Correspondence*: renanmaestri@gmail.com

** Artigo publicado no periódico *Journal of Biogeography* (2016) 43: 1192-1202 (doi: 10.1111/jbi.12718)

Abstract

Aim Body-size variation in animal assemblages is a widely addressed pattern in biogeographical studies, and is affected by both environmental gradients and phylogenetic constraints. However, no study has yet explored to what extent the association between body-size variation and environmental gradients across broad spatial scales is influenced by the biogeographical distribution of different phylogenetic lineages. In this study, we discriminate the influences of environmental variables and phylogenetic community composition on body-size variation in South American sigmodontine rodents.

Location South America.

Methods We computed the mean body mass of sigmodontine species co-occurring in 1 x 1° cells across South America. For each cell we recorded mean values for three environmental variables. We characterized the phylogenetic composition of sigmodontine assemblages within each cell using phylogenetic fuzzy-weighting and principal coordinates of phylogenetic structure (PCPS). We then partitioned out the influence of environmental factors and the phylogenetic community composition on mean body size.

Results Mean body-size variation was mostly explained by shared influence of phylogenetic community composition (PCPS) and environmental factors (68%), while exclusive influence of PCPS was low (19%), and of environment was even lower (0.47%). Increases in body size were related to increases in annual mean temperature, and the influence of environment on body size was mediated by the distribution of sigmodontine lineages across South America.

Main Conclusions Environment alone was not sufficient to explain body-size variation in sigmodontine assemblages. Rather, environmental gradients interacted with historical processes to determine body-size variation in the Neotropical assemblages. These results

have implications for the way we think of body-size gradients across species assemblages, because any gradient in a trait may be a result of differences in the biogeographical distribution of lineages across space, which should be considered in an explicit context.

Keywords: Bergmann's rule, biogeographical distribution, functional biogeography, macroecology, phylogenetic fuzzy-weighting, phylogenetic uncertainty, variation partitioning.

Introduction

Understanding how the geographical distribution of species traits is affected by both evolutionary history and environmental factors is one of the most exciting and challenging topics in ecology. Macroecological studies on geographical variation in species traits have historically aimed to understand macro-environmental correlates across space (Blackburn & Gaston, 2001; Rodríguez *et al.*, 2008), while macroevolutionary studies have focused on finding evolutionary trends in trait change across phylogeny and time (Cooper & Purvis, 2010; Raia *et al.*, 2010). Macroecology and macroevolution are nevertheless closely connected in attempts to explain spatial and temporal trends in traits. Further, the biogeographical history of lineages potentially affects patterns of trait variation in both space and time (Wiens & Donoghue, 2004). Thus, the variation in species traits could be dependent on the evolutionary history traced by lineages across space, making the phylogenetic background an important determinant of variation in species' life-history strategies across geographical space.

Geographical patterns of body size have been documented for a large number of taxa at the intraspecific level (Martinez *et al.*, 2013; Schiaffini, 2015), across species (Medina *et al.*, 2007; Adams & Church, 2008), and in assemblages (Blackburn &

Hawkins, 2004; Rodríguez *et al.*, 2006; Rodríguez *et al.*, 2008; Olalla-Tárraga *et al.*, 2009; Olalla-Tárraga *et al.*, 2010). One of the most frequently recognized patterns of body-size variation across broad scales is predicted by Bergmann's rule. This rule predicts that the body mass of homeothermic animals tends to increase with latitude and related ecological processes, as a mechanism to optimize heat retention (Bergmann, 1847; Meiri, 2011). This empirical generalization seems to fit well for land mammals of the Northern Hemisphere (Blackburn & Hawkins, 2004; Rodríguez *et al.*, 2006; O'Keefe *et al.*, 2013), although it poorly predicts mammal body-size variation in the Southern Hemisphere (Medina *et al.*, 2007; Rodríguez *et al.*, 2008; Schiaffini, 2015). Rodríguez *et al.* (2008) tested Bergmann's rule across the Americas, discovering that different environmental factors are responsible for variation in body mass of mammals from the Northern and Southern Hemispheres. In the Neotropical region, the largest mammals occur in lowlands at lower latitudes, and body mass is positively related with mean annual temperature, which contradicts Bergmann's rule (Medina *et al.*, 2007; Rodríguez *et al.*, 2008). Furthermore, the universality of Bergmann's rule has been contested due to its low effectiveness in explaining body-size clines in amphibians (Adams & Church, 2008) and other ectothermic organisms (Ashton & Feldman, 2003; Pincheira-Donoso, 2010), and in some bird and mammal lineages (Meiri & Dayan, 2003; Meiri *et al.*, 2004). Moreover, the rule seems to be less strong for small mammals weighing less than 500 g, such as rodents (Freckleton *et al.*, 2003; Meiri & Dayan 2003). The evolution of body mass in different mammalian lineages has been influenced by a complex combination of geography, climate and history (Cooper & Purvis, 2010). Depending on the mammalian clade or region of the planet, a better-adjusted specific model of evolution across time combines the macroecological and macroevolutionary approaches necessary to understand body-mass variation in space and evolution (Cooper & Purvis, 2010).

Therefore, we might expect that patterns of body mass across space are shaped by both ecological (e.g. environment) and evolutionary processes (e.g. biogeographical distribution of lineages in space, model of trait evolution across time).

Sigmodontine rodents generally comprise the largest component of species diversity and biomass of terrestrial mammals in South-American communities. These small mammals occupy a wide range of habitats, with a striking history of colonization and diversification in the Southern Hemisphere. The subfamily Sigmodontinae (family Cricetidae) became one of the most diverse rodent taxa, with at least 400 extant species in 86 genera (Salazar-Bravo *et al.*, 2013; Lessa *et al.*, 2014). This subfamily is distributed mainly across South America, with one genus endemic to Central America (D'Elía, 2003). Today, the most plausible scenario for the arrival of the sigmodontines in South America involves the transoceanic dispersal of one or a few lineages during the Miocene (from Central America), before the closing of the Panamanian Isthmus (Steppan *et al.*, 2004; Parada *et al.*, 2013; Leite *et al.*, 2014). The ancestral sigmodontine lineages began to diversify during the middle to late Miocene, generating an explosive radiation that resulted in the proliferation of the several tribes of Sigmodontinae (Leite *et al.*, 2014). At the time of radiation, the South American small-mammal fauna was represented exclusively by opossums and caviomorph rodents, and the sigmodontine group then had a variety of ecological opportunities to occupy empty niches or to compete for occupied niches. These opportunities resulted in the appearance of adaptations to exploit a wide range of habitats, with the development of arboreal, cursorial, scansorial and semiaquatic lifestyles (Parada *et al.*, 2013; Leite *et al.*, 2014). This remarkable diversity of species and habitats makes this group highly representative of mammals and ideal for studies on large spatial scales.

In this study, we evaluated the influence of macroecological (i.e. environment) and historical factors (i.e. phylogenetic composition of assemblages) on body-mass variation in the Neotropical sigmodontine rodents. We first tested for the phylogenetic signal of body mass across species. Testing for this signal allows us to assess if this trait is (1) conserved (greater resemblance between close relatives than expected under a Brownian model; Losos, 2008), (2) fits a Brownian motion model (Blomberg *et al.*, 2003), (3) fits, to some degree, an Ornstein-Uhlenbeck (OU) model (i.e. the trait evolves under stabilizing selection; Hansen, 1997; Butler & King, 2004; Raia *et al.*, 2010), or (4) the trait is randomly distributed across phylogeny (i.e. complete absence of phylogenetic signal). Then, we partitioned out the influence of macroecological factors and phylogenetic community composition on mean body-mass variation. Variation partitioning sought to determine the strength of both exclusive and shared influences of ecological and evolutionary factors (related to the historical distribution of lineages) for predicting variations in body mass in Sigmodontinae. Some studies have associated body-size variation with environmental variables; more recently, others have taken into account phylogenetic effects on these traits, in order to remove phylogenetic non-independence (Ashton & Feldman, 2003; Diniz-Filho *et al.*, 2007; Olalla-Tárraga *et al.*, 2009; Olalla-Tárraga *et al.*, 2010; Terribile *et al.*, 2012). Nonetheless, to our knowledge, no study has yet explored how the distribution of phylogenetic lineages across geographical space affects the variation in mean body size.

Depending on the model of trait co-variation among species, coupled with the biogeographical history of different species of Sigmodontinae, different geographical patterns can arise. In the simplest scenario, the species are randomly distributed across the continent (i.e. their spatial distribution has no phylogenetic structure), which generates a pattern that can potentially be explained exclusively by environmental variables.

Otherwise, if phylogeny structures the geographical distribution, this pattern may influence the body-size distribution across space, more or less integrated with the effects of environmental variables. Therefore, we ask whether the pattern of body-mass variation across space (when explored in the context of an assemblage) is explained only by environmental variables, or whether it also depends on the biogeographical distribution of lineages across space. We suggest some scenarios that might account for our results. If phylogeny does not structure species across the continent, we would predict that the mean body size by site will be explained by the environment exclusively. However, if phylogeny does structure species assemblages across the continent, the mean body mass by site will depend on a shared effect between the phylogenetic composition of the fauna at particular sites and the environment; under this scenario, the strength of the phylogenetic influence on mean body mass will depend on how strongly the body mass is conserved in phylogeny. If body mass is a highly conserved attribute, we predict that the phylogenetic composition of the fauna at each site will be highly informative in explaining body-mass variation. Otherwise, if body mass is randomly distributed across phylogeny, we predict a small or nonexistent influence of the phylogenetic composition by site on mean body size. If body mass concords with a Brownian motion model of evolution, we predict a notable influence of the phylogenetic composition of the fauna by site on this attribute across assemblages.

Materials and Methods

Occurrence data and body mass of sigmodontine species

Range maps for 245 species of sigmodontines were obtained from IUCN Red List (2008) (available at http://www.iucnredlist.org/). We superimposed the range maps on a grid of 1° x 1° cells (~ 110 x 110 km) covering the entire South American continent.

Island portions and coastal cells containing less than 50% land mass were excluded. We also excluded cells that contained no species. By doing so we were able to define the incidence (presence/absence) of all sigmodontine rodent species in each 1° x 1° cell. A total of 1527 cells describing the occurrence of sigmodontine rodents across South America were used in the data analysis.

For each species, the mean body mass (in grams) was taken from Rodríguez *et al.* (2008) and Bonvicino *et al.* (2008) (Appendix S1 in Supporting Information). Then we computed the mean body mass for the species that co-occurred in each cell. All these procedures were carried out in SAM 4.0 – Spatial Analysis in Macroecology (Rangel *et al.*, 2010).

Phylogenetic tree

The phylogenetic relationships among the 245 sigmodontine species (the subfamily contains nearly 400 species) were reconstructed using the most recent and comprehensive phylogenetic hypothesis for rodents (Fabre *et al.*, 2012). Species not treated by Fabre *et al.* (2012) were embedded in the phylogeny following Parada *et al.* (2013). The phylogenetic tree was constructed using MESQUITE 2.75 (Maddison & Maddison, 2011). Due to absence of a dated phylogenetic hypothesis for this set of species, four nodes were dated using the ages (in millions of years) available in Parada *et al.* (2013). The basal North American sigmodontine *Sigmodon hispidus* was considered as the outgroup. The first dated node consists of the basal split between *S. hispidus* and the other sigmodontine species (15.41 Ma). The second node marks the origin of the tribe Thomasomini (8.24 Ma), while the third node marks the origin of Oryzomyini (7.72 Ma). The fourth node marks the appearance of the tribe Akodontini (7.36 Ma). Using these previously dated nodes, we extrapolated node ages over the entire phylogeny using the

bladj algorithm implemented in PHYLOCOM 4.2 (Webb *et al.*, 2008). Prior to the data analysis, the phylogenetic tree was transformed into an ultrametric tree. We then computed the phylogenetic pairwise patristic distance between species. Nomenclature followed the usage of Musser & Carleton (2005) updated when necessary (Weksler *et al.*, 2006; Patton *et al.*, 2015). We mapped body mass along the phylogeny using the method proposed by Revell (2013), in order to visualize changes in size across the phylogeny and reconstruct the ancestral character. To estimate the ancestral characters at internal nodes, we used a maximum-likelihood criterion (Revell, 2013). The complete tree with terminal tip nodes is available in Appendix S2 in Supporting Information. In order to account for the phylogenetic uncertainty stemming from the polytomies in the tree (the phylogenetic relationships of 92 species have polytomies, all at the genus level or below), we used the analytical strategy proposed by Rangel *et al.* (2015). This methodology consists of simulating a given number of trees. In each random tree, every *phylogenetically uncertain taxon* (PUT: in this study, the 92 species located on nodes with three or more branches) is inserted in a random position within its *most derived consensus clade* (MDCC: the clade in the phylogeny where there is no doubt that the PUT pertains). Thereby, for each polytomy, two branches are chosen at random and reassigned to the same node (within its MDCC), and then each remaining branch from the original polytomy is inserted sequentially, in random order, within the same node (Rangel et al., 2015). This process assures that all new trees are fully resolved. We generated 1,000 trees using this procedure, and subsequent statistical analyses were performed on the 1,000 trees, generating a mean value for each statistic used, and an associated confidence interval. Random trees were generated using the SUNPLIN software (Simulation with Uncertainty for Phylogenetic Investigations, available at http://wsmartins.net/sunplin/) and its integrated function in the R software (R Core Team, 2014).

Phylogenetic signal and phylogenetic structure

We tested the phylogenetic signal in body mass across all 245 mapped species, using the PSR curve (phylogenetic signal representation; Diniz-Filho *et al.*, 2012). This technique was used to test the strength of the phylogenetic signal in the body mass and to measure deviations from the evolutionary scenario based on Brownian motion. The PSR curve allows a comparison of the observed phylogenetic signal with expectations from either the Brownian or the Ornstein-Uhlenbeck (OU) model (Diniz-Filho *et al.*, 2012). The PSR curve consists of a sequential inclusion of eigenvectors from a phylogenetic eigenvector regression (PVR), in a regression between R^2 obtained from PVR and the cumulative eigenvalues of phylogenetic eigenvectors. A linear relationship (45° line) is expected when the trait has evolved under a Brownian motion model of evolution. Deviations from this line indicate either a faster (higher R^2 - positive PSR Area) or a slower (lower R^2 - negative PSR Area) evolution of the trait than that expected under Brownian motion (Diniz-Filho *et al.*, 2012). We also used the Blomberg's K statistic (Blomberg *et al.*, 2003) to test the phylogenetic signal. Values of K less than one indicate less similarity in the attribute than expected under Brownian evolution, whereas K greater than one indicates more similarity in the attribute than expected under Brownian evolution (Blomberg *et al.*, 2003). The phylogenetic-signal tests were conducted in R 3.1.1 (R Core Team, 2014), using the PVR package (Santos *et al.*, 2013), and the "phytools" package (Revell, 2012), on the 1,000 resolved trees, one at a time.

The phylogenetic composition of Sigmodontinae in the grid cells was characterized using the fuzzy-weighting method developed by Pillar & Duarte (2010). Accordingly, the species occurrence in each cell was weighted by their phylogenetic relatedness, resulting in a matrix **P** (1,000 matrices **P**) whose cells are phylogenetic fuzzy

sets defined by rodent species. Then, by running a principal coordinates analysis (PCoA) on matrix **P**, we computed the principal coordinates of phylogenetic structure (PCPS; Duarte, 2011), which describes orthogonal phylogenetic gradients across the array of grid cells (Duarte *et al.*, 2012). The PCPS with higher eigenvalues usually describes broader phylogenetic gradients (i.e. related to the deepest nodes of the phylogenetic tree), while the PCPS with smaller eigenvalues describes finer phylogenetic gradients. A forward-selection procedure was performed to select PCPS that significantly explain the variation in body mass. From 1001 PCPS generated by PCoA on matrix **P**, the forward procedure selected a different subset of PCPS for each phylogenetic tree, usually two or three that typically accounted for more than 50% of the total variation in body mass (PCPS 1 and 9, and sometimes 6). PCPS were generated in R v3.1.1 (R Core Team, 2014), with the "PCPS" package (Debastiani & Duarte, 2014), and forward selection was conducted in the package "packfor" (Dray *et al.*, 2013).

Environmental Variables

We initially selected 15 environmental variables summarizing temperature, elevation, precipitation, evapotranspiration and normalized difference vegetation index. The variables were taken from the WorldClim bioclimatic database (Annual Mean Temperature, Mean Diurnal Temperature Range, Isothermality, Mean Temperature of Warmest Quarter, Mean Temperature of Coldest Quarter, Mean Relative Humidity, Mean Annual Precipitation, Precipitation Seasonality, Precipitation in Wettest Quarter, Precipitation in Driest Quarter; Hijmans *et al.*, 2005), the National Geophysical Data Center (Normalized Difference Vegetation Index, Topographic Range, Topographic Average; http://www.ngdc.noaa.gov/), and the Atlas of the Biosphere (Annual Actual Evapotranspiration, Potential Evapotranspiration; http://www.sage.wisc.edu/atlas/index.

php). Some of these variables have been shown to be important in explaining variation in mammalian body size across the Americas (Blackburn & Hawkins, 2004; Medina *et al.*, 2007; Rodríguez *et al.*, 2008). Environmental variables were summarized through a principal components analysis (PCA) on the correlation matrix in SAM v.4.0 (Rangel *et al.*, 2010), in order to avoid collinearity between predictors. We then selected the orthogonal axes that explained more than 5% of the variation (first three axes) and used the most closely correlated variables within each axis as explanatory variables in the variation partitioning. The first three axes of the PCA analysis summarized ~ 85% of the total environmental variability. The variables selected were Annual Mean Temperature (axis I), Precipitation Seasonality (axis II), and Topographic Average (axis III).

Statistical Analyses

Initially, we tested for spatial autocorrelation on body mass using Moran's *I* test. A Moran's correlogram was constructed using the criterion of equal number of pairs within classes, and the default number of classes provided by SAM v.4.0 (Rangel *et al.*, 2010), and can be found in Appendix S3. To avoid problems of statistical independence of data caused by autocorrelation (Legendre, 1993), we used the method of principal coordinates of neighborhood matrices (PCNM) in redundancy-analysis and variation-partitioning procedures (Borcard & Legendre, 2002). We calculated PCNM variables, performing a principal coordinates analysis on the truncated distance matrix connecting all sites. This procedure generated 544 PCNM variables. Each PCNM represents an independent spatial filter. PCNM having higher eigenvalues represent broad-scale spatial gradients, while PCNM with low eigenvalues represent small-scale gradients (Borcard & Legendre, 2002). Then, we performed a stepwise redundancy analysis (RDA) using all PCNM variables as explanatory factors, and the selected PCPS (PCPS 1, 9 and 6) plus

the three selected environmental variables as response variables. This procedure selected 40 PCNM variables as descriptors of environmental and phylogenetic gradients. Further analysis was performed using the remaining 504 PCNM variables that are not selected in the stepwise procedure (i.e. unrelated to environmental or phylogenetic gradients) as the spatial component potentially responsible for spatial autocorrelation in our response variable (mean body mass per cell). The PCNM analysis was performed with the software SAM v4.0 (Rangel *et al.*, 2010), and the selection of PCNM variables was performed with the R software v3.1.1 (R Development Core Team, 2014), using the forward selection implemented in the packfor package (Dray *et al.*, 2013).

A variance partitioning analysis (Borcard *et al.*, 1992) was performed to estimate the relative contribution of phylogenetic structure (the selected PCPS) and environment (Annual Mean Temperature, Precipitation Seasonality, and Topographic Average) to the mean body mass variation among sites (1 x 1º cell). The 504 PCNM variables were used as covariables in order to control for spatial autocorrelation. Variation partitioning was performed 1,000 times (one analysis for each tree) in R software v3.1.1 (R Development Core Team, 2014), with the vegan package (Oksanen *et al.*, 2013). Linear regressions were used to evaluate the relationship between mean body mass by site and degrees of latitude and longitude.

Results

The species body mass ranged from 12.5 g (*Salinomys delicatus*) to 239.8 g (*Nectomys rattus*). Small- and medium-sized species were recorded throughout the phylogenetic tree (Fig. 1). The three largest species (more than 180 grams) belonged to the tribe Oryzomyini. Body-size of species in tribe Thomasomyini (mean= 73.18; median= 77; SD= 22.38), Oryzomyini (mean= 59.86; median= 55.75; SD= 39.78) and

Clade C (mean= 62.17; median= 58.02; SD= 25.02) are the biggest in average, while tribes Phyllotini (mean= 41.40; median= 42.5; SD= 22.14), Akodontini (mean= 45.34; median= 35; SD= 28.29) and Clade B (mean= 40.59; median= 37.6; SD= 15.95) have the smallest species.

The phylogenetic signal in sigmodontine body mass produced a mean PSR area equal to -0.29 ±0.0026 (min. -0.297, max. -0.275). The PSR area for the original tree (with polytomies) was -0.25. The hypothesis that the PSR area is equal to the null expectation (i.e. absence of any relationship in a trait among species) was rejected ($\bar{P}$ < 0.01), while the probability that the PSR area is equal to a Brownian expectancy was accepted ($\bar{P}$ = 0.98). A somewhat different result was found when we performed Blomberg's K statistic (Blomberg *et al.*, 2003), which had a mean of 0.0004 ±0.0006 ($\bar{P}$ = 0.14), indicating absence of a phylogenetic signal. The original polytomic tree had returned a K = 0.46 (P = 0.001). The PSR area and K statistics are correlated (Diniz-Filho *et al.*, 2012), although the presence of polytomies in phylogenetic trees has a strong effect on K (Davies *et al.*, 2012), while the PSR curve seems to be more robust in the presence of polytomies. According to the PSR curve, body-mass variation across phylogeny carries a phylogenetic signal nearest to a Brownian motion model of evolution. Indeed, the distribution of eigenvalues along the PSR plot (Fig. 2) may indicate that close relatives are less similar than would be expected under the Brownian model of evolution. The evidence of trait plasticity arise because the shape of the PSR curve departs from the Brownian motion towards the null expectation.

The mean body mass per grid cell ranged from 26.82 to 158.9 g. Mean body mass showed a positive relationship to latitude (F = 1077; R^2 = 0.41; $P \leq 0.001$ – Fig. 3). Sites with heavier species (in average) occurred at lower latitudes, mainly in the Caatinga, Cerrado and Amazonia. Lightweight species occurred at sites at high as well as low

latitudes, but were mainly distributed in higher latitudes (Fig. 3). These regions comprised most of the Atlantic Forest biome as well as the Andes, Pampas and Patagonia. The longitudinal gradient had a low influence on the mean assemblage body mass (R^2adj = 0.14; F = 261.4; $P \leq 0.001$).

The relationship between PCPS 1 (34.98% of total variation) and PCPS 2 (21.04%) revealed the dissimilarity between sites according to the differential frequency of given sigmodontine tribes (Fig. 4). Positive values along PCPS 1 characterized sites comprising species belonging to Oryzomyini and Clade C (e.g. *Anotomys* spp., *Ichthyomys* spp.). PCPS 2 segregated sites composed by species of Akodontini and Thomasomyini (negative correlations) from those associated with Phyllotini, Clade B (e.g. *Chelemys* spp., *Abrothrix* spp., *Auliscomys* spp.), and Clade A (e.g. *Euneomys* spp., *Rhagomys* spp.) (positive correlations).

The geographical variation in the phylogenetic composition of sites depicted by PCPS 1 is shown in Fig. 5. Positive values describe mainly sites in Amazonia, Caatinga, and north of Cerrado biome, which showed a distinctive phylogenetic composition owing to the high frequencies of species belonging to Oryzomyini and Clade C. Higher values of annual mean temperature were also associated with Amazonia, Caatinga, and north of Cerrado biome (Fig. 5).

Partitioning out the effects of environment and phylogenetic composition revealed that the shared portion explained the largest variation in mean body mass (Table 1). The independent influences of environment and phylogenetic composition were similar, and each explained a small percentage of total variation. This means that the effect of the environment on body mass depends on the phylogenetic composition at each site. Spatial autocorrelation corresponds to a negligible fraction of the total variation. The standard error resulting from the 1,000 randomized trees, for each R^2, was negligible (always lower

than 1×10^{-5}), which is probably because all polytomies solved were in the shallower nodes of the tree (i.e. genus level), whereas the principal information captured by the key PCPS (PCPS 1 and 2) was related to the deeper nodes of the phylogeny.

PCPS 1 was the most influential phylogenetic predictor of body-mass variation among sites (Table 1). PCPS 6 and 9 showed smaller percentages of explanation. Increases in the dissimilarities in the phylogenetic composition between sites increased the differences in mean body mass across cells. The main environmental factor explaining body mass variation was annual mean temperature, and in a lesser degree topographic average and precipitation seasonality (Table 1).

Discussion

The results showed that historical processes linked to the distribution of sigmodontine lineages across South America affected the pattern of geographical variation in body mass as much as did the ecological variables. Body-mass patterns were highly dependent on the phylogenetic relationships among rodents in Neotropical assemblages, as well as on the degree of phylogenetic conservation in body mass through sigmodontine lineages. This indicates that the phylogenetic identity of species occurring at a given site can represent an important historical factor explaining why some regions had assemblages containing taxa with higher mean body mass than others. Therefore, ignoring the variation in the biogeographical distribution of main lineages may lead to biased estimates of factors explaining trait-variation patterns across space. In our study, the different phylogenetic clades of Sigmodontinae showed complementary patterns of biogeographical distribution. These patterns, coupled with a model of size evolution that agrees with a Brownian pattern, suggest that a simple scenario is plausible, where different tribes exhibit differences in mean body mass (i.e. some tribes contain heavier

species than others do), and each tribe has a larger number of species in particular geographical regions of the continent. Sites at lower latitudes (e.g. Amazonia, Caatinga, and north of Cerrado biome) have species that are on average larger than species from higher latitudes.

The main result presented here (i.e. the shared effect between environment and phylogenetic composition of assemblages) have implications for the way that we think of body size gradients in the context of a species assemblage. Accordingly, it has implications for the validation of the most studied pattern: Bergmann's rule. In North America, for example, Bergmann's rule seems to fit the body-size patterns of mammals well (Blackburn & Hawkins, 2004; Rodríguez *et al.*, 2008). In this region, the patterns show sharp increases in body mass with increasing latitude. The predictions of this rule do not fit well for mice in South America, since body mass tends to decrease with latitude (Fig. 3). This is unsurprising, since the patterns found here are in agreement with previous studies (e.g. Meiri & Dayan, 2003) showing that rodent lineages and mammal taxa weighing 4-500 g fail to conform to Bergmann's rule, while most mammal orders and families conform to the general pattern predicted by this rule (Meiri & Dayan, 2003; lineages of Neotropical rodents were not included in the dataset used by Meiri & Dayan). Since mammal assemblages from South America are dominated by an impressively diverse fauna of rodents with low body mass, the absence of a body-size gradient that agrees with the Bergmann expectation seems to be a logical result. Furthermore, the dominance of rodents is deeply rooted in the historical processes of South American mammalian colonization. Our results suggest that variations in body mass do not depend exclusively on adjustments between body mass and environmental constraints. The distribution of lineages also structures body-mass patterns and community assemblages across the continent, which could blur the effects of environment on body mass.

Therefore, the absence of the effect expected by Bergmann's rule may also be a result of the different biogeographical distributions of lineages across South America. Clades containing species with higher weights on average could be part of the same communities (i.e. Oryzomyini in Amazonia) simply due to historical processes (i.e. dispersal, vicariance), which may have generated the observed body-mass patterns. Nonetheless, in some situations, environmental conditions may have shaped the body mass of species because of natural selection acting through evolutionary time. The shared effect of environmental and phylogenetic community variance affects the pattern of body-mass distribution, and we cannot discriminate between these possibilities. However, we contend that the particular environment of Amazonia, Caatinga and Cerrado contributes to determine the relatively large body mass of the species that are present there, where the higher temperatures probably select for large sizes in mammals (Rodríguez *et al.*, 2008).

While this pattern found here clearly contradicts Bergmann's rule (and this is unsurprising, for the reasons discussed above), it is worth remembering that we are treating Bergmann's rule in an assemblage-based approach. The rule is probably most applicable at the intraspecific level, less so between closely related species, and even less so for this assemblage (Meiri, 2011). Indeed, there is evidence that the rule fits well at the intraspecific level for some South-American mammal species (Gay & Best, 1996; Martinez *et al.*, 2013), although not for others (Schiaffini, 2015). Our study sheds light on the long-standing discussion (Mayr, 1956; James, 1970; Blackburn *et al.*, 1999; Meiri, 2011) of on what level Bergmann's rule should be treated, and helps to show that some early suspicions may be valid, i.e. that differences in size between unrelated species may evolve for reasons that may be unrelated to temperature or latitude (Meiri, 2011). Further, we have shown that any study of body-size at an assemblage scale must take into account

the phylogenetic composition of the assemblages, in order to detect if the biogeographical history of the species involved affect in some way the size pattern found, whether or not it is concordant with Bergmann's rule.

From a historical perspective, biogeographical patterns exhibited by sigmodontine lineages are very complex, owing to the uncertainties regarding the phylogenetic relationships among species and the great diversity linked to their explosive radiation to several habitats and regions (Pardiñas *et al.*, 2002; Schenk *et al.*, 2013). This leads to controversies, and we are still far from a consensus regarding where the origin of the main tribes took place, and how their diversification occurred (D'Elía, 2003; Parada *et al.*, 2013). Despite this, we found that each main sigmodontine lineage is associated with a particular South American region. Concerning the trait variation, studies have frequently found that mammalian body size is strongly heritable across phylogeny (see Smith *et al.*, 2004). Notably, for mammals with a small body size (in general, all sigmodontine species), stronger phylogenetic constraints would be expected than for medium-sized mammals, owing to restrictions in trophic strategies due to the phylogenetically conserved high metabolic rate and the necessity for a continuous supply of high-energy food (Smith *et al.*, 2004). Also, the optimal-body-size theory suggests that mammals should converge to a 100 g weight (Brown *et al.*, 1993; Raia *et al.*, 2010), which would generate a process of stabilizing selection in body size. The PSR curve showed a pattern of body mass across phylogeny that, although it agrees with a Brownian motion model, tends toward lability, which is probably the result of some degree of OU restraining force acting on the trait, generating a stabilizing selection at the shallower nodes of the phylogeny (Fig. 2). This restraining force acting on the trait, and the forcing body mass to an adaptive peak, eventually limits the variation and therefore loses the phylogenetic signal (Bini *et al.*, 2014), as evidenced by the K value and the PSR curve.

Overall, our results suggest that the geography of body size should consider the distribution of lineages in an explicit context. The distribution of lineages and differences in phylogenetic composition among rodent assemblages strongly influenced body-size patterns across space and, consequently, community assemblage. An obvious implication of our results is that environment alone is not sufficient to explain processes that generated body-size patterns in an assemblage-based approach. We also suggest testing the influence of the community phylogeny of mammal clades from the Northern Hemisphere, where patterns of body size conform to Bergmann's rule and small sigmodontine rodents do not occur (but other small Cricetidae rodents occur). In addition, an exploration of community phylogeny across several vertebrate lineages (i.e. all mammals, birds) could lead to better understanding of body-size patterns across broad scales, helping to distinguish between the strength of the historical and environmental processes influencing the body-size variation and community assemblage.

Acknowledgments

We are grateful to Bruce D. Patterson for his helpful suggestions and comments on the manuscript, to Vanderlei J. Debastiani for his help with the R functions, and to Taís F.R. Guimarães for her help with Figure 3. We also thank François Guilhaumon, Pablo A. Martinez, and three anonymous referees for their constructive criticisms and helpful comments that improved the quality of this manuscript. R.M., A.L.L. and L.D.B. received student fellowships from the Coordenadoria de Aperfeiçoamento de Pessoal de Nível Superior (CAPES). S.M.H. and L.D.S.D. received financial support from the Conselho Nacional de Desenvolvimento Científico e Tecnológico (CNPq – grants 306816/2010-5 and 303534/2012-5). T.R.O.F. received financial support from CNPq, CAPES, and the Fundação de Amparo à Pesquisa do Estado do Rio Grande do Sul (Fapergs). This study

was initially developed during a postgraduate course on community phylogenetics at the Universidade Federal do Rio Grande do Sul, supported by the Programa de Pós-Graduação em Ecologia.

References

Adams, D.C. & Church, J.O. (2008) Amphibians do not follow Bergmann's rule. *Evolution*, **62**, 413-420.

Ashton, K.G. & Feldman, C.R. (2003) Bergmann's rule in non-avian reptiles: turtles follow it, lizards and snakes reverse it. *Evolution*, **57**, 1151-1163.

Bergmann, C. (1847) Über die Verhältnisse der Wärmeokönomie der Thiere zu ihrer Grösse. *Göttinger Studien*, **3**, 595-708.

Bini, L.M., Villalobos, F. & Diniz-Filho, J.A.F. (2014) Explorando patrones en rasgos macroecológicos utilizando regresión secuencial de autovectores filogenéticos. *Ecosistemas*, **23**, 21–26.

Blackburn, T.M. & Gaston, K.J. (2001) Linking patterns in macroecology. *Journal of Animal Ecology*, **70**, 338-352.

Blackburn, T.M., Gaston, K.J. & Loder, N. (1999) Geographic gradients in body size: a clarification of Bergmann's rule. *Diversity and Distributions*, **5**, 165-174.

Blackburn, T.M. & Hawkins, B.A. (2004) Bergmann's rule and the mammal fauna of northern North America. *Ecography*, **27**, 715-724.

Blomberg, S.P., Garland, T. & Ives, A.R. (2003) Testing for phylogenetic signal in comparative data: behavioral traits are more labile. *Evolution*, **57**, 717-745.

Bonvicino, C.R., Oliveira, J.A. & D'Andrea, P.S. (2008) *Guia dos roedores do Brasil, com chaves para gêneros baseadas em caracteres externos*. Rio de Janeiro, Centro Pan-Americano de Febre Aftosa, OPAS/OMS.

Borcard, D. & Legendre, P. (2002) All-scale spatial analysis of ecological data by means of principal coordinates of neighbor matrices. *Ecological Modelling*, **153**, 51-68.

Borcard, D., Legendre, P. & Drapeau, P. (1992) Partialling out the spatial component of ecological variation. *Ecology*, **73**, 1045-1055.

Brown, J.H., Marquet, P.A. & Taper, M.L. (1993) Evolution of body size: consequences of an energetic definition of fitness. *The American Naturalist*, **142**, 573-584.

Butler, M.A. & King, A.A. (2004) Phylogenetic comparative analysis: a modeling approach for adaptive evolution. *The American Naturalist*, **164**, 683-695.

Cooper, N. & Purvis, A. (2010) Body size evolution in mammals: complexity in tempo and mode. *The American Naturalist*, **175**, 727-738.

Davies, T.J., Kraft, N.J.B., Salamin, N. & Wolkovich, E.M. (2012) Incompletely resolved phylogenetic trees inflate estimates of phylogenetic conservatism. *Ecology*, **93**, 242-247.

D'Elía, G. (2003) Phylogenetics of Sigmodontinae (Rodentia, Muroidea, Cricetidae), with special reference to the akodont group, and with additional comments on historical biogeography. *Cladistics*, **19**, 307-323.

Debastiani, V.J. & Duarte, L.D.S. (2014) PCPS – an R package for exploring phylogenetic eigenvectors across metacommunities. *Frontiers of Biogeography*, **6**, 144-148.

Diniz-Filho, J.A.F., Bini, L.M., Rodríguez, M.Á., Rangel, T.F.L.V.B. & Hawkins, B.A. (2007) Seeing the forest for the trees: partitioning ecological and phylogenetic components of Bergmann's rule in European Carnivora. *Ecography*, **30**, 598-608.

Diniz-Filho, J.A.F., Rangel, T.F., Santos, T. & Bini, L.M. (2012) Exploring patterns of interspecific variation in quantitative traits using sequential phylogenetic eigenvector regressions. *Evolution*, **66**, 1079-1090.

Dray, S., Legendre, P. & Blanchet, G. (2013) *Packfor: Forward selection with permutation*. R package version 0.0-8. R Foundation for Statistical Computing, Vienna, Austria. Available at: https://www.R-project.org/ (accessed 14 December 2015).

Duarte, L.D.S. (2011) Phylogenetic habitat filtering influences forest nucleation in grasslands. *Oikos*, **120**, 208-215.

Duarte, L.D.S., Prieto, P.V. & Pillar, V.D. (2012) Assessing spatial and environmental drivers of phylogenetic structure in Brazilian *Araucaria* forests. *Ecography*, **35**, 952-960.

Fabre, P., Hautier, L., Dimitrov, D. & Douzery, E.J.P. (2012) A glimpse on the pattern of rodent diversification: a phylogenetic approach. *BMC Evolutionary Biology*, **12**, 88.

Freckleton, R.P., Harvey, P.H. & Pagel, M. (2003) Bergmann's rule and body size in mammals. *The American Naturalist*, **161**, 821-825.

Gay, S.W. & Best, T.L. (1996) Relationships between abiotic variables and geographic variation in skulls of pumas (*Puma concolor*: Mammalia, Felidae) in North and South America. *Zoological Journal of the Linnean Society*, **117**, 259-282.

Hansen, T.F. (1997) Stabilizing selection and the comparative analysis of adaptation. *Evolution*, **51**, 1341-1351.

Hijmans, R.J., Cameron, S.E., Parra, J.L., Jones, P.G. & Jarvis, A. (2005) Very high resolution interpolated climate surfaces for global land areas. *International Journal of Climatology*, **25**, 1965-1978.

James, F.C. (1970) Geographic size variation in birds and its relationship to climate. *Ecology*, **51**, 365-390.

Legendre, P. (1993) Spatial autocorrelation: trouble or new paradigm? *Ecology*, **74**, 1659-1673.

Leite, R.N., Kolokotronis, S., Almeida, F.C., Werneck, F.P., Rogers, D. & Weksler, M. (2014) In the wake of invasion: tracing the historical biogeography of the South American cricetid radiation (Rodentia, Sigmodontinae). *PLoS ONE,* **9**, e100687.

Lessa, E.P., Cook, J.A., D'Elía, G. & Opazo, J.C. (2014) Rodent diversity in South America: transitioning into the genomics era. *Frontiers in Ecology and Evolution*, **2**, 39.

Losos, J.B. (2008) Phylogenetic niche conservatism, phylogenetic signal and the relationship between phylogenetic relatedness and ecological similarity among species. *Ecology Letters*, **11**, 995-1007.

Maddison, W.P. & Maddison, D.R. (2011) *Mesquite: A modular system for evolutionary analysis*. Version 2.75. http://mesquiteproject.org.

Martinez, P.A., Marti, D.A., Molina, W.F. & Bidau, C.J. (2013) Bergmann's rule across the equator: a case study in *Cerdocyon thous* (Canidae). *Journal of Animal Ecology*, **82**, 997-1008.

Mayr, E. (1956) Geographical character gradients and climatic adaptation. *Evolution*, **10**, 105-108.

Medina, A.I., Martí, D.A. & Bidau, C.J. (2007) Subterranean rodents of the genus *Ctenomys* (Caviomorpha, Ctenomyidade) follow the converse to Bergmann's rule. *Journal of Biogeography*, **34**, 1439-1454.

Meiri, S. (2011) Bergmann's rule – what's in a name? *Global Ecology and Biogeography*, **20**, 203-207.

Meiri, S. & Dayan, T. (2003) On the validity of Bergmann's rule. *Journal of Biogeography*, **30**, 331-351.

Meiri, S., Dayan, T. & Simberloff, D. (2004) Carnivores, biases and Bergmann's rule. *Biological Journal of the Linnean Society*, **81**, 579-588.

Musser, G.G. & Carleton, M.D. (2005) "Superfamily Muroidea". *Mammal species of the world: A taxonomic and geographic reference* (ed. by D.E. Wilson and D.M. Reeder), pp. 894-1531. Johns Hopkins University Press, Baltimore, USA.

O'Keefe, F.R., Meachen, J., Fet, E.V. & Brannick, A. (2013) Ecological determinants of clinal morphological variation in the cranium of the North American gray wolf. *Journal of Mammalogy*, **94**, 1223-1236.

Oksanen, J., Blanchet, F.G., Kindt, R., Legendre, P., Minchin, P.R., O'Hara, R.B., Simpson, G.L., Solymos, P., Stevens, M.H.H. & Wagner, H. (2013) *Vegan: Community Ecology package*. R package version 2.0-10.

Olalla-Tárraga, M.Á., Bini, L.M., Diniz-Filho, J.A.F. & Rodríguez, M.Á. (2010) Cross-species and assemblage-based approaches to Bergmann's rule and the biogeography of body size in *Plethodon* salamanders of eastern North America. *Ecography*, **33**, 362-368.

Olalla-Tárraga, M.Á., Diniz-Filho, J.A.F., Bastos, R. & Rodríguez, M.Á. (2009) Geographic body size gradients in tropical regions: water deficit and anuran body size in the Brazilian Cerrado. *Ecography*, **32**, 581-590.

Parada, A., Pardiñas, U.F.J., Salazar-Bravo, J., D'Elía, G. & Palma, R.E. (2013) Dating an impressive Neotropical radiation: molecular time estimates for the Sigmodontinae (Rodentia) provide insights into its historical biogeography. *Molecular Phylogenetics and Evolution*, **66**, 960-968.

Pardiñas, U.F.J., D'Elía, G. & Ortiz, P.E. (2002) Sigmodontinos fósiles (Rodentia, Muroidea, Sigmodontinae) de América del Sur: estado actual de su conocimiento y prospectiva. *Mastozoología Neotropical*, **9**, 209-252.

Patton, J.L., Pardiñas, U.F.J. & D'Elía, G. (2015) *Mammals of South America Volume 2: Rodents*. University of Chicago Press, Chicago.

Pillar, V.D. & Duarte, L.D.S. (2010) A framework for metacommunity analysis of phylogenetic structure. *Ecology Letters*, **13**, 587-596.

Pincheira-Donoso, D. (2010) The balance between predictors and evidence and the search for universal macroecological patterns: taking Bergmann's rule back to its endothermic origin. *Theory in Biosciences*, **129**, 247-253.

R Core Team (2014) R: a language and environment for statistical computing. R Foundation for Statistical Computing, Vienna, Austria. Available at: https://www.R-project.org/ (accessed 14 December 2015).

Raia, P., Carotenuto, F. & Meiri, S. (2010) One size does not fit all: no evidence for an optimal body size on islands. *Global Ecology and Biogeography*, **19**, 475-484.

Rangel, T.F., Diniz-Filho, J.A.F. & Bini, M. (2010) SAM: a comprehensive application for Spatial Analysis in Macroecology. *Ecography*, **33**, 46-50.

Rangel, T.F., Colwell, R.K., Graves, G.R., Fučíková, K., Rahbek, C. & Diniz-Filho, J.A.F. (2015) Phylogenetic uncertainty revisited: implications for ecological analyses. *Evolution*, **69**, 1301-1312.

Revell, L.J. (2012) phytools: an R package for phylogenetic comparative biology (and other things). *Methods in Ecology and Evolution*, **3**, 217-223.

Revell, L.J. (2013) Two new geographical methods for mapping trait evolution on phylogenies. *Methods in Ecology and Evolution*, **4**, 754-759.

Rodríguez, M.Á., López-Sañudo, I.L. & Hawkins, B.A. (2006) The geographic distribution of mammal body size in Europe. *Global Ecology and Biogeography*, **15**, 173-181.

Rodríguez, M.Á., Ollala-Tárraga, M.Á. & Hawkins, B.A. (2008) Bergmann's rule and the geography of mammal body size in the Western Hemisphere. *Global Ecology and Biogeography*, **17**, 274-283.

Salazar-Bravo, J., Pardiñas, U.F.J. & D'Elía, G. (2013) A phylogenetic appraisal of Sigmodontinae (Rodentia, Cricetidae) with emphasis on phyllotine genera: systematics and biogeography. *Zoologica Scripta*, **42**, 250-261.

Santos, T., Diniz-Filho, J.A.F., Rangel, T.F. & Bini, M. (2013) PVR: *Computes phylogenetic eigenvectors regression (PVR) and phylogenetic signal-representation curve (PSR) (with null and Brownian expectations).* R package version 0.2.1. R Foundation for Statistical Computing, Vienna, Austria. Available at: https://www.R-project.org/ (accessed 14 December 2015).

Schenk, J.J., Rowe, K.C. & Steppan, S.J. (2013) Ecological opportunity and incumbency in the diversification of repeated continental colonizations by muroid rodents. *Systematic Biology*, **62**, 837-864.

Schiaffini, M.I. (2016) A test of the Resource's and Bergmann's rules in a widely distributed small carnivore from southern South America, *Conepatus chinga* (Molina, 1782) (Carnivora: Mephitidae). *Mammalian Biology*, **81,** 73-81.

Smith, F.A., Brown, J.H., Haskell, J.P., Lyons, S.K., Alroy, J., Charnov, E.L., Dayan, T., Enquist, B.J., Ernest, S.K.M., Hadly, E.A., Jones, K.E., Kaufman, D.M., Marquet, P.A., Maurer, B.A., Niklas, K.J., Porter, W.P., Tiffney, B. & Willing, M.R. (2004) Similarity of mammalian body size across the taxonomic hierarchy and across space and time. *The American Naturalist*, **163**, 672-691.

Steppan, S.J., Adkins, R.M. & Anderson, J. (2004) Phylogeny and divergence-date estimates of rapid radiations in muroid rodents based on multiple nuclear genes. *Systematic Biology*, **53**, 533-553.

Terribile, L.C., Diniz-Filho, J.A.F., Lima-Ribeiro, M.S. & Rodríguez, M.Á. (2012) Integrating phylogeny, environment and space to explore variation in macroecological

traits of Viperidae and Elapidae (Squamata: Serpentes). *Journal of Zoological Systematics and Evolutionary Research*, **50**, 202-209.

Webb, C.O., Ackerly, D.D. & Kembel, S.W. (2008) Phylocom: software for the analysis of phylogenetic community structure and trait evolution. *Bioinformatics*, **24**, 2098-2100.

Weksler, M., Percequillo, A.R. & Voss, R.S. (2006) Ten new genera of Oryzomyine rodents (Cricetidae: Sigmodontinae). *American Museum Novitates*, **3537**, 1-29.

Wiens, J.J. & Donoghue, M.J. (2004) Historical biogeography, ecology and species richness. *Trends in Ecology and Evolution*, **19**, 639-644.

Supporting Information

Additional Supporting Information may be found in the online version of this article:

Appendix S1. Body mass for each of the 245 sigmodontine species used in this study.

Appendix S2. Phylogenetic tree used for this study.

Appendix S3. Moran's correlogram for body mass.

Tables

Table 1. Variation partitioning results with mean body mass of sigmodontine rodents by site as the response variable, against environmental variables by site and phylogenetic composition of each site as the explanatory variables. Standard coefficients and *F* statistics for each predictor separately are also shown. The values shown are the arithmetic mean for the statistics extracted from the variation partitioning performed on each of the 1,000 randomized trees. Standard error for each mean value was always lower than 1×10^{-5}.

	Mean Body Mass by cell			
Source of variation	$\bar{r}^2_{adj}$	$\bar{S}$td. Coeff.	$\bar{F}$	$\bar{P}$
Environment	**0.0047**		**473.78**	**0.001**
Annual Mean Temperature		0.738	1401.3	
Precipitation Seasonality		0.017	1.84	
Topographic Average		0.069	309.18	
Phylogenetic composition	**0.1938**		**891.62**	**0.001**
PCPS1		0.736	1801.8	
PCPS6		-0.162	41.26	
PCPS9		-0.263	113.52	
Shared component	**0.6836**			
Spatial Filters	-0.0873		1.32	
Residuals	0.2052			
Total	1.000			

Figures

Figure 1. Distribution of body mass (grams) across the phylogeny of the Neotropical sigmodontine rodents classified into main tribes. Ancestral characters were estimated using maximum likelihood. Clade A, B and C refers to species that are not formally assigned to a tribe. *Sigmodon hispidus* appears as outgroup. Phylogenetic topology follows Fabre *et al.* (2012), and was complemented and dated according to Parada *et al.* (2013).

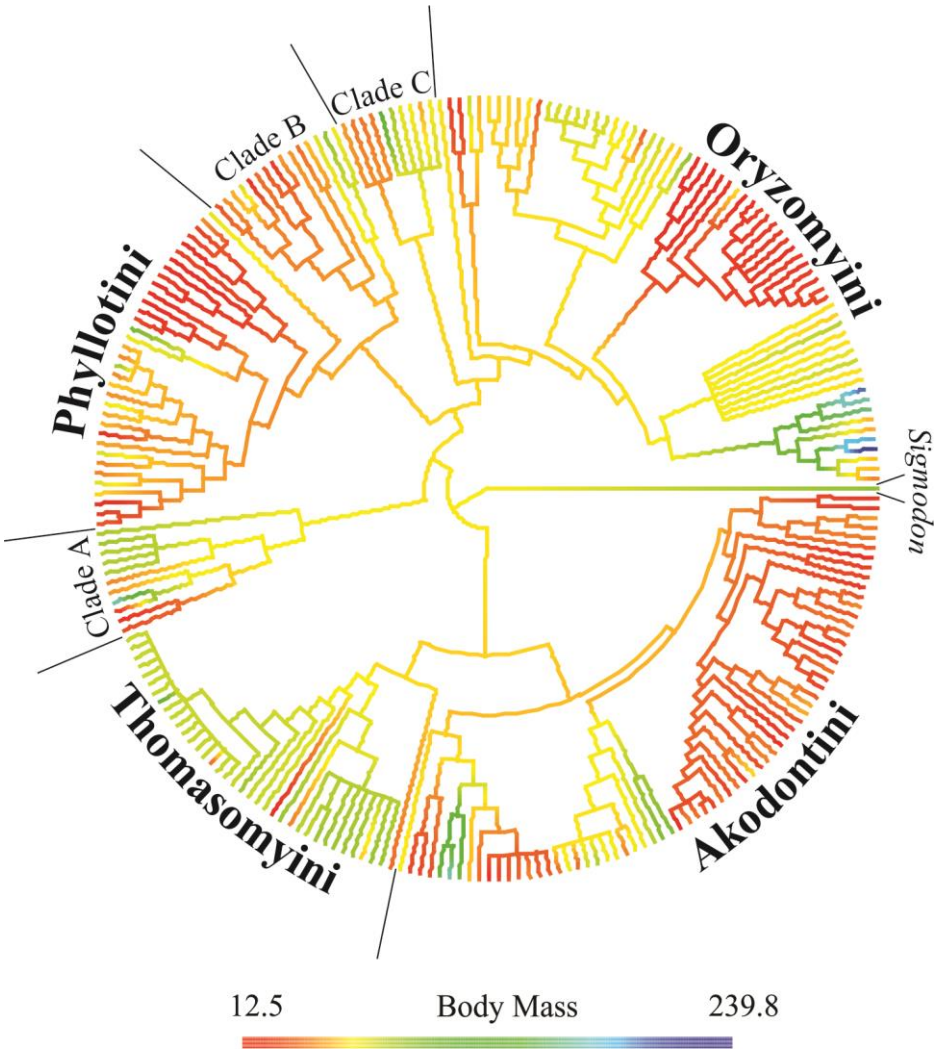

Figure 2. Phylogenetic signal-representation (PSR) curve derived from phylogenetic eigenvector regression on body mass. Black dots show the PSR curve for the body mass. Black dotted line shows the expected curve under Brownian movement, and gray dotted line indicates the null expectation.

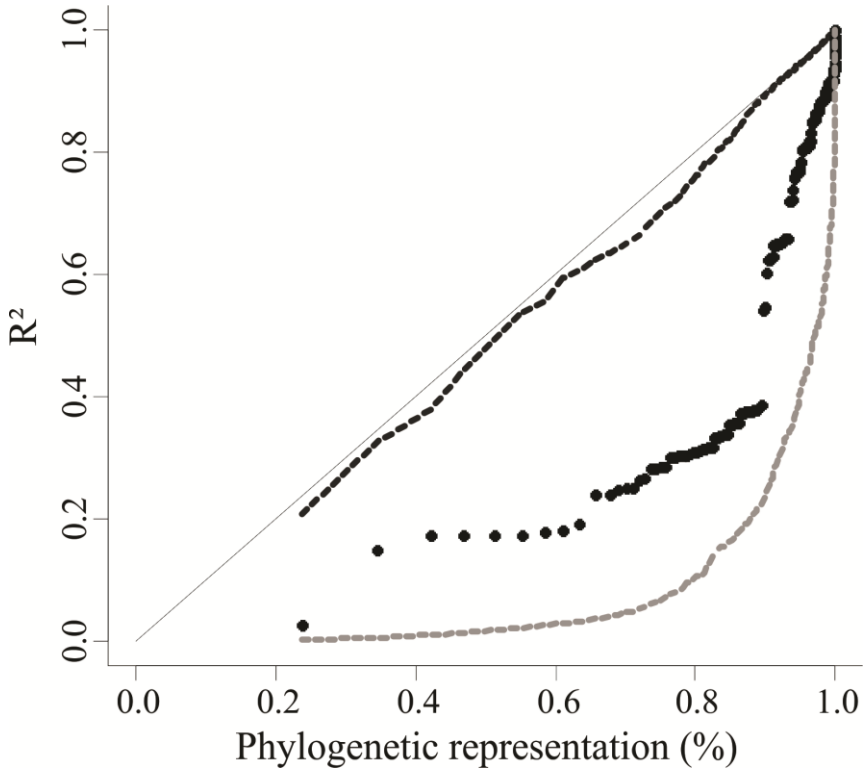

Figure 3. Geographical pattern of mean body mass (g) of sigmodontine rodents across 1527 cells in South America (left). For each cell, the colour depicts a mean of all the mean body-size of each species with presence in that cell. The relationship between mean body mass by site and degrees of latitude (right).

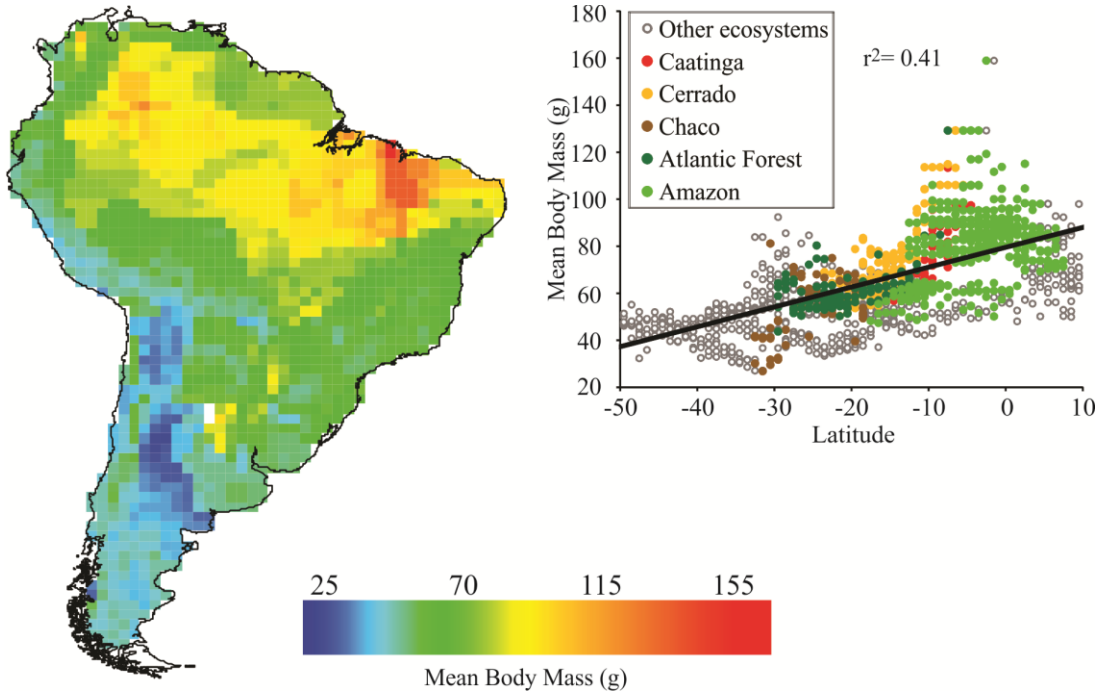

Figure 4. Correlogram of main axes of variation in phylogenetic structure of sigmodontine rodents across South America. Main clades of Sigmodontinae are shown. Sites are omitted.

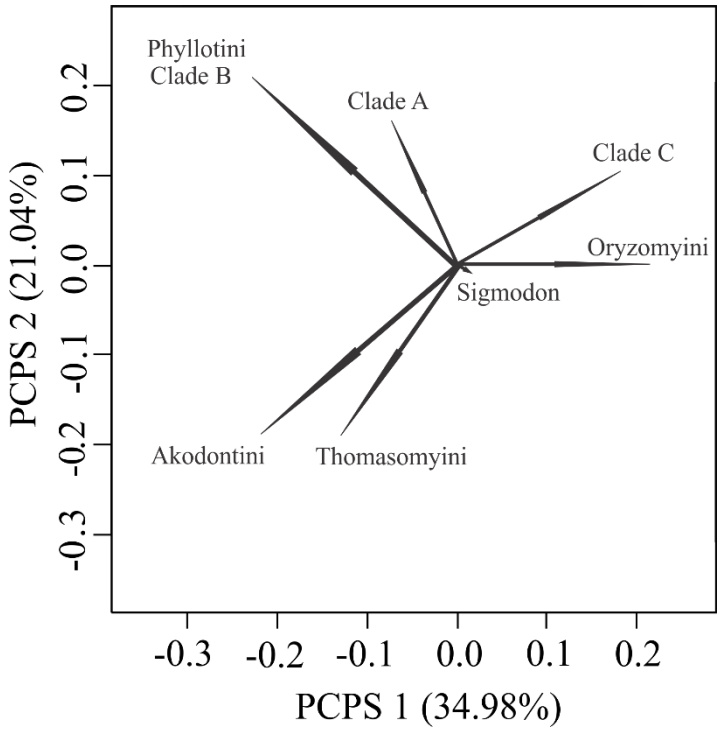

Figure 5. Geographical pattern of PCPS 1 (left) and Annual Mean Temperature (right). Scale bar of PCPS represents the variation in the orthogonal axis, from negative to positive values.

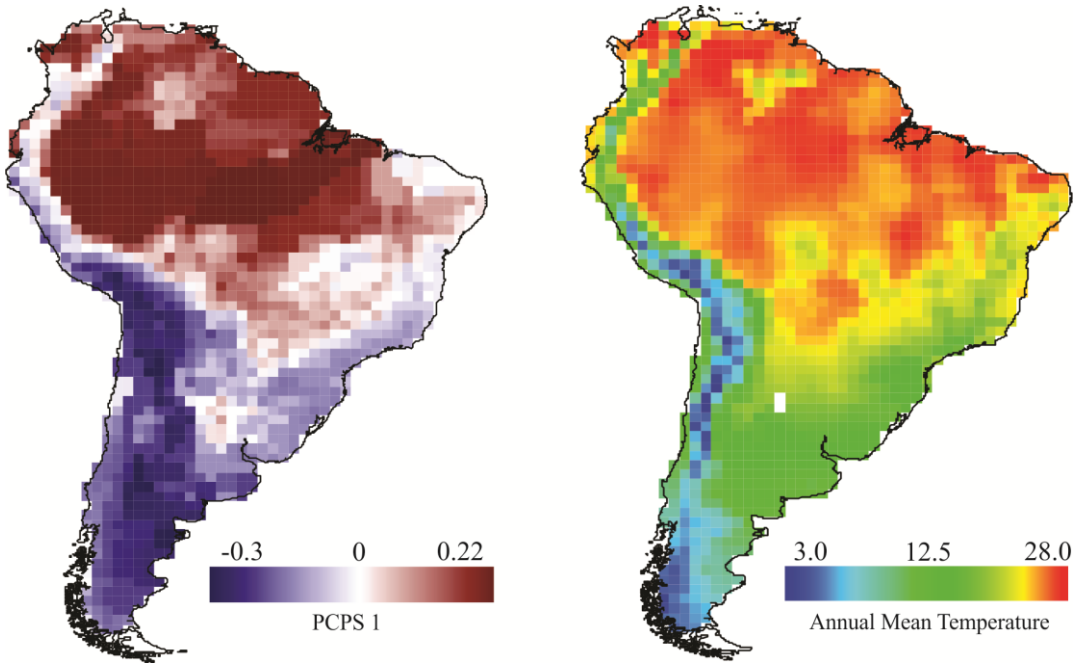

Supporting Information

Appendix S1. Body mass (in grams) for each of the 245 sigmodontine species (Rodentia, Sigmodontinae) used in the study, plus the place of each species within tribes (see Appendix S2).

Species	Mass (grams)	Tribe
Abrawayaomys ruschii	63.00	Clade A
Abrothrix illuteus	47.80	Clade B
Abrothrix lanosus	32.50	Clade B
Abrothrix longipilis	37.60	Clade B
Abrothrix sanborni	24.70	Clade B
Aepeomys lugens	37.00	Thomasomyini
Akodon aerosus	60.00	Akodontini
Akodon affinis	24.90	Akodontini
Akodon albiventer	21.80	Akodontini
Akodon azarae	25.00	Akodontini
Neomicroxus bogotensis	13.00	Clade A
Akodon boliviensis	27.50	Akodontini
Akodon budini	26.90	Akodontini
Akodon cursor	39.90	Akodontini
Akodon dayi	32.50	Akodontini
Akodon dolores	50.50	Akodontini
Akodon fumeus	22.70	Akodontini
Akodon iniscatus	28.70	Akodontini
Akodon juninensis	39.00	Akodontini
Akodon kofordi	29.50	Akodontini
Akodon latebricola	39.00	Akodontini
Akodon mimus	24.00	Akodontini
Akodon molinae	33.00	Akodontini
Akodon mollis	30.40	Akodontini
Akodon montensis	44.10	Akodontini
Akodon neocenus	42.40	Akodontini
Akodon orophilus	39.00	Akodontini
Akodon paranaensis	32.40	Akodontini
Akodon reigi	30.10	Akodontini
Akodon sanctipaulensis	27.10	Akodontini
Akodon serrensis	28.30	Akodontini
Akodon siberiae	34.60	Akodontini
Akodon simulator	42.50	Akodontini
Akodon spegazzinii	28.60	Akodontini
Akodon subfuscus	30.40	Akodontini
Akodon sylvanus	39.00	Akodontini
Akodon toba	51.20	Akodontini
Akodon torques	39.00	Akodontini
Akodon varius	40.00	Akodontini
Andalgalomys pearsoni	25.40	Phyllotini
Andalgalomys roigi	32.90	Phyllotini
Andinomys edax	69.70	Clade A
Anotomys leander	66.40	Clade C
Auliscomys pictus	54.70	Phyllotini
Auliscomys sublimis	38.00	Phyllotini
Bibimys chacoensis	28.00	Akodontini
Bibimys labiosus	30.00	Akodontini
Bibimys torresi	28.00	Akodontini
Blarinomys breviceps	36.00	Akodontini

Brucepattersonius albinasus	20.00	Akodontini
Brucepattersonius griserufescens	27.00	Akodontini
Brucepattersonius guarani	32.00	Akodontini
Brucepattersonius igniventris	35.00	Akodontini
Brucepattersonius iheringi	43.00	Akodontini
Brucepattersonius misionensis	34.00	Akodontini
Brucepattersonius soricinus	33.00	Akodontini
Calomys boliviae	27.00	Phyllotini
Calomys callidus	27.00	Phyllotini
Calomys callosus	45.00	Phyllotini
Calomys hummelincki	27.00	Phyllotini
Calomys laucha	14.00	Phyllotini
Calomys lepidus	26.60	Phyllotini
Calomys musculinus	20.10	Phyllotini
Calomys sorellus	20.00	Phyllotini
Calomys tener	13.80	Phyllotini
Chelemys macronyx	73.30	Clade B
Chelemys megalonyx	50.80	Clade B
Chibchanomys trichotis	50.00	Clade C
Chilomys instans	19.00	Thomasomyini
Chinchillula sahamae	169.80	Clade A
Delomys dorsalis	67.50	Clade A
Delomys sublineatus	90.00	Clade A
Deltamys kempi	26.40	Akodontini
Eligmodontia moreni	18.00	Phyllotini
Eligmodontia morgani	16.50	Phyllotini
Eligmodontia puerulus	28.50	Phyllotini
Eligmodontia typus	17.30	Phyllotini
Euneomys chinchilloides	87.60	Clade A
Euneomys fossor	83.00	Clade A
Euneomys mordax	82.00	Clade A
Euneomys petersoni	83.00	Clade A
Galenomys garleppi	59.30	Phyllotini
Geoxus valdivianus	31.50	Clade B
Graomys domorum	102.00	Phyllotini
Graomys griseoflavus	67.50	Phyllotini
Holochilus brasiliensis	155.00	Oryzomyini
Holochilus chacarius	204.00	Oryzomyini
Holochilus sciureus	163.50	Oryzomyini
Ichthyomys hydrobates	66.40	Clade C
Ichthyomys pittieri	69.10	Clade C
Ichthyomys stolzmanni	84.70	Clade C
Ichthyomys tweedii	118.50	Clade C
Irenomys tarsalis	43.10	Clade A
Juliomys pictipes	22.90	Clade A
Juscelinomys guaporensis	97.30	Akodontini
Juscelinomys huanchacae	97.30	Akodontini
Gyldenstolpia fronto	168.00	Akodontini
Kunsia tomentosus	115.60	Akodontini
Lenoxus apicalis	53.60	Akodontini
Loxodontomys micropus	72.70	Phyllotini
Loxodontomys pikumche	43.00	Phyllotini
Melanomys caliginosus	41.00	Oryzomyini
Melanomys robustulus	53.50	Oryzomyini
Melanomys zunigae	53.50	Oryzomyini
Microryzomys altissimus	13.50	Oryzomyini
Neacomys dubosti	14.00	Oryzomyini
Neacomys guianae	14.20	Oryzomyini
Neacomys paracou	14.00	Oryzomyini
Neacomys spinosus	19.00	Oryzomyini

Necromys lactens	32.90	Akodontini
Necromys lasiurus	39.90	Akodontini
Necromys obscurus	40.70	Akodontini
Necromys temchuki	47.20	Akodontini
Nectomys rattus	239.80	Oryzomyini
Nectomys squamipes	190.70	Oryzomyini
Neusticomys monticolus	39.50	Clade C
Neusticomys mussoi	40.00	Clade C
Neusticomys peruviensis	40.00	Clade C
Neusticomys venezuelae	47.10	Clade C
Notiomys edwardsii	21.30	Clade B
Oecomys bicolor	34.00	Oryzomyini
Oecomys cleberi	73.40	Oryzomyini
Oecomys concolor	61.60	Oryzomyini
Oecomys flavicans	73.40	Oryzomyini
Oecomys mamorae	62.50	Oryzomyini
Oecomys paricola	73.40	Oryzomyini
Oecomys phaeotis	73.40	Oryzomyini
Oecomys rex	73.40	Oryzomyini
Oecomys roberti	73.40	Oryzomyini
Oecomys rutilus	73.40	Oryzomyini
Oecomys speciosus	73.40	Oryzomyini
Oecomys superans	73.40	Oryzomyini
Oecomys trinitatis	73.40	Oryzomyini
Oligoryzomys andinus	25.20	Oryzomyini
Oligoryzomys arenalis	25.20	Oryzomyini
Oligoryzomys chacoensis	23.00	Oryzomyini
Oligoryzomys delticola	29.40	Oryzomyini
Oligoryzomys destructor	25.20	Oryzomyini
Oligoryzomys eliurus	30.00	Oryzomyini
Oligoryzomys flavescens	21.30	Oryzomyini
Oligoryzomys fulvescens	25.00	Oryzomyini
Oligoryzomys griseolus	25.20	Oryzomyini
Oligoryzomys longicaudatus	27.00	Oryzomyini
Oligoryzomys magellanicus	25.20	Oryzomyini
Oligoryzomys microtis	22.50	Oryzomyini
Oligoryzomys nigripes	20.50	Oryzomyini
Oligoryzomys stramineus	25.00	Oryzomyini
Nephelomys albigularis	60.50	Oryzomyini
Handleyomys alfaroi	33.30	Oryzomyini
Nephelomys auriventer	60.50	Oryzomyini
Oreoryzomys balneator	60.50	Oryzomyini
Transandinomys bolivaris	60.50	Oryzomyini
Oryzomys couesi	69.30	Oryzomyini
Oryzomys gorgasi	60.50	Oryzomyini
Mindomys hammondi	60.50	Oryzomyini
Nephelomys keaysi	58.30	Oryzomyini
Nephelomys levipes	60.50	Oryzomyini
Euryoryzomys macconnelli	58.00	Oryzomyini
Hylaeamys megacephalus	57.80	Oryzomyini
Euryoryzomys nitidus	55.20	Oryzomyini
Hylaeamys perenensis	57.80	Oryzomyini
Eremoryzomys polius	60.50	Oryzomyini
Euryoryzomys russatus	91.00	Oryzomyini
Hylaeamys laticeps	75.73	Oryzomyini
Cerradomys subflavus	50.00	Oryzomyini
Transandinomys talamancae	55.00	Oryzomyini
Aegialomys xanthaeolus	79.80	Oryzomyini
Hylaeamys yunganus	60.50	Oryzomyini
Oxymycterus akodontius	68.00	Akodontini

Oxymycterus angularis	68.00	Akodontini
Oxymycterus delator	81.50	Akodontini
Oxymycterus hiska	68.00	Akodontini
Oxymycterus hispidus	36.80	Akodontini
Oxymycterus hucucha	68.00	Akodontini
Oxymycterus inca	35.00	Akodontini
Oxymycterus nasutus	68.00	Akodontini
Oxymycterus paramensis	42.00	Akodontini
Oxymycterus roberti	83.40	Akodontini
Oxymycterus rufus	75.40	Akodontini
Pearsonomys annectens	45.83	Clade B
Phyllotis amicus	20.20	Phyllotini
Phyllotis andium	53.00	Phyllotini
Phyllotis bonaeriensis	42.50	Phyllotini
Phyllotis caprinus	50.80	Phyllotini
Phyllotis darwini	50.80	Phyllotini
Phyllotis definitus	89.00	Phyllotini
Phyllotis haggardi	42.50	Phyllotini
Phyllotis magister	68.50	Phyllotini
Phyllotis osgoodi	45.10	Phyllotini
Phyllotis osilae	49.00	Phyllotini
Phyllotis wolffsohni	42.50	Phyllotini
Phyllotis xanthopygus	56.30	Phyllotini
Pseudoryzomys simplex	51.20	Oryzomyini
Punomys lemminus	84.80	Clade A
Reithrodon auritus	70.90	Reithrodontini
Rhagomys longilingua	30.00	Thomasomyini
Rhagomys rufescens	21.20	Thomasomyini
Rhipidomys austrinus	89.00	Thomasomyini
Rhipidomys caucensis	89.00	Thomasomyini
Rhipidomys couesi	89.00	Thomasomyini
Rhipidomys fulviventer	89.00	Thomasomyini
Rhipidomys latimanus	57.50	Thomasomyini
Rhipidomys leucodactylus	80.00	Thomasomyini
Rhipidomys macconnelli	41.60	Thomasomyini
Rhipidomys mastacalis	77.50	Thomasomyini
Rhipidomys nitela	89.00	Thomasomyini
Rhipidomys venezuelae	90.00	Thomasomyini
Rhipidomys venustus	89.00	Thomasomyini
Rhipidomys wetzeli	89.00	Thomasomyini
Salinomys delicatus	12.50	Phyllotini
Scapteromys tumidus	146.00	Akodontini
Scolomys melanops	26.50	Oryzomyini
Scolomys ucayalensis	26.50	Oryzomyini
Sigmodon hispidus	92.40	Sigmodontini
Tapecomys primus	71.50	Phyllotini
Thalpomys cerradensis	24.00	Akodontini
Thalpomys lasiotis	24.00	Akodontini
Thaptomys nigrita	19.90	Akodontini
Thomasomys aureus	88.00	Thomasomyini
Thomasomys baeops	77.00	Thomasomyini
Thomasomys bombycinus	114.50	Thomasomyini
Thomasomys cinereiventer	77.00	Thomasomyini
Thomasomys cinereus	77.00	Thomasomyini
Thomasomys daphne	77.00	Thomasomyini
Thomasomys eleusis	77.00	Thomasomyini
Thomasomys gracilis	77.00	Thomasomyini
Thomasomys hylophilus	77.00	Thomasomyini
Thomasomys incanus	77.00	Thomasomyini
Thomasomys ischyurus	77.00	Thomasomyini

Thomasomys kalinowskii	77.00	Thomasomyini
Thomasomys ladewi	77.00	Thomasomyini
Thomasomys laniger	35.50	Thomasomyini
Thomasomys monochromos	77.00	Thomasomyini
Thomasomys niveipes	77.00	Thomasomyini
Thomasomys notatus	77.00	Thomasomyini
Thomasomys paramorum	77.00	Thomasomyini
Thomasomys pyrrhonotus	77.00	Thomasomyini
Thomasomys rhoadsi	77.00	Thomasomyini
Thomasomys silvestris	77.00	Thomasomyini
Thomasomys taczanowskii	77.00	Thomasomyini
Thomasomys vestitus	76.50	Thomasomyini
Wiedomys pyrrhorhinos	46.70	Wiedomyini
Wilfredomys oenax	46.80	Clade A
Zygodontomys brevicauda	52.20	Oryzomyini
Zygodontomys brunneus	75.60	Oryzomyini

Appendix S2. Phylogenetic tree for 245 species of sigmodontine rodents based on Fabre et al. 2012 phylogeny. See text for further explanation on tree construction.

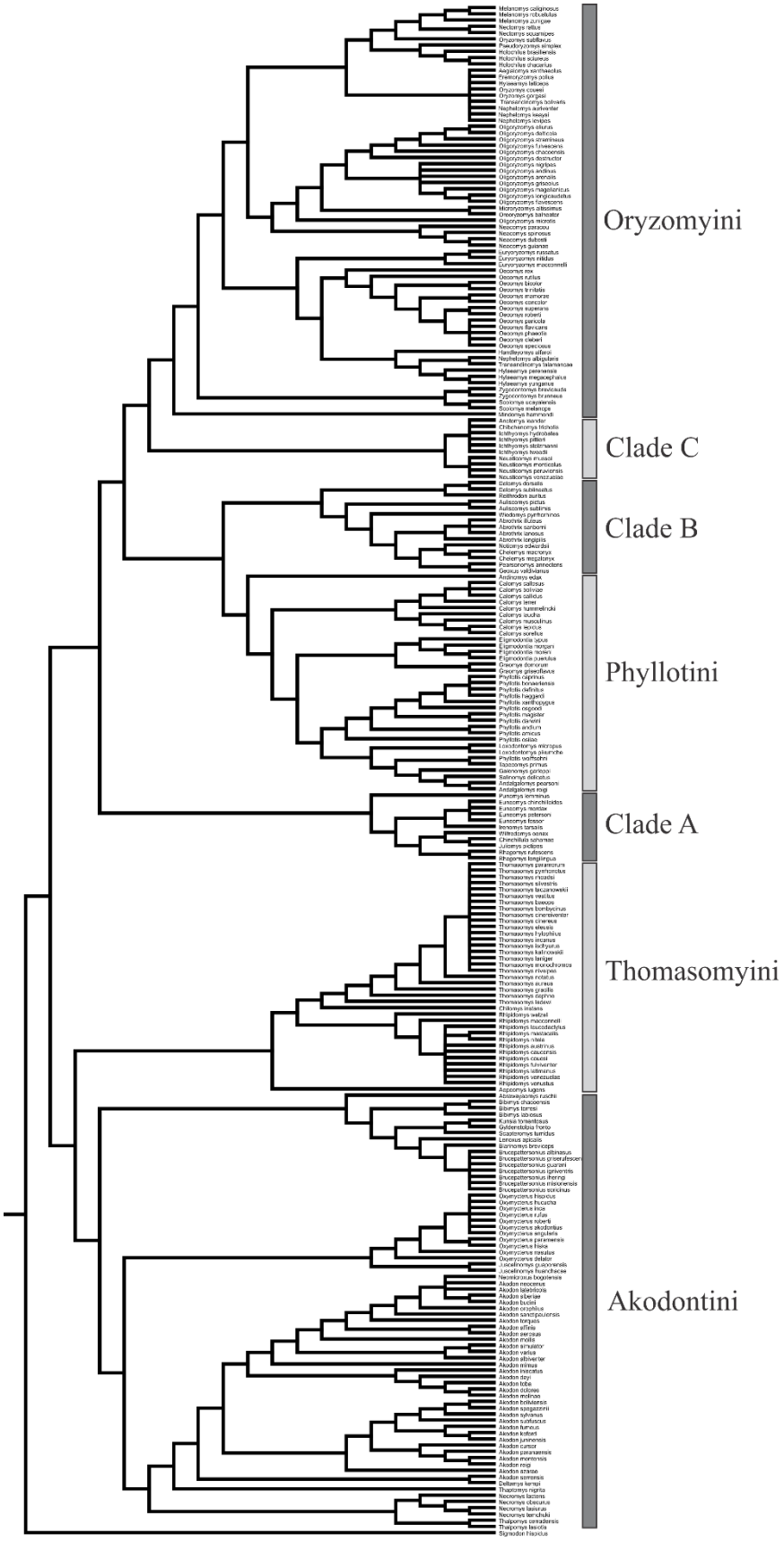

Appendix S3. Moran's correlogram for body mass across assemblages.

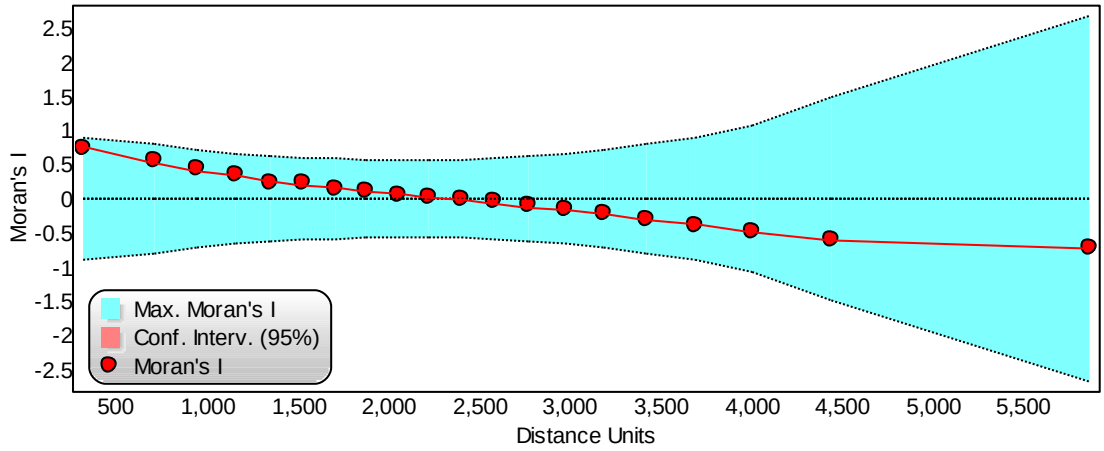

Capítulo 5

Geometric morphometrics meets metacommunity ecology: environment and lineage distribution affects spatial variation in shape**

Renan Maestri[1*], Leandro Rabello Monteiro[2], Rodrigo Fornel[3], Thales Renato Ochotorena de Freitas[1,4], Bruce D Patterson[5]

[1]*Programa de Pós-Graduação em Ecologia, Universidade Federal do Rio Grande do Sul, Porto Alegre, RS 91501-970, Brazil.*

[2]*Laboratório de Ciências Ambientais, CBB, Universidade Estadual do Norte Fluminense, Campos dos Goytacazes, RJ 28013-620, Brazil.*

[3]*Programa de Pós-Graduação em Ecologia, Universidade Regional Integrada do Alto Uruguai e das Missões, Campus Erechim, Erechim RS 99709-910, Brazil.*

[4]*Departamento de Genética, Universidade Federal do Rio Grande do Sul, Porto Alegre, RS 91501-970, Brazil.*

[5]*Integrative Research Center, Field Museum of Natural History, Chicago, IL 60605, USA*

* *Correspondence*: renanmaestri@gmail.com

** Artigo submetido para publicação no periódico *Ecography* em novembro de 2016

Abstract

Patterns of univariate trait variation across metacommunities are widely explored, as are searches for their underlying causes. Surprisingly, patterns of multivariate shape remain unknown, and the search for drivers of functional traits of communities often neglect the biogeographical distribution of phylogenetic clades. Our aim was to investigate multivariate shape distribution across metacommunities and to determine the main environmental drivers of shape beyond/taking into account the phylogenetic distribution of lineages. We obtained mean skull and mandible shape for 228 species of Neotropical sigmodontine rodents through geometric morphometrics (GM), and then calculated mean shapes for 1°x1° cells across the Neotropics based on the incidence of sigmodontines. We investigated the effects of lineage distribution on mean trait variation by using phylogenetic fuzzy weighting to calculate Principal Coordinates of Phylogenetic Structure (PCPS). Effects of environmental variables on shape variation incorporating phylogenetic composition were realized through redundancy analysis. We found that the different distributions of major lineages throughout the Neotropics were responsible for much of the mean shape variation. The association of landscape features with tribal groupings (Oryzomyini with Amazonia and Phyllotini and Abrotrichini with the Andes) were standouts. Environmental variables and lineage distribution explain the same (i.e. shared) portion of shape variation, suggesting phylogenetic niche conservatism at the metacommunity level. Seasonality in temperature and land cover were the best environmental predictors of mean shape: larger tympanic bullae, incisive foramina, and check teeth are all associated with highly seasonal and less vegetated areas. Our new approach of using GM shape across metacommunities was demonstrably useful in understanding large-scale biogeographical patterns of shape variation and identifying its underlying causes. The overlap between environmental variables and phylogenetic

lineage distribution suggests that a process of niche conservatism is likely: the phenotype-environment correlation is mediated by the differential biogeographical distribution of the main clades.

Keywords: functional biogeography, metacommunity biogeography, community phylogenetics, phylogenetic niche conservatism, shape variation, Sigmodontinae.

Introduction

Functional biogeography is an emerging discipline that seeks to understand the distribution of traits and functions across space and the mechanisms that generated those patterns (Violle et al. 2014). At the community level, trait variation can be investigated through the average of trait values among constituent members (i.e. community weighted means, CWM; Ricotta and Moretti 2011). Such an approach is useful to understand the factors responsible for both the structure of communities and the drivers of trait diversity (Fig. 1). A number of factors are responsible for the composition of species in communities (matrix W), which ultimately will determine the CWM. Historical factors (e.g. dispersal, vicariance, extinction), attributes of the species, and the environment are the main factors that influence the structure of communities and the CWM (Leibold et al. 2010, de la Sancha et al. 2014, Lawing et al. 2016). Commonly, evolutionary history (i.e. phylogeny) also affects trait variation among species (Fig. 1; Felsenstein 1985). However, it is still a question how phylogenetic relationships among species directly affect the mean trait variation across metacommunities (de Bello et al. 2015, Lawing et al. 2016, Duarte et al. 2016).

Patterns of trait variation across metacommunities are traditionally investigated using univariate traits. The most commonly investigated trait is size (e.g. body mass:

Rodriguez et al. 2008, body length: Olalla-Tárraga et al. 2010). Numerous competing hypotheses attempt to explain size variation across metacommunities, based on heat conservation, heat dissipation, and resource availability, among others (Blackburn and Hawkins 2004, Rodríguez et al. 2008). However, the understanding of shape variation across metacommunities is weak. Most ecological investigations of "shape" involve a ratio between two morphological variables or univariate measure of body parts, as in studies of some ecogeographical rules (Gaston et al. 2008).

The study of shape across geographical and ecological gradients is needed to detect hidden factors influencing morphological variation, which can shed new light on the evolutionary and ecological history of species. Myriad studies have shown that shape variation follows environmental gradients. At the intraspecific level, skull shape differences were flagged between rodent populations occupying different biomes (Monteiro et al. 2003), and variation is known to follow both elevational (Alvarado-Serrano et al. 2013) and climatic gradients (Cardini et al. 2007). Climatic factors explain the skull shape variation of several species of capuchin monkeys (Cáceres et al. 2013) and *Graomys* (Martínez and Cola 2011) across South America. Moreover, size and shape variation present complex relationships with each other, and can be decoupled—in the sense that different factors can influence size and shape along geographical transects (Cardini and Elton 2009; Maestri et al. 2016a). This suggests that an understanding of the factors guiding morphological variation is needed for "size-free" shape. The interaction between historical and ecological processes that influence trait at an assemblage scale can illuminate the organisms' functions and evolution in a given environment, and at the same time enhance understanding of assembly rules.

The main purpose of this paper is two-fold: (i) to investigate multivariate shape variation across metacommunities, and (ii) to understand the environmental drivers of

shape variation after taking into account the phylogenetic composition of metacommunities. As our understanding of shape is quintessentially multivariate (Zelditch et al. 2012), geometric morphometrics offers the only methodology that can satisfy our concept of shape: “all the geometric information that remains when location, scale and rotational effects are filtered out from an object” (Kendal 1977). However, analyses of multivariate shape are difficult to conduct at the metacommunity level. This is especially true at biogeographical scales, where a large number of specimens (representing many species) must be sampled from each community, and communities differ in species composition, enlarging that number further. Thus, we remain ignorant of even the most basic patterns and potential environmental drivers of mean shape across metacommunities. Moreover, understanding how the distribution of lineages across space determines the composition of species in communities, and thereby affects mean trait distribution, is rarely considered. Such lineage distribution is likely to affect the relationship between mean trait variation (CWM) and environmental variables, and needs to be explicitly considered (Pillar and Duarte 2010, Maestri et al. 2016b).

A major framework has been used to investigate biogeographic patterns of variation in mean traits across large arrays of metacommunities. The assemblage-based approach (Gaston et al. 2008) uses range maps of species to determine their incidence in a given cell, making it feasible to assemble communities and investigate their trait variation at such large scales. The principal issue raised involves how to isolate the effects of phylogeny, environment, and geography, which can each affect trait variation (e.g., Diniz-Filho et al. 2009; Olalla-Tárraga et al. 2010). A common procedure removes phylogenetic non-independence before investigating trait variation (e.g., Diniz-Filho et al. 2007). However, by “removing” the phylogenetic component, this approach does not address how much of the CWM is jointly explained by phylogeny and environment at the

metacommunity scale, and thus fails to address phylogenetic niche conservatism (Pillar & Duarte 2010). Isolating phylogenetic information to understand the joint role of lineage distribution and environment is essential for a complete understanding of the factors shaping the CWM.

Recognizing that ecological communities are diverse systems with producers, consumers, and scavengers from multiple living kingdoms, most metrics of community ecology actually apply to more restricted sets of species, often guilds, assemblages, or ensembles (Fauth et al. 1996). Therefore, in the present paper, we use the term "community" in this loose sense and apply it to a diverse assemblage of rodents, all primary or secondary consumers. The term metacommunity refers to a set of communities connected via species dispersal (Leibold et al. 2004).

Here, we investigate mean skull and mandible shape variation, environmental variables, and phylogenetic lineage distribution across metacommunities composed by sigmodontines (Rodentia, Cricetidae) throughout the Neotropical region. Sigmodontinae is a subfamily of ~400 species of rats and mice that colonized South America in the late Miocene via transoceanic dispersal before the closure of the Panamanian isthmus (~10 Ma; Parada et al. 2013, Vilela et al. 2013). Given their widespread distribution across virtually all Neotropical habitats (Patton et al. 2015), high local richness and turnover (Maestri and Patterson 2016), and recent radiations (Schenk et al. 2013) guaranteeing comparable patterns of niche exploitation, sigmodontines are an excellent group for studying large-scale patterns of trait variation.

We predict that four scenarios may arise: (i) if environmental variables are the sole drivers of shape variation across metacommunities, effects of environment on shape should be strong even after accounting for lineage differences in regional occupation, and lineage occupation is not correlated with shape variation; (ii) however, if spatial patterns

of shape variation arise solely because random colonization of a given region by an ancestral species was followed by subsequent clade diversification there (Lawing et al. 2016), then we predict that lineage distribution will affect shape variation, but not environmental variables; (iii) if the effects of environmental variables on shape are indirect because of covariation between lineage distribution and shape (i.e. if/when environment and lineage distribution explain the same portion of shape), then the correlation of environment with shape should be nullified by controlling for the differential distribution of lineages, a pattern known as phylogenetic niche conservatism at the metacommunity level (Pillar and Duarte 2010); and (iv) if both environment and lineage distribution affect shape variation, but in an independent way, phylogenetic niche conservatism is unlikely (Pillar and Duarte 2010). For the lineage distribution to have an effect on shape variation across metacommunities in the first place, shape must be structured by phylogeny (i.e. a phylogenetic signal at the species level must exist), or else lineage distribution cannot structure shape across metacommunities. We thus evaluated phylogenetic signal at the species level, and then applied redundancy-analysis, considering spatial autocorrelation, to discriminate among the four scenarios.

Materials and Methods

Sampling and geometric morphometrics

We examined 2812 specimens from 73 genera and 228 species of sigmodontine rodents, including all tribes recognized by Patton et al. (2015). A list of museums housing the specimens examined, the catalogue numbers of these specimens, and the number of individuals analyzed for each species can be found in Supplementary material Appendix 1. Nomenclature and classification followed accounts in Patton et al. (2015), updated where needed (Pardiñas et al. 2016, Teta et al. 2016). We obtained two-dimensional

images of the skull in ventral and lateral views and the mandible in lateral view of each specimen using a digital camera (Nikon Coolpix P100). All specimens were positioned in the same plane, and the same distance was used from the camera to the subject. Two-dimensional approximations of a three-dimensional structure are a common procedure in geometric morphometric studies, and the error resulting from the 3D to 2D approximation proved to be negligible when tested in the skull and mandible of a rodent (Cardini 2014). Only adult specimens were examined, identified by the complete eruption (in occlusion) of the third molar. Because we are interested in patterns at a broad-scale interspecific level, and sexual dimorphism in sigmodontines are seldom explored and typically small or absent, we did not differentiate between sexes. On each specimen, we digitized 56 landmarks on the skull in ventral view, 20 landmarks on the skull in lateral view, and 13 landmarks on the mandible (see image and landmark description in Supplementary material Appendix 2). The digitization of landmarks was made in TpsDig2 software (Rohlf 2015). Different views of the skull and mandible were analyzed separately. The matrices of landmark coordinates were superimposed with a Generalized Procrustes Analysis (GPA) in order to remove undesirable effects of scale, position, and orientation (Rohlf and Slice 1990). Symmetry was imposed on the ventral view to eliminate unnecessary information caused by bilateral asymmetry (Klingenberg et al. 2002), and also considering that, for mammalian crania, structures on which symmetry was imposed carry virtually the same information as untransformed ones (Cardini 2017). An arithmetic mean of shape was calculated for each species. The visualization of shape changes were made with an outline interpolation (Klingenberg 2013), generated to help visualization but should be interpreted with caution, because the shape change information varies with the selection of the landmarks. Geometric morphometric procedures were carried out

using the geomorph package (Adams and Otarola-Castillo 2013) in the R environment (R Core Team 2016).

Metacommunity data

The entire Neotropical region (Morrone 2014), exclusive of islands, was split into 1°x1° cells (~110 x 110 km). Range maps for each of the 228 sigmodontine species with morphological information were obtained from *.shp files documented in Maestri and Patterson (2016; 218 maps for South American species generated from accounts in Patton et al. 2015) or IUCN Red List (2008; 10 maps for Central American species). Incidence (presence/absence) of each species was calculated using their polygons, for each of the 1770 cells. Using the mean shape of each species, we calculated the arithmetic mean shape of the assemblage in each cell by averaging the shapes of those species present there. A Principal Component Analysis (PCA) was conducted to explore mean shape variation for each skull and mandible view across sites (results in Supplementary material Appendix 3). The set of PCs of shape necessary to achieve 100% of variation (49 PCs for ventral view, 36 PCs for lateral view, and 22 PCs for mandible) were used as response variables in all subsequent analyses.

We were also concerned that richness differences among cells could influence the results of this paper; this is sometimes apparent for univariate traits (Meiri and Thomas 2007), leading us to implement a few other approaches. A median shape for each cell was also calculated (i.e. by taking the median shape of the species on each cell); medians of body size proved to be less affected than means by richness differences among cells (Meiri and Thomas 2007). Another suggested strategy is using richness per cell as a covariate in such assemblage-trait studies (Olson et al. 2009). Statistical analyses (see beyond) were conducted on both mean and median shape values for each cell, with and

without richness as a covariate. Because the results of all analyses were highly correlated, we show only the results using mean shape and do not include richness as a covariate in the main paper. The results of analyses conducted with median shape values and using richness per cell as a covariate are presented in Supplementary material Appendix 4. Spatial and geometric morphometric procedures were conducted in R (R Core Team 2016), and the visualization of maps was made using Spatial Analysis in Macroecology (SAM – Rangel et al. 2010).

Phylogenetic tree and phylogenetic signal

Phylogenetic relationships among the 228 sigmodontine species (Fig. 2; Supplementary material Appendix 5) were reconstructed in Mesquite 2.75 (Maddison and Maddison 2011) following the phylogenetic hypothesis of Parada et al. (2015). Parada et al. (2015) contains one of the most comprehensive published phylogenies of sigmodontines, is based on the mitochondrial cytochrome b and the nuclear IRBP genes, and its topology and dating are broadly consistent with those of previous studies (Fabre et al. 2012, Parada et al., 2013, Schenk et al. 2013, Leite et al. 2014). The tree was pruned to remove species not sampled here and was supplemented to include phylogenetic information for species not present in that phylogeny utilizing topologies in Fabre et al. (2012), Coyner et al. (2013), Machado et al. (2015), and Leite et al. (2015). Relationships involving members of the tribe Ichthyomyini still lacking genetic information were set according to morphological trees in Voss (1988). The addition of species without genetic samples, especially the fish-eating ichthyomines, is of great value to include the entire morphological diversity of sigmodontines in the analyses. Nodes of the tree were dated using ages (in millions of years) from Parada et al. (2015) and extrapolated over undated nodes using the *bladj* algorithm implemented in Phylocom 4.2 (Webb et al. 2008). The

inclusion of species not originally sampled, along with the extrapolation of dates, may generate some branches with arbitrary lengths, an undesirable feature. To investigate if the branch lengths of the tree can influence the results found in this study, we repeated all analyses using a topology-only tree (i.e., with all branch lengths set to 1.0), and included the results from that analysis in Supplementary material Appendix 6. The results varied little and the same conclusions hold using both trees.

The phylogenetic signal at the species level was calculated for each morphological dataset (i.e., skull shape in ventral and lateral views, and mandible shape) using the generalized K statistics (Adams 2014). Values of K=1 are consistent with the evolution of a trait by Brownian motion, while K<1 indicates less similarity in the trait than expected under Brownian evolution, and K>1 indicates greater similarity in the trait than expected under Brownian evolution (Blomberg et al. 2003). Phylogenetic signal tests were conducted using geomorph package (Adams and Otarola-Castillo 2013) in the R environment (R Core Team 2016).

Phylogenetic distribution of lineages

Principal Coordinates of Phylogenetic Structure (PCPS) offers a way to investigate how species membership in (phylogenetic) lineages varies across communities and affects mean trait variation (Pillar and Duarte 2010). The PCPS are eigenvectors extracted from a double-centered distance matrix based on species composition across communities (i.e. assemblages) weighted by their phylogenetic similarities (matrix P – Duarte 2011, Duarte et al. 2016). Thus, matrix P represents phylogenetic community composition. PCPS with higher eigenvalues are related to the basal nodes of phylogeny, and segregate the communities by expressing that basal fraction of phylogenetic community composition, while PCPS with lower eigenvalues

describe gradients in phylogenetic community composition more strongly influenced by terminal nodes (Duarte 2011). Therefore, the effect of the historical distribution of lineages on the trait distribution across metacommunities can be evaluated with a number of PCPS (Duarte et al. 2012, Maestri et al. 2016b).

Selection of the most important PCPS explaining mean shape variation were made using forward selection, taking mean shape as the response variables and all PCPS as explanatory variables. PCPS 1, 2, and 3 significantly explained (α= 0.05) mean shape in the three views, and were used in further analysis. All analyses were conducted in the R environment (R Core Team 2016), using the packages PCPS (Debastiani and Duarte 2014), and packfor (Dray et al. 2013).

Environmental and spatial variables

We selected six environmental variables that might conceivably be correlated with mean shape across metacommunities. Variables were selected based on intraspecific and cross-species studies that showed these variables are correlated with skull and mandible shape variation in mammals (temperature and temperature seasonality: Martínez and Cola 2011, Cáceres et al. 2013, Martínez et al. 2014, Meloro et al. 2014; elevation: Alvarado-Serrano et al., 2013, primary productivity: Cardini et al. 2007; land cover or vegetation type: Monteiro et al. 2003, Alvarado-Serrano et al. 2013). For each cell, we obtained mean values of temperature, temperature seasonality, mean elevation (obtained from Bioclim database – Hijmans et al. 2005), net primary productivity, Normalized Difference Vegetation Index (NDVI), and Land Cover (obtained from NASA: http://neo.sci.gsfc.nasa.gov/). The correlations among these environmental variables were examined and found to be not highly correlated with each other (all Pearson $r<0.6$).

We generated principal coordinates of neighbourhood matrices (PCNM) to assess the effect of spatial scale on our analysis (Borcard and Legendre 2002). Spatial gradients in environmental variables are not simply bias or noise to be controlled, but instead may reflect the true structure of nature (Legendre 1993, Hawkins 2012). Still, gradients may generate spatial autocorrelation in the residuals of the model of interest, inflating degrees of freedom (Borcard and Legendre 2002). PCNM variables are useful to control these effects across multiple scales, as they represent both broad (PCNM with high eigenvalues) and finer (PCNM with low eigenvalues) spatial gradients. We generated PCNM variables by performing a principal coordinates analysis on a truncated distance matrix connecting all sites, where the truncation distance (287.105 km) was defined under a minimum-spanning-tree criterion (Rangel et al. 2006). We performed a stepwise redundancy analysis between selected PCPS and environmental variables as response variables, and all PCNM as explanatory variables. From this, 21 PCNM were selected as descriptors of environmental and phylogenetic gradients. The remaining 900 PCNM not selected were used as covariates in further analyses, as they represent spatial variables not related to climate or lineage distribution, and so are potentially responsible for spatial autocorrelation in our response variables (the morphological datasets) (following Duarte et al. 2014). PCNM analysis and forward selection were performed using the packages vegan (Oksanen et al. 2015) and packfor (Dray et al. 2013) in the R environment (R Core Team 2016).

Statistical analyses

We performed independent Redundancy Analysis (RDA) between our response variables (PCs of shape in all views [independently] representing 100% of variation) and the selected PCPS to test the influence of the phylogenetic distribution of lineages

depicted by PCPS 1, 2 and 3 on mean shape variation. Then, we carried out RDA between mean shape and environmental variables, with and without controls for the phylogenetic distribution of lineages (i.e. by using PCPS as a condition variable). In all models, PCNM were used as covariates to control for residual spatial autocorrelation. In addition, we performed variation partitioning analyses to segregate the individual and shared contributions of the PCPS and the environmental variables on mean shape. RDAs and variance partitioning were conducted in R with the package vegan (Oksanen et al. 2015). Shape changes associated with the variables of interest were visualized after determining the regression coefficients for each model and plotting the shape changes associated with the combination of all PC scores for each view.

Results

Phylogenetic signal and phylogenetic lineage distribution

Analyses of phylogenetic signal returned a value of K= 0.90 for skull shape in ventral view, K= 0.88 for skull shape in lateral view, and K= 0.78 for mandible shape, all statistically significant at α= 0.05. These values indicate a phylogenetic signal at the species level that is close to Brownian expectation.

The most important differences in the distribution of lineages affecting mean shape across space are those related to PCPS 1, 2, and 3 (Table 1). PCPS 2 had the highest correlation with all shape views. It clearly separates members of the tribe Oryzomyini from members of other tribes, particularly Akodontini and Thomasomyini (Fig. 3). In geographic space, this translates to the difference between areas centered in Amazonia plus some parts of the Cerrado, the Guiana shield, and the Panamá region (where oryzomyines are dominant) versus other parts of the Neotropics (Fig. 4). Negative values of PCPS 2 (Amazonia, the oryzomyine region) correspond to skulls with a proportionally

shorter snout, smaller cheek teeth and incisive foramina, and a narrower neurocranium with smaller tympanic bullae; positive values of PCPS 2 show the opposite tendencies. Mandible shapes associated with negative values of PCPS 2 included a shorter but higher mandible (Fig. 4). PCPS 3 represents the gradient between phyllotines and abrotrichines (negative values) and akodontines and thomasomyines (positive values) (Fig. 3B). Communities dominated by tribes associated with negative values are located mainly to the west of the Andes and in southern South America, whereas positive values are associated with Atlantic Forest, Cerrado, and Caatinga biomes, and to a lesser degree, with the eastern Andes (Fig. 4). Skull shapes characterizing negative values (phyllotines and abrotrichines) have a wider neurocranium and larger tympanic bullae, larger incisive foramina, and a shorter snout, compared to changes associated with positive values in this axis (Fig. 4). Negative values of PCPS 3 are also associated with an elongation of the mandible and a longer condyloid process. PCPS 1 is responsible for the difference in phylogenetic community composition between the northernmost regions of Neotropics—associated with the non-Oryzomyalia sigmodontines (Schenk et al. 2013)—from the remainder of the Neotropics (Fig. 3A). This difference captures the most basal node of the phylogeny within Sigmodontinae (Fig. 2). Main shape differences are influenced mostly by species of Sigmodontini, resulting in wider but shorter skulls at the snout level, narrower skulls at the braincase level, and mandibles with larger coronoid, condyloid, and angular process associated with negative values, when compared to skulls and mandibles associated with positive values (Supplementary material Appendix 7).

Environmental variables

Major environmental predictors of mean shape variation were temperature seasonality and land cover (Table 2). Percentages of explanation were similar among skull

and mandible views. Main shape differences associated with temperature seasonality indicated that in highly seasonal regions, skulls present a wider neurocranium with much larger tympanic bullae, larger incisive foramina, bigger cheek teeth, and an elongated, narrow snout (Fig. 5). Mandibles of mice in highly seasonal environments present larger cheek teeth and elongated coronoid and angular processes. The opposite features are present in mice from more equable regions. Forested lands are populated by mice with a proportionally shorter, wider snout and shorter incisive foramina and tympanic bullae compared to those in more sparsely vegetated areas (Fig. 5). Mice in forested areas are also characterized by a longer coronoid and shorter condyloid and angular processes of the mandible compared to mice in more barren areas. Savanna and grassland mice presented skull and mandible features more or less intermediate to those of forest and sparsely vegetated areas, with the exception of a higher skull in lateral view (Fig. 5).

The explanatory percentages of environmental variables drop noticeably when using the PCPS (1, 2, and 3) as condition variables in the RDA (Table 2). This indicates that the distribution of clades and the environmental variables have a shared influence on mean shape in all views. This was confirmed by the variance partitioning analysis (Table 3), which indicates that the shared contribution of PCPS and environmental variables varied between 47% and 60% depending on the shape view, while the individual contributions of either predictor were between two to twelve times lower than their shared contribution (Table 3). Best environmental predictors based on R^2 differed slightly when controlling for the PCPS: NDVI and land cover appear among the best, with productivity also helping to explain skull shape views. Mean temperature is among the poorest predictors. NDVI represents a gradient from little to much green leaf growth, indicating a possible influence of vegetated areas on shape changes.

Discussion

We found that spatial shape variation among metacommunities is jointly explained by both environmental variables and the different, complementary distributions of sigmodontine lineages across South America. This agrees closely with our third scenario, a phylogenetic niche conservatism at the metacommunity level (Pillar and Duarte 2010). Under this interpretation, the variation in mean shape variables across metacommunities is roughly proportional to the amount of phylogenetic dissimilarity among communities, providing that shape is structured by phylogeny at the species level (i.e. there is a phylogenetic signal). At the same time, environmental variables are likely to affect the mean shape, both directly (when shape is considered an aggregated functional attribute of the community – Violle et al. 2014) and indirectly, through affecting the biogeographical distribution of lineages (Pillar and Duarte 2010).

Although these analyses ignore environmental influences on species-level shape, they nevertheless demonstrate that the environment has a biogeographic effect on mean shape that is mediated by the phylogenetic distribution of lineages across metacommunities. Phylogenetic niche conservatism at the species level (PNC – Losos 2008, Wiens 2008) is a different phenomenon from PNC at the metacommunity level (Pillar and Duarte 2010), so that each must be considered independently. The relationship between the two phenomena still needs to be better elucidated. An evaluation of metacommunity patterns in clades with distinct levels of phylogenetic signal and varied patterns of clade composition across space is needed to address the relationships among the PNCs and clarify which predictions could be made under this framework.

The phylogenetic dissimilarities between communities explained by PCPS 1, 2, and 3, which are related to basal nodes of the phylogeny, strongly account for mean shape variation. This indicates that the proportion of species belonging to a given higher-level

clade (notably the tribes Oryzomyini, Phyllotini, and Abrotrichini) in a community is responsible for the mean shape of that cell, and that phylogeny affects spatial patterns of trait variation. The proportional effects is higher for the basal nodes and lower for the distal or terminal nodes of the phylogeny.

Among environmental variables, temperature seasonality and land cover predict a sizable proportion of mean shape across space. These variables likely influence mean shape variation through niche conservatism at the level of metacommunity composition, because they share its explanation with phylogenetic lineage distribution. A simple explanation for metacommunity PNC may be that species of a given lineage occupy a particular region for historical or ecological reasons, and because they are adapted to the conditions of such region, these species and their descendants are likely to remain in that region. Larger tympanic bullae in less vegetated and highly seasonal areas may be an adaptation to live in xeric environments (Mares 1999, Monteiro et al., 2003). This relates to the function of the bullae, which increase sensitivity to sound, a necessary adaptation for predator avoidance and prey capture in open environments (Alhajeri et al. 2015, Bueno et al. 2015). This explains why enlarged tympanic bullae are common among desert rodents in particular (Prakash and Gosh 1975). The incisive foramina, also larger in species occupying highly seasonal and more open environments, have more uncertain functions, but may be related to the vomeronasal olfactory system (Matsunami and Buck 1997); they appear to serve sensorial purposes and transmit blood vessels in rodents (Quay 1954). The maintenance of such morphological features among phyllotines and abrotrichines is the basis for a metacommunity PNC process in those mainly seasonal and open environments.

A similar process of metacommunity niche conservatism may occur in the Amazonian region. Oryzomyines have colonized and become widespread throughout

Amazonia. There, relatively constant (i.e. less seasonal) temperatures may had influenced the predominance of oryzomyines and consequently the particular shape of Orzyomyini in such regions. Differences between oryzomyine-Amazonia traits and other clades-regions combinations are also reflected in the spatial distribution of body size among sigmodontines (Maestri et al. 2016b). On the other hand, over the highly seasonal and/or cold temperatures in the environment of southern South America and the western slope of the Andes, phyllotine-like skulls have become prevalent. Besides the tympanic bullae, it is also interesting that larger teeth (as we documented in highly seasonal environments) were also a characteristic of capuchin monkeys also inhabiting highly seasonal environments in South America (Cáceres et al. 2013); larger teeth were interpreted by those authors as an adaptation for consuming a greater variety of food types. Likewise, Salazar-Bravo et al. (2013) have already suggested that the particular environment of the Puna grasslands in the Andes may select for high hypsodonty in the teeth of sigmodontines.

Here, we have demonstrated that shape variation can be usefully studied in the framework of metacommunities, leading to a better understanding of prevailing patterns of shape variation across space. We showed that the main differences in shape were associated with metacommunities occupying forested, less seasonal Amazonian habitats – dominated by Oryzomyini – versus those in less vegetated, more seasonal areas to the south and in the Andean region, where Phyllotini and Abrotrichini are dominant. As these patterns represent a first step, many questions are left unanswered, such as which mechanisms are responsible for the observed relationships between environment and average skull shape in communities? The relationship between aridity and tympanic bullae is probably one factor, but others remain to be elucidated. Although size patterns have long been studied and are reasonably well understood, shape patterns are only now

being explored, and the various forces (e.g., climate, habitat type, diet, phylogenetic conservatism) that affect shape need to be better understood. It goes without saying that any trait studied within the framework of metacommunities needs to be understood in light of the group's phylogeny (Pillar and Duarte 2010, Maestri et al. 2016b), providing a more complete understanding of the random and non-random forces acting to shape functional traits across communities.

Aknowledgments

We thank Leandro D.S. Duarte for the insightful discussions about the PCPS. Andrea Cardini and two anonymous reviewers provided useful comments that improved the quality of the article. We are grateful to all curators and collection managers that provided access to specimens and assistance in finding specimens in their institutions: in addition to the FMNH, these include João A. de Oliveira (MNUFRJ), Mario de Vivo and Juliana Gualda (MZUSP), Diego H. Verzi and A. Itatí Olivares (MLP), Eileen Westwig (AMNH), and Darrin Lunde (NMNH). RM is supported by CAPES, LRM is supported by CNPq and FAPERJ, and TROF is supported by CAPES, CNPq, and FAPERGS.

References

Alhajeri, B. H. et al. 2015. Molecular systematics of gerbils and deomyines (Rodentia: Gerbillinae, Deomyinae) and a test of desert adaptation in the tympanic bulla. – J. Zool. Sys. Evol. Res. 53: 312-330.

Adams, D. C. 2014. A generalized K statistic for estimating phylogenetic signal from shape and other high-dimensional multivariate data. – Syst. Biol. 63: 685-697.

Adams, D. C. and Otárola-Castillo, E. 2013. geomorph: and R package for the collection and analysis of geometric morphometric shape data. – Methods Ecol. Evol. 4: 393-399.

Alvarado-Serrano, D. F. et al. 2013. Localized versus generalist phenotypes in a broadly distributed tropical mammal: how is intraspecific variation distributed across disparate environments? – BMC Evol. Biol. 13: 160.

Blackburn, T. M. and Hawkins, B. A. 2004. Bergmann's rule and the mammal fauna of northern North America. – Ecography 27: 715-724.

Blomberg, S. P. et al. 2003. Testing for phylogenetic signal in comparative data: behavioral traits are more labile. – Evolution 57: 717-745.

Borcard, D. and Legendre, P. 2002. All-scale spatial analysis of ecological data by means of principal coordinates of neighbor matrices. – Ecol. Model. 153: 51–68.

Bueno, A. D. A. and Motta-Junior, J. C. 2015. Behavioural and morphological strategies by small savannah rodents to avoid predation. – Mamm. Biol. 80: 401-408.

Cáceres, N. et al. 2013. Ecogeographical variation in skull shape of capuchin monkeys. – J. Biogeogr. 41: 501-512.

Cardini, A. et al. 2007. A geometric morphometric approach to the study of ecogeographical and clinal variation in vervet monkeys. – J. Biogeogr. 34: 1663-1678.

Cardini, A. et al. 2014. Missing the third dimension in geometric morphometrics: how to assess if 2D images really are a good proxy for 3D structures? – Hystrix 25: 73-81.

Cardini, A. 2017. Left, right or both? Estimating and improving accuracy of one-side-only geometric morphometric analyses of cranial variation. – J. Zool. Sys. Evol. Res. 55: 1-10.

Cardini, A. and Elton, S. 2009. Geographical and taxonomic influences on cranial variation in red colobus monkeys (Primates, Colobinae): introducing a new approach to 'morph' monkeys. – Global Ecol. Biogeogr. 18: 248-263.

Coyner, B. S. et al. 2013. Taxonomic validity of species groups in the genus *Akodon* (Rodentia, Cricetidae). – Zool. Scr. 42: 335-350.

De Bello, F. et al. 2015. On the need for phylogenetic 'corrections' in functional trait-based approaches. – Folia Geobot. 50: 349-357.

De la Sancha, N. U. et al. 2014. Metacommunity structure in a highly fragmented forest: has deforestation in the Atlantic Forest altered historic biogeographic patterns? – Divers. Distrib. 20: 1058-1070.

Debastiani, V. J. and Duarte, L. D. S. 2014. PCPS – an R-package for exploring phylogenetic eigenvectors across metacommunities. – Front. Biogeogr. 6: 144-148.

D'Elía, G. et al. 2007. Definition and diagnosis of a new tribe of sigmodontine rodents (Cricetidae: Sigmodontinae), and a revised classification of the subfamily. – Gayana 71: 187-194.

Diniz-Filho, J. A. F. et al. 2007. Seeing the forest for the trees: partitioning ecological and phylogenetic components of Bergmann's rule in European Carnivora. – Ecography 30: 598-608.

Diniz-Filho, J. A. F. et al. 2009. Climate history, human impacts and global body size of Carnivora (Mammalia: Eutheria) at multiple evolutionary scales. – J. Biogeogr. 36: 2222-2236.

Dray, S. et al. 2013. Packfor: Forward selection with permutation. R package version 0.0-8. R Foundation for Statistical Computing, Vienna, Austria. – <https://www.R-project.org/>.

Duarte, L. D. S. 2011. Phylogenetic habitat filtering influences forest nucleation in grasslands. – Oikos 120: 208-215.

Duarte, L. D. S. et al. 2012. Assessing spatial and environmental drivers of phylogenetic structure in Brazilian Araucaria forests. – Ecography 35: 952-960.

Duarte, L. D. S. 2014. Climate effects on amphibian distributions depend on phylogenetic resolution and the biogeographical history of taxa. – Global Ecol. Biogeogr. 23: 213-222.

Duarte, L. D. S. et al. 2016. Dissecting phylogenetic fuzzy weighting: theory and application in metacommunity phylogenetics. – Methods Ecol. Evol. 7: 937-946.

Fabre, P. et al. 2012. A glimpse on the pattern of rodent diversification: a phylogenetic approach. – BMC Evol. Biol. 12: 88.

Fauth, J. E. et al. (1996) Simplifying the jargon of community ecology: a conceptual approach. – Am. Nat. 147: 282-286.

Felsestein, J. 1985. Phylogenies and the comparative method. – Am. Nat. 125: 1-15.

Gaston, K. J. et al. 2008. Ecogeographical rules: elements of a synthesis. – J. Biogeogr. 35: 483-500.

Hawkins, B. A. 2012. Eight (and a half) deadly sins of spatial analysis. – J. Biogeogr. 39: 1-9.

Hijmans, R.J. et al. 2005. Very high resolution interpolated climate surfaces for global land areas. – Int, J. Climatol. 25: 1965–1978.

IUCN 2008. The IUCN Red List of Threatened Species. – <http://www.iucnredlist.org/technical-documents/spatial-data>.

Kendall, D. 1977. The diffusion of shape. – Adv. Appl. Probab. 9: 428–430.

Klingenberg, C. P. 2013. Visualizations in geometric morphometrics: how to read and make graphs showing shape changes. – Hystrix 24: 15-24.

Klingenberg, C. P. et al. 2002. Shape analysis of symmetric structures: quantifying variation among individuals and asymmetry. – Evolution 56: 1909-1920.

Lawing, A. M. et al. 2016. Community functional trait composition at the continental scale: the effects of non-ecological processes. – Ecography doi: 10.1111/ecog.01986.

Legendre, P. 1993. Spatial autocorrelation: trouble or new paradigm? – Ecology 74: 1659–1673.

Leibold, M. A. et al. 2010. Metacommunity phylogenetics: separating the roles of environmental filters and historical biogeography. – Ecol. Lett. 13: 1290-1299.

Leite, R. N. et al. 2014. In the wake of invasion: tracing the historical biogeography of the South American cricetid radiation (Rodentia, Sigmodontinae). – PloS ONE 9: e100687.

Leite, Y. L. R. et al. 2015. Evolutionary affinities of the “Lost World” mouse suggest a late Pliocene connection between the Guiana and Brazilian shields. – J. Biogeogr. 42: 706-715.

Losos, J. B. 2008. Phylogenetic niche conservatism, phylogenetic signal and the relationship between phylogenetic relatedness and ecological similarity among species. – Ecol. Lett. 11: 995-1003.

Machado, L. F. et al. 2015. Molecular phylogenetic position of endangered *Wilfredomys* within Sigmodontinae (Cricetidae) based on mitochondrial and nuclear DNA sequences and comments on Wiedomyini. – Zootaxa 3986: 421-434.

Maddison, W. P. and Maddison, D. R. 2011. Mesquite: A modular system for evolutionary analysis. Version 2.75. – <http://mesquiteproject.org>.

Maestri, R. and Patterson, B. D. 2016. Patterns of species richness and turnover for the South American rodent fauna. – PloS ONE 11: e0151895.

Maestri, R. et al. 2016a. Predictors of intraspecific morphological variability in a tropical hotspot: comparing the influence of random and non-random factors. – J. Biogeogr. 43: 2160-2172.

Maestri, R. et al. 2016b. Geographical variation of body size in sigmodontine rodents depends on both environment and phylogenetic composition of communities. – J. Biogeogr. 43: 1192-1202.

Mares, M. A. (ed.) 1999. Encyclopedia of Deserts. – Univ. Oklahoma Press.

Martínez, J. J. and Cola, V. D. 2011. Geographic distribution and phenetic skull variation in two close species of *Graomys* (Rodentia, Cricetidae, Sigmodontinae). – Zool. Anz. 250: 175-194.

Martínez, J. J. et al. 2014. Ecological preference between generalist and specialist rodents: spatial and environmental correlates of phenotypic variation. – Biol. J. Linn. Soc. 112: 180-203.

Matsunami, H. and Buck, L. B. 1997. A mutigene family encoding a diverse array of putative pheromone receptors in mammals. – Cell 90: 775-784.

Meiri, S. and Thomas, G. H. 2007. The geography of body size – challenges of the interspecific approach. – Global Ecol. Biogeogr. 16: 689-693.

Meloro, C. et al. 2014. In and out the Amazonia: evolutionary ecomorphology in howler and capuchin monkeys. – Evol. Biol. 41: 38-51.

Monteiro, L. R. et al. 2003. Environmental correlates of geographical variation in skull and mandible shape of the punaré rat *Thrichomys apereoides* (Rodentia, Echimyidae). – J. Zool. 261: 47-57.

Morrone, J. J. et al. 2014. Biogeographical regionalisation of the Neotropical region. – Zootaxa 3782: 1-110.

Oksanen, J. et al. 2015. vegan: community ecology package. R package version 2.3-1. – <http://CRAN.R-project.org/package=vegan>.

Olalla-Tárraga, M. Á. et al. 2010. Cross-species and assemblage-based approaches to Bergmann's rule and the biogeography of body size in *Plethodon* salamanders of eastern North America. – Ecography 33: 362–368.

Olson, V. A. et al. 2009. Global biogeography and ecology of body size in birds. – Ecol. Lett. 12: 249-259.

Parada, A. et al. 2013. Dating an impressive Neotropical radiation: molecular time estimates for the Sigmodontinae (Rodentia) provide insights into its historical biogeography. – Mol. Phylogenet. Evol. 66: 960-968.

Parada, A. et al. 2015. The influence of ecological and geographical context in the radiation of Neotropical sigmodontine rodents. – BMC Evol. Biol. 15: 172.

Pardiñas, U. F. J. et al. 2016. A new genus for *Habrothrix angustidens* and *Akodon serrensis* (Rodentia, Cricetidae): again paleontology meets neontology in the legacy of Lund. – Mastozool. Neotrop. 23: 93-115.

Patton, J.L. et al. (eds.) 2015. Mammals of South America, Vol. 2: rodents. – Univ. Chicago Press.

Pillar, V. D. and Duarte, L. D. S. 2010. A framework for metacommunity analysis of phylogenetic structure. – Ecol. Lett. 13: 587–596.

Prakash, I. and Ghosh, P. K. (eds.) 1975. Rodents in desert environments. – Dr. W. Junk publishers, the Hague.

Quay, W. B. 1954. The anatomy of the diastemal palate in microtine rodents. – Univ. Michigan Press.

R Core Team. 2014. R: a language and environment for statistical computing. R Foundation for Statistical Computing, Vienna, Austria. – <https://www.R-project.org/>.

Rangel, T. F. L. V. B. et al. 2006. Towards an integrated computational tool for spatial analysis in macroecology and biogeography. – Global Ecol. Biogeogr. 15: 321-327.

Rangel, T. F. et al. 2010. SAM: a comprehensive application for Spatial Analysis in Macroecology. – Ecography 33: 46–50.

Ricotta, C. and Moretti, M. 2011. CWM and Rao's quadratic diversity: a unified framework for functional ecology. – Oecologia 167: 181-188.

Rodríguez, M. Á. et al. 2008. Bergmann's rule and the geography of mammal body size in the Western Hemisphere. – Global Ecol. Biogeogr. 17: 274–283.

Rohlf, F. J. 2015. The tps series of software. – Hystrix 26: 9-12.

Rohlf, F. J. and Slice, D. 1990. Extensions of the Procrustes method for the optimal superimposition of landmarks. Syst. Zool. 39: 40-59.

Salazar-Bravo, J. et al. 2013. A phylogenetic appraisal of Sigmodontinae (Rodentia, Cricetidae) with emphasis on phyllotine genera: systematics and biogeography. – Zool. Scr. 42: 250-261.

Schenk, J. J. et al. 2013. Ecological opportunity and incumbency in the diversification of repeated continental colonizations by muroid rodents. – Syst. Biol. 62: 837-864.

Teta, P. et al. 2016. Phylogeny of the tribe Abrotrichini (Cricetidae, Sigmodontinae): integrating morphological and molecular evidence into a new classification. – Cladistics doi: 10.1111/cla.12164

Vilela, J. F. et al. (2013) Sigmodontine rodents diversified in South America prior to the complete rise of the Panamanian Isthmus. – J. Zool. Sys. Evol. Res. 52: 249-256.

Violle, C. et al. 2014. The emergence and promise of functional biogeography. – Proc. Natl. Acad. Sci. 111: 38.

Voss, R. S. (1988) Systematics and ecology of ichthyomyine rodents (Muroidea): patterns of morphological evolution in a small adaptive radiation. – Bull. Am. Mus. Nat. Hist. 188: 259-493.

Webb, C. O. et al. 2008. Phylocom: software for the analysis of phylogenetic community structure and trait evolution. – Bioinformatics 24: 2098-2100.

Wiens, J. J. 2008. Commentary on Losos (2008): niche conservatism déjà vu. – Ecol. Lett. 11: 1004-1005.

Zelditch, M. L. et al. 2012. Geometric morphometrics for biologists: a primer. 2nd edition. – Elsevier/Academic Press.

Supporting information

Additional Supporting Information may be found in the online version of this article:

Appendix S1. Number of specimens per species of sigmodontine rodents and museum catalogue numbers.

Appendix S2. Definition of landmarks placed on skull and mandible.

Appendix S3. Principal component analysis of shape among sites.

Appendix S4. Results of RDA analyses using median shape across cells.

Appendix S5. Phylogenetic relationships among sigmodontine species.

Appendix S6. Results of RDA analyses using a topology-only tree.

Appendix S7. Geographical variation of the PCPS 1 and associated shape changes.

Tables

Table 1. Redundancy Analysis of skull and mandible shape of sigmodontine rodents on gradients of phylogenetic composition of metacommunities (Principal Components of Phylogenetic Structure – PCPS). Spatial autocorrelation was controlled using PCNM as condition variables in the models.

	Shape Ventral		Shape Lateral		Shape Mandible	
	R^2	*P*	R^2	*P*	R^2	*P*
PCPS 2	0.274	0.001	0.285	0.001	0.350	0.001
PCPS 1	0.150	0.001	0.204	0.001	0.197	0.001
PCPS 3	0.163	0.001	0.112	0.001	0.124	0.001

Table 2. Redundancy Analysis of skull and mandible shape of sigmodontine rodents on environmental variables, with and without controlling for the gradients of phylogenetic composition of metacommunities (Principal Components of Phylogenetic Structure – PCPS). Spatial autocorrelation was controlled using PCNM as condition variables in all models.

Shape ~ Environment						
	Shape Ventral		Shape Lateral		Shape Mandible	
	R^2	*P*	R^2	*P*	R^2	*P*
Temperature Seasonality	0.311	0.001	0.329	0.001	0.428	0.001
Land Cover	0.310	0.001	0.326	0.001	0.370	0.001
Temperature	0.301	0.001	0.283	0.001	0.336	0.001
NDVI	0.180	0.001	0.203	0.001	0.255	0.001
Elevation	0.116	0.001	0.127	0.001	0.136	0.001
Productivity	0.068	0.001	0.085	0.001	0.127	0.001
Shape ~ Condition (PCPS) + Environment						
	Shape Ventral		Shape Lateral		Shape Mandible	
	R^2	*P*	R^2	*P*	R^2	*P*
NDVI	0.040	0.001	0.026	0.001	0.011	0.001
Land Cover	0.024	0.001	0.020	0.001	0.015	0.001
Temperature Seasonality	0.012	0.001	0.007	0.001	0.012	0.001
Productivity	0.024	0.001	0.017	0.001	0.011	0.001
Elevation	0.008	0.001	0.009	0.001	0.008	0.001
Temperature	0.009	0.001	0.007	0.001	0.008	0.001

Table 3. Variance partitioning analysis of skull and mandible shape of sigmodontine rodents on environmental variables and phylogenetic composition of metacommunities (Principal Components of Phylogenetic Structure – PCPS). The unique and shared portions of variation are shown.

	Shape Ventral		Shape Lateral		Shape Mandible	
	R^2	*P*	R^2	*P*	R^2	*P*
PCPS	0.102	0.001	0.076	0.001	0.058	0.001
Environment	0.167	0.001	0.210	0.001	0.172	0.001
Shared component	0.475		0.508		0.605	
Residuals	0.256		0.206		0.165	
Total	1.000		1.000		1.000	

Figures

Figure 1. A theoretic path showing how the composition of species in communities (matrix W) and the average of trait values in each of them (community-weighed means – CWM) are affected by multiple historical and environmental factors. Matrix P refers to community composition weighed by the phylogenetic relationships among species (Pillar & Duarte 2010).

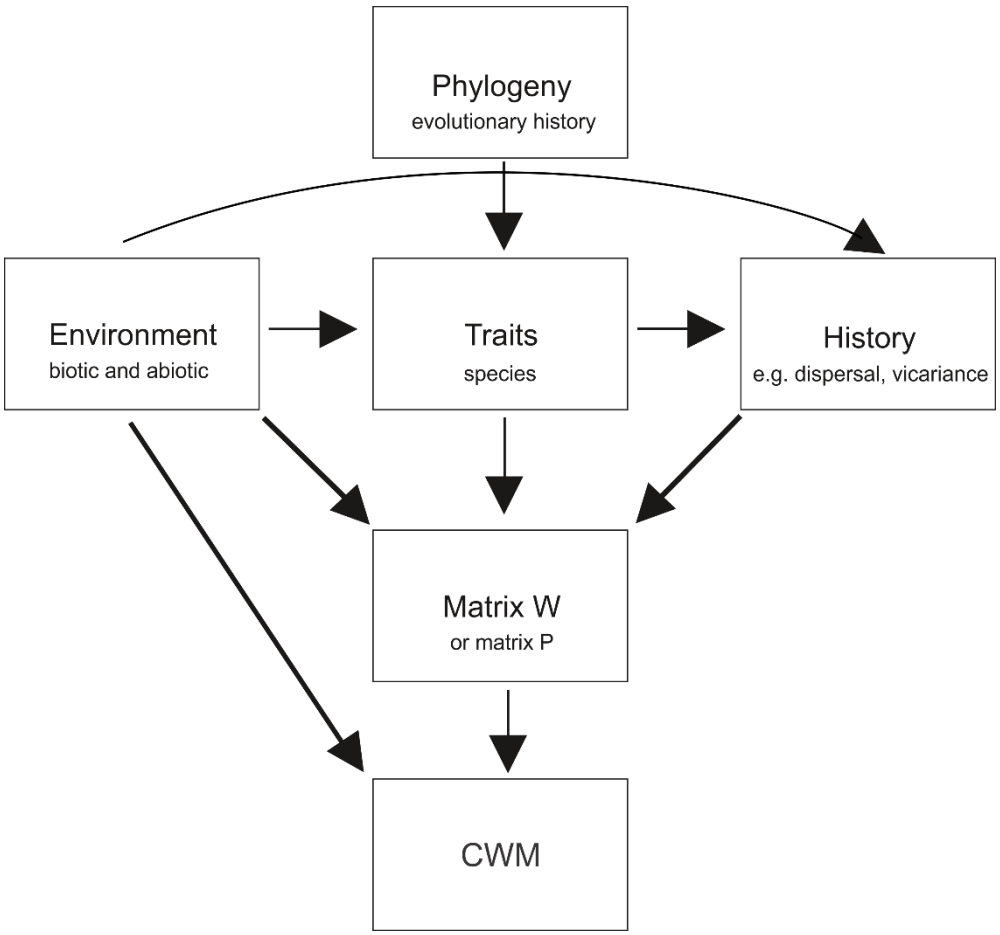

Figure 2. Phylogenetic relationships among 228 species of sigmodontine rodents. Different symbols refers to tribes: circles – white: Akodontini, black: Oryzomyini; stars – white: Phyllotini, black: Thomasomyini; squares – white: Sigmodontini, black: Abrotrichini; triangle – white: "*incertae sedis"* [uncertain placement], black: Ichthyomyini; diamonds – white: Wiedomyini, black: Reithrodontini. Classification follows accounts in Patton et al. (2015); phylogeny based on Parada et al. (2015).

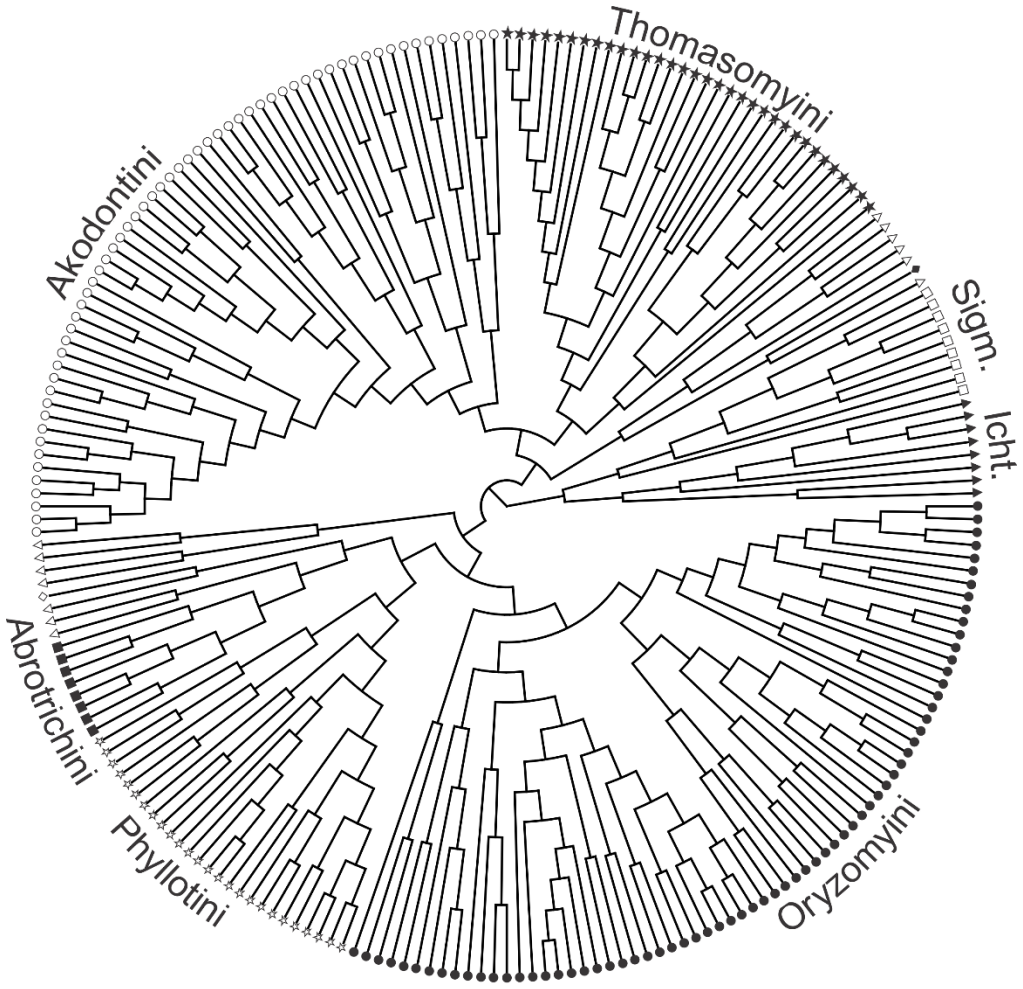

Figure 3. A) Plot of axes 1 and 2, and C) 2 and 3, of variation in phylogenetic structure of communities comprised by sigmodontine rodents across the Neotropics. Main clades of sigmodontines are shown. Sites were omitted. Acronyms are the names of the tribes abbreviated.

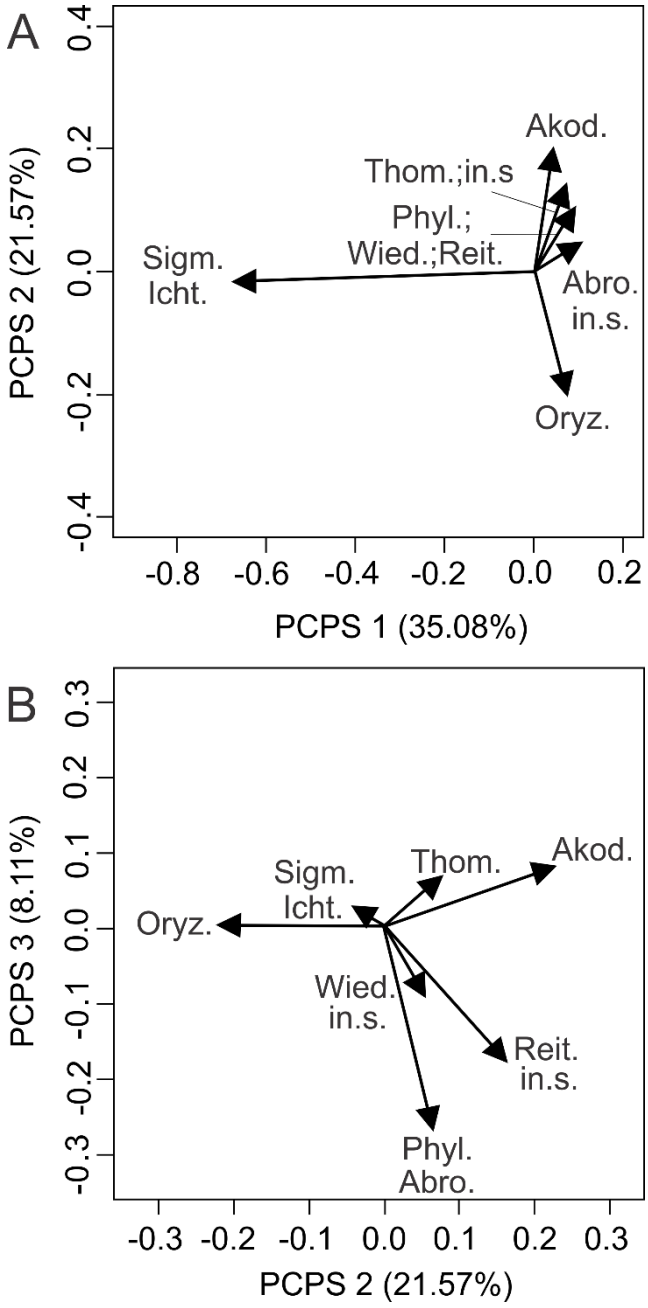

Figure 4. Geographical variation of principal coordinates of phylogenetic structure 2 (left) and 3 (right). Scale bar represents all variation in the orthogonal axis (see Fig. 3) from negative to positive values. Shape variation associated with negatives and positive values on each axis are shown.

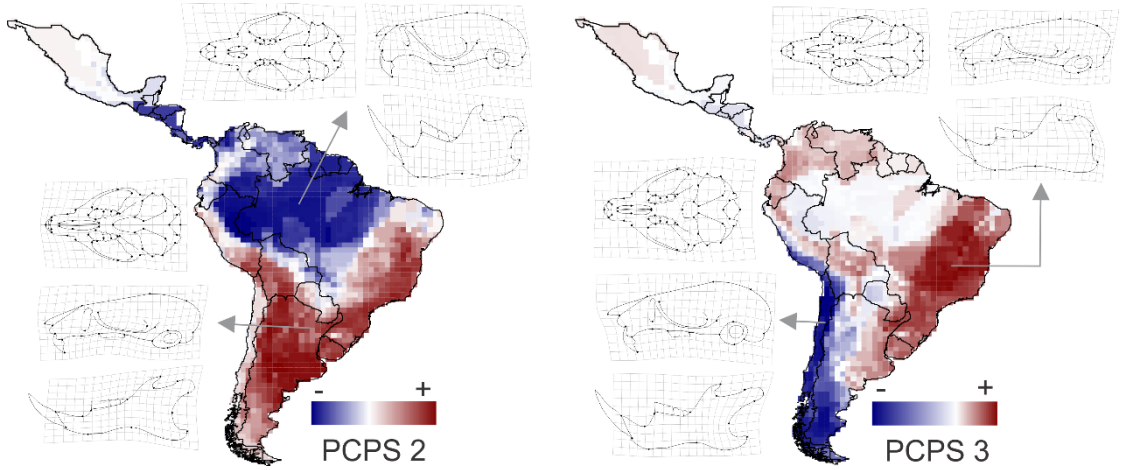

Figure 5. Geographical variation in temperature seasonality and land cover across the Neotropical region. These were the environmental variables most correlated with skull and mandible shape. Shape variation associated with each variable are shown.

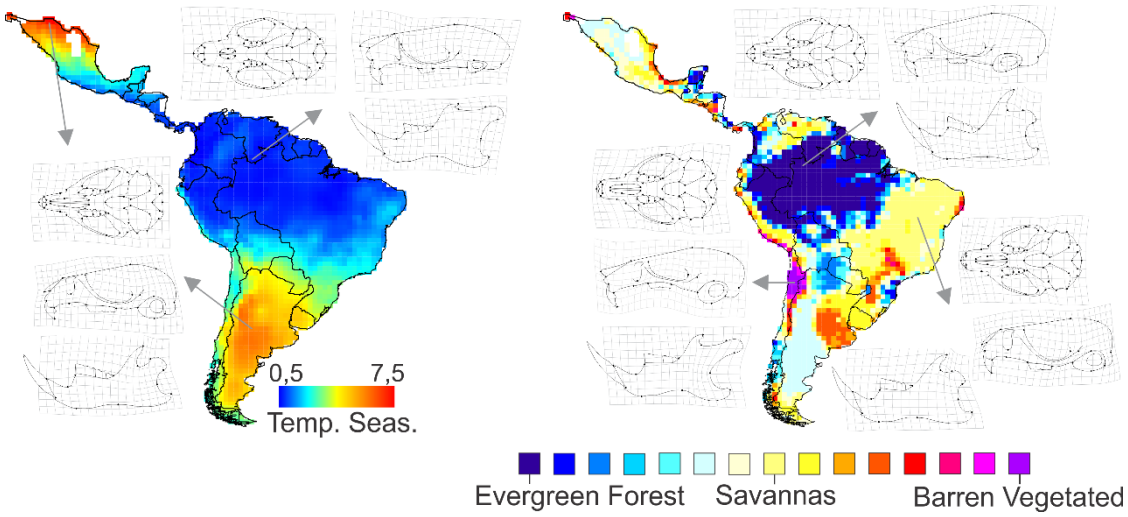

Supporting Information

Appendix S1. Number of specimens included per species of sigmodontine rodents, and the list of museums and catalogue numbers of specimens examined.

Genus	Species	Number of Individuals
Abrawayaomys		
	Abrawayaomys ruschii	6
Abrothrix		
	Abrothrix andina	4
	Abrothrix jelskii	5
	Abrothrix lanosa	6
	Abrothrix longipilis	5
	Abrothrix olivacea	10
Aegialomys		
	Aegialomys xanthaeolus	17
Aepeomys		
	Aepeomys lugens	13
Akodon		
	Akodon aerosus	142
	Akodon affinis	9
	Akodon albiventer	88
	Akodon azarae	101
	Akodon boliviensis	45
	Akodon budini	14
	Akodon caenosus	13
	Akodon cursor	94
	Akodon dayi	30
	Akodon dolores	19
	Akodon fumeus	20
	Akodon iniscatus	4
	Akodon juninensis	20
	Akodon kofordi	5
	Akodon lindberghi	13
	Akodon lutescens	8
	Akodon mimus	11
	Akodon mollis	48
	Akodon montensis	81
	Akodon mystax	32
	Akodon orophilus	23
	Akodon paranaensis	50
	Akodon reigi	2
	Akodon sanctipaulensis	14
	Akodon siberiae	7
	Akodon simulator	25
	Akodon spegazzinii	13
	Akodon subfuscus	65
	Akodon surdus	14
	Akodon sylvanus	2
	Akodon toba	36
	Akodon torques	67
	Akodon varius	10
Andalgalomys		
	Andalgalomys pearsoni	10
Andinomys		
	Andinomys edax	14
Anotomys		
	Anotomys leander	5

Auliscomys		
	Auliscomys boliviensis	10
	Auliscomys pictus	8
	Auliscomys sublimis	11
Blarinomys		
	Blarinomys breviceps	2
Brucepattersonius		
	Brucepattersonius iheringi	3
	Brucepattersonius soricinus	2
Calomys		
	Calomys callosus	13
	Calomys laucha	6
	Calomys lepidus	5
	Calomys musculinus	9
	Calomys sorellus	8
	Calomys venustus	2
Castoria		
	Castoria angustidens	33
Cerradomys		
	Cerradomys langguthi	3
	Cerradomys maracajuensis	11
	Cerradomys scotti	5
Chelemys		
	Chelemys megalonyx	2
Chibchanomys		
	Chibchanomys trichotis	2
Chilomys		
	Chilomys instans	10
Chinchillula		
	Chinchillula sahamae	11
Delomys		
	Delomys dorsalis	5
	Delomys sublineatus	6
Deltamys		
	Deltamys kempi	16
Eligmodontia		
	Eligmodontia morgani	10
Eremoryzomys		
	Eremoryzomys polius	7
Euneomys		
	Euneomys chinchilloides	8
	Euneomys petersoni	6
Euryoryzomys		
	Euryoryzomys legatus	6
	Euryoryzomys macconnelli	8
	Euryoryzomys nitidus	10
	Euryoryzomys russatus	10
Galenomys		
	Galenomys garleppi	7
Geoxus		
	Geoxus valdivianus	16
Graomys		
	Graomys domorum	6
	Graomys griseoflavus	20
Handleyomys		
	Handleyomys alfaroi	17
	Handleyomys intectus	5
Holochilus		
	Holochilus brasiliensis	9
	Holochilus sciureus	5

Hylaeamys		
	Hylaeamys megacephalus	9
	Hylaeamys oniscus	1
	Hylaeamys perenensis	10
	Hylaeamys yunganus	8
Ichthyomys		
	Ichthyomys hydrobates	10
	Ichthyomys pittieri	2
	Ichthyomys tweedii	7
Irenomys		
	Irenomys tarsalis	24
Juliomys		
	Juliomys pictipes	1
Juscelinomys		
	Juscelinomys huanchacae	7
Kunsia		
	Kunsia tomentosus	4
Lenoxus		
	Lenoxus apicalis	17
Loxodontomys		
	Loxodontomys micropus	24
Lundomys		
	Lundomys molitor	5
Melanomys		
	Melanomys caliginosus	15
	Melanomys robustulus	3
	Melanomys zunigae	3
Microryzomys		
	Microryzomys altissimus	8
	Microryzomys minutus	18
Neacomys		
	Neacomys guianae	1
	Neacomys spinosus	21
	Neacomys tenuipes	6
Necromys		
	Necromys amoenus	8
	Necromys lactens	2
	Necromys lasiurus	11
	Necromys lenguarum	10
	Necromys obscurus	1
	Necromys urichi	6
Nectomys		
	Nectomys apicalis	13
	Nectomys rattus	9
	Nectomys squamipes	10
Neomicroxus		
	Neomicroxus bogotensis	25
Neotomys		
	Neotomys ebriosus	16
Nephelomys		
	Nephelomys albigularis	9
	Nephelomys auriventer	1
	Nephelomys devius	9
	Nephelomys keaysi	7
	Nephelomys levipes	9
	Nephelomys maculiventer	6
	Nephelomys meridensis	7
	Nephelomys moerex	2
	Nephelomys pectoralis	2
Neusticomys		

	Neusticomys monticolus	12
	Neusticomys venezuelae	1
Oecomys		
	Oecomys bicolor	11
	Oecomys concolor	1
	Oecomys flavicans	9
	Oecomys mamorae	7
	Oecomys paricola	8
	Oecomys phaeotis	7
	Oecomys roberti	6
	Oecomys speciosus	1
	Oecomys superans	10
	Oecomys trinitatis	2
Oligoryzomys		
	Oligoryzomys andinus	3
	Oligoryzomys arenalis	11
	Oligoryzomys chacoensis	10
	Oligoryzomys destructor	10
	Oligoryzomys flavescens	10
	Oligoryzomys fulvescens	9
	Oligoryzomys griseolus	9
	Oligoryzomys longicaudatus	19
	Oligoryzomys magellanicus	11
	Oligoryzomys microtis	11
	Oligoryzomys nigripes	26
	Oligoryzomys vegetus	2
Oreoryzomys		
	Oreoryzomys balneator	1
Oryzomys		
	Oryzomys couesi	13
Oxymycterus		
	Oxymycterus dasytrichus	42
	Oxymycterus delator	7
	Oxymycterus inca	7
	Oxymycterus nasutus	5
	Oxymycterus paramensis	13
	Oxymycterus quaestor	8
	Oxymycterus rufus	6
Paynomys		
	Paynomys macronyx	19
Phyllotis		
	Phyllotis amicus	12
	Phyllotis andium	11
	Phyllotis caprinus	4
	Phyllotis darwini	9
	Phyllotis definitus	3
	Phyllotis gerbillus	12
	Phyllotis haggardi	1
	Phyllotis limatus	10
	Phyllotis magister	11
	Phyllotis osilae	7
	Phyllotis xanthopygus	10
Podoxymys		
	Podoxymys roraimae	2
Pseudoryzomys		
	Pseudoryzomys simplex	6
Punomys		
	Punomys lemminus	2
Reithrodon		
	Reithrodon auritus	15

Rhagomys		
	Rhagomys longilingua	1
Rheomys		
	Rheomys raptor	4
Rhipidomys		
	Rhipidomys austrinus	3
	Rhipidomys caucensis	3
	Rhipidomys fulviventer	11
	Rhipidomys latimanus	7
	Rhipidomys leucodactylus	10
	Rhipidomys maconnelli	2
	Rhipidomys macrurus	1
	Rhipidomys mastacalis	1
	Rhipidomys modicus	4
	Rhipidomys venezuelae	5
	Rhipidomys venustus	13
Scapteromys		
	Scapteromys aquaticus	4
	Scapteromys tumidus	13
Scolomys		
	Scolomys melanops	5
Sigmodon		
	Sigmodon alstoni	10
	Sigmodon arizonae	6
	Sigmodon fulviventer	1
	Sigmodon hirsutus	13
	Sigmodon hispidus	10
	Sigmodon leucotis	4
	Sigmodon mascotensis	4
	Sigmodon peruanus	6
	Sigmodon toltecus	4
Sigmodontomys		
	Sigmodontomys alfari	11
Sooretamys		
	Sooretamys angouya	12
Thalpomys		
	Thalpomys lasiotis	2
Thaptomys		
	Thaptomys nigrita	49
Thomasomys		
	Thomasomys aureus	13
	Thomasomys baeops	12
	Thomasomys cinereiventer	14
	Thomasomys cinereus	14
	Thomasomys daphne	1
	Thomasomys gracilis	4
	Thomasomys hylophilus	11
	Thomasomys incanus	6
	Thomasomys ischyrus	11
	Thomasomys kalinowskii	7
	Thomasomys laniger	10
	Thomasomys monochromos	1
	Thomasomys niveipes	12
	Thomasomys notatus	6
	Thomasomys oreas	6
	Thomasomys paramarum	10
	Thomasomys pyrrhonotus	4
	Thomasomys taczanowskii	2
	Thomasomys vulcani	3
Transandinomys		

	Transandinomys bolivaris	4
	Transandinomys talamancae	15
Wiedomys		
	Wiedomys pyrrhorhinus	8
Wilfredomys		
	Wilfredomys oenax	2
Zygodontomys		
	Zygodontomys brevicaudata	21
	Zygodontomys brunneus	12
Total		**2812**

Box S1. List of museums housing the specimens examined with their catalogue numbers, organized by column. AMNH: American Museum of Natural History; FMNH: Field Museum of Natural History; MCNU: Museu de Ciências Naturais da Ulbra; MLP: Museo de la Plata; MN: Museu Nacional do Rio de Janeiro; MZUSP: Museu de Zoologia da Universidade de São Paulo; USNM: U.S. National Museum of Natural History.

Abrawayaomys	***Akodon cont.***	***Euneomys cont.***	***Oligoryzomys cont.***
MCNU3630	FMNH23357	FMNH50593	FMNH26600
MCNU3629	FMNH23356	FMNH50596	FMNH26601
MCNU3628	FMNH23352	***Euryoryzomys***	FMNH26604
MN23075	FMNH23355	FMNH162819	FMNH26612
MN73415	FMNH23351	FMNH162821	FMNH26613
USNM552416	FMNH23361	FMNH162823	FMNH26613
Abrothrix	FMNH21581	FMNH129265	FMNH26616
FMNH23143	FMNH21578	FMNH129267	FMNH26617
FMNH23144	FMNH21575	FMNH129266	FMNH26618
FMNH23146	FMNH21588	FMNH136915	FMNH14304
FMNH23147	FMNH74880	FMNH136906	FMNH18519
FMNH49386	FMNH74879	FMNH136905	***Oreoryzomys***
FMNH48389	FMNH74874	FMNH136911	USNM513570
FMNH49392	FMNH74876	FMNH136909	***Oryzomys***
FMNH49394	FMNH74875	FMNH136913	FMNH5347
FMNH49395	FMNH41284	FMNH143318	FMNH44702
FMNH50174	FMNH41285	FMNH143319	FMNH54160
FMNH50379	FMNH29127	FMNH117111	FMNH54161
FMNH50380	FMNH23673	FMNH117113	FMNH54162
FMNH50382	FMNH75561	FMNH26786	FMNH54163
FMNH50383	FMNH23671	FMNH117110	FMNH56006
FMNH50384	FMNH52544	FMNH139874	FMNH56007
FMNH127506	FMNH52556	FMNH141637	FMNH56008
FMNH127507	FMNH52555	FMNH141638	FMNH73521
FMNH127504	FMNH75483	FMNH141639	FMNH73522
FMNH127503	FMNH128296	FMNH141640	FMNH73523
FMNH127502	FMNH128298	FMNH141641	FMNH73525
FMNH131540	FMNH128293	FMNH141642	FMNH171227
FMNH131642	FMNH128297	FMNH141643	FMNH171228
FMNH131643	FMNH128295	FMNH141644	FMNH171230
FMNH131645	FMNH30195	FMNH141646	FMNH171231
FMNH131647	FMNH30194	FMNH141648	FMNH171232
FMNH131649	FMNH23384	MZUSP1844	FMNH7818
FMNH131651	FMNH23390	MZUSP1841	FMNH7819
FMNH131652	FMNH23392	MZUSP1894	FMNH7811
FMNH131654	FMNH23389	MZUSP20559	***Oxymycterus***
FMNH131655	FMNH23388	MZUSP20560	MZUSP10777

Aegialomys	FMNH23387	***Galenomys***	MZUSP2089
FMNH179528	FMNH49696	AMNH262814	MZUSP10721
FMNH51756	FMNH49697	AMNH246941	MZUSP29368
FMNH49012	FMNH21559	AMNH246942	MZUSP29374
FMNH51761	FMNH50975	AMNH246943	MZUSP29375
FMNH51763	FMNH20899	AMNH246945	MZUSP9891
FMNH51764	FMNH20902	AMNH246947	MZUSP9832
FMNH51765	FMNH20905	AMNH246946	MZUSP10207
FMNH51766	FMNH20909	***Geoxus***	MZUSP10189
FMNH51767	FMNH20908	FMNH133125	MZUSP10188
FMNH51769	FMNH20910	FMNH133115	MZUSP10187
FMNH51768	FMNH21144	FMNH133116	MZUSP10190
FMNH107377	FMNH81350	FMNH133124	MZUSP29364
FMNH107378	FMNH24481	FMNH134949	MZUSP29365
FMNH107379	FMNH24487	FMNH134948	MZUSP29366
FMNH107380	FMNH24489	FMNH127724	MZUSP29367
FMNH107381	FMNH24425	FMNH133097	MZUSP29369
FMNH107383	FMNH24427	FMNH133103	MZUSP29370
FMNH107386	FMNH24429	FMNH133104	MZUSP22483
FMNH81389	FMNH24431	FMNH124059	MZUSP22487
FMNH81390	FMNH24439	FMNH22499	MZUSP22488
FMNH81391	FMNH24441	FMNH22496	MZUSP22490
FMNH81392	FMNH24440	FMNH22495	MZUSP22491
FMNH81393	FMNH24438	FMNH133094	MZUSP22492
FMNH81394	FMNH24434	FMNH50538	MZUSP21572
FMNH81403	FMNH24432	***Graomys***	MZUSP21573
FMNH81404	FMNH24426	FMNH50961	MZUSP21574
FMNH81405	FMNH24430	FMNH50962	MZUSP10208
FMNH81407	FMNH26817	FMNH50963	MZUSP21575
Aepeomys	FMNH26834	FMNH50968	MZUSP26794
FMNH22154	FMNH26838	FMNH50969	MZUSP21595
FMNH22155	FMNH26846	FMNH21525	MZUSP21594
USNM579496	FMNH26847	FMNH157386	MZUSP23751
USNM579498	FMNH26848	FMNH157387	MZUSP22461
USNM579492	FMNH26851	FMNH157388	MZUSP845
USNM579494	FMNH26850	FMNH157393	MZUSP10085
USNM387954	FMNH26853	FMNH157394	MZUSP35158
USNM387957	FMNH26855	FMNH164754	MZUSP35157
USNM387961	FMNH26858	FMNH164749	MZUSP2771
USNM374597	FMNH29146	FMNH164750	MZUSP10650
USNM374598	FMNH29145	FMNH157385	MZUSP10651
USNM374603	FMNH35243	FMNH157382	FMNH145443
USNM374600	FMNH24535	FMNH164836	FMNH145442
Akodon	FMNH24500	FMNH164837	FMNH145441
USNM236310	FMNH24495	FMNH164838	FMNH145438
USNM236315	FMNH24774	FMNH164841	FMNH145437
USNM274275	FMNH24773	FMNH164842	FMNH53875
USNM274276	FMNH19754	FMNH164843	FMNH53874
USNM236259	FMNH129234	FMNH164844	FMNH175211
USNM236261	FMNH129236	FMNH164846	FMNH179217
USNM236266	FMNH19718	FMNH164850	FMNH175213
USNM236268	FMNH19717	FMNH164857	FMNH175215
USNM236299	FMNH19728	***Handleyomys***	FMNH172366
USNM236263	FMNH19726	FMNH64541	FMNH52622
USNM236269	FMNH19721	FMNH73543	FMNH84365
USNM236276	FMNH19722	FMNH73562	FMNH27652
USNM236300	FMNH19725	FMNH73545	FMNH29250
USNM271407	FMNH19729	FMNH73560	FMNH29253
USNM259611	FMNH94520	FMNH61679	FMNH52623
USNM259612	FMNH94515	FMNH61680	FMNH52630
USNM236314	FMNH29138	FMNH5371	FMNH52624
USNM172966	FMNH19135	FMNH70296	FMNH52633
USNM259622	FMNH30131	FMNH70302	FMNH52625
USNM259623	FMNH30122	FMNH70303	FMNH52626

USNM331060	FMNH30128	FMNH70304	FMNH52631
USNM276608	FMNH30109	FMNH70305	FMNH162837
USNM276609	FMNH30110	FMNH55904	FMNH162839
USNM290926	FMNH30113	FMNH56033	FMNH162841
USNM390141	FMNH30115	FMNH55896	FMNH162843
USNM390699	FMNH30117	FMNH55900	FMNH162845
USNM584503	FMNH29142	FMNH11137	FMNH26592
USNM584504	FMNH30119	FMNH11138	FMNH26595
USNM584505	FMNH30120	FMNH11139	FMNH26587
USNM584506	FMNH122686	FMNH11142	FMNH35354
USNM390160	FMNH29122	FMNH14111	FMNH34383
USNM390161	FMNH29123	***Holochilus***	FMNH23843
USNM390162	FMNH30181	FMNH145308	FMNH26757
USNM271433	FMNH30182	FMNH53948	FMNH26754
USNM290907	FMNH30184	FMNH53949	FMNH128320
USNM290927	FMNH30189	FMNH23307	FMNH128321
USNM236238	FMNH107797	FMNH23308	FMNH128322
USNM236241	FMNH107794	FMNH23311	FMNH128323
USNM238127	FMNH107793	FMNH23313	FMNH128324
USNM259603	FMNH107787	FMNH23314	FMNH122697
USNM141453	FMNH107727	FMNH23315	FMNH95138
USNM181333	FMNH107721	FMNH118811	FMNH136928
USNM181335	FMNH107719	FMNH118819	FMNH136929
USNM181338	FMNH107544	FMNH118816	***Paynomys***
USNM259615	FMNH107549	FMNH118820	FMNH132990
USNM259616	FMNH107546	FMNH118825	FMNH132979
USNM259617	FMNH107530	***Hylaeamys***	FMNH132940
USNM259618	FMNH107772	FMNH143304	FMNH132988
USNM259619	FMNH107777	FMNH143305	FMNH132987
USNM302998	FMNH107760	FMNH143306	FMNH132983
USNM303000	FMNH107754	FMNH143308	FMNH50530
USNM303001	FMNH107751	FMNH143309	FMNH50529
USNM304548	FMNH107747	FMNH143310	FMNH46153
USNM279457	FMNH107744	FMNH143313	FMNH46154
USNM279459	FMNH107703	FMNH143315	FMNH46155
USNM279461	FMNH107704	FMNH143316	FMNH132927
USNM513598	FMNH107705	FMNH63778	FMNH132931
USNM513599	FMNH107717	FMNH75222	FMNH132944
USNM513600	FMNH107718	FMNH75241	FMNH132956
USNM513601	FMNH170485	FMNH75243	FMNH132924
USNM513602	FMNH170487	FMNH75244	FMNH132930
USNM513603	FMNH170489	FMNH75246	FMNH132942
USNM513604	FMNH107803	FMNH75247	FMNH132953
USNM513605	FMNH107805	FMNH75248	***Phyllotis***
USNM364531	FMNH107807	FMNH75273	FMNH81260
USNM181334	FMNH107810	FMNH75269	FMNH81261
USNM181336	FMNH107814	FMNH75270	FMNH81263
USNM121380	FMNH107817	FMNH66401	FMNH19258
USNM121386	FMNH107818	FMNH75242	FMNH19259
USNM541492	FMNH43371	FMNH75253	FMNH19261
USNM304606	FMNH43372	FMNH72051	FMNH107390
USNM304607	FMNH83476	FMNH58778	FMNH107392
USNM309160	FMNH164159	FMNH58779	FMNH107391
USNM462077	FMNH164160	FMNH87970	FMNH107393
USNM462078	FMNH164161	FMNH72067	FMNH107394
USNM484227	FMNH164164	***Ichthyomys***	FMNH107396
USNM484229	FMNH164168	FMNH90293	FMNH19839
USNM484230	FMNH164169	USNM513625	FMNH19841
USNM484521	FMNH157211	USNM151288	FMNH19842
USNM485107	FMNH164101	USNM115315	FMNH19843
USNM485110	FMNH164118	USNM460684	FMNH81208
USNM485115	FMNH164119	USNM461078	FMNH81207
USNM259279	FMNH164136	USNM461094	FMNH81206
USNM259632	FMNH157192	USNM294985	FMNH81205

USNM194753	FMNH157194	USNM562980	FMNH81204
USNM194752	FMNH157197	USNM562981	FMNH81203
USNM194758	FMNH157199	AMNH71382	FMNH81202
USNM194757	FMNH157201	AMNH71383	FMNH41287
USNM195760	FMNH157203	AMNH71384	FMNH85847
USNM194762	FMNH157206	AMNH71385	FMNH85848
USNM194763	FMNH172223	AMNH46732	FMNH85849
USNM194666	FMNH172221	AMNH46730	FMNH119508
USNM196941	FMNH171861	AMNH46731	FMNH119507
USNM259272	FMNH171862	AMNH39594	FMNH22325
USNM259273	FMNH172231	AMNH64624	FMNH22326
USNM259274	FMNH172225	***Irenomys***	FMNH22328
USNM259275	FMNH172227	FMNH134969	FMNH133896
USNM259277	FMNH172229	FMNH134970	FMNH119512
USNM259278	FMNH172233	FMNH134964	FMNH35902
USNM194658	FMNH170501	FMNH134967	FMNH119505
USNM194672	FMNH170503	FMNH134963	FMNH21126
USNM194673	FMNH170506	FMNH133137	FMNH21127
USNM194675	FMNH170508	FMNH133139	FMNH21128
USNM194727	FMNH170509	FMNH133140	FMNH21916
USNM194735	FMNH170510	FMNH133154	FMNH81265
USNM194736	FMNH170511	FMNH133155	FMNH81266
USNM194739	FMNH170517	FMNH133142	FMNH81269
USNM194742	FMNH170519	FMNH50554	FMNH81270
USNM194743	FMNH170523	FMNH50567	FMNH81271
USNM194744	FMNH170524	FMNH50555	FMNH81275
USNM194746	FMNH170526	FMNH50557	FMNH81274
USNM194749	FMNH175021	FMNH50561	FMNH81273
USNM194751	FMNH175023	FMNH50563	FMNH81272
USNM194750	FMNH175025	FMNH50564	FMNH53306
USNM194645	FMNH170029	FMNH50565	FMNH107609
USNM194644	FMNH175031	FMNH50568	FMNH107574
USNM194655	FMNH175033	FMNH133166	FMNH107575
USNM194643	FMNH50980	FMNH133164	FMNH107598
USNM194694	FMNH50983	FMNH133148	FMNH49481
USNM194641	FMNH20981	FMNH133143	FMNH49482
USNM194657	MN33681	***Juliomys***	FMNH49484
USNM194639	MN33681	FMNH94552	FMNH49485
USNM194651	MN33681	***Juscelinomys***	FMNH49487
USNM194642	MN33681	USNM584510	FMNH49488
USNM194656	MN33681	USNM584508	FMNH35360
USNM324907	MN33681	USNM584509	FMNH49475
USNM324908	MN33681	USNM584511	FMNH107683
USNM390146	MN33703	USNM584512	FMNH107690
USNM390147	MN48026	USNM584514	FMNH107691
USNM390148	MN67123	USNM584513	FMNH107692
USNM390150	MN48882	***Kunsia***	FMNH107561
USNM390151	MN48882	FMNH122711	FMNH107611
USNM390152	MN48882	FMNH122710	FMNH107612
USNM390153	MN48882	USNM584515	FMNH107613
USNM390155	MN48882	USNM584516	FMNH107616
USNM390157	MN48882	***Lenoxus***	FMNH22342
USNM390158	MN48888	FMNH20106	FMNH50964
USNM555668	MN48889	FMNH52613	FMNH74870
USNM555669	MN50241	FMNH52612	FMNH50966
USNM194581	MN63121	AMNH72624	FMNH74871
USNM194583	MN48890	AMNH72620	FMNH74872
USNM194586	MN48891	AMNH72622	FMNH74873
USNM194593	MN50255	AMNH72618	FMNH107898
USNM194594	MN50281	AMNH72616	FMNH107900
USNM194595	MN50282	AMNH72615	FMNH107901
USNM194596	MN50283	AMNH72611	FMNH107902
USNM194599	MN50256	AMNH72610	FMNH107903
USNM194600	MN50257	AMNH72609	FMNH107904

USNM194601	MN50258	AMNH264855	FMNH107905
USNM194604	MN50259	AMNH264854	FMNH107929
USNM194609	MN50260	AMNH16553	FMNH107936
USNM194610	MN50261	AMNH16065	FMNH107939
USNM194612	MN50262	AMNH16558	USNM121143
USNM194613	MN50263	***Loxodontomys***	USNM121145
USNM194614	MN50264	FMNH132689	***Podoxymys***
USNM194615	MN50265	FMNH132692	AMNH75584
USNM194618	MN50266	FMNH132706	AMNH75585
USNM194619	MN50267	FMNH132746	***Pseudoryzomys***
USNM194621	MN50269	FMNH132747	FMNH118810
USNM194623	MN50270	FMNH132749	FMNH34236
USNM194626	MN50271	FMNH132751	USNM584585
USNM194627	MN50272	FMNH132752	USNM584586
USNM194628	MN50273	FMNH132668	USNM390668
USNM194629	MN50274	FMNH132666	AMNH262048
USNM194630	MN50275	FMNH132665	***Punomys***
USNM194631	MN50276	FMNH132787	AMNH156781
USNM194633	MN69565	FMNH132785	AMNH256780
USNM194635	MN69566	FMNH132783	***Reithrodon***
USNM194636	MN69567	FMNH132782	FMNH134180
USNM582136	MN69568	FMNH132780	FMNH134188
USNM582137	MN69569	FMNH132779	FMNH134189
USNM582138	MN69570	FMNH132778	FMNH134190
USNM582139	MN69571	FMNH132789	FMNH134225
USNM582141	MN69572	FMNH132791	FMNH134211
USNM582142	MN69573	FMNH132792	FMNH134222
USNM582143	MN69574	FMNH132800	FMNH134224
USNM582169	MN69575	FMNH132804	FMNH50577
USNM582171	MN69576	FMNH132807	FMNH50578
USNM182175	MN69585	***Lundomys***	FMNH124418
USNM290909	MN69586	FMNH29257	FMNH124420
AMNH268750	MN69587	FMNH29260	FMNH124417
AMNH268743	MN69588	FMNH29261	FMNH35339
AMNH268744	MN69589	FMNH29263	FMNH18192
AMNH268751	MN69590	USNM259641	***Rhagomys***
AMNH268745	MN69596	***Melanomys***	FMNH170687
AMNH268746	MN69599	FMNH66576	***Rheomys***
AMNH268747	MN59113	FMNH65577	USNM565826
AMNH268748	MN69602	FMNH65578	USNM396585
AMNH268752	MN69605	FMNH29454	USNM396586
AMNH268738	MN69606	FMNH41475	USNM520769
AMNH268739	MN69609	FMNH43228	USNM516939
AMNH268740	MN69613	FMNH128471	USNM516940
AMNH268741	MN69623	FMNH128472	AMNH185015
AMNH268742	MN69627	FMNH128476	AMNH189291
AMNH67428	MN69628	FMNH128477	AMNH185016
AMNH67431	MN69629	FMNH128488	AMNH185017
AMNH67462	MN69644	FMNH92459	AMNH205314
AMNH67466	MN69645	FMNH70358	AMNH205313
AMNH47567	MN69660	FMNH70364	AMNH205316
AMNH47568	MN69664	FMNH70366	AMNH205315
AMNH47566	MN69665	FMNH70370	AMNH205318
AMNH47556	MN48029	FMNH70347	AMNH205319
AMNH47558	MN48066	FMNH70350	AMNH208256
AMNH47563	MN75283	FMNH70352	AMNH182138
AMNH231302	MN75282	FMNH70354	AMNH205321
AMNH231298	MN48031	FMNH70355	AMNH182137
AMNH231296	MN48032	***Microryzomys***	AMNH207447
AMNH231300	MN48033	FMNH24698	***Rhipidomys***
AMNH71230	MN48034	FMNH24700	FMNH72882
AMNH71220	MN48035	FMNH24704	FMNH72881
AMNH71227	MN48036	FMNH24703	FMNH72883
AMNH71226	MN48041	FMNH24705	FMNH71738

AMNH76691	MN48067	FMNH24685	FMNH71736
AMNH92456	MN48070	FMNH24686	FMNH71744
AMNH260436	MN63110	FMNH24694	FMNH71487
AMNH260439	MN69675	FMNH175045	FMNH71488
AMNH260438	MN69676	FMNH175047	FMNH71720
AMNH260440	MN69677	FMNH175049	FMNH71722
AMNH260441	MN69679	FMNH175051	FMNH71723
AMNH260442	MN69681	FMNH175053	FMNH71724
AMNH260445	MN69682	FMNH175055	FMNH71725
AMNH268759	MN69683	FMNH175057	FMNH71726
AMNH268757	MN69685	FMNH175059	FMNH71727
AMNH262681	MN69686	FMNH71951	FMNH71728
AMNH262680	MN69687	FMNH71950	FMNH71729
AMNH262678	MN69695	FMNH71956	FMNH70235
AMNH262677	MN69700	FMNH71957	FMNH70237
AMNH262682	MN69701	FMNH71964	FMNH70238
AMNH206049	MN69705	FMNH71958	FMNH70241
AMNH206047	MN69710	FMNH71966	FMNH70244
AMNH206046	MN69714	FMNH71960	FMNH70247
AMNH206040	MN69715	FMNH71959	FMNH70249
AMNH206041	MN69716	FMNH71954	FMNH43211
AMNH206042	MN69719	***Neacomys***	FMNH41477
AMNH206043	MN69724	FMNH95643	FMNH125049
AMNH206056	MN69735	FMNH125030	FMNH53401
AMNH206050	MN69727	FMNH125033	FMNH41478
AMNH206052	MN69726	FMNH125036	FMNH68652
AMNH262690	MN69737	FMNH125038	FMNH75229
AMNH262718	MN69741	FMNH125039	FMNH24820
AMNH626692	MN69745	FMNH125041	FMNH24819
AMNH262717	MN71897	FMNH75364	FMNH24816
AMNH262714	MN62119	FMNH75362	FMNH53982
AMNH262711	MN62120	FMNH75360	FMNH53983
AMNH248998	MN54491	FMNH75359	FMNH211417
AMNH263640	MN69584	FMNH75361	FMNH128325
AMNH263630	MN69597	FMNH75363	FMNH140806
AMNH263632	MN69621	FMNH23746	FMNH140807
AMNH263631	MN60640	FMNH24761	FMNH140808
AMNH263642	MN60654	FMNH24762	FMNH19363
AMNH263641	MN69655	FMNH24763	FMNH70261
AMNH262648	MN69657	FMNH20088	FMNH7048
AMNH262685	MN69666	FMNH20089	FMNH21826
AMNH262687	MN69667	FMNH52711	FMNH21828
AMNH262695	MN69669	FMNH19360	FMNH29443
AMNH262719	MN69673	FMNH19691	FMNH71705
AMNH262704	MN63113	FMNH70116	FMNH71706
AMNH247794	MN63114	FMNH70123	FMNH71708
AMNH247789	MN51644	FMNH70124	FMNH71712
AMNH247795	MN71903	FMNH70125	FMNH71713
AMNH247796	MN48065	FMNH70126	FMNH71714
AMNH247797	MN77791	FMNH19653	FMNH71715
AMNH263300	MN71942	***Necromys***	FMNH71716
AMNH263298	MN48027	AMNH259916	FMNH71717
AMNH263295	MN48028	AMNH259917	FMNH71719
AMNH263294	MN42011	AMNH259919	FMNH19831
AMNH263291	MN48030	AMNH259920	FMNH18188
AMNH262745	MN60680	AMNH259921	FMNH21825
AMNH262746	MN60711	AMNH259922	***Scapteromys***
AMNH262747	MN35912	FMNH162771	FMNH29160
AMNH262748	MN35919	FMNH23366	FMNH98288
AMNH262751	MN35921	FMNH122687	FMNH98287
AMNH262753	MN35922	FMNH107836	FMNH122714
AMNH262754	MN35923	FMNH107838	FMNH122713
AMNH268777	MN35924	FMNH107862	USNM
AMNH268776	MN35926	FMNH107864	AMNH206221

AMNH268773	MN35927	FMNH107866	AMNH206223
AMNH268772	MN32637	FMNH10875	AMNH206222
AMNH268771	MN24592	FMNH107680	AMNH206216
AMNH268780	MN24594	FMNH107699	AMNH206209
AMNH268783	MN24595	FMNH25197	AMNH206219
AMNH268779	MN24616	FMNH25198	AMNH206230
AMNH268788	MN24617	FMNH25200	AMNH206244
AMNH268787	MN24627	FMNH26201	AMNH206245
AMNH268786	MN24630	FMNH128339	AMNH206240
AMNH268785	MN24631	FMNH128337	AMNH206231
AMNH231341	MN24632	FMNH128336	***Scolomys***
AMNH231340	MN24639	FMNH128335	USNM513582
AMNH231338	MZUSP29114	FMNH128334	USNM513583
AMNH231337	MZUSP29112	FMNH128333	USNM548381
AMNH231334	MZUSP29100	FMNH128331	USNM513581
AMNH231331	MZUSP29102	FMNH164415	AMNH57522
AMNH231329	MZUSP29103	FMNH164416	***Sigmodon***
AMNH231328	MZUSP29104	FMNH164414	FMNH18683
AMNH231326	MZUSP29105	FMNH164413	FMNH18686
AMNH231325	MZUSP29106	FMNH164411	FMNH18682
AMNH231324	MZUSP29107	FMNH164426	FMNH18693
AMNH231322	MZUSP29108	FMNH164422	FMNH22138
AMNH231318	MZUSP29109	FMNH164421	FMNH18648
AMNH231317	MZUSP29110	FMNH164419	FMNH20040
AMNH231403	MZUSP29111	FMNH164418	FMNH20041
AMNH231400	MZUSP29113	***Nectomys***	FMNH20042
AMNH231399	MZUSP29088	FMNH43208	FMNH20038
AMNH268766	MZUSP29089	FMNH43210	FMNH890
AMNH262724	MZUSP29090	FMNH41465	FMNH891
AMNH268803	MZUSP29091	FMNH41466	FMNH892
AMNH268809	MZUSP29092	FMNH41467	FMNH893
AMNH268810	MZUSP29093	FMNH65687	FMNH894
AMNH268816	MZUSP29094	FMNH65690	FMNH895
AMNH268818	MZUSP29096	FMNH65691	FMNH889
AMNH268819	MZUSP29097	FMNH78696	FMNH13223
AMNH268820	MZUSP29098	FMNH68643	FMNH13224
AMNH268795	MZUSP29099	FMNH68640	FMNH13226
AMNH268797	MZUSP29119	FMNH68639	FMNH44865
AMNH268801	MZUSP29120	FMNH65694	FMNH69157
AMNH268802	MZUSP29121	FMNH19645	FMNH54008
AMNH47486	MZUSP29122	FMNH19644	FMNH54007
AMNH47494	MZUSP29123	FMNH19643	FMNH34962
AMNH47501	MZUSP29124	FMNH19649	FMNH5005
AMNH207963	MZUSP29126	FMNH18549	FMNH34960
AMNH207966	MZUSP29101	FMNH46213	FMNH44009
AMNH207965	MZUSP29115	FMNH18542	FMNH44010
AMNH260579	MZUSP29116	FMNH61896	FMNH34972
AMNH260594	MZUSP29117	FMNH20110	FMNH7930
AMNH260578	MZUSP29118	FMNH61892	FMNH7931
AMNH260431	MZUSP938	FMNH26442	FMNH7934
AMNH260428	MZUSP939	FMNH140805	FMNH7918
AMNH260434	MZUSP942	FMNH20710	FMNH7920
AMNH260430	MZUSP30951	FMNH20711	FMNH7923
AMNH231476	MZUSP31013	FMNH20712	FMNH7925
AMNH231475	MZUSP30997	FMNH20713	FMNH7926
AMNH231472	MZUSP1773	FMNH94390	FMNH7944
AMNH231469	MZUSP1796	FMNH94387	FMNH7938
AMNH60594	MZUSP27226	FMNH94380	FMNH15181
AMNH264231	MZUSP27223	FMNH94385	FMNH14090
AMNH264232	MZUSP1794	FMNH94377	FMNH14089
AMNH264233	MZUSP27225	FMNH93049	FMNH14363
AMNH264238	MZUSP9469	***Neomicroxus***	FMNH8653
AMNH264239	MZUSP2772	FMNH71235	FMNH8656
AMNH264274	MZUSP29127	FMNH71239	FMNH8658

AMNH264272	MZUSP29128	FMNH71240	FMNH8662
AMNH91561	MZUSP30947	FMNH71243	FMNH81341
AMNH91565	MZUSP28965	FMNH71244	FMNH19216
AMNH91564	MZUSP28966	FMNH71247	FMNH81344
AMNH91569	MZUSP626	FMNH18573	FMNH81345
AMNH91577	MZUSP29255	FMNH18574	FMNH81346
AMNH91575	MZUSP29256	FMNH18671	FMNH81347
AMNH91574	MZUSP29257	FMNH18673	FMNH106540
AMNH91578	MZUSP29259	FMNH18675	FMNH106541
AMNH41816	MZUSP29260	USNM374609	FMNH106542
AMNH41803	MZUSP29261	USNM374611	FMNH106544
AMNH41682	MZUSP29262	USNM374613	FMNH73614
AMNH41692	MZUSP29263	USNM387966	FMNH73615
AMNH264296	MZUSP29264	USNM387967	FMNH73616
AMNH264288	MZUSP29247	USNM387969	FMNH73617
AMNH264281	MZUSP29225	USNM579559	FMNH73618
AMNH264293	MZUSP28388	USNM579560	FMNH73619
AMNH264282	MZUSP28379	USNM579562	FMNH73613
AMNH264290	MZUSP28357	USNM579563	***Sigmodontomys***
AMNH264295	MZUSP29239	USNM579564	FMNH70530
AMNH262294	MZUSP29240	USNM579565	FMNH70534
AMNH264292	MZUSP29241	USNM579566	FMNH70535
AMNH264285	MZUSP29242	USNM579567	FMNH70536
AMNH41752	MZUSP29243	***Neotomys***	FMNH90282
AMNH41832	MZUSP29244	FMNH24775	FMNH89563
AMNH41835	MZUSP29245	FMNH81238	FMNH70532
AMNH41675	MZUSP29246	FMNH24776	FMNH69193
AMNH41648	MZUSP29218	FMNH75580	FMNH69196
AMNH41651	MZUSP29219	FMNH49708	FMNH21829
AMNH41656	MZUSP29228	FMNH51262	FMNH53999
AMNH268857	MZUSP29229	FMNH51263	***Sooretamys***
AMNH268856	MZUSP29230	USNM541802	FMNH26752
AMNH268855	MZUSP29231	AMNH231645	FMNH26751
AMNH268850	MZUSP29232	AMNH231644	FMNH26750
AMNH268851	MZUSP29233	AMNH231641	FMNH26749
AMNH268854	MZUSP29234	AMNH231640	FMNH26748
FMNH65705	MZUSP29235	AMNH231639	FMNH26747
FMNH66402	MZUSP29237	AMNH231637	FMNH136919
FMNH68609	MZUSP29238	AMNH231636	FMNH136920
FMNH68612	MZUSP32429	AMNH231634	FMNH136922
FMNH68614	MZUSP32424	***Nephelomys***	FMNH18165
FMNH68616	MZUSP32427	FMNH71840	FMNH18166
FMNH78709	MZUSP29227	FMNH71845	FMNH18167
FMNH41474	MZUSP29226	FMNH71846	***Thalpomys***
FMNH43229	MZUSP3520	FMNH71847	FMNH128327
FMNH43232	MLP5.xi.92.37	FMNH71848	FMNH128326
FMNH19265	MLP5.xi.92.14	FMNH71849	***Thaptomys***
FMNH19268	MLP5.xi.92.28	FMNH71851	MN8780
FMNH19266	MLP5.xi.92.23	FMNH53342	MN8778
FMNH19757	MLP5.xi.92.38	FMNH53344	MN8775
FMNH78715	MLP5.xi.92.24	FMNH53336	MN8771
FMNH78714	MLP5.xi.92.19	FMNH123996	MN8769
FMNH78710	MLP5.xi.92.21	FMNH128415	MN8767
FMNH78720	MLP5.xi.92.18	FMNH128467	MN8764
FMNH75481	MLP5.xi.92.13	FMNH128462	MN8763
FMNH75480	MLP5.xi.92.17	FMNH128464	MN8805
FMNH75479	MLP5.xi.92.1	FMNH128466	MN8804
FMNH75478	MLP10.iii.79.1	FMNH128468	MN8803
FMNH75477	MLP10.iii.79.5	FMNH128469	MN8797
FMNH75476	MLP24.v.77.1	FMNH128470	MN8795
FMNH75475	MLP20.xii.00.16	FMNH170640	MN8792
FMNH75474	MLP16.v.01.10	FMNH170645	MN8788
FMNH75473	MLP16.v.01.9	FMNH170649	MN8787
FMNH75472	MLP30.v.02.2	FMNH170651	MN8785

FMNH75471	MLP14.xii.73.3	FMNH170654	MN8735
FMNH75470	MLP28.ix.95.5	FMNH170655	MN8734
FMNH75479	MLP1.x.70.18	FMNH170658	MN8731
FMNH75565	MLP11.ii.36.7	FMNH172358	MN8730
FMNH75225	MLP18.viii.74.2	FMNH172360	MN8729
FMNH24522	MLP18.viii.74.6	FMNH172362	MN2727
FMNH24525	MLP18.viii.74.4	FMNH171884	MN8724
FMNH24526	MLP18.viii.74.8	FMNH175171	MN8721
FMNH24532	MLP9.ii.99.1	FMNH174173	MN8720
FMNH24534	MLP24.v.96.2	FMNH175175	MN29100
FMNH24536	MLP30.viii.99.8	FMNH175177	MN29101
FMNH24538	MLP14.ix.99.34	FMNH175179	MN29104
FMNH24540	MLP14.ix.99.35	FMNH13213	MN29110
FMNH24542	MLP14.ix.99.3	FMNH13214	MN29096
FMNH24543	MLP14.ix.99.17	FMNH13215	MN29097
FMNH24502	MLP14.ix.99.37	FMNH13217	MN29098
FMNH24506	MLP14.ix.99.45	FMNH13220	MN29099
FMNH24503	MLP14.ix.99.42	FMNH13222	MN69838
FMNH24510	MLP14.ix.99.43	FMNH18646	MN77795
FMNH24512	MLP14.ix.99.30	FMNH18650	MN7041
FMNH78376	MLP14.ix.99.1	FMNH18651	MN7037
FMNH78375	MLP18.v.74.7	FMNH18652	MN7025
FMNH78377	***Andalgalomys***	FMNH18653	MN7033
FMNH52539	FMNH157341	FMNH18654	MN7096
FMNH52523	FMNH164192	FMNH18655	MZUSP29384
FMNH52522	FMNH164190	FMNH54004	MZUSP29385
FMNH52593	FMNH164184	FMNH93133	MZUSP29386
FMNH52294	FMNH164188	FMNH93134	MZUSP29387
FMNH52527	FMNH151997	FMNH20087	MZUSP29388
FMNH52526	AMNH262344	FMNH20085	MZUSP29383
FMNH52525	AMNH262345	***Nesoryzomys***	MZUSP23850
FMNH52524	AMNH262347	FMNH179526	MZUSP24008
FMNH52528	AMNH262346	FMNH30831	***Thomasomys***
FMNH52529	***Andinomys***	FMNH30843	FMNH70320
FMNH52541	FMNH23435	FMNH30832	FMNH70322
FMNH18180	FMNH132648	FMNH30835	FMNH70323
FMNH52538	FMNH132647	FMNH30838	FMNH70327
FMNH52107	FMNH132651	FMNH30839	FMNH70328
FMNH52531	FMNH162757	FMNH30840	FMNH70329
FMNH72100	FMNH162759	FMNH30841	FMNH70331
FMNH170423	FMNH162761	FMNH179527	FMNH70307
FMNH170427	FMNH51281	FMNH30848	FMNH70308
FMNH170428	FMNH51283	FMNH30855	FMNH70309
FMNH170429	FMNH51282	FMNH30854	FMNH70310
FMNH170431	FMNH51279	FMNH30852	FMNH70311
FMNH170408	FMNH29156	FMNH30856	FMNH70316
FMNH170413	FMNH29157	FMNH30859	FMNH90333
FMNH170414	FMNH74869	FMNH30873	FMNH90334
FMNH170415	***Anotomys***	FMNH30871	FMNH90335
FMNH170416	FMNH53367	***Neusticomys***	FMNH90339
FMNH170417	AMNH244607	FMNH71218	FMNH71478
FMNH170412	AMNH244606	FMNH71220	FMNH71480
FMNH170420	AMNH244605	FMNH71222	FMNH71481
FMNH170388	AMNH66202	FMNH71223	FMNH71482
FMNH170393	***Auliscomys***	FMNH71225	FMNH71475
FMNH170396	FMNH49769	USNM406123	FMNH71474
FMNH170397	FMNH49768	AMNH64632	FMNH71471
FMNH170399	FMNH49771	AMNH64633	FMNH71467
FMNH170400	FMNH49773	AMNH64629	FMNH71344
FMNH170403	FMNH49774	AMNH62920	FMNH71348
FMNH170368	FMNH49599	AMNH63376	FMNH71347
FMNH170369	FMNH49600	AMNH244609	FMNH71351
FMNH170371	FMNH49601	AMNH244608	FMNH71329
FMNH170377	FMNH49602	***Oecomys***	FMNH71336

FMNH170379	FMNH49604	FMNH116934	FMNH71337
FMNH170380	FMNH81284	FMNH116936	FMNH71339
FMNH170384	FMNH81228	FMNH116933	FMNH71352
FMNH170385	FMNH81282	FMNH116979	FMNH71353
FMNH170351	FMNH107764	FMNH116973	FMNH71354
FMNH170353	FMNH107748	FMNH116974	FMNH71355
FMNH170357	FMNH107716	FMNH116966	FMNH71356
FMNH170359	FMNH107694	FMNH116926	FMNH81332
FMNH170360	FMNH107678	FMNH116927	FMNH81333
FMNH170361	FMNH107767	FMNH116947	FMNH81337
FMNH172197	FMNH107769	FMNH116946	FMNH81338
FMNH172195	FMNH49550	FMNH87968	FMNH81339
FMNH172193	FMNH107696	FMNH69198	FMNH83444
FMNH172192	FMNH107674	FMNH69199	FMNH81334
FMNH172190	FMNH107675	FMNH69200	FMNH81330
FMNH129981	FMNH107711	FMNH92521	FMNH81329
FMNH129982	FMNH107763	FMNH92525	FMNH81328
FMNH129983	FMNH49546	FMNH92526	FMNH81327
FMNH129986	FMNH49540	FMNH92527	FMNH83446
FMNH129992	FMNH49544	FMNH92528	FMNH83449
FMNH129993	***Blarinomys***	FMNH92530	FMNH83450
FMNH129995	MZUSP34269	FMNH51913	FMNH172378
FMNH107876	USNM304577	FMNH21522	FMNH43393
FMNH52575	***Brucepattersonius***	FMNH25267	FMNH43392
FMNH107880	MZUSP34665	FMNH21524	FMNH70342
FMNH107879	FMNH94499	FMNH21523	FMNH71489
FMNH107890	MZUSP27227	FMNH117061	FMNH18565
FMNH53622	MZUSP10661	FMNH117060	FMNH18576
FMNH53623	MZUSP21129	FMNH94024	FMNH18578
FMNH53624	***Calomys***	FMNH136894	FMNH18580
FMNH107472	FMNH23341	FMNH143292	FMNH18584
FMNH107475	FMNH23393	FMNH136943	FMNH18586
FMNH107479	FMNH23377	FMNH143288	FMNH18588
FMNH107478	FMNH23376	FMNH143291	FMNH18587
FMNH107543	FMNH23373	FMNH143289	FMNH92554
FMNH107488	FMNH23430	FMNH143290	FMNH92558
FMNH107491	FMNH26790	FMNH84314	FMNH92560
FMNH107492	FMNH26792	FMNH68637	FMNH23725
FMNH107497	FMNH26796	FMNH68638	FMNH23731
FMNH107528	FMNH26799	FMNH170604	FMNH23728
FMNH107533	FMNH26795	FMNH172269	FMNH23730
FMNH107470	FMNH28361	FMNH170599	FMNH23732
FMNH107441	FMNH28362	FMNH170602	FMNH23734
FMNH107439	FMNH23404	FMNH175097	FMNH53244
FMNH170630	FMNH23405	FMNH84303	FMNH53407
FMNH107627	FMNH23407	FMNH175099	FMNH92000
FMNH107624	FMNH23409	FMNH88937	FMNH92001
FMNH107593	FMNH23410	FMNH72024	FMNH92002
FMNH107594	FMNH23413	FMNH72030	FMNH92003
FMNH107597	FMNH49551	FMNH62056	FMNH93148
FMNH107600	FMNH49552	FMNH41460	FMNH93150
FMNH107601	FMNH49553	FMNH41458	FMNH93152
FMNH107618	FMNH75420	FMNH41459	FMNH94991
FMNH107619	FMNH54743	FMNH72013	FMNH94993
FMNH107621	FMNH164672	FMNH72025	FMNH23738
FMNH107633	FMNH164723	FMNH72089	FMNH23724
FMNH107554	FMNH164724	FMNH72020	FMNH23739
FMNH107568	FMNH164737	FMNH72027	FMNH23736
FMNH107570	FMNH157322	FMNH72042	FMNH23737
FMNH107573	FMNH157342	FMNH72033	FMNH23735
FMNH107578	FMNH157343	FMNH24574	FMNH23723
FMNH107579	FMNH157352	FMNH24576	FMNH71452
FMNH107580	FMNH157364	***Oligoryzomys***	FMNH71457
FMNH107587	FMNH140812	FMNH20962	FMNH71458

FMNH162735	FMNH140813	FMNH20961	FMNH71459
FMNH162737	FMNH23751	FMNH20963	FMNH71461
FMNH162745	FMNH23752	FMNH19409	FMNH71454
FMNH162645	FMNH23654	FMNH19414	FMNH71455
FMNH162647	FMNH23753	FMNH19415	FMNH71456
FMNH162679	FMNH23757	FMNH19416	FMNH71443
FMNH162681	FMNH23758	FMNH19418	FMNH71444
FMNH162685	FMNH23760	FMNH19419	FMNH71445
FMNH162683	FMNH23763	FMNH19421	FMNH71446
FMNH162687	***Cerradomys***	FMNH19423	FMNH71408
FMNH162689	FMNH19507	FMNH19424	FMNH71409
FMNH162693	FMNH25246	FMNH19425	FMNH71413
FMNH162699	FMNH26446	FMNH19426	FMNH71414
FMNH162707	FMNH116909	FMNH157391	FMNH71416
FMNH162713	FMNH116822	FMNH164910	FMNH71415
FMNH162721	FMNH116823	FMNH164911	FMNH71417
FMNH162723	FMNH116824	FMNH164913	FMNH71419
FMNH162725	FMNH116825	FMNH164914	FMNH71420
FMNH23342	FMNH116826	FMNH164915	FMNH71423
FMNH23341	FMNH116827	FMNH164924	FMNH69190
FMNH23340	FMNH116887	FMNH145314	FMNH170693
FMNH23328	FMNH116888	FMNH26641	FMNH170796
FMNH23329	FMNH116889	FMNH26805	FMNH170697
FMNH23330	FMNH116895	FMNH29238	FMNH170699
FMNH23333	FMNH128310	FMNH122692	FMNH170701
FMNH23334	FMNH128311	FMNH27671	FMNH172380
FMNH23332	FMNH128312	FMNH27668	FMNH75224
FMNH23335	FMNH128313	FMNH27667	FMNH172376
FMNH23336	FMNH128315	FMNH27655	FMNH170707
FMNH23337	***Chelemys***	FMNH27654	FMNH175241
FMNH23339	FMNH22494	FMNH27651	FMNH175243
FMNH22233	FMNH23901	FMNH162807	FMNH175245
FMNH98283	***Chibchanomys***	FMNH162809	FMNH53236
FMNH98282	FMNH71226	FMNH162811	FMNH91984
FMNH95140	USNM442606	FMNH19768	FMNH91986
FMNH23344	***Chilomys***	FMNH19778	FMNH91987
FMNH23345	FMNH71600	FMNH19779	FMNH91988
FMNH23346	FMNH71621	FMNH19780	FMNH91989
FMNH23347	FMNH71607	FMNH19781	FMNH91992
FMNH23348	FMNH71606	FMNH19782	FMNH91993
FMNH23349	FMNH71604	FMNH19783	FMNH91991
FMNH23350	FMNH71602	FMNH143301	FMNH44309
FMNH29218	FMNH71605	FMNH143300	FMNH81296
FMNH29220	FMNH71499	FMNH143299	FMNH84439
FMNH29222	FMNH71495	FMNH143298	FMNH84438
FMNH29223	FMNH71496	FMNH143297	FMNH81295
FMNH29215	***Chinchillula***	FMNH143295	FMNH43249
FMNH29214	FMNH49401	FMNH143293	FMNH93146
FMNH29213	FMNH49402	FMNH29240	FMNH94992
FMNH29211	FMNH49403	FMNH27650	FMNH53980
FMNH29209	FMNH49404	FMNH27649	FMNH74867
FMNH29207	FMNH49405	FMNH27645	FMNH74866
FMNH29205	FMNH49406	FMNH29230	***Transandinomys***
FMNH29200	FMNH49409	FMNH29231	FMNH128493
FMNH29199	FMNH49410	FMNH29232	FMNH128490
FMNH29196	FMNH49411	FMNH29234	FMNH128491
FMNH29195	FMNH49417	FMNH29236	FMNH128492
FMNH27612	FMNH49418	FMNH1305	FMNH70504
FMNH29204	***Delomys***	FMNH73550	FMNH70496
FMNH29188	FMNH26597	FMNH73551	FMNH70497
FMNH29189	FMNH26598	FMNH73554	FMNH70526
FMNH27614	FMNH141628	FMNH72555	FMNH70522
FMNH27615	FMNH145383	FMNH73557	FMNH70492
FMNH27616	FMNH141629	FMNH73561	FMNH70489

FMNH27617	FMNH143287	FMNH73518	FMNH69207
FMNH27620	FMNH136932	FMNH73519	FMNH60211
FMNH27621	FMNH136934	FMNH89332	FMNH69203
FMNH27624	FMNH136936	FMNH18634	FMNH69204
FMNH27625	FMNH136937	FMNH18636	FMNH69205
FMNH27626	FMNH136939	FMNH18637	FMNH71057
FMNH27627	***Deltamys***	FMNH18638	FMNH72058
FMNH27628	MCNU15	FMNH18641	FMNH72059
FMNH27630	MCNU2	FMNH71969	***Wiedomys***
FMNH27631	MCNU9	FMNH71975	FMNH25249
FMNH27632	MCNU8	FMNH71967	FMNH136941
FMNH27633	MCNU6	FMNH71970	FMNH136942
FMNH27635	MCNU7	FMNH133211	USNM538314
FMNH27636	MCNU22	FMNH133217	USNM538306
FMNH27641	MCNU14	FMNH133215	USNM555761
FMNH27670	MCNU5	FMNH133218	USNM304584
FMNH27662	MCNU10	FMNH25312	USNM555760
FMNH27642	MCNU11	FMNH25313	***Wilfredomys***
FMNH27638	MCNUPCE5	FMNH22644	FMNH104933
FMNH27664	MCNU15	FMNH22645	AMNH206020
FMNH27619	MCNU7	FMNH22646	***Zygodontomys***
FMNH27669	MCNU25	FMNH22647	FMNH20051
FMNH52551	MCNU44	FMNH22649	FMNH20052
FMNH64339	***Eligmodontia***	FMNH22651	FMNH20053
FMNH52543	FMNH133029	FMNH133469	FMNH20054
FMNH52545	FMNH133034	FMNH133470	FMNH20055
FMNH52544	FMNH133035	FMNH133471	FMNH87990
FMNH162753	FMNH133036	FMNH133473	FMNH87999
FMNH162751	FMNH133037	FMNH133475	FMNH88004
FMNH162749	FMNH133038	FMNH133476	FMNH88006
FMNH107829	FMNH133041	FMNH133478	FMNH88008
FMNH107834	FMNH133044	FMNH50698	FMNH89014
FMNH107840	FMNH133045	FMNH50699	FMNH18482
FMNH107841	FMNH133046	FMNH50700	FMNH18483
FMNH107848	***Eremoryzomys***	FMNH124339	FMNH18487
FMNH107850	FMNH19763	FMNH127353	FMNH18484
FMNH107853	FMNH19764	FMNH50685	FMNH18485
FMNH107856	FMNH19766	FMNH50686	FMNH18486
FMNH10858	FMNH19767	FMNH50690	FMNH18568
FMNH107863	FMNH129243	FMNH50691	FMNH18630
FMNH107865	FMNH129245	FMNH50693	FMNH21832
FMNH107928	FMNH129242	FMNH50695	FMNH54010
FMNH107940	***Euneomys***	FMNH139838	FMNH70193
FMNH107943	FMNH134186	FMNH139844	FMNH70194
FMNH107944	FMNH134182	FMNH139839	FMNH70188
FMNH107969	FMNH133088	FMNH139842	FMNH70187
FMNH52564	FMNH134183	FMNH139845	FMNH70205
FMNH49699	FMNH133083	FMNH139847	FMNH70204
FMNH49700	FMNH133085	FMNH139848	FMNH70202
FMNH23362	FMNH134181	FMNH84341	FMNH70201
FMNH23363	FMNH133089	FMNH84342	FMNH70199
FMNH23364	FMNH50587	FMNH84343	FMNH70198
FMNH23365	FMNH50590	FMNH84344	FMNH70206
FMNH23360	FMNH50591	FMNH26593	FMNH70226
FMNH23359	FMNH50592	FMNH26599	

Appendix S2. Definition of landmarks placed on the skull and mandible views of all sigmodontine specimens.

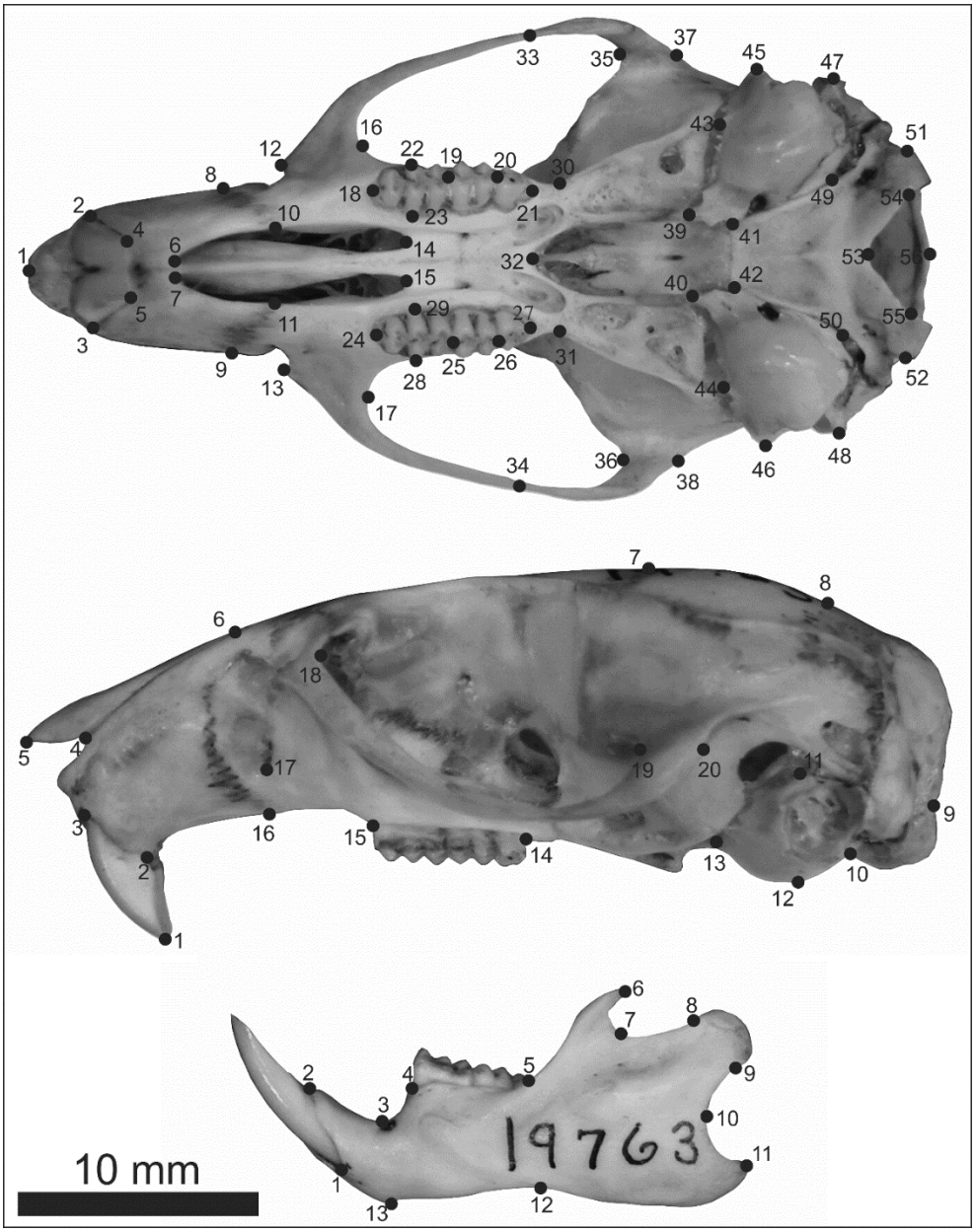

Description of landmarks of skull-ventral view:

L1: anteriormost point of the suture between nasals; **L2,3**: lateralmost point of the alveolus of the incisor; **L4,5**: lateral tip of the incisor; **L6,7**: anteriormost point of the incisive foramen; **L14,15**: posteriormost point of the incisive foramen; **L10,11**: medial extent of the suture between the premaxilla and maxilla lateral to the incisive foramen as seen in the ventral view; **L8,9**: lateralmost extent of suture between the premaxilla and

maxilla; **L12,13**: anterodorsal tip of zygomatic plate; **L16,17**: anteriormost point of the orbit; **L18,24**: anteriormost point of the molar row; **L19,25**: contact point between first and second molars; **L20,26**: contact point between second and third molars; **L21,27**: posteriormost point of the third molar; **L22,28**: lateral paracone of first molar; **L23,29**: medial paracone of first molar; **L30,31**: least post-palatal distance across the palatines; **L32**: posteriormost extent of palate at the midline; **L33,34**: suture between jugal and squamosal in the zygomatic arch as seen in the ventral view; **L35-36**: anteriormost point of the glenoid fossa; **L37,38**: posterior end of squamosal root of zygomatic bar; **L39-40**: anteriormost point of the eustachian tube; **L41,42**: suture between basisphenoid and basioccipital at point of contact with the auditory bulla; **L43-44**: anteriormost border of the paramastoid process; **L45,46:** anteriormost external border of the ectotympanic; **L47,48**: posteriormost margin of the masseteric tubercle; **L49,50**: opening of the basioccipital at the level of the occipital condyle; **L51,52**: lateralmost point of the occipital condyle; **L53**: anteriormost point of the foramen magnum along the midline; **L54**: posteriormost point of the foramen magnum on the midline; **L55,56**: anteriormost margin of the occipital condyle.

Description of landmarks of skull lateral view:

L1: tip of the incisor; **L2:** posteriormost point of the upper incisive alveolus; **L3:** inferiormost point of the upper incisive alveolus; **L4:** anteriormost point of the suture between the nasal and the premaxilla; **L5:** anterior tip of the nasal; **L6:** end of nasal line in lateral view; **L7:** dorsalmost point of the suture between the frontal and the parietal; **L8:** dorsalmost point of the suture between the parietal and the interparietal; **L9:** curvature at the limit between the occipital condyle and the occipital bone; **L10:** inferior extremity on the boundary between the occipital condyle and the tympanic bulla; **L11:**

superiormost point at the middle of the tympanic bulla; **L12:** ventralmost point at the middle of the tympanic bulla; **L13:** anteroventral limit of the tympanic bulla; **L14:** posteriormost point of the molar row; **L15:** anteriormost point of the molar row; **L16:** ventral extent of the suture between maxilla and premaxilla; **L17:** ventral extent of intraorbital foramen; **L18:** anteriormost point of the orbit; **L19:** anteriormost point of the glenoid fossa in the zygomatic bar; **L20:** posterior end of zygomatic bar.

Description of landmarks of mandible view:

L1: Anteroventral border of incisive alveolus; **L2:** Upper extreme anterior border of incisor alveolus; **L3:** Position of greatest inflection of the diastema; **L4:** Anterior edge of the alveolus of first molar; **L5:** Intersection between molar crown and coronoid process in lateral view; **L6:** Tip of the coronoid process; **L7:** Point of maximum curvature between the coronoid and condylar process; **L8:** Dorsal margin of the anterior edge of the articular surface of the condylar process; **L9:** Ventral edge of the articular surface of the condylar process; **L10:** Point of maximum curvature between condylar and angular processes; **L11:** Tip of the angular process; **L12:** Intersection between mandibular body and masseteric crest; **L13:** Ventral limits of the mandibular symphysis.

Appendix S3. Principal Component Analysis of shape among sites, showing the percentage of variance explained. Also shown is a graphical depiction of shape changes associated with the first principal component for each view.

Skull shape in ventral view

PC	Eigenvalues	% Variance	Cumulative %
1	0,00035529	53,613	53,613
2	0,00015509	23,403	77,016
3	0,00006389	9,641	86,657
4	0,00003302	4,982	91,639
5	0,00001630	2,460	94,100
6	0,00000697	1,051	95,151
7	0,00000636	0,960	96,111
8	0,00000549	0,829	96,940
9	0,00000357	0,539	97,478
10	0,00000292	0,440	97,918

Skull shape in lateral view

PC	Eigenvalues	% Variance	Cumulative %
1	0,00036422	46,044	46,044
2	0,00020444	25,846	71,890
3	0,00007841	9,913	81,803
4	0,00005864	7,414	89,217
5	0,00002466	3,118	92,334
6	0,00001944	2,458	94,792
7	0,00001061	1,342	96,134
8	0,00000578	0,731	96,865
9	0,00000477	0,603	97,468
10	0,00000387	0,490	97,957

Mandible shape

PC	Eigenvalues	% Variance	Cumulative %
1	0,00061185	54,194	54,194
2	0,00028392	25,148	79,342
3	0,00007941	7,034	86,376
4	0,00004421	3,916	90,292
5	0,00002551	2,260	92,551
6	0,00002264	2,005	94,557
7	0,00001672	1,481	96,037
8	0,00001193	1,057	97,094
9	0,00000822	0,728	97,822
10	0,00000563	0,499	98,321

Mean Shape Ventral

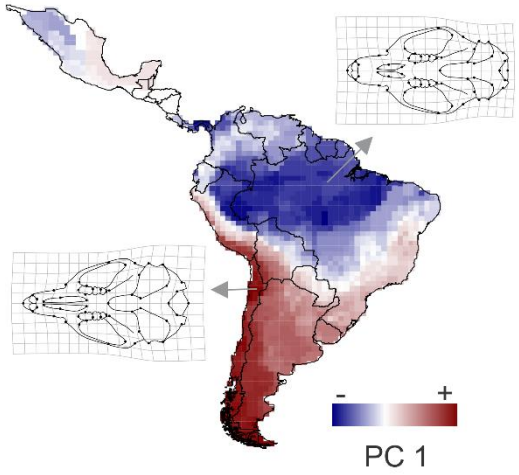

Median Shape Ventral

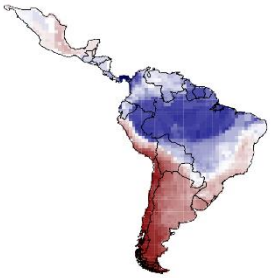

Mean Shape Lateral

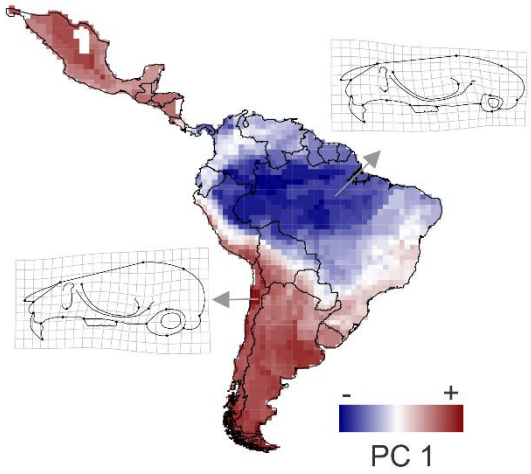

Median Shape Lateral

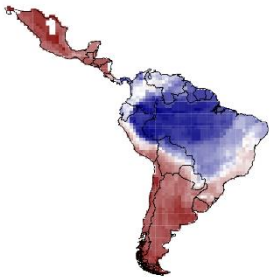

Mean Shape Mandible

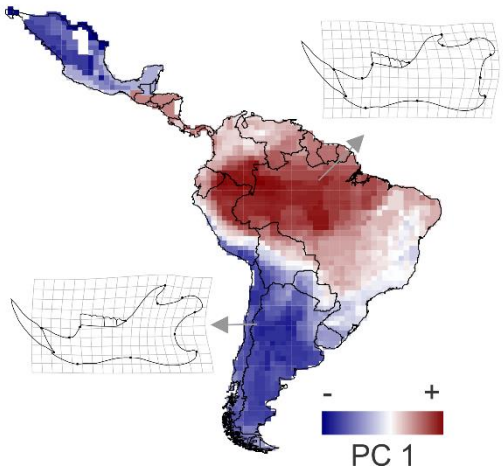

Median Shape Mandible

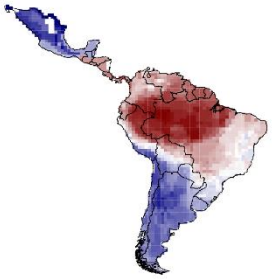

Appendix S4. Results of RDA analyses using the median shape across cells as response variables, and treating richness as a covariate.

Table S2. Redundancy analysis of median skull and mandible shape of sigmodontine rodents on gradients of phylogenetic composition of metacommunities (Principal Components of Phylogenetic Structure – PCPS). Spatial autocorrelation was controlled for by using PCNM as condition variables in the models.

Median shape ~ PCPS						
	Shape ventral		Shape Lateral		Shape Mandible	
	R^2	*P*	R^2	*P*	R^2	*P*
PCPS 2	0.27956	0.001	0.27427	0.001	0.3175	0.001
PCPS 1	0.14635	0.001	0.10895	0.001	0.19962	0.001
PCPS 3	0.16597	0.001	0.19389	0.001	0.11617	0.001

Table S2. Redundancy analysis of median skull and mandible shape of sigmodontine rodents on environmental variables with and without controlling for the gradients of phylogenetic composition of metacommunities (Principal Components of Phylogenetic Structure – PCPS). Spatial autocorrelation was controlled for by using PCNM as condition variables in all models.

Median shape ~ Environment						
	Shape ventral		Shape Lateral		Shape Mandible	
	R^2	*P*	R^2	*P*	R^2	*P*
Temp. Seas.	0.31172	0.001	0.3393	0.001	0.39438	0.001
Land Cover	0.30933	0.001	0.31867	0.001	0.34742	0.001
Temperature	0.32663	0.001	0.27816	0.001	0.30487	0.001
NDVI	0.18393	0.001	0.19285	0.001	0.23856	0.001
Elevation	0.12575	0.001	0.12769	0.001	0.13483	0.001
Productivity	0.06049	0.001	0.08337	0.001	0.11902	0.001
Median shape ~ Condition (PCPS) + Environment						
	Shape ventral		Shape Lateral		Shape Mandible	
	R^2	*P*	R^2	*P*	R^2	*P*
NDVI	0.03018	0.001	0.02214	0.001	0.0146	0.001
Land Cover	0.02253	0.001	0.02376	0.001	0.018	0.001
Temp. Seas.	0.01186	0.001	0.00902	0.001	0.01049	0.001
Productivity	0.01675	0.001	0.01323	0.001	0.0114	0.001
Elevation	0.00588	0.001	0.00915	0.001	0.00672	0.001
Temperature	0.00643	0.001	0.00637	0.001	0.0073	0.001

Table S3. Redundancy analysis of mean skull and mandible shape of sigmodontine rodents on gradients of phylogenetic composition of metacommunities (Principal Components of Phylogenetic Structure – PCPS). Richness was used as a condition variable. Spatial autocorrelation was controlled for by using PCNM as condition variables in the models.

Mean shape ~ Condition (Richness) + PCPS						
	Shape ventral		Shape Lateral		Shape Mandible	
	R^2	*P*	R^2	*P*	R^2	*P*
PCPS 2	0.27425	0.001	0.28487	0.001	0.35027	0.001
PCPS 1	0.0972	0.001	0.12088	0.001	0.11845	0.001
PCPS 3	0.16191	0.001	0.11099	0.001	0.12168	0.001

Table S4. Redundancy analysis of mean skull and mandible shape of sigmodontine rodents on environmental variables. Richness was used as a condition variable. Spatial autocorrelation was controlled for by using PCNM as condition variables in all models.

Mean shape ~ Condition (Richness) + Environment						
	Shape ventral		Shape Lateral		Shape Mandible	
	R^2	*P*	R^2	*P*	R^2	*P*
Temp. Seas.	0.29274	0.001	0.29842	0.001	0.39416	0.001
Land Cover	0.29175	0.001	0.29144	0.001	0.33282	0.001
Temperature	0.3131	0.001	0.2865	0.001	0.34048	0.001
NDVI	0.1678	0.001	0.17928	0.001	0.23005	0.001
Elevation	0.13877	0.001	0.16286	0.001	0.17297	0.001
Productivity	0.0526	0.001	0.06003	0.001	0.09882	0.001

Table S5. Redundancy analysis of median skull and mandible shape of sigmodontine rodents on gradients of phylogenetic composition of metacommunities (Principal Components of Phylogenetic Structure – PCPS). Richness was used as a condition variable. Spatial autocorrelation was controlled for by using PCNM as condition variables in the models.

Median shape ~ Condition (Richness) + PCPS						
	Shape ventral		Shape Lateral		Shape Mandible	
	R^2	*P*	R^2	*P*	R^2	*P*

PCPS 2	0.27959	0.001	0.27434	0.001	0.31759	0.001
PCPS 1	0.10026	0.001	0.12137	0.001	0.12439	0.001
PCPS 3	0.16542	0.001	0.10727	0.001	0.11469	0.001

Table S6. Redundancy analysis of median skull and mandible shape of sigmodontine rodents on environmental variables. Richness was used as a condition variable. Spatial autocorrelation was controlled for by using PCNM as condition variables in all models.

Median shape ~ Condition (Richness) + Environment						
	Shape ventral		Shape Lateral		Shape Mandible	
	R^2	*P*	R^2	*P*	R^2	*P*
Temp. Seas.	0.30537	0.001	0.30451	0.001	0.3579	0.001
Land Cover	0.29217	0.001	0.28193	0.001	0.30831	0.001
Temperature	0.32877	0.001	0.28268	0.001	0.30965	0.001
NDVI	0.17356	0.001	0.16762	0.001	0.21301	0.001
Elevation	0.14921	0.001	0.16458	0.001	0.17323	0.001
Productivity	0.0468	0.001	0.05774	0.001	0.09147	0.001

Appendix S5. Phylogenetic relationships among 228 sigmodontine species, showing species names and a scale bar in millions of years. See main text for details on tree construction.

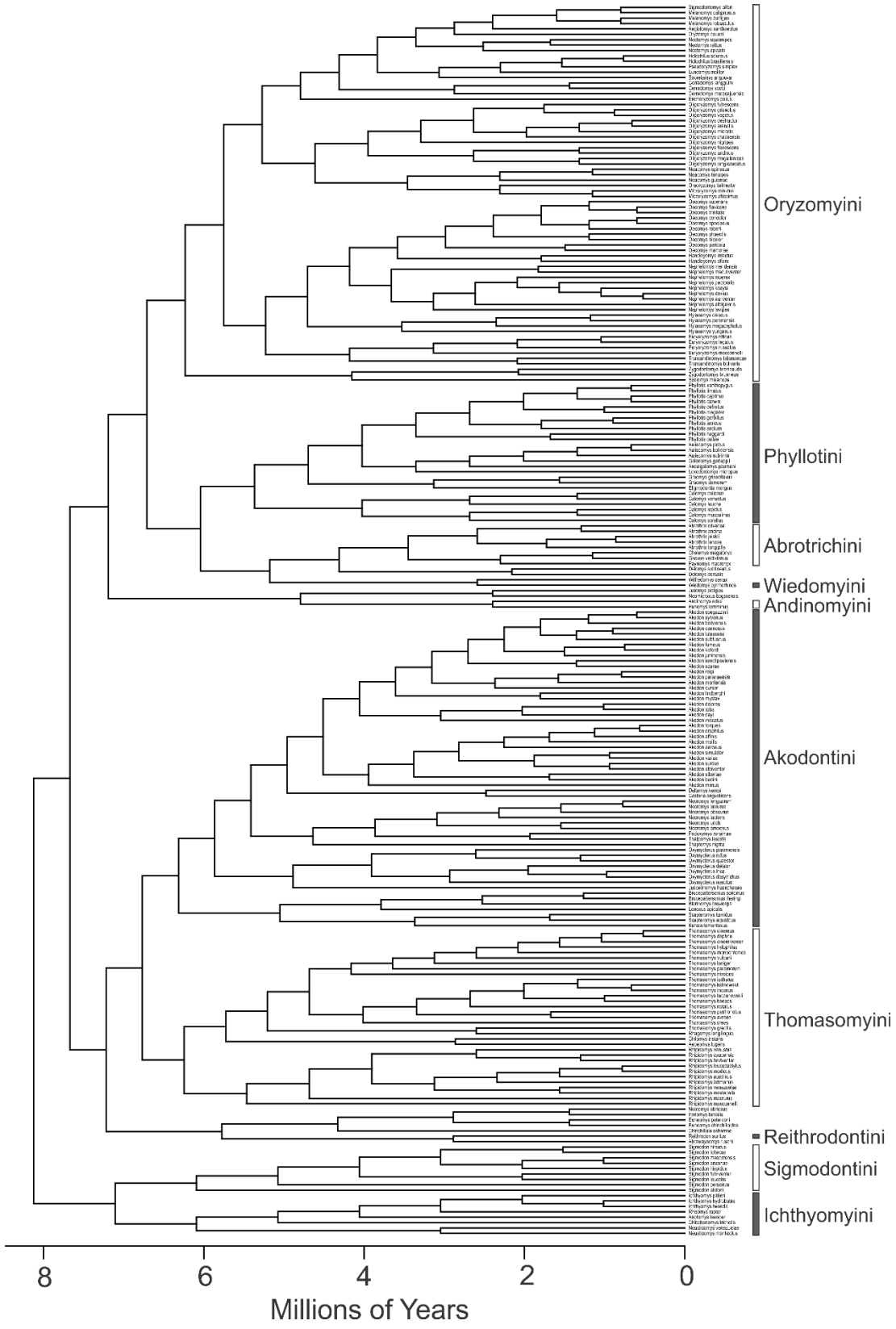

Appendix S6. Results of RDA analyses using the PCPS calculated upon a topology-only tree (with all branch lengths set to 1.0) as explanatory variables. Mean shape across cells was used as a response variable.

Table S3. Redundancy analysis of mean skull and mandible shape of sigmodontine rodents on gradients of phylogenetic composition of metacommunities (Principal Components of Phylogenetic Structure – PCPS) calculated under a topology-only tree. Spatial autocorrelation was controlled for by using PCNM as condition variables in the models.

Mean shape ~ PCPS						
	Shape ventral		Shape Lateral		Shape Mandible	
	R^2	*P*	R^2	*P*	R^2	*P*
PCPS 2	0.2657	0.001	0.3124	0.001	0.3876	0.001
PCPS 1	0.1099	0.001	0.1031	0.001	0.0957	0.001
PCPS 3	0.0515	0.001	0.0366	0.001	0.0413	0.001

Table S2. Redundancy analysis of mean skull and mandible shape of sigmodontine rodents on environmental variables controlling for the gradients of phylogenetic composition of metacommunities (Principal Components of Phylogenetic Structure – PCPS) calculated using a topology-only tree. Spatial autocorrelation was controlled for by using PCNM as condition variables in all models.

Mean shape ~ Condition (PCPS) + Environment						
	Shape ventral		Shape Lateral		Shape Mandible	
	R^2	*P*	R^2	*P*	R^2	*P*
NDVI	0.0056	0.001	0.0061	0.001	0.0048	0.001
Land Cover	0.0331	0.001	0.0221	0.001	0.0176	0.001
Temp. Seas.	0.0279	0.001	0.0152	0.001	0.0228	0.001
Productivity	0.0102	0.001	0.0094	0.001	0.0126	0.001
Elevation	0.0049	0.001	0.0052	0.001	0.0071	0.001
Temperature	0.0186	0.001	0.0146	0.001	0.0126	0.001

Appendix S7. Geographical variation of the PCPS 1 and associated shape changes.

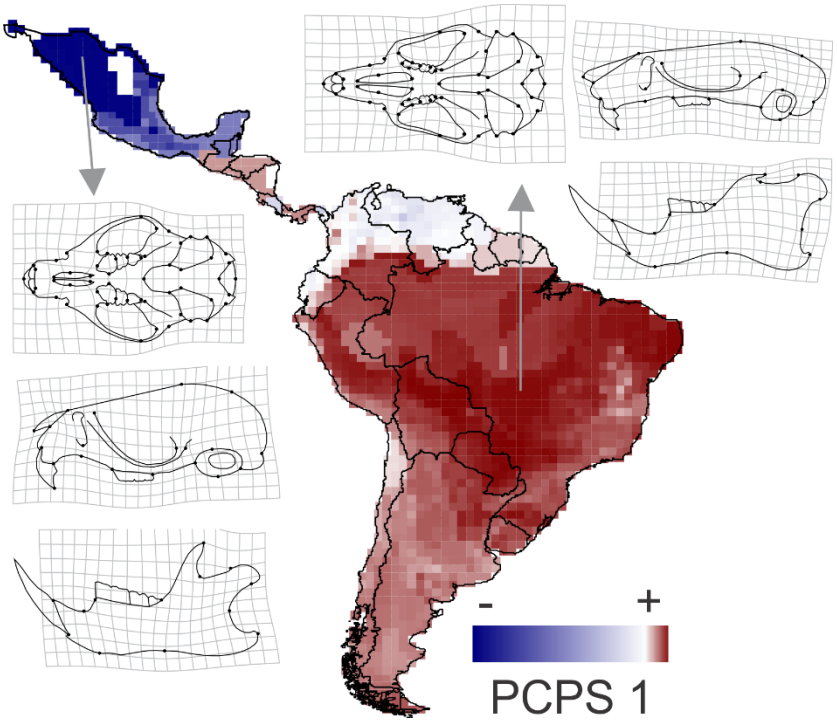

CONCLUSÕES

A parte I da presente tese mostrou que a radiação dos roedores sigmodontíneos no continente sul-americano difere das radiações tipicamente adaptativas, cujos melhores exemplos provêm de ilhas (e.g., Grant & Grant, 2008). A oportunidade ecológica, se presente, não levou à uma grande disparidade adaptativa nesses roedores. Efeitos alopátricos, possivelmente os maiores responsáveis pela especiação no clado (Maestri & Patterson, 2016), também parecem ser, por extensão, os principais determinantes da variação morfológica em sigmodontíneos (capítulo 1 da tese). A morfologia do crânio e mandíbula do grupo, apesar de apresentar relações funcionais com a força da mordida (capítulo 2 da tese), e apresentar uma influência da dieta (capítulos 1 e 2), não parece responder majoritariamente à uma diferenciação ecológica de dieta ou modo de vida, como seria esperado em uma radiação adaptativa (Schluter, 2000). A seleção natural divergente, portanto, não foi a principal responsável pela diferenciação morfológica de forma e tamanho do crânio nos roedores sigmodontíneos.

Essa síntese deriva da combinação de dois fatores: (i) os roedores sigmodontíneos, refletindo os murídeos (Rodentia: Muroidea: Cricetidae: Sigmodontinae; Schenck et al., 2013), apresentam um fenótipo generalista e bem adaptado às diversas condições ecológicas; e (ii) a própria estrutura de radiações evolutivas em escalas continentais parecem favorecer o aparecimento do padrão observado em sigmodontíneos. Um fenótipo generalista tal como o dos sigmodontíneos (Cox et al., 2012) requer pouca mudança seletiva para alcançar adaptação (capítulo 2), e portanto uma baixa diversificação morfológica pode ser esperada. E radiações continentais, em si mesmas, podem ter essa característica de baixa especialização ecológica refletida no fenótipo (Derryberry et al., 2011; Zelditch et al., 2015) quando comparadas às exuberantes radiações adaptativas ocorridas em ilhas (Schluter, 2000). Em grandes escalas espaciais, os efeitos geográficos

(i.e. barreiras à dispersão levando a alopatria) podem ser mais importantes do que a divergência ecológica (Zelditch et al., 2015; capítulo 1), simplesmente porque há mais espaço disponível. Espécies diferentes podem ocupar regiões geográficas diferentes (ainda que ecologicamente similares), gerando distribuições alopátricas e, portanto, evitando competição interespecífica (e consequentemente evitando a disparidade ecológica resultante do deslocamento de caracteres). Talvez uma característica central das radiações continentais seja justamente o fato de que os eventos de especiação podem ser ecologicamente incompatíveis (sob o princípio da exclusão competitiva), mas isso não faz diferença porque as espécies estão em alopatria.

Em sigmodontíneos, os efeitos do contato secundário e da simpatria sobre a evolução morfológica das espécies ainda merece maior atenção. Provavelmente esse contato foi recente, dada a pouca idade da radiação (~ 10 Ma), e ainda exista especialização ecológica incipiente no grupo. Sigmodontíneos insetívoros parecem de fato trilhar o caminho da especialização (parte I da tese). A pouca idade da radiação pode explicar a baixa quantidade de especialização morfológica atualmente refletida no fenótipo. Além disso, a versatilidade do fenótipo sigmodontíneo (*the one-to-many mapping between form and function*) pode permitir especialização ecológica com pouca especialização morfológica.

Na parte II da tese, nota-se uma consistência de explicações quando se passou do nível interespecífico para o intraespecífico. O fluxo gênico (e deriva genética; processos de acúmulo neutro de variação) tem um papel determinante para explicar a forma do crânio entre distintas populações de *Akodon cursor*. Desta forma, processos não-determinísticos explicam melhor a evolução morfológica (especialmente da forma do crânio e mandíbula) tanto no nível interespecífico (parte I) quanto no nível intraespecífico (parte II). O tamanho, no entanto, se mostrou uma característica mais lábil do que a forma,

e mais prontamente modificável por processos determinísticos. Isso fica evidente no capítulo 3, dentro de *Akodon cursor*, e também é notável, em menor grau, ao nível interespecífico, já que a evolução do tamanho parece ser influenciada pelo modo de vida e dieta das espécies (capítulo 1).

Na parte III da tese, os resultados dos capítulos 4 e 5 ressaltam a importância da composição filogenética das comunidades (i.e. das assembleias compostas por sigmodontíneos) em explicar a distribuição do tamanho e forma médios ao longo do espaço. Tanto o tamanho corporal (capítulo 4) quanto a forma do crânio e mandíbula (capítulo 5) são explicados por variação ambiental e pela distribuição de clados filogenéticos ao longo do espaço geográfico. As duas classes de preditores (ambiente e composição filogenética) parecem explicar a mesma proporção da variação na morfologia, o que parece indicar uma conservação filogenética de nicho ao nível de metacomunidades (Pillar & Duarte, 2010). Em outras palavras, o atributo morfológico médio em cada sítio depende de filtros ambientais e, dado que o atributo está estruturado na filogenia (sinal filogenético aproximadamente Browniano para a morfologia entre espécies) e os principais clados apresentam distribuição alopátrica, também depende da proporção de espécies pertencentes à cada clado filogenético em cada sítio.

De modo geral, os resultados da tese mostram que, para entender o processo de evolução fenotípica, é necessário considerar concomitantemente ecologia, filogenia e história biogeográfica. Minha expectativa é que esta tese estimule o debate sobre radiações evolutivas em escalas continentais, sobre a diferenciação morfológica dos roedores sigmodontíneos, e sobre o papel da distribuição filogenética de clados para entender a biogeografia funcional.

Referências

Cox, P.G., Rayfield, E.J., Fagan, M.J., Herrel, A., Pataky, T.C. & Jeffery, N. (2012) Functional evolution of the feeding system in rodents. *Plos One*, **7**, e36299.

Derryberry, E.P., Claramunt, S., Derryberry, G., Chesser, R.T., Cracraft, J., Aleixo, A., Pérez-Emán, J., Remsen Jr, J.V. & Brumfield, R.T. (2011) Lineage diversification and morphological evolution in a large-scale continental radiation: the Neotropical ovenbirds and woodcreepers (Aves: Furnariidae). *Evolution*, **65**, 2973-2986.

Grant, P.R. & Grant, B.R. (2008) *How and why species multiply: the radiation of Darwin's finches*. Princeton University Press, 272p.

Maestri, R. & Patterson, B.D. (2016) Patterns of species richness and turnover for the South American rodent fauna. *PLoS ONE*, **11**, e0151895.

Pillar, V.D. & Duarte, L.D.S. (2010) A framework for metacommunity analysis of phylogenetic structure. *Ecology Letters*, **13**, 587–596.

Schenk, J.J., Rowe, K.C. & Steppan, S.J. (2013) Ecological opportunity and incumbency in the diversification of repeated continental colonizations by muroid rodents. *Systematic Biology*, **62**, 837-864.

Schluter, D. (2000) *The ecology of adaptive radiation*. Oxford University Press, New York.

Zelditch, M.L., Li, J., Tran, L.A.P. & Swiderski, D.L. (2015) Relationships of diversity, disparity, and their evolutionary rates in squirrels (Sciuridae). *Evolution*, **69**, 1284-1300.

ANEXO

Anexo 1

Patterns of species richness and turnover for the South American rodent fauna**

Renan Maestri[1*], Bruce D Patterson[2]

[1]*Programa de Pós-Graduação em Ecologia, Universidade Federal do Rio Grande do Sul, Porto Alegre, RS 91501-970, Brazil.*

[2]*Integrative Research Center, Field Museum of Natural History, Chicago, IL 60605, USA*

* *Correspondence*: renanmaestri@gmail.com

** Artigo publicado no periódico *Plos One* (2016) 11: e0151895 (doi: 10.1371/journal.pone.0151895)

Abstract

Understanding the spatial distribution of species sheds light on the group's biogeographical history, offers clues to the drivers of diversity, and helps to guide conservation strategies. Here, we compile geographic range information for South America's diverse rodents, whose 14 families comprise ~50% of the continent's mammalian species. The South American rodent fauna is dominated by independent and temporally staggered radiations of caviomorph and sigmodontine groups. We mapped species richness and turnover of all rodents and the principal clades to identify the main predictors of diversity patterns. Species richness was highest in the Andes, with a secondary hotspot in Atlantic Forest and some regions of considerable richness in Amazonia. Differences in richness were evident between the caviomorphs and sigmodontines, the former showing the greatest richness in tropical forests whereas the latter show--and largely determine--the all-rodent pattern. Elevation was the main predictor of sigmodontine richness, whereas temperature was the principal variable correlated with richness of caviomorphs. Across clades, species turnover was highest along the Andes and was best explained by elevational relief. In South America, the effects of the familiar latitudinal gradient in species richness are mixed with a strong longitudinal effect, triggered by the importance of elevation and the position of the Andes. Both latitudinal and elevational effects help explain the complicated distribution of rodent diversity across the continent. The continent's restricted-range species—those seemingly most vulnerable to localized disturbance—are mostly distributed along the Andes and in Atlantic Forest, with the greatest concentration in Ecuador. Both the Andes and Atlantic Forest are known hotspots for other faunal and floral components. Contrasting patterns of the older caviomorph and younger sigmodontine radiations underscore the interplay of both historical and ecological factors in determining present-day diversity patterns.

Introduction

A central question in studies of biodiversity concerns how species richness is distributed in space and where it varies and changes the most. By studying aggregate species distributions, macroecological studies can access hidden patterns and help to reveal the main factors explaining these patterns. Diversity in this context can be roughly distinguished in two components: alpha and beta [1]. Alpha diversity is simply the number of species present at a single site or its *species richness*; beta diversity, or here, *species turnover*, concerns changes in species composition among sites [2, 3]. Both components are important to understand how diversity is distributed across space and reflect the group's biogeographic history as well as the ecological opportunities and challenges it has encountered over the course of its diversification. Additionally, both species richness and turnover provide critical information for conservation planning, identifying areas that should be conservation priorities [4].

One of the oldest and most general patterns of species richness is the latitudinal gradient of species richness [5-7]. Several hypotheses have been proposed to explain this richness pattern [8]. Among the most targeted in animal studies are the species-energy and the contemporary climate hypotheses. The species-energy hypothesis states that as the energy available in an ecosystem increases, it can therefore house more species [9, 10]. The species-energy hypothesis has (at least) three versions: the "productivity" and the "ambient-energy" hypotheses, which depend on whether energy influences richness through alimentary resources or thermoregulatory tolerances, respectively [8], and the "evolutionary speed" hypothesis, which relates energy with higher evolutionary rates in tropics ([5, 11] but see Bromham & Cardillo [12]). The contemporary climate hypothesis argues that climate-related features, including its stability, seasonality, and variability, act

to shape patterns of diversity [13, 14] and promote the emergence of the latitudinal diversity pattern [5]. Furthermore, researchers are increasingly noting the effects of topographic complexity (i.e. variation in topography) on both richness [15] and turnover [2], although rises in diversity with increases in topographical complexity has long been appreciated [16]. Consequently, measures of climatic and topographic variables are likely to jointly affect diversity patterns over large spatial scales [e.g., 17]. Whereas variation in species richness is comparatively well studied, patterns and causes for variation in species turnover across large spatial scales is still poorly known [2].

South America offers a special case for studies of macroecology. The continent spans 65 degrees of latitude, including the Equator, and presents a dizzying range of tropical, temperate, and even subantarctic habitats. It has been isolated for most of the last 65 million years, almost as an island, with episodic connections for faunal exchanges with other parts of the world [18]. And it is home to the Andes Mountains, stretching 7000 km along the continent's western margins, the longest continental mountain chain on Earth. These features have combined to generate the world's richest vertebrate faunas [19] and floras [20]. Paradoxically, the challenges of revising and mapping its hyper-diverse faunas and floras have limited macroecological studies in South America to a few relatively well-studied groups at coarse taxonomic scales [e.g., birds: 8], [mammals: 2, 21, 22], [angiosperms: 23].

Rodents comprise more than half of all Neotropical mammal species [24], and South America is home to about a quarter of all the world's rodent species. Most are either "caviomorphs" (relatives of African mole-rats and Old World porcupines) or "sigmodontines" (a Neotropical radiation of the muroid family Cricetidae). Caviomorph ancestors arrived in South America during the Eocene (~50 Ma) via transoceanic dispersal from Africa [25] and the group underwent extensive diversifications in the

Oligocene and Miocene [26]. Although many lineages are now extinct, nearly 250 species and 10 families range across the continent [27]. On the other hand, sigmodontine rodents (Cricetidae: Sigmodontinae) arrived in South America during the Miocene (~ 8 Ma, well before final closure of the Panamanian seaway), via island-hopping or transoceanic dispersal from North America [28-30]. Sigmodontines have radiated into 86 genera and nearly 400 species over this short time period [31]. Including squirrels, pocket mice, harvest mice and other groups, nearly 650 rodent species occur on the continent [27], exploiting fossorial, terrestrial, cursorial, arboreal, and semi-aquatic niches occupied by various mammal groups on other continents [32]. Caviomorphs and sigmodontines thus comprise the two principal monophyletic lineages of rodents in South America [33], with sharply contrasting histories of colonization of the continent [34]. Inside each radiation, phylogenetic analyses have established well-supported monophyletic lineages (i.e. clades) that are formally recognized and named. The older divergences among caviomorph lineages are recognized by placing their divisions into distinct superfamilies (Octodontoidea, Cavioidea, Chinchilloidea, and Erethizontidae [26]), whereas the younger sigmodontine lineages are recognized at the tribal level, grouping related genera within the subfamily Sigmodontinae (e.g. Oryzomyini, Akodontini, Thomasomyini, and Phyllotini [29, 35]).

An earlier analysis of rodent diversity in South America was based on distributions maintained by IUCN [22], which were produced in workshops during 2006 and 2007. Results pointed to four regions of high richness (the Andean yungas, western Amazonia, Atlantic Forest, and the Guianas) and to a modest concentration of threatened species in north-central Peru [22]. To date, no study has mapped the richness of the major clades of South American rodents [but see 26, which was also based on IUCN range maps] or explored their species turnover patterns. Recently, the taxonomy and

geographical distribution of all South American rodents was comprehensively reviewed and revised by taxonomic experts [27]. This new revision permits more accurate analyses of rodent diversity and offers potentially new insights into their biogeography and conservation.

Here, we compiled the range maps of 653 species of rodents according to their distributions as given in Patton et al. [27]. We investigated patterns of species richness and turnover of all South American rodents and the two main clades (caviomorphs and sigmodontines), as well as their components (superfamilies and principal tribes, respectively). Although richness patterns of all mammals in South America have been addressed [36-39], studies are lacking for the major clades of South American rodents, and for the turnover patterns of these clades. We also assessed the distributions of restricted-range species, the quarter with the smallest ranges [40]. We used multiple regressions to evaluate which abiotic predictors might better explain species richness and turnover for these taxonomic groupings.

Materials and Methods

Data Acquisition

Contributors to *The Mammals of South America, Vol. 2. Rodents* [27] revised both the taxonomy and spatial distribution of each species of rodent occurring in South America. This was the most comprehensive revision of taxonomy since [41] and of their geographic ranges since [42]. We used the maps presented in the book to generate a digital image of the map for each species. Range maps of each species were then digitized to create *.shp files using the GSC South America 1969 projection and ArcMap ver. 9.2 software.

The range maps were then mapped onto a grid of 0.5° by 0.5° cells (~ 55 km at the Equator) which was pruned to cover the South American continent. A matrix of presence/absence of each species in each cell was created: species were considered present in a cell if their range occupied at least 50% of the cell. Based on this matrix, we defined the species richness of each cell by summing all the species occurring in it. Species turnover was calculated for each cell as the mean of the beta-diversity values between a focal cell and each of its eight adjacent cells [2]. The metric used to calculate species turnover follows the framework proposed by Baselga [3], where the turnover and nestedness components of beta diversity are decomposed. The spatial turnover component, used in this study, is calculated as a Simpson-based dissimilarity index (β_{SIM}): $\min(b,c)/a+\min(b,c)$, where a is the number of species common to both cells, b is the number of species exclusive to the focal cell, and c is the number of species exclusive to the adjacent cell. We chose β_{SIM} because it is less sensitive to differences in species richness among cells [1].

Species turnover was quantified in R software [43], using the packages betapart [44] and CommEcol (package in development by Adriano S. Melo, available at: http://commecol.r-forge.r-project.org/). Because turnover values present a left-skewed distribution, we applied a square-root transformation of these values, which showed a normal distribution. Richness calculations and the diversity maps were constructed in SAM software [Spatial Analysis in Macroecology; 45]. All images generated were based on maps obtained from open sources (OpenStreetMap, free available at: http://www.openstreetmap.org/).

Environmental correlates

We extracted four environmental variables from the Bioclim database [46] to use as predictors of species richness and turnover: 1) Elevation; 2) Mean temperature; 3) Mean precipitation; and 4) Seasonality in temperature. Temperature is the variable most closely associated with the energy hypothesis [5], elevation sought to capture topographic effects [15], and precipitation and seasonality are productivity- and climate-related features [47]. We chose these variables because they are commonly used in analyses of diversity patterns; studies with mammals have shown them to be correlated with both richness [e.g., 14, 15, 48] and turnover [e.g., 2, 49]. We used values of the original variables in richness tests, on a cell-by-cell basis. However, the environmental variables were modified for correlations with species turnover: here, we employed mean differences of the values in the focal cell from its eight adjacent cells [see 2]. This approach sought to capture neighborhood differences in environmental metrics, and do so at the same spatial scale as the turnover metric itself. Hereafter, we refer to these variables in the text adding the suffix ".dif", to distinguish them from the original variables used in richness tests.

We tested multicollinearity among the predictors by examining the variance inflation factor (VIF). Heuristically, values lower than 10 are taken as evidence of low collinearity between predictors [50]. VIF for our four predictor variables always returned a value lower than 7 in all partial regression tests (see Statistical Analyses), so we opted to use all four variables as predictors. Variables were extracted for each cell using SAM [45]. Mean differences in predictor values of the focal cell from its adjacent cells were calculated using the *select.window* function of the CommEcol package in R [43]. VIF tests were performed with the function *vif.cca* of the package vegan [51].

Statistical analyses

We used multiple regressions to assess the effect of environmental variables on both species richness and turnover, as well as spatial terms to include spatial autocorrelation in the models. Spatial autocorrelation was first evaluated using Moran's I correlograms [52], for both species richness and turnover, for all rodents and for each clade in separate (Moran's correlograms appear in S1 Appendix). We then calculated principal coordinates of neighborhood matrices (PCNM) by performing a principal coordinate analysis (PCoA) on the truncated distance matrix connecting all sites [53]. Truncation distance was defined under a minimum-spanning-tree criterion [54]. Eigenvectors from this PCoA were then selected under the criterion of minimizing Moran's I residuals, and the selected eigenvectors were used in the regressions to correct estimated effects of the predictors, taking into account their spatial autocorrelation [55]. These eigenvectors (spatial filters) represent different spatial gradients, where those with higher eigenvalues characterize broad-scale spatial gradients, whereas eigenvectors with small eigenvalues characterize small scale gradients [53]. Each partial regression was carried out on species richness or turnover using a single environmental variable as predictor at a time, controlling for the effect of spatial filters and for the effects of the other environmental variables. In this way, the independent effect of each variable could be assessed. A model-selection technique based on information theory [56] was used as an alternative to partial regression in order to assess simultaneously the importance of all predictors included in the analysis. The Akaike information criterion (AIC) was used in model selection, and the relative importance of predictors in the best models were ranked by their standardized regression coefficients. PCNM extraction and partial regressions were performed in the R environment [43] with the package vegan [51], via *pcnm* and *rda* functions; model selection based on AIC was conducted with the package MuMIn

[57]. The relationships between diversity metrics with latitude and longitude were evaluated by simple Pearson's correlations.

Results

Species Richness

The overall pattern of rodent diversity is depicted in Fig 1a. High richness is concentrated along the Andes, from Colombia to northern Argentina, with a second hotspot in the Brazilian Atlantic Forest. Other regions, such as western and eastern Amazonia, also support substantial richness. Restricted-range rodents (the quartile of species with the smallest ranges, < 75.62 km^2; see S2 Appendix) are mostly distributed in the Andes, from Mérida (Venezuela) to Tucuman (Argentina), with a great concentration in Ecuador, as well as in the Atlantic Forest of Brazil and Argentina (Fig 2).

Species richness of caviomorphs is high along the Andes, through much of Amazonia and Atlantic Forest, and in some regions of central and northeastern Brazil (Fig 3a). Sigmodontines are rich all along the tropical Andes, with lesser peaks in Atlantic Forest and in the Cerrado (Fig 3b). It is noteworthy that these richness patterns are relative and ignore absolute differences in richness between caviomorphs and sigmodontines; the latter are richer across virtually all of South America. The richness pattern of sigmodontines strongly influences the overall richness pattern, based on 14 families of rodents.

Rodent richness is positively correlated with latitude (r = 0.39, Fig 4c). The pattern is strong for caviomorphs (r = 0.50, Fig 5a), and weaker for sigmodontines (r = 0.14, Fig 6a). Richness patterns are also influenced by elevation (rodents, r = 0.14; caviomorphs, r = -0.07; and sigmodontines, r = 0.31). This correlation and the presence of the Andes

along the continent's western margins mean that richness is also correlated with longitude. Relationships between elevation, longitude and species richness are shown in Fig 4. The plot of elevation on longitude (Fig 4a) shows the imprints of both the Andes in the west and the Serra do Mar in the east. The plot of rodent richness against longitude shows that peaks in elevation and species richness are largely coincident (Fig 4b). Nevertheless, there is considerable variation in richness across both longitude (Fig 4b) and elevation (Figs 4d), and neither variable explains much variation in species richness.

Caviomorph richness is instead highly associated with latitude and with temperature (r = 0.50, Fig 5b), and less influenced elevation (Fig 5d). Plots of caviomorph richness lack the imprint of Andes in their relationship with longitude (Fig 5c).

Sigmodontine patterns (Fig 6) strongly contribute to the rodent-wide patterns and show the same general associations. Despite scatter, there are obvious latitudinal, elevation and longitudinal relationships.

There was significant spatial autocorrelation in all response variables (i.e. richness and turnover for all rodents, caviomorphs and sigmodontines), with similar patterns of positive spatial autocorrelation at smaller scales and mostly negative autocorrelation at larger ones (see S1 Appendix). In general, both partial regressions and model-selection procedures returned similar results concerning the importance of each predictor in explaining diversity patterns (Tables 1 and 2). The main predictors of species richness for all rodents were mean elevation and mean temperature (Tables 1 and 2); positively associated with rodent richness. Caviomorph richness was mainly influenced by temperature, whereas sigmodontine richness was more strongly affected by elevation. Precipitation and seasonality in temperature had smaller influences on overall richness, but contributed modestly to models of caviomorph and sigmodontine richness (Table 2).

Maps of temperature (Fig 7a), elevation (Fig 7b), and topographic complexity (Fig 7c) for South America are shown in Fig.7.

Richness of caviomorph superfamilies in South America is shown in Fig 8. The richest superfamily, Octodontoidea (spiny rats and allies, 182 species), has diversity hotspots in Amazonia and the Atlantic forest, as well as in northern Argentina (Fig 8a). Cavioidea (guinea pigs and allies, 34 species) are rich in the central Andes and the Caatinga (Fig 8b). Living species of Chinchilloidea (chinchillas and pacaranas, 8 species) are restricted to western South America, mainly in the Andes (Fig 8c). Lastly, Erethizontidae (New World porcupines, 14 species) have disjunct centers of richness, with peaks in the Atlantic Forest of Brazil and the northern Andes of Colombia (Fig 8d).

The richness patterns of the main tribes of sigmodontines appear to be largely complementary to one another (Fig 9). Species of the largest tribe, Oryzomyini (rice rats, 121 species), are richest in northern South America, with hotspots of diversity in the northern and central Andes, western Amazonia, the Guianas, and the Cerrado (Fig 9a). In contrast, species of the Akodontini (field mice, 85 species) are concentrated in two hotspots, in the central Andes and the Atlantic forest (Fig 9b). Species of Thomasomyini (Thomas' mice, 74 species) are strongly concentrated in the northern and central Andes, where they overlap with oryzomyines but complement the Andean distributions of akodontines and phyllotines (Fig 9c). Species of Phyllotini (leaf-eared mice, 51 species) overlap with akodontines in the central Andes, but are richer toward the southern tip of the continent (Fig 9d).

Species turnover

Rodent turnover was generally highest all along the Andes, with the region of greatest turnover in the southern Andes (Fig 1b). Other regions, including the Atlantic

Forest-Pampas and Atlantic Forest-Cerrado ecotones, also presented moderate species turnover. The Guianas and most of Amazonia are characterized by low species turnover. This general pattern was evident for both caviomorphs and sigmodontines, exaggerated in the latter by their higher species richness (Fig 3c,d). Spatial differences between these groups include little caviomorph turnover across the Peruvian Andes, where turnover of sigmodontines is high, and far greater turnover of sigmodontines along the margins of the Brazilian Plateau, where Amazonia, Cerrado, Caatinga, and Atlantic Forest all abut one another. Both groups show strong turnover between interior portions of the Atlantic Forest and the more open formations to the west and south (Fig 3c,d).

The best predictor of species turnover (all rodents, caviomorphs, and sigmodontines) was elevation (Tables 1 and 2). Elevational relief is high along both slopes of the Andes mountain chain (Fig 4b), where it is associated with elevated species turnover in rodents (Figs 1b and 3c,d). The turnover component shows a correlation of 0.52 with elevation.dif, -0.24 with longitude, and -0.14 with latitude.

Discussion

The pattern of high species richness and turnover being associated with complex topographies has long been recognized and holds for many taxa [15, 16]. Many species of both Phyllostomidae (bats) and Cricetidae (rodents) reach their distributional range limits of species along the mountain chain [58]; this concentration brings various lowland and upland faunas into close proximity. Here we demonstrate that the Andes host both the highest species richness and species turnover of rodents in South America. Elevational measures offer the best explanations for both richness and turnover patterns for all rodents (Tables 1 and 2). By establishing barriers to dispersal and isolating populations, thus

leading to speciation [15], mountain ranges help generate a high richness and turnover [2,14,15].

The richness of rodents in general, and of sigmodontines in particular, is strongly affected by elevation, which is dominated by the Andes and introduces an indirect effect of longitude. The richness of caviomorphs, on the other hand, is positively associated with temperature, which correlates well with latitude. The turnover component is greatly affected by elevational relief, a pattern that holds across all clades (Tables 1 and 2). Thus, latitudinal effects on species richness of South American rodents are mixed with elevational effects, and consequently by longitude, while species turnover is more closely associated with elevation and less with latitude.

The species-energy hypothesis, therefore, fails to explain diversity patterns of rodents in South America. High-energy environments support great diversity, especially of caviomorphs, but low-energy mountains habitats can harbor an even greater diversity of rodents. Different mechanisms appear to explain these patterns. High-energy environments may contribute to increases in diversity though ecological mechanisms (e.g. productivity, evolutionary speed), as hypothesized. But elevation per se, by disrupting species ranges, may contribute to allopatric speciation and vicariant ecological replacements, even where overall productivity is low (cf. Fig1b). Differences between high- and low-elevation sites in diversity would be diminished if considered in terms of biomass, given the much larger average size of caviomorphs [32]. Disentangling the various mechanisms by which energy can act is beyond the scope of this paper.

The positive association of species richness with elevation is not universal though. In fact, for most groups, the decrease in energy availability with increasing elevation diminishes the number of species [see 5, 59 for reviews]. This is often not the case for mammals [15], as demonstrated here at a macroscale. The pattern of high richness

associated with high elevations was not clear indeed, especially because some exceptionally arid regions of the western Andes (Fig 6c,e) support low species despite their elevational complexity. Such differences may explain why some local or regional studies detect diminishing richness of rodents at higher elevations [e.g., 59].

Bats (Chiroptera) are the second-richest order of mammals in terms of species. Mammal-wide studies of diversity patterns demonstrate that bats have a strong influence on the latitudinal richness gradient [6, 60], and often exhibit the most pronounced latitudinal gradients [21, 61]. Although the latitudinal pattern also holds for non-volant taxa, rodents often do not follow this gradient [60]. We also recovered this pattern and identify elevational effects as a possible explanation.

The general rodent richness pattern is different from that presented in [22] using the IUCN database. That analysis reported higher species richness in Guianan forests, not evident in our analyses (Fig 1a), and lower richness in the Andes, especially to the south in Bolivia and northern Argentina. Nevertheless, these overall richness patterns are based on fundamentally different patterns shown by the continent's principal rodent radiations (caviomorphs and sigmodontines).

The four caviomorph superfamilies all date to the Oligocene [>32 Ma; 26] and each underwent substantial Cenozoic radiations in the absence of other rodents and various other groups [32]. In fact, more genera of Cavioidea, Chinchilloidea, and Erethizontoidea are known from the Miocene (23-5.3 Ma) than are extant in those groups today [62]. Most living genera of caviomorphs had already appeared by the end of the Miocene [26]. The caviomorph radiations can be considered mature and are obvious products of both speciation and extensive extinction. Although Chinchilloidea species are now limited to Andean and peri-Andean regions, fossils show that they were ubiquitous in the Miocene. The other superfamilies are generally diverse in the same regions (Fig 8):

western Amazonia, along the Andes, and along the Atlantic coast of Brazil. The present-day diversity patterns of caviomorphs can offer only a weak signal of their historic diversification patterns [but see 63, for reconstructions based on their phylogenetic patterns].

On the other hand, the sigmodontine tribes and genera appeared only in the late Miocene and Pliocene, 6-2.5 Ma [29, 30], so that their radiations are far younger than the caviomorphs. Although the sigmodontines are distributed throughout the continent, each of the major tribes has diversity hotspots that are largely complementary to one another (Fig 9). The central and southern Andes constitute the chief exception, being a region of overlap where all four major tribes exhibit elevated richness. The central location of this region allows the juxtaposition of different regional faunas, and its topographic complexity allows these to occupy diverse habitats that are zoned by elevation. By interrupting and limiting distributions, topographic complexity promotes both higher species richness and turnover. The complementarity of tribal distributions is also evident: oryzomyines are the dominant sigmodontines in Amazonia and range well into mountainous regions in western Amazonia and the Guiana shield, but exhibit lower richness along Brazil's Serra do Mar (Fig 9a). That same Atlantic Forest region houses a hotspot of akodontine richness, and this group is scarcely present in Amazonian forest (Fig 9b). These two rainforests are similar environmentally and share many widespread species [64]. Historical contingences are likely responsible for the geographically segregated but complementary diversity patterns of sigmodontines [see also 65]. Phylogenetic methods are now being applied to help resolve these relationships [35, 66].

The turnover pattern documented for all rodents are similar to that for all mammals depicted in Melo et al. [2]. Differences in elevation were the main predictor of turnover in their study, as in ours. South America has been called "The Rodent Continent" [R. S.

Voss in 27], and the dominance of rodents (~50% of all species) certainly contributes to these similarities between studies involving all mammals and those focusing solely on rodents. There are dramatic changes in rodent species composition along the Andes from one cell to another, both vertically and horizontally. Studies of widespread Andean forest birds have shown that their geographic distributions average 300 times longer than they are wide, following the ribbon-like distribution of suitable habitat along Andean slopes [67]. Flight allows these animals to cross the intervening river canyons that drain the Eastern Versant. But studies on rodents have shown that speciation often occurs by allopatric divergence in separate watersheds along the Andean versant [68, 69]; species may subsequently become closely juxtaposed via elevational zonation, producing both high richness and high turnover [70].

Elevation thus affects these distributions both historically, by limiting geographic ranges [58] and setting the stage for allopatric speciation, and ecologically, by creating a vertical succession of habitats suitable for a plethora of species [71]. The relative importance of historical or ecological components are apt to vary from place to place and across spatial scales.

Species with small geographic ranges are expected to be more vulnerable to habitat conversion and other localized anthropogenic threats [40]. Restricted-range species of rodents in this study occur mostly in the tropical Andes, especially Ecuador, as well as in the Atlantic Forest. These regions present elevated richness and turnover of rodents, and are characterized by substantial topographic relief that is dissected by river valleys. This spatial pattern was also documented for all terrestrial mammals [72], but it contrasts with recent proposals for rodents based on IUCN Redlist classifications. Using older IUCN distributions, [22] showed that vulnerable species were geographically scattered save for a small concentration in the Peruvian Andes. Because a number of the

restricted-range species used in our analysis do not yet have IUCN classifications, conducting reviews of their status (and reassessing this discrepancy) should be a high conservation priority.

Our study demonstrated that a latitudinal gradient in species richness is coupled with an elevational gradient of great importance in explaining rodent richness and turnover in South America. This finding highlights the importance of the Andes in shaping diversity patterns in the continent, and points to the role of elevation in forging macroecological gradients for terrestrial mammals. Richness, and especially species turnover, are better associated with elevational effects than with latitudinal effects. Caviomorphs and sigmodontines showed different richness patterns, which underscores the importance of treat different evolutionary radiations separately. Future studies might investigate the influence of stochastic processes on richness, such as the mid-domain effect [48]. We hope the newly generated information will help to guide strategies for conserving the extraordinary diversity and vulnerability of faunas in the tropical Andes, the southern Andes, and the Atlantic forest.

Acknowledgments

Primary thanks are due the systematists and biogeographers who are responsible for refining species limits and geographic ranges in South America. We also thank Jessica Mohlman for her work compiling species ranges from the accounts in [27], funded by the Barbara E. Brown Fund for Mammal Research (FMNH).

References

1. Lennon JJ, Koleff P, Greenwood J, Gaston KJ. The geographical structure of British bird distributions: diversity, spatial turnover and scale. J Anim Ecol. 2001; 70(6):966-79.
2. Melo AS, Rangel TFL, Diniz-Filho JAF. Environmental drivers of beta-diversity patterns in New World birds and mammals. Ecography. 2009; 32(2):226-36.
3. Baselga A. Partitioning the turnover and nestedness components of beta diversity. Global Ecol Biogeogr Let. 2010; 19(1):134-43.
4. McKnight MW, White PS, McDonald RI, Lamoreux JF, Sechrest W, Ridgely RS, et al. Putting beta-diversity on the map: broad-scale congruence and coincidence in the extremes. PLoS Biol. 2007; 5(10):e272.
5. Rohde K. Latitudinal gradients in species diversity: the search for the primary cause. Oikos. 1992:514-27.
6. Kaufman DM. Diversity of New World mammals: universality of the latitudinal gradients of species and bauplans. J Mamm. 1995; 76(2):322-34.
7. Rodríguez P, Arita HT. Beta diversity and latitude in North American mammals: testing the hypothesis of covariation. Ecography. 2004; 27(5):547-56.
8. Hawkins BA, Porter EE, Diniz-Filho JAF. Productivity and history as predictors of the latitudinal diversity gradient of terrestrial birds. Ecology. 2003; 84(6):1608-23.
9. Hutchinson GE. Homage to Santa Rosalia or why are there so many kinds of animals? Am Nat. 1959; 93:145-59.
10. Wright DH. Species-energy theory: an extension of species-area theory. Oikos. 1983; 41(3):496-506.
11. Tamma K, Ramakrishnan U. Higher speciation and lower extinction rates influence mammal diversity gradients in Asia. BMC Evol Biol. 2015; 15(1):11.

12. Bromham L, Cardillo M. Testing the link between the latitudinal gradient in species richness and rates of molecular evolution. Journal of Evolutionary Biology. 2003; 16(2):200-7.
13. Rahbek C, Graves GR. Multiscale assessment of patterns of avian species richness. Proc Natl Acad Sci U S A. 2001; 98(8):4534-9.
14. Tognelli MF, Kelt DA. Analysis of determinants of mammalian species richness in South America using spatial autoregressive models. Ecography. 2004; 27(4):427-36.
15. Badgley C. Tectonics, topography, and mammalian diversity. Ecography. 2010; 33(2):220-31.
16. Simpson GG. Species density of North American recent mammals. Syst Zool. 1964:57-73.
17. Jetz W, Fine PVA. Global gradients in vertebrate diversity predicted by historical area-productivity dynamics and contemporary environment. PLoS Biol. 2012; 10(3):e1001292.
18. Patterson BD, Costa LP, editors. Bones, Clones, and Biomes: The history and geography of Recent Neotropical mammals. Chicago: University of Chicago Press; 2012.
19. Jenkins CN, Pimm SL, Joppa LN. Global patterns of terrestrial vertebrate diversity and conservation. Proc Natl Acad Sci U S A. 2013; 110(28):E2602-E10.
20. Kier G, Kreft H, Lee TM, Jetz W, Ibisch PL, Nowicki C, et al. A global assessment of endemism and species richness across island and mainland regions. Proceedings of the National Academy of Sciences. 2009; 106(23):9322-7.
21. Pereira MJR, Palmeirim JM. Latitudinal diversity gradients in New World bats: are they a consequence of niche conservatism? PLoS One. 2013; 8(7):e69245.

22. Amori G, Chiozza F, Patterson BD, Rondinini C, Schipper J, Luiselli L. Species richness and distribution of Neotropical rodents, with conservation implications. Mammalia. 2013; 77(1):1-19.
23. Kerkhoff AJ, Moriarty PE, Weiser MD. The latitudinal species richness gradient in New World woody angiosperms is consistent with the tropical conservatism hypothesis. Proceedings of the National Academy of Sciences. 2014; 111(22):8125-30.
24. Patterson BD. Patterns and trends in the discovery of new Neotropical mammals. Divers Distrib. 2000; 6:145-51.
25. Rowe DL, Dunn KA, Adkins RM, Honeycutt RL. Molecular clocks keep dispersal hypotheses afloat: evidence for trans-Atlantic rafting by rodents. J Biogeogr. 2010; 37(2):305-24. doi: j.1365-2699.2009.02190.x.
26. Upham NS, Patterson BD. Evolution of caviomorph rodents: a complete phylogeny and timetree for living genera. In: Vassallo AI, Antenucci D, editors. Biology of caviomorph rodents: diversity and evolution. Buenos Aires: SAREM Series A; 2015. p. 63-120
27. Patton JL, Pardiñas UFJ, D'Elia G, editors. Mammals of South America, Vol. 2: Rodents. Chicago: University of Chicago Press; 2015.
28. Steppan SJ, Adkins RM, Anderson J. Phylogeny and divergence-date estimates of rapid radiations in muroid rodents based on multiple nuclear genes. Syst Biol. 2004; 53(4):533-53.
29. Parada A, Pardinas UFJ, Salazar-Bravo J, D'Elía G, Eduardo Palma R. Dating an impressive Neotropical radiation: Molecular time estimates for the Sigmodontinae (Rodentia) provide insights into its historical biogeography. Mol Phylogen Evol. 2013; 66:960-8.

30. Vilela JF, Mello B, Voloch CM, Schrago CG. Sigmodontine rodents diversified in South America prior to the complete rise of the Panamanian Isthmus. Journal of Zoological Systematics and Evolutionary Research. 2013; 52(3):249-56. doi: 10.1111/jzs.12057.
31. Lessa EP, Cook JA, D'Elía G, Opazo JC. Rodent diversity in South America: transitioning into the genomics era. Frontiers in Ecology and Evolution: Phylogenetics, Phylogenomics, and Systematics. 2014; 2(39):1-7. doi: 10.3389/fevo.2014.00039.
32. Mares MA, Ojeda RA. Patterns of diversity and adaptation in South American hystricognath rodents. In: Mares MA, Genoways HH, editors. Mammalian biology in South America. Pymatuning symposia in ecology. Pittsburgh: Pymatuning Laboratory of Ecology, University of Pittsburgh; 1982. p. 393-432.
33. Fabre PH, Hautier L, Dimitrov D, Douzery EJP. A glimpse on the pattern of rodent diversification: a phylogenetic approach. BMC Evol Biol. 2012; 12:88. doi: 10.1186/1471-2148-12-88.
34. Patterson BD, Upham NS. A study in contrasts: two extensive Neotropical radiations. Frontiers in Ecology and Evolution. 2014; 2:44. doi: 10.3389/fevo.2014.00044.
35. Leite RN, Kolokotronis S-O, Almeida FC, Werneck FP, Rogers DS, Weksler M. In the wake of invasion: tracing the historical biogeography of the South American cricetid radiation (Rodentia, Sigmodontinae). PLoS One. 2014; 9(6):e100687.
36. Ojeda RA. Diversity and conservation of Neotropical mammals. In: Levin SA, editor. Encyclopedia of Biodiversity, 2nd edition, Volume 2. Waltham, MA: Academic Press; 2013. p. 582-94.
37. Ruggiero A. Latitudinal correlates of the sizes of mammalian geographic ranges in South America. J Biogeogr. 1994; 21:545-59.

38. Ruggiero A, Kitzberger T. Environmental correlates of mammal species richness in South America: effects of spatial structure, taxonomy and geographic range. Ecography. 2004; 27(4):401-16.
39. Ruggiero A, Lawton JH, Blackburn TM. The geographic ranges of mammalian species in South America: spatial patterns in environmental resistance and anisotropy. J Biogeogr. 1998; 25(6):1093-103.
40. Terborgh J. Preservation of natural diversity: The problem of extinction-prone species. BioSci. 1974; 24:715-22.
41. Musser GG, Carleton MD. Superfamily Muroidea. In: Wilson DE, Reeder DAM, editors. Mammal species of the world: a taxonomic and geographic reference, 3rd ed. 2. Baltimore: Johns Hopkins University Press; 2005. p. 894-1531.
42. IUCN. IUCN Redlist of Threatened Species, 2010.2: International Conservation Union; 2008 [12 Aug 2010]. Available from: http://www.iucnredlist.org/.
43. R Core Team. R: a language and environment for statistical computing. Vienna, Austria: R Foundation for Statistical Computing; 2015.
44. Baselga A, Orme D, Villeger S, De Bortoli J, Leprieur F. betapart: Partitioning beta diversity into turnover and nestedness components. R package version 1.3. 2013.
45. Rangel TFLVB, Diniz-Filho JAF, Bini LM. SAM: a comprehensive application for Spatial Analysis in Macroecology. Ecography. 2010; 33:46-50.
46. Hijmans RJ, Cameron SE, Parra JL, Jones PG, Jarvis A. Very high resolution interpolated climate surfaces for global land areas. International Journal of Climatology. 2005; 25(15):1965-78.
47. Begon M. Ecology: from individuals to ecosystems, 4th edition. Oxford: Blackwell; 2006.

48. Stevens RD. Gradients of bat diversity in Atlantic Forest of South America: environmental seasonality, sampling effort and spatial autocorrelation. Biotrop. 2013; 45(6):764-70.
49. López-González C, Presley SJ, Lozano A, Stevens RD, Higgins CL. Ecological biogeography of Mexican bats: the relative contributions of habitat heterogeneity, beta diversity, and environmental gradients to species richness and composition patterns. Ecography. 2015; 38(3):261-72.
50. Gross J. Variance inflation factors. R News. 2003; 3:13-5.
51. Oksanen J, Blanchet FG, Kindt R, Legendre P, Minchin PR, O'Hara RB, et al. vegan: community ecology package. R package version 2.3.1. http://CRAN.R-project.org/package-vegan; 2015.
52. Sokal RR, Oden NL, Thomson BA. Local spatial autocorrelation in biological variables. Biol J Linn Soc. 1998; 65(1):41-61.
53. Borcard D, Legendre P. All-scale spatial analysis of ecological data by means of principal coordinates of neighbour matrices. Ecological Modelling. 2002; 153(1):51-68.
54. Rangel TFL, Diniz-Filho JAF, Bini LM. Towards an integrated computational tool for spatial analysis in macroecology and biogeography. Global Ecol Biogeogr Let. 2006; 15(4):321-7.
55. Diniz-Filho JAF, Bini LM. Modelling geographical patterns in species richness using eigenvector-based spatial filters. Global Ecol Biogeogr Let. 2005; 14(2):177-85.
56. Burnham KP, Anderson DR. Model selection and multimodel inference: a practical information-theoretic approach. New York: Springer Science & Business Media; 2002.

57. Bartoń K. MuMIn: multi-model inference. R package version 1.15.1. http://CRAN.R-project.org/package=MuMIn 2013.

58. Patterson BD, Solari S, Velazco PM. The role of the Andes in the diversification and biogeography of Neotropical mammals. In: Patterson BD, Costa LP, editors. Bones, Clones, and Biomes: The history and geography of Recent Neotropical mammals. Chicago: University of Chicago Press; 2012. p. 351-78.

59. Willig MR, Presley SJ. Biodiversity and metacommunity structure of animals along altitudinal gradients in tropical montane forests. J Trop Ecol. In press:DOI: 10.1017/S0266467415000589.

60. Buckley LB, Davies TJ, Ackerly DD, Kraft NJB, Harrison SP, Anacker BL, et al. Phylogeny, niche conservatism and the latitudinal diversity gradient in mammals. Proc R Soc Lond B. 2010; 277(1691):2131.

61. Willig MR, Patterson BD, Stevens RD. Patterns of range size, richness, and body size in the Chiroptera. In: Kunz TH, Fenton MB, editors. Bat ecology. Chicago: University of Chicago Press; 2003. p. 580-621.

62. Vucetich MG, Arnal M, Deschamps CM, Pérez ME, Vieytes EC. A brief history of caviomorph rodents as told by the fossil record. In: Vassallo AI, Antenucci D, editors. Biology of caviomorph rodents: diversity and evolution. Buenos Aires: SAREM Series A; 2015.

63. Upham NS, Patterson BD. Diversification and biogeography of the Neotropical caviomorph lineage Octodontoidea (Rodentia: Hystricognathi). Mol Phylogen Evol. 2012; 63:417-29. doi: 10.1016/j.ympev.2012.01.020.

64. Costa LP. The historical bridge between the Amazon and the Atlantic Forest of Brazil: a study of molecular phylogeography with small mammals. J Biogeogr. 2003; 30(1):71-86.

65. Patterson BD. Contingency and determinism in mammalian biogeography: the role of history. J Mamm. 1999; 80:345-60.

66. Parada A, D'Elía G, Palma RE. The influence of ecological and geographical context in the radiation of Neotropical sigmodontine rodents. BMC Evol Biol. 2015; 15(1):172.

67. Graves GR. Linearity of geographic range and its possible effect on the population structure of Andean birds. Auk. 1988; 105:47-52.

68. Patton JL, Myers P, Smith MF. Vicariant versus gradient models of diversification: the small mammal fauna of eastern Andean slopes of Peru. In: Peters G, Hutterer R, editors. Biogeography and systematics in the tropics, Bonn, June 5-8 1989. Bonn: Alexander Koenig Zoological Research Institute and Zoological Museum; 1990. p. 355-71.

69. Patton JL, Smith MF. mtDNA phylogeny of Andean mice: a test of diversification across ecological gradients. Evolution. 1992; 46(1):174-83.

70. Voss RS. A new species of *Thomasomys* (Rodentia: Muridae) from eastern Ecuador, with remarks on mammalian diversity and biogeography in the Cordillera Oriental. Amer Mus Novit. 2003; 3421:1-47.

71. Terborgh J. Distribution on environmental gradients. Theory and a preliminary interpretation of distribution patterns in the avifauna of the Cordillera Vilcabamba, Peru. Ecology. 1971; 52:23-40.

72. Schipper J, Chanson JS, Chiozza F, Cox NA, Hoffmann M, Katariya V, et al. The status of the world's land and marine mammals: diversity, threat and knowledge. Science. 2008; 322:225-30.

Supporting Information

S1 Appendix. Moran's I correlograms for rodent richness and turnover.

S2 Appendix. Range sizes of rodent species.

Tables

Table 1. Partial regression analysis of richness and turnover of rodents in South America.

Predictors	Richness					
	All Rodents		Caviomorphs		Sigmodontines	
	R^2	F	R^2	F	R^2	F
Global model	0.095	379.34	0.166	723.07	0.069	215.90
Elevation	**0.055**	**882.54**	0.043	762.27	**0.049**	**606.01**
Temperature	**0.044**	**714.00**	**0.107**	**1859.7**	0.011	142.26
Precipitation	0.024	382.72	0.011	191.88	0.017	213.32
Seasonality	0.010	169.02	0.018	324.80	0.007	94.412
Predictor	Turnover					
	All Rodents		Caviomorphs		Sigmodontines	
	R^2	F	R^2	F	R^2	F
Global model	0.110	319.90	0.060	147.74	0.087	232.65
Elevation.dif	**0.044**	**513.66**	**0.021**	**215.30**	**0.032**	**346.73**
Temperature.dif	0.002	26.401	0.001	16.867	0.001	19.52
Precipitation.dif	0.0009	11.446	0.0002	2.768	0.0001	0.06
Seasonality.dif	0.002	25.230	0.0008	8.779	0.002	24.56

The values of R^2 and F are provided for the global model and for each predictor after accounting for the others. Spatial autocorrelation was controlled by using spatial filters as a condition variable in all models (see Methods). Most important variables appear in bold.

Table 2. Multiple regression models for richness and turnover of rodents in South America.

Species richness							
	Elevation	Temperature	Precipitation	Seasonality	R^2	AICc	AIC_c w_i
All Rodents	0.521	0.553	0.266	0.343	0.61	401.3	0.99
Caviomorphs	0.463	0.835	0.105		0.64	281.2	0.99
Sigmodontines	0.49	0.28	0.225	0.177	0.50	365.7	0.99
Species turnover							
	Elev.dif	Temp.dif	Prec.dif	Seas.dif	R^2	AICc	AIC_c w_i
All Rodents	0.384	0.08	-0.037	-0.057	0.46	-163.4	0.98
Caviomorphs	0.27	0.069	-0.02	-0.036	0.37	-105.1	0.57
Sigmodontines	0.33	0.072		-0.059	0.41	-134.1	0.73

Only the models with lowest AICc are shown. The standardized regression coefficients of the predictors included in each model are provided, along with the R^2, AICc and the AIC weighting of each model (AIC_c w_i). Correction for spatial autocorrelation was made by including spatial filters as a fixed variable in all models.

Figures

Fig 1. Rodent richness and turnover across South America. (a) Rodent richness, and (b) its turnover. Turnover was calculated as the average of the Simpson-dissimilarity index (β_{SIM} - [3]) between a focal cell and each of its eight neighboring cells.

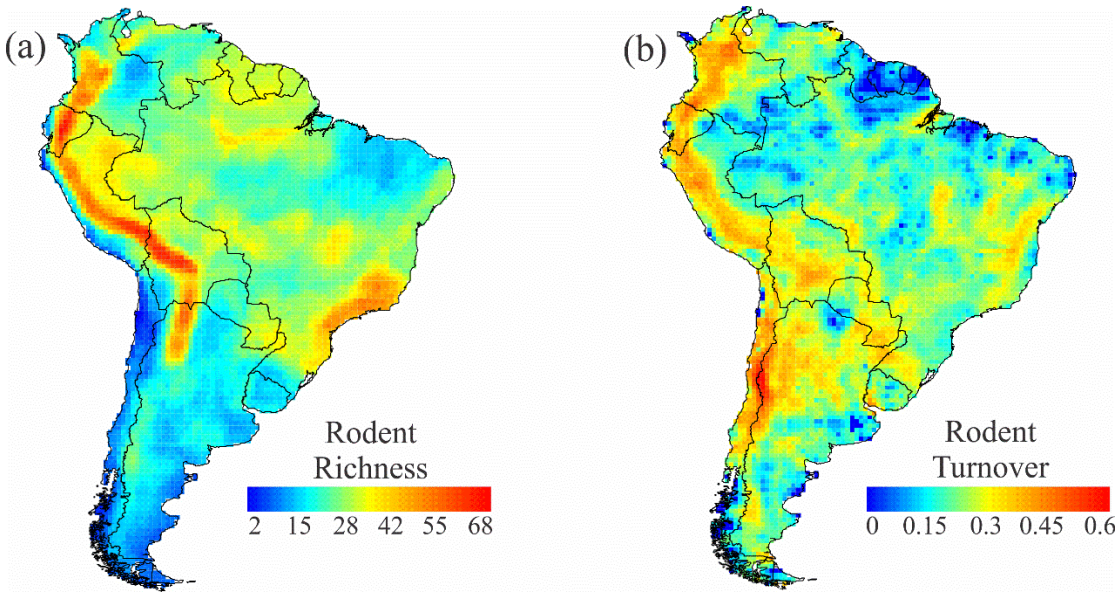

Fig 2. Richness of restricted-range species. Richness of the 25% of species with the smallest ranges (those less than 75.62 km^2).

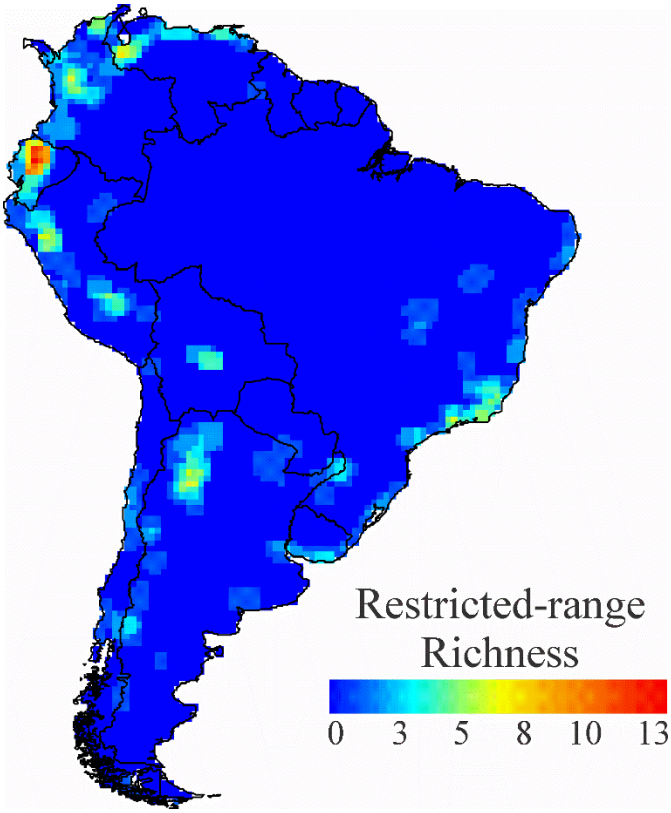

Fig 3. Richness and turnover of rodent clades across South America. (a) Caviomorph richness; (b) Sigmodontine richness; (c) Caviomorph turnover; (d) Sigmodontine turnover. Turnover was calculated as the average of the Simpson-dissimilarity index (β_{SIM} - [3]) between a focal cell and each of its eight neighboring cells.

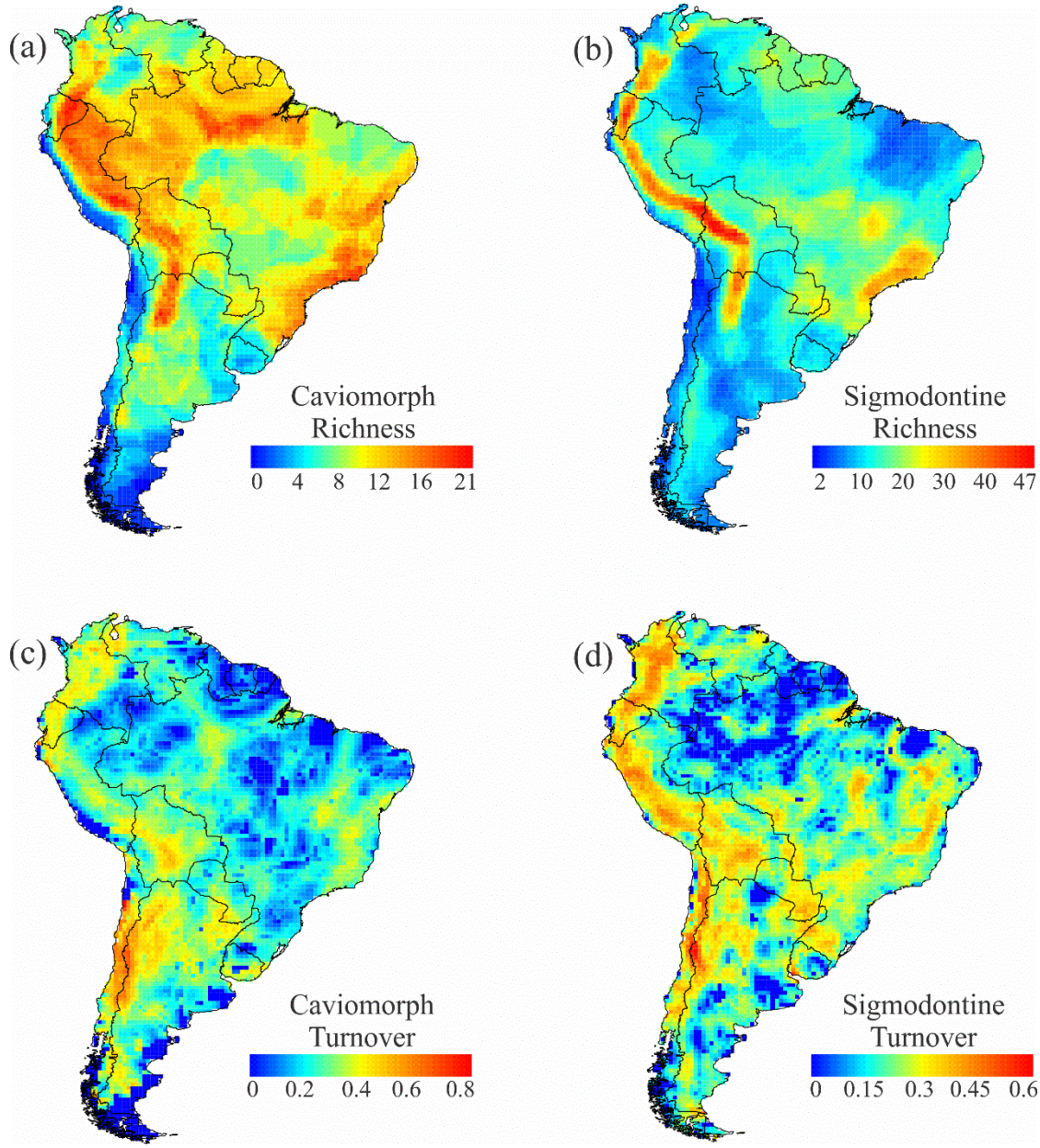

Fig 4. The relationship among rodent richness, latitude, longitude, and elevation. (a) The relationship between mean elevation (m) and longitude (r = -0.26), (b) rodent richness and longitude (r = 0.01), (c) rodent richness and latitude (r = 0.39), and (d) rodent richness and mean elevation (m) (r = 0.14).

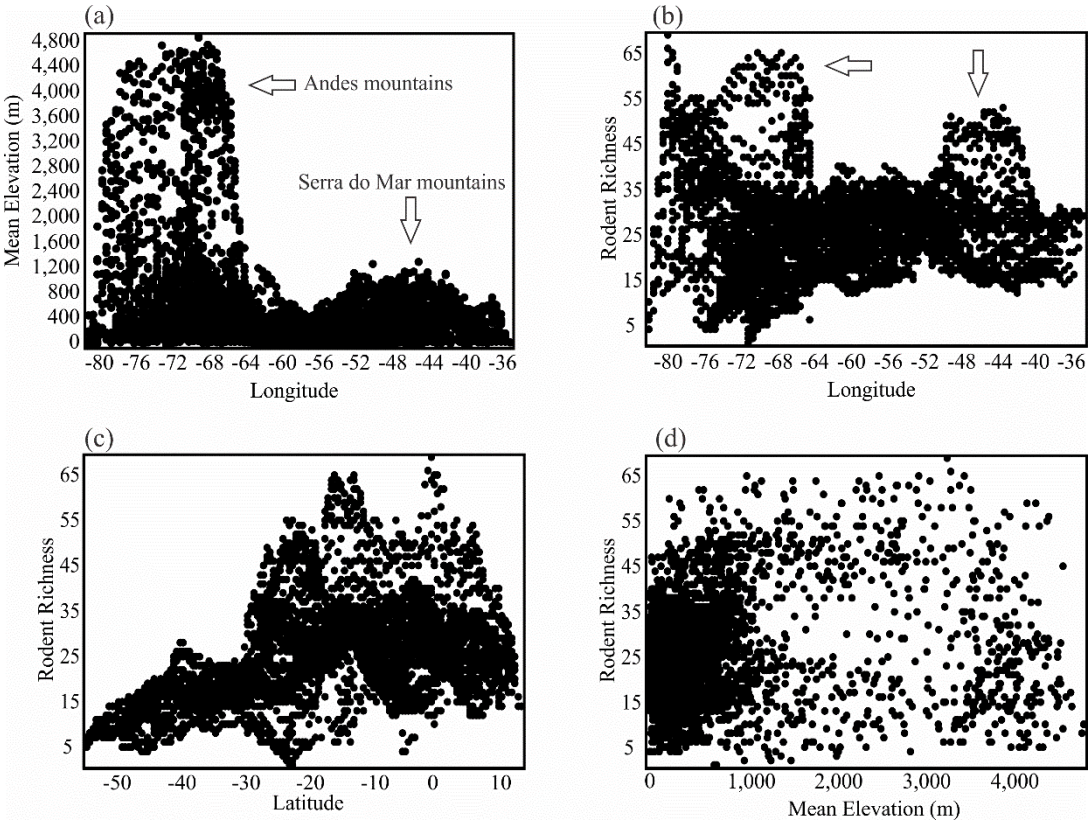

Fig 5. The relationship among caviomorph richness, latitude, longitude, temperature and elevation. (a) The relationship between caviomorph richness and latitude (r = 0.50), (b) caviomorph richness and mean temperature (C°) (r = 0.50), (c) caviomorph richness and longitude (r = 0.17), and (d) caviomorph richness and mean elevation (m) (r = -0.07).

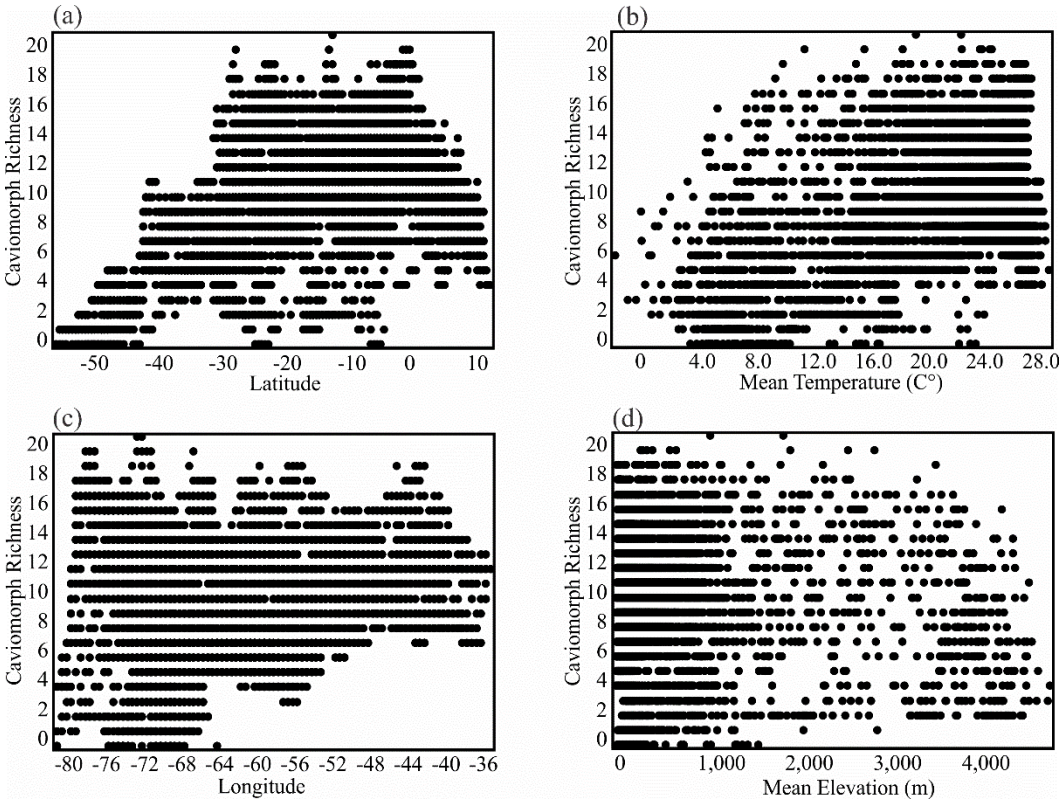

Fig 6. The relationship among sigmodontine richness, latitude, longitude, and elevation. (a) The relationship between sigmodontine richness and latitude (r= 0.14), (b) sigmodontine richness and longitude (r= 0.01), (c) sigmodontine richness and mean elevation (m) (r = 0.31). Cells highlighted in yellow in plots (b) and (c) are depicted in yellow in the corresponding maps (e) and (d), respectively.

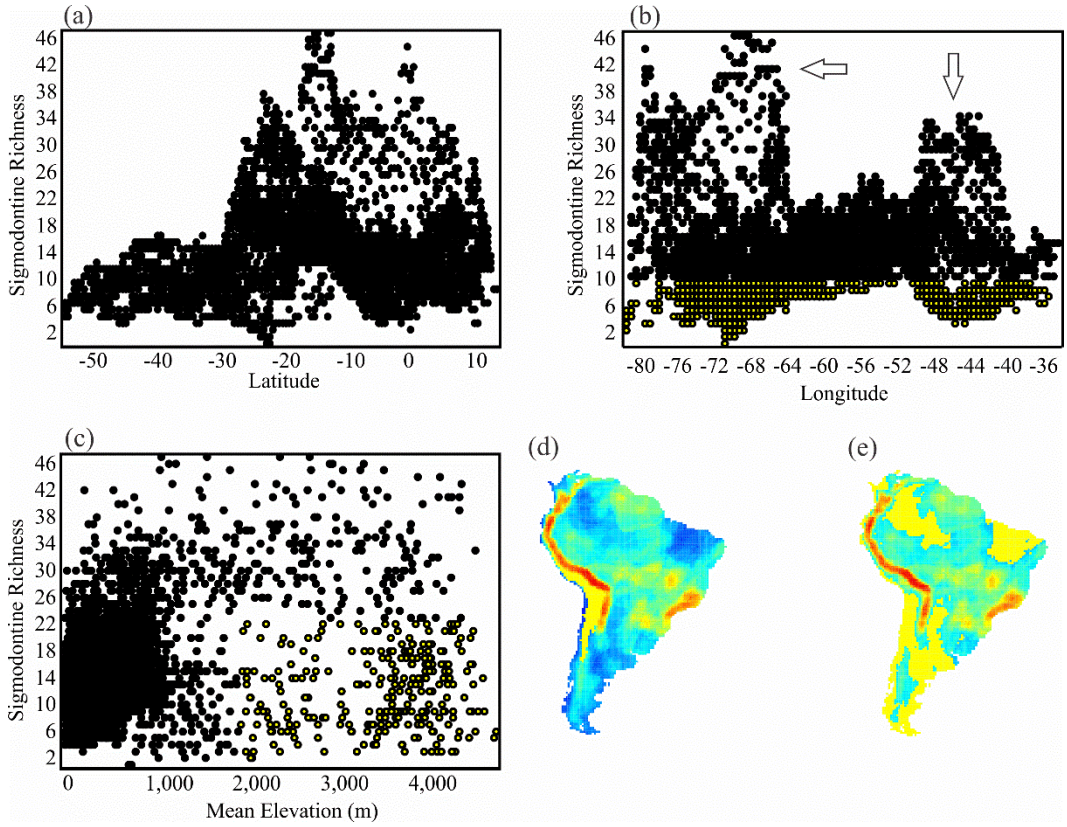

Fig 7. Predictors of rodent richness and turnover. (a) Mean Annual Temperature, one of the major predictors of rodent richness; (b) Mean elevation, one of the major predictors of rodent richness; (c) Differences in elevation between a focal cell and its neighbors, the main predictor of species turnover.

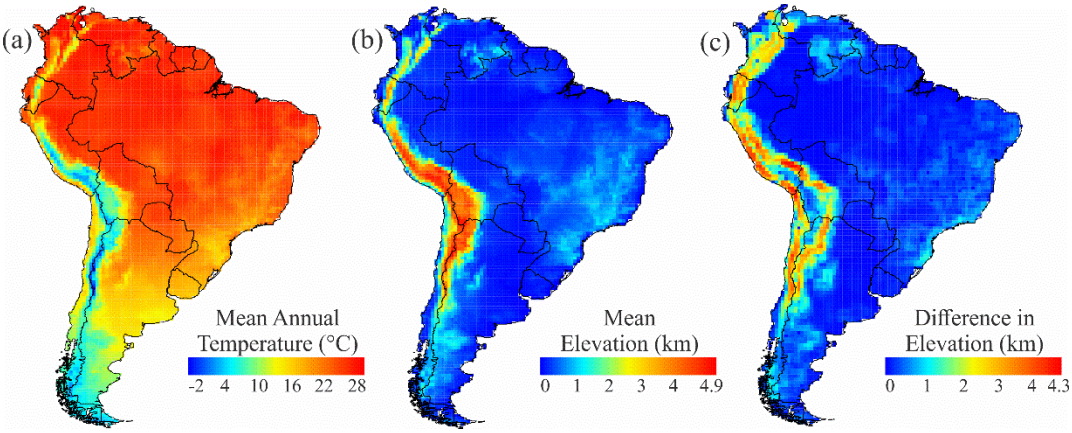

Fig 8. Richness of the four superfamilies of caviomorphs in South America. Richness of (a) Octodontoidea, (b) Cavioidea, (c) Chinchilloidea, and (d) Erethizontoidea in the South American portions of their ranges.

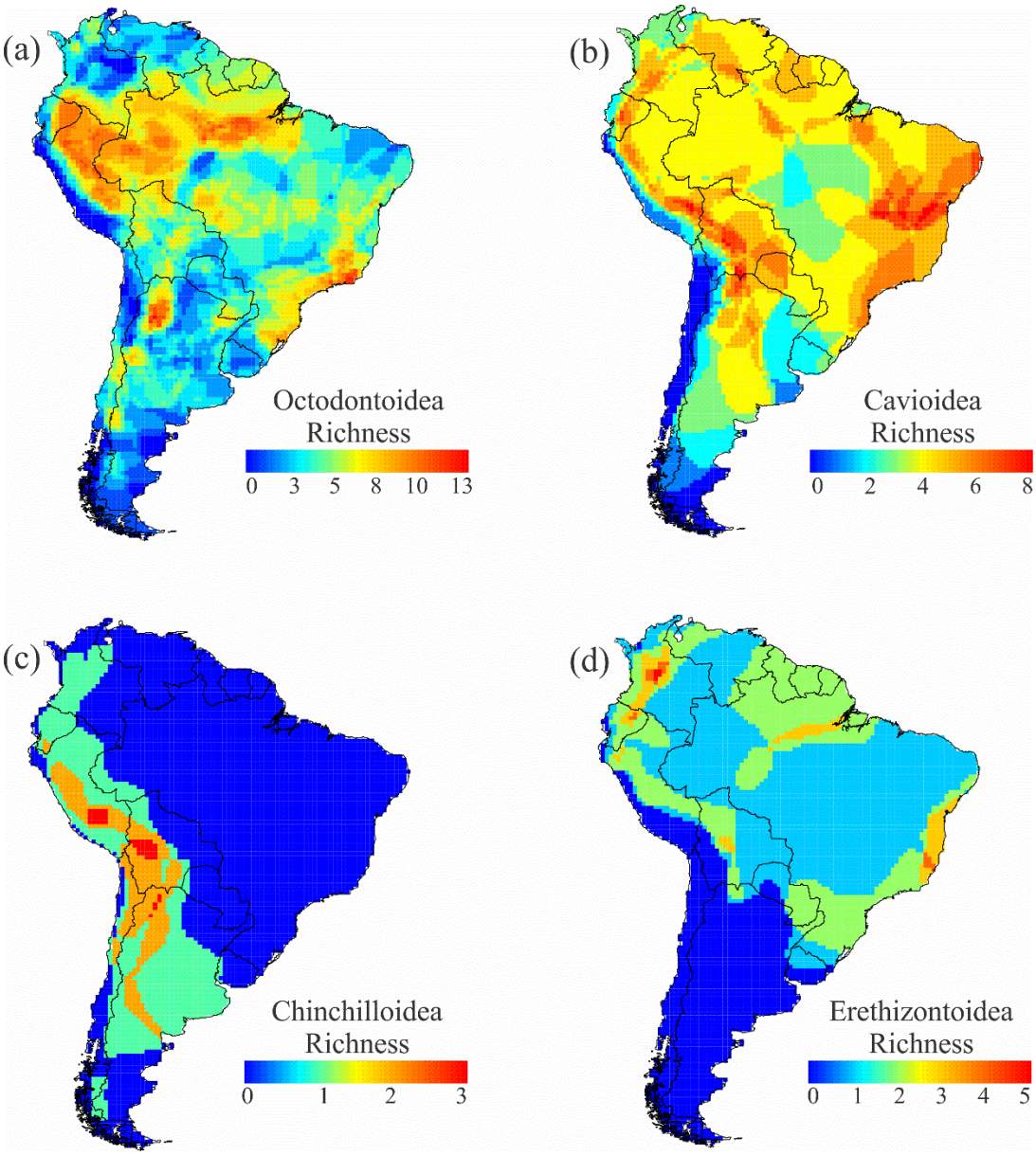

Fig 9. Richness of the main tribes of sigmodontines. Richness of (a) Oryzomyini, (b) Akodontini, (c) Thomasomyini, and (d) Phyllotini

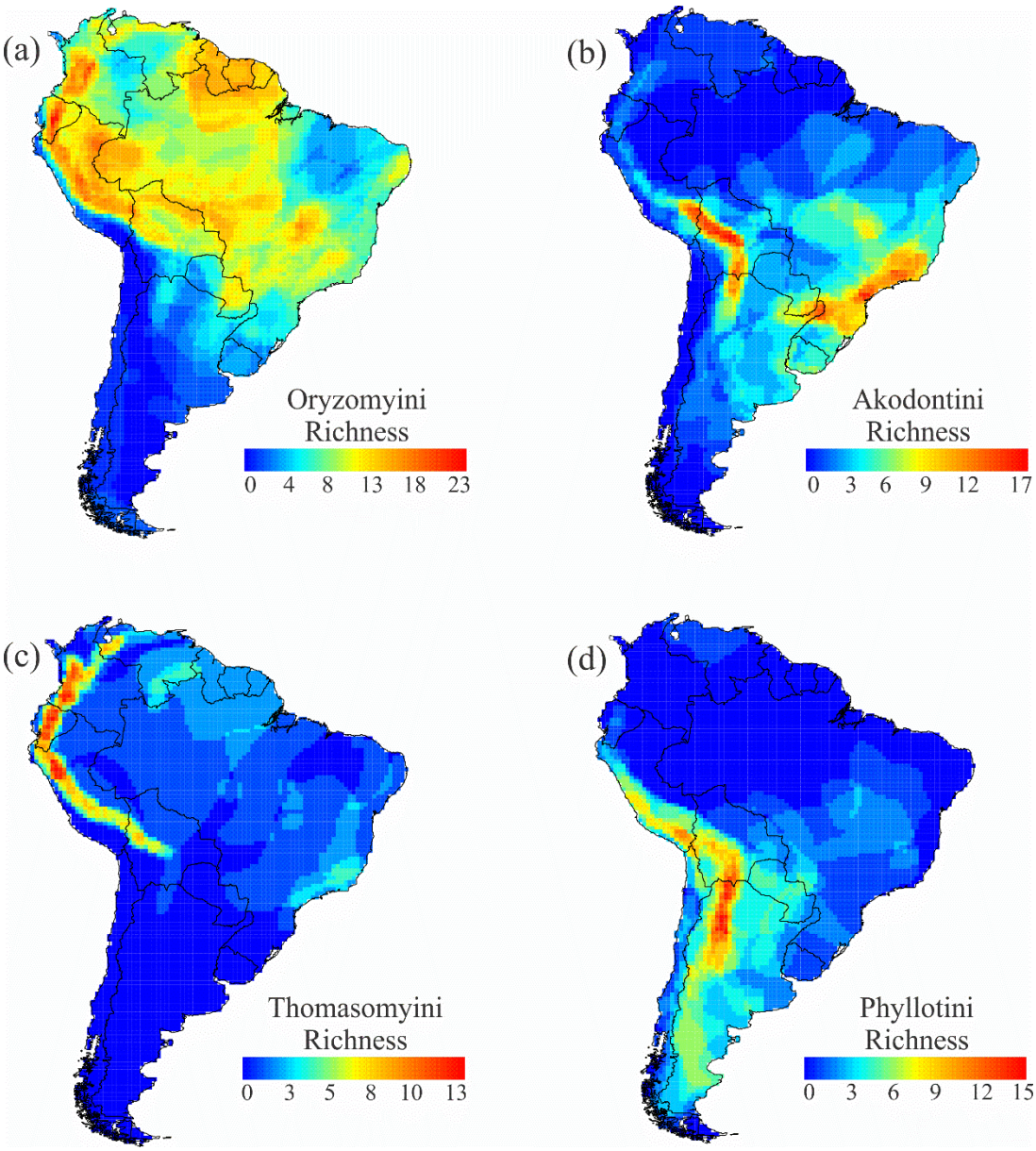

Supporting Information

Appendix S1. Moran's I correlogram for rodent richness and turnover. Figures S1 to S6 depict the Moran's correlogram for richness and turnover of all rodents, caviomorphs, and sigmodontiness. Moran's correlograms were constructed based on 24 distance classes set up according to a criterion of equal numbers of pairs within each class. Significant values were identified through 250 permutations. All distance classes in all rodents, caviomorphs, and sigmodontines, for alpha and beta diversity, returned a significant p-value at $\alpha<0.05$.

Figure S3. Moran's I correlogram for richness of all rodents.

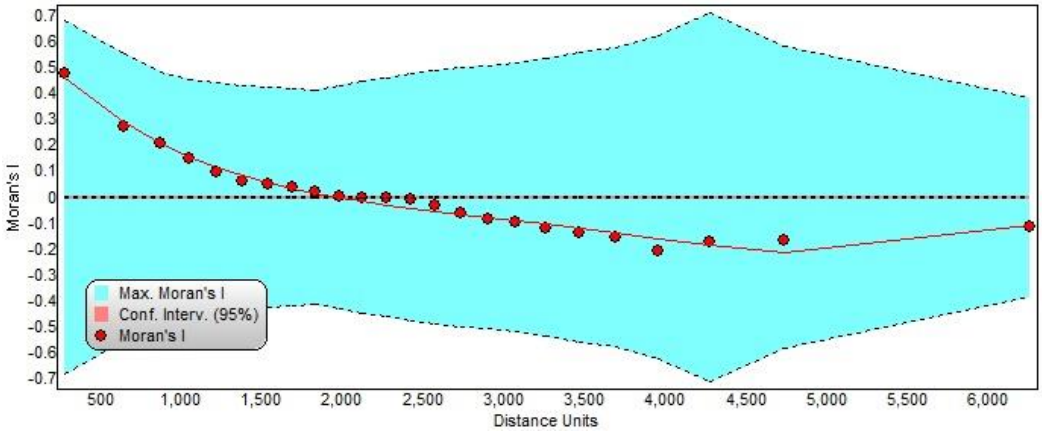

Figure S2. Moran's I correlogram for turnover of all rodents.

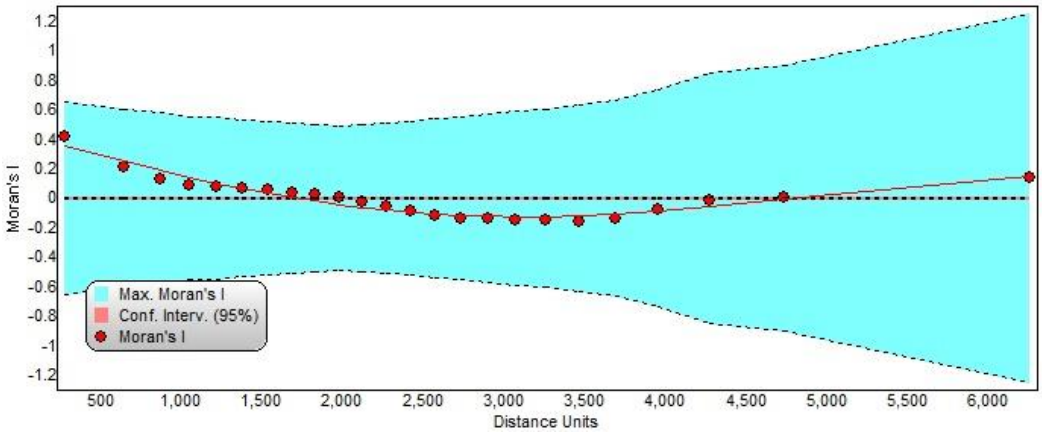

Figure S3. Moran's I correlogram for richness of caviomorphs.

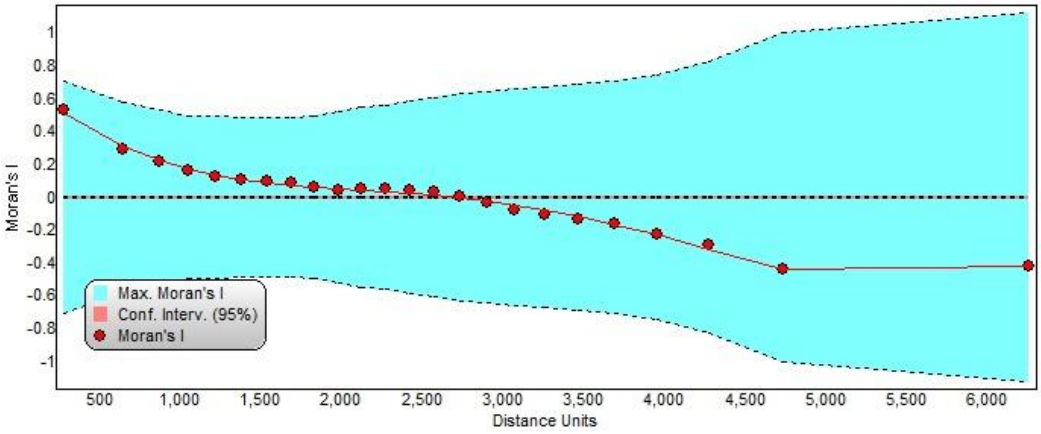

Figure S4. Moran's I correlogram for turnover of caviomorphs.

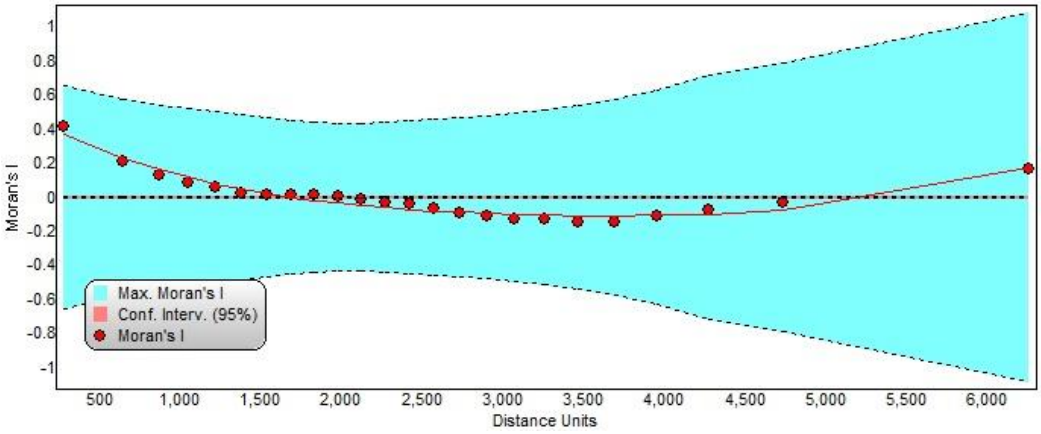

Figure S5. Moran's I correlogram for richness of sigmodontines.

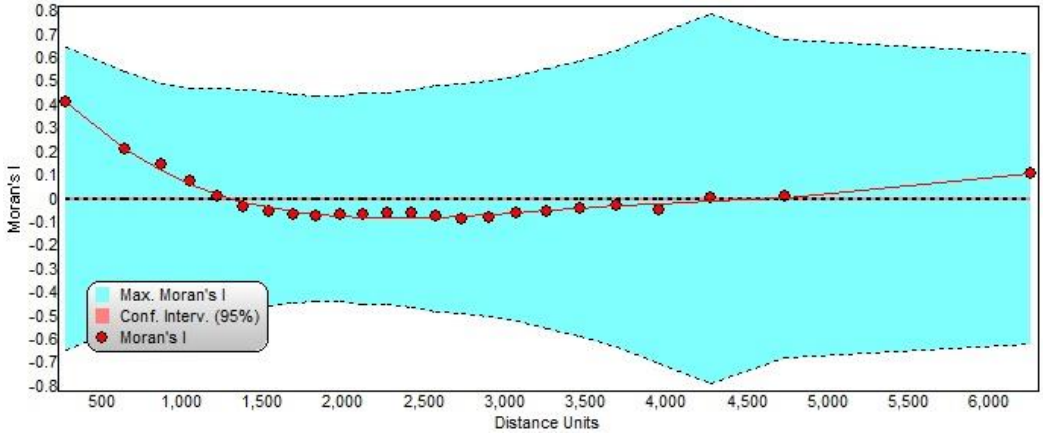

Figure S6. Moran's I correlogram for turnover of sigmodontines.

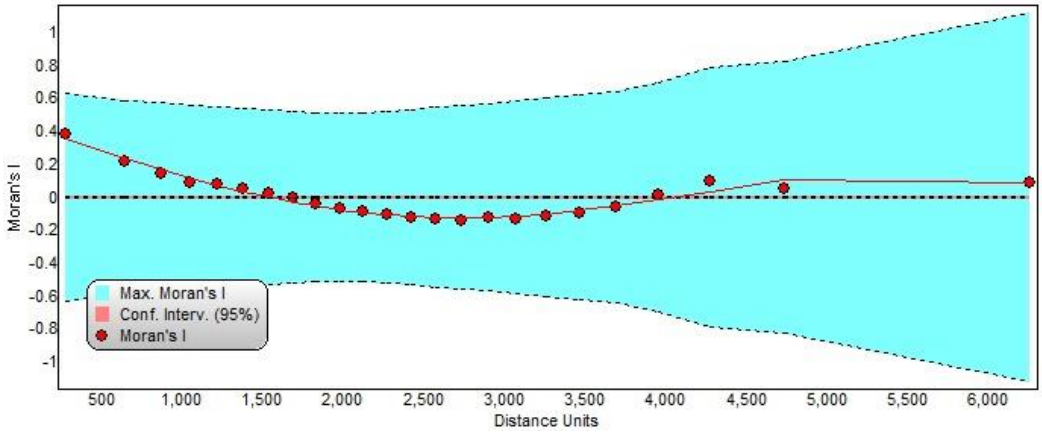

Appendix S2. Range sizes of rodent species. The box below presented each South American rodent species, their membership in higher taxa, range sizes in km², and the information if the species is a restricted-range species (RR – with range size < 43,000 km², or the quartile of species with the smallest ranges).

Species	Range Size km²	Family	Tribe Sigmodontines	Superfamily Caviomorphs	RR
O_dariensis	24,227	Geomyidae			Yes
H_anomalus	484,874	Heteromyidae			
H_australis	280,750	Heteromyidae			
H_catopterius	39,594	Heteromyidae			Yes
H_desmarestianus	6,035	Heteromyidae			Yes
H_oasicus	3,012	Heteromyidae			Yes
H_teleus	35,960	Heteromyidae			Yes
G_aestuans	3,415,431	Sciuridae			
G_brasiliensis	2,653,710	Sciuridae			
H_igniventris	2,251,883	Sciuridae			
H_pyrrhinus	1,261,138	Sciuridae			
H_spadiceus	3,289,344	Sciuridae			
M_flaviventer	2,672,822	Sciuridae			
M_isthmius	89,010	Sciuridae			
M_mimulus	14,790	Sciuridae			Yes
M_otinus	39,495	Sciuridae			Yes
M_sabanillae	27,605	Sciuridae			Yes
M_santanderensis	8,696	Sciuridae			Yes
M_similis	132,545	Sciuridae			
M_simonsi	16,389	Sciuridae			Yes
N_granatensis	1,057,918	Sciuridae			
N_pucheranii	2,847,307	Sciuridae			
S_nebouxii	61,293	Sciuridae			
S_pusillus	1,947,013	Sciuridae			
S_stramineus	41,586	Sciuridae			Yes
Syntheosciurus_sp	21,519	Sciuridae			Yes
A_andina	546,156	Cricetidae	Abrotrichini		
A_hershkovitzi	25,574	Cricetidae	Abrotrichini		Yes
A_illutea	59,774	Cricetidae	Abrotrichini		
A_jelskii	710,632	Cricetidae	Abrotrichini		
A_lanosa	283,682	Cricetidae	Abrotrichini		
A_longipilis	1,155,414	Cricetidae	Abrotrichini		
A_olivacea	1,585,401	Cricetidae	Abrotrichini		
A_sanborni	90,351	Cricetidae	Abrotrichini		
C_macronyx	550,231	Cricetidae	Abrotrichini		
C_megalonyx	71,017	Cricetidae	Abrotrichini		
G_valdivianus	610,488	Cricetidae	Abrotrichini		
N_edwardsii	440,649	Cricetidae	Abrotrichini		
P_annectens	19,341	Cricetidae	Abrotrichini		Yes
A_aerosus	252,666	Cricetidae	Akodontini		
A_affinis	59,706	Cricetidae	Akodontini		
A_albiventer	299,953	Cricetidae	Akodontini		
A_azarae	1,455,726	Cricetidae	Akodontini		
A_boliviensis	367,234	Cricetidae	Akodontini		
A_budini	69,053	Cricetidae	Akodontini		
A_caenosus	117,168	Cricetidae	Akodontini		
A_cursor	1,017,938	Cricetidae	Akodontini		
A_dayi	246,218	Cricetidae	Akodontini		
A_dolores	987,217	Cricetidae	Akodontini		
A_fumeus	260,109	Cricetidae	Akodontini		
A_iniscatus	544,187	Cricetidae	Akodontini		
A_josemariarguedasi	27,469	Cricetidae	Akodontini		Yes
A_juninensis	115,166	Cricetidae	Akodontini		
A_kofordi	72,559	Cricetidae	Akodontini		

A_lindberghi	242,971	Cricetidae	Akodontini	
A_lutescens	225,739	Cricetidae	Akodontini	
A_mimus	101,659	Cricetidae	Akodontini	
A_mollis	209,292	Cricetidae	Akodontini	
A_montensis	1,317,647	Cricetidae	Akodontini	
A_mystax	21,775	Cricetidae	Akodontini	Yes
A_orophilus	36,233	Cricetidae	Akodontini	Yes
A_paranaensis	487,883	Cricetidae	Akodontini	
A_pervalens	63,447	Cricetidae	Akodontini	
A_philipmyersi	9,760	Cricetidae	Akodontini	Yes
A_polopi	46,307	Cricetidae	Akodontini	
A_reigi	70,843	Cricetidae	Akodontini	
A_sanctipaulensis	24,150	Cricetidae	Akodontini	Yes
A_serrensis	461,471	Cricetidae	Akodontini	
A_siberiae	34,255	Cricetidae	Akodontini	Yes
A_simulator	195,697	Cricetidae	Akodontini	
A_spegazzinii	217,144	Cricetidae	Akodontini	
A_subfuscus	314,453	Cricetidae	Akodontini	
A_surdus	16,218	Cricetidae	Akodontini	Yes
A_sylvanus	27,089	Cricetidae	Akodontini	Yes
A_toba	733,122	Cricetidae	Akodontini	
A_torques	58,825	Cricetidae	Akodontini	
A_varius	285,467	Cricetidae	Akodontini	
Akodon_sp	337,146	Cricetidae	Akodontini	
B_breviceps	636,802	Cricetidae	Akodontini	
B_chacoensis	122,939	Cricetidae	Akodontini	
B_griserufescens	52,147	Cricetidae	Akodontini	
B_guarani	21,408	Cricetidae	Akodontini	Yes
B_igniventris	15,756	Cricetidae	Akodontini	Yes
B_iheringi	188,627	Cricetidae	Akodontini	
B_labiosus	362,223	Cricetidae	Akodontini	
B_misionensis	18,283	Cricetidae	Akodontini	Yes
B_paradisus	18,788	Cricetidae	Akodontini	Yes
B_soricinus	120,213	Cricetidae	Akodontini	
B_torresi	18,761	Cricetidae	Akodontini	Yes
D_kempi	337,917	Cricetidae	Akodontini	
G_fronto	71,662	Cricetidae	Akodontini	
G_planaltensis	198,067	Cricetidae	Akodontini	
J_candango	56,677	Cricetidae	Akodontini	
J_huanchacae	128,250	Cricetidae	Akodontini	
K_tomentosus	1,429,280	Cricetidae	Akodontini	
L_apicalis	94,088	Cricetidae	Akodontini	
N_amoenus	311,798	Cricetidae	Akodontini	
N_lactens	295,757	Cricetidae	Akodontini	
N_lasiurus	7,473,449	Cricetidae	Akodontini	
N_lenguarum	859,364	Cricetidae	Akodontini	
N_obscurus	50,227	Cricetidae	Akodontini	
N_punctulatus	164,355	Cricetidae	Akodontini	
N_urichi	1,426,790	Cricetidae	Akodontini	
O_amazonicus	1,229,399	Cricetidae	Akodontini	
O_caparaoe	20,658	Cricetidae	Akodontini	Yes
O_dasytrichus	1,170,852	Cricetidae	Akodontini	
O_delator	3,167,534	Cricetidae	Akodontini	
O_hiska	157,107	Cricetidae	Akodontini	
O_hucucha	11,650	Cricetidae	Akodontini	Yes
O_inca	616,070	Cricetidae	Akodontini	
O_josei	25,096	Cricetidae	Akodontini	Yes
O_juliacae	145,064	Cricetidae	Akodontini	
O_nasutus	332,189	Cricetidae	Akodontini	
O_nigrifrons	82,764	Cricetidae	Akodontini	
O_paramensis	289,547	Cricetidae	Akodontini	
O_quaestor	570,542	Cricetidae	Akodontini	
O_rufus	841,914	Cricetidae	Akodontini	
O_wayku	33,086	Cricetidae	Akodontini	Yes
S_aquaticus	347,515	Cricetidae	Akodontini	
S_tumidus	491,204	Cricetidae	Akodontini	
T_cerradensis	851,228	Cricetidae	Akodontini	

T_lasiotis	1,470,485	Cricetidae	Akodontini	
T_nigrita	946,574	Cricetidae	Akodontini	
A_leander	10,986	Cricetidae	Ichthyomyini	Yes
C_orcesi	149,478	Cricetidae	Ichthyomyini	
C_trichotis	70,917	Cricetidae	Ichthyomyini	
I_hydrobates	166,715	Cricetidae	Ichthyomyini	
I_pittieri	33,332	Cricetidae	Ichthyomyini	Yes
I_stolzmanni	237,736	Cricetidae	Ichthyomyini	
I_tweedii	66,921	Cricetidae	Ichthyomyini	
N_ferreirai	214,284	Cricetidae	Ichthyomyini	
N_monticolus	255,805	Cricetidae	Ichthyomyini	
N_mussoi	22,636	Cricetidae	Ichthyomyini	Yes
N_oyapocki	434,076	Cricetidae	Ichthyomyini	
N_peruviensis	50,700	Cricetidae	Ichthyomyini	
N_venezuelae	649,557	Cricetidae	Ichthyomyini	
P_roraimae	18,824	Cricetidae	Ichthyomyini	Yes
A_chebezi	56,053	Cricetidae	incertae sedis	
A_edax	579,279	Cricetidae	incertae sedis	
A_ruschii	360,985	Cricetidae	incertae sedis	
C_sahamae	265,358	Cricetidae	incertae sedis	
D_dorsalis	514,333	Cricetidae	incertae sedis	
D_sublineatus	457,613	Cricetidae	incertae sedis	
E_chinchilloides	64,288	Cricetidae	incertae sedis	
E_fossor	30,026	Cricetidae	incertae sedis	Yes
E_mordax	85,185	Cricetidae	incertae sedis	
E_petersoni	647,412	Cricetidae	incertae sedis	
I_tarsalis	238,561	Cricetidae	incertae sedis	
J_ossitenuis	215,996	Cricetidae	incertae sedis	
J_pictipes	669,028	Cricetidae	incertae sedis	
J_rimofrons	13,174	Cricetidae	incertae sedis	Yes
N_bogotensis	57,124	Cricetidae	incertae sedis	
N_ebriosus	983,884	Cricetidae	incertae sedis	
N_latebricola	32,494	Cricetidae	incertae sedis	Yes
P_ferrugineus	41,024	Cricetidae	incertae sedis	Yes
P_kofordi	45,457	Cricetidae	incertae sedis	
P_lemminus	55,851	Cricetidae	incertae sedis	
W_oenax	506,172	Cricetidae	incertae sedis	
A_galapagoensis	303	Cricetidae	Oryzomyini	Yes
A_savamis	22,262	Cricetidae	Oryzomyini	Yes
A_xanthaeolus	441,557	Cricetidae	Oryzomyini	
C_goytaca	10,168	Cricetidae	Oryzomyini	Yes
C_langguthi	566,796	Cricetidae	Oryzomyini	
C_maracajuensis	2,261,084	Cricetidae	Oryzomyini	
C_marinhus	55,829	Cricetidae	Oryzomyini	
C_scotti	2,543,721	Cricetidae	Oryzomyini	
C_subflavus	819,260	Cricetidae	Oryzomyini	
C_vivoi	588,227	Cricetidae	Oryzomyini	
D_albimaculatus	141,739	Cricetidae	Oryzomyini	
E_emmonsae	610,821	Cricetidae	Oryzomyini	
E_lamia	193,021	Cricetidae	Oryzomyini	
E_legatus	251,517	Cricetidae	Oryzomyini	
E_macconnelli	5,879,653	Cricetidae	Oryzomyini	
E_nitidus	1,820,334	Cricetidae	Oryzomyini	
E_polius	48,061	Cricetidae	Oryzomyini	
E_russatus	1,855,704	Cricetidae	Oryzomyini	
H_acritus	220,766	Cricetidae	Oryzomyini	
H_alfaroi	415,549	Cricetidae	Oryzomyini	
H_brasiliensis	560,532	Cricetidae	Oryzomyini	
H_chacarius	1,332,585	Cricetidae	Oryzomyini	
H_fuscatus	18,651	Cricetidae	Oryzomyini	Yes
H_intectus	13,132	Cricetidae	Oryzomyini	Yes
H_lagigliai	15,302	Cricetidae	Oryzomyini	Yes
H_laticeps	273,594	Cricetidae	Oryzomyini	
H_megacephalus	6,485,969	Cricetidae	Oryzomyini	
H_oniscus	76,953	Cricetidae	Oryzomyini	
H_perenensis	2,187,051	Cricetidae	Oryzomyini	
H_sciureus	7,906,350	Cricetidae	Oryzomyini	

H_tatei	17,620	Cricetidae	Oryzomyini	Yes
H_venezuelae	433,872	Cricetidae	Oryzomyini	
H_vulpinus	1,036,054	Cricetidae	Oryzomyini	
H_yunganus	6,281,253	Cricetidae	Oryzomyini	
L_molitor	202,576	Cricetidae	Oryzomyini	
M_altissimus	391,720	Cricetidae	Oryzomyini	
M_caliginosus	413,157	Cricetidae	Oryzomyini	
M_columbianus	39,177	Cricetidae	Oryzomyini	Yes
M_hammondi	17,154	Cricetidae	Oryzomyini	Yes
M_minutus	812,097	Cricetidae	Oryzomyini	
M_robustulus	124,762	Cricetidae	Oryzomyini	
M_transitorius	21,463	Cricetidae	Oryzomyini	Yes
M_zunigae	11,149	Cricetidae	Oryzomyini	Yes
N_albigularis	142,758	Cricetidae	Oryzomyini	
N_apicalis	940,123	Cricetidae	Oryzomyini	
N_auriventer	129,186	Cricetidae	Oryzomyini	
N_caracolus	27,403	Cricetidae	Oryzomyini	Yes
N_childi	141,932	Cricetidae	Oryzomyini	
N_darwini	900	Cricetidae	Oryzomyini	Yes
N_dubosti	268,174	Cricetidae	Oryzomyini	
N_fernandinae	418	Cricetidae	Oryzomyini	Yes
N_g_grandis	32,603	Cricetidae	Oryzomyini	Yes
N_guianae	477,945	Cricetidae	Oryzomyini	
N_indefessus	848	Cricetidae	Oryzomyini	Yes
N_keaysi	306,151	Cricetidae	Oryzomyini	
N_levipes	141,280	Cricetidae	Oryzomyini	
N_maculiventer	20,229	Cricetidae	Oryzomyini	Yes
N_meridensis	65,576	Cricetidae	Oryzomyini	
N_minutus	335,337	Cricetidae	Oryzomyini	
N_moerex	8,364	Cricetidae	Oryzomyini	Yes
N_musseri	221,072	Cricetidae	Oryzomyini	
N_narboroughi	341	Cricetidae	Oryzomyini	Yes
N_nimbosus	18,332	Cricetidae	Oryzomyini	Yes
N_p_palmipes	5,822	Cricetidae	Oryzomyini	Yes
N_p_tatei	33,656	Cricetidae	Oryzomyini	Yes
N_paracou	1,065,939	Cricetidae	Oryzomyini	
N_pectoralis	118,847	Cricetidae	Oryzomyini	
N_rattus	9,687,543	Cricetidae	Oryzomyini	
N_spinosus	3,997,135	Cricetidae	Oryzomyini	
N_squamipes	1,927,498	Cricetidae	Oryzomyini	
N_swarthi	594	Cricetidae	Oryzomyini	Yes
N_tenuipes	293,127	Cricetidae	Oryzomyini	
Nectomys_grandis	113,500	Cricetidae	Oryzomyini	
O_andinus	229,760	Cricetidae	Oryzomyini	
O_arenalis	216,855	Cricetidae	Oryzomyini	
O_auyantepui	1,310,293	Cricetidae	Oryzomyini	
O_balneator	70,241	Cricetidae	Oryzomyini	
O_bicolor	8,258,727	Cricetidae	Oryzomyini	
O_brendae	112,167	Cricetidae	Oryzomyini	
O_catherinae	1,470,321	Cricetidae	Oryzomyini	
O_chacoensis	850,398	Cricetidae	Oryzomyini	
O_cleberi	636,692	Cricetidae	Oryzomyini	
O_concolor	948,944	Cricetidae	Oryzomyini	
O_couesi	58,415	Cricetidae	Oryzomyini	
O_delicatus	886,330	Cricetidae	Oryzomyini	
O_destructor	908,962	Cricetidae	Oryzomyini	
O_flavescens	2,998,800	Cricetidae	Oryzomyini	
O_flavicans	440,015	Cricetidae	Oryzomyini	
O_fornesi	22,280	Cricetidae	Oryzomyini	Yes
O_gorgasi	171,005	Cricetidae	Oryzomyini	
O_griseolus	14,183	Cricetidae	Oryzomyini	Yes
O_longicaudatus	957,670	Cricetidae	Oryzomyini	
O_magellanicus	215,404	Cricetidae	Oryzomyini	
O_mamorae	1,455,448	Cricetidae	Oryzomyini	
O_mattogrossae	1,436,684	Cricetidae	Oryzomyini	
O_messorius	550,657	Cricetidae	Oryzomyini	
O_microtis	2,457,941	Cricetidae	Oryzomyini	

O_moojeni	221,557	Cricetidae	Oryzomyini		
O_nigripes	2,459,421	Cricetidae	Oryzomyini		
O_paricola	3,193,732	Cricetidae	Oryzomyini		
O_phaeotis	483,063	Cricetidae	Oryzomyini		
O_rex	1,309,244	Cricetidae	Oryzomyini		
O_roberti	6,094,553	Cricetidae	Oryzomyini		
O_rupestris	497,448	Cricetidae	Oryzomyini		
O_rutilus	1,018,612	Cricetidae	Oryzomyini		
O_speciosus	591,171	Cricetidae	Oryzomyini		
O_stramineus	1,112,290	Cricetidae	Oryzomyini		
O_superans	1,298,882	Cricetidae	Oryzomyini		
O_sydandersoni	120,337	Cricetidae	Oryzomyini		
O_trinitatis	8,496,080	Cricetidae	Oryzomyini		
O_utiaritensis	546,068	Cricetidae	Oryzomyini		
P_simplex	3,776,962	Cricetidae	Oryzomyini		
S_alfari	404,011	Cricetidae	Oryzomyini		
S_angouya	1,467,951	Cricetidae	Oryzomyini		
S_melanops	157,785	Cricetidae	Oryzomyini		
S_ucayalensis	536,353	Cricetidae	Oryzomyini		
T_aphrastus	11,482	Cricetidae	Oryzomyini		Yes
T_bolivaris	201,236	Cricetidae	Oryzomyini		
T_talamancae	713,870	Cricetidae	Oryzomyini		
Z_brevicauda	2,673,751	Cricetidae	Oryzomyini		
Z_brunneus	104,738	Cricetidae	Oryzomyini		
A_olrogi	22,617	Cricetidae	Phyllotini		Yes
A_pearsoni	136,784	Cricetidae	Phyllotini		
A_pictus	435,601	Cricetidae	Phyllotini		
A_roigi	115,168	Cricetidae	Phyllotini		
A_sublimis	446,243	Cricetidae	Phyllotini		
Auliscomys_boliviensis	125,397	Cricetidae	Phyllotini		
C_apicalis	13,120	Cricetidae	Phyllotini		Yes
C_callidus	819,241	Cricetidae	Phyllotini		
C_callosus	1,454,043	Cricetidae	Phyllotini		
C_cerqueirai	48,364	Cricetidae	Phyllotini		
C_expulsus	1,238,577	Cricetidae	Phyllotini		
C_hummelincki	388,603	Cricetidae	Phyllotini		
C_laucha	2,490,235	Cricetidae	Phyllotini		
C_lepidus	881,915	Cricetidae	Phyllotini		
C_musculinus	2,716,001	Cricetidae	Phyllotini		
C_sorellus	292,036	Cricetidae	Phyllotini		
C_tener	2,718,279	Cricetidae	Phyllotini		
C_tocantinsi	223,044	Cricetidae	Phyllotini		
C_venustus	175,719	Cricetidae	Phyllotini		
Calomys_boliviae	266,457	Cricetidae	Phyllotini		
E_bolsonensis	84,304	Cricetidae	Phyllotini		
E_dunaris	23,733	Cricetidae	Phyllotini		Yes
E_hirtipes	240,447	Cricetidae	Phyllotini		
E_moreni	276,958	Cricetidae	Phyllotini		
E_morgani	661,763	Cricetidae	Phyllotini		
E_puerulus	206,441	Cricetidae	Phyllotini		
E_typus	989,215	Cricetidae	Phyllotini		
G_chacoensis	1,220,355	Cricetidae	Phyllotini		
G_domorum	253,794	Cricetidae	Phyllotini		
G_edithae	29,457	Cricetidae	Phyllotini		Yes
G_garleppii	70,532	Cricetidae	Phyllotini		
G_griseoflavus	1,387,979	Cricetidae	Phyllotini		
L_micropus	666,425	Cricetidae	Phyllotini		
P_alisosiensis	29,624	Cricetidae	Phyllotini		Yes
P_amicus	230,122	Cricetidae	Phyllotini		
P_andium	285,497	Cricetidae	Phyllotini		
P_anitae	31,167	Cricetidae	Phyllotini		Yes
P_bonariensis	30,508	Cricetidae	Phyllotini		Yes
P_caprinus	84,083	Cricetidae	Phyllotini		
P_darwini	223,656	Cricetidae	Phyllotini		
P_definitus	18,309	Cricetidae	Phyllotini		Yes
P_gerbillus	37,236	Cricetidae	Phyllotini		Yes
P_haggardi	23,814	Cricetidae	Phyllotini		Yes

P_limatus	305,237	Cricetidae	Phyllotini	
P_magister	277,454	Cricetidae	Phyllotini	
P_osgoodi	17,386	Cricetidae	Phyllotini	Yes
P_osilae	557,273	Cricetidae	Phyllotini	
P_xanthopygus	2,250,743	Cricetidae	Phyllotini	
S_delicatus	170,812	Cricetidae	Phyllotini	
T_primus	40,013	Cricetidae	Phyllotini	Yes
T_wolffsohni	152,520	Cricetidae	Phyllotini	
R_auritus	1,680,505	Cricetidae	Reithrodontini	
R_typicus	338,660	Cricetidae	Reithrodontini	
S_alstoni	1,584,424	Cricetidae	Sigmodontini	
S_hirsutus	542,943	Cricetidae	Sigmodontini	
S_inopinatus	16,302	Cricetidae	Sigmodontini	Yes
S_peruanus	77,340	Cricetidae	Sigmodontini	
A_lugens	26,725	Cricetidae	Thomasomyini	Yes
Aepeomys_reigi	11,713	Cricetidae	Thomasomyini	Yes
C_fumeus	46,035	Cricetidae	Thomasomyini	
C_instans	268,032	Cricetidae	Thomasomyini	
R_austrinus	173,319	Cricetidae	Thomasomyini	
R_cariri	261,111	Cricetidae	Thomasomyini	
R_caucensis	69,252	Cricetidae	Thomasomyini	
R_couesi	223,621	Cricetidae	Thomasomyini	
R_emiliae	1,268,242	Cricetidae	Thomasomyini	
R_fulviventer	62,875	Cricetidae	Thomasomyini	
R_gardneri	383,799	Cricetidae	Thomasomyini	
R_ipukensis	87,259	Cricetidae	Thomasomyini	
R_itoan	109,216	Cricetidae	Thomasomyini	
R_latimanus	333,877	Cricetidae	Thomasomyini	
R_leucodactylus	5,214,252	Cricetidae	Thomasomyini	
R_longilingua	94,461	Cricetidae	Thomasomyini	
R_macconnelli	134,297	Cricetidae	Thomasomyini	
R_macrurus	1,898,998	Cricetidae	Thomasomyini	
R_mastacalis	752,539	Cricetidae	Thomasomyini	
R_modicus	72,977	Cricetidae	Thomasomyini	
R_nitela	1,591,548	Cricetidae	Thomasomyini	
R_ochrogaster	16,807	Cricetidae	Thomasomyini	Yes
R_rufescens	379,040	Cricetidae	Thomasomyini	
R_similis	49,192	Cricetidae	Thomasomyini	
R_tenuicauda	11,577	Cricetidae	Thomasomyini	Yes
R_tribei	39,404	Cricetidae	Thomasomyini	Yes
R_venezuelae	216,021	Cricetidae	Thomasomyini	
R_venustus	47,378	Cricetidae	Thomasomyini	
R_wetzeli	130,324	Cricetidae	Thomasomyini	
Rhagomys_sp	49,112	Cricetidae	Thomasomyini	
T_andersoni	41,237	Cricetidae	Thomasomyini	Yes
T_apeco	21,903	Cricetidae	Thomasomyini	Yes
T_aureus	628,600	Cricetidae	Thomasomyini	
T_auricularis	35,203	Cricetidae	Thomasomyini	Yes
T_australis	29,286	Cricetidae	Thomasomyini	Yes
T_baeops	232,923	Cricetidae	Thomasomyini	
T_bombycinus	20,922	Cricetidae	Thomasomyini	Yes
T_caudivarius	65,610	Cricetidae	Thomasomyini	
T_cinereiventer	43,633	Cricetidae	Thomasomyini	
T_cinereus	74,436	Cricetidae	Thomasomyini	
T_cinnameus	168,516	Cricetidae	Thomasomyini	
T_contradictus	50,889	Cricetidae	Thomasomyini	
T_daphne	136,917	Cricetidae	Thomasomyini	
T_dispar	26,512	Cricetidae	Thomasomyini	Yes
T_eleusis	31,737	Cricetidae	Thomasomyini	Yes
T_emeritus	25,102	Cricetidae	Thomasomyini	Yes
T_erro	18,117	Cricetidae	Thomasomyini	Yes
T_fumeus	9,307	Cricetidae	Thomasomyini	Yes
T_gracilis	44,887	Cricetidae	Thomasomyini	
T_hudsoni	14,350	Cricetidae	Thomasomyini	Yes
T_hylophilus	22,364	Cricetidae	Thomasomyini	Yes
T_incanus	92,433	Cricetidae	Thomasomyini	
T_ischyrus	66,933	Cricetidae	Thomasomyini	

T_kalinowskii	102,830	Cricetidae	Thomasomyini		
T_ladewi	48,270	Cricetidae	Thomasomyini		
T_laniger	53,627	Cricetidae	Thomasomyini		
T_macrotis	16,077	Cricetidae	Thomasomyini		Yes
T_monochromos	7,446	Cricetidae	Thomasomyini		Yes
T_nicefori	46,805	Cricetidae	Thomasomyini		
T_niveipes	28,032	Cricetidae	Thomasomyini		Yes
T_notatus	194,311	Cricetidae	Thomasomyini		
T_onkiro	22,973	Cricetidae	Thomasomyini		Yes
T_oreas	214,083	Cricetidae	Thomasomyini		
T_paramorum	69,352	Cricetidae	Thomasomyini		
T_popayanus	35,233	Cricetidae	Thomasomyini		Yes
T_praetor	49,830	Cricetidae	Thomasomyini		
T_princeps	16,138	Cricetidae	Thomasomyini		Yes
T_pyrrhonotus	52,191	Cricetidae	Thomasomyini		
T_rosalinda	18,931	Cricetidae	Thomasomyini		Yes
T_silvestris	38,848	Cricetidae	Thomasomyini		Yes
T_taczanowskii	149,462	Cricetidae	Thomasomyini		
T_ucucha	16,917	Cricetidae	Thomasomyini		Yes
T_vestitus	24,868	Cricetidae	Thomasomyini		Yes
T_vulcani	23,507	Cricetidae	Thomasomyini		Yes
W_cerradensis	220,465	Cricetidae	Thomasomyini		
W_pyrrhorhinos	530,563	Cricetidae	Thomasomyini		
C_aperea	6,575,296	Caviidae		Cavioidea	
C_fulgida	763,762	Caviidae		Cavioidea	
C_intermedia	6,594	Caviidae		Cavioidea	Yes
C_magna	110,013	Caviidae		Cavioidea	
C_paca	13,472,855	Cuniculidae		Cavioidea	
C_patzelti	17,268	Caviidae		Cavioidea	Yes
C_taczanowskii	836,245	Cuniculidae		Cavioidea	
C_tschudii	924,033	Caviidae		Cavioidea	
D_azarae	3,801,213	Dasyproctidae		Cavioidea	
D_croconota	388,295	Dasyproctidae		Cavioidea	
D_fuliginosa	3,409,373	Dasyproctidae		Cavioidea	
D_guamara	8,803	Dasyproctidae		Cavioidea	Yes
D_iacki	40,813	Dasyproctidae		Cavioidea	Yes
D_kalinowskii	54,254	Dasyproctidae		Cavioidea	
D_leporina	4,836,314	Dasyproctidae		Cavioidea	
D_patagonum	1,300,159	Caviidae		Cavioidea	
D_prymnolopha	2,001,873	Dasyproctidae		Cavioidea	
D_punctata	744,559	Dasyproctidae		Cavioidea	
D_salinicola	731,789	Caviidae		Cavioidea	
D_variegata	438,515	Dasyproctidae		Cavioidea	
G_comes	135,471	Caviidae		Cavioidea	
G_flavidens	46,369	Caviidae		Cavioidea	
G_leucoblephara	2,018,295	Caviidae		Cavioidea	
G_musteloides	292,476	Caviidae		Cavioidea	
G_spixii	1,707,066	Caviidae		Cavioidea	
H_hydrochaeris	13,534,101	Caviidae		Cavioidea	
H_isthmius	337,601	Caviidae		Cavioidea	
K_acrobata	75,812	Caviidae		Cavioidea	
K_rupestris	761,350	Caviidae		Cavioidea	
M_acouchy	1,082,813	Dasyproctidae		Cavioidea	
M_australis	1,911,418	Caviidae		Cavioidea	
M_niata	168,048	Caviidae		Cavioidea	
M_pratti	3,324,728	Dasyproctidae		Cavioidea	
M_shiptoni	42,649	Caviidae		Cavioidea	Yes
C_chinchilla	489,377	Chinchillidae		Chinchilloidea	
C_lanigera	33,782	Chinchillidae		Chinchilloidea	Yes
D_branickii	1,716,807	Dinomyidae		Chinchilloidea	
L_ahuacaense	15,242	Chinchillidae		Chinchilloidea	Yes
L_crassus	47,279	Chinchillidae		Chinchilloidea	
L_maximus	1,477,712	Chinchillidae		Chinchilloidea	
L_viscacia	1,957,976	Chinchillidae		Chinchilloidea	
L_wolffsohni	60,195	Chinchillidae		Chinchilloidea	
C_bicolor	540,218	Erethizontidae		Erethizontoidea	
C_ichillus	148,879	Erethizontidae		Erethizontoidea	

C_insidiosus	168,410	Erethizontidae	Erethizontoidea	
C_melanurus	1,465,296	Erethizontidae	Erethizontoidea	
C_nycthemera	342,984	Erethizontidae	Erethizontoidea	
C_prehensilis	13,044,939	Erethizontidae	Erethizontoidea	
C_pruinosus	247,446	Erethizontidae	Erethizontoidea	
C_quichua	507,609	Erethizontidae	Erethizontoidea	
C_roosmalenorum	164,725	Erethizontidae	Erethizontoidea	
C_rufescens	495,759	Erethizontidae	Erethizontoidea	
C_speratus	19,788	Erethizontidae	Erethizontoidea	Yes
C_spinosus	1,193,740	Erethizontidae	Erethizontoidea	
C_subspinosus	259,724	Erethizontidae	Erethizontoidea	
C_vestitus	16,332	Erethizontidae	Erethizontoidea	Yes
A_bennettii	146,536	Abrocomidae	Octodontoidea	
A_cinerea	510,834	Abrocomidae	Octodontoidea	
A_famatina	7,084	Abrocomidae	Octodontoidea	Yes
A_fuscus	43,753	Octodontidae	Octodontoidea	
A_porteri	23,434	Octodontidae	Octodontoidea	Yes
A_sagei	50,467	Octodontidae	Octodontoidea	
A_schistacea	9,165	Abrocomidae	Octodontoidea	Yes
A_uspallata	5,226	Abrocomidae	Octodontoidea	Yes
A_vaccarum	5,511	Abrocomidae	Octodontoidea	Yes
Abrocoma_boliviensis	17,659	Abrocomidae	Octodontoidea	Yes
Abrocoma_budini	6,709	Abrocomidae	Octodontoidea	Yes
C_argentinus	245,465	Ctenomyidae	Octodontoidea	
C_ashaninka	15,559	Abrocomidae	Octodontoidea	Yes
C_australis	43,373	Ctenomyidae	Octodontoidea	Yes
C_azarae	263,598	Ctenomyidae	Octodontoidea	
C_bergi	84,794	Ctenomyidae	Octodontoidea	
C_boliviensis	69,905	Ctenomyidae	Octodontoidea	
C_bonettoi	36,890	Ctenomyidae	Octodontoidea	Yes
C_brasiliensis	8,276	Ctenomyidae	Octodontoidea	Yes
C_colburni	203,097	Ctenomyidae	Octodontoidea	
C_coludo	46,286	Ctenomyidae	Octodontoidea	
C_conoveri	118,328	Ctenomyidae	Octodontoidea	
C_coyhaiquensis	16,876	Ctenomyidae	Octodontoidea	Yes
C_dorbignyi	90,295	Ctenomyidae	Octodontoidea	
C_dorsalis	47,094	Ctenomyidae	Octodontoidea	
C_emilianus	26,832	Ctenomyidae	Octodontoidea	Yes
C_famosus	45,080	Ctenomyidae	Octodontoidea	
C_flamarioni	50,026	Ctenomyidae	Octodontoidea	
C_fochi	40,544	Ctenomyidae	Octodontoidea	Yes
C_fodax	44,401	Ctenomyidae	Octodontoidea	
C_frater	210,698	Ctenomyidae	Octodontoidea	
C_fulvus	107,589	Ctenomyidae	Octodontoidea	
C_goodfellowi	54,533	Ctenomyidae	Octodontoidea	
C_haigi	231,022	Ctenomyidae	Octodontoidea	
C_ibicuiensis	12,959	Ctenomyidae	Octodontoidea	Yes
C_johannis	46,599	Ctenomyidae	Octodontoidea	
C_juris	47,798	Ctenomyidae	Octodontoidea	
C_knighti	47,476	Ctenomyidae	Octodontoidea	
C_lami	17,432	Ctenomyidae	Octodontoidea	Yes
C_laticeps	1,808,980	Echimyidae	Octodontoidea	
C_latro	87,430	Ctenomyidae	Octodontoidea	
C_leucodon	78,893	Ctenomyidae	Octodontoidea	
C_lewisi	58,319	Ctenomyidae	Octodontoidea	
C_magellanicus	274,820	Ctenomyidae	Octodontoidea	
C_mariafarelli	62,096	Ctenomyidae	Octodontoidea	
C_maulinus	92,568	Ctenomyidae	Octodontoidea	
C_mendocinus	426,738	Ctenomyidae	Octodontoidea	
C_minutus	56,522	Ctenomyidae	Octodontoidea	
C_nattereri	245,722	Ctenomyidae	Octodontoidea	
C_oblativus	19,250	Abrocomidae	Octodontoidea	Yes
C_occultus	46,479	Ctenomyidae	Octodontoidea	
C_opimus	316,073	Ctenomyidae	Octodontoidea	
C_osvaldoreigi	46,574	Ctenomyidae	Octodontoidea	
C_paraguayensis	49,312	Ctenomyidae	Octodontoidea	
C_pearsoni	40,046	Ctenomyidae	Octodontoidea	Yes

C_perrensi	1,853	Ctenomyidae	Octodontoidea	Yes
C_perrensi_complex	52,532	Ctenomyidae	Octodontoidea	
C_peruanus	73,054	Ctenomyidae	Octodontoidea	
C_pictus	37,312	Echimyidae	Octodontoidea	Yes
C_pilarensis	48,591	Ctenomyidae	Octodontoidea	
C_pontifex	76,742	Ctenomyidae	Octodontoidea	
C_porteousi	66,041	Ctenomyidae	Octodontoidea	
C_pundti	117,493	Ctenomyidae	Octodontoidea	
C_rionegrensis	92,479	Ctenomyidae	Octodontoidea	
C_roigi	37,807	Ctenomyidae	Octodontoidea	Yes
C_rondoni	107,029	Ctenomyidae	Octodontoidea	
C_rosendopascuali	72,270	Ctenomyidae	Octodontoidea	
C_saltarius	82,940	Ctenomyidae	Octodontoidea	
C_scagliai	72,263	Ctenomyidae	Octodontoidea	
C_sericeus	34,159	Ctenomyidae	Octodontoidea	Yes
C_sociabilis	28,677	Ctenomyidae	Octodontoidea	Yes
C_steinbachi	69,476	Ctenomyidae	Octodontoidea	
C_sulcidens	1,803,485	Echimyidae	Octodontoidea	
C_talarum	428,201	Ctenomyidae	Octodontoidea	
C_torquatus	235,493	Ctenomyidae	Octodontoidea	
C_tuconax	62,420	Ctenomyidae	Octodontoidea	
C_tucumanus	65,364	Ctenomyidae	Octodontoidea	
C_tulduco	56,658	Ctenomyidae	Octodontoidea	
C_validus	67,060	Ctenomyidae	Octodontoidea	
C_viperinus	66,378	Ctenomyidae	Octodontoidea	
C_yolandae	67,080	Ctenomyidae	Octodontoidea	
Ctenomys_bicolor	55,566	Ctenomyidae	Octodontoidea	
D_boliviensis	391,116	Echimyidae	Octodontoidea	
D_caniceps	46,032	Echimyidae	Octodontoidea	
D_dactylinus	4,382,849	Echimyidae	Octodontoidea	
D_labilis	132,509	Echimyidae	Octodontoidea	
D_peruanus	233,664	Echimyidae	Octodontoidea	
E_chrysurus	1,493,625	Echimyidae	Octodontoidea	
E_saturnus	113,286	Echimyidae	Octodontoidea	
E_spinosus	1,071,738	Echimyidae	Octodontoidea	
E_vieirai	94,883	Echimyidae	Octodontoidea	
H_gymnurus	207,895	Echimyidae	Octodontoidea	
I_barbarabrownae	26,281	Echimyidae	Octodontoidea	Yes
I_bistriata	1,844,783	Echimyidae	Octodontoidea	
I_negrensis	609,719	Echimyidae	Octodontoidea	
I_orinoci	146,637	Echimyidae	Octodontoidea	
I_pagurus	245,650	Echimyidae	Octodontoidea	
I_sinnamariensis	162,005	Echimyidae	Octodontoidea	
K_amblyonyx	676,648	Echimyidae	Octodontoidea	
L_emiliae	322,561	Echimyidae	Octodontoidea	
M_coypus	2,870,255	Echimyidae	Octodontoidea	
M_didelphoides	4,894,281	Echimyidae	Octodontoidea	
M_hispidus	5,232,543	Echimyidae	Octodontoidea	
M_leniceps	49,408	Echimyidae	Octodontoidea	
M_macrura	2,597,869	Echimyidae	Octodontoidea	
M_occultus	75,919	Echimyidae	Octodontoidea	
M_stimulax	406,791	Echimyidae	Octodontoidea	
O_albicaudus	161,387	Echimyidae	Octodontoidea	
O_bridgesii	134,622	Octodontidae	Octodontoidea	
O_degus	63,584	Octodontidae	Octodontoidea	
O_edax	18,153	Echimyidae	Octodontoidea	Yes
O_gliroides	508,286	Octodontidae	Octodontoidea	
O_lunatus	31,547	Octodontidae	Octodontoidea	Yes
O_mimax	123,288	Octodontidae	Octodontoidea	
Octodon_pacificus	2,411	Octodontidae	Octodontoidea	Yes
P_blainvilii	658,028	Echimyidae	Octodontoidea	
P_brasiliensis	53,869	Echimyidae	Octodontoidea	
P_brevicauda	1,836,935	Echimyidae	Octodontoidea	
P_canicollis	135,176	Echimyidae	Octodontoidea	
P_carrikeri	191,006	Echimyidae	Octodontoidea	
P_chrysaeolus	160,051	Echimyidae	Octodontoidea	
P_cuvieri	3,637,416	Echimyidae	Octodontoidea	

P_dasythrix	267,947	Echimyidae	Octodontoidea	
P_decumanus	87,485	Echimyidae	Octodontoidea	
P_echinothrix	1,066,447	Echimyidae	Octodontoidea	
P_flavidus	1,350	Echimyidae	Octodontoidea	Yes
P_gardneri	493,504	Echimyidae	Octodontoidea	
P_goeldii	1,480,204	Echimyidae	Octodontoidea	
P_guairae	339,075	Echimyidae	Octodontoidea	
P_guyannensis	1,913,731	Echimyidae	Octodontoidea	
P_hoplomyoides	150,511	Echimyidae	Octodontoidea	
P_kerri	17,607	Echimyidae	Octodontoidea	Yes
P_kulinae	175,886	Echimyidae	Octodontoidea	
P_lamarum	444,602	Echimyidae	Octodontoidea	
P_longicaudatus	1,609,756	Echimyidae	Octodontoidea	
P_lundi	6,808	Echimyidae	Octodontoidea	Yes
P_mantiqueirensis	11,264	Echimyidae	Octodontoidea	Yes
P_medius	923,862	Echimyidae	Octodontoidea	
P_mincae	19,454	Echimyidae	Octodontoidea	Yes
P_nigrispinus	426,967	Echimyidae	Octodontoidea	
P_occasius	513,759	Echimyidae	Octodontoidea	
P_oconnelli	55,992	Echimyidae	Octodontoidea	
P_pattoni	585,425	Echimyidae	Octodontoidea	
P_punctatus	59,677	Echimyidae	Octodontoidea	
P_quadruplicatus	1,205,299	Echimyidae	Octodontoidea	
P_roberti	2,097,851	Echimyidae	Octodontoidea	
P_semispinosus	306,382	Echimyidae	Octodontoidea	
P_semivillosus	78,747	Echimyidae	Octodontoidea	
P_simonsi	2,001,152	Echimyidae	Octodontoidea	
P_steerei	1,641,293	Echimyidae	Octodontoidea	
P_sulinus	618,481	Echimyidae	Octodontoidea	
P_thomasi	14,566	Echimyidae	Octodontoidea	Yes
P_trinitatis	27,643	Echimyidae	Octodontoidea	Yes
P_unicolor	21,685	Echimyidae	Octodontoidea	Yes
Proechimys_pattoni	122,341	Echimyidae	Octodontoidea	
Proechimys_sp	57,748	Echimyidae	Octodontoidea	
S_cyanus	103,738	Octodontidae	Octodontoidea	
S_rufodorsalis	10,913	Echimyidae	Octodontoidea	Yes
T_a_albispinus	431,496	Echimyidae	Octodontoidea	
T_a_minor	47,901	Echimyidae	Octodontoidea	
T_apereoides	272,471	Echimyidae	Octodontoidea	
T_barrerae	285,342	Octodontidae	Octodontoidea	
T_dimidiatus	35,994	Echimyidae	Octodontoidea	Yes
T_eliasi	20,592	Echimyidae	Octodontoidea	Yes
T_g_bonafidei	10,943	Echimyidae	Octodontoidea	Yes
T_g_gratiosus	78,447	Echimyidae	Octodontoidea	
T_grandis	371,616	Echimyidae	Octodontoidea	
T_iheringi	29,269	Echimyidae	Octodontoidea	Yes
T_inermis	691,922	Echimyidae	Octodontoidea	
T_kirchnerorum	5,669	Octodontidae	Octodontoidea	Yes
T_laurentius	890,396	Echimyidae	Octodontoidea	
T_loschalchalerosorum	12,573	Octodontidae	Octodontoidea	Yes
T_mirapitanga	26,605	Echimyidae	Octodontoidea	Yes
T_moojeni	10,075	Echimyidae	Octodontoidea	Yes
T_pachyurus	937,455	Echimyidae	Octodontoidea	
T_paratus	38,120	Echimyidae	Octodontoidea	Yes
T_rhipidurus	137,361	Echimyidae	Octodontoidea	
T_s_elegans	139,005	Echimyidae	Octodontoidea	
T_s_setosus	442,134	Echimyidae	Octodontoidea	
T_yonenagae	34,220	Echimyidae	Octodontoidea	Yes
Thrichomys_sp	527,024	Echimyidae	Octodontoidea	
Tympanoctomys_aureus	12,150	Octodontidae	Octodontoidea	Yes